COLLECTED PAPERS ISEC 2017

5-9 November Miyazaki City, Japan

DOI: 10.5281/zenodo.7966154

Ion Transfer at the Interface between Water and a Fluorous Solvent 1,1,1,2,3,4,4,5,5,5-Decafluoropentane

Kohei UEMATSU[1,*], Hajime KATANO[1], Yasuhiro KURODA[1] and Toshiyuki OSAKAI[2]
[1]*Department of Bioscience, Fukui Prefectural University, Eiheiji, Fukui 910-1195, Japan;*
[2]*Department of Chemistry, Kobe University, Nada, Kobe 657-8501, Japan*

Ion-transfer reactions at the interface between fluorous solvent 1,1,1,2,3,4,4,5,5,5-decafluoropentane (DFP) and water (W) were investigated voltammetrically. Within the potential window at the DFP | W interface, various non-fluorinated ions, including tetraphenylarsonium (Ph_4As^+) and tetraphenylborate (Ph_4B^-), and fluorinated ions gave reversible voltammetric waves for their ion transfer across the DFP | W interface. Based on the Ph_4As^+-Ph_4B^- assumption, the formal potentials of their ion transfer could be determined in terms of Galvani potential difference. The formal Gibbs energies for the transfer of ions from DFP to W, which would provide the criteria necessary for evaluating the fluorophilicity/hydrophilicity of ions were calculated from the formal potentials, and were compared with the transfer energies from 1,2-dichloroethane to W and those from DFP to the organic solvent, as quantitative scales of the ion's lipophilicity/hydrophilicity and fluorophilicity/lipophilicity.

1. Introduction

Electrochemical processes at a liquid | liquid or non-aqueous solvent | W interface have been studied extensively, because of the wide range of applicability of the systems in chemistry and biology. It is necessary for the non-aqueous solvent that it is immiscible with W and forms stable interface, and that it dissolves high concentration of electrolyte to give a high conductivity. To date, nitrobenzene (NB), 1,2-dichloroethane (DCE), and their analogues have been used as non-aqueous solvents in liquid-liquid electrochemistry. In a previous paper [1], we examined the applicability of a fluorous solvent DFP as a non-aqueous phase for ion-transfer voltammetry. In this study, we have investigated the transfer of various monovalent ions across the DFP | W interface. Interestingly, unlike the DCE | W and NB | W interfaces, Ph_4As^+ and Ph_4B^- ions gave voltammetric waves within the potential window of the DFP | W interface. The voltammograms could be attributed to the reversible transfer of monovalent ions, and the reversible half-wave potentials, ${}_{\mathrm{r}}E_{1/2}(Ph_4As^+)$ and ${}_{\mathrm{r}}E_{1/2}(Ph_4B^-)$, were determined. On the basis of the Ph_4As^+-Ph_4B^- extrathermodynamic assumption, the formal potentials for the transfer of these ions in terms of the Galvani potential difference at the DFP | W interface, $\Delta^{\mathrm{W}}_{\mathrm{DFP}}\phi^{0\prime}(Ph_4As^+)$ and $\Delta^{\mathrm{W}}_{\mathrm{DFP}}\phi^{0\prime}(Ph_4B^-)$, were calculated from the ${}_{\mathrm{r}}E_{1/2}$ values. Other ions (j^z, z being the charge number including sign) also gave reversible voltammetric waves, and their $\Delta^{\mathrm{W}}_{\mathrm{DFP}}\phi^{0\prime}(j^z)$ values were determined. From the $\Delta^{\mathrm{W}}_{\alpha}\phi^{0\prime}(j^z)$ values (α = DFP, DCE, and NB), the formal Gibbs transfer energy of j^z ion from the α to the W phase, $\Delta G^{0\prime}_{\mathrm{tr},\alpha\rightarrow\mathrm{W}}(j^z)$, were calculated by

$$\Delta G^{0,}_{\mathrm{tr},\alpha\rightarrow\mathrm{W}}(j^z) = -zF\Delta^{\mathrm{W}}_{\alpha}\phi^{0,}(j^z). \quad (1)$$

Although DFP is miscible with DCE (and NB), the transfer energy of j^z ion from DCE to DFP is calculated by

$$\Delta G^{0,}_{\mathrm{tr,DCE}\rightarrow\mathrm{DFP}}(j^z) = \Delta G^{0,}_{\mathrm{tr,DCE}\rightarrow\mathrm{W}} - \Delta G^{0,}_{\mathrm{tr,DFP}\rightarrow\mathrm{W}}. \quad (2)$$

The $\Delta G^{0,}_{\mathrm{tr,DFP}\rightarrow\mathrm{W}}$, $\Delta G^{0,}_{\mathrm{tr,DCE}\rightarrow\mathrm{W}}$, and $\Delta G^{0,}_{\mathrm{tr,DCE}\rightarrow\mathrm{DFP}}$ values can be useful as quantitative scales of the affinities for the fluorous solvent, water, and the non-fluorinated organic solvent, that is, fluorophilicity, hydrophilicity and lipophilicity of ions. These values of non-fluorinated and fluorinated ions were compared with each other.

2. Experimental

2.1 Reagents

The purification of DFP and the preparation of supporting electrolytes for the DFP phase, tetra-*n*-octylammonium bis(nonafluorobutanesulfonyl)imide (Oct_4NBNSI) and tetrabutylammonium tetrakis[3,5-bis(trifluoromethyl)phenyl]borate (Bu_4NTFPB) were described in Ref. 1. $Ph_4AsBNSI$ and Bu_4N^+ salts with $[(C_nF_{2n+1}SO_2)_2N]^-$ at n = 1, 2, and 3 ($BTSI^-$, $BPSI^-$ and $BHSI^-$) were prepared in a manner similar to that used to prepare Oct_4NBNSI or Bu_4NBNSI. Other chemicals were of reagent grade and used as received.

2.2 Measurements

Ion-transfer reactions across the DFP | W interface have been studied by means of cyclic voltammetry using a three-electrode system. Cells I and II represent the electrochemical cells used to record the cyclic voltammograms (CVs) of the transfer of the Ph_4As^+ and Ph_4B^- ions across the DFP | W interface, respectively.

cell I:

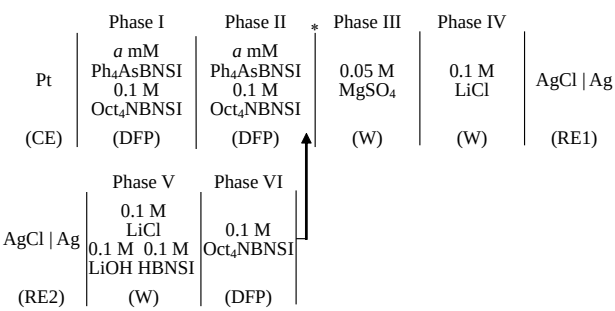

cell II:

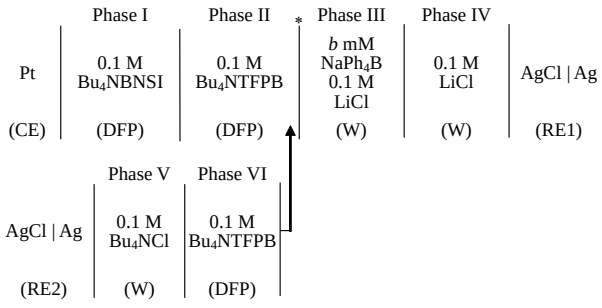

The test DFP | W interface is indicated by an asterisk. The electrolysis cell is described in Ref. 1. The solution resistance between the two reference electrodes was about 2 kΩ for cells I and II. E was controlled by a potentiostat furnished with a positive feedback iR compensation circuit. In this paper, the E value is reported against the ${}_{\mathrm{r}}E_{1/2}$ for transfer of the tetramethylammonium (Me_4N^+) ion across the DFP | W interface, which was determined to be ${}_{\mathrm{r}}E_{1/2}(Me_4N^+)$ = –0.276 V with cell I and 0.334 V with cell II. All electrochemical measurements were carried out at 25±1°C.

3. Results and Discussion

3.1 Physical properties of DFP

At 25°C, the solubility of W in DFP is 0.049 wt% [1], and the density of DFP is 1.58 g cm^{-3}. Therefore, DFP formed a stable interface with W. The relative permittivity of DFP is 6.72, which is lower than those of DCE (10.45) and NB (34.78). Despite the low permittivity, DFP dissolves an electrolyte Oct_4NBNSI at the 0.1 M level, and the conductivity of the 0.1 M Oct_4NBNSI (DFP) was 220 μS/cm, which is comparable to those of the DCE and NB solutions (910 and 690 μS/cm). The viscosity of DFP was determined to be 0.90 cP by a vibro viscometer. The value is very close to that of W. On the basis of Walden rule, the ratio of the diffusion coefficient of a j^z ion in the W phase to that in the DFP phase, D_j^W/D_j^{DFP}, is assumed to be $D_j^W/D_j^{DFP} \approx 1$ in the determination of $\Delta_{DFP}^W\phi^{0'}(j^z)$ below.

3.2 Transfer of Ph_4As^+ and Ph_4B^- ions at the DFP | W interface

Curve (a) in Figure 1 shows a CV obtained with cell I at a = 0, that is, the base current of the 0.1 M Oct_4NBNSI (DFP) | 0.05 M $MgSO_4$ (W) interface at the scan rate of ν = 0.1 V s^{-1}. A polarizable potential window was observed. Curve (b) in the figure shows a CV obtained with cell I at a = 0.5 and ν = 0.1 V s^{-1}. Within the potential window, a pair of well-defined cathodic and anodic peak currents were observed, corresponding to the transfer of the Ph_4As^+ ion from the DFP to the W phase and back to the DFP phase, respectively. The dependence of the height of anodic peak current and the potential peak separation on ν indicates that the voltammogram can be assigned to a reversible CV of monovalent ion transfer. By taking that the reversible half-wave potential is equal to the midpoint potential, the ${}_rE_{1/2,}(Ph_4As^+)$ was determined to be –0.387±0.004 V *vs.* ${}_rE_{1/2,}(Me_4N^+)$.

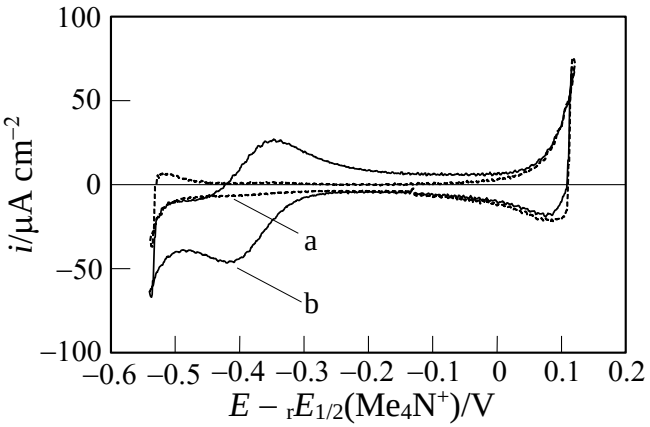

Figure 1. Cyclic voltammograms (CVs) at the 0.1 M Oct_4NBNSI (DFP) | 0.05 M $MgSO_4$ (W) interface in the (a) absence and (b) presence of 0.5 mM $Ph_4AsBNSI$ in the DFP phase. Scan rate, ν = 0.1 V s^{-1}.

Curve (a) in Figure 2 shows a CV obtained with cell II at b = 0. By the replacement of the electrolyte anion, the anodic final rise was shifted to a more positive potential range. Curve (b) in the figure shows a CV obtained with cell II at b = 0.1. The anodic and cathodic voltammetric waves can be attributed to the transfer of the Ph_4B^- ion from the W to the DFP phase and back to the W phase, respectively. The voltammogram can be assigned to a reversible CV of monovalent ion transfer, and the reversible half-wave potential ${}_rE_{1/2,}(Ph_4B^-)$ was determined to be 0.067±0.005 V *vs.* ${}_rE_{1/2,}(Me_4N^+)$.

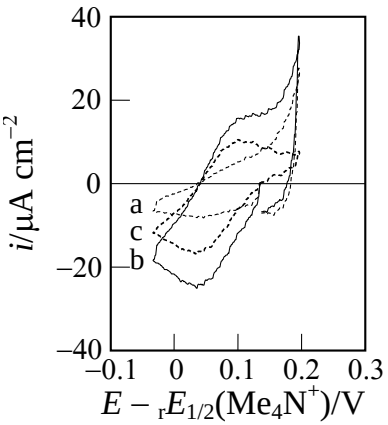

Figure 2. CVs at the 0.1 M Bu_4NTFPB (DFP) | 0.1 M LiCl (W) interface in the (a) absence and (b) presence of 0.1 mM $NaPh_4B$ in the W phase. ν = 0.1 V s^{-1}. (c), (b) – (a).

The reversible half-wave potential of a j^z ion, ${}_rE_{1/2}(j^z)$, can be related to $\Delta^W_{DFP}\phi^{0'}(j^z)$, as given by

$${}_rE_{1/2}(j^z) = \Delta^W_{DFP}\phi^{0'}(j^z) + (RT/zF)\ln[(D_j^W/D_j^{DFP})^{1/2}] + \Delta E_{ref}, \quad (3)$$

where ΔE_{ref} is determined by the reference electrode system for cells I and II. R, T, and F are used in the usual meaning. By taking $D_j^W/D_j^{DFP} = 1$, that is, $(RT/zF)\ln[(D_j^W/D_j^{DFP})^{1/2}] = 0$, and $\Delta^W_{DFP}\phi^{0'}(Ph_4As^+) + \Delta^W_{DFP}\phi^{0'}(Ph_4B^-) = 0$, the formal potentials are calculated to be $\Delta^W_{DFP}\phi^{0'}(Ph_4As^+) = -0.227\pm0.006$ V, $\Delta^W_{DFP}\phi^{0'}(Ph_4B^-) = 0.227\pm0.006$ V, and $\Delta^W_{DFP}\phi^{0'}(Me_4N^+) = 0.160\pm0.006$ V. Also, ΔE_{ref} values were calculated to be −0.365 and 0.174 V for cells I and II, respectively.

3.3 Formal potentials for the transfer of ions at DFP | W interface

The CVs of the transfer of choline (Ch^+), acetylcholin (ACh^+), tetraethylammonium (Et_4N^+), tetrapropylammonium (Pr_4N^+), and Bu_4N^+ cations and 2,4,6-trinitrophenolate (TNP^-), 2,4-dinitrophenolate (DNP^-), ClO_4^-, SCN^-, I^-, NO_3^-, and Br^- anions at the DFP | W interface were recorded with cell I, in which Phase III (W) was replaced by 0.50 mM j^+Cl^- (j^+ = Ch^+, and ACh^+), j^+Br^- (j^+ = Et_4N^+, Pr_4N^+, and Bu_4N^+), or Na^+j^- (j^- = TNP^-, DNP^-, ClO_4^-, SCN^-, I^-, NO_3^-, and Br^-) and 0.05 M $MgSO_4$ (W), and Phases I and II were replaced by 0.1 M Oct_4NBNSI (DFP). These ions gave well-developed voltammetric waves within the potential window, and the voltammetric behaviors were of reversible nature. Using $\Delta E_{ref} = -0.365$ V, the $\Delta^W_{DFP}\phi^{0'}(j^z)$ values were determined as listed in Table 1 together with the reported values of $\Delta^W_{DCE}\phi^{0'}$[2] and $\Delta^W_{NB}\phi^{0'}$ [3-5].

Table 1. Formal potentials for the transfer of non-fluorinated ions at the DFP, DCE, and NB | W interfaces, $\Delta^W_{DFP}\phi^{0'}$, $\Delta^W_{DCE}\phi^{0'}$, and $\Delta^W_{NB}\phi^{0'}$ (in V)

ion	$\Delta^W_{DFP}\phi^{0'}$	$\Delta^W_{DCE}\phi^{0'}$ [a]	$\Delta^W_{NB}\phi^{0'}$ [b]
cation			
Ch^+	0.223±0.004	0.200	0.117
Me_4N^+	0.160±0.006	0.133	0.035
ACh^+	0.140±0.002	0.110	0.049
Et_4N^+	0.036±0.003	−0.013	−0.055
Pr_4N^+	−0.087±0.003	−0.141	−0.170
Bu_4N^+	−0.189±0.005	−0.278	−0.275
Ph_4As^+	−0.227±0.006	−0.341	−0.372
anion			
Ph_4B^-	0.227±0.006	0.345	0.372
TNP^-	−0.016±0.003	0.043	0.069
ClO_4^-	−0.097±0.003	−0.078	−0.082
DNP^-	−0.113±0.004	−0.083	−0.076
SCN^-	−0.197±0.003	−0.161	−0.164
I^-	−0.227±0.004	−0.179	−0.191
NO_3^-	−0.241±0.003	−0.258	−0.261
Br^-	−0.318±0.004	−0.289	−0.288

a) Ref. 2, b) Refs. 3-5.

Fluorocomplex anions, BF_4^- and PF_6^-, perfluoro-*n*-alkanoate anions, $C_nF_{2n+1}COO^-$ with n = 1, 2, 3, and 4 (TFA^-, PFP^-, HFB^-, and NFP^-, respectively), and $BTSI^-$ anion gave reversible CVs within the potential window at the 0.1 M Oct_4BNSI (DFP) | 0.05 M $MgSO_4$ (W) interface, and their formal potentials were determined as listed in Table 2. The formal potential for the transfer of the $BPSI^-$, and $BHSI^-$ were determined by the EMF measurement as listed in the table.

Table 2. $\Delta^W_{DFP}\phi^{0'}$ and $\Delta^W_{DCE}\phi^{0'}$ for fluorinated ions (in V).

ion	$\Delta^W_{DFP}\phi^{0'}$	$\Delta^W_{DCE}\phi^{0'}$
$BHSI^-$	0.317±0.001	0.206±0.004
$BPSI^-$	0.217±0.002	0.142±0.004
$BTSI^-$	0.132±0.002	0.078±0.004
PF_6^-	0.063±0.004	0.041±0.004
NFP^-	−0.099±0.002	−0.103±0.002
BF_4^-	−0.113±0.003	−0.097±0.003
HFB^-	−0.156±0.002	−0.140±0.002
PFP^-	−0.199±0.002	−0.181±0.002
TFA^-	−0.264±0.003	---[a]

a) Out of the potential window.

3.4 Formal Gibbs transfer energy

The possible ion-pair formation of tested ions with electrolyte ions in DFP is currently studied, so at present we cannot make a meticulous discussion of the standard potentials for the transfer of ions at the DFP | W interface. However, the determined formal potentials, though

involving the contribution of ion-pair formation, may be useful to discuss the hydrophilic, hydrophobic, or fluorophilic nature of the ions. From the values of $\Delta^{W}_{DFP}\phi^{0'}$ and $\Delta^{W}_{DCE}\phi^{0'}$, $\Delta G^{0'}_{tr,DFP\rightarrow W}$, $\Delta G^{0'}_{tr,DCE\rightarrow W}$, and $\Delta G^{0'}_{tr,DCE\rightarrow DFP}$ were calculated by Eqs. (1) and (2), as listed in Table 3.

In Fig. 3, $\Delta G^{0'}_{tr,DFP\rightarrow W}$ for non-fluorinated ions is plotted against $\Delta G^{0'}_{tr,DCE\rightarrow W}$ as shown by the filled circles. The plot gives the regression line:

$$\Delta G^{0'}_{tr,DFP\rightarrow W}\ /\text{kJ mol}^{-1} = (0.84\pm0.040)(\Delta G^{0'}_{tr,DCE\rightarrow W}\ /\text{kJ mol}^{-1}) + (-4.9\pm0.9), \quad (4)$$

with the correlation coefficient of 0.993. Despite the differences in the sign of the charge and in the structure among the ions tested, an excellent linear relationship was observed between $\Delta G^{0'}_{tr,DFP\rightarrow W}$ and $\Delta G^{0'}_{tr,DCE\rightarrow W}$. Such an excellent linear relationship was also observed between $\Delta G^{0'}_{tr,DFP\rightarrow W}$ and $\Delta G^{0'}_{tr,NB\rightarrow W}$.

Despite the richness of fluorine atoms, TFA^-, PFP^-, HFB^-, BF_4^-, and NFP^- ions gave negative $\Delta G^{0'}_{tr,DFP\rightarrow W}$ values. Since their $\Delta G^{0'}_{tr,DCE\rightarrow W}$ values were also negative, and these ions can be categorized as hydrophilic. This category of ions is not bulky, so their surfaces have higher electric field strength. Therefore, the electrostatic (*i.e.*, coulomb and polarization) ion–solvent interactions would contribute significantly to the Gibbs transfer energy. On the other hand, the PF_6^-, $BTSI^-$, $BPSI^-$, and $BHSI^-$ ions gave positive $\Delta G^{0'}_{tr,DCE\rightarrow W}$ values, and thus can be categorized as hydrophobic. The $\Delta G^{0'}_{tr,DFP\rightarrow W}$ for fluorinated ions is plotted against $\Delta G^{0'}_{tr,DCE\rightarrow W}$ as shown by the open circles in Fig. 3. The $\Delta G^{0'}_{tr,DFP\rightarrow W}$ values for the hydrophilic fluorinated ions are close to their $\Delta G^{0'}_{tr,DCE\rightarrow W}$. However, the $\Delta G^{0'}_{tr,DFP\rightarrow W}$ values for the hydrophobic fluorinated ions are higher than those predicted from Eq. (4) with increasing $\Delta G^{0'}_{tr,DCE\rightarrow W}$, that is, the hydrophobicity of the ions.

As another representation, the values of $\Delta G^{0'}_{tr,DCE\rightarrow DFP}$ are plotted against those of $\Delta G^{0'}_{tr,DCE\rightarrow W}$ in Fig. 4. $\Delta G^{0'}_{tr,DCE\rightarrow DFP}$ could be used as a quantitative scale of fluorophilicity/lipophilicity of ions. The plots of $\Delta G^{0'}_{tr,DCE\rightarrow DFP}$ for hydrophilic ions are concentrated in the vicinity of the abscissa axis, *i.e.*, at $\Delta G^{0'}_{tr,DCE\rightarrow DFP} = 0$. The $\Delta G^{0'}_{tr,DCE\rightarrow DFP}$ for hydrophobic fluorinated ions, however, shifted to more negative values with increasing $\Delta G^{0'}_{tr,DCE\rightarrow W}$, *i.e.*, the hydrophobicity of the ions. On the other hand, $\Delta G^{0'}_{tr,DCE\rightarrow DFP}$ for hydrophobic non-fluorinated ions shifted to more positive values with increasing $\Delta G^{0'}_{tr,DCE\rightarrow W}$. These results suggest that fluorophilicity of ions should be a physical property incompatible with both lipophilicity and hydrophilicity.

Table 3. Formal Gibbs transfer energy of tested ions from DFP to W, $\Delta G^{0'}_{tr,DFP\rightarrow W}$, from DCE to W, $\Delta G^{0'}_{tr,DCE\rightarrow W}$, and from DCE to DFP, $\Delta G^{0'}_{tr,DCE\rightarrow DFP}$ (in kJ mol^{-1}).

ion	$\Delta G^{0'}_{tr,DFP\rightarrow W}$	$\Delta G^{0'}_{tr,DCE\rightarrow W}$	$\Delta G^{0'}_{tr,DCE\rightarrow DFP}$
cation			
Ch^+	−21.5	−19.3	2.2
Me_4N^+	−15.4	−12.8	2.6
ACh^+	−13.5	−10.6	2.9
Et_4N^+	−3.5	1.3	4.7
Pr_4N^+	8.4	13.6	5.2
Bu_4N^+	18.2	26.8	8.6
Ph_4As^+	21.9	32.9	11.0
anion			
Ph_4B^-	21.9	33.3	11.4
TNP^-	−1.5	4.1	5.7
ClO_4^-	−9.4	−7.5	1.8
DNP^-	−10.9	−8.0	2.9
SCN^-	−19.0	−15.5	3.5
I^-	−21.9	−17.3	4.6
NO_3^-	−23.3	−24.9	−1.6
Br^-	−30.7	−27.9	2.8
fluorinated			
$BHSI^-$	30.6	19.9	−10.7
$BPSI^-$	20.9	13.7	−7.2
$BTSI^-$	12.9	7.5	−5.4
PF_6^-	6.1	4.0	−2.1
NFP^-	−9.6	−9.9	−0.4
BF_4^-	−10.9	−9.4	1.5
HFB^-	−15.1	−13.5	1.5
PFP^-	−19.2	−17.5	1.7

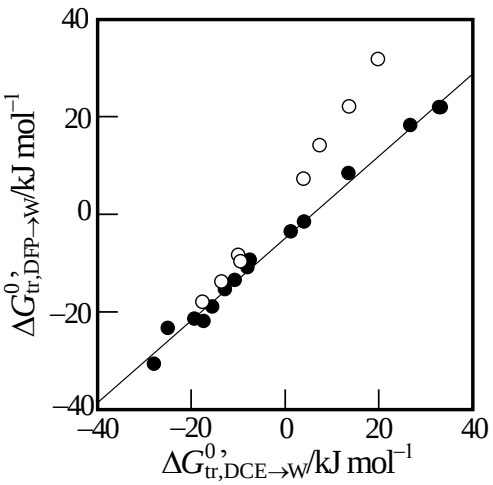

Figure 3. Plots of the formal Gibbs transfer energy from DFP to W, $\Delta G^{0,}_{tr,DFP\rightarrow W}$, against that from DCE to W, $\Delta G^{0,}_{tr,DCE\rightarrow W}$, for non-fluorinated (●) and fluorinated (○) ions.

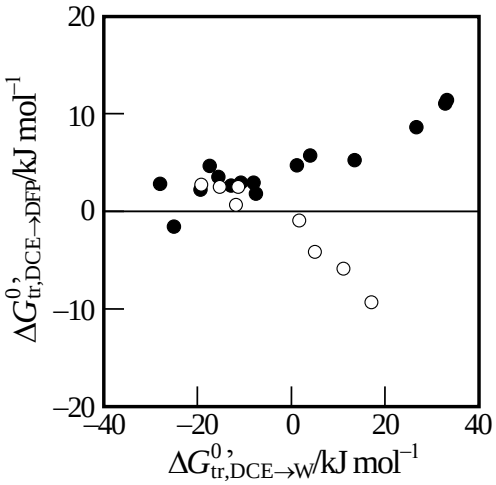

Figure 4. Plots of the formal Gibbs transfer energy from DCE to DFP, $\Delta G^{0,}_{tr,DCE\rightarrow DFP}$ against $\Delta G^{0,}_{tr,DCE\rightarrow W}$, for non-fluorinated (●) and fluorinated (○) ions.

4. Conclusions

The transfer of ions at the interface between a fluorous solvent DFP and water could be studied voltammetrically, and the electrochemical data gave the formal Gibbs transfer energy of various ions from DFP to water or organic solvents, which can provide useful criteria for evaluating the fluorophilicity, lipophilicity, and hydrophilicity of ions. The transfer energy would be also useful to understand the interfacial process in solvent extraction using fluorous solvents and compounds.

References

1) H. Katano, Y. Kuroda, K. Uematsu, *J. Electroanal. Chem.*, **788**, 232-234 (2017).
2) H. Katano, H. Tatsumi, M. Senda, *Talanta*, **63**, 185-193 (2004) 185.
3) T. Osakai, K. Ebina, *J. Phys. Chem. B*, **102**, 5691-5968 (1998).
4) J. Koryta, *Electrochim. Acta*, **29**, 445-452 (1984).
5) Z. Samec, D. Homolka, V. Mereček, L. Kavan, *J. Electroanal. Chem.*, **145**, 213-218 (1983).

Binary Droplet Coalescence – Influence of Ions and Mass Transfer

Jens S. HEINE[1,*], Felix GEBAUER[1], Christian WECKER[2], Eugeny Y. KENIG[2] and Hans-Jörg BART[1]

[1]*Chair of Separation Science and Technology, University of Kaiserslautern, Kaiserslautern, 67663, Germany;* [2]*Chair of Fluid Process Engineering, Paderborn University, Paderborn, 33098, Germany*

The behavior of coalescence in liquid/liquid systems is determined by multiple factors, including the concentration and type of any continuous phase ions present. Their influence on the film drainage time was captured with a high speed imaging system. Higher coalescence probabilities were found to correlate with a simple drainage model. Another focus was the mass transfer during droplet formation. Here in situ analytics in the system toluene/acetonitrile/water was applied for the mass transfer direction from the dispersed to the continuous phase. Marangoni effects during droplet formation are the reason that more than 75 % of the mass transfer occurs in the first 5 seconds, which agrees with the literature data reporting up to 80 %. Therefore, initial droplet formation (< 5 seconds) was also investigated by in silico experiments. The corresponding CFD studies were based on volume capturing methods.

1. Introduction

In chemical, biochemical and petrochemical processes, mass transfer in liquid/liquid extraction is of vital importance. The process efficiency and product quality in technical processes are substantially influenced by the interfacial area, which depends on the competitive dynamic phenomena of droplet breakage and coalescence. Despite comprehensive scientific research efforts, the influencing factors (e.g. pH value, salts, mass transfer), especially for coalescence, are not fully understood, and thus predictive modelling is not yet possible [2, 3].

The influence of the drainage on coalescence outcomes has been described in literature by various models. The most widely used approach of Coulaloglou and Tavlarides [4] assumes the coalescence probability as a ratio of drainage to contact time. A simplified relation [4] was used to describe the dependence of coalescence probability λ on the ratio of drainage $t_{drainage}$ to contact time $t_{contact}$, and the model of Coulaloglou and Tavlarides [4] is expanded via an additional exponent χ:

$$\lambda_{C\&T} = \exp\left(-\frac{t_{drainage}}{t_{contact}}\right)^{\chi} \quad (1)$$

The influence of ionic species on coalescence is reported, but scarcely systemically investigated [5]. A classification according to Hofmeister [6] is based on the precipitation effect, which distinguishes between cosmotropic and chaotropic ions. In the following sequence, cosmotropic ions are placed left and chaotropic right:

$$F^- \approx SO_4^{2-} < HPO_4^{2-} < CH_3COO^- < Cl^- < NO_3^- < Br^- < Clo_3^- < I^- < ClO_4^- < SCN^- < Cl_3CCOO^- \quad (2)$$

Structure forming ions (cosmotropic) intensify hydropobic effects, which are responsible for the separation of oil/water mixtures.

Regarding the mass transfer, a local (tangential) shear stress condition (e.g. a concentration dependent interfacial tension gradient) reflects a strong coupling between the velocity and the concentration fields. Marangoni instabilities (interfacial flow) are observed [7] when interfacial tension gradients are inducted by gradients in the solute concentration. In such cases, up to 80 % of the mass transfer occurs already during droplet formation [8].

The concentration profile in a droplet can be described as [9, 10]:

$$Fo_{tu} \leq 0.15: \qquad \frac{y(t)-y_I}{y_0-y_I} = 1-6\cdot\sqrt{\frac{Fo_{tu}}{\pi}}+3\cdot Fo_{tu} \tag{3}$$

with $Fo_{tu} = \frac{4\cdot D_{tu}\cdot t}{d^2}$ and $D_{tu} = T\cdot D$

where *Fo* stays for Fourier number, *y* for mass fraction of the transfer component, *D* for diffusion coefficient, *t* for time, *d* for droplet diameter, *T* for intensification factor.

When applying Equation 3 to describe experimental data, *T* is regarded as an adjustable parameter, since the turbulent eruptions have not yet been quantified. Model improvements require a high spatial and temporal resolution of the local phenomena, which is difficult to achieve experimentally. The possibility to overcome these limitations is given by computational fluid dynamics (CFD) simulations. In our study, the open-source CFD package OpenFOAM® was used. A standard volume-of-fluid (VOF) solver was extended with the mass transfer model of Haroun [11], adjusted boundary conditions and some improvements for the curvature approximation to reduce spurious currents.

2. Materials and methods

2.1 Experimental setup

The influence of ionic species and pH on coalescence was investigated with sodium chloride (Merck 1.06404), sodium nitrate (VWR chemicals 27955.295), sodium perchlorate (Merck 1.06564), sodium thiocyanate (Sigma-Aldrich S7757-250G) and sodium sulfate (VWR chemicals 28114.296). Sodium hydroxide (Merck 1.09956) was used to adjust the pH value. Water and toluene were mutually saturated in order to avoid additional mass transfer. Acetonitrile (ACN) as solute and toluene as solvent were of a purity > 99.8 % (CHROMANORM®). Water (conductivity of < 0.5 $\mu S\cdot cm^{-1}$) was purified by reserved osmosis (Hydrotec, Hydromos UO 50 W) and ion exchange (Hydrotex, Hydromos VE 17).

Constant and reproductive test conditions for the droplet generation (precision syringe pump, PSD/3-Mini module, from Hamilton®), detachment and interaction were ensured with a coalescence cell after Kamp and Kraume [12]. A high speed camera (Photron Fastcam APX RS) recorded videos with a resolution of 256x256 pixels and a frame rate of 30000 fps. The size of the rising droplet d_b (at constant rising height of 0.5 mm to the hanging droplet d_u) was systematically varied, in order to adjust the equivalent droplet diameter d_{eq}:

$$d_{eq}=2\cdot\frac{d_u \cdot d_b}{d_u + d_b} \quad (4)$$

The mass transfer and the effect of Marangoni convection during droplet formation was identified by measuring the interfacial tension as a function of time, as well as by measuring the concentration inside the droplet by non-invasive confocal Raman spectroscopy.

Measurement methods:

- A newly designed test cell for single droplet mass transfer [13] was made of stainless steel and PTFE, with a capillary height of 2 mm and the inner dimensions of 33 mm*23 mm*33 mm (*L*W*D*). The droplet is formed on a capillary, which has an inner diameter of 0.8 mm and an outer diameter of 1 mm. A precision syringe pump (PSD/3-Mini module) from Hamilton® was used to generate well-defined droplets with a volume rate of $\dot{V}$=12.5 µL·s^{-1}. The solute concentration inside the droplet was measured via a confocal Raman spectrometer HR800 from Horiba (532 nm laser from Quantum, type torus 532, software LabSpec6).
- The pendant drop method was used to determine the interfacial tension (OCA 15; Dataphysics) with a syringe in the surrounding phase in which the contact angles of a single droplet were measured. The curved syringe is used for the investigation of the pendant drops with an inner diameter of 0.69 mm and an outer diameter of 1.07 mm and a Hellma® glass-measuring cell [13] with the inner dimensions of 50 mm*50 mm*10 mm (*L*W*D*). The respective droplets were formed at a volumetric rate of $\dot{V}$= 2 µL·s^{-1}.

3. Results and discussion

3.1 Experimental

3.1.1 Ion species and strength

Experimentally determined coalescence probabilities and times are compared with the simplified correlation (s. Equation 1) in Figure 1. The coalescence probability was observed to decrease with increasing coalescence times for each ion species investigated, when adjusting the exponent χ = 1.6. An average contact time of 25 ms was used for the calculations of the theoretical coalescence probability. This assumption was chosen in accordance with the calculations of Villwock et al. [14].

Experimental outliers can be attributed to the high sensitivity of the coalescence process to marginal changes in the test system, which may

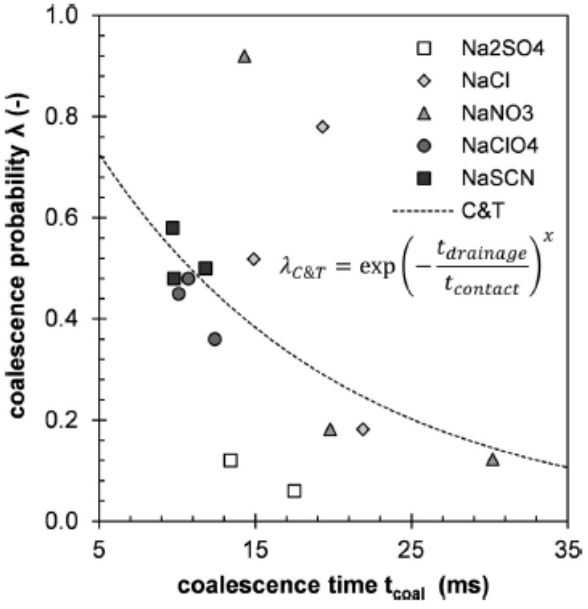

Figure 1. Effect of ionic species the coalescence time t_{coal}, for all d_{eq} [1]

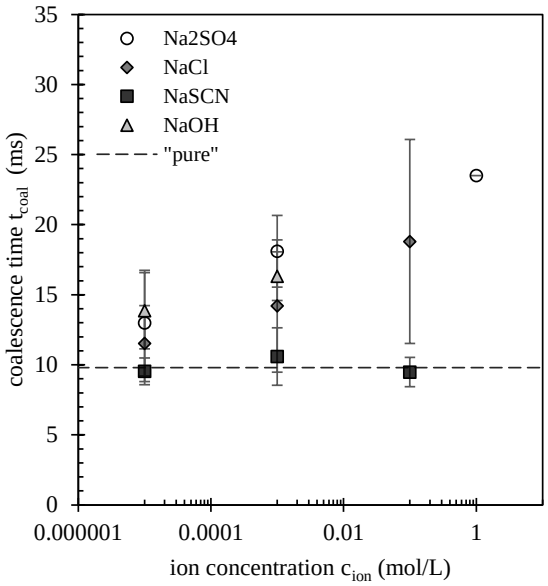

Figure 2. Coalescence probability vs. coalescence time for different ion species ($d_{eq} = 2.5\ mm$) [1]

Along with the influence of the ion species, the concentration is also of relevance (s. Figure 2). Increasing the concentration of chaotropic ion species (e.g. NaSCN) had a negligible effect on the coalescence time. In contrast, the coalescence time increased with the addition of cosmotropic anions (e.g. Na_2SO_4).

A description of the ion influence is required that is independent of the equivalent droplet diameter is possible, through the extension of the model of Prince et al. [15] with the newly developed Equation 5. Here the coalescence time is mapped over the entire range of salt concentrations using c_1 and c_2 to correlate different ion species:

not lead to a measureable change in physical properties (e.g. interfacial tension).

According to the aforementioned Hofmeister anion species classification (s. Equation 2), cosmotropic, structure-forming, anions were observed to slow down the drainage rate. For example, the addition of sodium sulfate increased the coalescence time as compared to the "pure" system (s. Figure 2). Chaotropic, structure-destroying, anions, such as SCN^-, have a significantly lower impact on the coalescence time.

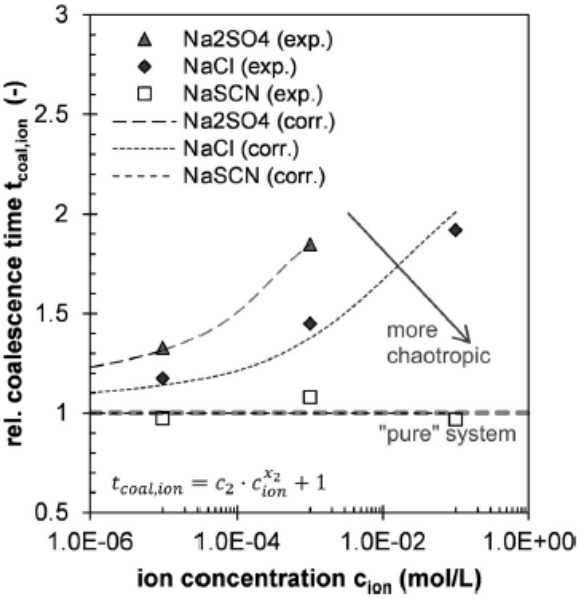

Figure 3. Effect of NaCl concentration on the coalescence time compared to correlation, Equation 5 [1]

$$t_{coal,P\&B^*,NaCl} = \left[\frac{\left(\frac{d_{eq}}{2}\right)^3 \cdot \rho_c}{16 \cdot \sigma}\right]^{\frac{1}{2}} \cdot \ln\left(\frac{h_0}{h_{crit}}\right) \cdot (c_1 \cdot c_{ion}^{c_2} + 1) \quad (5)$$

where t_{coal} is coalescence time, d_{eq} is equivalent droplet diameter, ρ is density, σ is interfacial tension, h_0 is film thickness at the point of contact, h_{crit} is critical film thickness, c_{ion} is ion concentration and c_1, c_2 are constants.

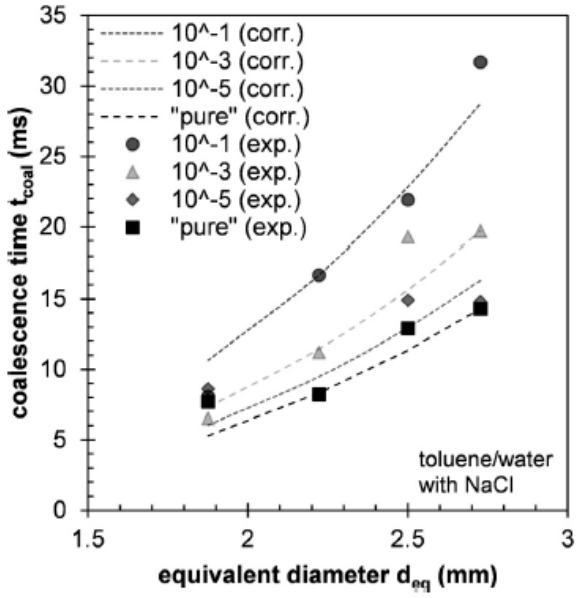

Figure 4. Effect of increasing NaCl concentration on the coalescence time according to Equation 5 [1]

3.1.2 Mass transfer measurement with Raman spectroscopy

The confocal Raman spectroscopy measurement in a droplet with an initial solute concentration of $c_{ACN} = 10$ w.-% and a volume of 4.2 µL shows a decrease of the solute concentration over time (s. Figure 5). It can be seen that the concentration decreases very fast, so that 90 % of the mass transfer occurs during the first 5 seconds. This fast decrease in concentration can be described with Equation 3 for turbulent mass transfer ($T = 25$) and follows the measurement results in the first 10 seconds very well.

The change in the coalescence time with the addition of e.g. sodium chloride ($c_1 = 1.652$, $c_1 = 0.214$) shown in Figure 3. Equation 5 enables a description of the coalescence time for changing ion concentrations of sodium chloride without adjustment (s. Figure 4).

However, Equation 5 is only valid below ionic concentrations of 10^{-1} mol/L and in the range of equivalent droplet diameters of 1.87 mm < d_{eq} < 2.73 mm for the EFCE standard test system toluene/water.

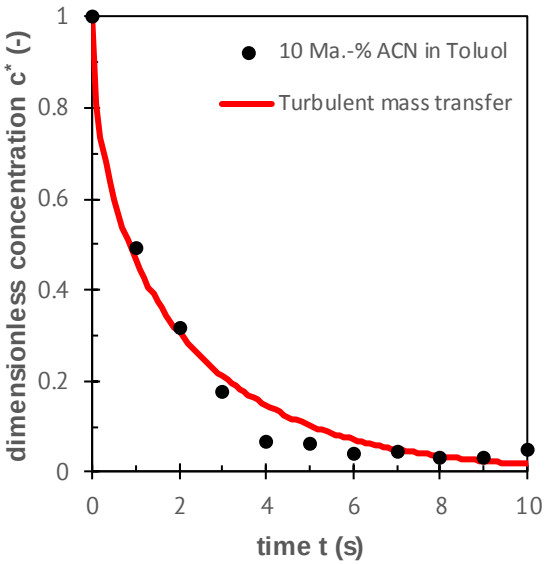

Figure 5. Transient development of the solute concentration on a droplet ($V = 4.2$ µL) with an initial solute concentration of $c_{ACN} = 10$ w.-% and a flow rate $\dot{V} = 12.5$ µL·s^{-1}

3.1.3 Mass transfer measurement via interfacial tension

Interfacial tension measurements need a higher droplet volume compared to Raman spectroscopy, and hence, droplet formation has to be slower, otherwise the droplet will be detached from the needle. However, after about 7.5 seconds the droplet has gained its final shape with a corresponding stable mass transfer behavior. The measurement with an initial solute concentration of $c_{ACN} = 10$ w.-% and a volume of 15 µL shows that the first measurement points (s. Figure 6) lead to either decreased or increased interfacial tension. Therefore, the dimensionless concentration is either too high or too low in the first seconds. Nevertheless, in the first 5 seconds more than 75 % of the mass transfer occurred. However, the correlation (s. Equation 3) with $T = 8$ fits the measurement results after 20 seconds very well.

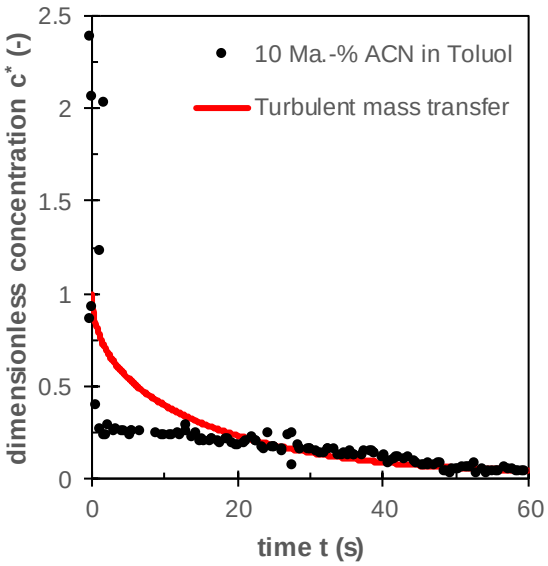

Figure 6. Interfacial tension measurements of the solute concentration on a droplet (V = 15 µL) with an initial solute concentration of c_{ACN} = 10 w.-% and a flow rate $\dot{V}$ = 2 µL·s^{-1}

As could be seen, both methods were unable to monitor mass transfer in the first seconds of droplet formation. Raman spectroscopy has its focus on measurement inside the droplet and interfacial tension on measurement the surface of the droplet; thus deviations between these measurements exists. Thereto, in silico experiments with small time steps are necessary. Here, CFD methods can be applied to reveal temporal and spatial details.

3.2 Numerical simulations

Coalescence

In respect to droplet coalescence of e.g. two differently sized droplets (pendant with 2.2 mm and top with 3 mm), simulation using a modified VOF code, (s. Figure 7, top) were compared with the experimental data (s. Figure 7, bottom) [16]. The simulated sequence of the simulation is given by a 2D plot as a cut through the center of the domain. Before the droplets enter into actual contact, the increasing pressure in the film between them leads to an elliptical droplet deformation. After 19.1 ms, similar droplet shapes and film rupture can be observed both in the simulations and in the experiments.

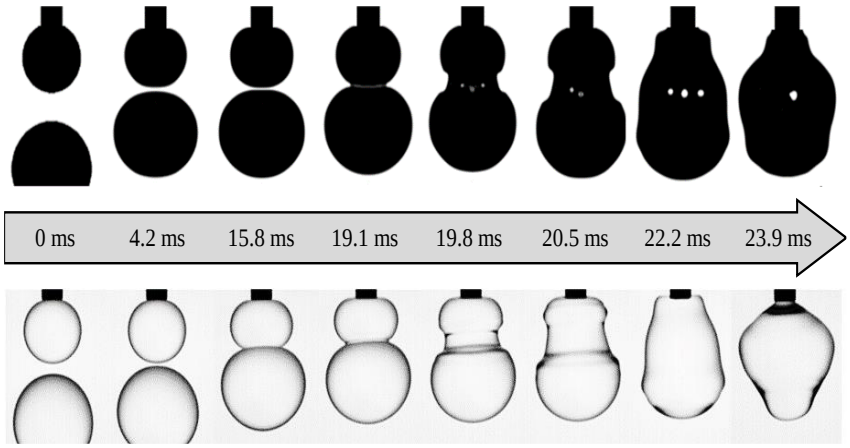

Figure 7. Coalescence toluene/water; CFD (top); exp. (bottom) [16].

Mass transfer

At first, the extended solver has to be validated to ensure that the results are confident. Therefore, a VOF simulation of a single falling droplet (d = 2.5 mm) in a quiescent liquid was performed. The concentration decrease over the time was compared with a validated level-set code from Engberg [17] (s. Figure 8). The standard test system cyclohexane/water/acetic acid in which water represents the continuous phase and acetic acid the transition component was studied in a two dimensional mode. As can be seen, the mass transfer model yields restorable results, but it seems to be important to reduce the spurious currents. For simulation of droplet formations, further studied will follow.

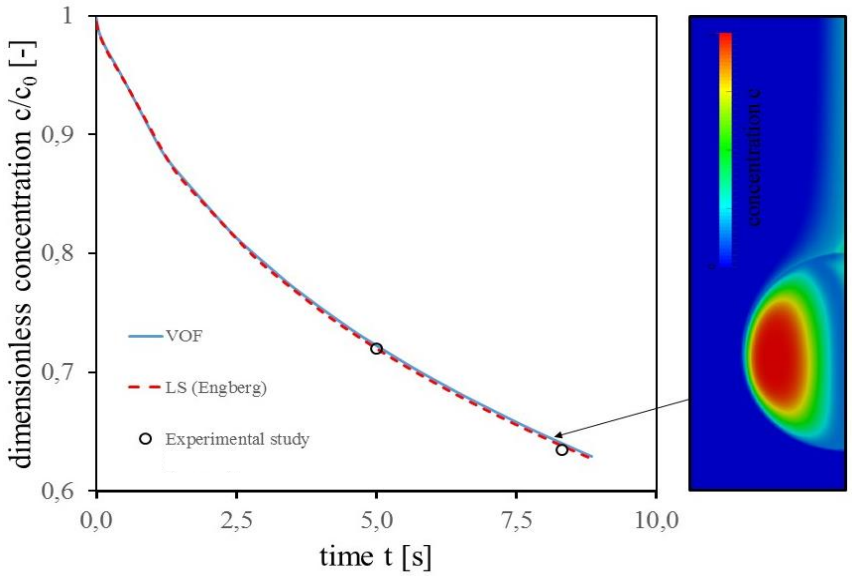

Figure 8. Dimensionless average concentration in the droplet over time (left); concentration field after eight seconds (right)

4. Conclusions

Systematic experiments to investigate the dynamic coalescence of two organic droplets were carried out, with the focus on the variation of the ionic strength and ion species. To meet the high requirements of reproducibility and purity, a standardized and validated experimental setup was used. Characteristic coalescence times were measured using a high speed camera with high temporal and spatial resolution. Cosmotropic anions lead to a significant increase in the coalescence time, the addition of chaotropic anions did not change the coalescence time. Based on the present experimental results, a correlation was developed to predict the dependency of the coalescence time on both the equivalent droplet diameter and ion concentration.

The influence of the Marangoni convection on the mass transfer during droplet formation was evaluated with the chemical system toluene/acetonitrile/water applying two different analytical methods. In the first method, the measurement of the solute concentration inside the droplet at a defined area was performed by confocal Raman spectroscopy. The measurement of the mass transfer inside a single droplet (V = 4.2 µL) showed that, with a droplet formation time of 0.34 seconds and an initial solute concentration of c_{ACN} = 10 w.-%, about 90 % of the mass transfer occurred during the first 5 seconds. However, this is not consistent with the interfacial tension measurements at the droplet surface. Under similar concentration conditions with a droplet formation time of 7.5 seconds (V = 15 µL), a value of 75 % of the initial surface concentration was reached in the first 5 seconds.

This discrepancy between the interfacial tension measurements and the confocal Raman spectroscopy can be explained by the difference in droplet formation time, droplet volume and the measurement inside and on the surface of the droplet. On the other hand, similar trends can be obtained with both measurement methods, which means that a large part of the mass transfer after the droplet formation is

completed in the first seconds. For these first seconds, in silico experiments offer the possibility to enable a more detailed analysis.

The numerical investigation of single droplet interactions opens up several possibilities for the model development. On the one hand, local spatial and time resolved information about the hydrodynamics and the film drainage will allow a better understanding of the coalescence behavior. On the other hand, detailed numerical VOF based simulations will help to determine surface and bulk droplet concentrations with high temporal resolution thus allowing a deep insight into mass transfer and droplet formation phenomena.

Acknowledgement

The authors gratefully acknowledge the financial support of the German Research Foundation (DFG) for this work (BA 1569/73-1, KE 837/28-1).

References

[1] F. Gebauer, J. Villwock, M. Kraume, H.-J. Bart, *Chem. Eng. Res. Des.*, **115**, 282 – 291 (2016).
[2] R. T. Eiswirth, Binary coalescence of free rising droplets, *Dissertation*, TU Kaiserslautern (2014).
[3] M. Henschke, *Chem. Eng. J.*, **85**, 369 – 378 (2002).
[4] C. A. Coulaloglou, L. L. Tavlarides, *Chem. Eng. Sci.*, **32**, 1289 – 1297 (1977).
[5] A. Pfennig, A. Schwerin, *Ind. Eng. Chem. Res.*, **37**, 3180 – 3188 (1998).
[6] F. Hofmeister, *Archiv f. experiment. Pathol. u. Pharmakol*, **25**, 1 – 30 (1888).
[7] M. Wegener, A. R. Paschedag, *Int. J. Multiphase Flow*, **37**, 76 – 83 (2011).
[8] L. Steiner, G. Oezdemir, S. Hartland, *Ind. Eng. Chem. Res.*, **29**, 1313 – 1318 (1990).
[9] A. B. Newman, *Trans. AIChE ,***27**, 310 – 333 (1931).
[10] A. B. Newman, *Trans. AIChE ,***27**, 203 – 220 (1931).
[11] Y. Haroun, Etude du transfert de masse réactif Gaz-Liquide le long de plans corrugués par simulation numérique avec suivi d'interface, *Dissertation*, Université de Toulouse (2008).
[12] J. Kamp, M. Kraume, *Chemical Engineering Research and Design*, **92**, 635 – 643 (2014).
[13] J. S. Heine, C. Wecker, E. Y. Kenig, H.-J. Bart, *Stofftransport bei der binären Tropfenkoaleszenz*, Jahrestreffen der Fachgruppe Extraktion, Köln (2017).
[14] J. Villwock, F. Gebauer, J. Kamp, H.-J. Bart, M. Kraume, *Chem. Eng. Technol.*, **37**, 1103 – 1111 (2014).
[15] M. J. Prince, H. W. Blanch, *AIChE J.*, **36**, 1485 – 1499 (1990).
[16] F. Gebauer, M. W. Hlawitschka, H.-J. Bart, *Chin. J. Chem. Eng.*, **24**, 249 – 252 (2016).
[17] R. F. Engberg, Einzeltropfen in Flüssig-flüssig-Systemen: Numerische Untersuchungen zu Fluiddynamik, Stofftransport und Marangonikonvektion, *Dissertation*, Universität Paderborn (2016).

Measurement of the Aggregates of Anionic Porphyrin with Cationic Surfactants at the Supercritical Carbon Dioxide/Water Interface by Total Internal Reflection Spectroscopy

Akira OHASHI*, Masaki ENDO, Kouhei YAMAGISHI, Haeng-Boo KIM
College of Science, Ibaraki University, Bnkyo 2-1-1, Mito, Ibaraki 310-8512, Japan

A total internal reflection (TIR) spectrometric devise was developed for direct measurement of adsorbates at the supercritical carbon dioxide (SC-CO_2)/water interface. The aggregation of diprotonated 5,10,15,20-tetraphenyl-21H,23H-porphinetetrasulfonic acid (H_4tpps^{2-}) with cationic surfactants, cetyltrimethylammonium ion (CTA^+), at the SC-CO_2/water interface was studied using this devise. Dependence of the TIR absorption spectra on CTA^+ concentration and CO_2 pressure were investigated, and the interfacial CTA^+ concentration was found to cause changes in the interfacial H_4tpps^{2-} species present. Increasing the CO_2 pressure changed the interfacial species from the H_4tpps^{2-} monomer to the H_4tpps^{2-} J-aggregate because the interfacial CTA^+ concentration increased as the pressure increased.

1. Introduction

Supercritical fluid extraction (SFE) of organic compounds and metal complexes from aqueous media has become a feasible separation method alternative to solvent extraction [1,2]. Among the supercritical fluids used in SFE, supercritical carbon dioxide fluid (SC-CO_2) has been widely used as the extraction medium, since it is non-toxic, cheap, environmentally acceptable and has a relatively mild critical point. Many studies on supercritical carbon dioxide (SC-CO_2) extraction of analytes from liquid matrix have been reported in recent years [3,4]. Clarification of chemical reactions at the SC-CO_2/water interface is important to understand the SC-CO_2 extraction mechanism and kinetics. However, studies on the SC-CO_2/water interface have been performed only by the interfacial tension determination [5,6]. Therefore, the development of spectroscopy analysis of the SC-CO_2/water interface is demanded, because the spectroscopy analysis allows us to obtain the much information about chemical species at the SC-CO_2/water interface. In this study, we developed the total internal reflection (TIR) spectroscopic system for measurement of the reaction at SC-CO_2/water interface and investigated the aggregation of water-soluble porphyrin with cationic surfactants at the SC-CO_2/water interface.

2. Experimental

2.1 Reagents

Cetyltrimethylammonium chloride (CTAC) was purchased from Tokyo Kasei (Japan). 5,10,15,20-Tetraphenyl-21H,23H-porphinetetrasulfonic acid disulfuric acid tetrahydrate ($H_6tpps•2H_2SO_4•4H_2O$) was purchased from Dojindo (Japan). Each stock solution was prepared in

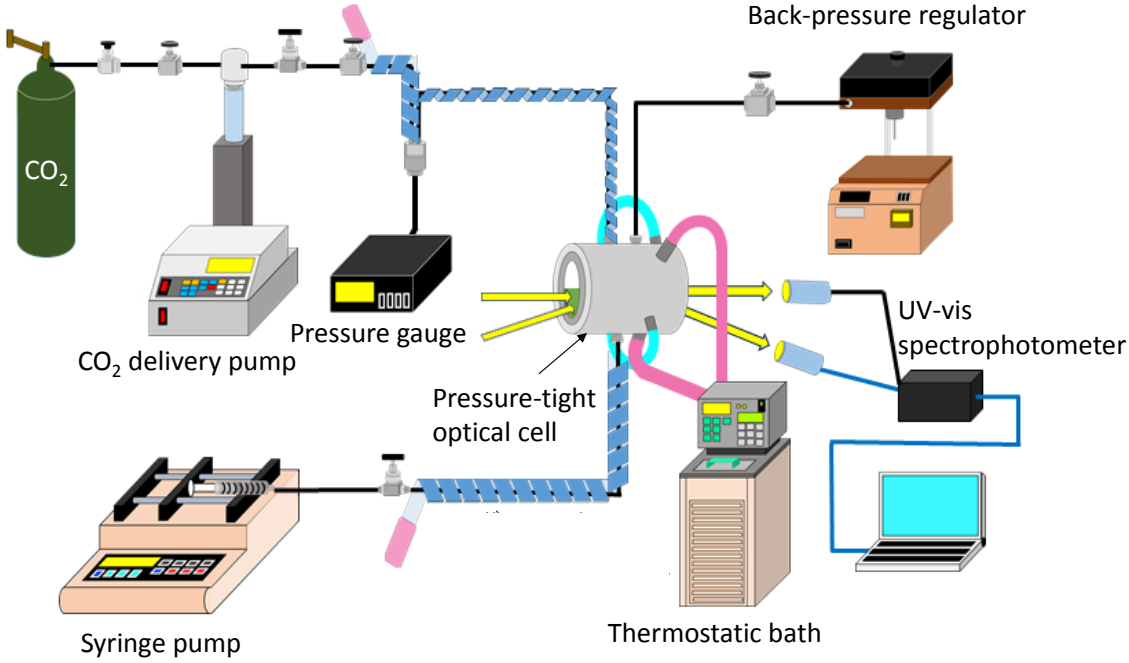

Figure 1. Schematic of the apparatus used to measure TIR spectra from the supercritical CO_2/water interface.

pure water. Liquid CO_2 (99.99%) was purchased from Taiyo Nissan Co. Ltd. Water was double distilled and purified further using a Milli-Q system (Millipore). All other chemicals were of analytical reagent grade and were used without further purification.

2.2 Apparatus

Figure 1 is a schematic of the TIR spectroscopic system developed in this study. The system has a CO_2 delivery pump (SCF-Get; Jasco), a syringe pump (KD210; Muromachi), a pressure tight optical cell (Jasco), a UV–vis spectrophotometer (USB3000; Ocean Optics), an arc lamp light source (APEX SOURCE ARC 150W XE OF; Newport), and a back-pressure regulator (880-80; Jasco). The pressure-tight optical cell is cylindrical and made of stainless steel with a 10 cm^3 inner volume, 15 mm path length, a pair of quartz windows (22 mm diameter, 15 mm thick), and a water jacket to control the temperature. Optical fibers and a focus lens are used to irradiate the sample and collect the reflected light. A polarization prism is placed between the pressure-tight optical cell and optical fiber on the irradiation side. Temperature of the pressure-tight optical cell is monitored using a digital temperature indicator (Fenwal), and pressure inside the cell is monitored using a digital pressure gauge (Toyo Sokki).

2.3 Measurement of total internal reflection spectra at the SC-CO_2–water interface

An aqueous solution (5.7 mL) containing H_2tpps^{4-} and CTA^+ was added to the pressure-tight optical cell using a syringe pump. CO_2 was then introduced into the cell using a CO_2 delivery pump, and the cell pressure was controlled using a back-pressure regulator. Temperature inside the cell was maintained at 318 K using a water jacket and a thermostat-controlled water circulator. The system was left to equilibrate for 7 h, light was irradiated obliquely to the interface from the aqueous medium side,

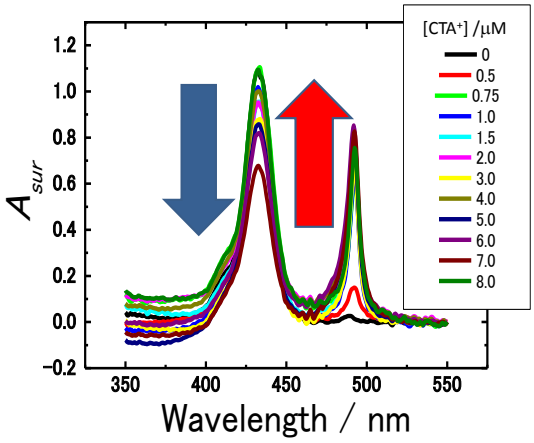

Figure 2. s-Polarized TIR spectra of H_4tpps^{2-} at the various CTA^+ concentrations. [H_2tpps^{4-}] = 2.0 μM; pressure = 10 MPa; temperature = 318 K.

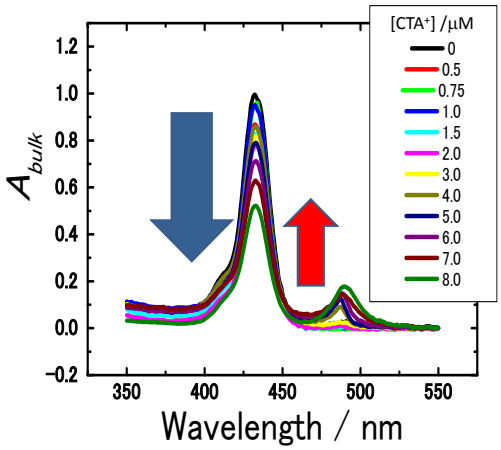

Figure 3. Absorption spectra of H_4tpps^{2-} in the aqueous phase at the various CTA^+ concentrations. [H_2tpps^{4-}] = 2.0 μM; pressure = 10 MPa; temperature = 318 K.

and the TIR spectrum was measured. The refractive index of water (1.34) are larger than those of CO_2 and SC-CO_2 (1.02–1.12, respectively [7]). The incidence angle was fixed at 68°. The TIR absorbance, A_{TIR}, was defined as $\log(R_0/R)$, where R_0 and R are the reflectivities in the absence and presence of the absorbate, respectively. The absorption spectrum of the aqueous phase was measured simultaneously. H_2tpps^{4-} concentration was maintained at 2.0 μM, and CTAC concentration was varied from 0 to 9 μM. Pressure was varied from 1 to 10 MPa, and CO_2 pressure and temperature were maintained within 0.2 MPa and 0.1 °C, respectively, of the desired value.

3. Results and Discussion

3.1 Aggregation behavior of H_4tpps^{2-} with CTA^+ at the SC-CO_2/water interface

Figures 2 and 3 show s-polarized TIR and the aqueous phase's absorption spectra, respectively, at the various CTA^+ concentrations measured using the apparatus developed in this study. Two bands at 434 nm and 492 nm in Figures 2 and 3 were assigned to the H_4tpps^{2-} monomer in the aqueous phase and the H_4tpps^{2-} J-aggregate at the SC-CO_2/water interface. The TIR absorbance at 434 nm decreased and that at 492 nm increased with an increase in the CTA^+ concentration as shown in Figure 2. A similar spectral change in the aqueous phase was observed in Figure 3. However, the absorbance at 492 nm in Figure 3 was much smaller than that in Figure 2. This result indicated that the H_4tpps^{2-} J-aggregate was mainly formed at the SC-CO_2/water interface. The TIR absorption spectrum of the H_4tpps^{2-} J-aggregate at the SC-CO_2/water interface could be obtained by the deduction of the absorption spectrum in the aqueous phase. Figure 4 shows the plots of the TIR absorbance at 492 nm of the H_4tpps^{2-} J-aggregate at the SC-CO_2/water interface after the deduction of the absorbance in the aqueous phase against the concentration of CTA^+. The TIR absorbance at 492 nm became constant near 1 μM of CTA^+. This result indicated that the interfacial concentration of H_4tpps^{2-} J-aggregate was saturated about 1 μM of CTA^+.

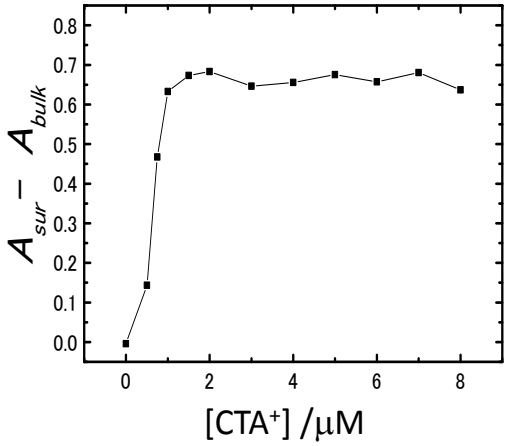

Figure 4. Dependency of the TIR absorbance of the interfacial H_4tpps^{2-} J-aggregate on the CTA^+ concentration. $[H_2tpps^{4-}]$ = 2.0 μM; pressure = 10 MPa; temperature = 318 K.

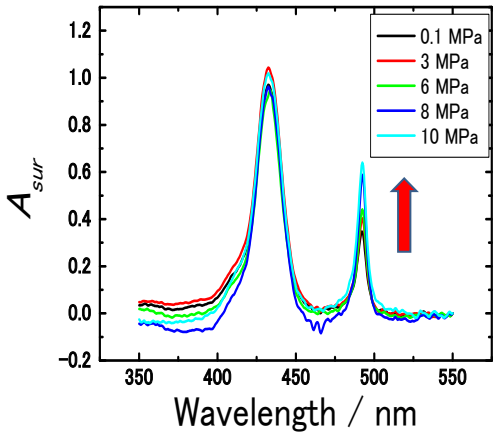

Figure 5. s-Polarized TIR spectra of H_4tpps^{2-} at the various pressures. $[H_2tpps^{4-}]$ = 2.0 μM; $[CTA^+]$ = 1 μM; temperature = 318 K.

Pressure-dependent TIR absorption spectra were measured at a constant CTA^+ concentration (1 μM) to determine the effect the CO_2 pressure on H_4tpps^{2-} aggregation at the SC-CO_2–water interface. Figure 5 shows the s-polarized TIR spectra at the various CO_2 pressures. The TIR absorbance at 492 nm increased with an increase in the CO_2 pressure. As the pressure increases, the adsorptivity of CTA^+ at the SC-CO_2/water interface may become higher [8]. That is, the interfacial concentration of CTA^+ at high pressure is higher than that at low pressure. This may cause the higher interfacial concentration of H_4tpps^{2-} and the formation of H_4tpps^{2-} J-aggregate with CTA^+. The result obtained implies that it is possible to change the interfacial chemical species by changing the pressure in the SC-CO_2/water system.

4. Conclusion

In this study, we developed a TIR spectrometric devise for direct measurement of the adsorbate at the SC-CO_2/water interface. The aggregation of H_4tpps^{2-} with CTA^+ at the SC-CO_2/water interface was studied using this devise. The TIR spectra of the H_4tpps^{2-} J-aggregate formed at the SC-CO_2/water interface could be observed. The method developed in this study allows us to obtain much information on the chemical species at the SC-CO_2/water interface. Therefore, this may promote further development on the investigation in the supercritical CO_2 extraction.

Acknowledgement

This work was supported by JSPS KAKENHI Grant Number 26410143.

References

1) F.V. Bright, M.E.P. McNally, “Supercritical Fluid Technology: Theoretical and Applied

Approaches to Analytical Chemistry", 1992, ACS, Washington DC.

2) L.T. Taylor, "Supercritical Fluid Extraction", 1996, John Wiley & Sons, New York.
3) A. Ohashi, K. Ohashi, *Solvent Extr. Res. Dev., Jpn.*, **15**, 11-20 (2008).
4) F.Y. Lin, D.G. Liu, S.M. Das, N. Prempeh, Y. Hua, J.G. Lu, *Ind. Eng. Chem. Res.*, **53**, 1866–1877 (2014).
5) S.R.P. da Rocha, K.P. Johnston, *Langmuir*, 16, 3690-395 (2000).
6) M. Sagisaka, T. Fujii, Y. Ozaki, S. Yoda, Y. Takebayashi, Y. Kondo, N. Yoshino, H. Sakai, M. Abe, K. Otake, K. *Langmuir*, 20, 2560-2566 (2004).
7) Y. Sun, B.Y. Shekunov, P. York, *Chem. Eng. Comm.*, 190, 1-14 (2003).
8) X. Chen, S.S. Adkins, O.P. Nguyen, A.W. Sanders, K.P. Johnston, *J. Supercrit. Fluid.*, 55, 712-723 (2010).

Co-extraction and Concentration of Dyes into the Ionic Liquid Formed in an Aqueous Solution

Kenji CHAYAMA*, Nobuhiko OOI, Jun KAWAMURA, Mari TOYAMA and Satoshi IWATSUKI
Faculty of Science and engineering, Konan University
Okamoto8-9-1, Higashinada, Kobe 658-8501, Japan

The novel methodology of ionic liquid extraction of chemical species was investigated. To form the ionic liquid in an aqueous solution, 1-butyl-3-methylimidazolium chloride solution was added to the aqueous solution of a dye, then the solution of lithium bis(trifluoromethylsulfonyl)imide was added into the solution. Another phase of ionic liquid 1-butyl-3-methylimidazolium bis(trifluoromethylsulfonyl)imide appeared immediately. Some dyes such as ethyl violet, rhodamine B were simultaneously concentrated into the ionic liquid phase. On the other hand, fast green, new coccine, tartrazin and some dyes were not exracted at all. The distribution behaviors of dyes were related to their chemical structures.

1. Introduction

The studies of the ionic liquids (ILs) have been developed in a few decades. Because of the character of vapourless and insoluble in water, ILs are required as the extraction solvents for the separation and concentration of the chemical compounds[1-3]. So far, almost all ILs were synthesized and purified, and then, used as the liquid-liquid extraction media. However, the costs of ILs are much more expensive than the usual organic solvents. Although, researchers seek to examine a lot of

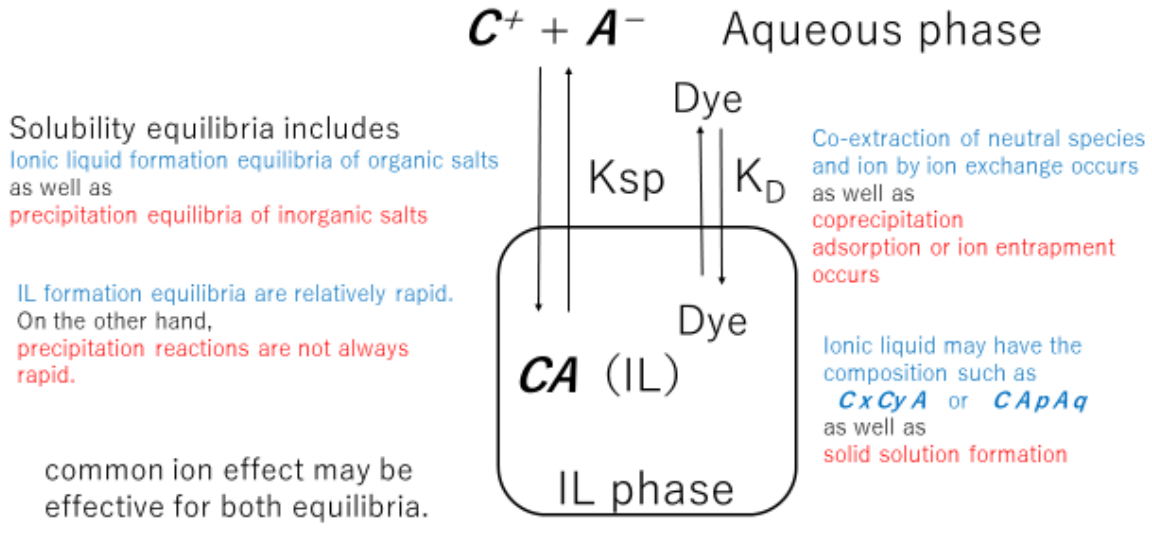

Scheme1 Phenomena of hetero phase formation equilibria of IL comparing those of precipitation equilibria

combination of cations such as imdazoiums, pyridiniums or alkyl ammoniums ...etc and anions such as bis(trifluoromethylsulfonyl)imide ion, tetrafluoroborate ion and so many kinds of anions. Because, one of the advantage of the ILs as the solvents might be the variety of the chemical character changeable by means of substitute the part of the cation or of the anion. It is impossible to synthesize and purify so many kinds of ILs for each experiments.

As shown in scheme 1, ILs are insoluble salts like inorganic salts such as AgCl. If the cation and the anion were supersaturated over their solubility of the salt, ILs, organic liquid salts formed another phase in the aqueous solution, like the precipitation of an inorganic solid salts. Chemical reactions using the precipitation equilibrium shall be applicable for ILs formation equilibrium, because both are same hetero phase formation equilibria. Authors focused on the reaction of forming ILs in an aqueous solution. At same time, co-extraction (as well as the co-precipitation in the precipitation reaction) of some chemical organic species will be accompanied by the ILs formation reaction.

In this study, combination of 1-butyl-3-methylimidazolium [BMIm] chloride or 1-octyl-3-methylimidazolium [OMIm] chloride aqueous solution and the lithium bis(trifluoromethylsulfonyl)imide [NTf_2] solution were examined to form the ILs phase in the aqueous solution including dyes. Co-extraction behaviors of some dyes were examined. These compounds to form Ils are shown in Figure1

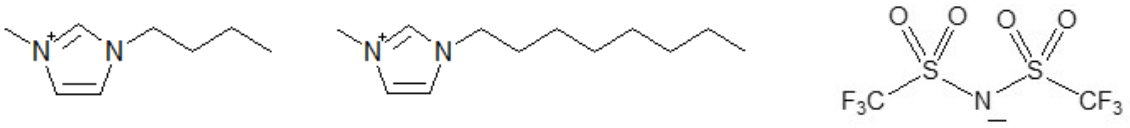

[BMIm] ion [OMIm] ion [NTf2] ion

Figure 1. Structures of the cations and an anion forming the ILs in this study.

2. Experimental

2.1.1 Reagents to form ILs

Reagents for forming ILs were purchased as follows; 1-butyl-methylimidazorium [BMIm] chloride from Wako pure chemical, 1-methyl-3-n-octylimidazorium [OMIm] chloride from Tokyo Kasei Co., and lithium bis(trifluoromethylsulfonyl)imide [NTf_2] from Tokyo Kasei Co.. All reagents were more than 98% purity. The aqueous solution of 1 M [BMIm]Cl, [OMIm]Cl and Li [NTf_2] were diluted with a distilled water.

2.1.2 Dyes

Dyes used were acid red 52 ($C_{27}H_{29}N_2NaO_7S_2$) purchased from Wako pure chemical Co., ethyl violet ($C_{31}H_{42}ClN_3$ $0.5ZnCl_2$) from Tesque Co., crystal violet ($C_{25}H_{30}ClN_3$) from Nacalai Tesque Co., Brilliant green ($C_{27}H_{34}N_2O_4S$) from Tesque Co., basic violet ($C_{24}H_{28}ClN_3$) from Tokyo chemical industry Co., malachite green ($C_{24}H_{25}O_2N_2$) from Wako pure chemical Co., methylene blue ($C_{16}H_{18}N_3SCl$) from Tesque Co., rose Bengal ($C_{20}H_2Cl_4I_4Na_2O_5$) from Wako pure chemical Co., rhodamine B ($C_{28}H_{31}ClN_2O_3$) from Wako pure chemical Co., erythrosine B ($C_{20}H_6I_4Na_2O_5$) from Wako pure chemical Co., phloxine B ($C_{20}H_2Br_4Cl_4Na_2O_5$) from Kishi Kasei Co., bromocresol green ($C_{21}H_{14}Br_4O_5S$) from Nacalai Tesque Co., bromocresol purple ($C_{21}H_{16}Br_2O_5S$) from Wako pure chemical Co., methyl red ($C_{15}H_{15}N_3O_2$) from Wako pure chemical Co., lithol rubine B ($C_{18}H_{12}CaN_2O_6S$) from Kishi Kasei Co., fluorescein ($C_{20}H_{12}O_5$) from Wako pure chemical Co., sunset yellow FCF ($C_{16}H_{10}N_2Na_2O_7S_2$) from

Wako pure chemical Co., bordeaux S ($C_{20}H_{11}N_2Na_3O_{10}S_3$) from Wako pure chemical Co., new coccine ($C_{20}H_{11}N_2Na_3O_{10}S_3$) from Wako pure chemical Co., tartrazine ($C_{16}H_{19}N_4Na_3O_9S_2$) from Wako pure Chemical Co., allura red AC ($C_{18}H_{14}N_2Na_2O_8S_2$) from Wako pure chemical Co., metacresol purple ($C_{21}H_{18}O_5S$) from Wako pure chemical Co., fast green ($C_{37}H_{34}N_2Na_2O_{10}S_3$) from Wako pure chemical Co., indigo carmine ($C_{16}H_8N_2Na_2O_8S_2$) from Wako pure chemical Co., brilliant blue ($C_{37}H_{34}N_2Na_2O_9S_3$) from Wako pure chemical Co.. Bromocresol green, bromocresol purple, metacresol purple, methylene blue, fluorescein, methyl red and tetrabromotetrachloro-fluorescein were dissolved with a small portion of 1 M (mol/dm^3) sodium hydroxide solution. Lithol rubin B was dissolved with diluted sulfuric acid. Other dyes were dissolved and diluted with distilled water.

2.2 Apparatus

Absorption spectra of the aqueous solution of dyes were measured by Hitachi U3310 spectrophotometer. The pH of an aqueous solution was measured by Toa DKK HM25R pH meter. Freeze drying machine was used to eliminate water in ILs by Eyla freeze dryer FD1000.

2.3 Procedure for the ionic liquid formation in an aqueous solution

The 1 M 1-buthyl-3-methylimidazorium [BMIm] chloride solution and the 1 M lithium bis(tri-fluoromethylsulfonyl)imide [NTf_2] solution were added to the aqueous solution containing the $5x10^{-6}$ M dye, to be the concentration of [BMIm] ; 0.1 M and [NTf_2] ; 0.1 M in an aliquiot (10 mL) of the solution. The solution were shaken with the mechanical shaker with 180 spm, and then centrifuged with 2000 rpm. As an IL phase appeared under the water phase, it was collected with the pipet and the concentration of the dye in the aqueous phase were determined spectrophtometrycally. The weight of IL phase was determined after the collection and freezedrying. The concentrations of [BMIm]Cl solutions and Li[NTf_2]solutions were changed, and the amount of the IL phase were measured.

3. Results and Discussion

3.1 Ionic liquid formation

The small volume of an IL phase appeared under the aqueous phase. In order to determine the weight of IL phase, it was collected and freeze dried and weighed. The aqueous solution containing 0.1 M [BMIm] and 0.1 M [NTf_2] in 10 mL formed the IL phase of 0.252$\pm$0.0082 mL (n=10). As the concentration of [BMIm] and [NTf_2] increased up to 0.3 M, the volume of the IL increased lineally, and the line followed the calculated line considering the K_{sp} value of [BMIm] [NTf_2]. If a compound like malachite green were distributed and concentrated into the IL phase, concentration ratio would be 40 times as usual equal volume extraction.

3.2 Co-extraction of a dye into the IL

As shown in Figure 2, after adding the [BMIm] and [NTf_2] solution, IL phase of [BMIm] [NTf_2] was separated from the aqueous solution. The dye, ethyl violet was co-extracted into the IL phase. Table 1. shows percent extraction and the distribution ratio D of dyes between IL and aqueous solution.

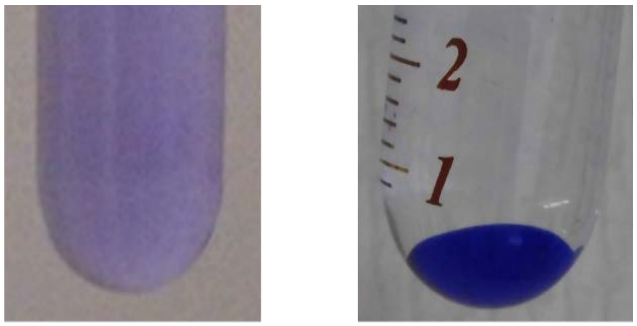

Figure 2. Photos of the solutions before and after the addition of [BMIm] and [NTf2] into the ethyl violet solution.

Table 1 Distribution of dyes between water and Ils

	[BMIm][NTf2]			[OMIm][NTf2]		
	pH	%E	logD	pH	%E	logD
malachite green	8.00	99.7	4.16	7.39	98.9	3.37
methylene blue	8.01	99.4	3.85	7.33	97.1	2.95
crystal violet	8.00	98.7	3.47	7.40	99.2	3.52
basic violet	7.81	97.4	3.16	7.60	96.6	2.89
ethyl violet	8.03	96.9	3.09	7.35	97.4	3.01
brilliant green	8.10	94.4	2.82	7.38	99.4	3.64
rhodamine B	8.06	93.3	2.74	7.46	95.4	2.74
rose bengal	7.90	20.0	0.99	7.33	98.0	3.12
acid red	8.12	12.7	0.76	7.40	46.8	1.37
fast green FCF	8.06	3.3	0.13	7.47	4.2	0.23
bromocresol purple	9.75	0.7	-	9.63	5.3	0.17
erythrosine B	8.01	0.3	-	7.42	86.6	2.24
phloxine B	7.97	0.3	-	7.45	92.7	2.53
Br4Cl4-fluorecein	8.03	0.0	-	7.80	91.0	2.43
bromocresol green	9.76	0.0	-	9.73	41.6	1.28
methyl red	8.00	0.0	-	7.55	35.4	1.17
lithol rubine B	7.52	0.0	-	5.05	15.9	0.7
fluorecein	8.01	0.0	-	7.42	0.5	-
sunset yellow	8.15	0.0	-	7.47	0.0	-
bordeaux S	8.05	0.0	-	7.44	0.0	-
new coccine	8.19	0.0	-	7.40	0.0	-
tartrazine	8.07	0.0	-	7.42	0.0	-
allura red	7.83	0.0	-	7.42	0.0	-
metacresol purple	10.89	0.0	-	10.47	0.0	-
indigo carmine	8.22	0.0	-	7.48	1.0	-
brilliant blue	8.05	0.0	-	7.38	0.0	-

The distribution ratio D is expressed as equation (1).

$$D = [\text{dye}]_{IL} / [\text{dye}]_{aq} \quad (1)$$

Where $[\text{dye}]]_{IL}$ is the concentration of the dye in the IL phase, and $[\text{dye}]_{aq}$ is the concentration of the dye in the aqueous phase. The percent extraction $\%E$ of the dye is expressed as equation (2)

$$\%E = 100D/(D+ (V_W/V_{IL})) \quad (2)$$

Where V_W is the volume of the aqueous phase, and V_{IL} is the volume of the IL phase.

As shown in Table 1, some dyes were well co-extracted into the IL phase for both case of the formation

of [BMIm][NTf_2] and [OMIm][NTf_2]. The structures of such dyes are shown in Figure 3.

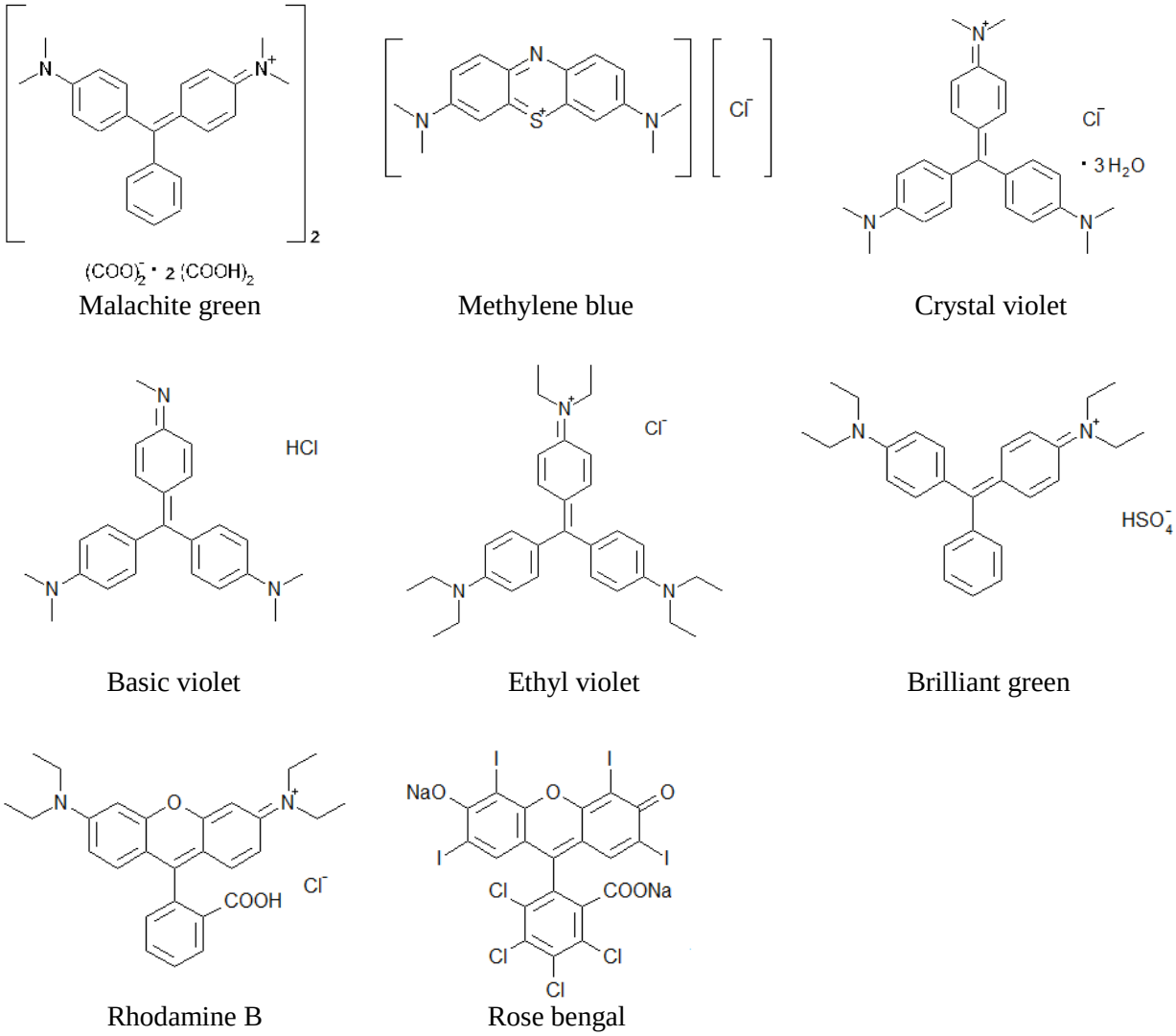

Figure 3. Chemical structures of dyes well co-extracted when the formation of both [BMIm][NTf_2] and [OMIm][NTf_2].

Those dyes have chemical structures which is hydrophobic and their cation center are on the nitrogen atoms seem to delocalized to aromatic rings with the exception of basic violet and rose bengal. Because, the structure of protonated basic violet has similar structure to that of crystal violet, it may be co-extracted well. The difference of %*E*s between brilliant green and rhodamine B may be caused by the introduction of carboxyl group into the structure of brilliant green. In the case of formation of [BMIm][NTf_2], the values of %*E* are quite different. It is interesting to focus for the effect of the length of alkyl chains between the BMIm and OMIm for these two dyes. On the other hand, Figure 4 shows the structures of dyes which are well extracted with [OMIm][NTf_2], not extracted well with [BMIm][NTf_2]

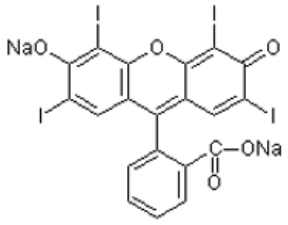

Erythrosine B

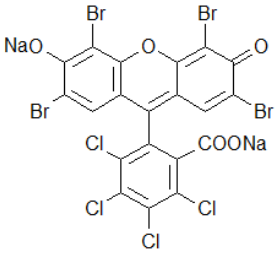

Phloxine B

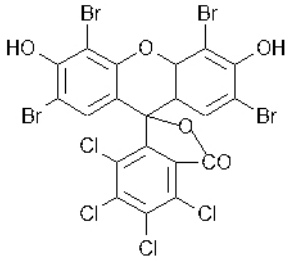

Br4Cl4-fluorecein

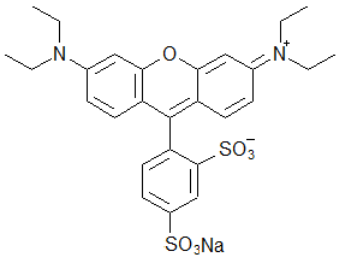

Acid red

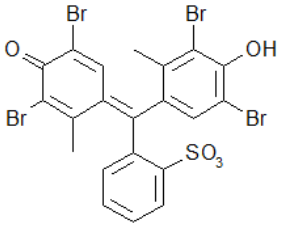

Bromocresol green

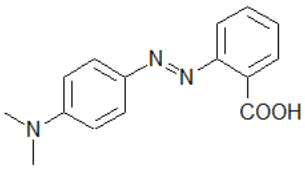

Methyl red

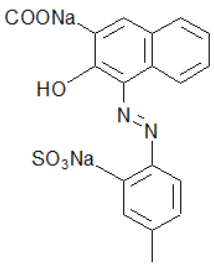

Lithol rubine B

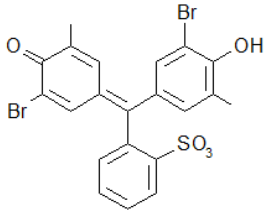

Bromocresol purple

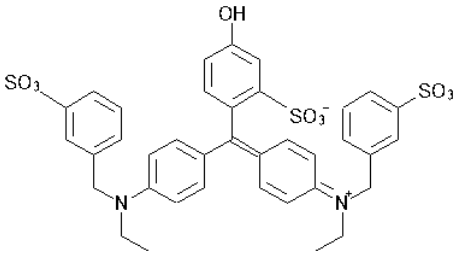

Fast green

Figure 4. Chemical structures of dyes well co-extracted when the formation of [OMIm][NTf_2] not co-extracted well with [BMIm][NTf_2] .

The results of Table 1 and the structures on Figure 4 indicate the importance of the alkyl chain length different between OMIm and BMIm on the co-extraction. Erythrosine B, phloxine B and Br_4Cl_4-fluorecein have hydrophobic part in their molecules. These dyes were co-extracted with [OMIm][NTf_2], however not co-extracted with [BMIm][NTf_2]. The dyes which have a sulfo group in their molecules, it is hard to be co-extracted with [BMIm][NTf_2] and even with [OMIm][NTf_2]. Lithol rubine, bromocresol purple and fast green not co-extracted with both ILs. Figure 5 shows the photograph of the fast green solution of high concentration when [BMIm][NTf_2] formed in the solution. It is clear the dye which have a few sulfo groups in the molecule are not co-extracted at all. Figure 6 shows the structures of dyes which are not co-extracted at all with both of [BMIm][NTf_2] and [OMIm][NTf_2]

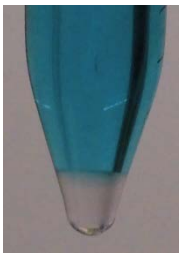

Figure 5. Fast green with IL

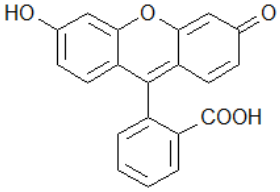

Fluorecein

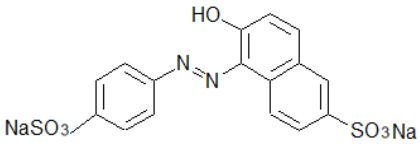

Sunset yellow

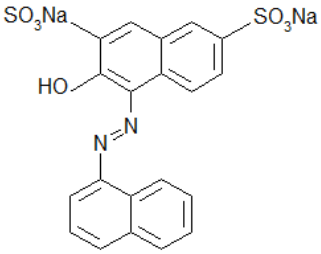

Bordeaux S

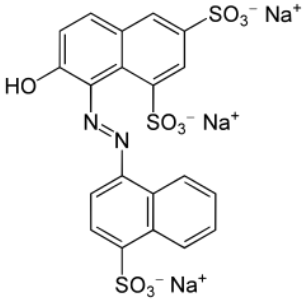

New coccine

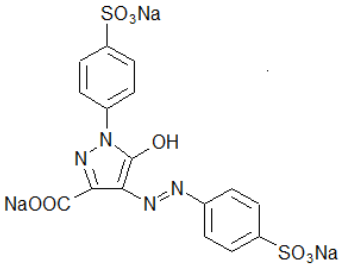

Tartrazine

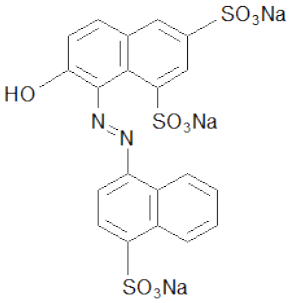

Allura red

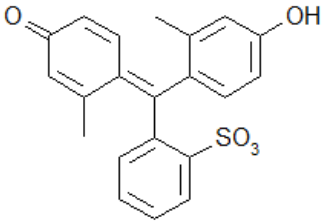

Metacresol purple

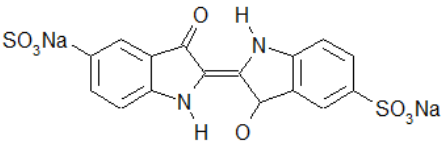

Indigo carmine

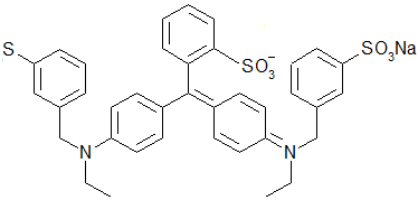

Brilliant blue

Figure 6. Chemical structures of dyes not co-extracted at all when the formation of [OMIm][NTf_2] and [BMIm][NTf_2] .

Almost all dyes in Figure 6 are water soluble and have some hydrophilic groups such as hydroxyl, carboxyl and sulfo groups in their molecules. It seems, at least two hydrophilic groups in a molecule may be helpful to surround the dye by the water network which defend to move over the water-IL interface. It can be possible to separate between the dyes in Figure 4 and those in Figure 6. Further, it would be possible to concentrate the dye to determine the concentration by spectrophotometrically.

4. Conclusion

The methodology developed in this study for IL extraction might save the time of IL extraction, because it shortcuts the synthesis and purification of IL in as much as those processes were not necessary. Some of analytical method such as extraction spectrophotometry may be taken place with those methods. Further, the applications for the chemical processes such as separations of products during synthesis,

specific extraction of biomaterials in order to use a specific groups in the compartment cation or anion would be possible.

Acknowledgement

Authors are thankful to Mr. Daisuke Maezawa, CEO of Kishi Kasei Co.Ltd., for giving a sample of phloxine B and lithol rubine B.

References

1) M. L. Dietz, *Sep. Sci. Technol.*,**41**, 2047-2063 (2006)
2) N. Papaiconomow, J. M. Lee, J. Salminen, M. Stosch, J. M. Prausnitz, *Ind. Eng. Chem. Res.*,**47**, 5080-5086(2008).
3) K. Chayama, Y. Sano, S. Iwatsuki, *Anal., Sci.*, **31**, 1-3(2015)
4) X. Sun, H. Luo, and S. Dai, *Chem. Rev.*, **112**, 2100-2118(2012)
5) *Ionic Equilibria in Analytical Chemistry* H. Freiser, Q. Fernando, Robert E. Krieger publishing company, Huntington, New York 1979. ISBN 0-88275-955-8

Tutorial Videos on Solvent Extraction

Andreas PFENNIG

University of Liège, Department of Chemical Engineering - Products, Environment, and Processes (PEPs), Quartier Agora, Allée du Six Août, 11, 4000 Liège, Belgium, http://chemeng.ulg.ac.be/pfennig

Recording basic lectures on separation processes as well as expert presentations on video and uploading them to corresponding video platforms is described. The basic setup preparing expert videos consists of a large TV screen, a HD video camera, corresponding soft-box lighting, and a wav field recorder with 24 bit resolution. The advantages of this setup are described. The topics covered deal with fundamental design principles of solvent and reactive extraction processes. First videos describe systematic solvent selection. Then details of drop behavior are covered, which is the basis for understanding the major challenges in extraction as a basis for knowledge-based design and operation. Drop-based design methods are presented in detail together with the corresponding lab-scale experiments to characterize system behavior. Finally companies and experts are invited to contribute to this video series with photos, graphs, and videos or to contribute with their expertise e.g. on practical issues.

1. Introduction

To support students studying Chemical Engineering, the ordinary lectures of the author had originally been recorded on video. To this end a suitable high-resolution video camera and a spot light had been used over several years. From each lecture the videos were then prepared with the help of a suitable software and the videos uploaded to university-internal repositories. This was very much appreciated by the students. Of course preparing the recording and also the final cutting of the videos every year was quite some effort. At the same time, it was realized that the quality was limited, if the standard situation in a classroom was recorded. Even with the spotlight, the lighting situation could only partially be optimized. Finally, it occurred that within the own research group many elaborate presentations had been prepared over the years, including dedicated workshops for industry. This apparently was fleeting effort. Thus it was realized that preparing dedicated presentation in the best possible quality and supplying them publicly, e.g. on YouTube, would be a similar effort as previously, enhance the video quality significantly, and would ensure that all knowledge collected over the years in the group could be delivered to everybody interested in a didactically suitable way.

2. Realization

As a start a variety of configurations for recording videos have been tried out. It was e.g. tested, if the ordinary lecture configuration could be enhanced with additional and advanced lighting options. Unfortunately it turned out that either the presenting person is only dimly lit or the wall projection of

the PowerPoint slides significantly looses contrast because of the bright lighting. In case the presenting person is not properly lit, the facial expression cannot be recognized or there are too strong shadows in the face. Also in some situations the picture of the projector turned out to be too bright, so that details of the diagrams were lost in the video recording. Thus, no lighting situation using an ordinary projector led to acceptable results.

It was then proposed to use greenscreen technology. This has actually not been tested, because the lecturer is no professional actor used to such technology, but the proposal led to formulate the detailed goals for a good video recording. These requirements were defined as:

- the person delivering should be clearly visible also with his/her facial expression and should be able to interact with the projected slides while explaining their content, because this would facilitate a vivid presentation of the lecture content,
- the diagrams shown should be sufficiently rich in contrast in order to realize enough detail, where this actually also sets up boundary conditions for the slides presented,
- when writing notes, e.g. during derivations, the text written should always be clearly visible to enhance that students can follow the content, and
- the sound recording should be of sufficient quality, especially to allow maximizing recording level without decreasing the signal-to-noise ratio.

To reach these goals especially different lighting setups have been tested. Optimal quality was finally reached by using a large TV screen for projecting the presentation slides and to use a tablet or convertible with a suitable writing program for presenting the derivations. This is shown exemplarily in Figure 1. This way also a direct interaction between presenter and presentation is apparently easily possible and derivations can be recorded from the same TV screen. Sound recording is performed with a condenser microphone and a recording device which allows wav-recording with 24-bit resolution.

Figure 1. Recording environment (photo by: Olivier Borsu, IFRES (Institut de Formation et de Recherche en Enseignement Supérieur), Université de Liège)

With this setup a series of videos is currently being recorded, which starts out with the basics of thermal unit operations, which will also include extraction, phase separation, etc. In the meantime already the basic design principles have been made available on YouTube [1], e.g. including a generalized McCabe-Thiele method. An example screen from a video is shown in Figure 2, which shows that many of the requirements are very well fulfilled with this setup. The screen of the convertible laptop can be switched with the push of a button between the presentation and a journal file used for the manual derivations. The sound is recorded separately with a Roland Edirol R-09 with 24 bit resolution. It turns out that such a recording environment, which at the University of Liège is kindly supplied by the Training and Research Institute for Higher Education (IFRES), can be obtained including a suitable convertible laptop with a comparably low budget of well below 10 000 Euro. IFRES meanwhile is using this optimal setup for other video recordings as well.

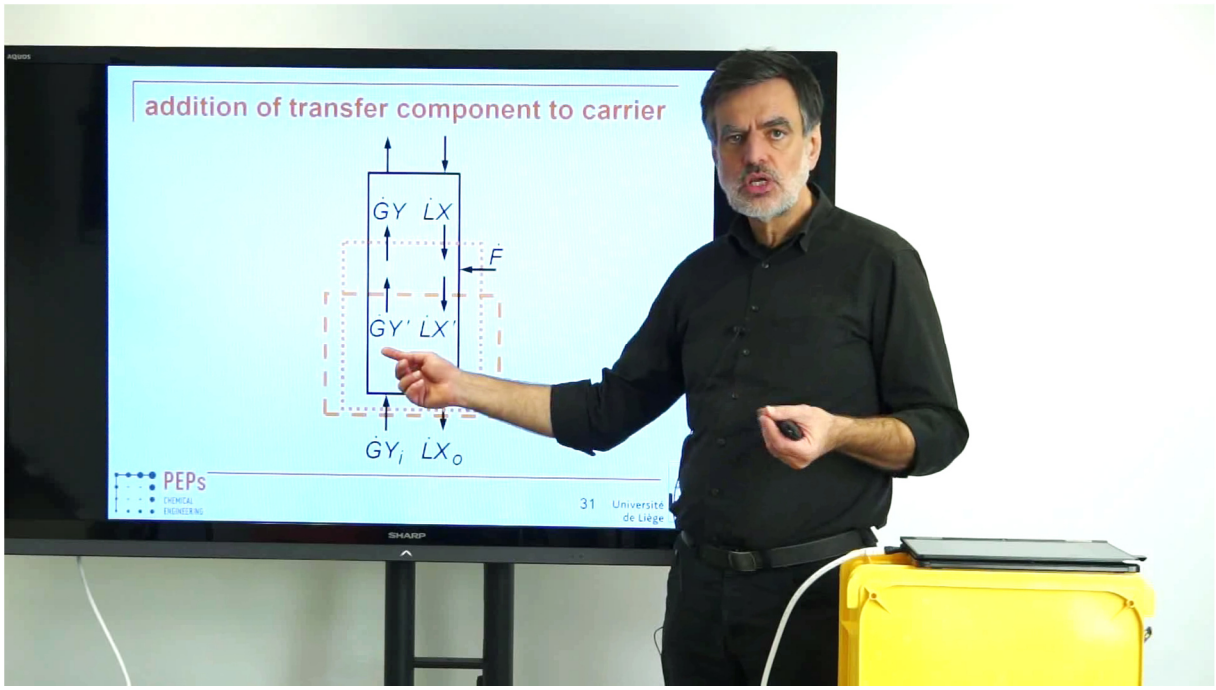

Figure 2. Resulting screen of a video

After the raw recording the video is cut with an available software. The soundtrack from the Edirol is added after preliminary steps performed with the open-source software audacity [2], which include normalization, level adjustment and slight compression. The videos are then produced in high quality and uploaded to YouTube.

This is an ongoing project. At the start the first lectures from the lecture ‘Thermal Spearation Processes’ have been recorded, which begins with topics of distillation. As a second large chapter general considerations have been collected, which include among others a very fundamental description of the McCabe-Thiele method in a way that it can be applied to essentially all counter-current separation processes. Special emphasis is placed on the systematic derivations, which include a thorough discussion of the assumptions. It should be mentioned that this has already been

very valuable in an industry cooperation, where in industrial practice overall mass flowrates and mass ratios (loads) had been used to determine the number of theoretical stages of a real equipment, which led to surprising results. This combination unfortunately does not comply with the assumptions made in deriving the McCabe-Thiele method. Only after the appropriate basis had been chosen and systematically applied, i.e. the mass ratios were combined with the flowrates of the carrier components, i.e. water and an organic solvent, correct and meaningful values were obtained. The strong difference in this case was a result of the high load of the transfer component transferred between the pahses.

It has also been realized that in the research group several excellent presentations on advanced topics have been prepared in the past and delivered on various occasions including expert workshops. Also very basic knowledge, e.g. on the influence of electrolytes on interaction of interfaces thus strongly influencing coalescence or on the origin and behavior of mass-transfer induced instabilities has been collected over the last years. This knowledge is dispersed over a variety of scientific publications. The nature of such publications does not allow proper didactic presentation of the findings. Correspondingly this knowledge is hard to access for the novice. Thus the final goal of this project is to collect in the videos all expertise acquired in the research group, e.g. on extractant selection, coalescence and phase separation, including design of reactive steps. This effort is supported by supplying the lecture manuscripts as PDF file on our website [3]. This way a collection of easily accessible and complete teaching and advanced-training material will be made available in the future. The level of the presentations is on the one hand side basic, i.e. the goal is that every novice can follow. This includes detailed derivations of a variety of aspects, since it is believed that for a proper university education, where the students are educated to be able to cope with new situations, also the full background of the fundamental cases needs to be delivered. On the other hand significant detail is supplied, which is relevant for the advanced scholar and expert.

Currently large effort is put into obtaining picture and graphical material for utilization in the videos taking the copyright issues appropriately into account. From a variety of companies e.g. photographs of their internals have been obtained. These new diagrams will be used to substitute those which have until now been presented in the lectures, which were collected from the internet and textbooks. This will simultaneously significantly enhance the quality of the presentations.

Finally it should be mentioned that meanwhile the first of these videos have been synchronized in Brazilian Portuguese.

3. Invitation

Since in a university environment e.g. large-scale equipment as well as a variety of practical issues like trouble-shooting cannot be properly addressed, the author invites other experts in the field to contribute, e.g. by contributing videos, which can be recorded in our studio. Also it turns out that it is significant effort to obtain photos and videos of large-scale equipment and test facilities. While all companies addressed so far were quite supportive, nevertheless for each individual photo, diagram, video, etc. the copyright issues need to be addressed. Here also support from companies with respect to real-world photos, graphs, and videos is very welcome. Of course appropriate credits will be given.

Since also problematic cases with e.g. corroded examples would be welcome, confidential treatment of the source can be ensured as well.

Of course everybody is also invited to watch the videos, which are published under the creative-commons license by-nc-sa, i.e. attribution, non-commercial, and share alike. As mentioned, in the future the content will grow and increasingly also include expert topics.

4. Conclusion

After more than 25 videos of mostly between 20 and 45 minutes length have been produced, it can be concluded that this approach is quite feasible. The video recording and production is admittedly some effort. From experience it can be said that every video is generally recorded twice, since during the first recording the small inefficiencies in the manuscript and the slides become obvious, which apparently cannot be avoided even with very careful preparation. These inefficiencies are then removed for the second recording. Thus as a consequence it is found that also the material used, i.e. the PowerPoint slides as well as the manuscript are significantly enhanced by the video recording.

References

1) A. Pfennig, Thermal Unit Operations. YouTube Playlist (2017) https://www.youtube.com/playlist?list=PLEivQtB6FVkfUbs81p-i42FtjEl_2NWZY
2) audacity, https://sourceforge.net/projects/audacity/
3) http://chemeng.ulg.ac.be/PUO1

Enhanced Extraction of Nickel from a Concentrated Nitrate Aqueous Matrix Using LIX 63 / Versatic 10 / nonyl-4PC

Mike HUTTON-ASHKENNY[1]*, Keith R. BARNARD[2], and Don IBANA[3]

[1]Hatch, 144 Stirling Street, Perth, 6000, WA, Australia (previously Curtin University, WA School of Mines); [2]CSIRO Mineral Resources, 7 Conlon Street, Waterford, 6152, WA, Australia; [3]Curtin University, WA School of Mines, Kalgoorlie, 6430, WA, Australia.

Recent development of nitrate-based leaching techniques for nickel laterite ores has sparked interest in the solvent extraction of nickel and cobalt from such leach solutions. Solvent extraction from concentrated magnesium nitrate-based aqueous phases using LIX 63/Versatic 10/nonyl-4PC at low pH results in a higher deportment of nickel to the organic phase compared to zinc and cobalt, offering a novel method to separate nickel from cobalt. The present investigation into this phenomenon found that increasing nitrate concentrations in the aqueous phase increased distribution of nickel to the organic phase at a given pH for a range of solvent extraction reagents. Co-extraction of nitrate with nickel was also found to increase with decreasing pH for LIX 63/Versatic 10/nonyl-4PC from near 0 at pH 3 to a NO_3:Ni ratio of 1.27 at pH 1. UV-Vis analysis demonstrated that the nickel complex extracted from a concentrated nitrate matrix using only LIX 63 was octahedral with a spectrum comparable to $[Ni(HL)_3]Cl_2$ where HL is hydroxyoxime. These results are consistent with additional nickel uptake occurring at lower operating pH due to extraction of a nickel-nitrate salt such as $[Ni(HL)_3](NO_3)_2$.

1. Introduction

The advent of nitric acid–based processes such as the Direct Nickel process [1] or the nitric acid pressure leach [2] has generated interest in the purification of nickel and cobalt from nitric acid leach solutions. Solvent extraction directly from a nitrate leach liquor, after iron and aluminium removal, is a potential alternative to mixed hydroxide or mixed sulfide precipitation that bypasses the generation of an intermediate solid.

Previous studies have shown that extraction of certain metals from nitrate-based aqueous feeds occurs at a lower pH than corresponding sulfate-based aqueous feeds [3-6]. A comparative investigation by the present authors showed that, in general, the extraction pH_{50} value of base metals by acidic solvent extraction reagents decreases by 0.5 units on moving from a moderate ionic strength (1 M) sulfate to comparable nitrate matrix [7].

The expected nitrate concentration in the Direct Nickel solvent extraction feed could be as high as 9 M [8]. The effect of this high ionic strength matrix on the extraction of base metals by common solvent extraction reagents is not well understood.

We have previously investigated metal extraction from a moderate ionic strength nitrate matrix

(1 M $NaNO_3$) using the combination of LIX 63/Versatic 10. Nonyl-4PC was additionally used to enhance nickel kinetics in place of tributyl phosphate [9]. Nickel was extracted preferentially over cobalt and zinc under these conditions [10], contrary to the sulfate system where nickel and cobalt are extracted at the same pH [11]. This result prompted the development of a process to separate nickel from cobalt and zinc in a nitrate matrix at low pH (pH 1.5 to 2) using LIX 63/Versatic 10/nonyl-4PC [9]. The present paper aimed to further investigate the effects of increasing the aqueous phase magnesium nitrate concentration on the solvent extraction of nickel as may be applicable to a Direct Nickel-type process.

2. Experimental

2.1 Aqueous and Organic Solutions

Organic solutions were prepared using technical grade reagents diluted with ShellSol D70 (Shell Chemicals). Extractants used were: Versatic 10 (iso-decanoic acid, 99%, Shell Chemicals), LIX®63 (5,8-diethyl-7-hydroxy-6-dodecanone oxime, 55%, BASF), and nonyl-4PC (nonyl-4-pyridinecarboxylate, 95%, China Central South University). LIX 63 concentration was determined by gas chromatography flame ionisation detection (GC-FID) using pure *anti*-hydroxyoxime standard as described elsewhere [12].

Pure *anti*-hydroxyoxime was prepared following the nickel method of Tammi [13]. The remaining reagents were used as supplied and the quoted purities were obtained from either the MSDS or the manufacturer.

Solutions of nickel nitrate (AR) were made up in various matrices containing combinations of reagent grade magnesium nitrate or magnesium sulfate. Adjustment of pH was carried out using solutions of either sodium hydroxide (AR), sulfuric acid (AR), or nitric acid (AR).

2.2 Determination of metal extraction from varying matrix compositions

For slope analysis work, equilibrium nickel extraction (1.0 mM as nitrate) using LIX 63, Versatic 10, LIX 63/Versatic 10, Versatic 10/nonyl-4PC, and LIX 63/Versatic 10/nonyl-4PC all diluted to 0.35 M in ShellSol D70 was determined at various pH values depending on the organic composition used. The extraction tests were carried out from four different aqueous matrices of varying nitrate concentration but constant ionic strength assuming full dissociation of ions.

Further test work attempting to determine the extraction of nitrate via analytical methods was carried out from a 6 M magnesium nitrate solution containing 18 mM of nickel nitrate. Higher nickel concentrations were used for this work to allow greater extraction of nitrate and so improve the analytical resolution of the experiment.

All extraction tests were carried out in a water bath at 40 °C at an organic to aqueous ratio (O:A) of 1:1 using an overhead mixer (40 mm diameter impeller) at 900 rpm (tip speed 1.88 m/s) in a square stainless steel mixing box. The dispersion pH was measured using a pH probe (Ionode, IJ44-A). Samples of the dispersion were taken with a glass syringe and filtered through Whatman 1PS paper. The pH was adjusted using sodium hydroxide (10 g/L or 100 g/L) or sulfuric acid (100 g/L or 350 g/L). Sampled organic phases were stripped (50 g/L sulfuric acid, O:A 1:3, 40 °C, 40 minutes, or 62.5 g/L sulfuric acid, O:A = 1:4, 60 °C, 60 minutes for LIX 63 only) in a shaker-incubator operating at

250 rpm to allow calculation of mass balances and determination of organic phase nitrate concentrations.

2.3 Analytical Methods

Nickel, cobalt, and zinc were determined using atomic absorption spectroscopy (AAS) on an Agilent 240 FS spectrophotometer. Ultraviolet–visible (UV-Vis) spectroscopy was carried out on a Varian Cary 1C spectrophotometer.

Nitrate concentrations in the aqueous strip solutions were determined using a colorimetric method measuring UV-Vis absorbance at 410 nm after formation of a salicylic acid complex [14] with standards generated using potassium nitrate. Nitrate results were referenced against selected samples analysed using capillary electrophoresis (Beckman-Coulter, MDQ model).

3. Results and Discussion

3.1 Slope analysis for nickel extraction

Nickel extraction was carried out from aqueous phases of variable nitrate concentration but constant Ni concentration (1 mM) and ionic strength. The ionic strength was maintained using magnesium sulfate. The resulting log nickel distribution versus the log nitrate concentration is given in Figure 1.

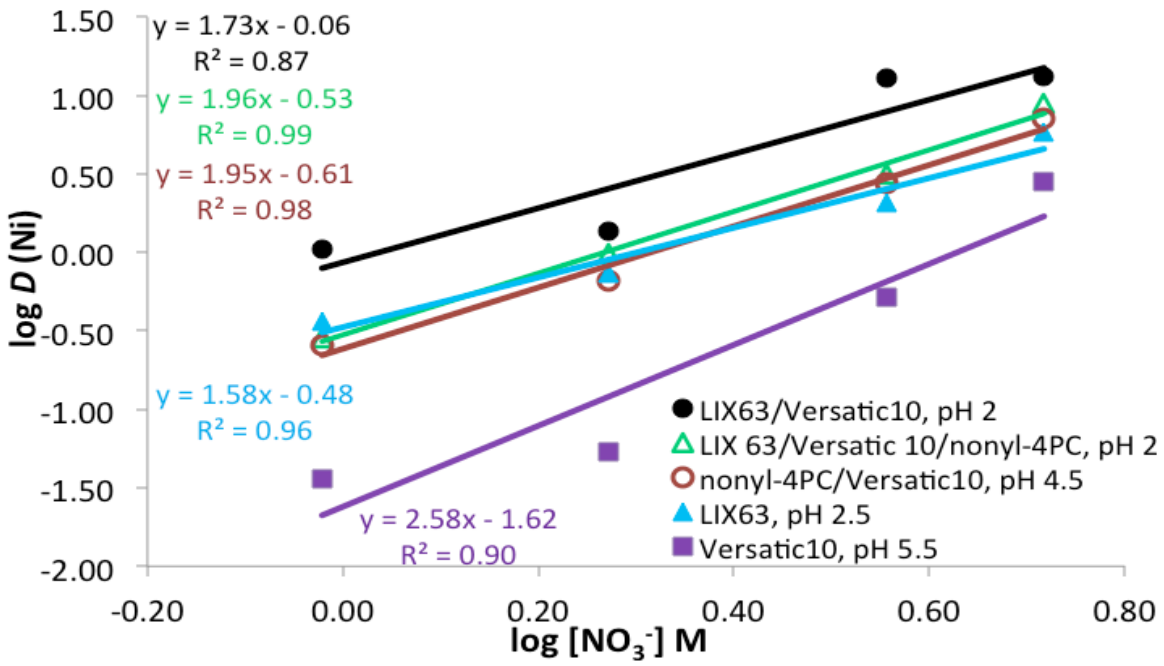

Figure 1. Effect of log nitrate concentration at constant ionic strength (9 M, balanced with magnesium sulfate) on log*D* of nickel extracted by various solvent extraction reagents in ShellSol D70.

The slopes of log*D* versus log[NO_3^-] in the five organic systems varied between 1.6 and 2.6 with a mean value of 1.96. R^2 values ranged from 0.87 to 0.99. Based on slope analysis techniques, the slope of the trend line in Figure 1 should represent the average number of nitrate anions extracted per

nickel ion into the organic phase. The prediction of two nitrate anions extracted per nickel ion would be consistent with a solvating system extracting both nickel and nitrate into the organic phase, such as $[Ni(HL)_3](NO_3)_2$ or $Ni(HL)_2(NO_3)_2$ where HL represents the neutral hydroxyoxime extractant.

Results from slope analysis should always be treated with some caution. High reagent concentrations, like those used in the present study, lead to non-ideality. Altering the type of anion in the aqueous matrix can also have a substantial effect on aqueous phase activity coefficients despite constant calculated ionic strength [15]. Corrections for activity coefficients for nickel in the distribution ratio based on these considerations can make significant differences to the obtained slope [15]. In addition, at high concentrations, full dissociation of ions may not be an accurate assumption. Some uncertainties therefore exist in relation to the true ionic strength of the test solutions. Despite these concerns, an increase in nickel uptake with increased nitrate concentration is clear in Figure 1. Further work was therefore carried out to determine if nitrate was being extracted into an organic phase nickel complex.

3.2 Investigation of nitrate incorporation into an organic phase nickel complex

Slope analysis above indicated that nitrate may be extracted into the organic phase at a molar ratio of nitrate to nickel of 2:1. Analysis of nickel (18 mM) extraction from 6 M magnesium nitrate using a mixture of the three reagents tested (LIX 63/Versatic 10/nonyl-4PC), however, showed that the molar ratio of nitrate to nickel in the organic phase was well below 2 at the three pH points used (Table 1). Further, nitrate extraction into the organic phase decreased to near zero with increasing pH in Table 1, and therefore with increased nickel loading. The maximum nitrate to nickel ratio of 1.27 occurred at the lowest pH tested (pH 1), and was about half that expected from the slope analysis results in Figure 1.

At lower pH, especially near pH 1, Versatic 10 proton dissociation will be unfavourable. Co-ordination of nitrate anions in place of a negatively charged organic acid [16, 17] may then be able to occur in the organic phase. This suggests that two competing nickel complexes were present in the organic phase, one charge balanced with nitrate and one with deprotonated Versatic 10. The increasing nitrate/nickel ratio further suggested that the relative concentration of the nitrate complex increased with decreasing pH. Extraction of nickel can therefore continue to occur at lower pH values by forming a nickel complex charge balanced with nitrate, such as $[Ni(HL)_3](NO_3)_2$ or $Ni(HL)_2(NO_3)_2$.

Table 1: Nickel and nitrate extractions of LIX 63/Versatic 10/nonyl-4PC. Nitrate extraction calculated by subtracting the nitrate obtained from contacting with a nickel-free aqueous.

pH	Nickel Extracted mM	Net Nitrate Extracted mM	Molar Ratio of nitrate / nickel
3	17.5	2.1	0.12
2	15.0	7.8	0.52
1	8.1	10.3	1.27

3.3 Ultraviolet-visible analysis of the organic phase nickel complex

UV-vis analysis was used as an investigative technique to further understand the different

nickel complexes formed with the pure *anti*-hydroxyoxime in LIX 63. Synergistic extraction of nickel using mixtures of LIX 63 and organic acids such as Versatic 10 results in the formation of octahedral mixed reagent complexes [17]. The UV-Vis spectrum for such a nickel complex, with a major peak at 600 nm, is shown in Figure 2. Nickel extracted by LIX 63 as a single reagent from a sulfate-based matrix at low acidity forms a square planar orange NiL_2 complex [18], where L is the deprotonated hydroxyoxime. This NiL_2 complex has a UV-Vis spectrum with a major peak at 440 nm (Figure 2).

At high sulfuric acid concentrations, nickel extracted with LIX 63 hydroxyoxime (HL) can form an insoluble octahedral $[Ni(HL)_3]SO_4$ salt, which readily precipitates [19]. Although the analogous $[Ni(HL)_3](NO_3)_2$ salt does not readily precipitate at high acidity, a short chain analogue has been successfully isolated by Barnard *et al.* [19], indicating that this complex can also exist. It was further found that a stable nickel salt with a nickel:chloride ratio of 1:2 is extracted from hydrochloric acid solutions [19]. The UV-Vis spectrum of the resulting organic phase nickel-hydroxyoxime-chloride complex closely resembles that of the octahedral nickel-hydroxyoxime-Versatic 10 complex (Figure 2), suggesting that the nickel chloride complex is also octahedral. Additional unpublished work has established a 3:1 HL:Ni ratio in the extracted nickel complex, allowing the stoichiometry to be established as $[Ni(HL)_3]Cl_2$.

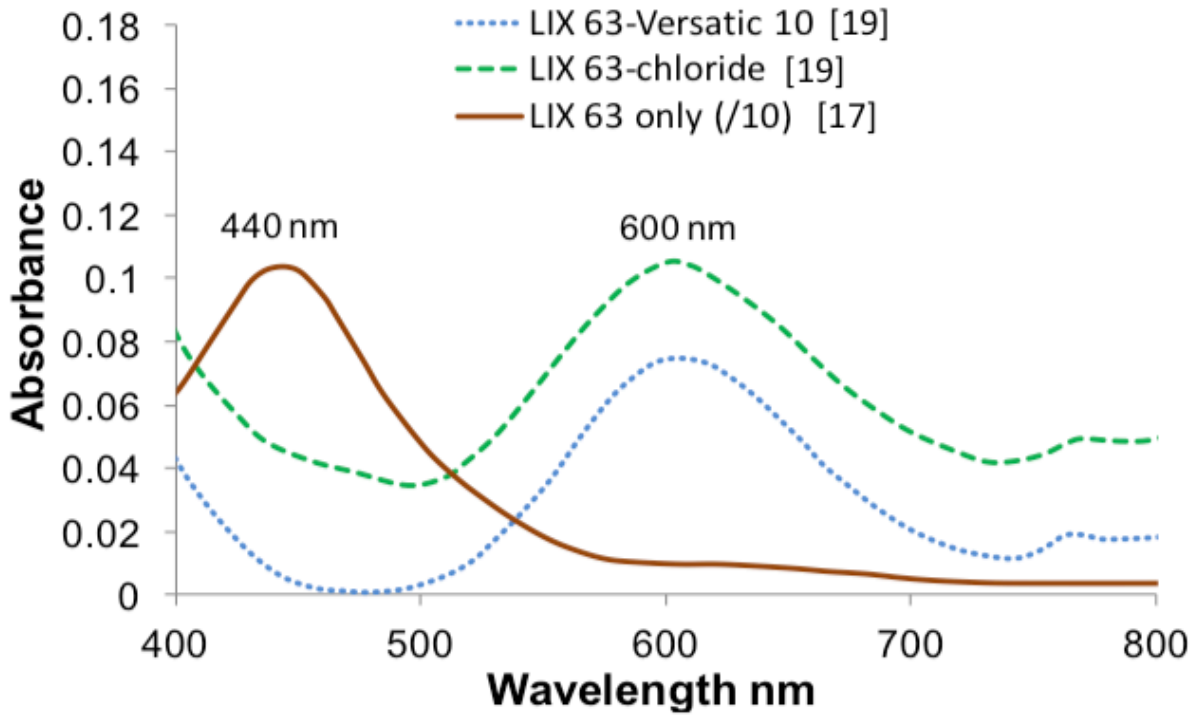

Figure 2: UV-Vis spectra for different nickel-LIX 63 complexes. Adapted from [17, 19]. Baseline of unloaded organic was manually subtracted in cited papers.

The UV-Vis spectrum of the nickel complex extracted from the concentrated nitrate matrix using *anti*-hydroxyoxime in the present investigation had a major peak at 613 nm (Figure 3) signifying that an octahedral nickel complex similar to that of nickel-hydroxyoxime-chloride, possibly of the

form $[Ni(HL)_3](NO_3)_2$, had been generated in the organic phase. Contacting the organic phase with concentrated magnesium sulfate resulted in the pale blue organic solution turning brown. This is reflected in Figure 3 with the peak at 613 nm being suppressed and the appearance of a new peak at 430 nm, resembling that of the NiL_2 square planar complex in Figure 2. Two different coordination environments (octahedral and square planar) therefore existed for nickel between the nitrate extract organic and the sulfate washed organic.

The obtained UV-Vis spectra coupled with the absence of any $[Ni(HL)_3]SO_4$ precipitate are consistent with the sulfate matrix removing nitrate from the organic phase and concurrent deprotonation of hydroxyoxime to maintain charge neutrality. The small residual peak around 600 nm after the sulfate wash in Figure 3 indicated that some residual nitrate remained in the organic phase after a new equilibrium had been established with the sulfate aqueous wash solution.

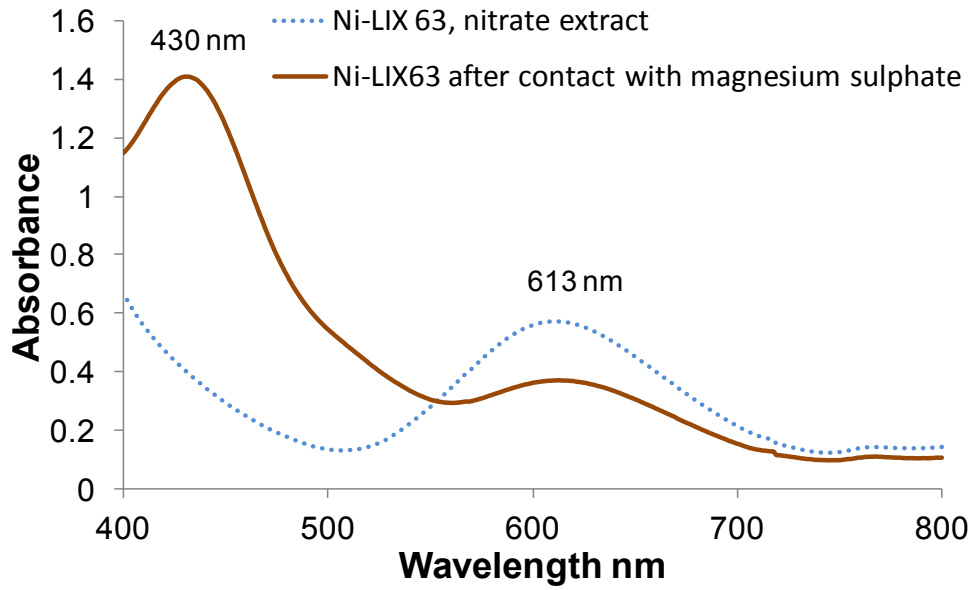

Figure 3: Change in UV-Vis spectrum of Ni-LIX 63 extracted from a nitrate matrix after washing with a concentrated sulfate solution ([Ni(II)] = 18 mM, [*anti*-hydroxyoxime] = 310 mM, magnesium salt concentrations = 2.5 M).

Nitrate anions in the aqueous phase can, therefore, potentially be co-extracted into organic systems containing LIX 63 at low to moderate pH to stabilise an octahedral nickel complex (either with or without Versatic 10 present) by forming an organic salt. This effect would be particularly promoted for nickel over other metals, which has a high octahedral ligand field stabilisation energy [20] and hence a preference for octahedral geometry. In the present study using LIX 63/Versatic 10/nonyl-4PC, co-ordination of a deprotonated Versatic 10 would take preference at higher pH values and nickel extraction would behave as expected using LIX 63/Versatic 10 in a sulphate matrix. As the pH decreases a new equilibrium between a nitrate counter-ion and a deprotonated Versatic 10 counter-ion will be established, increasing the nickel–nitrate ratio in the organic phase and thereby enhancing nickel extraction in the presence of high nitrate concentrations.

4. Conclusion

The present work has shown that nickel extraction using LIX 63 hydroxyoxime can occur via the use of both inorganic (nitrate) and organic (Versatic 10) counter-ions Operation at pH levels sufficiently high to encourage deprotonation of Versatic 10 favour its incorporation into a nickel-hydroxyoxime complex. At lower pH levels, where Versatic 10 deprotonation is not favored, nickel extraction can proceeed via incorporation of a suitable inorganic counter-ion, such as nitrate, into an organic phase complex. Increasing nitrate concentration in the aqueous phase therefore favoured increased nickel uptake via this mechanism for systems containing LIX 63.

UV-vis analysis of organic phase nickel complexes extracted using pure *anti*-hydroxyoxime revealed that an octahedral nickel complex, similar to the synergistic nickel complex formed using LIX 63/Versatic 10, was extracted from a concentrated nitrate matrix. The spectum obtained also aligned closely with $[Ni(HL)_3]Cl_2$ as presented in earlier work, suggesting that the nickel-nitrate complex formed was $[Ni(HL)_3](NO_3)_2$. This potential for some inorganic anions to co-ordinate with nickel-hydroxyoxime complexes at low pH values explains continued nickel extraction from a nitrate matrix with decreasing pH.

Practically, operation of a solvent extraction circuit from a concentrated nitrate aqueous phase at pH 1.5 will allow a greater separation of nickel from cobalt and zinc using LIX 63/Versatic 10/nonyl-4PC than from a comparable sulfate aqueous phase. This can be exploited to provide a novel method for separation of nickel from cobalt.

Acknowledgement

This study was supported by the Curtin University International Postgraduate Research Scholarship, the CSIRO Minerals Resources Flagship and Direct Nickel.

References

1. F. McCarthy, G. Brock. "The Direct Nickel process continued progress on the pathway to commercialisation". *ALTA Nickel / Cobalt*. Perth: ALTA Metallurgical Services. (2011).
2. B. Ma, W. Yang, B. Yang, C. Wang, Y. Chen, Y. Zhang, *Hydrometallurgy*, **155**. 88-94 (2015).
3. N.E. El-Hefny, J.A. Daoud, *Solvent Extr. Ion Exch.*, **25**. 831-843 (2007).
4. M.D. Lanagan, D.C. Ibana, *Miner. Eng.*, **16**. 237-245 (2003).
5. A.C. du Preez, J.S. Preston, *Solvent Extr. Ion Exch.*, **10**. 207-230 (1992).
6. J.S. Preston, A.C. du Preez, *Hydrometallurgy*, **58**. 239-250 (2000).
7. M. Hutton-Ashkenny, D. Ibana, K.R. Barnard. "Evidence for a predictable difference between nitrate and sulphate anions in the solvent extraction of base metals by acidic extractants". *International Solvent Extraction Conference*. Würzburg: Dechema. (2014).
8. F. McCarthy, *(personal communications)*. (2012).
9. M. Hutton-Ashkenny, K.R. Barnard, D. Ibana, *Hydrometallurgy*, **153**. 74-82 (2015).
10. M. Hutton-Ashkenny, D. Ibana, K.R. Barnard, *Miner. Eng.*, **77**. 42-51 (2015).

11. C.Y. Cheng, *Hydrometallurgy*, **84**. 109-117 (2006).
12. K.R. Barnard, M. Urbani, *Hydrometallurgy*, **89**. 40-51 (2007).
13. T.T. Tammi, *Hydrometallurgy*, **2**. 371-380 (1977).
14. D.A. Cataldo, M. Maroon, L.E. Schrader, V.L. Youngs, *Commun. Soil Sci. Plant Anal.*, **6**. 71-80 (1975).
15. B.A. Moyer, W.J. McDowell, B.C.F. Jr., G.N. Case, F.I. Case, *Solvent Extr. Ion Exch.*, **9**. 833-864 (1991).
16. J.M. Castresana, M.P. Elizalde, M. Aguilar, M. Cox, *Solvent Extr. Ion Exch.*, **6**. 265-274 (1988).
17. K.R. Barnard, G.L. Nealon, M.I. Ogden, B.W. Skelton, *Solvent Extr. Ion Exch.*, **28**. 778-792 (2010).
18. M.E. Keeney, K. Osseo-Asare, *Polyhedron*, **3**. 641-649 (1984).
19. K.R. Barnard, D.W. Shiers, M.J. McIldowie, B.W. Skelton, M.I. Ogden, *Ind. Eng. Chem. Res.*, **53**. 8208-8214 (2014).
20. F.A. Cotton, G. Wilkinson, "Advanced Inorganic Chemistry ". 4th Edition ed., USA: John Wiley and Sons. (1980)

Solvent Extraction in Different Lithium Recovery Processes

Sami VIROLAINEN[1,*], Mojtaba FALLAH FINI[1], Antero LAITINEN[2] and Tuomo SAINIO[1]

[1]Lappeenranta University of Technology, P.O. Box 20, 53851 Lappeenranta, Finland; [2]Technical Research Centre of Finland, P.O. Box 1000, 02044 VTT (Espoo), Finland

As Li exists often as Li^+ cation, Li-rich solutions can be purified from divalent metals with conventional cation exchange reagents. This approach is utilized in purification of Li-rich solutions originating from natural brines, and producing pure Li raffinate from Li-ion battery waste leachates. In this paper both of these processes are demonstrated in continuous bench scale experiments. Another industrially used solvent extraction purification process for Li-rich brine is removal of B, which is done by alcohol reagents, and the process is well known from 1960's. Li can be also directly extracted from natural brines and even seawater with solvating reagents. Adding ionic liquids improves often important Li/Mg selectivity. However, these direct solvent extraction processes have not been utilized industrially. The B removal process and the direct solvent extraction processes are discussed based on literature references.

1. Introduction

Currently Li is one of the most interesting metals in markets. This is due to its use in state-of-the-art battery technology, Li-ion batteries, and since societies are moving towards electric vehicles the demand of Li among Li-ion batteries is probably increasing dramatically within next decades [1]. The most important natural sources of Li are natural brines [2], chloride solutions, which contain 5–11 wt.-% Na and 10–1600 mg/kg Li. From purification point of view most significant impurities are Mg (30–31000 mg/kg, Ca (20–3900 mg/kg) and B (30–710 mg/kg) [3]. Currently, recovering Li from these brines is done by concentrating with solar energy, and purifying the obtained concentrate by different hydrometallurgical methods [4]. Solvent extraction may be used in this process for removal of B by alcohol reagent [5], and in final purification step for removal of Mg and Ca [6]. In this article solvent extraction removal of Mg and Ca in final purification step is demonstrated in bench scale continuous counter-current operation with synthetic Li-rich brine. The solvent extraction of B from Li containing brines is discussed based on literature survey.

Use of solvent extraction has not been popular in hydrometallurgical processes for recovering Li from ores. For example, recent review article by Choubey *et al.* [7] mention solvent extraction only with one reference [8], in which Li was extracted from zinnwaldite waste leachate with mixture of LIX-54 and TOPO. However, in many Li extraction processes from ores, there are problems with Li yield or purity of the Li product [7], for which problems solvent extraction could offer help.

As the solar evaporation based process is time consuming due to long residence times in the evaporation pools, Li producers are interested in direct recovery of Li from these brines, and there

solvent extraction, either by conventional reagents or by ionic liquids, is one of the most promising methods. These direct methods will be discussed in this article based on literature.

Since the amount of needed metal for Li-ion batteries is increasing, the amount of used batteries will be increasing at the same time as the lifespan of typical Li-ion battery is under 10 years [9]. This means that huge amounts of batteries become available as secondary source of Li (and other metals), but for example in 2011 the recycling rate of Li from all the end-of-life products was only 3% [10]. In hydrometallurgical processing of the used batteries, after acid leaching, solvent extraction is needed in removal of impurity metals (*e.g.* Cu, Al, Fe) [11] and in fractionation of Li+Co+Ni mixture [12]. Typical composition of battery waste is: Li 2–15%, Co 15–30%, Ni ≤10% Ni, Cu 7–17%, Al 3–10%, Fe ≤20% [13], and composition of typical sulfate leachate is: Co 21 g/L, Ni 0.5 g/L, Li 2.5 g/L, Fe 3.6 g/L, Cu 1.8 g/L, pH 3.5 [14]. In this paper producing over 99.6% pure Ni, Co and Li from synthetic battery waste leachate is demonstrated in bench-scale counter-current solvent extraction experiments.

2. Experimental

2.1 Chemicals and solutions

Chemicals used in the experiments, with their suppliers and purities (if available) were: $CoSO_4 \cdot 7H_2O$ (Outokumpu OY, Technical grade with 22% Co content), $NiSO_4 \cdot 6H_2O$ (Sigma-Aldrich Co., 99%), $Li_2SO_4 \cdot H_2O$ (Alfa-Aesar, 99%), LiCl (VWR International, 98%), $MgCl_2 \cdot 4.5H_2O$ (VWR International, 97%), $CaCl_2$ (VWR International, 98%), NaCl (VWR International, 98%), H_2SO_4 95-97% (Merck KGaA, Pro analysi), HCl 37% (Merck KGaA, Pro analysi), HNO_3 65% (Merck KGaA, Pro analysi), NH_3 25% (Merck KGaA, Pro analysi), NaOH (VWR International, 98%), Exssol D80 (ExxonMobil Chemical), Shellsol D70 (Shell Chemicals), Cyanex 272 (Cytec Solvay Group, 88%), Trioctylamine (Sigma-Aldrich Co., 98%), Tributylphosphate (Sigma-Aldrich Co., 97%), di-(2-ethylhexyl)phosphoric acid (D2EHPA), neodecanoic acid (Versatic 10).

The synthetic Li-rich brine solutions were prepared by dissolving the chloride salts of Li, Ca, and Mg to purified water. Chloride concentration was topped up to 200 g/L with NaCl. According to the analyses, their compositions were as follows: Li 26.0–34.0 g/L, Ca 1.17–1.55 g/L, Mg 0.022–0.075 g/L, pH 7.5. The synthetic battery waste leachates were prepared by dissolving sulfate salts of Li, Co and Ni to purified water, and the composition was: Co 14 g/L, Ni 0.5 g/L, Li 2.8 g/L.

2.2 Continuous counter-current experiments

The continuous counter-current solvent extraction experiments were performed in bench scale pilot equipment (SX Kinetics Inc.) having 270 mL settlers and 1050 mL mixers. The phase ratio in the mixer was monitored during the runs, and adjusted if needed by internal circulations. The flowsheet of the equipment is given in references [6] and [12].

Temperatures and pH's were monitored online, and adjusted if needed. The pH control was done by pre-neutralization of the organic phases using aqueous ammonia (25%) or 5 M NaOH, or in the battery waste leachate case by dropwise addition of concentrated H_2SO_4 (95-97%).

In the Li-rich brine case D2EHPA and Versatic 10 were used as extractants. Residence time in the mixer was 2.0–6.1 min, A/O phase ratio in loading stage 1.5–0.6, and temperature was 23 or 31 °C. With D2EHPA the pH varied between 3.7 and 4.1, and with Versatic 10 between 6.2 and 7.4. At least 50 mixer

volumes of the brine was treated in every run, and this amount was observed to be enough for achieving steady-state in the dynamic process.

The organic phase in battery waste leachate case was 1 M Cyanex 272 in Exssol D80 containing 5% v/v of a phase modifier (TOA or TBP). Residence time in the mixer was 10 min, which is, based on literature, enough to achieve equilibrium. Temperature was 23 °C. Loading (three runs), scrubbing (one run) and stripping (four runs) steps were studied in separate runs. Steady-state was again achieved in every run with fed amounts of 65 mixer volumes in loading and stripping runs, and 20.3 mixer volumes in the scrubbing run. The exact run parameters are given with the results in Tables 1 and 2.

2.3 Analytics

Metal analyses were carried out from 14% or 1 M HNO_3-media using inductively coupled plasma atomic emission spectroscopy (ICP-AES, device: IRIS Intrepid Duo, Thermo Electron Corporation), or by Thermo-Scientific iCE™ 3300 AAS Atomic Absorption Spectrometer. The organic phase metal concentrations were analyzed after stripping them with 14% HNO_3 (A/O = 10:1).

3. Results and Discussion

3.1 Solvent extraction removal of Ca and Mg from Li-rich brines

In conventional natural brine utilizing Li recovery process impurities are removed by precipitation methods, but their drawbacks are in inefficient purification and/or high Li losses, *i.e.* in selectivity [6]. On the other hand, solvent extraction seems to be feasible option for the final purification step, as in general the cation exchange reagents prefer divalent metals over monovalent, and the main impurities in the concentrated brines are Ca and Mg. In 1992 Bukowsky *et al.* [15] published a research in which Ca was removed from concentrated brine by D2EHPA. Therefore, it was decided to develop a flowsheet for solvent extraction removal of Ca and Mg by solvent extraction. Discussion below is based on authors' own experimental work.

Based on laboratory scale equilibrium experiments D2EHPA and Versatic 10 were identified as viable candidates for the purification task [6]. Nine continuous counter-current (2 stages) bench scale runs were done to study optimal run parameters (pH, phase ratio, residence time). Goal was to reduce Ca and Mg levels from 1.3 g/L and 50 mg/L, respectively, to under 20 mg/L, or preferably to ppm level.

With D2EHPA the pH adjustment (pre-neutralization) needs to be done so that the pH in both extraction stages is 3.6–3.8 (Table 1). If the pH is higher, Li losses are too high (Run D-1), and if it is lower, Mg yield decreases. For Versatic 10 the behavior is similar (and reasonable); increasing the pH increases Li losses (Run V-1), but these are in general lower than with D2EHPA.

In operation with two counter-current stages optimal phase ratio with both reagents is near unity. However, the yield for Mg can be increased by increasing the organic phase low, and at the same time the Li losses are increased a little bit. Decreasing the residence time from 5.1 to 2.0 min had positive effect to Mg extraction yield, but at the same time Li losses were also increased (Runs V-5 and V-6). With D2EHPA no significant effects with residence time were observed.

Table 1. Bench scale experiments for studying solvent extraction removal of Ca and Mg from Li-rich brine [6]. In Run-id. D stands for D2EHPA and V for Versatic 10.

Run id.	pH 1st	pH 2nd	A/O	τ, min	E_{Ca}, %	E_{Mg}, %	E_{Li}, %
D-1	3.9	4.1	0.85	6.0	99	94	9.1
D-2	3.7	3.6	1.25	6.1	99	90	4.0
D-3	3.7	3.8	1.20	2.0	98	86	5.3
V-1	6.7	7.1	1.00	4.5	100	95	4.6
V-2	6.2	6.8	1.25	6.1	97	34	1.4
V-3	6.9	7.4	1.35	6.0	99	50	2.1
V-4	6.4	6.9	1.25	2.0	99	40	2.1
V-5	6.6	6.9	0.60	5.1	100	90	3.3
V-6	6.4	6.9	0.60	2.0	100	98	5.5

In general, the performance of solvent extraction purification was satisfactory. Li purity increase from 95.1–96.6% to 99.9% was achieved with both of the reagents, and the Ca and Mg concentrations in raffinates were in ppm level (excluding Runs V-2, V-3 and V4 in Table 1). The Li losses in the effective purification runs were typically 5% or less, which is also much better than the 10% or more losses in the conventional precipitation purifications. With Versatic 10 a bit more pure raffinates were obtained as 100% Ca extractions and over 95% Mg extractions were recorded. The needed residence time is low (*e.g.* 2.0 min) meaning that high brine volumes could be treated with reasonable sized reactors.

3.2 Solvent extraction removal of B from Li-rich brines

B content in Li-rich brines is typically 30–710 mg/kg [3], which needs to be reduced to ppm level in order to obtain battery grade Li_2CO_3. In that purification step solvent extraction has been extensively used. Discussion below is based exclusively on literature references.

First industrial B recovery process from brines was operated already in 1960's [16–17]. The chemistry of the process has not been changed since then, and alcohols, especially polyols, have been almost exclusive used as extractants [18]:

$$H_3BO_3\,(aq) + 2R(OH)_2\,(org) \rightleftarrows R_2BO_4^-M^+\,(org) + 3H_2O + H^+ \qquad (1)$$

Diluent has some effect to the separation efficiency, but with kerosene the efficiency is not significantly worse than with some other suggested diluents [18–19]. Therefore it would be probably preferred in industrial operation, like it was used in the first B extraction plants [16–17].

Kumar *et al.* [18] suggested recently, based on laboratory experiments, a solvent extraction process for B removal from Uyuni salar brine (B 450 mg/L, Li 1100 mg/L). 2,2,4-trimethyl-1,3-pentanediol in chloroform is used as an extractant, and the extraction is most efficient (~100%) in pH range 3–5. Scrubbing was done successfully with 0.1 M H_2SO_4 with minor B losses, and stripping with 99% efficiency with 25% aqueous ammonia. Final purity of the B product is not given, but it can be assumed to be very high due to mentioned efficient scrubbing.

Patent literature contains few methods for the B removal from Li-rich brines. All of them use

simple fatty alcohols in kerosene as extractants [20–22]. In a patent by Perez *et al.* [22] TBP (5–20%) is used as modifier. The B removal is efficient with abovementioned organic phases, and for example over 99% overall yield from 7.85 g/L B containing Salar de Atacama Li-rich brine is reported in a journal article of Orrego *et al.* [23]. In these processes stripping of B is done by NaOH.

3.3 Direct solvent extraction of Li from naturally occurring brines and seawater

Discussion below is based exclusively on literature references. TBP is most conventionally used as a direct Li extractant. It needs some salt (typically $FeCl_3$ is used) to form an extractable ion pair (Equation 2). Typical problem with the TBP is selectivity, and Na, K and Mg salts hinder the extraction [24]. Kerosene is usually used as a diluent, but for example using MIBK can increase the distribution coefficient of Li [25].

$$Li^+ (aq) + FeCl_4^- (aq) + nTBP (org) \rightleftarrows LiFeCl_4 \cdot nTBP (org) \quad (2)$$

Gabra and Torma [26], and Bukowsky and Uhlemann [27] suggest using alcohols as Li extractant from brines. Gabra and Torma have gotten 99.6% purity Li from synthetic brine containing Na, K and Ca as impurities. If high selectivity over Mg is needed, diols can be added [27]. β-diketone mixed with TOPO has been suggested in patent of Baldwin and Seeley [28], which was inspired by journal article of Lee *et al.* [29], in which the extraction mechanism has been proposed to be adduct formation between Li, dibenzoylmethane and TOPO. With this synergistic system selectivities over alkali metals (*e.g.* K, Na) are high, but selectivities over Ca and Mg have not been studied.

Ionic liquids have been extensively studied for direct Li extractants from brines. Gao *et al.* used 1-butyl-3-methyl-imidazolium hexafluorophosphate ($[C_4mim][PF_6]$), 1-butyl-3-methylimidazolium bis(trifluoromethylsulfonyl) imide ($[C_4mim][NTf_2]$) and 1-ethyl-3-methylimidazolium bis(trifluoromethylsulfonyl) imide ($[C_2mim][NTf_2]$) in TIBP (triisobutyl phosphate) and kerosene to extract Li from 2.3 g/L Li and 77 g/L Mg containing brine. High selectivity over Mg was obtained and reusability of the organic phase was successfully tested in ten consequent extraction-stripping cycles. The extraction mechanism was studied with spectroscopic methods and claimed to be solvation of LiCl by TIBP [30]. Shi *et al.* [31–33] have used 1-octyl-3-methyl-imidazolium hexafluorophosphate ($[C_8mim][PF_6]$), $[C_4mim][NTf_2]$ and $[C_4mim][PF_6]$ with TBP and also gotten decent selectivity over Mg. In these articles the mechanism is claimed to be cation exchange reaction, in which the cation of ionic liquid is transferred to the aqueous phase. With all of these ionic liquid extractions, the Mg/Li ratio after stripping is low enough so that pure Li can be obtained by precipitation.

In article by Harvianto *et al.* [34] using ionic liquids for direct Li extractants from seawater has been suggested. With mixture of thenoyltrifluoroacetone (TTA) and TOPO in kerosene over 65% yield was obtained, but Mg needs to be precipitated first, and problems appear also with durability of the extractant. Extraction of Li from seawater by different membrane processes has been studied extensively in Japan. One of the processes utilizes ionic liquids as carrier between the membranes. The ionic liquid (N,N,N-trimethyl-N-propylammonium-bis(trifluorometaani-sulfonyl) imide, TMPA-TFSI) rejects Li transfer, but carries the other metals (Na, K, Ca, Mg) through the membrane [35].

3.4 Solvent extraction fractionation of battery waste leachate

In fractionation step for producing pure metals from battery waste leachates, Ni is often present in the feed, and thus solvent extraction with bis(2,4,4-trimethylpentyl)phosphinic acid (Cyanex 272, Mextral 272P, P507) is seen as the best choice. Although, this kind of process has been proposed previously [36–37], it was decided to seek for simpler flowsheet, higher purities, and to demonstrate the process in bench scale. Discussion below is based on authors' own experimental work.

Based on laboratory equilibrium experiments, Cyanex 272, with 5% TOA (or TBP in Run L-3, Table 2) as phase modifier, was chosen as extractant. Suggested flowsheet had mutual loading for Co and Ni, Li scrubbing and selective Ni stripping steps. The fractionation was demonstrated in bench scale with three loading, one scrubbing and four stripping runs.

Co and Ni were effectively loaded to the organic phase (Runs L-2 and L-3 in Table 2) in two extraction stages from the synthetic battery waste leachate at equilibrium pH around 7. However, the flowrate of the organic feed needs to be higher than the flowrate of the aqueous phase (compare Runs L-2 and L-1), and also the amount of co-extracted Li is high. The amount of co-extracted Li could be lowered by adding more loading stages, but here an approach of having Li scrubbing by acidic (pH 1.3) $NiSO_4$ solution was taken. The results are not shown here, but the scrubbing removed Li efficiently without significant losses of Co or Ni [12]. With TOA as a modifier, the Li losses in loading were lower than with TBP (Runs L-2 and L-3). The high Co and Ni yields mean also high Li purity in raffinate, which was 99.9% in Runs L-2 and L-3.

In two stage stripping, either the purity of the Co in organic phase, or Ni in aqueous phase remained under 99% (Runs S-1 and S-2 in Table 2). Therefore, it was decided to add one more stage. With this configuration a bit lower equilibrium pH was achieved (Run S-4) yielding less Co losses to the aqueous phase (higher Ni purity) while still having high Ni stripping percentage resulting at the same time high purity Co in organic phase.

Table 2. Bench scale experiments for studying solvent extraction fractionation of Co, Ni and Li from battery waste leachate [12]. In Run-id. L stands for loading and S for stripping. In stripping runs *P* stands for phase purity in target phase (org. for Co and aq. for Ni). In run L-3 phase modifier was 5% TBP instead of TOA.

Run id.	pH 1st	pH 2nd	pH 3rd	A/O	E_{Co}, %	E_{Ni}, %	E_{Li}, %
L-1	5.0	7.2	-	0.95	100	80.1	7.6
L-2	6.8	7.1	-	0.77	100	99.6	17.3
L-3	6.7	7.0	-	0.77	100	99.9	26.2
					P_{Co}, %	P_{Ni}, %	
S-1	6.3	5.2	-	0.65	99.6	97.6	-
S-2	6.3	5.4	-	0.67	98.7	99.6	-
S-3	6.3	6.1	5.4	0.67	98.2	99.9	-
S-4	6.0	5.8	5.0	0.65	99.6	99.7	-

4. Conclusion

Li exists in aqueous solutions mostly as Li^+ cation, and therefore it is not strongly extracted with cation exchange reagents. However, this feature can be utilized in purification of Li-rich brines from divalent cations. The process for effective removal of Ca and Mg has been demonstrated in this article with continuous bench scale runs using D2EHPA as extractant. The other solvent extraction utilizing purification stage in producing battery grade Li salts from natural brines is removal of B. Diols are used here as solvating extractants. The approach of having the pure Li product as raffinate can be used in producing 99.9% pure Li from battery waste leachates. Also this process has been demonstrated in this article with continuous bench scale runs.

Li^+ cation is not very strongly hydrated, which is probably the reason why it can be extracted fairly selectively from different solutions with solvating extractants, with or without ionic liquids in the organic phase. Though, for example with TBP $FeCl_4^-$ is needed as counter-ion, and the system does not have the desired high selectivity over Mg. With ionic liquids in organic phase direct cation exchange reaction with cation of the ionic liquid, or ionic liquid promoted solvation have been proposed as possible extraction mechanisms. With these systems, the selectivity over Mg is high, and from stripping solutions battery grade Li salts can be precipitated. However, the ionic liquids are expensive, and in the systems with the cation exchange mechanism the cation of ionic liquid needs to be recovered from the stripping solution.

Acknowledgement

Outotec (Finland) Oyj and particularly Mr. Marko Limnell are acknowledged for their support with the continuous bench scale equipment. B.Sc. Tommi Huhtanen, B.Sc. Marko Hirvelä, and B.Sc. Henri Vainio are acknowledged for their experimental assistance.

References

1) L.F. Cabeza, A. Gutierrez, C. Barreneche, S. Ushak, Á.G. Fernández, A. Inés Fernádez, M. Grágeda, *Renew. Sustain. Energy Rev.*, **42**, 1106–1112 (2015).
2) S.E. Kesler, P.W. Gruber, P.A. Medina, G.A. Keoleian, M.P. Everson, T.J. Wallington, *Ore Geol. Rev.*, **48**, 55–69 (2012).
3) J.W. An, D.J. Kang, K.T. Tran, M.J. Kim, T. Lim, T. Tran, *Hydrometallurgy*, **117–118**, 64–70 (2012).
4) D.E. Garrett, *Part 1 — Lithium, Handbook of Lithium and Natural Calcium Chloride*, Academic Press, Oxford, 1–235 (2004).
5) P.M. Brown, D.A. Boryta, *US5219550 A* (1993).
6) S. Virolainen, M. Fallah Fini, V. Miettinen, A. Laitinen, M. Haapalainen, T. Sainio, *Hydrometallurgy*, **162**, 9–15 (2016).
7) P.K. Choubey. M-S. Kim, R.R. Srivastava, J-C. Lee, J-Y. Lee, *Min. Eng.*, **89**, 119–137 (2016).
8) J. Jandová, P. Dvořák, H.N. Vu, *Hydrometallurgy*, **103**, 12–18 (2010).
9) J.B. Goodenough, K.S. Park, *J. Am. Chem. Soc.*, **135**, 1167–1176 (2013).
10) L. Talens Peiró, G. Villalba Mendez, R.U. Ayres, *JOM*, **65**, 986–996 (2013).
11) T. Suzuki, T. Nakamura, Y. Inoue, M. Niinae, J. Shibata, *Sep. Purif. Technol.*, **98**, 396–401 (2012).

12) S. Virolainen, M. Fallah Fini, A. Laitinen, T. Sainio, *Sep. Purif. Technol.*, **179**, 274–282 (2017).
13) X. Zeng, J. Li, N. Singh, *Crit. Rev. Environ. Sci. Technol.*, **44**, 1129–1165 (2014).
14) L. Chen, X. Tang, Y. Zhang, L. Li, Z. Zeng, Y. Zhang, *Hydrometallurgy*, **108**, 80–86 (2011).
15) H. Bukowsky, E. Uhlemann, K. Gloe, P. Mühl, *Hydrometallurgy*, **28**, 323–329 (1992).
16) C.R. Havighorst, *Chem. Eng.*, **70**, 228–232 (1963).
17) R.K. Klopfenstein, D.S. Arnold, *Journal of Metals*, **18**, 1195–1197 (1966).
18) J.R. Kumar, C-J. Kim, H-S. Yoon, D-J. Kang, J-Y. Lee, *Korean J. Met. Mater.*, **53**, 578–583 (2014).
19) K. Poslu, W.L. Dudeney, *Hydrometallurgy*, **10**, 47–60 (1983).
20) P.M. Brown, S.J. Beckerman, *US4980136 A* (1990).
21) P.M. Brown, D.A. Boryta, *US5219550 A* (1993).
22) W.A. Perez, H.A.C. Barrientos Ruiz, *US20130101484 A1* (2013).
23) P. Orrego, C. Goldman, P. Reveco, E. Valdes, M.E. Flores, D. Bustos, D. Jandragholica, *Nucleotecnica*, **14**, 39–46 (1994).
24) G. Zeming, Z. Shenlin, *Chinese Journal of Chemical Engineering*, **6**, 124–129 (1998).
25) Z. Zhou, W. Qin, W. Fei, *J. Chem. Eng. Data*, **56**, 3518–3522 (2011).
26) G.G. Gabra, A.E. Torma, *Hydrometallurgy*, **3**, 23–33 (1978).
27) H. Bukowsky, E. Uhlemann, *Sep. Sci. Technol.*, **28**, 1357–1360 (1993).
28) W. Baldwin, F. Seeley, *US3793433 A* (1974).
29) D.A Lee, W.L. Taylor, W.J. McDowell, J.S. Drury, *Journal of Inorganic and Nuclear Chemistry*, **30**, 2807–2821 (1968).
30) D. Gao, X. Yu, Y. Guo, S. Wang, M. Liu, T. Deng, Y. Chen, N. Belzile, *Chem. Res. Chin. Univ.*, **31**, 621–626 (2015).
31) C. Shi, Y. Jia, Y, Jing, *CIESC J.*, **66**, 253–259 (2015).
32) C. Shi, Y. Jing, Y. Jia, *J. Mol. Liq.*, **215**, 640–646 (2016).
33) C. Shi, Y. Jia, C. Zhang, H. Liu, Y. Jing, *Fusion Engineering and Design*, **90**, 1–6 (2015).
34) G. Harvianto, S.-H. Kim, C.-S. Ju, *Rare Met.*, 1–6 (2015).
35) T. Hoshino, *Fusion Engineering and Design*, **88**, 2956–2959 (2013).
36) V.T. Nguyen, J.C. Lee, J. Jeong, B.S. Kim, B.D. Pandey, *Met. Mater. Int.*, **20**, 357–365 (2014).
37) V.T. Nguyen, J.C. Lee, J. Jeong, B.S. Kim, B.D. Pandey. *Korean Chem. Eng. Res.*, **53**, 137–144 (2015).

Selective Extraction of Scandium from Other REEs Using Binary Extractant of PC-88A and Versatic 10 from Nitrate Media

Maha Sharaf [1], Wataru Yoshida[1], Fukiko Kubota[1] and Masahiro Goto[1, 2*]

[1]*Department of Applied Chemistry, Graduate School of Engineering*,

[2]*Center for Future Chemistry, Kyushu University, 744 Motooka, Fukuoka 819-0395, Japan*

Comparative study for the extraction of rare earth metals was conducted using some binary extractant systems, in which PC-88A was used as the main extractant. The binary systems showed a different extraction behavior of synergism or antagonism depending on several factors such as the structure of extractant, the mechanism of extraction, interaction between the extractant and the coordinated ligand and others. Based on the results obtained, the binary system composed of PC-88A and Versatic 10 enables to achieve the selective extraction of Sc(III) from other rare earth metals and to enhance the stripping efficiency even with using a mild acidic solution, which was thought to be difficult from a solvent including PC-88A alone.

1. Introduction

The demand of scandium (Sc) has been increasing in high-technology industries [1], however its supply is not enough because Sc(III) is difficult to be purified and recovered. Organophosphorous extractants such as 2-ethylhexylphosphonic acid mono-2-ethylhexyl ester (PC-88A) have been commercially often used for the separation of rare earth metals, however it exhibits too high affinity towards the extraction of Sc(III), which results in difficulty in stripping operation with a mild acidic condition [2]. To control the extraction and separation efficiency, it is sometimes effective to use a binary extractant system, which shows a synergistic or an antagonistic effect between the two mixed extractants [3,4,5].

The extraction of metal cation M^{x+} by the acidic extractant HA could be expressed by the formation of the MA_x chelate in the organic phase. Combined synergistic behavior of two extractants (HA, Z) in the binary system will be appeared if the MA_xZ_n adduct is formed, which is extracted with a high efficiency rather than the acidic extractant alone. On the other hand, antagonistic behavior will be observed if HA and Z interacts among themselves, reducing the initial available amount of HA ready for complex formation [6].

In the present study, we investigated the extraction behavior of rare earth metals using several binary extractant systems composed mainly of PC-88A and another extractant with a different extraction mode such as solvation, chelation and an ionic interaction mechanism. Moreover, we will report the selective extraction and recovery of Sc(III) from other rare earth metals by using a mixture of PC-88A and an alkyl-monocarboxylic acid, Versatic 10.

2. Experimental

2.1 Reagents

Extractants PC-88A, Primene JM-T, TBP, Cyanex 272 and Versatic 10 were purchased from Wako Pure Chemical Industries Ltd. (Osaka, Japan) and used without any purification. n-Dodecane, ammonium nitrate and nitric acid were supplied by Kishida Chemical Co., Ltd (Osaka, Japan). All the other chemicals were of analytical grade. The molecular structures of the extractants used in this study are shown in Figure 1.

2.2 Extraction experiments

Aqueous feed phases containing 0.1 mM of Sc ion and other rare earth metal ions (Y^{3+}, La^{3+}, Nd^{3+}, Eu^{3+} and Dy^{3+}) were prepared by dissolving the nitrate salts of the metals in 0.1 M HNO_3 and 0.1 M ammonium nitrate. The pH values in the aqueous phases were adjusted by mixing the two solutions. Extraction phases were prepared by dissolving a given amount of PC-88A and/other targeted extractant in the organic diluent (n-dodecane).

Equal volumes (2 ml) of the organic extraction phase and the feed aqueous phase were put into a sealed tube. The samples were mixed first for 1 min using a vibrating mixer then were shaken at 298 K for 1 h in a temperature-controlled bath to assure equilibrium. The equilibrium pH of the aqueous phase after extraction was measured by a pH meter (HM-60 G, DKK-TOA Co.). The stripping of metal ions from the extraction phase was achieved using an acid solution with the same procedure of extraction. Metal concentrations in the aqueous phases were estimated using an inductively coupled plasma (ICP)-atomic emission spectrometer (Optima 8300; Perkin Elmer Inc., MA, USA). The extraction ratio of the metal ions (E [-]) was calculated by Eq. (1):

$$E = \frac{[M]_{ex.eq}}{[M]_{aq.0}} = \frac{[M]_{aq.0} - [M]_{aq.eq}}{[M]_{aq.0}} \quad (1)$$

The distribution coefficient D [-] was defined as shown in Eq. (2):

$$D = \frac{[M]_{ex.eq}}{[M]_{aq.eq}} = \frac{[M]_{aq.0} - [M]_{aq.eq}}{[M]_{aq.eq}} \quad (2)$$

where [M] is the metal concentration, and subscripts aq and ex symbolize the feed aqueous and extraction phases, respectively. The subscripts 0 and eq denote the initial and the equilibrium state, respectively.

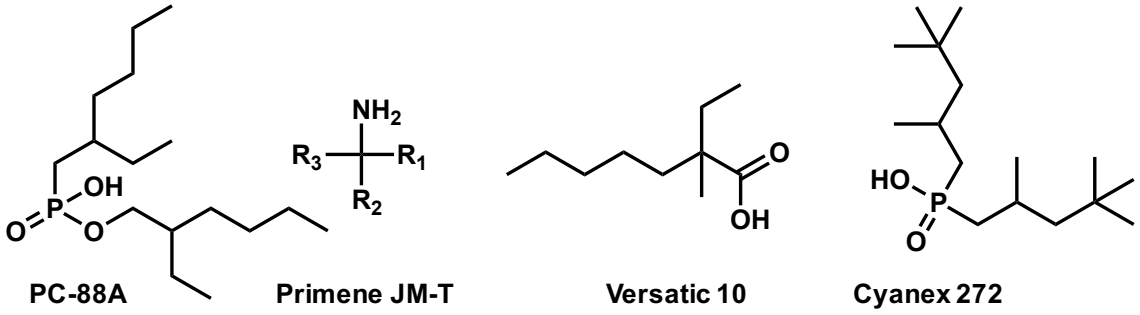

Figure 1. Molecular structures of extractants used in this study.

3. Results and Discussion

3.1 Extraction using individual PC-88A

The extraction ratio for the rare earth ions into the organic phase using 1 mM PC-88A alone is shown in Figure 2. Based on the results in Figure 2, PC-88A shows a high affinity towards Sc^{3+}; the extraction occurs from a high acidity (pH=zero), which is thought to be difficult to perform stripping operation from the Sc-loaded organic phase.

3.2 Extraction using different binary systems

Extraction isotherm equilibria using a binary mixture of PC-88A and TBP (solvating extractant) /or cyanex 272 (acidic chelating extractant) /or primene JM-T (basic extractant) are shown in Figure 3. Figure 3(a) shows the extraction behavior of 1 mM PC-88A and 5 mM primene JM-T, the addition of Primene JM-T delays the extraction of scandium, but on the other hand it enhances clearly the extraction of all Y, Dy and Eu ions, which is called the synergistic effect. We should notice that the extraction ratio of 5 mM Primene JM-T alone with the same concentration towards the rare earths ions is very low. Apparently, the last mentioned binary system decreases the selectivity towards Sc ion compared to that of PC-88A alone. While, the extraction ratio of Sc ion using the binary extractant of 1 mM PC-88A and 5 mM Cyanex 272 is obviously decreased indicating the strong antagonistic effect of adding Cyanex 272 to PC-88A for the extraction of Sc ion as shown in Figure 3(b). The addition of Cyanex 272 completely changes the extraction mode of PC-88A as the system becomes more selective to Y ion after pH 3 and enhances the extraction of other rare earths at the same time. The extraction using 5 mM Cyanex 272 alone shows very low extraction ability to rare earth ions, however, the addition of Cyanex 272 to PC-88A reduces the extraction ratio of Sc (antagonistic effect). The possible interaction between PC-88A and Cyanex 272 could be the reason for the antagonistic effect towards Sc ion but the extent of interaction had not been studied yet. The degree of interaction between the two extractants in the binary system can be deduced from the extent of the antagonistic effect, whereas in a synergistic effect, an additional extractant in return enhances the degree of extraction for some metal ions depending on the nature of extractant itself. Figure 3(c) demonstrates the effect of adding TBP (solvating agent) to PC-88A towards rare earth ions extraction. The results indicate the weak effect of adding TBP in the binary system that resembles the extraction by only PC-88A except for only Dy ion.

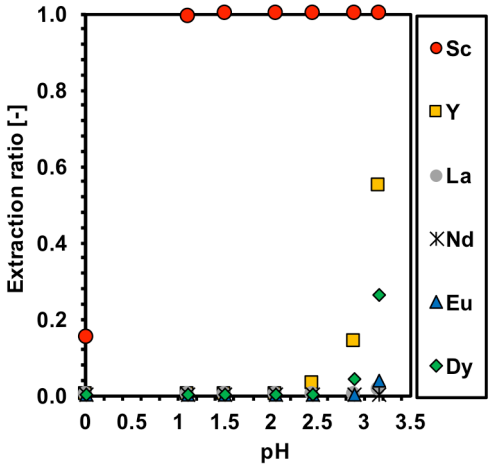

Figure 2. Extraction ratio of REE ions using 1 mM PC-88A alone, an aqueous phase: 0.1 mM M^{n+}.

Mixed extractant systems offer an interesting extraction behavior, which needs further investigation to elucidate the detailed reasons for the dissimilar features under set conditions. There are many factors, which will govern the extraction behavior such as the ligand effect, the mechanism

of extraction, the structure of extractant, solubility parameters of metal chelate, a diluent effect, hydrogen bond formation in the extractant phase, a self adduct formation, miscellaneous combination when using a base extractant, coordination of two extractants to the metal ion and so on.

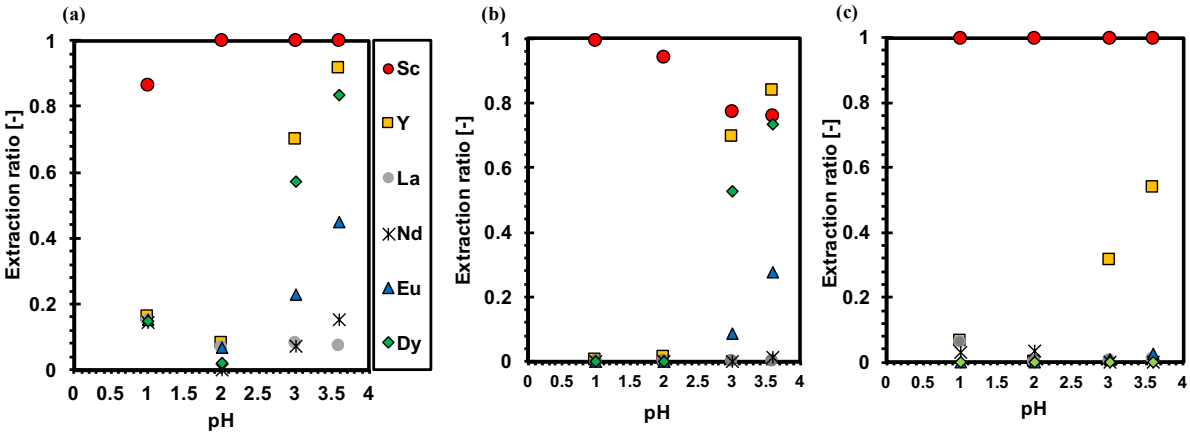

Figure 3. Extraction ratio of REE ions using (a) 1 mM PC-88A and 5 mM primene JM-T, (b) 1 mM PC-88A and 5 mM Cyanex 272 and (c) 1 mM PC-88A and 5 mM TBP in *n*-dodecane. Aqueous phase: 0.1 mM M^{n+}.

Interestingly, the binary system composed of 1 mM PC-88A and carboxylic acid extractant; 100 mM Versatic 10 delays the extraction of Sc ion more than the other binary systems used as shown in Figure 4. The addition of Versatic 10 to PC-88A causes the antagonistic effect i.e., the distribution coefficient of metal ions using the binary mixture is lower than the sum of that using the individual extractant. The extraction using only 100 mM Versatic 10 which attained less than 10 % extraction for Sc at pH 3.6. Shibata et al [7] reported the extraction of Sc using a high concentration of Versatic 10 (0.5 M) and quantitative extraction was achieved at high pH around 6. However, in the present study, we conducted extraction experiments in a low pH region to avoid the formation of Sc precipitation. It is proved in our study that the addition of Versatic 10 to PC-88A causes the antagonistic effect i.e., the distribution coefficient of metal ions using the binary mixture is lower than the sum of that using an individual extractant i.e ($D_{mix} < D_A+D_B$). We succeeded to carry out the selective extraction of Sc ion at an appropriate pH using the binary mixture 1 mM PC-88A+100 mM Versatic 10. Using the last binary system, we will overcome the problem of difficulty in the stripping process when using PC-88A alone as the extractant for Sc. In the case, a high acidic solution is required for both extraction and stripping processes and which also

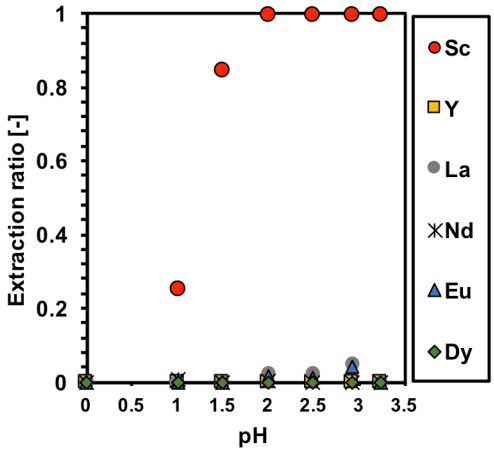

Figure 4. Extraction ratio of REE ions using 1 mM PC-88A+100 mM Versatic 10, an aqueous phase: 0.1 mM M^{n+}.

arises emulsification in the extraction operation [8]. After choosing the binary extractant; 1 mM PC-88A+100 mM Versatic 10 as the best combination to achieve the selective extraction of Sc at an appropriate pH. The stripping test was carried out from the Sc-loaded organic phases 1 mM PC-88A and the binary extractants with different nitric acid concentrations 0.5 M HNO_3, 0.75 M HNO_3, 1 M HNO_3 and 2 M HNO_3 at O/A=1, and at room temperature. Table 1 illustrates the stripping ratios after extraction. We found that 96% of scandium could be stripped from the binary mixture, whereas 49% of scandium was stripped from 1 mM PC-88A with 0.75 M HNO_3. The addition of Versatic 10 to PC-88A succeeded to achieve the complete scandium stripping with a mild acid consumption in one step, while 2 M nitric acid is required for achieving stripping of Sc from a 1 mM PC-88A solvent. Different acids were used to compare the stripping ability from the loaded organic phases and the stripping efficiency was increased in the order $HNO_3 \geq HCl > H_2SO_4$. It was confirmed that the stripping efficiency was improved using the last binary system rather than using PC-88A alone and the reason is the antagonistic effect, which could be due to the possible interaction between the two extractants in the organic phase that reduces available amount of free PC-88A ready for extraction.

Table 1. Stripping of Sc ion from the loaded organic phase .

Extraction systems (mM)	$[HNO_3](M)$			
	0.5	0.75	1	2
[PC-88A] (1 mM)	30%	49%	60%	90%
[PC-88A] (1 mM) + [Versatic 10] (100 mM)	86%	96%	100%	100%

4. Conclusion

The extraction behavior of rare earth metal ions was investigated using several binary extractant systems composed mainly from PC-88A and another extractants, which follows a different mechanism for rare earth metals extraction. PC-88A is an acidic extractant, which interacts with a metal cation via a metal complex formation at very low pH. On the other hand, primene JM-T, TBP and Cyanex 272 are basic, solvating and acidic chelating agents, respectively. When mixing the two extractants, the new binary mixture could exhibit interesting behavior of synergism or antagonism towards the rare earth extraction as in case of adding primene JM-T, Cyanex 272 and Versatic 10 or shows no obvious change as for adding TBP. The addition of carboxylic acid type Versatic 10 to PC-88A causes the antagonistic effect that managed to achieve the selective extraction of scandium at anappropriate pH and improved stripping efficiency using a mild acid concentration overcoming the difficulties resultant from using PC-88A alone for extraction. In conclusion, among the studied binary combinations, PC-88A and Versatic 10 system is the best candidate to attain both high extraction and stripping under favorable conditions. The new binary system achieves high selectivity, high loading efficiency, and prevents crud formation at the interface, indicating its potential for economic industrial applications.

Acknowledgments

This work was supported by Grants-in-Aid for Science Research (grant numbers 25420806 and 16K14462) from the Ministry of Education, Culture, Sports, Science and Technology of Japan, and the Environment Research and Technology Development Fund (ERTDF, grant number 3-1710) of the Ministry of the Environment, Japan.

References

1) J. Røyset and N. Ryum, Scandium in aluminium alloys. *Int. Mater. Rev.,* **50,** 19–44 (2005).
2) M. Karve and B. Vaidya, *Sep. Sci. Technol*., **43**, 1111–1123 (2008).
3) Y. Liu and M. S. Lee, *Solvent Extr. Ion Exch.,* **34,** 74–85 (2016).
4) P. Tkac, G. F. Vandegrift, G. J. Lumetta, and A. V. Gelis, *Ind. Eng. Chem. Res.,* **51,** 10433–10444 (2012).
5) Y. Li,. J. Hu, M. Fu, J. Tang, L. Dong and S. Liu. *RSC Adv.*, **6**, 56772-56779 (2016).
6) R. Sarkar, S. Ray and S. Basu, *J. Chem. Bio. Phy. Sci. Sec.*, **4**, 3156-3181 (2014).
7) J. Shibata, K. Moriyama, Y. Uesusuki, and N. Murayama, *Kagaku Kogaku Ronbunshu*, **41**, 362-367 (2015).
8) J. E. Quinn, K. H. Soldenhoff, G. W. Stevens, N.A. Lengkeek, *Hydrometallurgy*., **157**, 298–305 (2015).

Recovery of Rare Earth elements by solvent extraction vs precipitation method: The Maboumine project

Sarah BÉLAIR*, Denis BELTRAMI, Julie GÖRGE, Valérie WEIGEL and Fabien BURDET[1]
[1]*ERAMET Research, 1 avenue Albert Einstein, B.P. 120, F-78193 Trappes Cedex, France*

An alternative route to the rare earth elements precipitation was implemented in the Maboumine process. The rare earth elements are directly extracted from the pregnant leach solution by liquid-liquid extraction process using 17.5% v/v primene JM-T, 5% v/v isotridecanol in isane IP 185 as solvent. The rare earth elements stripped solution contains more than 98% of rare earth elements initially present in the pregnant leach solution whereas only 95% of rare earth elements are recovered in the precipitation process.

1. Introduction

The Maboumine project aims at recovering uranium (0.03%), niobium (1.2%) and Rare Earth Elements (REE) (1.4%) from a polymetallic deposit in Gabon. [1] In the free fluoride hydrometallurgical process developed by ERAMET Research, the ore is pasted with sulfuric acid and roasted. The valuable elements are solubilized, the niobium / tantalum are then precipitated as a concentrate (12% w/w Nb and 0.3% w/w Ta) while REE (2.7 g L^{-1}) and uranium (90 mg L^{-1}) remain in solution. [2] The niobium / tantalum concentrate is then treated be solvent extraction or precipitation. [3, 4, 5] Classical REE double salt precipitation method allows to recover nearly 90% of the REE present in the Pregnant Leach Solution (PLS) but only 70% of medium (Sm, Eu, Gd, Tb, Dy) and 20% of heavy (Ho, Er, Tm, Yb, Lu, Y) rare earth elements. Those residual REE can be recovered after an aluminum bleed as phosphate REE concentrate that have to be purified. In this way, three units are necessary to recover 95% of REE from the PLS. [6, 7]

An alternative route to the REE precipitation was implemented in the process. REE are directly extracted from the PLS by liquid-liquid extraction process using 17.5% v/v primene JM-T (a $C_{19}H_{41}N$ primary amine), 5% v/v isotridecanol (a phase modifier) in isane IP 185 (a C_{11}-C_{14} isoparaffinic diluent) as solvent. After some laboratory tests and a first short pilot plant trial, a longer continuous pilot plant trial was carried out over 10 days. The results obtained during this pilot are presented in this paper.

2. Experimental

2.1 Reagents

The primene JM-T was supplied by ROHM and HAAS, the isotridecanol was supplied by EXXONMOBIL and the isane IP185 was supplied by TOTAL.

The PLS used in this study was provided by ERAMET Research (France) and comes from the

Maboumine hydrometallurgical process. [7, 8, 9] The PLS underwent some treatments in order to simulate the best performances of the Maboumine upstream process. First, the PLS was reduced by adding iron powder at 70°C during 2 h. The reduced PLS was then doped in REE (La, Ce, Pr, Nd, Gd, Y) using rare earth nitrates supplied by Solvay. The rare earth nitrates solutions were mixed in right proportions with sodium hydroxide for 2 h. After centrifugation and water washing, the solid obtained was added to the reduced PLS. Finally, the solution was doped in aluminum using aluminum sulfate octadecahydrate (97%) supplied by VWR.

Sulfuric acid solution (VWR, 96%), sodium hydroxide solution (VWR, 50%), hydrochloric acid solution (CARLO ERBA, 37%) and sodium chloride (MERCK, >99.5%) were used as received.

2.2 Process description and flowsheet piloted

According to the previous results obtained in our laboratory on the REE recovery by solvent extraction from the Maboumine PLS, the process flowsheet given in Figure 1 was piloted. The organic solvent is composed of 17.5% v/v primene JM-T, 5% v/v isotridecanol in isane IP 185. The organic on aqueous ratio (O/A) for each section is given and all the solvent extraction system was thermostated at 40°C. Moreover, in order to be able to cycle the organic phase, it has to undergo a regeneration process that includes a titanium/scandium stripping followed by a regeneration step allowing to deprotonate the primene. Indeed, the accumulation in the solvent of titanium, scandium and sulfuric acid causes a decrease in the REE extraction yield.

The REE extraction by the primene is strongly dependent on the acidity of the solution. Indeed, in sulfuric acid media, as the Maboumine PLS, the primene can be protonated under two species, [R-NH^{3+}; HSO_4^-] (eq.(1)) and [$(R\text{-}NH^{3+})_2$; SO_4^{2-}] (eq.(2)). At high acidity ([H^+] ≥ 4 mol L^{-1}), the first species is predominant, while at low acidity ([H^+] = 0.5 mol L^{-1}) the second one is. As the REE are preferably extracted by the [$(R\text{-}NH^{3+})_2$; SO_4^{2-}] species, it is better to keep the feed at low acidity.

The protonation reactions for the primene are the following:

$$\overline{RNH_2} + H_2SO_4 \leftrightarrow \overline{RNH_3^+, HSO_4^-} \quad (1)$$

$$2\,\overline{RNH_2} + H_2SO_4 \leftrightarrow \overline{(RNH_3^+)_2, SO_4^{2-}} \quad (2)$$

Finally, under our conditions, the affinity order of the primene JM-T for the different elements present in the Maboumine PLS is Sc > Ti > Fe(III) > REE > Al > Mn.

The main extraction reactions are the following:

$$\overline{(RNH_3^+)_2, SO_4^{2-}} + 2\,[REE(SO_4)_2]^- \leftrightarrow 2\,\overline{RNH_3^+, [REE(SO_4)_2]^-} + SO_4^{2-} \quad (3)$$

$$\overline{(RNH_3^+)_2, SO_4^{2-}} + 2\,[Fe(SO_4)_2]^- \leftrightarrow 2\,\overline{RNH_3^+, [Fe(SO_4)_2]^-} + SO_4^{2-} \quad (4)$$

$$\overline{(RNH_3^+)_2, SO_4^{2-}} + 2\,[Sc(SO_4)_2]^- \leftrightarrow 2\,\overline{RNH_3^+, [Sc(SO_4)_2]^-} + SO_4^{2-} \quad (5)$$

$$\overline{(RNH_3^+)_2, SO_4^{2-}} + [TiO(SO_4)_2]^{2-} \leftrightarrow \overline{(RNH_3^+)_2, [TiO(SO_4)_2]^{2-}} + SO_4^{2-} \quad (6)$$

While the main stripping reactions are the following:

$$\overline{RNH_3^+, [REE(SO_4)_2]^-} + H_2SO_4 \leftrightarrow \overline{RNH_3^+, HSO_4^-} + [REE(SO_4)_2]^- + H^+ \quad (7)$$

$$\overline{RNH_3^+, [Fe(SO_4)_2]^-} + H_2SO_4 \leftrightarrow \overline{RNH_3^+, HSO_4^-} + [Fe(SO_4)_2]^- + H^+ \quad (8)$$

$$\overline{RNH_3^+, [Sc(SO_4)_2]^-} + HCl \leftrightarrow \overline{RNH_3^+, Cl^-} + [Sc(SO_4)_2]^- + H^+ \quad (9)$$

$$\overline{(RNH_3^+)_2, [TiO(SO_4)_2]^{2-}} + 2\ HCl \leftrightarrow 2\,\overline{RNH_3^+, Cl^-} + [TiO(SO_4)_2]^{2-} + 2\,H^+ \quad (10)$$

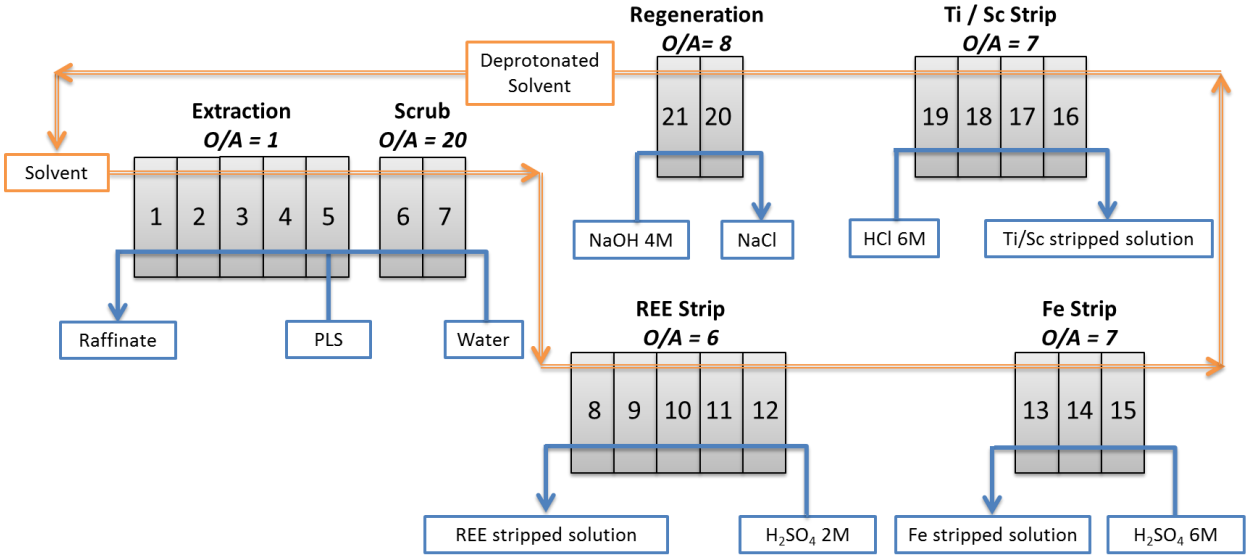

Figure 1. Process flowsheet piloted for the recovery of REE from the Maboumine PLS.

2.3 Elements analysis

The aqueous solutions at the input and the output of each section were analyzed directly while the organic phases were totally stripped using a hydrochloric acid solution at 5 mol L^{-1} and those stripped solutions were analyzed in order to calculate the section yield and the mass balances for each element. The concentrations of iron (Fe), aluminum (Al), titanium (Ti), phosphorus (P), sulfur (S), zirconium (Zr), manganese (Mn), scandium (Sc), lanthanum (La), cerium (Ce), praseodymium (Pr), neodymium (Nd), gadolinium (Gd) and yttrium (Y) were determined by ICP-OES using an iCAP 6000 series spectrometer (Thermo Scientific). Samples were diluted in 2% (v/v) HNO_3 for analysis. The Fe(III) concentration was determined by colorimetry method.

3. Results and Discussion

3.1 Extraction step

The mean composition of the PLS over the 30 -8 h- shifts of the pilot is presented in Table 1 with the standard and relative deviations. The high concentration variation observed for the zirconium is due to its value close to the quantification limit. The variation of the iron(III) concentration is due to its re-oxidation with time. The relative deviation for all the other elements except for the light REE (La, Ce, Pr, Nd) is lower than 5% and is attributed to the analytical error of the measurement by IPC-OES. The relative deviation observed for the light REE is certainly due to a slight precipitation as rare earth sodium sulfate double salt with time as 2 g L^{-1} of sodium are present in the PLS.

Table 1. Mean composition of the PLS used in this pilot study.

	Fe^{III}	Al	Ti	P	S	Zr	Mn
Mean PLS composition (mg L^{-1})	325	12548	271	2500	62600	3	3751
Standard deviation	94.8	540.3	11.7	89.7	2723	0.8	164.1
Relative deviation (%)	29.1	4.3	4.3	3.6	4.4	24.0	4.4

	Sc	La	Ce	Pr	Nd	Gd	Y
Mean PLS composition (mg L^{-1})	14	677	1575	166	670	210	265
Standard deviation	0.4	35.7	97.0	13.8	46.6	5.5	8.1
Relative deviation (%)	2.9	5.3	6.2	8.3	7.0	2.6	3.1

The mean extraction yields obtained, on five mixer-settlers and an O/A = 5, over the 30 -8 h-shifts of the pilot are presented in Table 2 with the standard and relative deviations. The well extracted elements (> 90%) – Sc, La, Ce, Pr, Nd, Gd and Y – have a steady extraction yield over the 30 shifts as shown by the low values of the standard and relative deviations. All the REE are very well extracted, the REE mean extraction yield is greater than 99.3% with a maximal standard deviation of 0.1%. These limitations are due to the analytical quantification limit but the mass balance for each REE ranges between 100% and 120% meaning that the analytical quantification limit is not a real problem. The mass balances for the other elements (Ti, Al, Mn and P) are comprised between 90% and 114% which is more than acceptable. No interpretation on the iron behavior can be made as only the iron(III) should be extracted and the analyses obtained are greatly overestimated leading to unacceptable mass balances. This could be due to an inopportune re-oxidation of the solution due to the pilot technology used. It can be fairly well supposed that, at an industrial scale, the re-oxidation could be avoided by using adequate equipment. As a consequence, no results are given on the iron extraction yield.

Previous studies carried out at the laboratory have shown that a part of the titanium was extracted. K. C. Sole indicates that the titanium species extractible in our conditions is $TiO(SO_4)_2^{2-}$ (eq.(6)).[10] The titanium extraction yield for this pilot is steady (the standard deviation is lower than 5%) and close to 64%.

Aluminum, phosphorus and manganese are weakly extracted and this does not affect the REE extraction whereas the sulfate is widely extracted with a concentration in the organic phase reaching 35.7 g L^{-1}. This represents 70% of the active solvent load.

Finally, the scandium is quantitatively extracted by the primene JM-T, its extraction yield reaches 92% due to the quantification limit.

Table 3. Mean extraction yield of the extraction step.

	Fe^{III}	Al	Ti	P	S	Zr	Mn
Mean extraction yield (%)	/	7.6	64.2	5.2	3.9	31.4	7.9
Standard deviation	/	6.7	2.6	2.1	8.9	13.5	7.2
Relative deviation (%)	/	88.8	4.0	41.1	230.8	42.9	91.0

	Sc	La	Ce	Pr	Nd	Gd	Y
Mean extraction yield (%)	92.1	99.8	99.9	99.3	99.8	99.5	99.6
Standard deviation	0.7	0.0	0.0	0.1	0.0	0.0	0.0
Relative deviation (%)	0.7	0.0	0.0	0.1	0.0	0.0	0.0

3.2 Scrubbing step

The aim of this scrubbing step with water is to remove the weakly extracted elements, namely aluminum, phosphorus and manganese but also the mechanical entrainment. This section is composed of two mixer-settlers and an O/A = 20. The mean concentrations of aluminum, phosphorus and manganese in the organic phase entering the scrubbing section are respectively 136 mg L^{-1}, 31 mg L^{-1} and 36 mg L^{-1}. After the scrubbing, the concentrations decrease to 4 mg L^{-1} for Al, 3.5 mg L^{-1} for P and 0.4 mg L^{-1} for Mn, proving that the washing is very efficient for those three elements.

The REE are very weakly scrubbed with analyses below the quantification limits almost all the time. This low REE loss is anyway sent back to the extraction section.

3.3 REE stripping step

The REE are stripped with a sulfuric acid solution at 2 mol L^{-1}. This section is composed of five mixer-settlers and an O/A = 6. The stripping yield of REE reaches the target of 98%. The residual concentrations of lanthanum, cerium, gadolinium and yttrium in the organic phase are respectively 10 mg L^{-1}, 50 mg L^{-1}, 1.5 mg L^{-1} and 1.5 mg L^{-1}.

Around 60% of the extracted iron is stripped in this stage meaning that its residual concentration in the organic phase is about 350 mg L^{-1}. An iron stripping step will then be necessary in the process.

Table 4 gives the mean composition of the REE stripped solution. This solution contains 29 g L^{-1} of REE and the main impurity is iron.

Table 4. Mean composition of the REE stripped solution.

	Fe^{III}	Al	Ti	P	S	Zr	Mn
Mean REE stripped solution composition (mg L^{-1})	3516	13	27	25	66934	3	2
Standard deviation	451.8	5.9	45.5	4.9	7455	0.7	1.1
Relative deviation (%)	12.9	47.1	167.1	19.7	11.1	27.1	68.3

	Sc	La	Ce	Pr	Nd	Gd	Y
Mean REE stripped solution composition (mg L^{-1})	11	5610	12600	1348	5756	1660	2063
Standard deviation	5.0	661.1	2019	207.9	877.5	94.2	119.9
Relative deviation (%)	45.7	11.8	16.0	15.4	15.2	5.7	5.8

3.4 Iron stripping step

The iron remaining in the organic phase is stripped with a solution of sulfuric acid at 6 mol L^{-1}. This section is composed of three mixer-settlers and an O/A = 7. The iron stripping yield is steady and greater than 90% all along the 30 -8 h- shifts. The organic phase leaving this section contains less than 50 mg L^{-1} of iron.

3.5 Titanium and scandium stripping step

In order to reuse the organic solvent as in any solvent extraction process, it has to be regenerated, that is to say, stripping all the elements that have been extracted. As titanium and scandium are strongly extracted by the primene JM-T, a specific stripping section has to be implemented. The only way to totally strip Sc and Ti from the organic phase is to use a hydrochloric acid solution at 6 mol L^{-1} as the stripping solution in four mixer-settlers with an O/A = 7. In that case, the stripping yield of titanium and scandium is greater than 90%. The mean composition of the Ti/Sc stripped solution is given in Table 5. As the scandium concentration is quite high, it could be interesting to separate it from titanium by solvent extraction. [11, 12]

Table 5. Mean composition of the Sc/Ti stripped solution.

	Fe^{III}	Al	Ti	P	S	Zr	Mn
Mean Sc/Ti stripped solution composition (mg L^{-1})	120	8	1018	2	139000	6	1
Standard deviation	88.1	6.2	576.2	0.3	17320	7.3	0.1
Relative deviation (%)	73.4	74.2	56.6	12.4	12.5	129.1	10.2

	Sc	La	Ce	Pr	Nd	Gd	Y
Mean Sc/Ti stripped solution composition (mg L^{-1})	178	1	11	1	2	1	1
Standard deviation	23.3	0.3	8.9	0.1	0.8	0.3	0.1
Relative deviation (%)	13.1	20.4	82.0	10.2	49.4	20.4	10.2

3.6 Solvent regeneration step

After the Ti/Sc stripping section, chlorides are present in the organic phase and have to be removed before sending back the solvent to the extraction section. Sodium hydroxide is then used at a concentration of 4 mol L^{-1} in two mixer-settlers with an O/A ratio of 8. The primene JM-T is then deprotonated and the chlorides are eliminated by forming sodium chloride salt. The acidity in the PLS

at the extraction stage is high enough to reprotonate the primene for another cycle.

4. Conclusion

This pilot validates the entire flowsheet of the recovery of REE by solvent extraction with primene JM-T. In the extraction step, more than 99.4% of REE are recovered. The scrubbing step allowed the elimination of manganese, phosphorus and aluminum. More than 98% of the REE are recovered in the stripped solution with a REE concentration of 29 g L^{-1}, 10 times more concentrated than the PLS. A specific iron stripping step is then necessary as iron(III) is strongly extracted. However, at industrial scale, the iron extraction could be limited by using an adequate equipment allowing to avoid an inopportune oxidation of the solution as only the iron(III) is extracted. After this step, the iron residual concentration in the organic phase is less than 50 mg L^{-1}. Finally, the organic phase has to be regenerated in two steps in order to remove titanium and scandium. At the end of these steps, the residual concentrations of Ti and Sc are respectively less than 10 mg L^{-1} and 1 mg L^{-1}.

This flowsheet can be improved especially concerning the titanium/scandium stripping step where the use of sodium chloride solution instead of hydrochloric acid has to be tested in order to decrease the operating cost.

Acknowledgement

The financial support for this work from ERAMET Company (France) is gratefully acknowledged.

References

1) D. Beltrami, G. J.-P. Deblonde, S. Bélair, V. Weigel, *Hydrometallurgy*, **157**, 356-362 (2015).
2) G. J.-P. Deblonde, V. Weigel, Q. Bellier, R. Houdart, F. Delvallée, S. Bélair, D. Beltrami, *Separation and Purification Technology*, **162**, 180-187 (2016).
3) G. J-P. Deblonde, A. Chagnes, M-A. Roux, V. Weigel and G. Cote, *Dalton Transactions*, **45**, 19351-19360, (2016).
4) G. J.-P. Deblonde, A. Chagnes, V. Weigel and G. Cote, *Hydrometallurgy*, **165**, Part 2, 345-350 (2016).
5) G. J-P. Deblonde, WO Patent **2017085404A1**, (2017).
6) D. Beltrami, S. Bélair, V. Weigel, *Proceedings of the 28th International Mineral Processing Congress* (IMPC 2016), ISBN: **978-1-926872-29-2**, September 11-15, 2016, Quebec City, Canada, Canadian Institute of Mining, Metallurgy and Petroleum.
7) J. Agin, N. Durupt, A. Greco, F. Hammy, G. Laroche, J. Thiry, FR Patent **2970265A1** (2012).
8) S. Belair, V. Weigel, *Proceedings of the 53rd Annual Conference of Metallurgists* (COM 2014), ISBN: **978-1-926872-24-7**, September 28 – October 1st, 2014, Vancouver, Canada, Canadian Institute of Mining, Metallurgy and Petroleum.
9) L. Donati, B. Courtaud, V. Weigel, *Proceedings of the 7th International Symposium Hydrometallurgy 2014* (HYDRO 2014), ISBN: **978-1-926872-22-3**, June 22-25, 2014, Victoria, Canada, Canadian Institute of Mining, Metallurgy and Petroleum.

10) K. C. Sole, *Hydrometallurgy*, **51**, 239-253 (1999).
11) W. Wang, Y. Pranolo, C. Y. Cheng, *Separation and Purification Technology*, **108**, 96-102 (2013).
12) D. Beltrami, D. Moussa-Ragueh, S. Bélair and V. Weigel, Proceedings of the 28th International Mineral Processing Congress (IMPC 2016), ISBN: **978-1-926872-29-2**, September 11-15, 2016, Quebec City, Canada, Canadian Institute of Mining, Metallurgy and Petroleum.

Steady State Population Balance Modeling of Zinc Extraction in a Kühni Liquid-liquid Extraction Column

Samer ALZYOD[1], Christian KORB[1], Menwer ATTARAKIH[1,2] and Hans-Jörg BART[1*]

[1]Chair of Separation Science and Technology , The University of Kaiserslautern, Kaiserslautern 67637, Germany; [2]Department of Chemical Engineering/School of Engineering, The University of Jordan,, Amman 11942, Jordan

A reduced steady state population balance model, based on the Spatially Mixed-Sectional Quadrature Method Of Moments (SM-SQMOM), is developed to model the reactive extraction process of zinc with D2EHPA in a Kühni liquid-liquid extraction column. The numerical flux vectors of the hydrodynamic transport equations are closed using one quadrature point, where an analytical solution based on the algebraic velocity model is used to calculate the required dispersed phase mean droplet velocity along the column height. In addition to this, a multi-sectional grid (w.r.t. droplet diameter) is used to approximate the source terms of the hydrodynamic transport equations, while one section (w.r.t. droplet solute concentration) is used to model the steady state reactive mass transfer behavior inside the column. The proposed model is validated with the experimental data using $ZnSO_4$/D2EHPA in isododecane EFCE chemical test system. The effect of changing the rotational speed, phase ratio and the total throughput on the column performance is investigated. The SM-SQMOM is found able to reconstruct the shape of the droplet size distribution and to predict the zinc reactive concentration profiles along the column height as compared with the experimental data.

1. Introduction

Liquid-liquid extraction is a commonly used separation process for recovery of heavy metals [1, 2]. In contrast to the physical extraction, the mass transfer process occurring during reactive extraction is superimposed by a chemical reaction when using liquid ion exchangers [1, 3]. An alternative to the commonly used mixer-settlers is the use of columns with the advantage of lower foot-print and solvent inventory. Their performance is determined by the coupled hydrodynamics and reactive mass transfer phenomena. In addition to this, the droplet size distribution is the major factor, which affects the available interfacial area and the droplets residence time inside a column. As a result of this, more attention is needed to model the coupled droplet-droplet interactions and the reactive mass transfer phenomena. A first attempt to simulate a reactive extraction column was done by Veglio and Slater [4]. The authors proposed a numerical design procedure and concluded that the most important design factor, which affects the column height, is the zinc ions mass transfer coefficient in the continuous phase. Ji et al. [5] studied the role of kinetics of zinc extraction in a packed bed liquid-liquid extraction column. The authors used the backmixing approach to model the reactive extraction process of zinc with D2EHPA,

where they assumed constant dispersed phase integral properties (dispersed phase holdup and mean droplet diameter). Neto and Mansur [6] modeled the reactive extraction of zinc with D2EHPA in a short Kühni liquid-liquid extraction column. The authors used the back and forward mixing models, where the required dispersed phase integral properties were calculated using published correlations [6]. However, assuming constant dispersed phase integral properties is not realistic because the dispersed phase properties change along the column height due to mass transfer and droplet breakage and coalescence. As a result of this, a rigorous mathematical model to describe the dispersed phase behavior is needed. To shed more light on the dispersed phase behavior, Attarakih et al. [7, 8] introduced a comprehensive reduced non-equilibrium bivariate population balance model based on the discrete Sectional Quadrature Method of Moments (SQMOM) which is called OPOSPM. This model was developed to simulate the simultaneous reversible chemical reaction and extraction process of an industrial scale high-pressure oil-splitting reactor with a first-order reversible kinetics. The authors showed that the proposed framework was able to describe the column hydrodynamics as well as the reactive mass transfer behavior as demonstrated by different case studies where the reactor was represented by a spray column in the absence of static or moving internals. Since the droplet size distribution is nearly constant in spray columns, the proposed reduced model conserves the total number concentration (zero moment) and total mass (dispersed phase holdup) of the droplet size distribution and hence no extra droplet-droplet interaction mechanisms are required to reconstruct the shape of the droplet size distribution.

In this contribution, a reduced steady state bivariate population balance algorithm is developed to model the reactive extraction process of zinc with D2EPHA in a lab scale Kühni liquid-liquid extraction column. In this regard, the Spatially Mixed-Sectional Quadrature Method Of Moments (SM-SQMOM) [9], which is based on the SQMOM as a discrete framework for modelling particulate systems [10], is utilized and implemented. To facilitate the source terms implementation, an analytical solution [9], which is based on the algebraic velocity model, is used to calculate the required dispersed phase mean droplet velocity inside the column. The resulting integral spatial numerical flux vector is closed using the mean mass droplet diameter (d_{30}), while the hydrodynamics source terms are closed using the Two-Equal Weight Quadrature (TEqWQ) formula [10]. A multi-sectional grid (w.r.t droplet diameter) is used to approximate the integral hydrodynamics source terms, where 20 sections were found enough to reconstruct the shape of the droplet size distribution. In addition to this, one section is used to model the steady state reactive mass transfer behavior inside the column. At the experimental validation level, the model prediction is compared with the experimental data using the reactive ZnSO4/D2EHPA/isododecane EFCE chemical test system. The SM-SQMOM was found able to predict the column hydrodynamics as well as the mass transfer profiles when compared with the experimental data.

2. Experimental investigations

2.1 Experimental procedure

The experimental investigations were carried out at TU Kaiserslautern using a countercurrent Kühni DN32 liquid-liquid extraction column, where the column dimensions are shown in Table. 1. The

chemical test system used in the investigations is $ZnSO_4$ / D2EHPA/ isododecane chemical test system as recommended by Bart et al. [1]. The column is initially filled with the aqueous phase, and then the rotor is started and after that the dispersed phase has been fed to the bottom of the column. In all cases, the dispersed organic phase (here isododecane) was fed at the bottom of the column using a finger distributer with 8 holes, while the continuous aqueous phase was fed at the top of the column. The dispersed phase holdup was measured in the active height of the column using the corresponding pressures method, while a high-speed camera was used to detect the droplet size distribution at the upper settling zone of the column. In this regard, the effect of changing the rotational speed, phase ratio and the total throughput on the column performance is investigated. The zinc ion concentrations and the pH values were measured at five different positions along the column height, where the column was operated at 80 percent away from the flooding point.

Table 1. Kühni column dimensions (all dimensions are in m).

Column diameter	Compartment height	Blade diameter	Stator diameter
0.032	0.028	0.0195	0.026

2.2 Chemical reaction kinetics

The EFCE chemical test system $ZnSO_4$/D2EHPA is commonly used as a standard test system for the extraction of zinc from aqueous solutions [1]. The chemical reaction of the zinc ions and D2EHPA occurs at the liquid-liquid interface as follows [1, 6]:

$$Zn^{2+} + 1.5\,\overline{(RH)}_2 = \overline{ZnR_2(RH)} + 2H^+ \qquad (1)$$

where $\overline{(RH)}$ and $\overline{ZnR_2(RH)}$ denote the D2EHPA and the zinc complex in the organic phase (see bar) respectively. Here, the D2EHPA dimer and the zinc ions diffuse toward the liquid-liquid interface and react to form the zinc complex in the organic phase and two protons in the aqueous phase. The equilibrium constant of the zinc extraction reaction is given by [1, 5, 6] and depends on the concentration of the pH value:

$$K = \frac{\left[\overline{ZnR_2(RH)}\right]\cdot\left[H^+\right]^2}{\left[Zn^{2+}\right]\cdot\left[\overline{(RH)}_2\right]^{1,5}} \qquad (2)$$

It is assumed that both phases are immiscible and the water solubility in the dispersed phase is neglected. In all cases, the zinc (Zn^{2+}) inlet concentration was fixed at a constant value of 0.01mol/l, while the D2EHPA concentration is fixed at 0.25 mol/l as recommended by many authors [1, 5, 6]. In addition to this, the sulfuric acid (H_2SO_4) was added to adjust the pH value inside the column. The physical properties of the chemical test system are shown in in Table (2).

Table 2. Physical properties of the extraction reaction chemical test system.

Chemical compound	Density (kg/m^3)	Viscosity (Pa.s)	Interfacial tension (N/m)
$ZnSO_4$/water	999.6	0.000913	-
D2EHPA/ isododecane	764.8	0.001543	0.02087

3. Mathematical model

Following the efforts of Attarakih et al. [10], Alzyod et al. [9] extended the Sectional Quadrature Method Of Moments (SQMOM) to solve the bivariate nonhomogeneous population balance equation, where they developed a steady state algorithm to model the hydrodynamics and mass transfer behavior of liquid-liquid extraction columns based on the Specially-Mixed Sectional Quadrature Method Of Moments (SM-SQMOM). The steady state moment's system of equations which describe the coupled hydrodynamics and mass transfer along the spatial domain is given by [9]:

$$\frac{\partial}{\partial z}\left(\bar{F}^{\langle i\rangle}_{r,m}-D_y\frac{\partial \mu^{\langle i\rangle}_{r,m}}{\partial z}\right)=\hat{S}^{\langle i\rangle}_{r,m}\quad r,m=0,..,2\times N_q-1 \tag{3}$$

Here, the superscript i represents the i^{th} section of the internal coordinate, N_q is the number of secondary particles, D_y is the dispersed phase axial dispersion coefficient, $\mu^{\langle i\rangle}_{r,m}$ is a two dimensional moment transformation (w.r.t droplet diameter and solution concentration), $\bar{F}^{\langle i\rangle}_{r,m}$ is transformed numerical flux and $\hat{S}^{\langle i\rangle}_{r,m}$ is the transformed source term. In this work, the transformed source term and the mixed numerical flux vectors are given as follows [9, 10]:

$$\hat{S}^{\langle i\rangle}_{r,m}=u^{in}_y\mu^{\langle i\rangle}_{in}c^m_{yin}\delta\left(z-z_y\right)+S^{\langle i\rangle}_{B,r,m}+S^{\langle i\rangle}_{C,r,m}+S^{\langle i\rangle}_{M,r,m} \tag{4}$$

$$\bar{F}^{\langle i\rangle}_{r,m}=\sum_{j=1}^{Nq}\sum_{n=1}^{Nq}\left[u_y\left(d_{j,n},\alpha_y,P\right)d^r_{j,n}c^m_{y,n}w_{j,n}\right]^{\langle i\rangle} \tag{5}$$

where u^{in}_y is the superficial inlet velocity of the dispersed phase, c^m_{yin} is the solute concentration in the dispersed phase, $S^{\langle i\rangle}_{B,r,m}$ and $S^{\langle i\rangle}_{C,r,m}$ are the breakage and coalescence source terms respectively and $S^{\langle i\rangle}_{M,r,m}$ is the transformed reactive mass transfer source term. The transformed hydrodynamics and mass transfer source terms are given by [9, 10]:

$$S^{\langle i\rangle}_{B,r}=-Dr^{\langle i\rangle}\left[\Gamma^{\langle i\rangle}\bullet w^{\langle i\rangle}\right]^T+\sum_{m=i}^{N_{pp}}C^{\langle i,m\rangle}_r\left[\Gamma^{\langle i\rangle}\bullet w^{\langle i\rangle}\right]^T \tag{6}$$

$$S^{\langle i\rangle}_{C,r,1}=\sum_{k=1}^{i\times N_q}\left\{\sum_{j=k}^{i\times N_q}\psi^{\langle i\rangle}_{k,j,r}\omega_{j,k}w'_jw'_k-\theta_k\times\sum_{n=1}^{N_q\times N_{pp}}\left(d'^r_k\right)\omega_{k,n}w'_kw'_n\right\}, \tag{7}$$

$$S^{\langle i\rangle}_{M,r,m}=m\sum_{n=1}^{N_{sp}}c_y^{m-1}\left(\partial c_y/\partial t\right)w_n \tag{8}$$

For more details regarding the source terms, the reader can refer to [9, 10]. In this work, the mixed numerical flux vector is closed using the mean mass droplet diameter (d_{30}) and the resulting set of hydrodynamics moments conservation equations are given by [9]:

$$\frac{\partial \bar{F}^{\langle i\rangle}_{r,0}}{\partial z}=\frac{\partial}{\partial z}\left(u^{\langle i\rangle}_y\left(d^{\langle i\rangle}_{30},\alpha_y,P\right)\mu^{\langle i\rangle}_{r,0}\right)=\hat{S}^{\langle i\rangle}_{r,0}\quad r=0,..,2\times \mathrm{N}_q-1 \tag{9}$$

where α_y is the dispersed phase volume fraction and P is the physical properties vector. The mean mass

droplet diameter can be directly calculated from Equation (9) as follows [9]:

$$d_{30}^{\langle i \rangle} = \sqrt[3]{\frac{\overline{F}_{3,0}^{\langle i \rangle}\left(d_{30}^{\langle i \rangle}\right)}{\overline{F}_{0,0}^{\langle i \rangle}\left(d_{30}^{\langle i \rangle}\right)}} \tag{10}$$

In this work, the hydrodynamics source terms are closed using the analytical Two Equal Weight Quadrature (TEqWQ) formula as follows [9, 10]:

$$d_{1,2}^{\langle i \rangle} = \hat{F}_{1,0}^{\langle i \rangle} \mp \frac{1}{\sqrt{3}} \sqrt{\frac{\hat{F}_{3,0}^{\langle i \rangle}}{\hat{F}_{1,0}^{\langle i \rangle}} - \left(\hat{F}_{1,0}^{\langle i \rangle}\right)^2} \tag{11}$$

$$w_{1,2}^{\langle i \rangle} = \frac{1}{2}\hat{F}_{0,0}^{\langle i \rangle} \tag{12}$$

Finally, the required dispersed phase mean droplet velocity to close the hydrodynamics model equations is given by [9]:

$$u_y^{\langle i \rangle}\left(F_{3,0}^{\langle i \rangle}, d^{\langle i \rangle}\right) = \frac{1}{3} \cdot \lambda_1^{\langle i \rangle} - \lambda_2^{\langle i \rangle} \tag{13}$$

where λ_1 and λ_2 are functions of droplet diameter, continuous phase velocity and the column internal geometry. For more information, the reader can refer to [9].

4. Results and discussion

In this section, the performance of the presented spatially mixed framework is tested, where the model prediction is validated using the steady state experimental data. The column dimensions and the chemical test system physical properties are discussed in detail in section 2. The simulations were carried out using two different inlet flow ratios ($\lambda_d = Q_d/Q_c = 0.2$ and 1.0 respectively), while the rotational speed was varied from 100 to 300 rpm. In this case study, the single droplet velocity model is given by Vigness velocity model [11]. The slowing effects due to the column internals and droplet's swarm is given by Steinmetz [12]. Concerning the droplet-droplet interactions, the coalescence mechanism between two liquid droplets is modeled using Coulaloglou and Tavlarides [13], while the droplet breakage probability function is given by Fang et al. [14]. Figure 1 shows a comparison between the calculated dispersed phase holdup and the experimental data using different rotational speed values. It can be clearly observed that a higher phase ratio results in a higher holdup values. In addition to this, the holdup values increase with increasing the rotational speed.

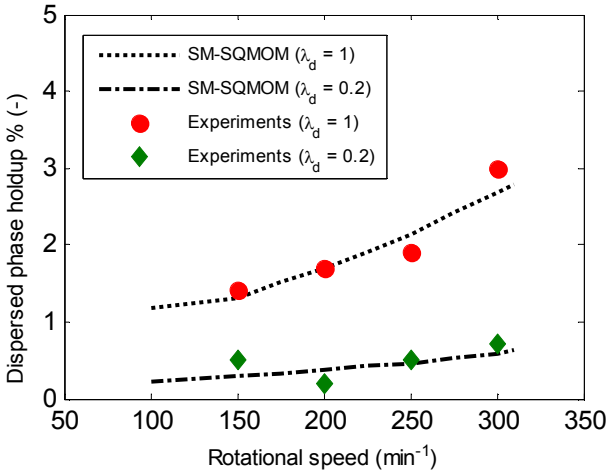

Figure 1. Comparison between the simulated and experimental dispersed phase hold up.

Figure 2 shows a comparison between the simulated droplet size distribution and the experimental data at the top of the column. The simulation was carried out at 350 rpm and a flow ratio of λ_d =1. It can be clearly observed that the SM-SQMOM retains the required information concerning the shape of the droplet size distribution, where 20 sections are found enough to reconstruct the shape of the size distribution. In addition to this, the column hydrodynamics is found dominated by the breakage phenomena at high rotor speeds.

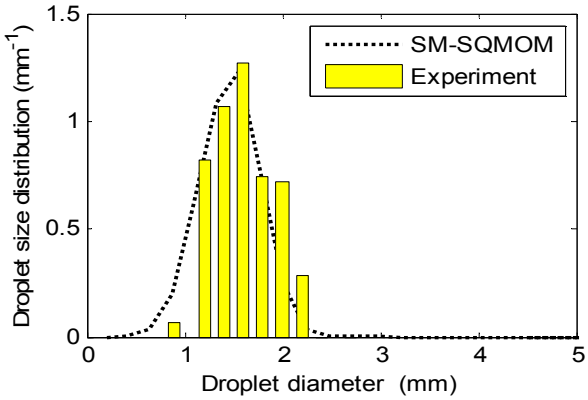

Figure 2. Comparison between the simulated and experimental droplet size distribution.

Based on the converged steady state droplet size distribution, the reactive solute mass transfer profiles can be predicted along the column height. This can be done by adjusting the coalescence model parameters to fit the predicated droplet size distribution at the top of the column with the experimental data. In this case study, the coalescence model parameters are given by c_1 = 0.02 and c_2 = 1.33×10^{11} m^{-2} respectively.

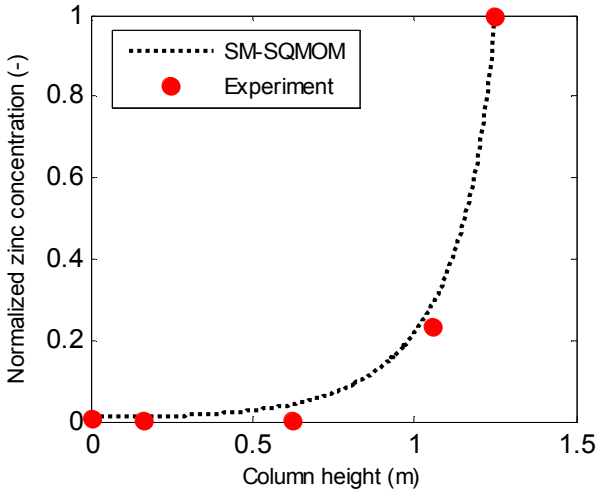

Figure 3. Comparison between the simulated and experimental Zn^{2+} concentration profiles.

Figure 3 shows a comparison between the simulated zinc ions concentration in the aqueous phase and the experimental data. In this case study, the correlation of Heertjes [15] is used to calculate the zinc ions local mass transfer coefficient in the continuous phase, while the correlation of Handlos and Baron [16] is used to calculate the D2EHPA local dispersed phase mass transfer coefficient. As expected the zinc ions concentration decreases along the column height (from the inlet point at the top to the bottom) due to the chemical reaction and the mass transfer process inside the extraction column. In addition to this, one section based on the solute concentration as an internal coordinate is found enough to predict the solute mass transfer profiles as compared with the experimental data.

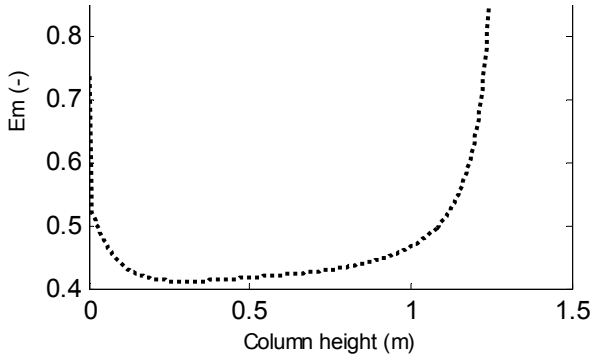

Figure 4. The ratio of the mass transfer resistance to the total resistance.

Figure 4 shows the ratio between the mass transfer resistance and the total resistance (*Em*) along the column height. It can be clearly observed that the extraction process is controlled by the mass transfer mechanism the top of the column, while the extraction process in controlled by the chemical reaction and mass transfer mechanisms at the bottom and the middle of the extraction column.

Figure 5 depicts a comparison between the simulated pH values and the experimental data at five different points along the column height using the same simulation conditions. The pH values decrease along the column height (from top to bottom of the column) until it reach a constant value (around 1.4). A very good agreement between the simulation results and the experimental data is obtained.

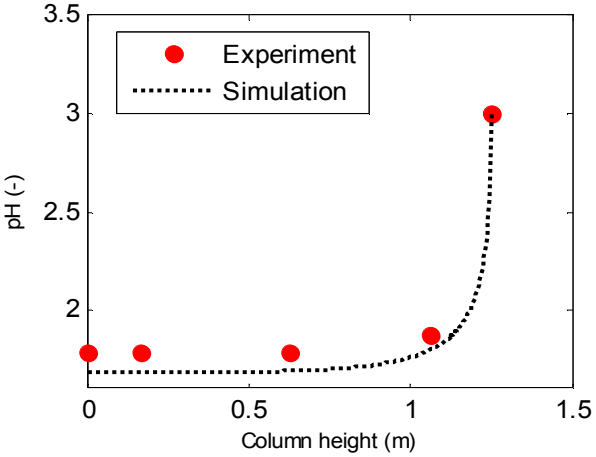

Figure 5. Comparison between the simulated and experimental pH profiles.

4. Conclusions

In this work, a steady state framework to model the reactive extraction process of zinc with D2EHPA in liquid-liquid extraction columns is developed, where the SM-SQMOM is utilized as a reduced population balance mathematical framework. The proposed framework is found able to describe the column hydrodynamics as well as the reactive mass transfer behavior. In this regard, 20 sections (w.r.t droplet diameter) are found enough to predict the column hydrodynamics, while one section (w.r.t solute concentration) is found enough to predict the reactive solute mass transfer profiles as compared with the experimental data. As a final conclusion, the SM-SQMOM is considered as a promising reduced population balance model for the two-phase flow problems.

Acknowledgement

The authors would like to acknowledge the financial support from the Process Engineering and Technology Network of Competence (Verfahrenstechnik-Pro3.de) and the Deutsche Forschungsgemeinschaft (DFG). This work has been carried out during the sabbatical leave granted to the coauthor professor Menwer Attarakih during the academic year 2017/2018.

References

1) H.-J. Bart, H.-P. Rousselle, *Hydrometallurgy*, **51**, 285-298 (1999).
2) M. Attarakih, S. Al-Zyod, M. Abu-Khader, H.-J. Bart, *Procedia Engineering*, **42**, 1445-1462 (2012).
3) H.-J. Bart, R. Marr, J. Scheks, M. Koncar, *Hydrometallurgy*, **31**, 13-28 (1992).
4) F. Veglio, M. Slater, *Hydrometallurgy*, **42**, 177-195 (1996).
5) J. Ji, K.H. Mensforth, J.M Perera, G.W Stevens, *Hydrometallurgy*, **84**, 139-148 (2006).
6) P. Neto, M.B Mansur, *Chemical Engineering Research and Design*, **91**, 2323-2332 (2013).
7) M. Attarakih, T. Albaraghthi, M.. Abu-Khader, Z. Al-Hamamre, H.-J. Bart, *Chemical Engineering Science*, **84**, 276–291 (2012).

8) M. Attarakih, H. Jildeh, M. Mickler, H.-J. Bart, *Computer Aided Chemical Engineering*, **31**, 1216-1220 (2012).
9) S. Alzyod, M. Attarakih, H.-J. Bart, *Chemical Engineering Research and Design*, **117**, 549-556 (2017).
10) M. Attarakih, C. Drumm, H.-J. Bart, *Chemical Engineering Science*, **64**, 742-752 (2009).
11) A. Vigness, *Genie Chim*, **93**, 129-42 (1965).
12) T. Steinmetz, Tropfenpopulationsbilanzgestütztes Auslegungsverfahren Zur Skalierung Einer Gerührten Miniplant Extraktionskolonne. Dissertation. TU, Kaiserslautern, Kaiserslautern, Germany (2007).
13) C. Coulaloglou, L. Tavlarides, *Chemical Engineering Science*, **32**, 1289-1297 (1977).
14) J. Fang, J.C. Godfrey, Z.Q. Mao, M.J. Slater, C. Gourdon, *Chem. Eng. Technol*, **18**, 41-48, (1995).
15) P. Heertjes, W. Holve, H. Talsma, *Chemical Engineering Science,* **9**, 122–142 (1954).
16) A. Handlos, T. Baron, *A.I.Ch.E. J.*, **3**, 127-136 (1957).

Effective Parameters in Extraction of Sulfuric Acid by Trioctylamine (TOA) as Organic Extractant

Aidin HEIDARI[1], Shahryar SHAHINI[1], Davoud H. FATMEHSARI [1], and Eskandar K. ALAMDARI [1,*],

[1] *Department of Mining and Metallurgical Engineering, Amirkabir University of Technology, P.O. Box. 15875-4413, Tehran, Iran*

Trioctylamine (TOA) is used as organic extractant in this research. In this study, the effects of several parameters such as concentration of trioctylamine (TOA) as the extractant, concentration of octanol as the modifier, temperature and ratio of organic phase (V_{org}) to aqueous phase (V_{aq}) were investigated. At the end, the stoichiometric coefficients of reaction were estimated by applying slope method analysis. Also, two equations are proposed (developed) for the extraction of sulfuric acid with TOA by statistical modeling.

1. Introduction

Acids, among other chemicals, are used in many industries for several purposes. So recovery of acids has been investigated in chemical industries [1]. Till date, several acids such as acetic acid, sulfuric acid, lactic acid, adipic acid, myristic acid, succinic acid, chloroacetic acid and glycolic acid were recovered from their dilute solutions. Also recovery of acids can be done by several methods. Membrane processes, electro-dialysis (ED), pervaporation, reverse osmosis (RO), biological processes, ion exchange/adsorption, reactive separation, reactive distillation, reactive chromatography (RC) and solvent extraction are important methods for recovery of acids [1-8]. Acid structure, economical efficiency and other conditions are the effective parameters to choose one of those methods.

Solvent Extraction is one of the most effective methods for separation/ recovery of metallic ions from the aqueous media. In recent years, this technique has been used for the recovery of different acids including sulfuric acid. Sulfuric acid has been widely used in metallurgical industries. As a result, large amounts of waste sulfuric acid solution have been generated, causing environmental problems. The waste sulfuric acid solution may contain valuable metals such as Fe, Ni, and Co. It is thus appropriate to develop an alternative method to recover sulfuric acid and the metals, simultaneously Recovery of sulfuric acid by solvent extraction has been investigated yet by TEHA, Alamine 336, Alamine 308 and Cyanex 923 as organic extractants [2,9-11]. Researches shows amines are more effective for extraction of sulfuric acid [12]. Extraction of sulfuric acid by solvent extraction has not been investigated yet by trioctylamine (TOA) as organic extractant. Trioctylamine (TOA) is used as organic extractant and the effects of several parameters were investigated in this research.

2. Experimental

2.1 Reagents

Commercial extractant trioctylamine (TOA) was supplied by Merck Co., kerosene was supplied by Tehran refinery Co. as the diluent, and octanol were supplied by Merck Co. as the modifier. Sulfuric acid (95-98vol%) was purchased from Scharlau (by titration, it was found that it is 98vol%) which is used with distillated water to prepare aqueous solutions. Potassium hydroxide (KOH) titrisol was supplied by Carlo Erba which is used with distillated water to prepare titrant solution for titration. Also phenolphthalein was purchased from Daejung as indicator.

2.2 Preparation of solution and experiments

Experiments were carried out in flasks containing 25 mL of aqueous and organic solutions. Initial concentrations of sulfuric acid in the aqueous phase varied from 20 to 380 g/L. Trioctylamine volume percentages in organic phase were set at 10, 25 and 40%. Moreover, the octanol volume percentages were 5, 10 and 15%. The volume was adjusted with kerosene as diluent. The mixtures were agitated at different temperatures of 5, 20 and 35˚C and different phase ratios. Samples were then retained in the flask for 30 min to allow complete separation of the phases. Potassium hydroxide titration was employed to determine sulfuric acid concentration in the aqueous and organic solutions, using phenolphthalein as an indicator.

3. Results and Discussion

3.1 Initial analysis of extraction behavior

For initial analysis of extraction behavior of sulfuric acid by TOA, experiments were done in a wide range of initial acid concentration from 20 to 380 g/l and three organic phases of 5, 10 and 15 volume percentage of TOA respectively and constant 10 volume percent for octanol. Figure 1 shows that by increasing the concentration of TOA, extraction of sulfuric acid increases. But for initial sulfuric acid concentration of more than 200 g/l, increasing in extraction of sulfuric acid is not considerable and TOA was closed to its loading capacity. Therefore, Subsequent experiments were done with acid concentrations of lower than 200 g/l as shown in Table 1.

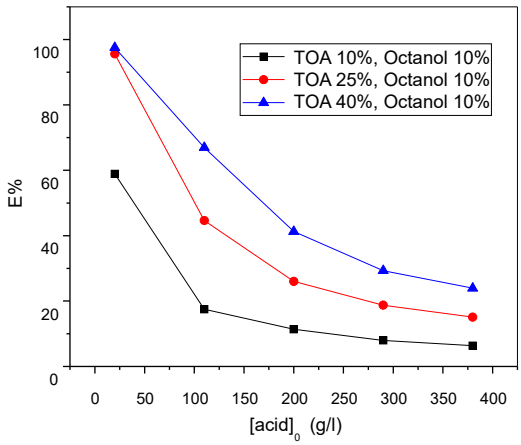

Figure 1. Extraction percentage of sulfuric acid against initial concentration of sulfuric acid; *T*=20 ºC; octanol=10vol%.

Table 1. Experiments and investigated parameters.

no	Acid concentration (g/l)			TOA concentration (volume percent)			Octanol concentration (volume percent)			Temperature (°C)			V_{org}/V_{aq}		
1	20	85	150	10	25	40		10			20			1	
2	20	85	150		25		5	10	15		20			1	
3	20	85	150		25			10		5	20	35		1	
4	20	85	150		25			10			20		0.5	1	2

3.2 Effect of TOA concentration on sulfuric acid extraction

Figure 2 shows that the sulfuric acid extraction increases with increasing in TOA concentration. But for sulfuric acid with 20 g/l concentration, extraction was completed by TOA with 25vol% concentration and extraction percent is about 100%. It should also be noted that viscosity of organic phase increases with increasing extractant concentration, which makes the separation process difficult. So TOA with 25vol% concentration was used in next experiments for investigation of other parameters.

3.3 Effect of modifier concentration (octanol) on sulfuric acid extraction

For this solvent extraction system, the presence of octanol is necessary to modify the organic phase. Figure 3 shows that increasing octanol concentration has no effect on sulfuric acid extraction and just accelerated separation of organic and aqueous phases and so two curves were superposed. But systems with octanol of 5vol% or less, resulted in a third phase formation. Thus octanol with concentration higher than 5vol% is necessary for this system. In subsequent experiments octanol with 10vol% was used for investigation of other parameters.

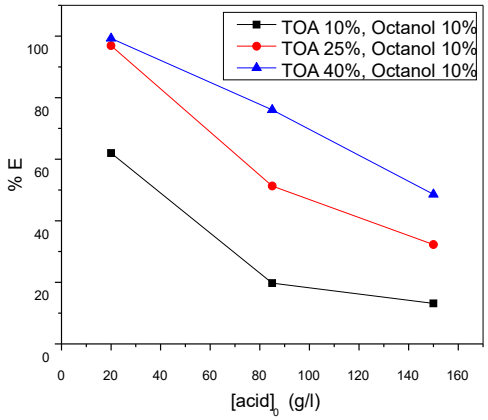

Figure 2. Effect of TOA concentration on extraction percentage of sulfuric acid against initial concentration of sulfuric acid; T=20°C; octanol=20vol%.

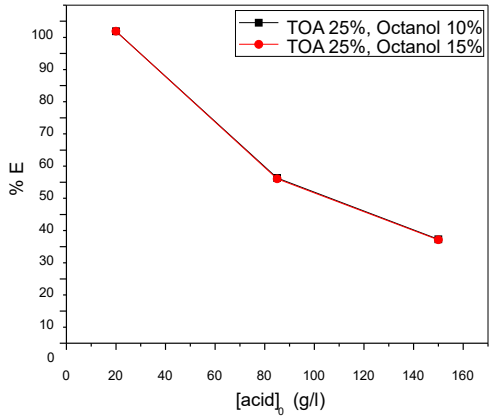

Figure 3. Effect of octanol concentration on extraction percentage of sulfuric acid against initial concentration of sulfuric acid; T=20°C; TOA=25vol%.

3.4 Effect of temperature on sulfuric acid extraction

Figure 4 shows the effect of temperature on sulfuric acid extraction. Although experiments show the extraction reaction is exothermic, effect of temperature was not considerable and the curves of these three temperatures were approximately superposed. So, later experiments for investigation of other parameters were done in 20°C.

3.5 Effect of V_{org}/V_{aq} on sulfuric acid extraction

Figure 5 shows that the sulfuric acid extraction increases with increasing in V_{org}/V_{aq} ratio. But for sulfuric acid with 20 g/l concentration, extraction percent of sulfuric acid with V_{org}/V_{aq}=1 was about to 100% thus for this sulfuric acid concentration and less, V_{org}/V_{aq}>1 is not required. Also separation of organic and aqueous phases is more difficult by increasing ratio of V_{org}/V_{aq}.

3.6 Extraction mechanism

Extraction mechanism of sulfuric acid by TOA is performed according to reaction 1:

$$TOA + n\,H_2SO_4 \rightleftharpoons TOA \cdot nH_2SO_4 \quad (1)$$

Equilibrium constant of reaction 1 is written as follows:

$$K = \frac{[TOA \cdot nH_2SO_4]}{[TOA]\,[H_2SO_4]^n} \times \frac{\gamma_{TOA \cdot nH_2SO_4}}{\gamma_{TOA}\,\gamma^n_{H_2SO_4}} = \frac{[TOA \cdot nH_2SO_4]}{[TOA]\,[H_2SO_4]^n} \times Q \quad (2)$$

Where Q is the ratio of activity coefficients and n is the number of sulfuric acid molecules extracted by one molecule of TOA. Equation 2 can be written like below:

$$\log\frac{K}{Q} = \log[TOA \cdot nH_2SO_4] - \log[TOA] - n\log[H_2SO_4] \quad (3)$$

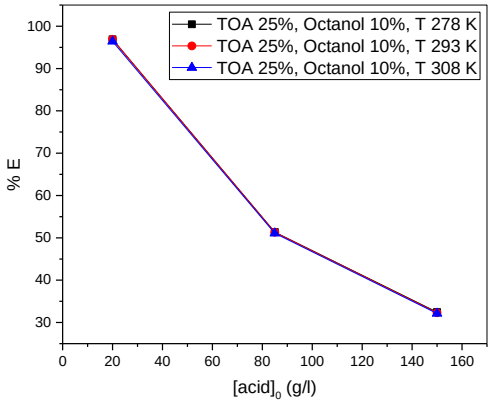

Figure 4. Effect of temperature on extraction percent of sulfuric acid against initial concentration of sulfuric acid; TOA=25vol%; octanol=10vol%.

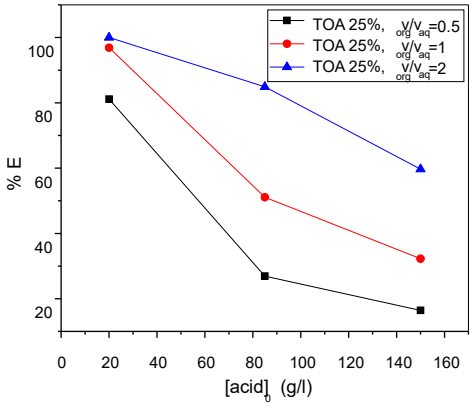

Figure 5. Effect of V_{org}/V_{aq} on extraction percentage of sulfuric acid against initial concentration of sulfuric acid; TOA=25vol%; octanol=10vol%.

According to stoichiometric coefficients of reaction:

$$[Acid]_{org} = n \times [TOA \cdot nH_2SO_4]$$
$$[Acid]_{aq} = [H_2SO_4] \quad (4)$$
$$[TOA] = [TOA]_0 - [TOA \cdot nH_2SO_4]$$

In which $[Acid]_{aq}$ and $[Acid]_{org}$ are sulfuric acid concentration in aqueous and organic phases

respectively. By substituting equation 4 in equation 3, equation 5 is obtained:

$$\log\frac{K}{Q} = \log\frac{[Acid]_{org}}{n} - \log([TOA]_0 - \log\frac{[TOA]_{org}}{n}) - n\ \log[Acid]_{aq} \quad (5)$$

By rewriting equation 5, equation 6 is obtained:

$$f(Acid) = \log\frac{[Acid]_{org}}{n} - n\log([TOA]_0 - \frac{[Acid]_{org}}{n}) = n\log[Acid]_{aq} + \log\frac{K}{Q} \quad (6)$$

according to equation 6, n can be obtained by slope analysis method. By guessing a number for n and plotting f(acid) against $\log[Acid]_{aq}$ a linear graph should be obtained, the slope of this graph should be n. So when the guessed number for n is equal to the slope of the related linear graph, it is the number of extracted sulfuric acid molecules extracted by one molecule of TOA. Using the above method by guessing n=0.83 this guessed number is equal to the slope of the related graph. The resulting graph is shown in Figure 6.

4. Conclusions

Initial studies indicated that at concentrations of more than 1.5 moles per liter (approximately 150 grams per liter) concentration of acid in the organic phase remains nearly fixed. This result is then used in the design of experiments. Extraction percentage and acid concentration in the organic phase increases with increasing in concentration of TOA. At acid concentrations of 20 g/l with TOA concentration of 25% extraction was almost complete and extraction percentage was close to 100.

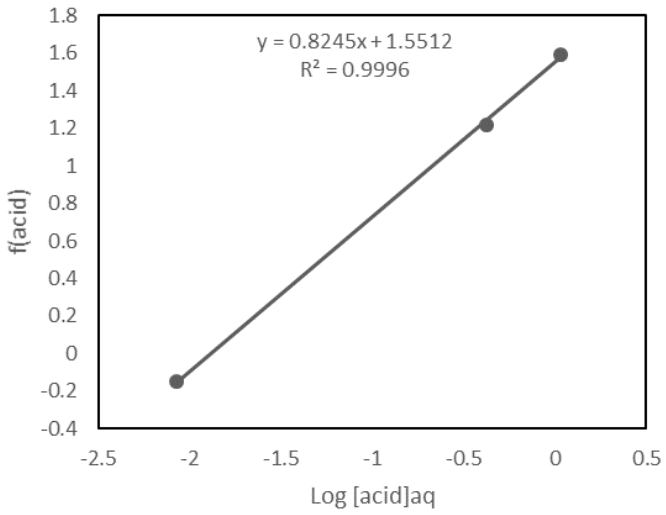

Figure 6. Application of slope analysis method for n=0.83

Therefore, to extract the acid concentrations of less than this amount TOA concentration of 25% seems to be suitable. Presence of octanol as modifier has no effect on the acid extraction and only facilitates the separation of the two phases. In extraction systems with octanol concentrations of 5% and less forms a three-phase mixture. Therefore, octanol concentrations of more than 5% should be used to prevent forming this three-phase mixture. Changes in temperature do not affect the absorption of sulfuric acid

by TOA. With increase in V_{org}/V_{aq} extraction percentage increases. At acid concentration of 20 g/l with TOA concentration of 25% and V_{org}/V_{aq} = 1 extraction was almost complete and extraction percentage was close to 100. Thus, for concentrations of 20 g / l and less, increase in this ratio will have no effect on the extraction. Since the temperature and volume fraction of octanol have no effect on extraction percent, for sulfuric acid extraction percent modeling through solvent extraction process with TOA, only initial sulfuric acid concentration and TOA volume percentage considered as effective parameters. Using the experimental results and formulation of them, the extraction percentage can be calculated as follows:

$$acid\ EXT\% = 49.9 - 25.2[acid]_0 + 19.82(\%TOA) + 11.35[acid]_0^2 - 5.14(\%TOA)^2 \quad (7)$$

In this equation, the initial acid concentration should be between -1 (lowest initial acid concentration, or 20 grams per liter) to 1 (maximum concentration of acid or 150 grams per liter) and TOA volume percent should be between -1 (lowest percentage of TOA or 10%) to 1 (maximum TOA percentage or 40%). The obtained model for acid concentration in organic phase is as follows:

$$[acid]_{org}\left(\frac{g}{L}\right) = 42.28 + 15.73[acid]_0 + 16.85(\%TOA) - 6.96[acid]_0^2 - 3.91(\%TOA)^2 + 12.43[acid]_0 \times (\%TOA) \quad (8)$$

Extraction number is equal to 1, calculated using slope analysis method and so the reaction seems to be:

$$TOA + H_2SO_4 \rightleftharpoons TOA \cdot H_2SO_4 \quad (9)$$

References

1) V. D. Talnikar, Y. S. Mahajan, *Korean J. Chem. Eng.*, **31**, 1720-1731 (2014).
2) D. F. Haghshenas, D. Darvishi, H. Rafieipour, E. K Alamdari, A.A. Salardini, *Hydrometallurgy*, **97**, 173-179 (2009).
3) A. Amornchai, K. Kittipong, A. Suttichai, *J. Ind. Eng. Chem.*, **14**, 796-803 (2008).
4) T. Xu, W. T. Yang, *J. Membr. Sci.ce*, **183**, 193-200 (2001).
5) N. Senad, K. Teeraporn, D. K. Klaus, *J. Membr. Sci.*, **166**, 99-104 (2000).
6) W. Zhixin, L. Yunbai, Y. Ping, *J. Membr. Sci.*, **280**, 134-137 (2006).
7) D. J. Benedict, S. J. Parulekar, P. T. Shih, *J. Membr. Sci.*, **281**, 435-445 (2006).
8) Y. Lixin, G. Qingfeng, H. Jihua, J. Weijun, *Desalination*, **129**, 283-288 (2000).
9) F.J. Alguacil, F.A. Lopez, *Hydrometallurgy*, **42**, 245-255 (1996).
10) K. Viljoen, K. C. Sole, L. J. Bryson, *Fif. SAIMM. Bas. Met. Conf.*, Btwn. (2009).
11) F. W. Ntengwe, Int. J. Chemtech. Res, **2**, 2131-2139 (2010).
12) L.Sadoun; F.Hassaine-sadi, *Desalination*, **167**, 159-163 (2004).

Selective Recovery of Molybdenum from Rhenium Containing Sulphate Model Solutions by Solvent Extraction with Organophosphorus and Oxime Reagents

Toni HELBIG[1,*], Christiane SCHARF[1]

[1]*Helmholtz-Zentrum Dresden-Rossendorf e.V., Helmholtz Institute Freiberg for Resource Technology, Chemnitzer Strasse 40, 09599 Freiberg, Germany*

In various primary or secondary raw materials, for example in molybdenite or in so called "Theisenschlamm", rhenium and molybdenum appear together. Consequently, processing of those materials can lead to aqueous solutions containing both elements. In order to obtain a separation of these elements the selective recovery of molybdenum by organophosphorus (D2EHPA, Cyanex 272) and oxime (LIX 63, LIX 84, LIX 860, LIX 984) reagents diluted in kerosene is investigated. The selectivity for the extraction of molybdenum over rhenium is compared and D2EHPA, Cyanex 272 as well as LIX 984 are chosen for extraction tests from sulphate model solutions containing zinc(II), iron(III), copper(II), molybdenum(VI), rhenium(VII), antimony(V), germanium(IV) and cobalt(II). Cyanex 272 achieves the highest selectivity for molybdenum. Due to that extraction isotherms of molybdenum with Cyanex 272 are constructed.

1. Introduction

The "Theisenschlamm" is a secondary raw material of the former copper shale processing in Germany. A total amount of 220,000 tons has been deposited between the years 1978 and 1990. Besides about 16 wt.-% zinc, 14 wt.-% lead and minor amounts of copper and tin, this material also contains valuable strategic elements, like about 0.05 wt.-% molybdenum and 100 ppm rhenium. Leaching tests in sulphate medium reveal that the acidic leaching solution contains both rhenium and molybdenum. Our results and also other investigations show that rhenium can be efficiently recovered with tertiary amines [1]. However molybdenum is co-extracted by these amines. The modification of the amine extraction system with tributyl phosphate (TBP) to selectively extract rhenium under alkaline conditions [2] or the separation of rhenium and molybdenum using only TBP as the active extractant [3, 4] have been reported. An approach that seems promising is the selective removal of molybdenum from rhenium containing solutions since there are a number of investigations reporting the ability of various extractants to recover molybdenum selectively over e.g. copper, iron, aluminium, uranium, cobalt or nickel. The applied extractants are, e.g. LIX 63 (5,8-diethyl-7-hydroxy-dodecan-6-oxime) [5, 6], LIX 84 (2-hydroxy-5-nonylacetophenone oxime) [7, 8], LIX 984N (1:1 mixture of LIX 84 and LIX 860N (5-nonylsalicylaldoxime) [3], LIX 622N (5-nonylsalicylaldoxime with tridecanol) [9], D2EHPA (di-(2-ethylhexyl)phosphoric acid) [10, 11], PC-88A (2-ethylhexyl phosphonic acid mono-2-ethylhexyl ester) [12, 13] or Cyanex 272 (bis(2,4,4-trimethylpentyl)-phosphinic acid) [13, 14] all diluted in poorly water soluble organic diluents, e.g. kerosene. However,

reports including rhenium are rare. Valenzuela et al. found that PC-88A extracts molybdenum selectively from solutions containing rhenium, copper and iron [12]. Srivastava et al. reported the selective extraction of molybdenum over rhenium from chloride solutions with Cyanex 272 [14]. This study intends to further evaluate the suitability of organophosphorus and oxime reagents to selectively recover molybdenum over rhenium. For this purpose the following extractants are applied for extraction tests from acidic sulphate model solutions: LIX 63, LIX 84, LIX 860 (5-dodecyl-salicylaldoxime), LIX 984 (1:1 mixture of LIX 84 and LIX 860), D2EHPA and Cyanex 272.

2. Experimental

2.1 Reagents

The model solutions were prepared by using the following chemicals: NH_4ReO_4 (Alfa Aesar, 99.999%), $Na_2MoO_4 \cdot 2H_2O$ (Merck, ≥ 99.5%), $Fe_2(SO_4)_3$ (VWR Chemicals, > 99%), $CuSO_4 \cdot 5H_2O$ (Merck, > 99.5%), $ZnSO_4 \cdot 7H_2O$ (Merck, > 99%), $NaSbO_3 \cdot 3H_2O$ (Alfa Aesar, > 98%), GeO_2 (PPM Pure Metals GmbH, 99.999%), $CoSO_4 \cdot 7H_2O$ (Alfa Aesar, 99.999%), H_2SO_4 (Carl Roth GmbH, 98%), NaOH (pellets, Carl Roth GmbH, ≥ 99%). Kerosene (light distillate, J.T. Baker) was used as diluent in the organic phase to dissolve the extractants: LIX 63 (BASF, 70%), LIX 84 IC (BASF, 65%), LIX 860 (BASF, 70%), D2EHPA (Alfa Aesar, 95%), Cyanex 272 (Cytec, 85%). The molar concentration of the respective extractant in the organic phase was adjusted considering the concentration of the active component in the supplied product (see percentage value in brackets). All chemicals were applied as supplied by the manufacturer.

2.2 Methods

The extraction experiments were carried out by mixing aqueous and organic phase in a beaker with an overhead stirrer followed by separation in separating funnels and analysis of the aqueous phase with ICP-OES. Unless otherwise specified the experiments were performed with 100 mL of each phase (phase ratio A/O = 1), 10 min mixing time, a stirring speed of 400 min^{-1} and a temperature of 20 ± 2°C. The pH value was adjusted with 9.2 M H_2SO_4 and 15 M NaOH. The percentage extraction (E) was calculated with Eq. (1) and the element concentration in the organic phase (c^n_{org}) for a certain loading stage (n) with Eq. (2).

$$E = \left(1 - \frac{V^t_{aq} \cdot c^t_{aq}}{V^\circ_{aq} \cdot c^\circ_{aq}}\right) \cdot 100\ \% \qquad (1)$$

$$c^n_{org} = \sum_{i=1}^{n} \left(\frac{V^{\circ,i}_{aq} \cdot c^\circ_{aq} - V^{t,i}_{aq} \cdot c^{t,i}_{aq}}{V^i_{org}}\right) \qquad (2)$$

(with: V – volume, c – concentration, aq – aqueous phase, org – organic phase, ° – initial state, t – state after a certain mixing time, n – loading stage of the organic phase)

3. Results and Discussion

3.1 Selectivity for Mo(VI) over Re(VII) comparing different extracting agents

In order to decide a suitable extractant to efficiently separate Mo(VI) and Re(VII), extraction tests with a model solution containing 1400 mg/L Mo(VI) and 150 mg/L Re(VII) are performed. The Mo(VI) concentration is chosen to include the possibility of polymolybdate formation whereas the

Re(VII) concentration refers to the intended concentration after cross-current Theisenschlamm leaching.

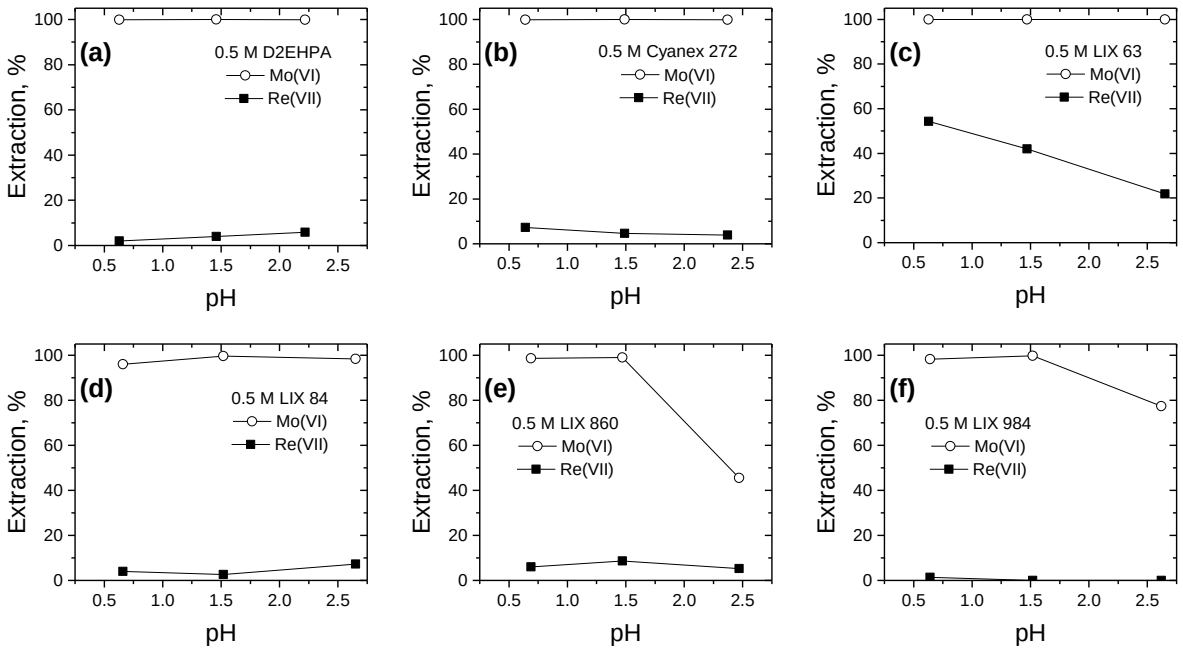

Figure 1. (a) – (f): Comparison of extracting agents based on the extraction of Mo(VI) and Re(VII) at different pH values from a model solution containing 1400 mg/L Mo(VI) and 150 mg/L Re(VII).

Figure 1 shows the results of the extraction of Mo(VI) and Re(VII) with D2EHPA, Cyanex 272, LIX 63, LIX 84, LIX 860 and LIX 984 with a concentration of 0.5 M each. Besides LIX 63 all of the tested extractants show a low Re(VII) extraction between 0% and 8.7% in the pH range 0.6 to 2.2. In the same pH range the organophosphorus reagents Cyanex 272 and D2EHPA extract Mo(VI) quantitatively. Regarding the oxime reagents LIX 84 and LIX 63 show quantitative Mo(VI) extraction in the considered pH range. However with LIX 860 Mo(VI) extraction decreases at pH values > 1.5 from 99% to 45% at pH 2.5. Since LIX 860 is one component of LIX 984 the effect of a decrease in Mo(VI) extraction at pH values > 1.5 appears as well but less distinct. However compared to LIX 84 and LIX 860 the Re(VII) extraction is lower with LIX 984.

The poor Re(VII) extraction can be explained with the presence of the $[ReO_4]^-$ anion. Neither the cation exchange mechanism of Cyanex 272 and D2EHPA nor the mechanism of chelate formation of the oxime reagents extract the negatively charged Re(VII) complex. In contrast to rhenium, molybdenum forms a variety of species, e.g. at pH < 2.5 and 21.2 mM Mo(VI): $[H_6Mo_2O_8]^{2+}$, $[H_3MoO_4]^+$, H_2MoO_4 and $[Mo_7O_{21}(OH)_3]^{3-}$ [15]. The species formation depends on both the molybdenum concentration and the pH value. However, it is often assumed that at low pH values the $[MoO_2]^{2+}$ cation is extracted by the organic reagents [7, 16]. So the Mo(VI) extraction can be expressed by Eqs. (3) and (4) according to the cation exchange mechanism of the dimeric organophosphorus reagents ($(HR)_2$) and the chelate formation mechanism for the oxime reagents (HL).

$$[MoO_2]^{2+}{}_{(aq)} + 2\ (HR)_{2\ (org)} \leftrightarrow MoO_2(R{\cdot}HR)_{2\ (org)} + 2\ H^+{}_{(aq)} \quad (3)$$

$$[MoO_2]^{2+}{}_{(aq)} + 2\ HL_{\ (org)} \leftrightarrow MoO_2L_{2\ (org)} + 2\ H^+{}_{(aq)} \quad (4)$$

3.2 Mo(VI) extraction from multi element sulphate model solution

Due to the results shown in Figure 1 Cyanex 272, D2EHPA and LIX 984 are chosen for further investigations. A multi element sulphate model solution (MES I) is prepared based on first results of the Theisenschlamm leaching. Table 1 shows the composition of this solution. The Re(VII) content has not reached the intended concentration yet.

Table 1. Composition of the multi element sulphate model solution (MES I).

	Zn(II)	Fe(III)	Cu(II)	Mo(VI)	Co(II)	Re(VII)	Sb(V)	Ge(IV)
Concentration, mg/L	3190	1765	250	150	12	9	9	6

This multi element model solution is used to further characterise the selected extractants regarding the selectivity for Mo(VI) depending on the pH value. The investigations are performed with extractant concentrations of 0.1 M and 0.5 M respectively.

Figure 2 shows the results of the mainly extracted elements of the model solution (MES I). In the investigated pH range of 0.5 < pH < 2.0 Co(II) is not extracted with these extractants. LIX 984 shows the lowest affinity for Zn(II) with a maximum of 5% extraction and D2EHPA as well as Cyanex 272 achieve the best selectivity over Cu(II) with a maximum of 5% Cu(II) extraction.

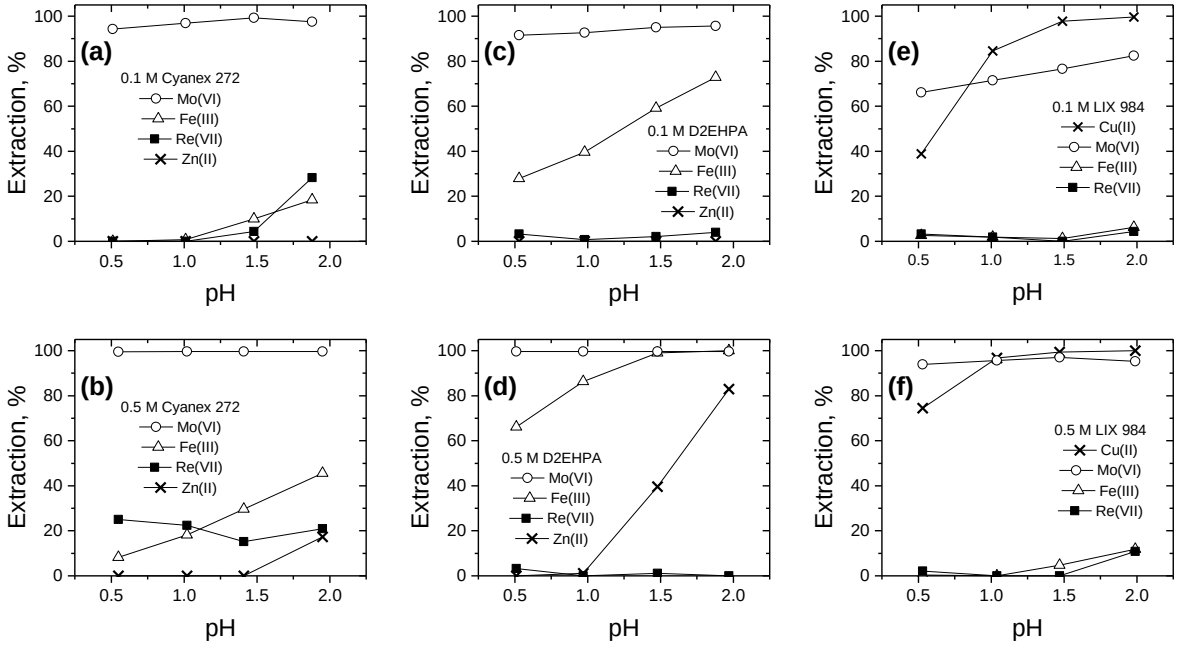

Figure 2. (a) – (f): Comparison of Cyanex 272, D2EHPA and LIX 984 based on the extraction of various elements from the multi element model solution (MES I).

Figures 2 (a) and (b) indicate that Cyanex 272 achieves the most selective Mo(VI) extraction at pH ≤ 1

with both 0.1 M and 0.5 M extractant concentrations. An increase in Cyanex 272 concentration leads to an increased extraction of Fe(III) and Re(VII) as well as Zn(II) co-extraction at pH > 1.5, as shown in Figure 2 (b). Figures 2 (c) and (d) show that with D2EHPA the Re(VII) co-extraction is the lowest among these extractants and within the investigated pH range. However, D2EHPA intensively co-extracts Fe(III) even at a low extractant concentration. At a D2EHPA concentration of 0.5 M and pH > 1 also Zn(II) is co-extracted. As shown in Figures 2 (e) and (f) LIX 984 achieves good selectivity over Fe(III) and Re(VII) at pH < 1.5. But it is also a well-known Cu(II) extractant so that Mo(VI) and Cu(II) are co-extracted. Figure 2 (e) indicates that a concentration of 0.1 M LIX 984 is not sufficient to extract Mo(VI) quantitatively. With an increase in LIX 984 concentration to 0.5 M a Mo(VI) extraction of > 95% can be achieved.

Consequently, D2EHPA is not suitable for the selective extraction of Mo(VI) if the solution contains Fe(III) and/or Zn(II) and also LIX 984 is not suitable in case the solution contains Cu(II). Hence Cyanex 272 is chosen for more detailed investigations.

3.3 Time dependence with Cyanex 272

Figure 3 shows the influence of the mixing time on the extraction of Mo(VI) and the mainly co-extracted elements with Cyanex 272 at pH 1.5. The results in Figure 3 reveal that a short mixing time is favourable since an increase leads to higher co-extraction of Fe(III) and Re(VII). This behaviour is more distinct for 0.5 M than for 0.1 M Cyanex 272. However, to reach a Mo(VI) extraction > 95% mixing times of 5 min and 1.5 min are necessary in case of 0.1 M and 0.5 M Cyanex 272, respectively.

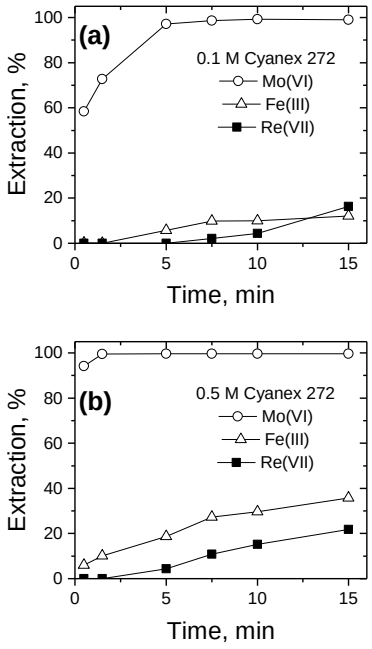

Figure 3. Influence of the mixing time on the extraction with (a) 0.1 M and (b) 0.5 M Cyanex 272 at pH 1.5.

3.4 Extraction isotherms with Cyanex 272

Extraction isotherms are constructed by using the method of contacting the organic phase several times with a fresh aqueous multi element sulphate model solution (MES II) with the composition shown in Table 2 [17, 18]. For all loading stages the aqueous to organic phase ratio is 1:1 and the equilibrium pH = 1. A mixing time of 5 min is adjusted to reduce co-extraction of Re(VII) and Fe(III) but still achieve a high Mo(VI) extraction with 0.1 M Cyanex 272. The element concentration in the organic phase after n loading stages is calculated according Eq. (2). Due to the low Mo(VI) concentration in the MES II the maximum loading capacity is not reached after 10 loading stages.

Table 2. Composition of the multi element sulphate model solution (MES II).

	Zn(II)	Fe(III)	Cu(II)	Mo(VI)	Co(II)	Re(VII)	Sb(V)	Ge(IV)
Concentration, mg/L	3650	1930	242	146	10	10	10	5

So only the first part of the extraction isotherms is constructed. Figure 4 shows that in the range of low Mo(VI) concentrations in the aqueous phase the extraction isotherms for Cyanex 272 concentrations of 0.3 M and 0.5 M are considerably steeper compared to that of 0.1 M. The higher slope is favourable because a low Mo(VI) concentration in the raffinate can be achieved with less extraction stages. Table 3 indicates that after 10 loading stages a cumulative Mo(VI) extraction of respectively 74.2%, 95.9% and 98.2% is reached with 0.1 M, 0.3 M and 0.5 M Cyanex 272. Thus an increase in Cyanex 272 concentration enables a more efficient Mo(VI) extraction and enrichment in the organic phase. However the increase from 0.3 M to 0.5 M leads only to a slightly improved Mo(VI) extraction. Table 3 also shows that, besides Mo(VI), other elements of the MES II accumulate in the organic phase as well. As already stated in Figures 2 (a) and (b), an increase in Cyanex 272 concentration also increases the co-extraction of not only Fe(III) but also Zn(II), Re(VII) and Sb(V). Less than 1 mg/L of Ge(IV), Cu(II) and Co(II) is present in the organic phase after 10 loading stages without being influenced by the Cyanex 272 concentration. In order to improve the purity of Mo(VI) in the organic phase previous investigations show that scrubbing of the loaded organic phase with sulfuric acid can reduce the Fe(III) content signifcantly [13]. Other approaches to reduce the impurity content in 0.3 M and 0.5 M Cyanex 272 are a shorter mixing time, compare Figure 3, and/or lowering the equilibrium pH value, compare Figures 2 (a) and (b).

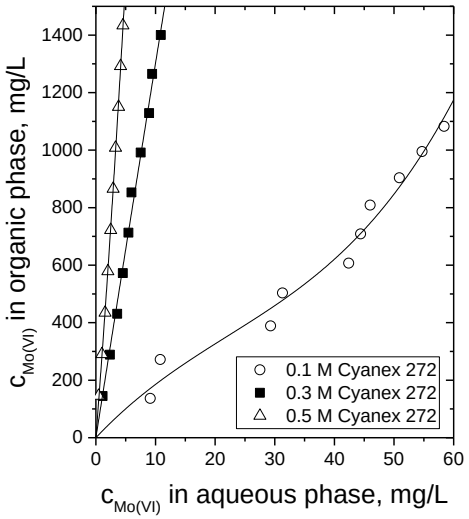

Figure 4. Extraction isotherms for Mo(VI) from multi element model solution (MES II) and 0.1, 0.3 and 0.5 M Cyanex 272, pH_{eq} = 1, V_a:V_o = 1, mixing time: 5 min.

Table 3. Concentration in the organic phase (c_{org} in mg/L) and cumulative extraction (E in %) after 10 loading stages with MES II, pH_{eq} = 1, V_a:V_o = 1, mixing time: 5 min.

Elements	Concentration of Cyanex 272 in kerosene					
	0.1 M		0.3 M		0.5 M	
	c_{org}	E	c_{org}	E	c_{org}	E
Mo(VI)	1082.7	74.2	1400.2	95.9	1433.8	98.2
Fe(III)	180.0	0.9	830.0	4.3	890.0	4.6
Zn(II)	0.0	0.0	130.0	0.4	150.0	0.4
Re(VII)	1.2	1.2	4.1	4.2	5.2	5.4
Sb(V)	1.0	1.0	2.9	3.0	3.1	3.1
Ge(IV)	0.5	0.9	0.3	0.6	0.0	0.0
Cu(II)	0.0	0.0	0.0	0.0	0.0	0.0
Co(II)	0.0	0.0	0.0	0.0	0.0	0.0

4. Conclusion

The investigation reveals that among the considered extractants Cyanex 272, D2EHPA and LIX 984 are the most promising ones for a selective extraction of Mo(VI) over Re(VII). Comparing the Mo(VI) extraction with these extractants from sulphate model solutions containing Zn(II), Fe(III), Cu(II), Mo(VI), Re(VII), Sb(V), Ge(IV) and Co(II) it is found that Cyanex 272 is the most selective. D2EHPA shows a significant co-extraction of Fe(III) and Zn(II) and LIX 984 extracts Cu(II) better than Mo(VI). The highest selectivity for Mo(VI) can be obtained with low Cyanex 272 concentrations (e.g. 0.1 M) at $pH_{eq.} \leq 1$ and short mixing times (e.g. 5 min). In order to improve selectivity the mixing time has to be adjusted depending on the Cyanex 272 concentration (e.g. 1.5 min at 0.5 M Cyanex 272). The construction of extraction isotherms for Mo(VI) by repeated loading of the organic phase shows that Cyanex 272 concentrations of 0.3 M and 0.5 M are more favourable for an efficient Mo(VI) extraction than a concentration of 0.1 M. With 0.1 M, 0.3 M and 0.5 M Cyanex 272 cumulative extractions of respectively 74.2%, 95.9% and 98.2% Mo(VI) and a low extraction of respectively 1.2%, 4.2% and 5.4% Re(VII) are achieved after 10 loading stages. Similar to Re(VII) also Fe(III) co-extraction increases with increasing Cyanex 272 concentration. Therefore a scrubbing step with sulfuric acid is required. These results form a basis for further investigations with real leaching solutions and the aim to achieve a Mo(VI) enrichment in the organic phase as well as an improvement of the selectivity which could be possible by e.g. reducing the contact time and/or lowering the $pH_{eq.}$ value.

Acknowledgement

The authors thank the BMBF (Federal Ministry of Education and Research, Germany) r^4-project “Theisenschlamm” (project number: 033R137E) for financial support and the CYTEC SOLVAY Group as well as BASF for the supply with solvent extraction reagents.

References

1) Z.S. Abisheva, A.N. Zagorodnyaya, N.S. Bekturganov, *Hydrometallurgy*, **109**, 1–8 (2011).
2) C. Zhan-fang, Z. Hong, Q. Zhao-hui, *Hydrometallurgy*, **97**, 153–157 (2009).
3) A. Khoshnevisan, H. Yoozbashizadeh, M. Mohammadi, A. Abazarpoor, M. Maarefvand, *Minerals and Metallurgical Processing*, **30**, 53–58 (2013).
4) E. Keshavarz Alamdari, D. Darvishi, D.F. Haghshenas, N. Yousefi, S.K. Sadrnezhaad, *Separation and Purification Technology*, **86**, 143–148 (2012).
5) P. Zhang, K. Inoue, K. Yoshizuka, H. Tsuyama, *Hydrometallurgy*, **41**, 45–53 (1996).
6) A. Trujillo, H. Freiser, *Solvent Extraction and Ion Exchange*, **7**, 1–14 (1989).
7) D. Mishra, G.R. Chaudhury, D.J. Kim, J.G. Ahn, *Hydrometallurgy*, **101**, 35–40 (2010).
8) K.-H. Park, H.-I. Kim, P.K. Parhi, *Separation and Purification Technology*, **74**, 294–299 (2010).
9) T.A. Lasheen, M.E. Ibrahim, H.B. Hassib, A.S. Helal, *Hydrometallurgy*, **146**, 175–182 (2014).
10) Z. Qingyuan, F. Huihao, *Hydrometallurgy*, **16**, 263–270 (1986).
11) X. Li, Z. Deng, C. Wei, C. Li, M. Li, G. Fan, H. Huang, *Hydrometallurgy*, **154**, 40–46 (2015).

12) F.R. Valenzuela, J.P. Andrade, J. Sapag, C. Tapia, C. Basualto, *Minerals Engineering*, **8**, 893–904 (1995).
13) P. Zhang, K. Inoue, H. Tsuyama, *Energy & Fuels*, **9**, 231–239 (1995).
14) R.R. Srivastava, M. Kim, J. Lee, *Ind. Eng. Chem. Res.*, **55**, 8191–8199 (2016).
15) M.A. Olazabal, M.M. Orive, L.A. Fernández, J.M. Madariaga, *Solvent Extraction and Ion Exchange*, **10**, 623-635 (1992).
16) Y. Sato, F. Valenzuela, T. Tsuneyuki, K. Kondo, F. Nakashio, *Journal of Chemical Engineering of Japan*, **20**, 317-321 (1987).
17) G.M. Ritcey, *Solvent Extraction Vol. 1*, 58–63 (2006).
18) G.M. Ritcey, *Solvent Extraction Vol. 2*, 10–13 (2006).

Developing Solvent Extraction for the Future of the Energy Industry

Mike HUTTON-ASHKENNY[1]*, Chris PANAOU[2]

[1]*Hatch, 144 Stirling Street, Perth, 6000, WA, Australia;* [2]*Hatch, 61 Petrie Terrace, Brisbane, QLD, 4000, Australia.*

The energy industry of the modern world is changing. Uranium and lithium consumptions are expected to increase in order to allow carbon-free energy sources to provide a higher proportion of global energy requirements. In order to meet the expected increase in demand for these commodities and to keep energy costs low, efficiency improvements during metallurgical processing will be required. Solvent extraction is a key processing step for generating high purity chemical products and already has widespread acceptance in the uranium industry. Recent improvements in solvent extraction in the uranium and lithium industries, including improvements in organic phase compositions and phase separation, are reviewed in this paper and are exemplified by recent project experiences within Hatch. Innovators and early adopters of the improved efficiencies offered by the discussed improvements should be well placed to lead the way diversifying the energy market.

1. Introduction

Coal production in China likely reached its peak in 2014 [3]; global production is expected to continue to fall as concerns over carbon dioxide emissions push energy production towards low carbon energy sources. Two alternatives to fossil fuels are nuclear energy and renewable energy.

Nuclear energy has the potential to supply a convenient base load for electricity generation to national grids. Recent work by Hatch has demonstrated that portable nuclear reactors could be used to power remote industrial sites. Nuclear reactors, however, are not currently suitable for use in commercial transportation, which, according to the World Bank, accounts for 20% of total carbon emissions. In contrast, renewable energy sources are typically intermittent. Lithium-based batteries are promoted as a method to smooth out intermittent electrical supply. This idea has been implemented in the mining industry; Sandfire Resources installed a 10 MW solar generation facility with 4 MW / 1.8 MWh of lithium battery storage at their DeGrussa operation in Western Australia [4]. In addition, demand for lithium-based batteries to power vehicles is currently growing at an exponential rate [5]. This has manifested as an increased demand for lithium, primarily for use in batteries (Figure 1).

Solvent extraction (SX) was first commercialized for the recovery of uranium in the 1950's [6] and is a key processing step in the production of many metals. More recently, SX for recovery of lithium from salar brines has started to become of interest [7]. SX can be used to avoid time consuming and weather dependent solar-evaporation and reduce the capital outlay required for pond construction (~35% of capital costs in Hatch's experience). This has the potential to greatly reduce the cost of lithium refining and production ramp up, predominantly in salar brine applications where 18 –

24 months ramp up is common. The chemistry of novel extraction techniques for uranium and lithium industries is therefore continually being developed in order improve efficiency and to reduce processing costs. Although lithium recovery via SX has yet to be commericalised, there has been pilot work completed to develop the technology for salar brines [8]. SX has also been applied to boron removal in the refining of lithium to generate battery grade lithium products [9].

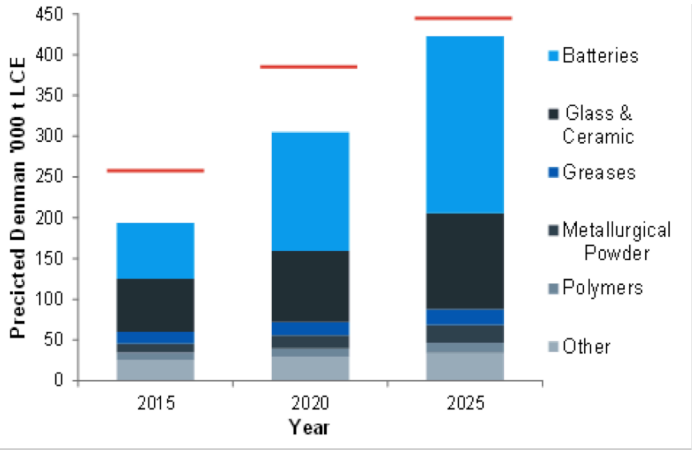

Figure 1: Predicted Lithium Demand by Product Type (Red Lines Represent Predicted Mine Capacity).

In addition to improving the chemistry of solvent extraction circuits, there has been considerable research into optimizing the contact and separation of the two liquid phases. In the uranium industry, both settlers and columns have been used for phase contact in the extract circuit. Columns are suitable to the extract stage [10] due to the particularly fast kinetics of uranium extraction using amines. Despite this, Hatch believes that mixer-settlers are the preferred technology for phase contact due to: (1) the ability to easily alter internal O:A ratios in response to changes in plant chemistry and liquor tenors, (2) the ability to handle larger flows, and (3) less onerous testwork requirements [10-12].

A key aspect of solvent extraction using mixer-settlers is the optimization of the separation of the two liquid phases. Improving the separation efficiency reduces capital costs by reducing the required settling area. It can also improve the quality of the product by reducing entrainment of raffinate into the strip solution. Several innovations for settling and phase separation that can decrease the cost and improve the efficiency of solvent extraction circuits have been proposed and implemented in recent years. Examples include the Hatch distribution array [13], Outotec deep dispersion gate (DDG) [14], and the CSIRO optimized picket fence [15].

Improvements to the solvent extraction of lithium and uranium have the potential to reduce the cost of future electricity generation and supply. There have been many recent advances in the solvent extraction chemistry of these elements as well as in the design of traditional mixer-settlers used in the solvent extraction industry. This paper therefore reviews these advances to provide a summary of the state of the art with references to the authors' experiences.

2. Developments in Solvent Extraction Chemistry for Uranium and Lithium

2.1 Uranium Solvent Extraction

Uranium recovery from primary ores is commonly practiced using amine-based solvent extraction reagents, the most common being trioctyl amine (TOA) [6, 16]. Uranium is then traditionally stripped using ammonia [16]. During ammonia stripping there is a risk of precipitating ammonium diuranate in the mixer-settler, causing crud and loss of valuable product. Ammonia must

also be recovered from the strip solution to minimize operating costs and to meet stringent nitrogen discharge limits [6, 17]. Further, the stripped amine reagent must be re-protonated before the extract stage and ultimately regenerated in a strong base strip mixer-settler, adding further costs. Research by Hatch has shown that although ammonia strip stages exhibit good phase separation compared with the extract stages, the regeneration stage exhibits very poor phase separation (Figure 2) and hence requires conservative settler specific flux (SSF) rates in design (< 3.5 $m^3/h/m^2$).

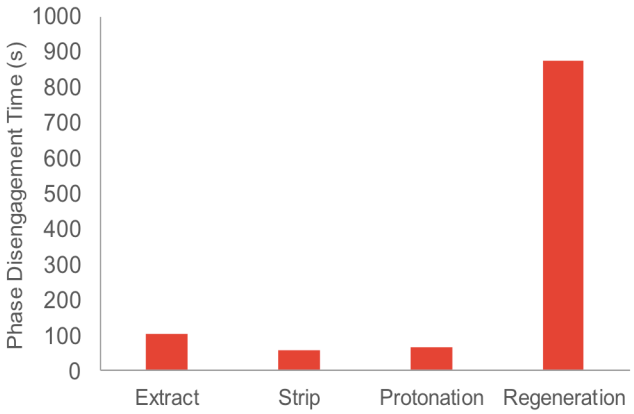

Figure 2: Phase Disengagement Times for Each Circuit from USX Testwork by Hatch.

Alternatives to ammonia stripping of amines that use different stripping chemicals or different organic reagents are being investigated. Different reagents are similarly being promoted for high chloride aqueous feeds due to strong competition between chloride and uranyl sulphate for the extractant. For example, Ballestrin *et al.* [18] combined TOA, TBP and di-2-ethylhexyl phosphoric acid (D2EHPA) in ShellSol 2046 for application to the Uranium One Honeymoon operation. This reagent mixture was able to extract uranium even in the presence of high chlorides. The inclusion of D2EHPA unfortunately increased iron co-extraction into the organic phase. To avoid stripping with ammonia, this system was stripped using sodium carbonate. Tight pH control was necessary to avoid third phase formation and phase separation issues, comparable to those noted for regeneration stages in conventional USX (Figure 2).

Morais *et al.* [19] suggested stripping of TOA with 4 M sulfuric acid to avoid ammonia stripping. Previous researchers have additionally promoted alternative reagents to TOA that can be effectively stripped using sulphuric acid. Zhu *et al.* [20] presented a solvent system containing D2EHPA and the ionic liquid CyphosIL-101. This system resulted in high uranium extraction (85%) at pH 0.5. Although iron co-extraction was acceptable (15%), vanadium co-extraction was particularly high (55%). Strong (4 M) sulfuric acid was required for effective stripping. Dogmane *et al.* [21] similarly researched uranium extraction with Cyanex 272 and subsequent stripping with strong sulfuric acid.

Sulfuric acid-based loaded strip solutions require neutralisation with lime, to generate gypsum, before uranium yellowcake precipitation can occur. Extensive washing of the gypsum would be necessary before disposal to recover uranium in the precipitate. Additionally, the stripping acid is destroyed in the process and cannot be recycled. In response to this, Zhu *et al.* [17] developed a method to recover uranium from strong acid (4 M) with transfer to weak acid (0.5 M) for subsequent neutralisation and yellowcake recovery. This method employs SX of uranium from the strong acid strip using 10% Cyanex 923 and 10% isodecanol. Unfortunately, many stages were required for both extraction (4) and stripping (5), suggesting that a high capital outlay may be required for this process.

Research by Hatch has shown that a strong acid contact with a USX organic phase could be designed at a much higher SSF (> 5 $m^3/h/m^2$) compared with the regeneration stage, thus requiring smaller settling areas and reducing capital costs. If a process for recycling the strong sulfuric acid required for uranium stripping can be successfully commercialized, then this process route appears to be an attractive option for future USX installations.

2.2 Lithium Solvent Extraction

Alternative purification techniques to extract lithium directly from salt lake brines or sulfate-based leach liquors, such as ion exchange or solvent extraction, can improve product quality by generating upgraded lithium solutions before precipitation of the final product. SX is considered a preferred method for lithium extraction over ion exchange, as it is able to treat higher concentrations of lithium (1 – 5 g/L) and higher solution volumes typically encountered in lithium refining.

Historical research into solvent extraction of lithium focused on using TBP with ferric chloride as a co-extractant [22, 23]. The use of ferric chloride as a co-extractant poses several operational problems, not least a requirement to acidify the entire process stream to avoid hydrolysis of the ferric ion. This would be a significant additional expense. In treatment of sulfate-based leach solutions of lithium-bearing minerals, the addition of ferric chloride to the process would increase the required bleed to avoid high levels of recirculating chloride. Further, to avoid third phase formation, highly polar diluents with low flash points, such as methyl iso-butyl ketone [24, 25], have been used, which would require additional design complexity for nitrogen blanketing to reduce fire risk.

To avoid the use of ferric chloride, other researchers have promoted the use of fatty alcohols for lithium recovery. Examples include the use of butanol [26] and octanol [27]. Processes promoting fatty alcohols were not adopted by the industry, presumably due to high solubility of the alcohol in the aqueous phase, and relatively low separation factors (< 3) of lithium over sodium, calcium and magnesium [26].

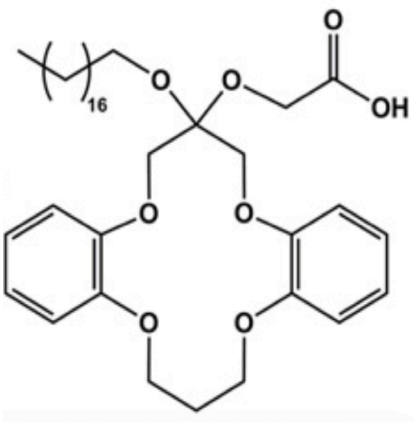

Figure 3: Functionalized Crown Ether used for Lithium Recovery

In response to these historically proposed techniques for lithium solvent extraction, Pranolo *et al.* [28] developed a solvent extraction process using commercially available reagents and diluents. The process was based on the extraction of lithium using trioctyl phosphine oxide (TOPO) and a beta-diketone dissolved in benzene [29]. Pranolo *et al.* [28] propose using LIX 54 (a commercial beta-diketone) and Cyanex 923 (a branched, liquid version of TOPO) dissolved in ShellSol D70 (100% aliphatic diluent). The lithium-sodium separation factor was 1500 at 1 g/L lithium and 80 g/L sodium. Extraction was carried out at pH 11 in 3-4 stages. Stripping was carried out using 0.5 M HCl in 2 stages. This method of selectively recovering lithium using commercially available solvent extraction reagents is believed to be a promising advancement in the lithium refining industry.

The most recent research trend for lithium recovery has targeted ionic liquids. Although many of these systems are not yet commercially applicable, they have the benefits of very selective

lithium extraction. Further, ionic liquid diluents have negligible vapor pressures and hence greatly improved health and safety characteristics. Crown ethers (Figure 3) are particularly attractive for lithium recovery as the size of the cavity can be tuned specifically for a lithium ion. Combining these two concepts, Torrejos *et al.* [2] report the application of a functionalized crown ether (Figure 3) dissolved in Cyphos IL 109 that offers separation factors of lithium over sodium of 2000. Although these ideas are still in their infancy, they are exciting developments that have the potential to improve the efficiency of lithium refining.

3. Developments in Phase Separation

Mixer-settlers are popular for phase contact because the degree of extraction of target metal and impurities can be easily controlled via three variables: (1) the residence time, (2) the agitation power, and (3) the phase volume ratio. In Hatch's experience, the operational benefits of mixer-settlers are also significant. These include ease of inspection of the mixer and settler units and ease of access for crud removal and sampling.

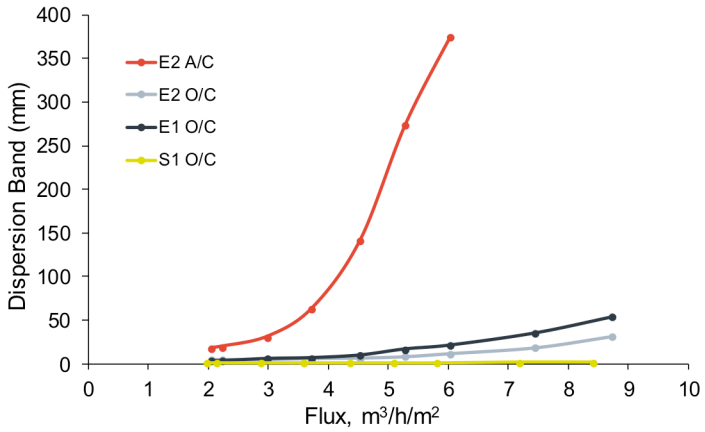

Figure 4: Dispersion Band Height for USX Stages at Varying SSF

One disadvantage of mixer-settlers is that during mixing a homogenous dispersion is created that must be separated. Phase separation rates differ depending on the two phases being mixed, kinetics and energy put into creating the dispersion. The rates of phase disengagement will therefore be different between extract and strip, and within each of their respective stages. This means that different mixer settlers should not always be sized at the same flux rate. This philosophy has been applied by Hatch previously to the design of uranium [10] and boron solvent extraction plants. Laboratory data collected comparing the settler flux rates versus the height of the dispersion band at the weir end of a test settler demonstrate the significant differences in achievable flux rates for different SX conditions (Figure 4).

Modifications to the settler itself can improve the separation characteristics of the two phases. If settling performance can be improved by modifying the settler, thus flattening the curves in Figure 4, then smaller setting areas can be used, or in existing circuits, additional throughput achieved. Computational fluid dynamic (CFD) modeling has recently been used in the solvent extraction industry to test these settler modifications without construction of a test settler. Research by the CSIRO has further demonstrated that CFD models can predict real settler performance with sufficient accuracy to allow design and screening of proposed improvements [15].

Hatch has exploited CFD modeling over a number of years to improve setter design. Similarly, the CSIRO (Australia) has also applied CFD modeling to propose modifications to the

design of a picket fence for a copper SX operation. The outcomes of some of this modeling are presented here as changes to settler design that improve phase separation in solvent extraction circuits, and thus reduce required settling area and ultimate capital costs of new projects. In existing operations, application of these principles can reduce operating costs, increase throughputs and improve the SX plant operability.

3.1 Feed Distribution

The Hatch feed distribution array [13] incorporates sets of panels arranged across the width of the settler. The number of sequential panels in each set and the number of sets of panels will depend on the particular application. Typically, two sets of two panels can achieve even distribution of the feed flow across the settler width. The multiple arrays encourage coalescence much like a picket fence.

This technology is currently being applied to a copper solvent extraction circuit where the redesign of the current picket fence is required to reduce entrainment at a given flux and therefore increase settler throughput. Variation in design combined with careful positioning of each array results in even distribution of flow to the settler. Even distribution of the created dispersion and parallel flow can then be achieved with minimal dynamic head loss avoiding upgrading of pump mixers.

3.2 Organic Weir

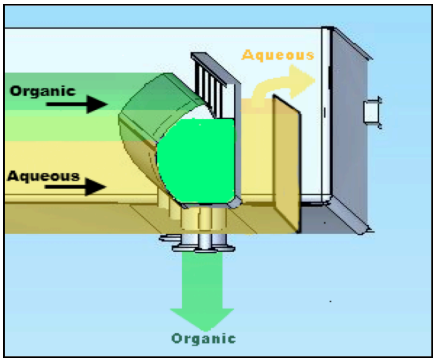

Figure 5: Hatch 'Bull Nose' Phase Splitter

Plant observation and measurement combined with CFD modelling have been utilised to develop improvements to the organic weir. The conventional vertical organic weir was observed to induce a recirculation in the organic phase at the weir end of the settler. This increases horizontal and vertical velocity in the organic phase, significant increasing entrainment. These problems are duplicated in the typical aqueous discharge arrangement.

The Hatch bull nose phase splitter (Figure 5) can be integrated into the organic launder. It presents a convex 'bull nose' profile to the separating phases with the apex positioned at the interface [30]. This profile prevents the formation of recirculating flow patterns in both separating phases, thereby reducing fluid velocities and hence entrainments.

4. Conclusions

There have been many recent developments in the chemistry of solvent extraction of both lithium and uranium, two key elements for the modernization of the energy industry. The drawbacks of conventional stripping of uranium loaded organic phases with ammonia can be avoided by stripping with strong (4 M) sulphuric acid. For this to be successful, a method for the recovery of uranium from the loaded strip solution must be developed. Recent advances in this area, using solvent extraction to transfer uranium from strong to weak acid, are promising. There have similarly been improvements in the solvent extraction of lithium. The most commercially relevant option recovers lithium using a

mixture of LIX 54 and Cyanex 923 dissolved in a high flashpoint aliphatic diluent.

In addition to improvements in solvent extraction chemistry, the solvent extraction of lithium and uranium will benefit from recent improvements in settler designs. Application of CFD modelling to the design of settlers has resulted in innovations in settler internals that can increase the achievable flux and therefore reduce the required settling area and SX plant capital outlay. Examples of these internals include the Hatch distribution array, the Outotec deep dispersion gate, and the Hatch bull nose organic weir.

References

1. J. Hykawy, T. Chudnovsky. "Lithium, cobalt and other relevant battery materials - where do these markets go?". *8th Lithium Supply and Markets Conference*. Las Vegas. (2016).
2. R.E.C. Torrejos, G.M. Nisola, H.S. Song, J.W. Han, C.P. Lawgon, J.G. Seo, S. Koo, H. Kim, W.J. Chung, *Hydrometallurgy*, **164**. 362-371 (2016).
3. Y. Qi, N. Stern, T. Wu, J. Lu, F. Green, *Nat. Geosci.*, **9**. 564-566 (2016).
4. Sandfire Resources, *Sandfire Resources NL: A quality copper-gold company*, in http://www.sandfire.com.au/images/SFR_juwi_Aug10.pdf. (2015).
5. B. Swain, *Sep. Purif. Technol.*, **172**. 388-403 (2017).
6. M. Mackenzie. "The solvent extraction of uranium with an eye to the future". *ALTA 2014*. Perth: ALTA Metallurgical Services. (2014).
7. P.K. Choubey, M. Kim, R.R. Srivastava, J.C. Lee, J.Y. Lee, *Miner. Eng.*, **89**. 119-137 (2016).
8. J. Lipp, B. Grinbaum, "Process for metal ions removal of from aqueous solutions". WO/2013/065050. (2013)
9. Galaxy Resources, *Galaxy Quaterly Report*, in http://www.galaxyresources.com.au/Investor/GXYSep2012Quarterly_000.pdf. (2012).
10. S. Poulter, N. Johns, R. Fraser, V. Brady. "Critical aspects for consideration in the deisgn on a uranium SX circuit ". *ALTA 2014*. Perth: ALTA Metallurgical Services. (2013).
11. A. Taylor. "Evolution of mixer-settler design for USX". *ALTA 2014*. Perth: ALTA Metallurgical Services. (2014).
12. E. Robles, S. Poulter, R. Haywood, I. Cronje, M. Leon. "The future of SX plant design for modern hydrometallurgical refineries". *Gecamin*. Viña del Mar, Chile: Gecamin. (2009).
13. S. Poulter, R. Haywood, W.A. Taylor, "Distribution array for use in a settler area of a mixer-settler". USPO United States of America US2014/0083956. (2014)
14. R. Kuusisto, P. Pekkala, G.J. Karcas. "Outokumou SX EW technology package". *Third Southern African Base Metals Conference*. Kitwe, Zambia: SAIMM. (2005).
15. G.L. Lane, K. Mohanarangam, W. Yang, D.J. Robinson, K.R. Barnard, *Chem. Eng. Res. Des.*, **109**. 200-214.
16. G. Kordosky, M. Virnig, P. Crane, K. Dudley, A. Feather. "Solvent exraction from acidic sulfate leach solutions using tertiary amines". *SME Annual Meeting*. Denver, CO: SME. (2007).
17. Z. Zhu, Y. Pranolog, C.Y. Cheng, *Miner. Eng.*, **89**. 77-83 (2016).

18. S. Ballestrin, R. Low, G. Reynaud, P. Crane. "Honeymoon mine Australia: Commissioning and operations of the process plant using a novel solvent extraction reagent mixture in a high chloride environment. ". *ALTA 2014*. Perth: ALTA Metallurgical Services. (2014).
19. C.A. Morais, L.A. Gomiero, W.S. Filho, H.J. Rangel, *Miner. Eng.*, **18**. 1331-1333 (2005).
20. Z. Zhu, K. Tulpatowicz, Y. Pranolog, C.Y. Cheng. "Uranium recovery from sulphate leach solutions containing chloride using a mixed system of D2EHPA and Cyphos IL-101". *ALTA 2014*. Perth: ALTA Metallurgical Services. (2014).
21. S.D. Dogmane, R.K. Singh, D.D. Bajpai, J.N. Mathur, *J. Radioan. Nucl. Chem.*, **253**. 477-482 (2002).
22. C. Shi, Y. Jing, J. Xiao, X. Wang, J. Yongzhong, *Hydrometallurgy*, **169**. 314-320 (2017).
23. L. Ji, Y. Hu, L. Li, D. Shi, J. Li, N. Feng, F. Song, Z. Zeng, W. Sun, Z. Lui, *Hydrometallurgy*, **162**. 71-78 (2016).
24. W. Xiang, S. Liang, Z. Zhou, W. Qin, W. Fei, *Hydrometallurgy*, **166**. 9-15 (2016).
25. A. Zhou, W. Qin, W. Fei, *J. Chem. Eng. Data*, **56**. 3518-3522 (2011).
26. G.G. Gabra, *Hydrometallurgy*, **3**. 23-33 (1978).
27. P.M. Brown, S.J. Beckerman, "Production of lithium metal grade lithium chloride from lithium-containing brine". USPO United States of America 4980136. (1990)
28. Y. Pranolo, Z. Zhu, C.Y. Cheng, *Hydrometallurgy*, **154**. 33-39 (2015).
29. F.G. Seeley, W.H. Baldwin, "Extraction of lithium from neutral brines using a beta diketone and trioctylphosphine oxide". USPO 3793433. (1974)
30. R. Haywood, S. Poulter, "Phase Splitter". USPO United States of America US2014/0110359. (2014)

Understanding of Uranium Extraction Mechanisms from Phosphoric and Sulfuric Media using DEHCNPB

Boris FRIES[1], Cécile MARIE[1], Vincent PACARY[1], Hamid MOKHTARI[2], Laurence BERTHON[1], Christian SOREL[1] and Marie-Christine CHARBONNEL[1]

[1] CEA, Nuclear Energy Division, Research Department on Processes for Mining and Fuel Recycling, 30207 Bagnols-sur-Cèze, France; [2]AREVA Mines, Service d'Etude de Procédés et Analyses (SEPA), B.P. 71 87250 Bessines-sur-Gartempe, France

The extraction of uranium(VI) from phosphoric and sulfuric acid solutions using DEHCNPB (butyl-1-[*N*,*N*-bis(2-ethylhexyl)carbamoyl]nonyl phosphonic acid) was studied to understand the influence of the original acidic medium on uranium extraction (phosphoric acid 5 mol/L or sulfates 1.6 mol/L at pH=1). Uranium(VI) extraction isotherms highlight different extraction behaviors depending on the initial medium with a lower [DEHCNPB]/[U] ratio reached at saturation with the phosphoric medium. Slope analysis showed different average stoichiometries: 1.9 and 3.3 for the phosphate and sulfate experiments respectively. The co-extraction of water with uranyl was evidenced by Karl-Fischer titrations and ESI-MS measurements and ESI-MS analysis confirmed the presence of uranyl/DEHCNPB complexes with one molecule of water, probably in the first coordination sphere.

1. Introduction

Phosphoric acid is largely produced from phosphate ores, which contain a small concentration of uranium (from 30 to 300 ppm) but are abundant. Therefore, there is a substantial quantity of uranium potentially recoverable from phosphate rocks (around 4 Mt), which constitutes an important secondary source for uranium production [1]. Recovering uranium from wet-phosphoric acid would allow the decontamination of phosphoric acid from uranium and the valorization of uranium for the nuclear industry. The extraction of uranium from wet phosphoric acid was carried out at an industrial scale using various processes and extractants [2]. For instance, the synergistic mixture HDEHP/TOPO is a well know system used for this purpose since the 1950s [3]. Nevertheless, those systems present several drawbacks, like the distribution ratio of uranium(VI) which is not high enough to develop a compact process, and the selectivity towards iron which could be improved. Such processes should enable the recovery of uranium from concentrated phosphoric acid (high complexation effect of uranium in the aqueous phase) while showing high selectivity versus impurities. Indeed, high concentrations of iron and aluminum are present in phosphate rocks (about 2 to 6 g/L), so extraction systems with high U(VI)/Fe(III) selectivity are expected in order to reach specifications for uranium decontamination.

The extractant DEHCNPB (butyl-1-[*N*,*N*-bis(2-ethylhexyl)carbamoyl]nonyl phosphonic acid, structure Figure 1) was recently developed [4] and showed good performances for the extraction of

U(VI) from phosphate media with very high selectivity for U(VI) towards iron (about 30 times higher than with the mixture HDEHP/TOPO) [5, 6]. DEHCNPB is also considered as a suitable extractant for uranium recovery from conventional ores. The main difference in this latter perspective is that uranium should be extracted from a sulfuric medium (leaching solutions) [7]. In order to develop an efficient process to recover uranium from a sulfuric medium, there is a need for understanding and characterizing the different extraction mechanisms of uranium depending on the initial medium (phosphoric or sulfuric). Though the extraction of uranium from a phosphoric medium using DEHCNPB was extensively studied during the development of the process [8, 9], the extraction mechanisms of uranium are still misunderstood and there are few data published on the extraction of uranium from a sulfuric medium [10]. DEHCNPB is a cationic exchanger and the extraction mechanism should involve the exchange of two protons from the phosphonic acid function as depicted in the following equation:

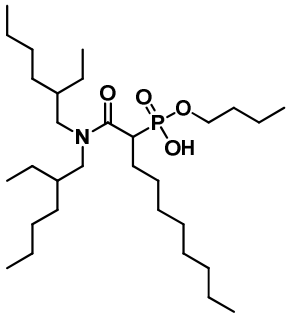

Figure 1. Molecular structure of DEHCNPB extractant.

$$UO_2^{2+} + n\overline{HL} \leftrightarrow \overline{UO_2L_2(HL)_{(n-2)}} + 2H^+ \qquad \text{n=2 to 3} \qquad (1)$$

Previous studies showed that this simple extraction mechanism is not sufficient to describe extraction of uranium from a phosphoric acid solution, especially at high uranium concentration range in the organic phase where polymetallic species should be taken into account [4]. Concerning the characterization of complexes formed in the organic phase, the participation of the amide function to the coordination in the first coordination sphere at high concentration of uranium was also considered [8]. In the present study, extraction data of uranium from both phosphoric and sulfuric media using DEHCNPB are reported and compared (slope analysis and extraction isotherms). Water extraction was also investigated and complexes formed in the organic phase were characterizes by ESI-MS to provide more understanding on the impact of the initial medium (phosphate or sulfate) on uranium extraction behavior.

2. Experimental

2.1. Materials and Sample preparation

Batch solvent extraction experiments were performed in order to study the influence of uranium and acid total concentrations on uranium distribution ratios. Organic phases were prepared by diluting DEHCNPB (synthesized by Pharmasynthese and purified by preparative chromatography, purity ~99 % determined by GC-FID) at 0.1 mol/L in hydrogenated tetrapropylene (TPH purchased from NOVASEP, France). The concentration of DEHCNPB in the organic phases was determined accurately by titration using sodium hydroxide 0.1 mol/L (AVS Titrinorm), in ethanol/water mixture (60/40%$_{v/v}$). Aqueous solutions of uranium phosphate were prepared from uranyl nitrate $UO_2(NO_3)_2$ (purchased from PROLABO) dissolved in water and precipitated into uranyl hydroxide by addition of sodium hydroxide. The isolated $UO_2(OH)_2$ precipitate was then washed three times with deionized

water and dissolved in 5 mol/L phosphoric acid (PROLABO). For sulfate solutions, uranium peroxide was dissolved in 0.6 mol/L sulfuric acid solution. Aqueous phases were then prepared by dilution of the concentrated uranium mother solution in sulfuric acid (PROLABO) and sodium sulfate (Sigma-Aldrich) solutions to adjust to pH=1 with a total concentration of sulfates equal to 1.6 mol/L (comparable with industrial leaching solutions).

2.2. Batch extraction experiments

For all extraction experiments, aqueous solutions were contacted until equilibrium was reached (20 min) at 25±1°C with equal volumes of organic phase (V_{aq} = V_{org}) by means of an automatic vortex shaker equipped with a thermostated cell. After phase separation by centrifugation, aqueous phases were diluted in 0.3 mol/L HNO_3 and organic phases in TPH. Uranium concentration was measured by ICP-AES (Perkin Elmer Optima 8300DV) in the initial and equilibrium aqueous phases. Selected wavelengths for uranium were 386, 367, 409, 393 and 424 nm. Scandium was introduced in all diluted samples as an internal standard at 5 mg/L. Aqueous phases containing low uranium concentrations (below 1 ppm) were analyzed by ICP-MS (Perkin Elmer Q-ICP-MS Elan DRCe). Organic phases at equilibrium were analyzed by the same ICP-AES instrument after dilution in TPH, using a parallel path micronebulizer (Burgener MiraMist) for sample introduction into the plasma torch. Total concentrations of phosphoric acid in aqueous phases were determined by potentiometric titration using NaOH, and pH was measured at equilibrium for all extraction tests from sulfate solutions. The H_2O content in organic phases was determined by Karl-Fischer titrations.

2.3. Characterization of complexes in the organic phase

Mass spectra of organic phases were acquired after dilution (100 fold) in methanol using Bruker micrOTOF-QII equipped with an electrospray ionization source and a time-of-flight analyzer.

3. Results and Discussion

3.1. Extraction experiments

3.1.1 Uranium extraction isotherms

Uranium extraction isotherm from a phosphoric medium was acquired during a previous study [4] by increasing the concentration of uranium (from 1 mmol/L up to 0.55 mol/L) in the initial solution of phosphoric acid 5 mol/L. These data are compared in Figure 2 with uranium extraction isotherm from a sulfuric medium ($C_{(SO4)2-}$= 1.6 mol/L, pH= 1) established in the present work. Uranium extraction isotherms show different behaviors depending on the aqueous medium. The saturation of the organic phase is obtained when 0.056 mol/L of uranium is extracted from a phosphoric medium ($C_{DEHCNPB}/C_U^{org}$ = 1.8). Whereas, the maximum uranium concentration loaded in the organic phase is 0.045 mol/L ($C_{DEHCNPB}/C_U^{org}$ = 2.2) when extracted from a sulfuric medium. In both cases, this lower ratio at saturation suggests that new complexes are formed with around two molecules of DEHCNPB for the extraction of one uranyl cation. As mentioned in our previous study [4], it is necessary to take into account the formation of bimetallic species $\overline{(UO_2)_2L_4}$ to better model extraction isotherm saturation from the phosphoric medium. The shape of the extraction isotherm suggests that the saturation of the organic phase is not reached in the sulfuric experiment, but it was difficult to prepare more concentrated solutions of uranium in sulfates. In addition, the

extraction isotherms do not show the same behavior between 0.03 mol/L and 0.05 mol/L of uranium in the organic phase. In fact, the isotherm acquired from a sulfuric medium takes shape of a Langmuir isotherm, while the one acquired from a phosphoric medium shows a more complex behavior. Since the complexation effect is more important in the phosphate medium compared with the sulfate, the saturation of the organic phase should be reached faster when increasing the concentration of uranium in the initial aqueous phase, which is not the case. Those results suggests that different extraction mechanisms should take place depending on the initial medium. Nevertheless, no phosphate or sulfate was observed to be co-extracted with uranyl cation. Extraction of phosphoric acid in the organic phase was investigated by means of ^{31}P-NMR measurements, showing that phosphoric acid is not involved in the extraction mechanism of uranium [10]. For sulfates, direct measurements of sulfur in loaded organic phases were investigated by ICP-AES and showed no significant signal for sulfur. Additional data are then required to better understand differences in extraction mechanisms.

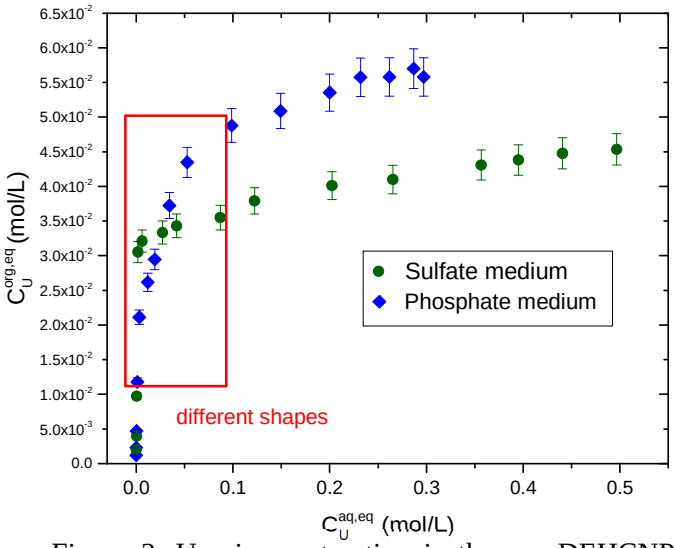

Figure 2. Uranium extraction isotherms. DEHCNPB 0.1 mol/L in TPH. Phosphate medium: $[H_3PO_4]$= 5 mol/L ; sulfate medium: $C_{(SO4)2-}$ = 1.6 mol/L ; pH= 1; O/A= 1 ; T= 25 °C.

3.1.2 Influence of DEHCNPB concentration on uranium(VI) extraction

The influence of DEHCNPB concentration on uranium(VI) extraction from a phosphoric medium was already reported in a previous study [10]. Those data are reported in Figure 3 and compared with the same experiment performed from a sulfuric medium. The determination of free extractant concentration in the organic phase using ^{31}P-NMR was performed as described before.[10] The average stoichiometry of the complexes formed in the organic phase was estimated using slope analysis. Activity coefficients and speciation in the aqueous phase were calculated using a dedicated Scilab program. Based on the general extraction mechanism (Equation 1), the extraction constant can be defined by equation (2):

$$K_{ex} = \frac{[\overline{UO_2L_2(HL)_{(n-2)}}].[H^+]^2}{[UO_2{}^{2+}].[\overline{HL}]^n} \cdot \frac{\gamma(\overline{UO_2L_2(HL)_{(n-2)}}).\gamma(H^+)^2}{\gamma(UO_2^{2+}).\gamma(\overline{HL})^n} \quad (2)$$

While the distribution ratio of uranium can be expressed as follows:

$$D_U = \frac{C_U^{org}}{C_U^{aq}} = \frac{[\overline{UO_2L_2(HL)_{(n-2)}}]}{[UO_2^{2+}](1+\sum_i [A^{z-}]^{\nu}.\beta_i)} \quad (3)$$

In those equations, γ_I is the activity coefficient of species I, A is the anion participating in the formation

of aqueous complex i, z its charge, υ its stoichiometric coefficient, and β_i the formation constant of complex i. Activity coefficients in the organic phase are supposed to be equal to unity. By combining equations (2) and (3), the following relationship may be proposed:

$$K_{ex}^{app} = \frac{D_U.[H^+]^2.(1+\sum_i [A^{z-}]^{\upsilon}.\beta_i)}{[\overline{HL}]^n} \frac{\gamma(H^+)^2}{\gamma(UO_2^{2+})} \quad (4)$$

$$\log(D_U) \underbrace{- 2.pH + \log(1+\sum_i [A^{z-}]^{\upsilon}.\beta_i) + 2.\log\gamma(H^+) - \log\gamma(UO_2^{2+})}_{X} = n.\log([\overline{HL}]_{free}) + \log(K_{ex}^{app}) \quad (5)$$

In equation (5), n is the average stoichiometric coefficient of DEHCNPB and can be measured as the slope obtained when plotting $\log(D_U) + X$ as a function of $\log[\overline{HL}]_{free}$ as shown in Figure 3. For the extraction of uranium from a phosphoric medium, the slope analysis shows a linear behavior with a slope of 1.9, which indicates the formation of a 1:2 complex between the ligand and the uranyl cation. Concerning the extraction of uranium from a sulfuric medium, a slope of 3.3 is obtained. This observation would suggest the extraction of uranium by three molecules of DEHCNPB in average (or three dimers). As this stoichiometric coefficient is not an integer, uranium may be extracted from a sulfuric medium according to a complex mechanism, involving the formation of multiple complexes in the organic phase. However, this average stoichiometry shows that more DEHCNPB molecules are required to extract uranium from a sulfuric medium compared to phosphoric acid, and thus different mechanisms could be involved depending on the initial medium. Slope analysis is also consistent with uranium extraction isotherms, showing that a higher [DEHCNPB]/[U] ratio is reached at saturation when uranium is extracted from a sulfate medium.

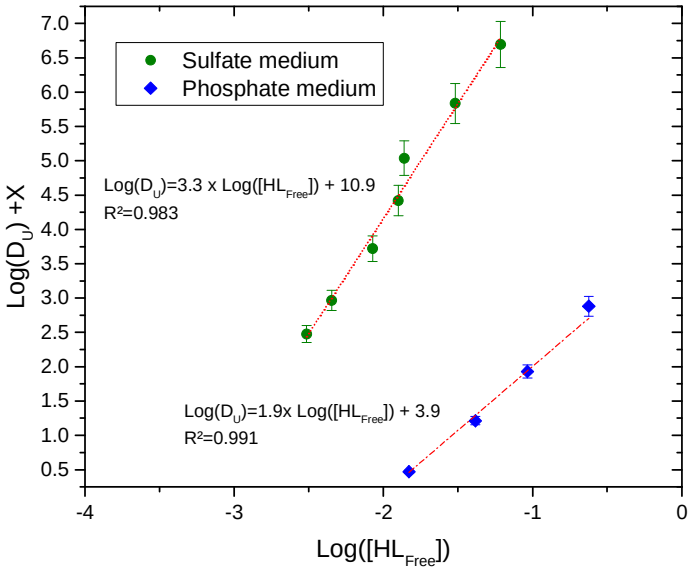

Figure 3. Slope analysis: $\log(D_U) + X$ as a function of free DEHCNPB concentration logarithm. Phosphate medium: C_U= 1.2 g/L; $[H_3PO_4]$= 5 mol/L; sulfate medium: C_U= 1.0 g/L; $C_{(SO4)2-}$= 1.6 mol/L; $pH_{initial}$ =1; O/A=1; T=25 °C.

3.1.3 Extraction of water

The content of water extracted in the organic phase as a function of uranium concentration was determined starting from a solution of phosphoric acid 5 mol/L or a solution of sulfates (1.6 mol/L at pH=1) and results are reported in Figure 4. The quantity of water extracted increases when uranium

content loaded in the organic phase gets higher. This observation suggests that there is some water co-extracted in the organic phase with uranium. This tendency is observed for both media. The ratio of water over uranium content in the organic phase tend to 1, which means that around one molecule of water is co-extracted with one uranyl cation. Species like $\overline{UO_2(H_2O)L_2(HL)_{2n-2}}$ could be formed in both cases. But in the case of uranium extraction from phosphoric acid, a maximum is reached (53 mM of water for 40 mmol/L of uranium) before decreasing at higher concentration of uranium. This behavior would suggest that a non-hydrated complex appears when the organic phase is saturated. This is also an additional indication showing that different extraction mechanisms are involved when uranium is extracted from a phosphoric medium, with different hydration of extracted complexes when the concentration of uranium reaches saturation.

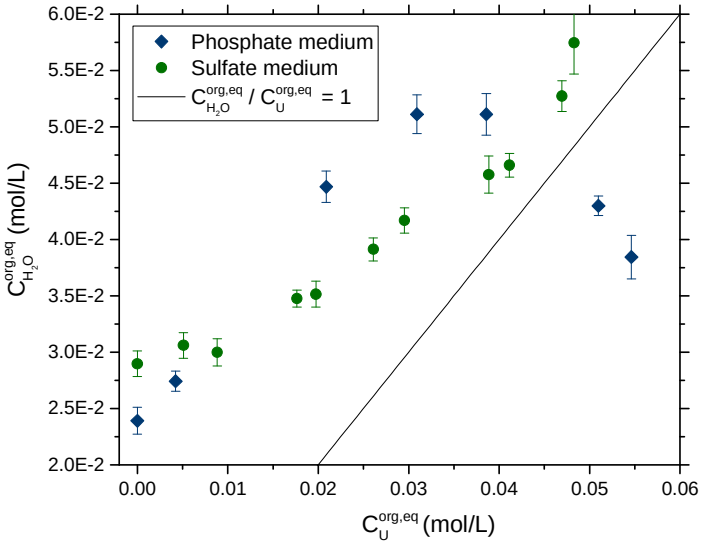

Figure 4. Evolution of water content in organic phases as a function of uranium concentration. Phosphate medium: $[H_3PO_4]$= 5 mol/L; sulfate medium: $C_{(SO4)2-}$= 1.6 mol/L; $pH_{initial}$ = 1; O/A=1; T=25 °C.

3.2. Characterization of uranium complexes in the organic phase by ESI-MS

Electrospray ionization (ESI) is a soft ionization technique that allows the transfer of pre-existing ions from the solution into the gas phase so that speciation information in solution can be obtained. This technique has been used successfully to characterize metal-ligand complexes in solution involving liquid-liquid extraction systems containing uranyl cation [11, 12]. Loaded organic phases of DEHCNPB 0.1M in TPH were analyzed by ESI-MS after dilution in methanol to characterize species formed after extraction of uranium from both media ($[H_3PO_4]$= 5 mol/L and $C_{(SO4)2-}$= 1.6 mol/L at pH=1). In the phosphoric medium experiment, almost all the DEHCNPB ions detected contain uranium and only one ion of protonated DEHCNPB $[HL.H]^+$ remains (L corresponding to the deprotonated form of DEHCNPB). Whereas in the sulfuric medium experiment, the most abundant ions correspond to Na^+ adducts such as $[HL.Na]^+$, $[(HL)_2.Na]^+$ and $[(HL)_3.Na]^+$. The aqueous phase is prepared from sodium sulfate whereas the phosphoric solution is only made of phosphoric acid explaining why higher amounts of sodium could be present in the sulfate experiment. Monometallic species where observed in the phosphate medium extraction: $[(HL)_2.UO_2]^{2+}$ and $[HL.L.UO_2]^+$ and $[L.UO_2.H_2O.CH_3OH]^+$. The most intense species is $[L.UO_2.H_2O.CH_3OH]^+$ containing one molecule of water and one molecule of methanol. This observation confirms the potential participation of water to the complexes formed in the organic phase. Moreover, the fragmentation of this ions has been performed, and leads to $[L.UO_2.H_2O.]^+$ and $[L.UO_2.(H_2O)_2.]^+$ respectively with the loss of a methanol molecule and with the exchange of a methanol molecule with a water molecule remaining in the gas

phase. Water was also found in the $[L_2.(UO_2)_2.(H_2O)_2.]^{2+}$ bimetallic species. The formation of $[L.UO_2.H_2O.CH_3OH]^+$ is also observed in the sulfuric medium experiment but with a lower intensity. Those results consolidate the hypothesis that some water is co-extracted with uranium and is strongly bound to uranyl (potentially in the first coordination sphere) since no loss of water molecule was observed during fragmentation experiments. Many polymetallic species could be observed in the phosphoric experiment ($[L_2.(UO_2)_2.(H_2O)_2.]^{2+}$, $[HL.L_2(UO_2)_2]^{2+}$, $[L_4.(UO_2)_3]^{2+}$, $[HL.L_4.(UO_2)_3]^{2+}$ and $[(HL)_2.L_4.(UO_2)_2]^{2+}$), which confirm the hypothesis proposed before to model the behavior of uranium extraction isotherm at saturation.[4] Two polymetallic species could also be observed in the sulfate experiment: $[(HL)_2.L_3.(UO_2)_2.Na]_2^+$ and $[(HL).L_5.(UO_2)_3.Na]^{2+}$. Other uranyl species were detected in the sulfate experiment with sodium like $[(HL)_2UO_2Na_2]^{2+}$, $[(HL)_2.L_2.UO_2.Na_2]^{2+}$ and $[HL.L_2UO_2Na]^+$ with only one uranyl center. Those ESI-MS experiments confirm the possible formation of hydrated uranyl complexes and bimetallic species at high concentration of uranium in the organic phase after extraction from a phosphoric and sulfuric media. Those species are less intense in the case of sulfuric medium but it might be due to a lower concentration of uranium in the organic sample (lower saturation of the extractant) and the presence of sodium, which might interfere in the response factor of species formed during ionization in the gas phase.

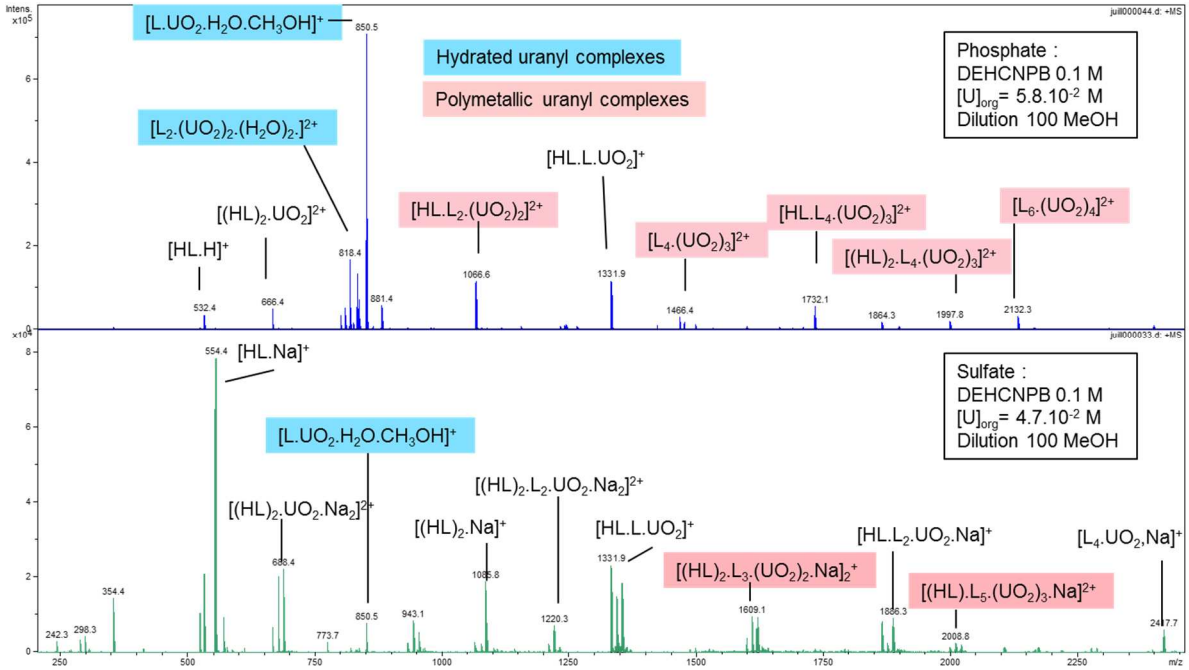

Figure 5. ESI-MS spectra of loaded organic phases (0.1 mol/L DEHCNPB in TPH, HL=DEHCNPB) with uranium after dilution 100 in methanol. Phosphoric medium: C_U^{ini} = 75 g/L ; $[H_3PO_4]$= 5 mol/L; sulfate medium : C_U^{ini} = 135 g/L; $C_{(SO4)2-}$= 1.6 mol/L; $pH_{initial}$ = 1; O/A= 1; T = 25 °C.

4. Conclusion

Uranium extraction isotherms acquired with the solvent DEHCNPB 0.1 mol in TPH from phosphoric acid 5 mol/L or sulfate medium (1.6 g/L of sulfates at pH=1) showed different behaviors. A higher saturation of the extractant DEHCNPB could be reached starting from the phosphoric acid

solution with a [DEHCNPB]/[U] ratio of 1.8 instead of 2.2 for the sulfuric experiment. Since the complexation effect is more important in the phosphate medium, this result highlights different extraction mechanisms depending on the initial medium. No evidence could be found for phosphate or sulfate counter anions co-extraction with uranyl (the extraction mechanism should then rely exclusively on a cation exchange mechanism). Slope analysis showed different average stoichiometries: 1.9 and 3.3 for the phosphate and sulfate experiments respectively, which is consistent with the lower [DEHCNPB]/[U] ratio reached in the uranium isotherm experiment from phosphoric acid. Karl-Fischer measurements showed that some water molecules are co-extracted with uranyl cation and that the uranyl/water ratio is close to one at saturation. But with phosphates, the behavior is different at saturation and the water content decreases when C_U^{org} > 40 mmol/L. Finally, ESI-MS measurements confirmed the presence of complexes with one molecule of water per uranyl cation in the loaded organic phases.

Acknowledgement

This work is financially supported by AREVA Mines. The authors are grateful to Claude Berthon for NMR measurements.

References

1) S. Gabriel, A. Baschwitz, G. Mathonnière, T. Eleouet, F. Fizaine, *Ann. Nucl. Energy,* **58**, 213-220 (2013).

2) D. Beltrami, G. Cote, H. Mokhtari, B. Courtaud, B.A. Moyer, A. Chagnes, *Chem. Rev.,* **114**, 12002-12023 (2014).

3) F.J. Hurst, D.J. Crouse, K.B. Brown, *Ind. Eng. Chem. Process Des. Dev.,* **11**, 122-128 (1972).

4) M. Miguirditchian, G. Bernier, V. Pacary, C. Balaguer, C. Sorel, R. Berlemont, B. Fries, M. Bertrand, B. Camès, A. Leydier, R. Turgis, G. Arrachart, S. Pellet-Rostaing, H. Mokhtari, *Solvent Ext. Ion Exch.,* **34**, 274-289 (2016).

5) M. Miguirditchian, G. Bernier, C. Balaguer, X. Hérès, V. Pacary, M. Bertrand, B. Camès, H. Mokhtari, *Proceedings ISEC 2014,* (2014).

6) G. Arrachart, N. Aychet, G. Bernier, F. Burdet, A. Leydier, M. Miguirditchian, S. Pellet-Rostaing, G. Planque, R. Turgis, E. Zekri, *Patent,* WO2013EP59352 20130506 (2013).

7) P. Baron, G. Bernier, D. Hartmann, C. Laluc, M. Marbet, *Patent,* WO2014139869 A2014139861 (2013).

8) O. Pecheur, D. Guillaumont, S. Dourdain, L. Berthon, R. Turgis, C. Fillaux, G. Arrachart, F. Testard, *Solvent Ext. Ion Exch.,* **34**, 260-273 (2016).

9) R. Turgis, A. Leydier, G. Arrachart, F. Burdet, S. Dourdain, G. Bernier, M. Miguirditchian, S. Pellet-Rostaing, *Solvent Ext. Ion Exch.,* **32**, 685-702 (2014).

10) B. Fries, C. Marie, V. Pacary, C. Berthon, M. Miguirditchian, H. Mokhtari, M.C. Charbonnel, *Procedia Chem.,* **21**, 93-100 (2016).

11) L.W. McDonald, J.A. Campbell, T. Vercouter, S.B. Clark, *Anal. Chem.,* **88**, 2614-2621 (2016).

12) F. Rodrigues, G. Ferru, L. Berthon, N. Boubals, P. Guilbaud, C. Sorel, O. Diat, P. Bauduin, J.P. Simonin, J.P. Morel, N. Morel-Desrosiers, M.C. Charbonnel, *Mol. Phys.,* **112**, 1362-1374 (2014).

Lithium Solvent Extraction (LiSX™) Process Evaluation using Tenova Pulsed Columns (TPC)

Jonathan LIPP[1,*]

[1]*Tenova Advanced Technologies Ltd., Yokneam, Israel*

Conventional lithium recovery relies almost solely on solar evaporation technology. As lithium prices have exploded in the last couple of years and as this old technology suffers from several drawbacks, the search for a new technology is on. Solvent extraction (SX) bears high promise to be a superior alternative.

Although SX is widely used in mineral processing, SX for lithium was not available until recently. This new process was evaluated in recent years over lab scale tests and its applicability was demonstrated. However, a larger scale evaluation has to be performed if this technology is to be adopted as the chosen alternative for lithium recovery.

It was therefore, the objective of this work, to evaluate the performance of the lithium solvent extraction (LiSX™) process on a larger scale, using Tenova Pulsed Columns (TPC) with a cross section diameter of 40 mm and 100 mm. The results showed that although high pH is required to facilitate the extraction stage, complete lithium recovery is achievable even for neutral raffinate pH. Scrubbing indicated that practically all alkali metal impurity is removed from the loaded solvent, and the striping stage demonstrated the ability of the process to produce saturate lithium salt solution. Overall the LiSX™ process demonstrated its ability to extract, purify and saturate lithium, showing its attractiveness as the new generation lithium recovery process.

1. Introduction

Electric cars are expected to become ever more popular in the coming years [1]. As the key component in its battery is lithium, lithium production is gaining ever increasing interest. Old-school production is based on a series of evaporation ponds with residence time of roughly 18 month [2]. In addition to that, low lithium recovery is but another drawback that this conventional technology has [3].

These drawbacks have initiated a worldwide search for an alternative technology. Although solvent extraction is commonly used in hydrometallurgical processes, it was not considered as an alternative until recently. This new emerging solvent extraction process for the recovery of lithium, LiSX™, was tested on a laboratory scale [4]. The results of the laboratory scale showed that the proprietary Tenova Advanced Technologies (TAT) solvent has a maximum loading capacity of 1.75 g/L lithium (0.25 M). It was also indicated that, the process should be executed in aqueous continuity and that practically 100% of the lithium is recovered when extraction is carried out at pH=12. Stripping was indicated to remove all lithium from the loaded solvent (LS) even at pH=7.

Although promising, these test results required to be validated on a larger scale testing if this technology is to be implemented on a commercial scale. It is therefore the objective of this paper to

further the evaluation of this process, and to elucidate the performance of the LiSX™ using small scale industrial equipment – Tenova Pulsed Columns (TPC), in the production of a saturated and pure Li_2SO_4 solution.

2. Experimental

2.1 Reagents

All chemical used in the line of the current work (reagent grade) were used as received. Both aqueous and organic solutions used were synthetically prepared. The aqueous feed solution was synthesized to imitate the expected composition fed to the LiSX™ process when operating with a typical South American lithium solution. As these brines normally contain alkaline earth elements, which are preferably extracted, the synthesized solution was prepared without these elements. In the commercial process this elimination is achieved by an upstream TAT process (LiP™). Feed composition is displayed in Table 1 below.

Table 1 – Aqueous Feed Stream composition

Element	Li	Na	K	B	Cl	S.G.
Units	mg/L	g/L	g/L	mg/L	g/L	
Value	720	115	8.4	500	195	1.235

2.2 Analysis

Analyses of Li, Na, K and B were performed using ICP or Atomic Absorption (AA), while titration was used for Cl^- determination. As a rule, high concentrations of a metal interfere with the determination of other metals that are present in very low concentrations. Therefore, standard solutions were used. These solutions contained a background of the ion present in high concentration in order to determine the ions present in low concentrations. For example, in the case of low lithium concentrations in the presence of high sodium concentrations (mainly for the determination of Li in the aqueous phase) analyses were performed by using standard solutions of Li containing similar Na concentrations to the concentrations in the diluted samples. The lowest concentration of Li that can be determined in this manner is 3 mg/L. In a similar way, low concentrations of other elements were quantified. It should be noted that the analytical accuracy of this method is ±10%. Organic solutions were stripped quantitatively using nitric acid solutions and the resulting aqueous solutions were analyzed. The concentrations in the organic solutions were calculated using the phase ratio in the stripping.

2.3 Hydraulic Test

Hydraulic tests, for all stages of the process, were conducted in counter current using a TPC with 100 mm cross-section diameter – having a total active section height of 7 m (PVDF disk-and-doughnut internals 7 X 90 cm PVDF sections separated by 10 cm glass sections), glass decanters with a diameter of 150 mm (top) and 110 mm (bottom). A mechanical pulsator (piston from PTFE) 120 mm in diameter, pulsating in a frequency of 1 Hz, was used to deliver pulsation to the column. All streams were pumped to the column using VFD controlled FMI (metering) or Peristaltic pumps. Pulsation intensity (PI – the product of the frequency and pulse amplitude) and flux were

changed in order to determine the optimal operating parameters. Holdup (the fraction of dispersed phase in the total volume) values were monitored by periodically sampling in order to ascertain the optimal flux and pulsation intensity. For each of the solvent extraction stages (Extraction, Scrubbing and stripping) the test focused on the more challenging side of the column. Hence, for the extraction stage LS was tested with the feed brine (expected conditions at the upper part of the extraction column); for the scrubbing stage LS versus spent scrub solution (expected conditions at the lower part of the scrubbing column) were evaluated and for the stripping stage the purified solvent was tested with the Li_2SO_4 product stream (expected conditions at the lower part of the stripping column).

2.4 Mass Transfer Test

Mass transfer tests, for all stages of the process, were conducted in counter current using a TPC having a 40 mm cross-section diameter – and a total active section height of 7 m (PVDF disk-and-doughnut internals, glass sections), and top and bottom glass decanters having 80 mm in cross-section diameter. A mechanical pulsator (piston of PTFE) with a cross-section diameter of 69 mm, pulsating in a frequency of 1 Hz, was used to deliver pulsation to the column. All streams were pumped to the column using VFD controlled FMI (metering) or Peristaltic pumps. For all tests organic and aqueous samples were periodically collected and analyzed.

For the extraction stage, the lithium feed concentration is 720 mg/L, which sets the extraction organic to aqueous ratio (O:A) at 0.41 (calculated as lithium feed concentration divided by maximum lithium level in the LS). This ratio was maintained throughout the test work. As was previously reported [4] basic pH is required in order to facilitate the extraction process. Therefore, NaOH was added to the feed solution, resulting in feed brine pH of 12.5. In the scrubbing stage 0.73% H_2SO_4 solution was used to scrub the LS. Tests were conducted at O:A=10. While in the stripping stage, the purified solvent (PS) was stripped using a solution containing 61.25 g/L of H_2SO_4 and 246 g/L of Li_2SO_4 at O:A=5.

3. Results and Discussion

3.1 Hydraulic Tests

Extraction hydraulic test were conducted for fluxes raging 10-45 $m^3/m^2/h$. At a flux of 40 $m^3/m^2/h$, or grater, column operation proved to be unstable and flooding was observed regardless of the pulsation intensity (PI) used. The maximal flux which permitted continuous operation without flooding was 35 $m^3/m^2/h$ with a pulsation amplitude of 4mm, which corresponds to column PI=350 mm/min. At these conditions holdup values along the column were between 15-20%.

Scrubbing hydraulics was tested for flux values of 5-20 $m^3/m^2/h$. Flooding was observed at flux of 15 $m^3/m^2/h$ and above at any PI. Maximal flux that enabled continuous operation was 12.5 $m^3/m^2/h$ with an amplitude of 3mm, which corresponds to PI=260 mm/min. At these conditions holdup values along the column were between 25-30%.

Stripping hydraulics was tested for flux values of 5-30 $m^3/m^2/h$. At fluxes above 25 $m^3/m^2/h$, the column was flooded, indicating that the maximal flux that enables continuous operation is 25 $m^3/m^2/h$ with a pulsation amplitude of 3mm, which corresponds to column PI=260 mm/min. At these conditions holdup values along the column were between 25-30%.

3.2 Mass Transfer Tests

Similarly to other metal extraction process, lithium extraction is a chemical process. Thus, solvent deprotonation, achieved by basic pH at the feed brine, facilitates lithium extraction. This process, eliminate proton from the extracting agent and creates an active area on the solvent capable of chemically bonding with the lithium ions from the brine. The extraction profile is display in Table 2 and in Figure 1. As can be seen, near the organic entrance (at the lower section) to the column, the lithium content of the aqueous phase is minimal. In this area the solvent is being loaded with all other impurities, especially sodium. As the solvent flows up the column, lithium replaces those impurities, thus loading the solvent with lithium and removing co-extracted impurities at the same time. The solvent leaving the column is at maximum loading level regarding lithium and minimal loading with regards to other impurities. Those impurities will need, in any case, to be scrubbed out if purified lithium is to be produced.

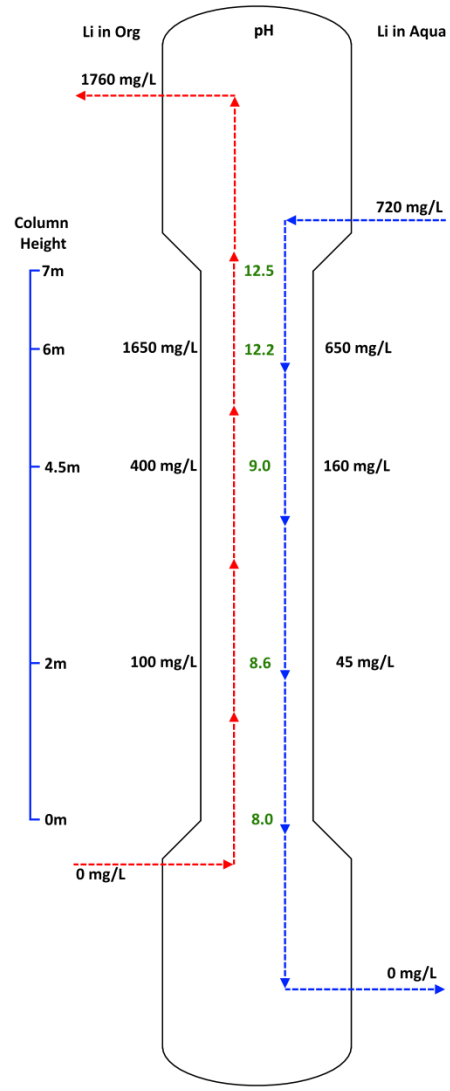

Figure 1 – Extraction Column Profile

Due to the extraction mechanism, a pH profile develops in the column. As protons are released from the organic into the aqueous phase the pH is reduced along the column until the raffinate

leaves the column at practically neutral pH. This column pH profile is achieved by an optimal addition of NaOH. Excessive addition would result in higher pH level in the raffinate, whereas the outcome of inadequate addition will be incomplete lithium extraction due to insufficient active extraction sites on the solvent, and subsequently lithium loses to the raffinate.

As lithium concentration in the raffinate is driven below the detection limit, these results indicate that lithium was completely extracted from the feed. Moreover, the lithium purity, from feed brine to loaded solvent, was increase from roughly 0.6% to 92% on metal base, or from ca. 1.4% to 92% on either LiCl or Li_2SO_4 basis, which further highlights the advantages the solvent extraction process bears for lithium production.

Table 2 – Extraction Column Profile

Height	Stream	Li	Na	K	B	Cl	pH
m		mg/L	mg/L	mg/L	mg/L	mg/L	
7	LS	1760	365	23	<3	<3	12.5
	Feed	720	115000	8400	500	195000	
6	Org	1650	455	37	15	<3	12.2
	Aqu	650	110000	8200	490	190000	
4.5	Org	400	2885	45	23	25	9.0
	Aqu	160	108000	8300	510	195000	
2	Org	100	5630	70	64	60	8.6
	Aqu	45	105000	8000	500	195000	
0	BS	<3	<3	<3	<3	<3	8.0
	Raff	<3	109000	8300	500	200000	

The scrubbing process is aimed at removing the co-extracted impurities and producing highly pure lithium solution. This is achieved by partial stripping of the solvent. As the objective is to maximize the impurity levels in the spent scrub solution while minimizing its lithium content the exact acid concentration in the scrub solution is determined to allow pH=12 in the spent scrub. In this pH the lithium levels at the spent scrub solution are assumed to be minimal and as, in the industrial plant, this solution will be fed back to the extraction stage, this level would not increase the caustic demand.

As sodium is the major impurity, acid consumption is based solely on its concentration. In this process, each proton triggers the scrubbing of one sodium ion. pH=12 will be reached if sodium ions are in excess of 0.01 M over H^+ ions, which will induce proton elimination from the water resulting in a solution with OH^- concentration of 0.01 M.

The acid used in this stage will be the same acid used in the stripping stage in order to minimize the final product contamination. Therefore, H_2SO_4 was used as scrubbing acid. As the scrub solution is expected to be weak acidic one a specific gravity of 1 is assumed and O:A=10 is being taken into account in calculating the required acid concentration:

$$[\%H_2SO_4] = \frac{M_{W_{H_2SO_4}}\frac{g}{mol}}{2} \times \left(\frac{\left[Na_{org}\right]\frac{g}{l}}{M_{W_{Na}}\frac{g}{mol}} \times O{:}A - 0.01\frac{mol}{l} \right) \times 0.1\frac{l}{100gr}$$

Where $[\%H_2SO_4]$ is the acid concentration in the scrub solution, $M_{W_{H_2SO_4}}$ is the molecular

weight of the sulfuric acid, $[Na_{org}]$ is the sodium concentration in the LS, and $M_{w_{Na}}$ is the molecular weight of sodium. Calculating the required acid concentration for this case gives:

$$[\%H_2SO_4] = \frac{98\,\frac{g}{mol}}{2} \times \left(\frac{0.365\,\frac{g}{l}}{23\,\frac{g}{mol}} \times 10 - 0.01\,\frac{mol}{l}\right) \times 0.1\,\frac{l}{100gr} = 0.73\%$$

The results of the scrubbing test is displayed in Table 3, as can easily been seen all the impurities were successfully scrubbed out of the solvent resulting in PS containing practically only lithium. Additionally, lithium concentration in the spent scrub was indeed minimal. Nevertheless, there will be no lithium losses in the industrial scale, as this solution will be fed back to the extraction stage. The PS purity is adequate to allow for solvent stripping and production of the purified lithium solution.

Table 3 – Scrubbing results

Stream	Li	Na	K	B	Cl	pH
	mg/L	mg/L	mg/L	mg/L	mg/L	
LS	1760	365	23	<3	<3	
PS	1730	<3	<3	<3	<3	
Spent Scrub	250	3850	250	10	15	11.5

Similarly to scrubbing the stripping is a chemical neutralization reaction, where one proton is required to strip one lithium ion. The concentration of the strip solution is then derived from the designed O:A ratio, which is set on 5. This ratio is set in order to facilitate better phase dispersion in the column, and minimize axial mixing that would otherwise (in higher ratios) dominate column operation and may hinder lithium stripping. Thus, the required H_2SO_4 concentration is calculate as the product of O:A and lithium concentration in the PS (taken as 0.25 M), resulting in acid concentration of 1.25 N (0.625 M). In order to limit the demand for process water consumption, in the industrial plant, and to produce 40 g/L lithium solution (Li_2SO_4 solubility limit), part of the product stream is cycled back to the stripping and mixed with 98% H_2SO_4. Therefore the strip solution concentration is 61.25 g/L of H_2SO_4 and 246 g/L of Li_2SO_4. As the stripping process requires only one stage this mixing procedure bares no impact on the overall process.

The results of the stripping stage are shown in Table 4. As can be seen the target lithium concentration was achieved, and the product solution has a neutral pH which indicates complete proton consumption by the solvent from the aqueous solution. Impurity levels are minute and indicate lithium purity of 99.97% on metal base and 99.99% on Li_2SO_4 basis. This purity level significantly exceeds the 99.5% that is considered battery grade, and serves as an additional indication of the ability of the LiSX™ process to become the next generation technology for the production and recovery of lithium.

Table 4 – LiSX™ product composition

Li	Na	K	B	Cl	pH
g/L	mg/L	mg/L	mg/L	mg/L	
39.5	7	5	<3	<3	7.4

4. Conclusion

Lithium recovery via solvent extraction using TPC was evaluated. The solvent was shown to selectively extract the lithium where lithium purity of 0.6 (on metal basis) in the feed brine was elevated to 92% in the loaded solvent, with essentially obtaining 100% lithium recovery. Column pH profile revealed that although the feed brine entering the extraction stage is extremely basic (12.5) raffinate pH is practically neutral.

As some co-extraction takes place, scrubbing of alkali metals and other non-metallic impurities is required. 0.73% H_2SO_4 solution was used to scrub the loaded solvent. Virtually all impurities where scrubbed out were minimal lithium concentration was detected in the spent scrub solution. As this solution will be cycled to the extraction stage these lithium levels will not contribute to any lithium loses. The stripping of the purified solvent has produced saturated (40 g/L) and pure (99.97% on metal base) lithium sulfate solution.

The results presented in this paper indicate that the solvent extraction process outperforms the traditional solar evaporation technology. The current study continues to underline the validity of the LiSX™ process as an attractive alternative to the existing lithium production technology.

References

1) R. Baylis, *9th Lithium Supply & Markets Conference* (2017).
2) L. T. Peiro, G. V. Mendez, R. U. Ayres, *JOM*, **65(8)** 8, 986–996 (2013).
3) W. Tahil, *Meridian International Research*, 1-22 (2007)
4) J. Lipp, *proceedings of the International Solvent Extraction Conference – ISEC2014*, 338-343 (2014).

Slug Flow Extraction and Separation of Nickel and Cobalt with D2EHPA

Mikiya HINOUE[1], Hayato TOKUMOTO[1], Akira MATSUOKA[2], Koji NOSHIKI[3] and Akinori MUTO[1*]

[1]Graduate School of Engineering, Osaka Prefecture University, Sakai, Osaka, Japan; [2]Chemical & Environmental Technology Research Section, Kobe Steel, Ltd., Kobe, Hyogo, Japan; [3]Engineering Section, Kobe Steel, Ltd., Kobe, Hyogo, Japan

Slug flow is one of the typical flow patterns in microtube. The slug flow provides high mass transport due to the internal circulation within each segment. Additionally, it can precisely control the contact time between two phases. In this study, the slug flow was applied and discussed for the extraction and separation of Ni^{2+} and Co^{2+} from an aqueous solution into a cyclohexane phase, which contained di-(2-ethylhexyl) phosphoric acid (D2EHPA) as an extraction reagent. The extraction time of the maximum separation factor becomes longer with decreasing the flow velocity. These results suggest that the separation with high separation factor is available by adjusting of the extraction time.

1. Introduction

A liquid-liquid extraction process is widely used in the separation of rare metals, but conventional liquid–liquid extraction equipment (e.g., a continuous mixer–settler) tends to be quite large, as it requires a long time for phase separation after mixing the aqueous and organic solutions. In particular, the particle diameter of the dispersed phase has a large influence on the mass transfer rate. The dispersed phase coalesces and the particle size increases when it moves in the extraction column. In addition, the dispersed phase disperses axially as it travels through the extraction column. These phenomena reduce the mass transfer rate, and thus, design methods for such apparatus are complicated. This has led to increased interest in the use of slug flow (the alternating flow of two or more phases through a tube), [1-3] which offers a number of advantages in liquid–liquid extraction. Cobalt and nickel are important elements for charge/discharge devices such as lithium ion batteries [4], the demand for which has increased remarkably in recent years. This study explores the possibility of using slug flow to extract Cobalt and nickel ions (Co^{2+} and Ni^{2+}) from an aqueous solution into an organic phase consisting of cyclohexane with di-(2-ethylhexyl)phosphoric acid (D2EHPA) as an extraction reagent. This organic phase was selected because it is easily separated from the aqueous phase and has a high ability to extract alkaline metal ions [5].

2. Experimental

2.1 Reagents

Aqueous cobalt and/or nickel solutions were prepared by dissolving cobalt chloride (Wako Pure Chemical Industries Ltd. Japan) and / or nickel chloride (Wako Pure Chemical Industries Ltd. Japan) in deionized water. The organic phase was prepared by dissolving 40, 100 and 200 mM of D2EHPA (Tokyo Chemical Industries Ltd, Japan) was dissolved in cyclohexane as an organic solvent. Prior to be used, it was substituted H^+ of D2EHPA to Na^+ by adding 10 mM aqueous solution of sodium hydroxide (Wako Pure Chemical Industries Ltd. Japan).

2.2 Experimental apparatus and procedures

2.2.1 Batch extraction experiments

Equal volumes of the aqueous and organic solutions were poured into a snap-cap vial and agitated in at thermostatic batch at 25°C until equilibrated (more than 18 h). The concentrations of cobalt and Nickel in the aqueous phase were determined by atomic adsorption spectrophotometry and the pH of the aqueous phase was measured using a pH meter.

2.2.2 Continuous extraction experiments

Continuous extraction by slug flow was performed using the apparatus shown in Figure 1. Each solution was fed into the Y-junction at a constant total flow rate of 0.25 - 0.75 mL/min using a syringe pump and the two phases were then passed through the microtube. As the extraction time corresponds to the time needed for the liquids to flow from the Y-junction to the end of the microtube, the extraction times ere varied by simply adjusting the length of the microtube and flow rate. Continuous extraction experiment was conducted under same volume of the organic solution and the aqueous solution. All experiments were conducted three times using transparent polytetrafluoroethylene (PTFE) (i.d.: 1mm) microtube so that the flow pattern of liquid could be observed. The exhausted solution was collected in an 8-mm-diameter class receiver, which reduced the interface area between the aqueous and organic phases, causing them to instantly separate. As a preliminary experiment, the amount of extracted ions in the receiver was confirmed to be negligible when compared with the amount in the PTFE tube. After testing, the Co^{2+} and Ni^{2+} concentration in the exhausted aqueous phase was analyzed by atomic adsorption spectrophotometry. The details of the procedure are described elsewhere [6].

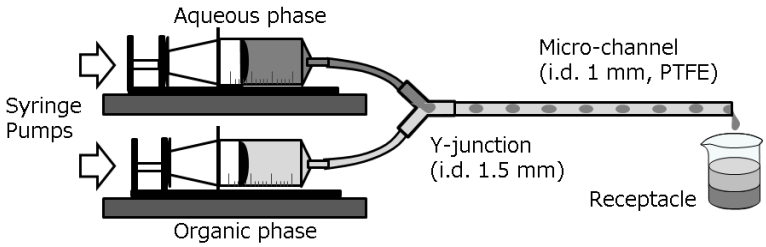

Figure 1 An illustration of continuous extraction experiment.

3. Results and Discussion

3.1 Distribution properties of Co^{2+} and Ni^{2+}

Distribution characteristics of Co^{2+} and Ni^{2+} in various concentrations of D2EHPA in cyclohexane were determined by batch experiments. Figure 2 shows the distribution characteristics of Co^{2+} and Ni^{2+} when D2EHPA concentrations are 40, 100 and 200 mM. The initial concentration of Co^{2+}

and Ni^{2+} in the aqueous phase was 1 mM, and an aqueous solution of a single component metal ion was dissolved in the experiment. As extraction progresses, H^+ of D2EHPA moves from the oil phase to the aqueous phase and the pH of the aqueous phase decreases. Here, a part of H^+ of D2EHPA was substituted in advance with Na^+ (0 to 60 mol%) before the experiment. Extraction rate *E* is defined as,

$$E = \frac{C_0 - C}{C_0} \quad (1)$$

Where *C* is metal concentration of the aqueous phase and C_0 is feed concentration. When the concentration of D2EHPA is high (200 mM), the distribution curves of Co^{2+} and Ni^{2+} show that the extraction rate increases as the pH of the aqueous phase is higher at pH 3.5-4.5. Co^{2+} is located on the side where pH is lower than Ni^{2+}. When the concentration of D2EHPA was 100 mM, the distribution curve of Ni^{2+} moved about 1 in the direction of higher pH. In D2EHPA showing high pH, that is, a high substitution rate of Na^+, the extraction rate became small and the maximum value was found. When the concentration of D2EHPA was 100 mM, the above tendency became remarkable. It was suggested that Co^{2+} can be selectively extracted at pH > 5. This indicates that highly selective extraction of Co^{2+} is possible by appropriately selecting the concentration of D2EHPA and the Na substitution rate of D2EHPA.

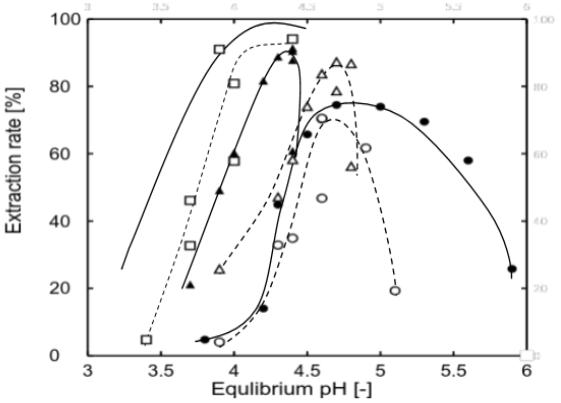

Figure 2 Distribution Curves of Co^{2+} and Ni^{2+}. Closed key; Co^{2+}, open key; Ni^{2+}. Concentrations of Co^{2+} and Ni^{2+} are 1.0 mM. Concentration of D2EHPA; circle is 40 mM, square is 20 mM, triangle is 100 mM.

Figure 3 shows the distribution curve by D2EHPA for a mixed solution of Co^{2+} and Ni^{2+}. As in the experiment Figure 2, a batch extraction experiment was conducted by replacing a part of H^+ in D2EHPA with Na^+. The concentration of D2EHPA was 200 mM, the concentrations of Co^{2+} and Ni^{2+} were 0.5 and 1.0 mM. When the metal ion concentration was more dilute, the distribution curve was shifted to the lower pH side. Therefore, the extraction rate of Co^{2+} was higher than that of Ni^{2+} at the same pH. Figure 4 shows the distribution curve of a mixed solution of Co^{2+} and Ni^{2+} when the concentration of D2EHPA is 40 mM. Ni^{2+} was

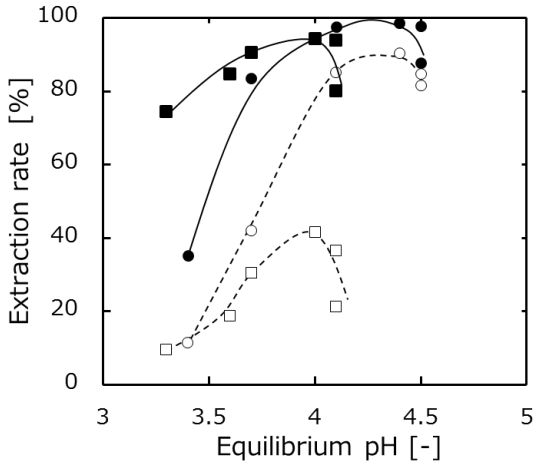

Figure 3 Distribution Curves of Co^{2+} and Ni^{2+}. Closed key; Co^{2+}, open key; Ni^{2+}. Concentrations of D2EHPA is 200 mM. Initial concentration of Co^{2+} and Ni^{2+}; circle is 0.5, mM, square is 1.0 mM.

scarcely extracted when pH < 4.3 and only Co^{2+} was selectively extracted.The continuous extraction experiments were carried out under the codition; D2EHPA concentarion was 40 mM, each concentarion of Co^{2+} and Ni^{2+} was 1.0 mM.

3.2 rate experiment

The overall volumetric mass transfer coefficient k_La is one of the parameters used to evaluate the extraction rate and can be obtained as follows. [7] First, the mass transfer rate N_A [mol/(L·s)] is determined using:

$$N_A = -\frac{dC}{dt} = -k_L a(C - C^*) \qquad (2)$$

where t is the extraction time [s] and C^* is the metal ion concentration [M] in the aqueous phase at extraction equilibrium. Integration of Eq. (2) gives:

$$-\ln(C - C^*) = k_L a t + A \qquad (3)$$

Substitution of Eq. (1) into Eq. (3) gives:

$$-\ln\left(1 - \frac{E}{E^*}\right) = k_L a\, t + A' \qquad (4)$$

where E^* are the extraction efficiencies at equilibrium.

$$E^* = \frac{C_0 - C^*}{C_0} \qquad (5)$$

A and A' are constants and C_0 is the feed concentration. As Eq. (5) shows that –ln (1 – E/E^*) is a linear function of extraction time t, experimental data for the extraction efficiency and extraction time were used to plot –ln(1 – E/E^*) against t. From the gradient of the linear plot, k_La was obtained.

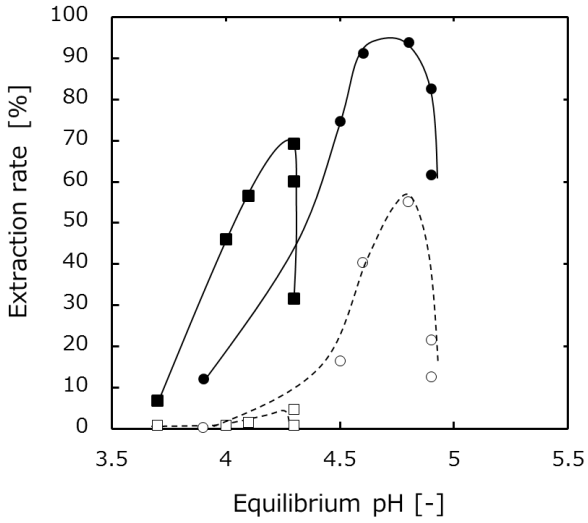

Figure 4 Distribution Curves of Co^{2+} and Ni^{2+}. Closed key; Co^{2+}, open key; Ni^{2+}. Concentrations of D2EHPA is 40 mM. Initial concentration of $Co2^{+}$ and Ni^{2+}; circle is 0.5, mM, square is 1.0 mM.

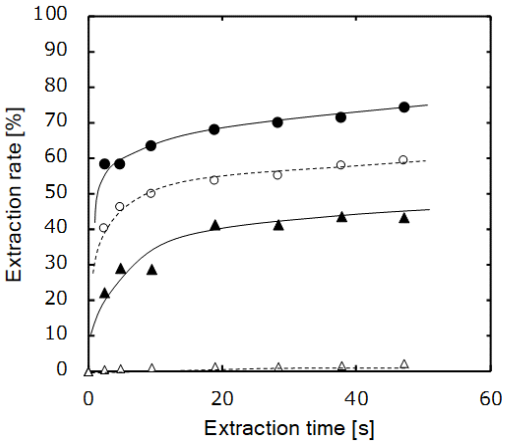

Figure 5 Continuous extraction of mono metal component. Closed mono-component, open key; mixture of Co^{2+} and Ni^{2+}. Concentration of the aqueous feed solution; 1.0 mM. D2EHPA concentration; 40 mM. Linear velocity; 0.021 m/s. Circle; Co^{2+}, triangle; Ni^{2+}.

The continuous extraction experiments by the slug flow were conducted under various feed concentration and linear velocity. The relationship between extraction time and extraction rate is shown in Figure 5. Figure 5 shows the extraction rate for the single metal ion component of Co^{2+} and Ni^{2+}. Each Co^{2+} and Ni^{2+} were quickly extracted just after the start of the extraction and gradually

approached the distribution equilibrium (cobalt; 75%, nickel; 65%, See Figure 2). The extraction experiment of the mixed solution of Co^{2+} and Ni^{2+} was carried out under the same conditions. The extraction rate of Co^{2+} decreasd somewhat with the influence of coexisting Ni^{2+}. On the cotrary, rate of Ni^{2+}extraction dramatically decreased with the influence of Co^{2+}. Li et al. report that the affinity of D2EHPA and Co^{2+} is larger than that of Ni^{2+} in an organic solvent. We think that this result affects difference rate of extraction of Co^{2+} and Ni^{2+}. The mass transfer capacity coefficients of Co^{2+} and Ni^{2+} were calculated From the experimental results. Figure 6 shows the relationship between the Reynolds number (*Re*, $=du\rho/\mu$, *d*; diameter of tube, *u*; liner flow rate, ρ; density of fluid, μ; viscosity of fluid) and the mass transfer capacity coefficient expressed by physical property values of the aqueous solution by experiments with different linear and oil phase linear velocities. The mass transfer capacity coefficient increased linearly with increasing of Reynolz number. We consider that the circulation flow in each segment of the oil phase and the aqueous phase increases and the extraction speed is increased as the linear velocity of the fluid increases,. When the linear flow velocity is small, the mass transfer capacity coefficient of nickel is close to zero. Therefore, high selective separation Co^{2+} and Ni^{2+} is available by the slug flow extraction.

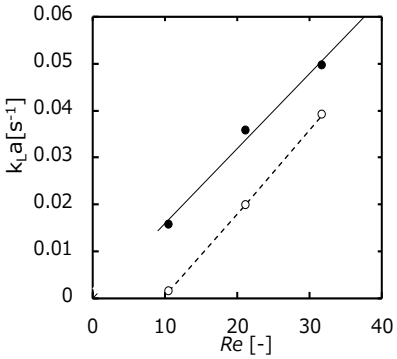

Figure 6 Effect of *Re* on volumetric mass transfer coefficient of Co^{2+} and Ni^{2+}. ●; Co^{2+}, ○; Ni^{2+}

Finary, Purity and separation facotor $\beta_{Co/Ni}$ is calculated for the extraction of mixed Co^{2+} and Ni^{2+}solution. The time dependence of the separation factor $\beta_{Co/Ni}$ is shown in Figure 7. $\beta_{Co/Ni}$ is defined as

$$\beta_{Co/Ni} = \left(\frac{C_{0,Co} - C_{Co}}{C_{Co}}\right) / \left(\frac{C_{0,Ni} - C_{Ni}}{C_{Ni}}\right) \quad (6)$$

The maximum values of $\beta_{Co/Ni}$ were 38 at 20 s when liner velocity was 0.032 m・s^{-1}, 38 at 40 s when liner velocity was 0.021 m・s^{-1}, and 80 at 40 s when liner velocity was 0.011 m・s^{-1}. The difinition of cobalt purity is ($C_{Co}{}^{2+}$ / $C_{Co}{}^{2+}$+ $C_{Ni}{}^{2+}$)) in the organic phase. The relationship between cobalt purity and extarction time is shown in Figure 8. The cobalt purity decreased with increasing of extration time. At just after the starting extraction, the exctraction of Co^{2+} is more rapid than Ni^{2+}, the cobalt purity was near to 1.0. The cobalt purity increased with decraesing of the flow linear velocity. The linear velocity was smaller, the ratio of volmetric

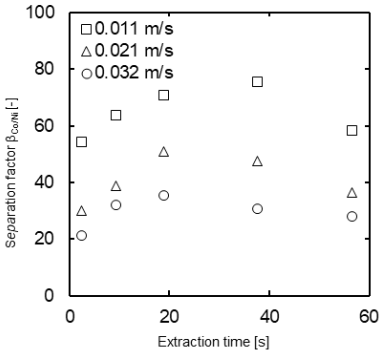

Figure 7 Time dependence of separation factor $\beta_{Co/Ni}$. Concentration of the aqueous feed solution; 1.0 mM. D2EHPA concentration; 40 mM.

mass transfer coefficient of Co^{2+} and Ni^{2+} is larger. These results suggests that the extraction by the slug flow can separate ions with high selectivity with controlling linear velocity and extraction time.

4. Conclusion

In this study, extraction and separation of Co^{2+} and Ni^{2+} by liquid-liquid extraction using a slug flow were investigated. The main conclusions drawn from this study are as follows:

(1) The distribution curves of Co^{2+} and Ni^{2+} were depended the concentration of the ions and the extract reagent (D2EHPA), and Na substitution rate of D2EHPA.

(2) The extraction rate of Co^{2+} which had high selectivity became slightly smaller even when Ni^{2+} coexisted. On the contrary, the extraction rate of Ni^{2+} dramatically decreased with coexisting of Co^{2+}.

(3) The overall mass transfer coefficient of Co^{2+} and Ni^{2+} increases linearly with increasing of *Re*.

(4) The purity and separation factor of Co^{2+} increased with decreasing linear flow rate and showed the maximum value depending on extraction time.

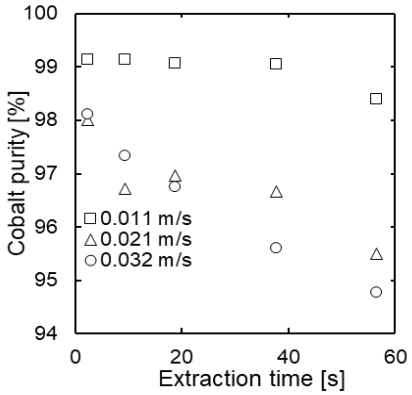

Figure 8 Time dependence of cobalt purity. Concentration of the aqueous feed solution; 1.0 mM. D2EHPA concentration; 40 mM.

References

1) V. Hessel, H. Löwe, F. Schönfeld, *Chem. Eng. Sci*. **60**, 2479-2501 (2005).
2) S. H. Wong, M. C. L. Ward, C.W. Wharton, *Sens. Actuators, B*, **100**, 359-379 (2004).
3) G. Dummann, U. Quittmann, L. Gröschel, D.W. Agar, O. Wörz, K. Morgenschweis, *Catal. Today*, **79-80**, 433-439 (2003).
4) K. Richa, C.W. Babbitt, G. Gaustad, X. Wang, *Resour. Conserv. Recycl*. **83**, 63-76 (2014).
5) O. Tamagawa, A. Muto, *Chem. Eng. J.*, **167,** 700-704 (2011).
6) A. Muto, Y. Hirayama, H. Tokumoto, A. Matsuoka, K. Noishiki, *Solvent Extr. Ion Exch.*, **35**, 61-73 (2017)
7) M. N. Kashid, Y.M. Harshe, D.W. Agar, *Ind. Eng. Chem. Res.*, **46**, 8420-8430 (2007).
8) Q. Li, P. Angeli, *Chem. Eng. Sci*., **143**, 276-286 (2016)

Rare-Earth-Element Removal from Leaching Solution of Ni–MH Battery

Masatoshi TAKANO* and Satoshi ASANO

Niihama Research Laboratories, Sumitomo Metal Mining Co., Ltd.
17-5 Isoura-choNiihma, Ehime, Japan 792-0002

We developed a recycling process for spent Ni–MH batteries using hydrometallurgical treatment. In this process, impure rare-earth elements (REEs) are removed using sulfuric-acid double-salt precipitation and solvent extraction. In this paper, we describe the removal of yttrium among other REEs.

1. Introduction

Ni–MH batteries have been used in hybrid or electric vehicles. The electrode materials of Ni–MH batteries contain nickel, cobalt, and rare-earth elements (REEs). In the future, recovering these valuable metals will be necessary by recycling spent Ni–MH batteries. We developed a Ni–MH battery-recycling process. Electrode powder, which is a mixture of negative and positive electrodes, was leached using sulfuric acid. The leaching solution contained nickel, cobalt, and REEs. To obtain a pure nickel and cobalt aqueous solution, which is an intermediate product of nickel or cobalt, we need to remove the REEs. We developed the REE-removal process from a Ni–MH battery leaching solution using precipitation and solvent-extraction methods. In this process, light REEs (LREEs) such as cerium or lanthanum were removed from the leaching solution using double-sulfate precipitation. LREE sulfates form insoluble double sulfate with an alkali metal sulfate [1]. By taking advantage of this property, LREEs can be separated from the solution as a precipitate. A part of contained yttrium, which is one of the heavy REEs, was removed from the leaching solution by co-precipitation with the double sulfate of alkali metal and LREEs. The removal efficiency depended on the mixing conditions such as temperature, mixing time, concentration of alkali metal sulfate, and ratio of LREEs to yttrium [2]. The residual yttrium was removed via solvent extraction. We selected D2EHPA as the extractant of yttrium. D2EHPA has a high affinity with yttrium [3]. Therefore, extracting yttrium with high extraction efficiency under a low-pH condition was made possible. In this paper, we will mainly explain the yttrium-removal step.

2. Experimental

2.1 Leaching solution

A leaching solution of spent Ni–MH battery powder was prepared using atmospheric sulfuric-acid leaching. The initial slurry concentration during leaching was 100 g/L. The leaching temperature was 80 °C. The leaching pH was 1.0. Sulfuric acid was used to maintain the 1.0 pH during

leaching. The end point of the leaching process was determined by the increase in the oxidation-reduction potential. The vessel used in the laboratory test was a 1-L-size separable flask made of Pyrex. In the pilot-plant test, the vessel was a 500-L-size tank made of stainless steel coated with polytetrafluoroethylene (PTFE) inside. Impellers were used in both tests for stirring. The chemical compositions of the leaching solution were approximately 1.0 pH, 50 g-Ni/L, 5.5 g-Co/L, 0.7 g-Y/L, 5.0 g -Ce/L, and 10 g-La/L.

2.2 Reagents

The extractant used was D2EHPA (Lanxess Co., Ltd.). The diluent used was Teclean N20, which is a naphthenic solvent (JX Nippon Oil & Energy Co.). The used sulfuric acid, sodium hydroxide, and sodium sulfate were of reagent grade (Wako Pure Chemical Industries, Ltd.).

2.3 Precipitation

The precipitation test was carried out on a laboratory scale using beakers. The double-sulfate salt was precipitated by adding sodium sulfate powder to the leaching solution. Stirring was performed by the impeller made of PTFE. The temperature was controlled by a water bath in which a thermostat was installed. The solid and liquid were separated by a 5C filter made of cellulose fiber (Advantech Co., Ltd.). The metal concentrations of the test samples were analyzed using inductively coupled plasma atomic emission spectroscopy (ICP-AES, PerkinElmer Co., Ltd., Optima 3300 DV).

2.4 Solvent extraction

The aqueous phase for extraction was the solution obtained after the solid and liquid separation in the precipitation test. The aqueous phase for back extraction was prepared using sulfuric acid and pure water. The range of the sulfuric-acid concentration was 3–6 mol-H_2SO_4/L. The organic phase was D2EHPA diluted by Teclean N20. The D2EHPA concentrations were 20–50 vol%. The laboratory-scale batch tests of the extraction and back extraction were performed using beakers and separatory funnels. The continuous test was performed using 1-L small mixer settlers made of polypropylene. The metal concentrations of the test samples were analyzed by ICP-AES.

3. Results and Discussion

3.1 Precipitation

Most of the LREEs precipitated as insoluble double-sulfate salt under any condition. The lanthanum and cerium concentrations in the leaching solution were 0.02 g-La/L and 0.007 g-Ce/L, respectively, after the precipitation. The yttrium-removal efficiency depended on the mixing time, temperature, and concentration of the added Na_2SO_4. Figure 1 shows the relationship between the mixing time and residual yttrium concentration at each temperature when 90 g-Na_2SO_4/L was added. The yttrium concentration decreased as the mixing time increased. Under the same mixing time, the yttrium concentration decreased when the temperature was higher. Figure 2 shows the relationship between the Na_2SO_4 and residual yttrium concentrations. The yttrium concentration decreased as the Na_2SO_4 concentration increased. We selected the temperature of 80 °C, mixing time of 20 min or longer, and Na_2SO_4 concentration of 90 g-Na_2SO_4/L as the pilot-plant precipitation conditions. The yttrium concentrations were 0.011–0.015 g-Y/L in the laboratory test under these conditions. However, in the Ni–MH battery recycling pilot plant, the concentrations were 0.1–0.2 g-Y/L, which was

presumed to be caused by the different stirring and mixing conditions between the laboratory and pilot tests. We believe that this problem can be avoided by optimizing the stirring condition. However, because the high affinity between D2EHPA and yttrium is well known, we considered that removal of yttrium via solvent extraction using D2EHPA was more reliable than optimizing the stirring condition in the pilot plant. Therefore, we selected the solvent-extraction method using D2EHPA, which could reliably remove yttrium.

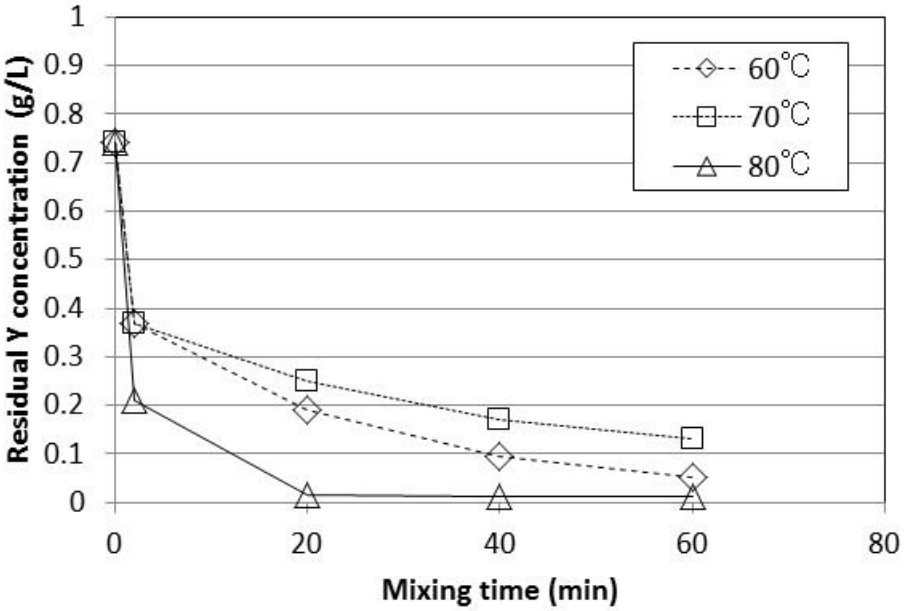

Figure 1. Relationship between the mixing time and residual yttrium concentration.

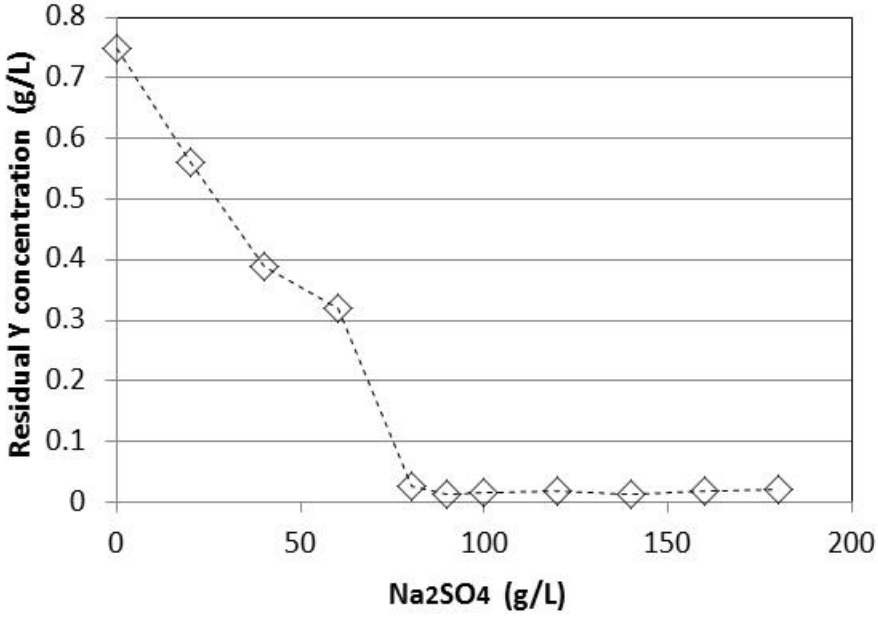

Figure 2. Relationship between the Na_2SO_4 and residual yttrium concentrations.

3.2 Solvent extraction

Figure 3 shows the yttrium-extraction isotherm. The D2EHPA concentration was 50 vol%, and the mixing time was 10 min. The pH was not adjusted in this test. The McCabe–Thiele diagram shows that if O/A is 0.013 or more, the yttrium concentration in the aqueous phase can be reduced from 0.2 to 0.01 g-Y/L or less via one-stage extraction. This result indicates that the D2EHPA has high affinity with yttrium. In the pilot-plant test, the D2EHPA concentration was set to 20 vol% to maintain lower viscosity in the organic phase. As a result of operating the mixer settler at O/A = 0.2, the yttrium concentration of the raffinate was reduced to 0.002 g-Y/L.

Figure 4 shows the relationship between the mixing time and back-extraction efficiency of Y. The D2EHPA concentration was 50 vol%, and the O/A was 0.03. The back-extraction efficiency of yttrium due to stirring and mixing for 15 min were 90% and 30% with 6 and 3 mol/L sulfuric acid, respectively. In the yttrium case, the equilibrium time of the back extraction was long. The back-extraction efficiency of yttrium increased with time in the 3 mol/L sulfuric acid. The higher the acid concentration was, the higher became the back-extraction efficiency. However, high acid concentration promotes extractant degradation and adversely affects the equipment. In the operation, we need to consider the optimization of sulfuric-acid concentration.

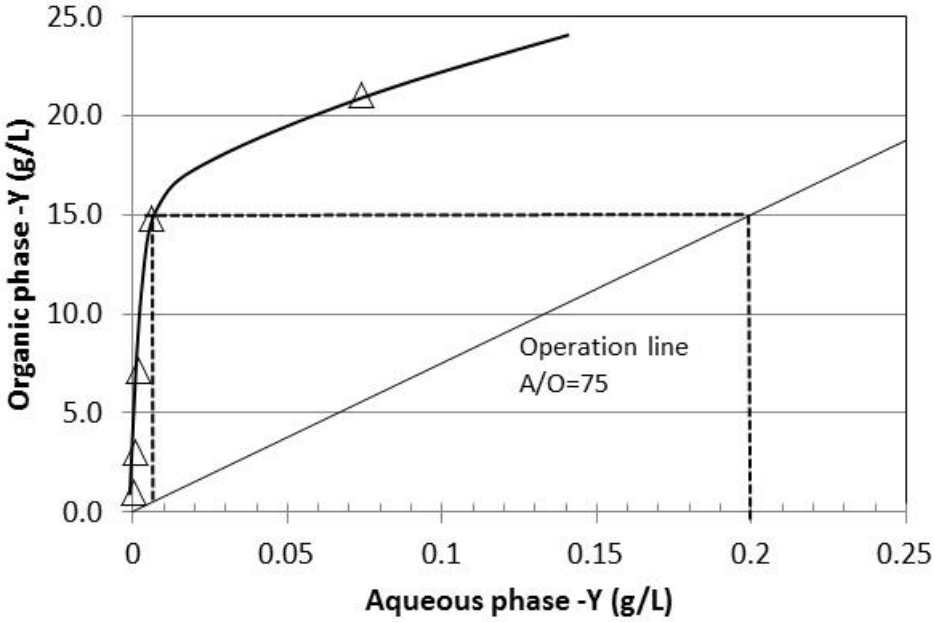

Figure 3. Yttrium-extraction isotherm.

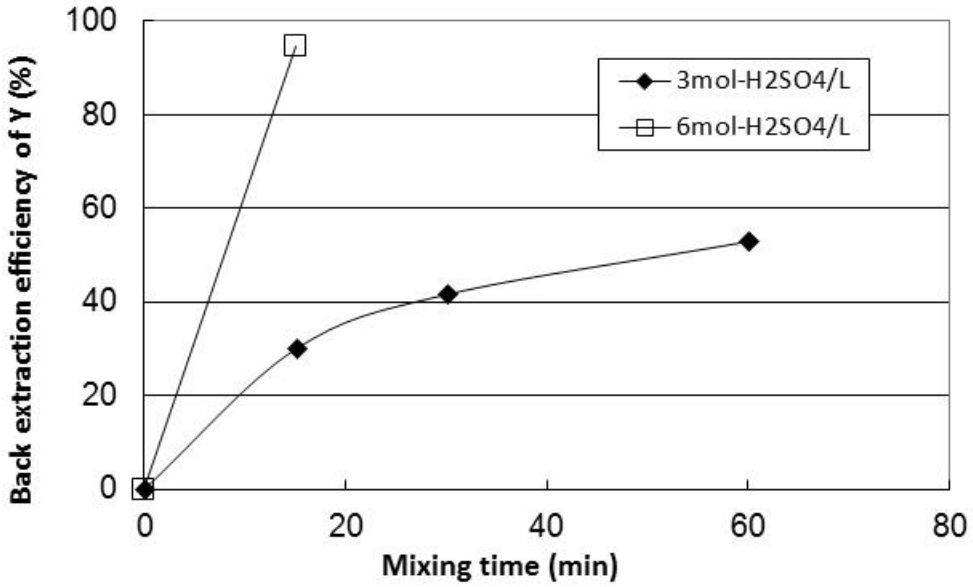

Figure 4. Relationship between mixing time and back-extraction efficiency of Y.

4. Conclusion

We have developed an REE-removal process from the leaching solution of Ni–MH battery electrode powder by combining double-sulfate precipitation and solvent extraction. LREEs such as cerium and lanthanum were removed from the leaching solution using double-sulfate precipitation. A part of yttrium was removed from the leaching solution by co-precipitation with double sulfate of alkali metal and LREEs. The residual yttrium was removed by solvent extraction using D2EHPA, which has high affinity with yttrium. Reducing yttrium in the leaching solution to 0.01 g-Y/L or less is possible. However, back extraction of yttrium from a loaded solvent is not easy. In the tests, we need to consider optimization of the sulfuric-acid concentration.

References

1) S. Mukai, *Tetsu-to-Hagane*, **71**, 633-644 (1985).1)
2) M. Takano, S. Asano, H. Ishida, Method for Recovering Heavy Rare Earth Element, Japan Patent JP5440569B2 (27 December, 2013).
3) M. Matsuda, A. Shibayama, K. Matsushima, Y. Jiang, T. Fujita, T. Kikukawa, *Shigen-to-Sozai*, **119**, 668-674 (2003).

Recovery of Palladium in Highly-Viscous Polymer Solution Using Precipitation of Water-Soluble Polymer

Takafumi KAJIWARA, Shintaro MORISADA, Keisuke OHTO,
Hidetaka KAWAKITA*
Department of Applied Chemistry, Saga University, 840-8502 Saga, Japan

To recovery palladium (mean size 6 nm) in acrylonitrile butadiene rubber (NBR) acetone solution, the solution of poly 2-(dimethylamino)ethyl methacrylate (poly(DMAEMA) (molecular weight 700,000) dissolved in water was added. Poly(DMAEMA) added to acetone solution captured palladium with amino group, then forming precipitation via dehydration by acetone. This technique using precipitation would possess a high-speed recovery of palladium in a high-viscous polymer solution.

1. Introduction

Palladium has been used as a catalyst for organic chemistry and polymer chemistry. Palladium is immobilized on the support such as silica particle and activated carbon. During the catalytic reaction, however, some of palladium immobilized is leaked to the reaction media [1]. After the reaction, leaked palladium needs to be recovered based on the economical view.

To recovery palladium, many researchers have studied the recovery of palladium in water media using solvent extraction [2], adsorption [3], and membrane [4] techniques. However, palladium in high-viscous solution, for instance in polymer solution, does not transfer; that is, there is a difficulty to recovery palladium in polymer solution because of the low mass transfer in viscous media. Thus, the high-speed recovery method of palladium in high-viscous solution have to be created.

Acrylonitrile butadiene rubber (NBR) is used for the polymer of automotive and aerospace industries [5]. Palladium is a catalyst for the change of double bond to single bond of NBR via hydrogenation reaction in organic media [6]. In this study, palladium in NBR dissolved in acetone was recovered using the precipitation of poly 2-(dimethylamino)ethyl methacrylate (poly(DMAEMA) in water. By addition of poly(DMAEMA) solution to palladium solution, amino group in poly(DMAEMA) captures palladium via dehydration with acetone, forming precipitation. This technique has the easiness of solid and liquid separation because of the formation of precipitation as well as the potential for the recovery of palladium at high speed.

2. Experimental

2.1 Reagents

Poly(acrylonitrile-butadiene) (average molecular weight 40,000, acrylonitrile composition: 37 – 39 wt%, NBR) was obtained from Sigma-Aldrich Co., MO, U. S. A. 2-(Dimethylamino) ethyl methacrylate (DMAEMA), activated alumina, ammonium persulfate (APS), and palladium(II) acetate

were purchased from Wako Pure Chemical Industries, Ltd., Japan. Polyvinyl pyrrolidone (average molecular mass: 40,000) was obtained from Tokyo Chemical Industry Co., Ltd., Japan. WA30 (porous spherical resin, functional group: tertiary amine) and HP20 (porous spherical resin, poly(styrene-divinylbenzene)) was purchased from Mitsubishi Chemical Corporation, Japan. Other chemicals were of analytical grade or higher.

2.2 Polymerization of poly(DMAEMA)

Nitrogen-bubbled DMAEMA (9.30 g), ammonium persulfate (APS, 0.33 g), and pure water (34.4 g) was mixed at 303 K with the rotation of 360 rpm for 24 h. The obtained polymer solution was added to acetone to obtained white gel-like precipitation. The purification of the obtained polymer was twice performed. The polymer weight was characterized using size-exclusion chromatography. The molecular weight of the obtained poly(DMAEMA) was approximately at 700,000.

2.3 Recovery of palladium particle by precipitation of poly(DMAEMA)

Palladium acetate (0.224 g), polyvinyl pyrrolidone (0.539 g) and ethanol (25 mL) were refluxed at 343 K for 2.0 h [7]. One mL of the synthesized palladium dispersed solution was diluted with acetone to 100 mL. The size of palladium was observed using transmission electron microscopy (JEOL-2100, JEOL Ltd., Japan). The mean size of the palladium particle was measured to be about 6 nm.

Palladium and NBR-containing-acetone solution were mixed in the glass vial (diameter: 2.2 cm, height 4.0 cm). Poly(DMAEMA) solution dissolved in pure water was dropped to the palladium solution at 303 K and 150 rpm. The concentration of palladium and NBR was changed. After the filtration to remove the precipitant of poly(DMAEMA), the concentration of palladium was determined by absorption spectroscopy (AA-6800, Shimadzu Corporation, Japan). For comparison, the commercially-available resins, HP20 and WA30, were used for palladium adsorption in batch mode. The amount of precipitation was determined in mass. The characterization of the precipitant was performed using ATR method of infrared spectroscopy (IRAffinity-1, Shimadzu Corporation, Japan). The recovery percentage of palladium particle was calculated using the following equation,

$$\text{Recovery percentage of palladium recovery [\%]} = 100\ (C_0\text{-}C)\ /C_0 \qquad (1)$$

where C_0 and C are the concentration of palladium before recovery and the concentration of palladium after recovery, respectively. The remained solution after the precipitation was dried and re-dissolved to acetone-D6 to analyze the interaction of NBR and poly(DMAEMA) by nuclear magnetic resonance (JEOL JNM-GX300).

3. Results and Discussion

3.1 Recovery of palladium by the precipitation of poly(DMAEMA)

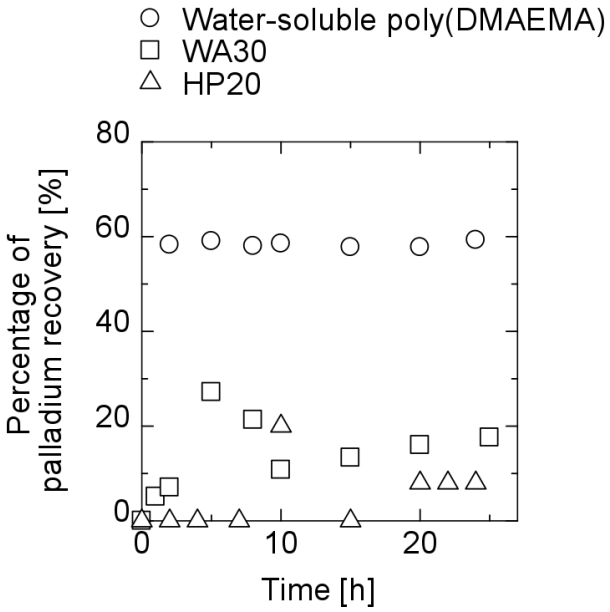

Figure 1. Time course curves of palladium recovery using adsorption and precipitation methods. Palladium solution (5 mL, 20 mg/L), concentration of NBR 22,000 mg/L, poly(DMAEMA) solution (0.1 mL, 0.1 g/mL), WA30 and HP20 100 mg.

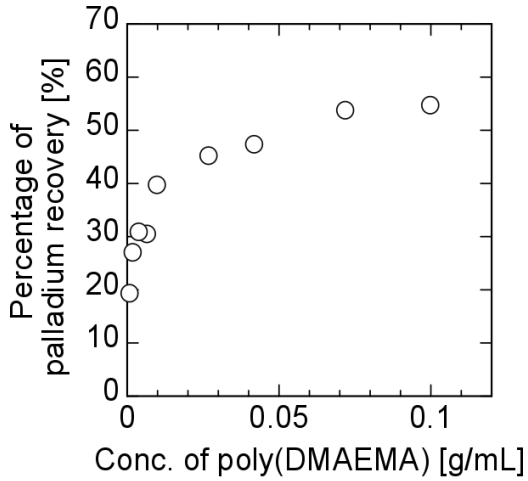

Figure 2. Effect of concentration of poly(DMAEMA) on recovery of palladium percentage. Palladium solution (5 mL, 20 mg/L), concentration of NBR 22,000 mg/L, poly(DMAEMA) solution (0.1 mL, 0.1 g/mL).

Palladium was dispersed in high viscous solution of NBR-acetone solution. Due to the high viscosity, palladium has the difficulty to move to the adsorbent. Figure 1 shows the time course curve of palladium recovery percentage using the commercially-available resins, WA30 and HP20, along with that of the proposed method in this study. In conventional adsorption, HP20 composed of poly(styrene divinylbenzene) had no ability to adsorb palladium. While WA30 with tertiary amino group had the adsorption percentage of 18% after 20 h. This indicated that amine group had the affinity to palladium. However, the conventional resin represented the slower speed of adsorption because NBR-containing-acetone solution had the high viscosity and palladium did not move to the resin faster. On the other hand, in the case of the addition poly(DMAEMA) solution, proposed in this study, the recovery percentage of palladium reached at 60% only for one hour. This technique includes the complexation with palladium in water-soluble poly(DMAEMA) and the dehydration of palladium-complexed polymer resulting in the precipitation formation. During this process, palladium could be captured quickly because of the faster binding with the amino group in poly(DMAEMA) as well as precipitation due to dehydration by acetone.

3.2 Concentration dependence of poly(DMAEMA) on recovery percentage of palladium

Poly(DMAEMA) in water has the hydrated structure with water. In palladium-acetone solution, hydrated water in poly(DMAEMA) moves to acetone forming a precipitation of poly(DMAEMA) binding with palladium. During capturing palladium, water has a critical role to change the phase transition of poly(DMAEMA) from soluble to insoluble states in acetone. Figure 2

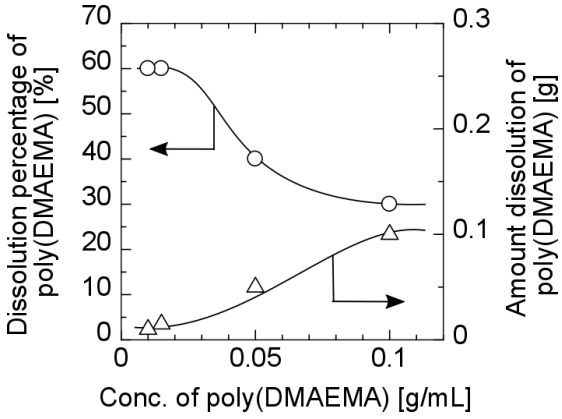

Figure 3. Effect of concentration of poly(DMAEMA) on dissolution of poly(DMAEMA) in NBR-acetone solution. Palladium solution (5 mL, 20 mg/L), concentration of NBR 22,000 mg/L, poly(DMAEMA) solution (0.1 mL, 0.1 g/mL).

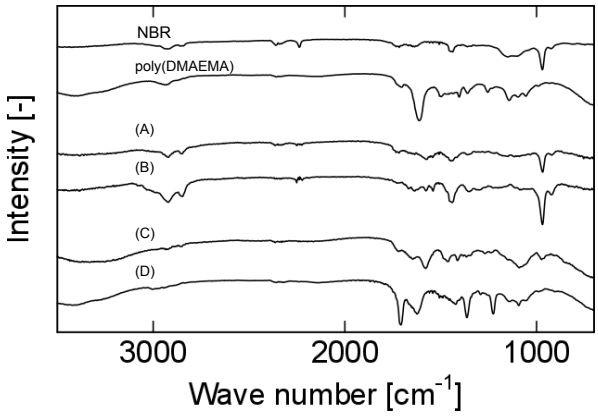

Figure 4. Infrared spectrograms of precipitants by adding poly(DMAEMA) solution. (A) 0.010 g/mL, (B) 0.015 g/mL, (C) 0.050 g/mL, (D) 0.10 g/mL.

shows the dependence of concentration of poly(DMAEMA) on the recovery percentage of palladium. With increasing the concentration of poly(DMAEMA) in water, the recovery percentage gradually increased and reached the percentage of 55%.

The dissolved poly(DMAEMA) added in NBR-acetone solution at the different concentrations of poly(DMAEMA) is shown in Figure 3. With increasing the concentration of poly(DMAEMA), the dissolution percentage of poly(DMAEMA) decreased. At lower concentration of poly(DMAEMA), there were much hydrated water around poly(DMAEMA) to make difficult form the precipitation. At higher poly(DMAEMA) concentration, the less water to hydrate, the less dissolution percentage in acetone.

To analyze the precipitant of mainly poly(DMAEMA), the precipitant was analyzed by infrared spectroscopy, as shown in Figure 4. NBR had peaks of 991 cm^{-1} and 2237 cm^{-1} assigned to C=C and C≡N groups, respectively [8]. At low concentration of poly(DMAEMA) as Figure 4 (A) and (B), the peaks at 991 cm^{-1} were clearly observed demonstrating that NBR would be co-precipitated with poly(DMAEMA). At higher concentration of poly(DMAEMA), the peaks of NBR disappeared because the more poly(DMAEMA) was precipitated by dehydration in acetone.

3.3 Interaction of poly(DMAEMA) and NBR with palladium

Water-soluble poly(DMAEMA) was not perfectly precipitated via dehydration as shown in Figure 3. The recovery percentage of palladium was 60%, shown in Figure 2, meaning that 40% of palladium was still dissolved in NBR-acetone solution. To enhance the recovery percentage of palladium, the interaction of poly(DMAEMA) with NBR or palladium need to be considered. The remained solution after the recovery of palladium was dried and re-dissolved in deuterated acetone to analyze them using nuclear magnetic resonance, as shown in Figure 5 (a) along with the assignments

to

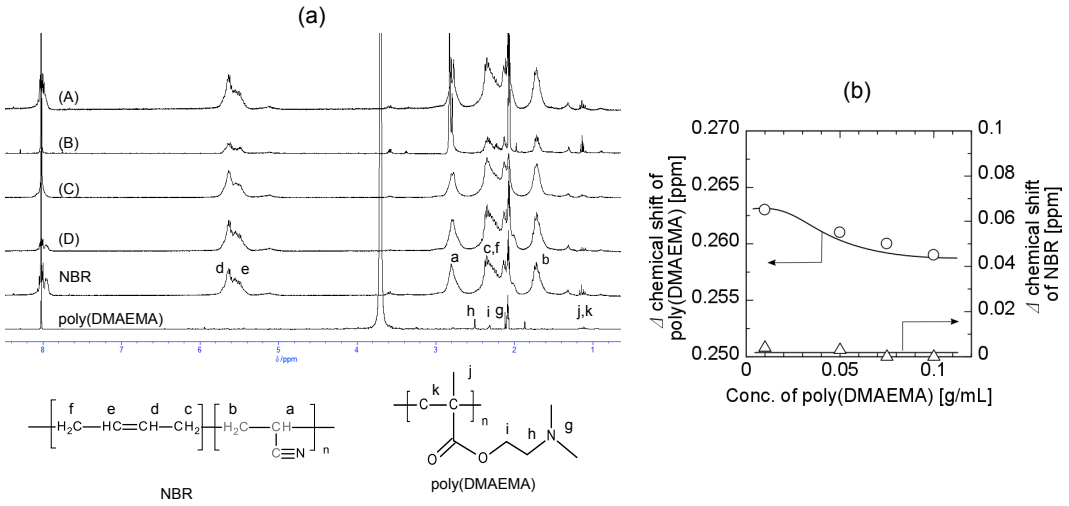

Figure 5. Interaction of polymers and palladium. (a) Spectra of nuclear magnetic resonance of remained NBR and poly(DMAEMA) solution after forming precipitation. (A) 0.1 g/mL poly(DMAEMA) added, (B) 0.075 g/mL poly(DMAEMA) added, (C) 0.050 g/mL poly(DMAEMA) added, (D) 0.010 g/mL poly(DMAEMA) added. Chemical shift standard used was $CHCl_3$. (b) Change of chemical shift of *h* in poly(DMAEMA and *a* in NBR.

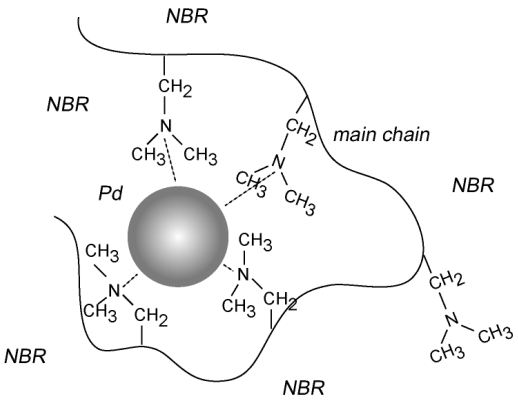

Figure 6. Pd complexation with poly(DMAEMA) in the presence of NBR.

NBR [9] and poly(DMAEMA) [10]. By the addition of poly(DMAEMA) the peaks of NBR were not changed, whereas the protons of *h* as two protons in poly(DMAEMA) were gradually shifted to the higher field with increasing the concentration of poly(DMAEMA) added. Change of chemical shift of *h*, *Δ* chemical shift, in change of concentration of poly(DMAEMA) is quantitatively shown in Figure 5 (b). On the other hand, the peak *a* in NBR of the assignment in Figure 5 (a) was not changed in increasing poly(DMAEMA) concentration, also as shown in Figure 5 (b). This indicated that tertiary amino group in poly(DMAEMA) would be interacted with palladium while NBR was not with poly(DMAEMA) and palladium as shown in Figure 6. The appropriate design of the functional group in monomer as well as the macroscopic structure of the polymer would be crucial for the sophisticated recovery of palladium in high-viscous solution using the precipitation method.

4. Conclusions

Palladium has been used as a catalysis for organic and polymer chemistry. During reaction, a part of palladium immobilized on the support is leaked to the media. In this study, palladium in high-viscous polymer acetone solution, acrylonitrile butadiene rubber, was recovered using the

precipitation of poly 2-(dimethylamino)ethyl methacrylate (poly(DMAEMA)). Compared with the conventional adsorption of palladium with the resin, this precipitation technique possessed the high-speed recovery of palladium. From the analysis of nuclear magnetic resonance, the amino group in poly(DMAEMA) would bind palladium.

References

1) C. M. Crudden, M. Sateesh, R. Lewis, *J. Amer. Chem. Soc.,* **127**, 10045-10050 (2005).
2) K. Ohto, H. Furugou, T. Yoshinaga, S. Morisada, H. Kawakita, K. Inoue, *Solv. Extr. Res. Dev., Jpn.*, **24**, 77-88 (2017).
3) Y. Yoshimura, K. Khunathai, A. Nozoe, K. Ohto, H. Kawakita, *J. Chem. Eng. Jpn.,* **45**, 178-181 (2012).
4) T. Yoshikawa, D. Umeno, K. Saito, T. Sugo, *J. Membr. Sci.*, **307**, 82-87 (2007).
5) G. A. S. Schultz, E. Comin, R. F. Souza, *J. Appl. Polym. Sci.*, **106**, 659-663 (2007).
6) M. Shirai, N. Suzuki, Y. Nishiyama, K. Torii, M. Arai, *Appl. Catal. A: General*, **177**, 219-225 (1999).
7) Y. Du, R. Chen, *Korean J. Chem. Eng.*, **32**, 1759-1765 (2015).
8) S. Zhou, H. Bai, J. Wang, *J. Appl. Polym. Sci.*, **91**, 2072-2078 (2004).
9) T. Suzuki, Y. Takegami, J. Furukawa, E. Kobayashi, Y. Arai, *Polym. J.*, **4**, 657-663 (1973).
10) J. Gao, G. Zhai, Y. Song, B. Jiang, *J. Appl. Polym. Sci.*, **107**, 3548-3556 (2008).

Effective Separation of Pt(IV), Pd(II), and Rh(III) in Acidic Solution by Using Phosphonium-based Ionic Liquid

Mochamad L FIRMANSYAH[1], Fukiko KUBOTA[1], Masahiro GOTO[1,2,*]

[1]Department of Applied Chemistry, Graduate School of Engineering, Kyushu University, 744 Motooka, Fukuoka, 819-0395, Japan; [2]Center for Future Chemistry, Kyushu University, 744 Motooka, Fukuoka, 819-0395, Japan

An interest in utilizing ionic liquids for solvent extraction has been increasing over these recent years. A novel phosphonium-based ionic liquid, trioctyl(dodecyl)phosphonium chloride ($P_{88812}Cl$) has developed and used for the extraction of platinum group metals (PGMs) (i.e Pt(IV), Pd(II), and RhIII) from HCl media, and then compared to that of commercial trihexyl(tetradecyl)phosphonium chloride ($P_{66614}Cl$). The extraction performance with $P_{88812}Cl$ was comparable to that of $P_{66614}Cl$. However, the extraction with $P_{88812}Cl$ was comparably faster than that of $P_{66614}Cl$, due to its lower viscosity than the latter. The stripping of metal-loaded ionic liquid could be achieved with HNO_3, $CS(NH_2)_2$, and HCl for Pt(IV), Pd(II) and Rh(III), respectively.

1. Introduction

Precious metals located in the columns V-VIII and period 5 and 6 are classified into platinum group metals (PGMs). Due to their unique physicochemical properties, various high-end technology industry requires PGMs[1]. Nowadays, primary production of PGMs is through mining. However, in few decades, PGMs would face a supply shortage due to the difficulty in substituting PGMs with other elements[2].

In recent years, researches in sustainable and environmentally friendly secondary production of PGMs has gained more interest. Solvent extraction has emerged as a suitable process for the recovery of PGMs. Various reagents have been studied and proposed, including quaternary ammonium salts, organophosphorus, and sulphides extractants[3,4]. Recently, many publications have appeared on the synthesis and applications of ionic liquids (ILs), which classified as green organic solvents due to their negligible vapor pressure. In a ILs extraction system, ILs were able to act not only as the solvent but also as the extracting agent. This was found to be appealing to replace the conventional extraction system, which uses massive amount of organic solvent. Various type of ILs has been explored, including ammonium, imidazolium, pyridinium, and phosphonium-based ILs. Not only possessed negligible vapor pressure, ILs are also non-flammable under normal storage conditions. ILs are therefore not expected to pollute the environment, safe to breathed and are neither flammable or explosives[5]. The most interesting feature of ILs is the tunability of their physicochemical properties by designing the structure of the cation and anion constituents. Various combination of cation and anion constituents was also one of the way to tune ILs properties.

ILs have also been used in PGMs extraction. Previously, imidazolium and phosphonium-based ILs have been able to quantitatively extract Au(III), Pt(IV), Pd(II), and Ir(IV)[6–8]. However, based on the previous results, Rh(III) was difficult to extract in a conventional extraction system with an organic solvent as a diluting agent. Different behavior of Rh(III) extraction was observed when using an undiluted ionic liquid. A phosphonium-based IL, namely trihexyl(tetradecyl)phosphonium chloride ($P_{66614}Cl$) was able to extract Rh(III) quantitatively in a single metal model solution.

It is required for ILs to use as extraction solvents that the ILs are hydrophobic and show low viscosity. The work presented here deals with the investigation of extraction and separation of Pt(IV), Pd(II), and Rh(III) based on the newly designed and synthesized phosphonium-based IL, trioctyl(dodecyl)phosphonium chloride ($P_{88812}Cl$). The physicochemical properties including the extraction performance was compared to that of commercially available $P_{66614}Cl$. The extraction behavior was investigated under the undiluted IL conditions.

2. Experimental

2.1 Reagents

Newly designed and synthesized ionic liquid, trioctyl(dodecyl)phosphonium chloride ($P_{88812}Cl$), obtained from Nippon Chemical Industrial Co. Ltd, (Tokyo, Japan) and commercial trihexyl(tetradecyl)phosphonium chloride ($P_{66614}Cl$) obtained from Ionic Liquids Technologies GmbH (Heibronn, Germany) were used as received. HCl, HNO_3, H_2SO_4, NH_4OH, $CS(NH_2)_2$, Pt(IV) and a Pd(II) standard solution were obtained from Wako Pure Chemical Ltd, (Osaka, Japan). A Rh(III) standard solution was purchased from Kanto Chemical Co. Inc (Tokyo, Japan).

2.2 Measurements

The fundamental properties of the ionic liquids, which were density, viscosity, and water content, were analyzed by using the density meter (DMA 35N, Anton Paar GmbH, Graz Austria), the viscometer (Lovis M/ME 200, Anton Paar GmbH, Graz Austria), the Karl-Fischer moisture meter (CA-200, Mitsubishi Chemical Analytec, Co. Ltd, Tokyo Japan), respectively. The concentration of each element in an aqueous phase was measured by the inductively coupled plasma optical emission spectrometer (ICP-OES, Optima 8300, Perkin-Elmer Co., MA, USA).

2.3 Extraction procedure

A set of aqueous phases in 0.1-5 mol L^{-1} HCl with 100 mg L^{-1} of each Pt(IV), Pd(II), and Rh(III) was prepared. An aqueous phase and an undiluted IL phase were mixed at volume ratio 2 in a PP tube, and then shaken mechanically at 160 rpm for 3 hours. All parameters were kept constant, unless mention otherwise. the stripping was conducted with various stripping solution (HCl, HNO_3, H_2SO_4, NH_4OH, and $CS(NH_2)_2$) at a similar manner. The distribution ratio of the metal in both phases, *D* (-), and the stripping percentage, *S* (%), were calculated as follows:

$$D = \frac{C_{org}}{C_{aq}} \quad (1)$$

$$S\% = \frac{C_{st}V_{st}}{C_{st}V_{St} + C_{org}V_{org}}\ x\ 100 \quad (2)$$

Where *V* and *C* were the volume and the metal concentration, respectively, and subscript *aq*, *org*,

and *st* denote the aqueous, the organic, and the stripping phase, respectively.

3. Results and Discussion

3.1 Extraction behavior of Pt(IV), Pd(II), and Rh(III) with a phosphonium IL.

Figure 1 shows the distribution ratio of Pt(IV), Pd(II), and Rh(III) with $P_{88812}Cl$ as a function of the HCl concentration. As observed, Pt(IV) and Pd(II) were quantitatively extracted, whereas the extraction performance of Rh(III) seemed to be very low. The *D* values were increasing along with the increase in the HCl concentration until it reaches the highest point at 0.5 mol L^{-1} HCl. Further increase in the HCl concentration caused a decrease in the *D* values of all the metal species. Rh(III) extraction seems to suffer the most upon the increase of the HCl concentration. The decrease in the high HCl concentration was probably due to the presence of massive amount of Cl ions. The high amount of Cl ions could also create extraction competition between metal and Cl ions[13], leading to the decrease in the extraction performance of the ionic liquids in a high HCl concentration.

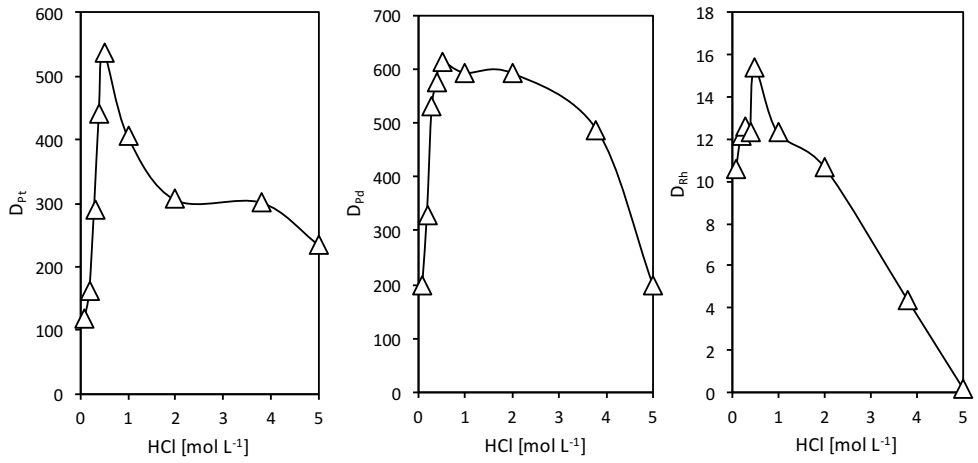

Figure 1. Effect of HCl concentration on the distribution ratio of the metals with $P_{88812}Cl$

The change in metal chlorocomplex species of Rh(III) was also one of the reason for the decrease in the extraction performance. According to the speciation diagram of several previous studies, in 5 mol L^{-1} HCl, Rh(III) mainly exists in the form of $RhCl_6^{3-}$ (70%) and $RhCl_5^{2-}$ (30%). With the decrease of the HCl content, the species composition has been changed to $RhCl_5^{2-}$ (80%) and $RhCl_6^{3-}$ (20%). The significant difference in molecular sizes of $RhCl_6^{3-}$ and $RhCl_5^{2-}$ would affect their charge to the size ratio or the charge density[14].The difficulty of the metal ion extraction was inversely proportional to their charge density. Thus, $RhCl_5^{2-}$, which has higher charge density was ready to extract compared to that of $RhCl_6^{3-}$. A similar extraction performance has been observed with commercial $P_{66614}Cl$.

3.2 Properties of ionic liquids

The physicochemical properties of the ionic liquids are important to use as extraction solvents because they affect the extraction performance. As shown in Table 1, the density of the novel $P_{88812}Cl$

was similar to that of $P_{66614}Cl$. However, it was found that $P_{88812}Cl$ possesses a significantly lower viscosity compare to that of $P_{66614}Cl$ (Table 1), which would be effective for the extraction process of metal ions due to the increase in the diffusion rate[9], as describe later.

Table 1. Physicochemical properties of the ILs

Ionic Liquid	Density [g mL^{-1}]	Viscosity [mPa.s]	Water Content [wt%]	Cation Release [mg L^{-1}]
$P_{88812}Cl$	0.8799	800.8	7.72	0.301
$P_{66614}Cl$	0.8767	1930.5	11.92	6.887

The water content of ionic liquids and the phosphorus (P) release into the aqueous phase after contacting ILs with water at the volume ratio of 2 (Water/IL) were analyzed and the results were listed in Table 1. The newly designed $P_{88812}Cl$ not only showed less P release, but also lower water content compared to those of $P_{66614}Cl$. The lower release property could be associated with higher hydrophobicity and smaller loss of the ionic liquid constituent compare to $P_{66614}Cl$[10]. Along with the low water content of $P_{88812}Cl$, which would minimize the cation aggregation, these factor would minimize the decrease in their extraction performance of $P_{88812}Cl$[11,12]. In addition, $P_{88812}Cl$ appear to be environmentally friendlier compare to $P_{66614}Cl$ due to the lower release of phosphorus (P) to the aqueous phase. As for P element is heavily regulated in water environment, such as waste water.

3.3 Extraction rate

Time course of the extraction percentage was measured with 200 mg L^{-1} metal concentration at 0.5 mol L^{-1} HCl at V_{aq}/V_{IL} 4. Novel $P_{88812}Cl$ could achieve the extraction equilibrium of Pt(IV) and Pd(II) within 30 min, whereas the conventional $P_{66614}Cl$ took more than 60-80 min to achieve the equilibrium. Although the extraction rate of Rh(III) was slower compared to that of Pt(IV) or Pd(II), the extraction equilibrium with $P_{88812}Cl$ was attained at arround 80 min, while more than 150 min was required to reach equilibrium with $P_{66614}Cl$. As described earlier, the viscosity of the ILs also affected to the diffusion rate of the metal ions into the ILs phase. Three hours were deemed enough for the extraction process to reach equilibrium. The kinetic parameter of the extraction was determined through the linear fitting at the initial stage through equilibrium of extraction according to Eq. (3).

$$\ln {C_f}/{C_i} = -kt \quad (3)$$

Where C_i and C_f are the metal concentration in the aqueous phase at beginning and after reaching equilibrium, respectively.

As listed in Table 2, $P_{88812}Cl$ exhibits a higher reaction rate constant compared to that of $P_{66614}Cl$. This supported the fact that $P_{88812}Cl$ achieved equilibrium faster than $P_{66614}Cl$. As expected, the Rh(III) rate constant was small compared to that of Pt(IV) and Pd(II). This result was in accordance with the degree of viscosity for each ionic liquid, which $P_{88812}Cl$ has a lower viscosity than that of $P_{66614}Cl$. This could affect the diffusion rate of the solutes, hence affecting the extraction rate using the ionic liquid.

Table 2. Reaction rate constants for both ionic liquids

Ionic Liquids	Reaction Rate Constant k [s^{-1}] (10^{-4})		
	Pt	Pd	Rh
$P_{88812}Cl$	6.73	7.55	1.23
$P_{66614}Cl$	4.82	4.98	0.93

3.4 Stripping behavior

Stripping of the meta-loaded extractant phase is an essential step for the metal recovery and an ionic liquid recycling. In this study, the ionic liquid extracted from 0.5 mol HCl was used for evaluating the stripping behavior, where the initial concentration of Pt(IV), Pd(II), and Rh(III) were 157, 175, 189 mg L^{-1}, respectively. Various strip solutions, such as 5 mol L^{-1} HCl, HNO_3, HCl, 0.5 mol L^{-1} NH_4OH, and 1 mol L^{-1} $CS(NH_2)_2$ in 1 mol L^{-1} HCl, were used. Table 3 presents the stripping results of $P_{88812}Cl$. Among them, 5 mol L^{-1} HNO_3 showed the highest percentage of Pt(IV), with 78.5% stripping from $P_{88812}Cl$. As for Pd(II), 1 mol L^{-1} $CS(NH_2)_2$ in 1 mol L-1 HCl was able to achieve the highest stripping percentage with 98.9%. In case of Rh(III), 5 mol L^{-1} HCl was able to selectively strip Rh(III), and more than 70% of the metal was recovered. Thus, HNO_3, $CS(NH_2)_2$ and HCl were effective for stripping Pt(IV), Pd(II) and Rh(III) from the meta-loaded ionic liquid phase. The performance in the stripping test was equal or comparable to that for $P_{66614}Cl$. After the stripping operation, neither emulsion nor precipitation were observed, and both phases were transparent and separated quickly.

Table. 3 Stripping from the ionic liquid with various strip solutions

Ionic Liquids	Metal	Stripping [%]				
		5 mol L^{-1}			0.5 mol L^{-1}	1 mol L^{-1}
		HCl	HNO_3	H_2SO_4	NH_4OH	$CS(NH_2)_2$
$P_{88812}Cl$	Pt	0.41	78.5	3.50	0.15	20.5
	Pd	0.06	0.28	2.09	39.1	98.9
	Rh	72.6	23.5	23.4	19.4	0.08
$P_{66614}Cl$	Pt	0.39	64.5	0.11	0.98	22.7
	Pd	0.74	0.21	0.25	31.8	92.7
	Rh	76.6	20.6	39.2	26.7	0.84

4. Conclusion

An ionic liquid having favorable properties in the liquid-liquid operation with two immisible solvents could be prepared by designing its alkylstructure. The extraction performance of newly designed trioctyl(dodecyl)phosphonium chloride ($P_{88812}Cl$) was comparable in the extraction of Pt(IV), Pd(II), and Rh(III) compared to that of commercial trihexyl(tetradecyl)phosphonium chloride ($P_{66614}Cl$). Both ionic liquids exhibit a significant decrease in Rh(III) extraction at a high HCl

concentration due to the extraction competition and the change of Rh(III) species with Cl^- in a high HCl concentration. $P_{88812}Cl$ was able to extract the metals faster than that of $P_{66614}Cl$ due to its low viscosity. It was also more hydrophobic and environmentally friendly due to the less release of phosphonium cation into the feed aqueous phase than $P_{66614}Cl$. The stripping test of the metals was achieved with HNO_3, $CS(NH_2)_2$, and HCl for Pt(IV), Pd(II), and Rh(III), respectively. Thus the obtained results indicate that $P_{88812}Cl$ possesses several advantages compared to $P_{66614}Cl$, as for a new task specific extractant.

Acknowledgement

This work was supported by a Grant-in-Aid for Scientific Research (No. 16K06830) from the Ministry of Education, Science, Sports, and Culture of Japan, and the Environment Research and Technology Development Fund (ERTDF, grant no. 3-1710) from the Ministry of the Environment, Japan. Mochamad L Firmaansyah was grateful for scholarship provided by the Ministry of Education, Science, Sports, and Culture of Japan (MEXT ID: 163644).

References

1) Rao C. R. M. and Reddi G. S., *TrAC- Trends Anal. Chem.*, **19**, 565–586, (2000).
2) European Commision, *On the review of the list of critical raw materials for the EU and the implementation of the raw materials initiative*, (2014).
3) Cieszynska A. and Wisniewski M., *Sep. Purif. Technol.*, **73**, 202–207, (2010).
4) Fraser K. J. and MacFarlane D. R., *Aust. J. Chem.*, **62**, 309–321, (2009).
5) Plechkova Natalia V. and Seddon Kenneth R., *Chem. Soc. Rev.*, **37**, 123–150, (2008).
6) Papaiconomou Nicolas, Vite Ghislain, Goujon Nicolas, Lévêque Jean-Marc and Billard Isabelle, *Green Chem.*, **14**, 2050, (2012).
7) Papaiconomou Nicolas, Genand-Pinaz Sebastien, Leveque Jean-marc and Guittonneau Sylvie, *Dalt. Trans.*, **42**, 1979–1982, (2013).
8) Nguyen Thi Hong, Sonu Chong Ho and Lee Man Seung, *Hydrometallurgy*, **164**, 71–77, (2016).
9) Germani Raimondo and Mancini Vincenza, *Tetrahedron Lett.*, **48**, 1767–1769, (2007).
10) Hamamoto T., Okai M. and Katsuta S., *J. Phys. Chem. B*, **119**, 6317–6325, (2015).
11) Tran Chieu D., De Paoli Lacerda Silvia H. and Oliveira Daniel, *Appl. Spectrosc.*, **57**, 152–157, (2003).
12) Martins Vitor L., Nicolau Bruno G., Urahata Sérgio M., Ribeiro Mauro C. C. and Torresi Roberto M., *J. Phys. Chem. B*, **117**, 8782–8792, (2013).
13) Rzelewska Martyna, Baczyńska Monika, Regel-Rosocka Magdalena and Wišniewski Maciej, *Chem. Pap.*, **70**, 454–460, (2016).
14) Rzelewska Martyna, Wiśniewski Maciej and Regel-Rosocka Magdalena, *Sep. Sci. Technol.*, DOI:10.1080/01496395.2017.1295996, (2017).

Metal Extractions by Diglycolamide-Type Tridentate Ligands

Yuji SASAKI[1*], Keisuke MORITA[1], Morihisa SAEKI[2], Shugo HISAMATSU[1], and Kazuharu YOSHIZUKA[3]
[1]*Japan Atomic Energy Agency, Tokai, Ibaraki 319-1195, Japan*
[2]*National Institutes for Quantum and Radiological Science and Technology, Tokai, Ibaraki 319-1106, Japan*
[3]*The University of Kitakyushu, Hibikino 1-1, Kitakyushu 808-0135, Japan*

Three tridentate extractants including soft and hard donor has been developed and examined. The extractants are termed as *N,N,N′,N′*-tetraoctyl-diglycolamide (TODGA), methylimino-*N,N′*-dioctylacetamide (MIDOA) and *N,N,N′,N′*-tetraoctyl-thiodiglycolamide (TDGA). The results of the present study indicate that TODGA can extract mainly hard acid metals, MIDOA can extract soft acid metals and oxyanions, and TDGA can extract soft acid metals. We can compare the distribution ratios of these metals obtained by TODGA, MIDOA, and TDGA. These results can be supported by some spectrometric studies, i.e., IR, and NMR and calculations of metal complexes.

1. Introduction

Recently, the tridentate diamide compounds were developed and their extraction performances were investigated worldwide [1-4] because of the strong extractability with not only actinide (An) and lanthanides (Ln) but also noble metals. The most famous tridentate diamide is TODGA (*N,N,N′,N′*-tetraoctyl-diglycolamide), which shows very high distribution ratio (*D*) of An from nitric acid and is very useful to recover An and Ln from high level radioactive waste. This compound has three oxygen donors (two carbonyl oxygen and an ether oxygen atoms), and shows very strong complexation with hard acid metals. Referring to the structure of TODGA, N and S donor extractants can be synthesized by substitution of their atoms to ether O atom in TODGA, N-compound is MIDOA (methylimino-*N,N′*-dioctylacetamide) and S-compound is TDGA (*N,N,N′,N′*-tetraoctyl-thiodiglycolamide), the structures of these extractants are described in Figure 1. Three compounds have their own extraction properties, O donor favors the complexation with hard acid metals and S and N donor favor the complexation with soft acid metals. Probably, S donor extractant may have difference with its extraction ability from that of N donor. In this work, we would like to see the difference among three extractants using extraction results, spectrophotometry and calculation.

2. Experimental

The extraction procedure was following that each extractant was dissolved in *n*-dodecane at room temperature. Each metal in the standard solution was evaporated and the residue was dissolved by the appropriate concentration of acids (HNO_3). The organic and aqueous phase were mixed and mechanically shaken at 1500 strokes/min for 30 min at 25 ± 0.1 °C. After centrifugation, the metal concentrations in the aliquots taken from the aqueous phases were measured by ICP-OES (SPS3100, Seiko Instruments Inc.). The metal concentrations in the organic phases were obtained by subtracting the aqueous concentration from the initial one. The *D* value is defined as the ratio of [M] in the organic phase to [M] in the aqueous phase.

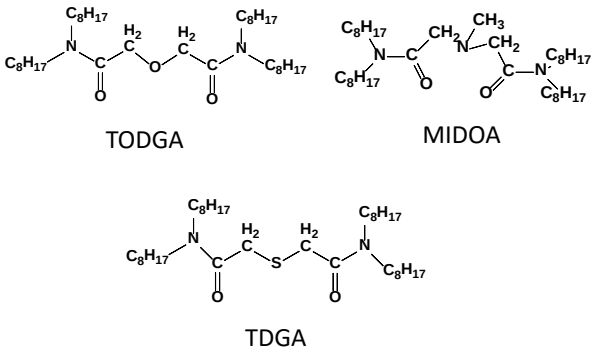

Figure 1 The structures of TODGA, MIDOA and TDGA

The sample preparation method for IR and NMR analysis was as follows: The extraction conditions at near-loading capacity were applied in order to reduce the concentration of free extractant in the organic phase. Here, the organic solvents, chloroform and carbon tetrachloride, are employed for NMR and IR measurements. After extraction and centrifugation, the organic phases containing metal complexes were used as the samples for IR (FT/IR4100, JASCO) and ^{1}H-NMR (JNM-ECA600, JEOL) studies.

All models of extractants, metal complexes and anions, were calculated *in vacuo* by using the Density Functional Theory (DFT) at the B3LYP/6-31g** level with the Gaussian03 series program, and the heats of formation of the metal complex, metal ion, extractant, and anion ($H_{f,metal\ complex}$, $H_{f,metal}$, $H_{f,L}$, $H_{f,anion}$) were obtained.

3. Results and Discussion

3.1 Matal extraction by three extractants

Results on metal extractions using TODGA and MIDOA are reported elsewhere [2,4]. In this work, we compare the results by three extractants and summarize the extractability trends from group 2 to group 16, the results are shown in Table 1. Columns in Table 1 show the kinds of metal, group No. stable valence of metals, HNO_3 concentration faced in extraction and extractability trends for three extractants. Concerning with this, from our experience, extraction behavior of fourth period (potassium-krypton line) is different from fifth (rubidium-xenon line) and sixth (cesium-radon line) period at the same group. So we should choose the metals in Table 1 from fifth and sixth periods.

From group 2 to 4, because of the hard acid metals, TODGA has very high *D* values, whose compound includes hard oxygen donor in the ether position of the structure. Lanthanides and actinides are included in these groups. Tetravalent Pu show high extraction ability with MIDOA as well as TODGA.

From group 5 to 10, MIDOA shows the highest extractability of all. Some metals at these groups form the oxonium anions (i.e., MoO_4^{2-} and TcO_4^{-}) and others are soft acid metals. Based on HSAB principle, these metals show the high preference by soft donor, like N and S donors. Nevertheless, TDGA including S donor show the low extractability for Tc, Ir, and Pt extractions than TODGA. Most of oxonium anions from this work are favorable to MIDOA rather than TDGA.

Table 1 Extractability trends for each metals among three extractants

Metals	group	valence	HNO_3 conc.	Extractability trend
Sr	2	2	3 M	TODGA >> MIDOA, TDGA
Nd	3	3	3 M	TODGA >> MIDOA, TDGA
Pu	3	4	3 M	TODGA ~ MIDOA > TDGA
Zr	4	4	3 M	TODGA > TDGA > MIDOA
Ta	5	5	0.2 M	MIDOA > TDGA > TODGA
Mo	6	6	0.2 M	MIDOA > TDGA > TODGA
Tc	7	7	0.2 M	MIDOA > TODGA > TDGA
Ru	8	3	0.2 M	MIDOA > TDGA > TODGA
Ir	9	3	3 M	MIDOA > TODGA > TDGA
Pd	10	2	0.2 M	MIDOA > TDGA > TODGA
Pt	10	4	3 M	MIDOA > TODGA > TDGA
Ag	11	1	3 M	TDGA >> TODGA, MIDOA
Au	11	3	3 M	TDGA > TODGA, MIDOA
Hg	12	2	0.2 M	TDGA > TODGA, MIDOA
In	13	3	3 M	TODGA > MIDOA, TDGA
Pb	14	2	3 M	TODGA > TDGA > MIDOA
Bi	15	3	3 M	TODGA > MIDOA > TDGA
Te	16	4	0.2 M	MIDOA > TODGA > TDGA

From group 11 to 12, TDGA shows the highest extractability of all. In addition, TDGA shows high *D* values for Pd in group 10, analog performance to MIDOA. Especially, TDGA has very high *D* value for Ag, other extractants show the negligibly small *D*(Ag). TDGA is an excellent extractant to recover Ag into organic phase from HNO_3.

From group 13 to 16, some metals are extractable by TODGA. Te in group 16 forms the oxonium anion, so N-donor extractants may indicate the high extractability.

Comparing the metal-extraction behavior of TODGA, MIDOA and TDGA, extraction by MIDOA indicates the decrease of *D* with HNO_3 concentration [3]. The reason that is the protonation of N donor in MIDOA, it comes up with competition reaction between protons and metal to N donor at high acid condition. This extraction behavior is different feature from those of other O and S donor-type ligands.

3.2 Spectrometric results by three extractants

We obtained the results for IR and NMR of three extractants, some of the results for TODGA and MIDOA are reported already [5-6]. The results of NMR study are shown in Figure 2. The chemical shifts for concerning protons can be seen in this figure. The columns, TDGA, TODGA and MIDOA, indicate the peak

positions for extractant alone and those with metals. From this figure, the spectrum ④ for TDGA and TODGA showing the large shift (0.19 ppm for TDGA and 0.267 ppm for TODGA to low magnetic field) suggest the metal complexation with S and O donors at the ether position in TDGA and TODGA. In addition, spectra ② and ④ for MIDOA sample shows the large shift before and after metal extractions (for spectrum ②, 0.572 and 0.615 ppm shift of Pd and Re extractions, and for spectrum ④, 0.861 and 0.965 ppm shift of Pd and Re extractions), which indicates N-donor in ether position may show the strong bond to Pd and Re. Saeki pointed out [6] that MIDOA may form H^+MIDOA (protonation to N donor in MIDOA) prior to solvent extraction. Not only protonation but also complexation of metal with N donor give large shift with appearance of MIDOA measurements.

We have also the results of IR for these samples. One of the representative peak of extractant is C=O stretching at 1600-1700 cm^{-1}. This peak is easy to identify and widely use for chemical shift between complexed and non-complexed samples. The results of chemical shifts are shown, TODGA: 1653 cm^{-1}, TODGA+La: 1624 cm^{-1}, MIDOA: 1646 cm^{-1}, MIDOA+Re: 1653 cm^{-1}, and TDGA: 1646 cm^{-1}, TDGA+Pd: 1644 cm^{-1}. From these results, TODGA sample has high difference (to red shift) between two samples. Because La is hard acid metal and may bond with carbonyl oxygen atom, then show the large shift. Other metals, Pd and Re, are soft acid metal or oxonium anion bond to S and N donor atoms, then show the weak bonding with carbonyl oxygen.

Chemical shift of NMR spectrum ③ and ④ for TDGA samples

	Spectra (③)	Spectra (④)
TDGA	3.3 ppm	3.49 ppm
+ Pd	3.38	3.68

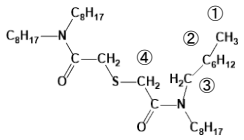

Chemical shift of NMR spectrum ③ and ④ for TODGA samples

	Spectra (③)	Spectra (④)
TODGA	3.153, 3.268 ppm	4.288 ppm
+ La	3.128, 3.284	4.555

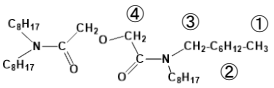

Chemical shift of NMR spectrum ③ and ④ for MIDOA samples

	Spectra (②)	Spectra (③)	Spectra (④)
MIDOA	2.545 ppm	3.235 ppm	3.555 ppm
+ Pd	3.117	3.282	4.416
+ Re	3.16	3.15	4.52

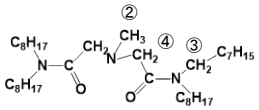

Figure 2 Peak positions of samples before and after metal extraction by ^{1}H-NMR

3.3 Calculation results by three extractants

In this work, the results of calculation for the complexes of TODGA, MIDOA and TDGA with Au, Pd, Zr and Tc are shown. Assuming that Au(III), Pd(II), Zr(IV), and Tc(VII) ions react with one to three molecules of extractant (see Table 2), the difference of the heat of formation during complex formation [ΔH_f/(kJ/mol)] can be calculated by

$$\Delta H_f = H_{f,\text{metal complex}} - (H_{f,\text{metal}} + nH_{f,L} + mH_{f,\text{anion}}). \quad (1)$$

where H_{fi} (i = metal complex, metal, L (TODGA, MIDOA, TDGA), and anion (NO_3^-)) are the relevant heat of formation of the species obtained by DFT calculations, and n and m are the stoichiometric coefficients of extractant and anion in metal complex. The $H_{f,L}$ (L: TODGA, MIDOA, TDGA) and $H_{f,anion}$ values for NO_3^- were calculated to be 20.5, 24.88, 13.95 and 4.58 kJ/mol, respectively, and the values were introduced into equation (1). The results of calculations are shown in Table 2. The apparent extraction constant, Int. y, can be inferred from the values of log y from the slope analysis of log D vs log [extractant]. The trend of ΔH_f decreasing with log y values can be referred from the previous paper [7]. The present results may be in agreement with the former studies that

Table 2 Relationship between Int. y and ΔHf among three extractants

	Extractant	No. of ligands	Int y	ΔHf
Au(III)	TODGA	1	0.964	322.26
	MIDOA	1	1.09	306.98
	TDGA	1	2.55	294.41
Pd(II)	TODGA	2	1.89	415.74
	MIDOA	2	5.05	341.28
	TDGA	1	3.71	287.99
Zr(IV)	TODGA	3	8.59	337.06
	MIDOA	2	3.81	352.1
	TDGA	2	1.5	377.06
Tc(VII)	TODGA	2	1.96	461.3
	MIDOA	1	2.71	251.42
	TDGA	1	1.8	314.95

indicates a negative relationship between ΔH_f and $\log K_{ex}$ [7]. The small difference obtained in this work from the previous paper might be the difference of No. of extractant associated in metal-complexes.

4. Summary

Three extractants, TODGA, MIDOA and TDGA, are compared to see the difference of extractabilities. From the present work, it is clear that metals of group 2-4 and 13-16 can be easily extracted by TODGA, metals of group 5-10 are for MIDOA and 11-12 are for TDGA. NMR and IR give the information on bonding of metals with donor atoms. The results of calculation for the heat of formation during complex formation give the reverse-correlation between ΔH_f and $\log K_{ex}$.

References

1) Y. Sasaki, Y. Sugo, S. Suzuki and S. Tachimori, *Solvent Extr. Ion Exch.*, **19**, 91-103 (2001).
2) Y. Sasaki, Y. Tsubata, Y. Kitatsuji, Y. Sugo, N. Shirasu, Y. Morita, T. Kimura, *Solvent Extr. Ion Exch.*, **31**, 401-415 (2013).
3) Y. Sasaki, M. Saeki, Y. Sugo, Y. Ikeda, T. Kawasaki, T. Suzuki, A. Ohashi, *Solvent Extr. Res. Dev. Jpn.* **22**, 37-45, (2015).
4) Y. Sasaki, K. Morita, M. Saeki, S. Hisamatsu, and K. Yoshizuka, *Hydrometallurgy* **169**, 576–584 (2017).
5) S. Murakami, M. Matsumiya, Y. Sasaki, S. Suzuki, S. Hisamatsu, K. Takao, Accepted in *Solvent Extr. Ion Exch.*
6) M. Saeki, Y. Sasaki, A. Nakai, A. Ohashi, D. Banerjee, A. C. Scheinost, H. Foerstendorf, *Inorg. Chem.* **51**, 5814−5821 (2012).
7) K. Uezu, K. Yoshizuka, *Solvent Extr. Res. Dev., Jpn.*, **2007**, *1-15*, 14.

Extraction of Nd and Y Using a Bifunctional Ionic Liquid

James QUINN[1,2], Karin H. SOLDENHOFF[1] and Geoffrey W. STEVENS[2]

[1]*ANSTO Minerals, Australian Nuclear Science & Technology Organisation, Sydney, Australia;* [2]*Department of Chemical & Biomolecular Engineering, University of Melbourne, Melbourne, Australia.*

The use of bifunctional ionic liquids for rare earth separations has attracted considerable interest in recent years. In this study, the extraction of Nd and Y by one such extractant is examined. The ionic liquid $R_4N^+EHEHP^-$ consists of the quaternary ammonium ion from Aliquat 336 (trioctyl/decylmethylammonium chloride) and the phosphonate ion from EHEHPA (2-ethylhexyl phosphonic acid 2-ethylhexyl mono ester). The interaction of the ionic liquid with acidic solutions, as well as the extraction of the rare earths is studied and complemented by $^{31}P\{^1H\}$ NMR and visible absorption spectroscopy. The results show that the extractant decomposes to a mixture of the protonated acid and quaternary ammonium chloride, with rare earths extracted through cation exchange by the phosphonic acid.

1. Introduction

The separation of the rare earth elements is a difficult task, most commonly achieved industrially by solvent extraction using EHEHPA (2-ethylhexyl phosphonic acid 2-ethylhexyl mono ester, also known by trade names P507, PC-88A and Ionquest 801). Recently, several reports have emerged of the use of 'bifunctional ionic liquids' (an ionic liquid containing a deprotonated cation exchanger and the cation from an anion exchanger) for rare earth separations [1-8]. There is debate about the exact mechanism for the extraction of rare earth elements, with some researchers pointing to neutral or solvating extraction mechanisms, and others suggesting cation exchange by the acidic component. Large separation factors for certain rare earth pairs have also been reported for some bifunctional ionic liquid extractants compared with traditional cation exchange reagents [2, 8] . This study investigates the process chemistry of one such extractant '$R_4N^+EHEHP^-$', consisting of the quaternary ammonium cation of Aliquat 336 (trioctyl/decylmethylammonium chloride), and the phosphonate anion of EHEHPA. The work was conducted at process relevant conditions to determine whether the use of an ionic liquid such as $R_4N^+EHEHP^-$ provides any advantages in practice when compared with EHEHPA.

2. Experimental

2.1 Reagents

Aliquat 336 (BASF), EHEHPA (SNF FloMin) and TOPO (trioctylphosphine oxide, Cytec) were used as received. Shellsol 2046 (Shell) was used as the diluent in all experiments except when

examining the interaction with acidic solutions (Section 3.1). In this case, toluene was used as the diluent to allow for comparisons with EHEHPA, which forms a third phase in Shellsol 2046 but not in toluene. Solutions of Nd and Y were prepared by dissolving the oxides (Nd_2O_3 and Y_2O_3, 99%) in HCl and diluting as required into the working solutions. All other reagents (NaCl, HCl, NaOH, KOH, isopropanol) were analytical grade reagents.

2.2 Preparation of Ionic Liquid

The reagent was synthesised using a modification of the procedure described by Sun et al. [9]. Aliquat 336 Cl (0.96 mol) was first added to a solution of KOH (0.96 mol) in isopropanol to convert to the quaternary ammonium hydroxide and precipitate KCl. This solution was then added to EHEHPA (0.79 mol) and mixed at 50 °C to form the quaternary ammonium phosphonate. The upper layer, which contained the extractant, was washed several times with water to remove the excess quaternary ammonium hydroxide and the solvent removed by rotary evaporation at 50 °C / 10 mbar.

2.3 Two-phase Titrations

A two-phase titration of $R_4N^+EHEHP^-$ was conducted by contacting the extractant (0.25 M) with a 1 M NaCl solution in a stirred beaker and adjusting the pH using 5 M HCl. The aqueous:organc phase ratio A:O was 1:1 and the temperature 21 °C. The pH of the dispersion was monitored using a Metrohm 6.0232.100 probe and 631 meter. The acid extraction (n_{HCl}) was determined by the difference between the acid added and that required for the measured pH change (as determined by a blank experiment with no extractant). The same process was conducted for EHEHPA, except that in this case the titrant was 1 M NaOH, and the moles of caustic consumed was calculated (n_{NaOH}). The results for both extractants were plotted as % protonation, defined as per Equations 1 and 2 (where $n_{R4N+EHEHP-}$ and n_{EHEHPA} are the moles of extractant present in the organic phase):

$$\%\ \text{Protonation}\ (R_4N^+EHEHP^-) = 100 \times \left(\frac{n_{HCl}}{n_{R4N+EHEHP-}} \right) \quad (1)$$

$$\%\ \text{Protonation}\ (\text{EHEHPA}) = 100 \times \left(1 - \frac{n_{NaOH}}{n_{EHEHPA}} \right) \quad (2)$$

2.4 Distribution Experiments

The distribution of Nd and Y between aqueous and organic phases was examined by first pre-equilibrating the organic phase (0.05 – 0.5 M $R_4N^+EHEHP^-$) with 1 M NaCl, with the pH of the dispersion controlled to the desired set point using 5 M HCl. A sample of the solvent was then withdrawn and the process repeated for successive pH set points. Each organic sample was then contacted with an aqueous phase containing 0.5 – 2.6 mM rare earths in 1 M NaCl / HCl solution for 30 minutes at the laboratory temperature (21 °C), at the same pH that the organic phase had been pre-equilibrated with. This ensured that the ionic strength of the aqueous phase remained constant in the distribution experiments, as otherwise the ionic liquid would have extracted HCl. The equilibrium pH was determined after the experiment. The A:O was 1:1 in all tests.

After the experiment, the organic phase was centrifuged and then stripped at an A:O of 2:1 using 5 M HCl. The feed solution, equilibrium aqueous and organic strip solutions were analysed by

ICP-MS (Perkin-Elmer Elan 9000) to determine the concentrations of Nd and Y.

2.5 Spectroscopy

$^{31}P\{^{1}H\}$ NMR spectra of 0.5 M EHEHPA and $R_4N^+EHEHP^-$ before and after loading with yttrium were recorded using a Bruker Avance DPX400. A coaxial insert containing 0.1 M H_3PO_4 in deuterated acetone was used for locking and referencing. Visible absorption spectra (560 – 620 nm) of 0.5 M EHEHPA and $R_4N^+EHEHP^-$ after loading with 21 - 23 mM Nd at pH 3 were recorded using a VWR UV-3100PC spectrophotometer. For comparison, the spectrum of 0.25 M TOPO loaded with 0.035 M Nd was also analysed.

3. Results and Discussion

3.1 Protonation of Ionic Liquid

The titration results reveal that the ionic liquid exhibits quite distinct acid base behavior when compared with EHEHPA (Figure 1). EHEHPA deprotonates sharply at around pH 7, consistent with formation of the sodium salt (Equation 3). Some dissociation of the sodium salt to the aqueous phase is also possible. However, the aqueous phase solubility of the closely related DEHPA (di-2-ethylhexylphosphoric acid) in alkaline media at salt concentrations of 5 % was reported to be quite low at 55 ppm (0.17 mM) [10]. The ionic liquid is initially fully deprotonated, and extracts acid in a considerably broader reaction between pH 1 and 8, reaching an acid:extractant molar ratio of 1:1. $^{31}P\{^{1}H\}$ NMR spectroscopy of the ionic liquid equilibrated at various pH values revealed a smooth downfield shift of the major resonance from 21.4 ppm (pH >8) to 30.2 ppm (pH <1). The NMR result is consistent with protonation of the phosphonate ion, and so it appears that Equation 4 is the appropriate expression for the extraction of acid by this extractant, that is protonation of phosphonate and formation of Aliquat 336-Cl as opposed to solvation of the acid (Equation 5).

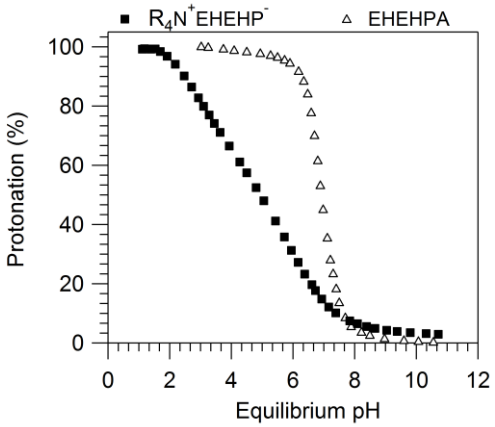

Figure 1. Protonation of 0.25 M extractants

$$\overline{HA} + NaOH \rightleftharpoons \overline{NaA} + H_2O \quad (3)$$

$$\overline{R_4N^+A^-} + HCl \rightleftharpoons \overline{R_4N^+Cl^-} + \overline{HA} \quad (4)$$

$$\overline{R_4N^+A^-} + HCl \rightleftharpoons \overline{R_4N^+A^- \cdot (HCl)} \quad (5)$$

The shift in protonation / deprotonation curve to lower pH, when compared with EHEHPA, is most likely to be due to ion pairing between the quaternary ammonium and phosphonate ions in the organic phase. The quaternary ammonium ion can be viewed as competing with protons for the available phosphonate ion. The change in acid-base behaviour means that the extractant is at least partially deprotonated in the expected region of interest for many rare earth separations (pH 1 – 5),

while for EHEHPA alone, the extractant remains almost fully protonated. The protonation reaction also has implications for recycling of the extractant after stripping with acidic solutions [11].

3.2 Extraction of Nd and Y

The effect of pH on the extraction of Nd and Y by $R_4N^+EHEHP^-$ is shown in Figure 2. The results show an increase in distribution ratios with increasing pH and extractant concentration. Yttrium is more strongly extracted than Nd, with a separation factor of around log $\beta_{Y/Nd}$ = 3.2. This is of a similar order as the literature separation factor for EHEHPA (log $\beta_{Y/Nd}$ = 2.9 [12]). The slope in the plot of log D vs pH ranged from around 1.6 to 1.8 for Nd (measured at D=1), with lower slopes measured at elevated pH (>3). For Y, measured between 0.1 and 1 M HCl, the slope was 2.6. Compared with data we have previously reported for 0.5 M EHEHPA under similar conditions, the extraction of yttrium by $R_4N^+EHEHP^-$ is weaker [13], meaning that it requires higher pH to achieve the same extraction.

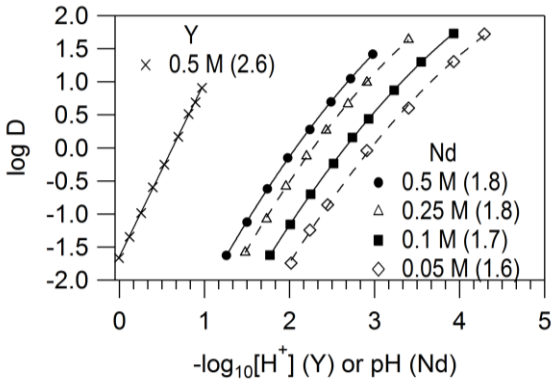

Figure 2. Effect of pH on extraction of Nd, Pr. ($R_4N^+EHEHP^-$ concentration as specified, slope of curve at pH_{50} in brackets)

The slope analysis indicates that at pH <1, the results are similar to what is generally observed for cation exchange by acidic extractants such as EHEHPA: i.e. a slope of approximately three in a plot of log D vs. pH (Equation 6). At elevated pH, however, the slopes are lower than this and the lines are concave down, which is not typically observed for EHEHPA.

$$RE^{3+} + 3\overline{H_2A_2} \rightleftharpoons \overline{RE(HA_2)_3} + 3H^+ \qquad (6)$$

An acid dependency in the extraction of rare earth elements has been reported for bifunctional ionic liquid extractants such as $R_4N^+EHEHP^-$ [2-7, 14]. It has been attributed either to the cation exchange behavior of the phosphonate ion, or to a neutral extraction mechanism for extraction of rare earths that is impacted upon by the co-extraction of acid (also by a neutral mechanism). In order to resolve this question, spectroscopic studies were carried out (Section 3.3). It should be possible to distinguish spectroscopically between a cation exchange complex formed with EHEHPA (i.e. $RE(HA_2)_3$) and a neutral complex of the form $RECl_3.(R_4N^+EHEHP^-)_n$.

3.3 Spectroscopy of complexes

The visible absorption spectra of Nd loaded EHEHPA and $R_4N^+EHEHP^-$ are compared in Figure 3.

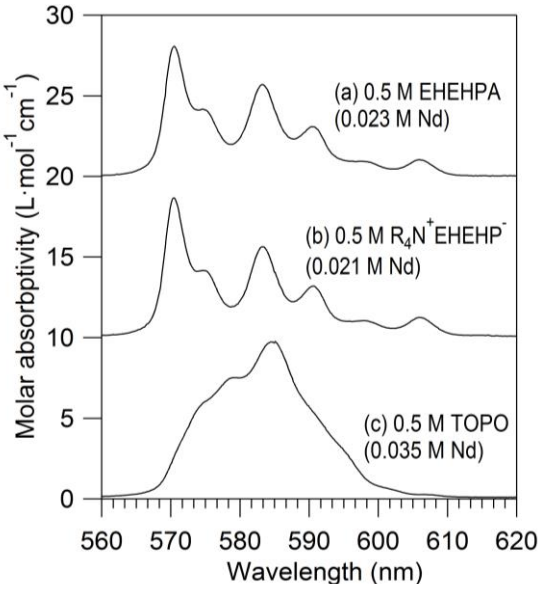

Figure 3. Visible absorption spectra of Nd loaded organic phases (spectra offset by 10 $L \cdot mol^{-1} \cdot cm^{-1}$)

The Nd^{3+} ion features a hypersensitive transition at around 570 nm. The spectrum for Nd loaded EHEHPA (Figure 3a) is similar to one previously reported, indicative of pseudo-octahedral geometry consistent with either $Nd(HA_2)_3$ or Nd_2A_6 [15]. Also shown in Figure 3c is the spectrum for a sample of Nd loaded TOPO (tri-n-octylphosphine oxide). The complex in this case would be of a $NdCl_3 \cdot (TOPO)_n \cdot (H_2O)_m$ adduct. The spectra are significantly different, with less well defined peaks with a maximum at approximately 585 nm in the Nd-TOPO spectrum. This is indicative of a change in coordination between the neutral complex compared with the cation exchange complex formed with EHEHPA. However, the spectrum for Nd loaded $R_4N^+EHEHP^-$ is indistinguishable from that of EHEHPA (Figure 3b).

$^{31}P\{^1H\}$ NMR was used to examine the chemical environment of the phosphorus containing ligands in EHEHPA and $R_4N^+EHEHP^-$. Spectra were recorded on neat samples of 0.5 M extractants before and after partially loading with yttrium (Figure 4). Yttrium was chosen in this case as Y^{3+} is diamagnetic and therefore there is no splitting of the $^{31}P\{^1H\}$ NMR spectrum. The approach is based on a similar study using DEHPA and lanthanum [16]. The EHEHPA spectrum prior to loading with yttrium reveals a single major signal at 30.7 ppm, with several minor peaks indicative of impurities of the commercial grade samples. After loading with yttrium, an additional signal is observed at 23.4 ppm, with considerable line broadening. The new complex is presumably the phosphonic acid associated with the yttrium complex, and the broadening indicates exchange between the free and complexed phosphonic acid. For $R_4N^+EHEHP^-$, the spectrum prior to loading (but after pre-equilibrating the extractant to pH 2), reveals a signal at 26.0 ppm. After loading, two signals are observed at 25.1 and 23.3 ppm. The former, based on integration of the signals, is consistent with the un-complexed phosphonate / phosphonic acid. The latter is in exactly the same position as the Y-EHEHPA signal. This suggests that:

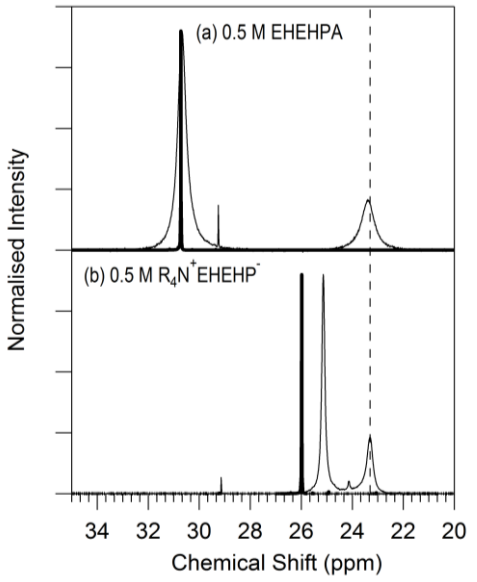

Figure 4. $^{31}P\{^1H\}$ NMR spectra of organic phases before and after loading with 26 mM Y (thick lines: prior to loading)

1) The chemical environment of the uncomplexed phosphonate / phosphonic acid is different from EHEHPA and changes with pH, consistent with results presented in Section 3.1, and
2) The chemical environment of the phosphonate ion complexed with yttrium is identical to that in the Y-EHEHPA complex.

3.4 Proposed Mechanism

The visible and NMR spectroscopy in Section 3.3 reveals that the chemical environment of the both the metal and ligand are identical for EHEHPA and $R_4N^+EHEHP^-$; in other words the complex formed is identical for the two extractants. However, the Nd and Y extraction data for $R_4N^+EHEHP^-$ (Section 3.2) is quite different from the cation exchange behavior of EHEHPA, with curved log D vs pH plots with slope <3, with the magnitude of the slope being dependent on the equilibrium pH. In

addition, the distribution ratios are depressed compared with EHEHPA alone.

Our hypothesis for this apparent discrepancy lies with the acid base behaviour evident in the results of Section 3.1. At low pH, the data indicates that the extractant is predominantly protonated, while as the pH increases the phosphonic acid is increasingly deprotonated favouring formation of the ionic liquid. If it is assumed that the dominant extraction mechanism is one of cation exchange by the phosphonic acid (as evident in the spectroscopic data), then increasing the pH would on one hand favour the extraction of rare earths (Equation 6), but on the other hand the free phosphonic acid concentration would decrease, which would decrease the extraction of rare earths. The latter explains the reduced slopes and curved nature of the plots at elevated pH, as well as the antagonism compared with EHEHPA alone. The proposed mechanism represented in Figure 5 is consistent with the slope analysis and spectroscopy data obtained in this study.

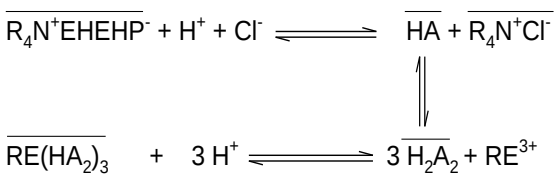

Figure 5. Proposed extraction mechanism

4. Conclusion

The results demonstrate that the ionic liquid extractant $R_4N^+EHEHP^-$ extracts acid and decomposes to a mixture of EHEHPA and $R_4N^+Cl^-$ after equilibration with HCl solutions. This has a pronounced effect on the extraction of rare earths, shifting the extraction to higher pH and lower slopes compared with EHEHPA. $^{31}P\{^1H\}$ NMR and visible absorption spectroscopy revealed that the extracted complex was identical to that formed upon extraction by EHEHPA. The proposed mechanism for the ionic liquid is one of extraction of rare earths through cation exchange by the phosphonic acid, moderated by the pH dependent interaction between the phosphonate and quaternary ammonium ions.

Acknowledgement

The authors acknowledge Patrick Yee (ANSTO) and the ANSTO Minerals analytical team for analysis of samples.

References

1) X. Sun, Y. Ji, F. Hu, B. He, J. Chen, D. Li, *Talanta*, **81**, 1877-1883 (2010).

2) J. Chen, L. Guo, Y. Deng, D. Li. In *Proceedings of the 52nd Conference of Metallurgists (COM)*, Montreal, Canada. London, I. M., Goode, J. R., Moldoveanu, G., Rayat, M. S., Eds. Canadian Institute of Mining, Metallurgy and Petroleum: Montreal, Canada, pp 367-374 (2013).

3) H. Yang, W. Wang, H. Cui, D. Zhang, Y. Liu, J. Chen, *J. Chem. Technol. Biotechnol.*, **87**, 198-205 (2012).

4) A. Rout, K. A. Venkatesan, T. G. Srinivasan, P. R. Vasudeva Rao, *Sep. Purif. Technol.*, **95**, 26-31 (2012).

5) V. V. Belova, A. A. Voshkin, A. I. Kholkin, A. K. Payrtman, *Hydrometallurgy,* **97**, 198-203 (2009).

6) A. Rout, J. Kotlarska, W. Dehaen, K. Binnemans, *Phys. Chem. Chem. Phys.*, **15**, 16533-16541 (2013).
7) L. Shen, J. Chen, L. Chen, C. Liu, D. Zhang, Y. Zhang, W. Su, Y. Deng, *Hydrometallurgy,* **161**, 152-159 (2016).
8) L. Guo, J. Chen, L. Shen, J. Zhang, D. Zhang, Y. Deng, *ACS Sustain. Chem. Eng.*, **2**, 1968-1975 (2014).
9) X. Sun, Y. Ji, Y. Liu, J. Chen, D. Li, *AIChE Journal*, **56**, 989-996 (2010).
10) C. A. Blake, K. B. Brown, C. F. Coleman *The extraction and recovery of uranium (and vanadium) from acidic liquors with di(2-ethylhexyl) phosphoric acid and some other organophosphorus acids*; ORNL-1903; Oak Ridge National Laboratory: 1955.
11) J. E. Quinn, K. H. Soldenhoff, G. W. Stevens, *Hydrometallurgy,* **169**, 306-313 (2017).
12) G. Xu, C. Huang, S. Gao, *Rare Earths (in Chinese)*. Metallurgical Industry Press: Beijing, China, Vol. 2, p 534, (1995).
13) J. E. Quinn, K. H. Soldenhoff, G. W. Stevens, N. A. Lengkeek, *Hydrometallurgy,* **157**, 298-305 (2015).
14) J. E. Quinn, K. H. Soldenhoff, G. W. Stevens, *Hydrometallurgy,* **169**, 621-628 (2017).
15) G. J. Lumetta, S. I. Sinkov, J. A. Krause, L. E. Sweet, *Inorg. Chem.*, **55**, 1633-1641 (2016).
16) C. Marie, B. Hiscox, K. L. Nash, *Dalton Trans*, **41**, 1054-1064 (2012).

Anomalously Suppressed Ion-exchange Extraction Behavior of Ni(II) into Ionic Liquids with Using *N*,*N*,*N'*,*N'*-Tetrakis(2-pyridylmethyl)ethylenediamine as a Neutral Chelator

Natsumi ASANO, Kotaro MORITA and Naoki HIRAYAMA*

Department of Chemistry, Faculty of Science, Toho University, Funabashi 274-8510, Japan

In use of *N*,*N*,*N'*,*N'*-tetrakis(2-pyridylmethyl)ethylenediamine (**tpen**) as a hexadentate neutral chelator, ion-exchange extractability for Ni(II) into an ionic liquid (IL), 1-butyl-3-methylimidazolium bis(trifluoromethanesulfonyl)imide (C_4mimTf_2N), was anomalously suppressed. From comparative extraction experiments with using different ILs and/or chelators corresponding to several substructures of **tpen**, it was suggested that **tpen** coordinates to Ni^{2+} as a tetradentate ligand in C_4mimTf_2N and that two 2-pyridylmethyl pendant arms in **tpen** without coordinating to Ni^{2+} resulted in the extraction suppression due to their relatively high protonation ability.

1. Introduction

Hydrophobic ionic liquids (ILs), including 1-alkyl-3-methylimidazolium bis(trifluoromethanesulfonyl)imide ($C_n$mimTf_2N, Figure 1), can extract many ionic species having hydrophobic and/or IL-philic nature from aqueous solutions via ion-exchange process. In extraction of metal cations into ILs via cation-exchange, their hydrophobization by forming complexes with monodentate neutral ligands or neutral chelators is imperative process.

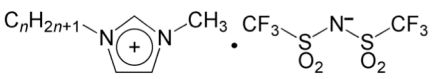

Figure 1. Chemical structure of $C_n$mimTf_2N.

N,*N*,*N'*,*N'*-Tetrakis(2-pyridylmethyl)ethylenediamine (**tpen**, Figure 2) is a hexadentate neutral chelator having four 2-pyridylmethyl pendant arms, and can form cationic complexes with many metal cations. Several researchers have studied its possible use for ion-pair extraction of several metal cations into organic solvents [1,2] and that for their cation-exchange extraction into ILs [3].

In study on cation-exchange extraction of several divalent metals into C_4mimTf_2N with using **tpen**, we wandered upon a curious fact that extraction of Ni(II) was dominantly suppressed. To clarify cause for the anomalous suppression, we investigated cation-exchange extraction behavior of Ni(II) with different chelators [*N*,*N'*-bis-(2-pyridylmethyl)ethylenediamine (**bpen**), bis(2-pyridyl-methyl)amine (**bpa**) and 2-(aminomethyl)pyridine (**ap**),

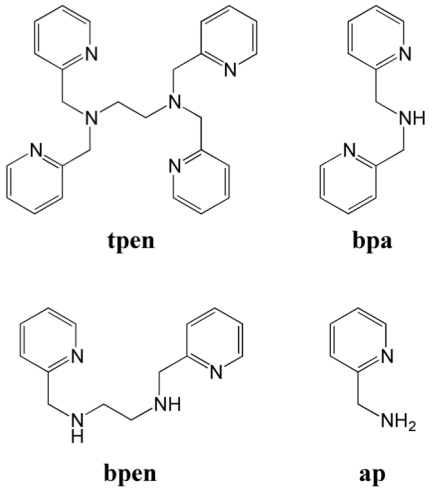

Figure 2. Chemical structures of the chelators used in this study.

Figure 2] corresponding to several substructures of **tpen**.

2. Experimental

2.1 Chemicals and apparatus

The three ILs (C_2mimTf_2N, C_4mimTf_2N and C_8mimTf_2N) were synthesized according to the previous reports [4,5]. The chelators (**tpen**, **bpen**, **bpa** and **ap**), nitrobenzene and other reagents were of reagent-grade materials purchased from Dojindo (Kumamoto, Japan), TCI (Tokyo, Japan) and other suppliers, and were used without further purification. High-purity water was produced with a Millipore Direct-Q water purification system.

A Thermo Fisher Model iCE3300 flame atomic absorption spectrometer was used for the determination of the metals in the aqueous phase. A Horiba Model F-72 pH meter equipped with a Horiba 9680-10D combined glass electrode was used to measure the pH values.

2.2 Extraction procedure

Aqueous phase (5 mL, pH 1–5) containing 2.0 μg mL^{-1} of Ni(II), Cu(II), Zn(II) or Mn(II), 0.1 M $NaClO_4$ (or KNO_3). 0.01M buffer (chloroacetic acid or acetic acid) was shaken to be equilibrated with extraction phase (1 mL, an IL or nitrobenzene) containing 1.0×10^{-3} M **tpen**, 2.0×10^{-3} M **bpen**, 2.0×10^{-3} M **bpa** or 4.0×10^{-3} M **ap**. On extraction at more acidic condition, suitable amount of HNO_3 was used instead of buffer and $-\log C_{HNO3}$ value was used instead of aqueous phase pH. After phase separation by centrifugation, the metal contents in the both phases were determined with using flame AAS, and extraction ratio (%*E*) and distribution ratio (*D*) for the metal were calculated. (The content in the extraction phase was determined after back-extraction into 1–3 M HNO_3.)

3. Results and Discussion

3.1 Extraction behavior of divalent metals into C_4mimTf_2N with tpen

Figure 3 shows extraction behavior of Ni(II), Cu(II), Zn(II) and Mn(II) into nitrobenzene and C_4mimTf_2N containing 1.0×10^{-3} M **tpen**. Changing $NaClO_4$ to KNO_3 in the nitrobenzene system resulted in the loss of metal extractability, whereas that in the C_4mimTf_2N system resulted in no change. Namely, the cationic **tpen** complexes were extracted as ion-pair with ClO_4^- in the former system and via cation-exchange mechanism in the latter system.

Cu(II), Zn(II) and Mn(II) showed similar extraction behavior between the nitrobenzene and C_4mimTf_2N systems. On the contrary, extraction of Ni(II) into C_4mimTf_2N was quite low compared to that into nitrobenzene. In addition, it was confirmed from slope analysis (log *D* vs. log $[\mathbf{tpen}]_e$) that the extracted species into nitrobenzene is

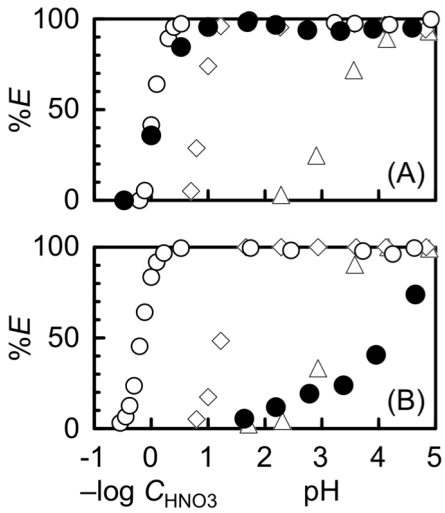

Figure 3. Extraction behavior of Ni (●), Cu (○), Zn (◇) and Mn (△) into nitrobenzene (A) or C_4mimTf_2N (B) with **tpen**.

M(**tpen**)$^{2+}$·2ClO_4^- ion-pair and that into C_4mimTf_2N is M(**tpen**)$^{2+}$ cation (except for Ni(II)).

3.2 Extraction behavior of Ni(II) into C_4mimTf_2N with bpen, bpa and ap

To make the suppression of Ni(II) extractability clear, extraction behavior of Ni(II) with using **bpen**, **bpa** and **ap** was investigated. On each experiment, chelator concentration was set based on the number of the 2-pyridylmethyl pendant arm.

The results are shown in Figure 4. In use of **bpa** and **ap**, the nitrobenzene system and the C_4mimTf_2N system showed similar extraction behavior. In use of **bpen**, intriguingly, the C_4mimTf_2N system showed high extractability for Ni(II), whereas the nitrobenzene system showed quite low one. Since **bpen** is a tetradentate chelator, Ni(**bpen**)$^{2+}$ complex seems to be coordinatively-unsaturated (hydrated) one. C_4mimTf_2N has lower hydrophobicity than nitrobenzene and, therefore, the **bpen**-C_4mimTf_2N seems to show relatively high Ni(II) extractability.

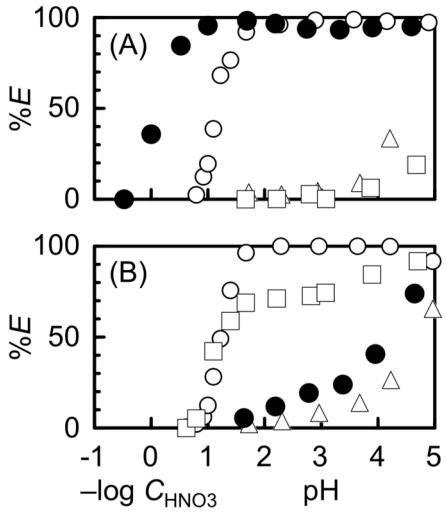

Figure 4. Extraction behavior of Ni(II) into nitrobenzene (A) or C_4mimTf_2N (B).
● **tpen**, □ **bpen**, ○ **bpa**, △ **ap**

On the contrary, hexadentate chelator **tpen** can form coordinatively-saturated complex with Ni(II). Namely, structure of the extracted cationic Ni(II)-**tpen** complex in the C_4mimTf_2N system seems to be different from that in the nitrobenzene system. In other words, it was suggested that the additional two 2-pyridylmethyl pendant arms in **tpen** play some role in the extraction suppression in the C_4mimTf_2N system.

3.3 Extraction behavior of Ni(II) into various ILs with bpen and tpen

To evaluate the relationship between Ni(II) extractability and relative hydrophobicity of extraction phase solvent, extraction behavior of Ni(II) with **bpen** and **tpen** into C_2mimTf_2N and C_8mimTf_2N was investigated. The results are shown in Figure 5 with the data for the C_4mimTf_2N and nitrobenzene systems.

In use of **bpen**, the order of Ni(II) extractability between solvents at pH 2–3 was C_2mimTf_2N > C_4mimTf_2N > C_8mimTf_2N > nitrobenzene, which is the inverse order of hydrophobicity of the solvents. This result is consistent with the relatively low hydrophobic nature of

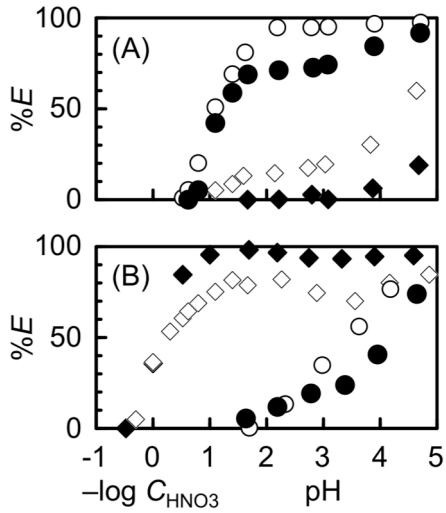

Figure 5. Extraction behavior of Ni(II) with **bpen** (A) and **tpen** (B) into C_2mimTf_2N (○), C_4mimTf_2N (●), C_8mimTf_2N (◇) or nitrobenzene (◆).

coordinatively-unsaturated (hydrated) Ni(**bpen**)$^{2+}$. In addition, the order between ILs, C_2mimTf_2N > C_4mimTf_2N > C_8mimTf_2N, accorded with conventional order in cation-exchange extraction into ILs [6].

In use of **tpen**, on the contrary, the order of Ni(II) extractability between solvents at pH 1–2 was nitrobenzene > C_8mimTf_2N >> C_4mimTf_2N ≈ C_2mimTf_2N. Interestingly, C_8mimTf_2N having higher hydrophobicity than C_4mimTf_2N showed similar Ni(II) extractability to nitrobenzene, whereas C_2mimTf_2N having lower hydrophobicity showed similar one to C_4mimTf_2N. Probably, coordinatively-saturated (unhydrated) hydrophobic Ni(**tpen**)$^{2+}$ complex prefers more hydrophobic solvents.

The pK_a values for H_4**tpen**$^{4+}$, H_3**tpen**$^{3+}$, H_2**tpen**$^{2+}$ and H**tpen**$^{+}$ are 2.95, 3.35, 4.86 and 7.19, respectively [7], whereas respective ones for the protonated **bpen** are 1.62, 1.81, 5.45 and 8.23 [8]. These values show that the pendant arms on **tpen** have high affinity for H^+ compared to those on **bpen**. In less-hydrophobic ILs such as C_4mimTf_2N and C_2mimTf_2N, it was suggested that **tpen** coordinates to Ni^{2+} not as a hexadentate ligand but as a tetradentate one to form relatively less-hydrophobic complex and that non-coordinating pyridine-N atoms on the free pendant arms are protonated, resulting in distribution of the more-charged (protonated) complex into the aqueous phase.

Acknowledgement

This study was financially supported in part by JSPS KAKENHI Grant No. JP26410162 from the Japan Society for the Promotion of Science, and MEXT-Supported Program for the Strategic Research Foundation at Private Universities (2012–2016) from the Ministry of Education, Culture, Sports, Science and Technology, Japan.

References

1) M. Watanabe, R. Mirvaliev, S. Tachimori, K. Takeshita, Y. Nakano, K. Morikawa, R. Mori, *Chem. Lett.*, 1230-1231 (2002).
2) N. Hirayama, S. Iimuro, K. Kubono, H. Kokusen, T. Honjo, *Anal. Chim. Acta*, **339**, 115-121 (1997).
3) K. Shimojo, H. Naganawa, F. Kubota, M. Goto, *Chem. Lett.*, **35**, 484-485 (2006).
4) S. V. Dzyuba, R. A. Bartsch, *ChemPhysChem*, **3**, 161-166 (2002).
5) A. K. Burrell, R. E. Del Sesto, S. N. Baker, T. M. McCleskey, G. A. Baker, *Green Chem.*, **9**, 449-454 (2007).
6) T. Hamamoto, M. Okai, S. Katsuta, *J. Phys. Chem. B*, **119**, 6317-6325 (2015).
7) G. Anderegg, F. Wenk, *Helv. Chim. Acta*, **50**, 2330-2332 (1967).
8) R. G. Lacoste, A. E. Martell, *Inorg. Chem.*, **3**, 881-884 (1964).

Selective Recovery of Zn(II) From Multimetal Acidic Chloride Solution with Hydrophobic Pyridine Derivatives

Aleksandra WOJCIECHOWSKA*, Karolina WIESZCZYCKA, Irmina WOJCIECHOWSKA
University of Technology, Institute of Chemical Technology and Engineering, Berdychowo St. 4, 60-965 Poznan, Poland

The main goal of this work was the application of derivatives of 1-(3-pyridyl)undecan-1-one as the selective extractants of zinc(II) ion from strong acidic chloride solutions containing also iron(II), iron(III) or lead(II). The effect of different variables influencing the extraction of zinc(II) ion such as the concentration of hydrochloric acid and chloride ion was investigated. The study also covered the selective stripping process. Laboratory-scale experiments were also performed and the obtained results indicated that the studied extractants were efficient and highly selective for zinc(II) and they can be proposed for the zinc ion removal from real spent pickling solution.

1. Introduction

Metal plating has been identified as an environmentally risky industrial sector concerning the potential hazardous nature of its waste streams since they often contain reasonable amounts of acids and heavy metals such as Zn, Pb, Fe, etc. The concentration of some metals in these wastes is relatively high thus making their recovery an interesting issue [1-3].

Solvent extraction is one of the most important techniques for the separation and recovery of metals in the industry. The undoubted advantage is the low power consumption and the ability to re-use extractants. This method is attractive from economic and environmental point of view. In recent years, a lot of novel compounds capable to coordinate the metal and to transfer the resulting complex to the hydrophobic organic solution have been proposed. These properties of the organic compounds are desirable both in analytical techniques and in metals extraction processes [4].

Derivatives of 1-(3-pyridyl)undecan-1-one are the most interesting group of non-commercial extracting agents. The pyridine ketoximes can form complexes with various metals ion, for example: zinc, copper, lead, iron, in the acidic solution. These compounds can form complexes with metals according to ion-pair and solvating mechanisms [5,6].

The aim of this work was to investigate the extraction properties of the pyridine derivatives towards Zn(II). The most important stage was to determine the effect of the different parameters on the selective Zn(II) removal from multimetal acidic chloride solutions.

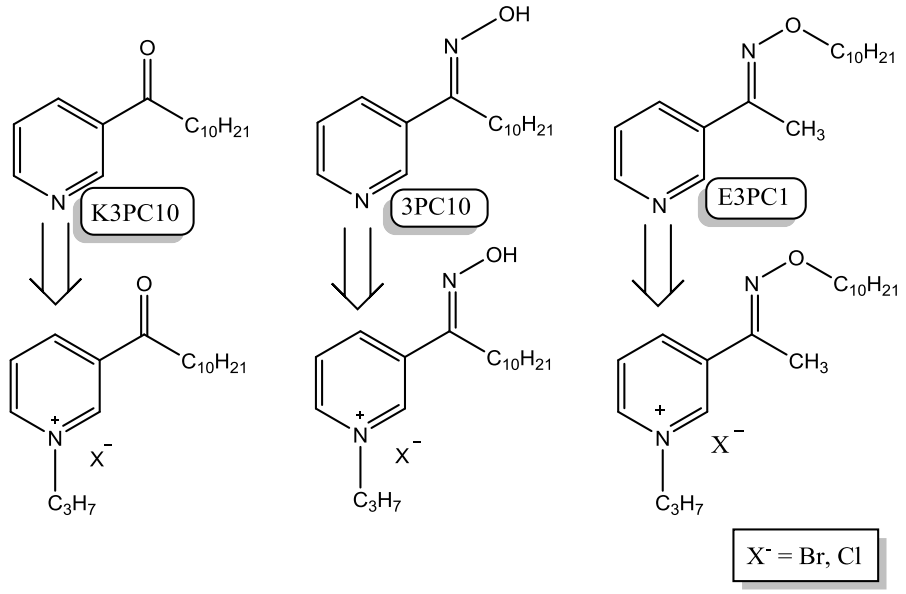

Figure 1. Structure of studied reagents.

2. Experimental

2.1 Reagents

- 1-(3-pyridyl)undecane-1-one (**K3PC10**),
- 1-propyl-3-undecanoylpyridinium bromide(**K3PC10-Br**),
- 1-propyl-3-undecanoylpyridinium chloride (**K3PC10-Cl**),
- 1-(3-pyridyl)undecan-1-one oxime (**3PC10**),
- 3-[1-(hydroxyimine)undecyl]-1-propylpyridinium bromide (**3PC10-Br**),
- 3-[1-(hydroxyimine)undecyl]-1-propylpyridinium chloride (**3PC10-Cl**),
- *N*-decyloxy-1-(3-pyridyl)ethanoimine (**E3PC1**),
- 3-[1-(N-decyloxyimine)ethyl]-1-propylpyridinium bromide (**E3PC1-Br**) and
- 3-[1-(N-decyloxyimine)ethyl]-1-propylpyridinium chloride (**E3PC1-Cl**) were synthesized according to procedure described in previous papers [5-10].

All reagents used in this study were of reagent grade. Toluene (POCH, Poland) and decan-1-ol (Merck, Germany) were used as components of the organic phase. Sodium chloride (Chempur, Poland), sodium nitrate(V) (Sigma-Aldrich, Germany), hydrochloric acid (38%) (POCH, Poland), nitric acid (70%) (POCH, Poland), zinc(II) chloride (anhydrous) (Sigma-Aldrich, Germany), iron(III) chloride (hexahydrate), iron(II) chloride (anhydrous) (Sigma-Aldrich, Germany), copper(II) chloride (hexahydrate) (Sigma-Aldrich, Germany) and lead(II) nitrate (Sigma-Aldrich, Germany) were used to compose the aqueous phase.

2.2 Extraction studies

Extraction studies of individual metal were carried out in a test tube using an organic to aqueous volume ratio (O/W) equal to 1. Both phases were shaken for 30 minutes at room temperature (21 -

23 ^{o}C) using a Bio-mix BWR04. Aqueous feed solutions were prepared by dissolving the appropriate amounts of the chloride or nitrate salts of zinc(II), sodium and lithium in ultrapure water. The research was carried out at a constant chloride ion concentration (4 mol/L) and various hydrochloric acid concentrations (from 0 to 4 mol/L), or at a constant mineral acid concentration (HCl or HNO_3, 0.5 mol/L) and various chloride ion concentrations (from 0 to 4 mol/L). The ionic strength of the aqueous solutions was constant I= 4 mol/L. The selectivity test was performed using the aqueous feed solution containing 1 g/L of Zn(II), Fe(II), Fe(III) and Pb(II) (1.91 g/L) ions and 1 or 4 mol/L HCl. Cumulative concentration of chloride ion was equal 4 mol/L. An organic phase used in the extraction studies contained synthesised compound and toluene with 10% (v/v) addition of decan-1-ol. The concentration of the extractant was 0.1 mol/L. A loaded organic solution containing 0.1 mol/L of the extractant was employed for stripping tests in which the organic phase was shaken with: water, 0.05, 0.1 and 0.5% of HCl, 5% Na_2SO_4 and 30% HNO_3, 1% oxalic acid, 1% sodium oxalate or their mixtures at phase ratio O/W equal to 1. The metal concentration was determined by the atomic absorption spectrometry using Z8200 (Hitachi) apparatus.

2.3 Calculations

Metal ion concentration in the organic phase $[M]_{org}$ were determined from the difference of the metal ion concentration in the aqueous phases before $[M]_{aq,0}$ and after the extraction $[M]_{aq}$. Distribution ratio (D), percentage extractions (%E) and separation factor of Zn towards Fe and Pb ions ($\beta_{Zn/M}$) were calculated from equations:

$$D = \frac{[M]_{org,eq}}{[M]_{aq,eq}} \quad (1)$$

$$\%E = \frac{[M]_{aq,o} - [M]_{aq,eq}}{[M]_{o,aq}} \times 100\% \quad (2)$$

$$\beta_{Zn/M} = \frac{D_{Zn}}{D_M} \quad (3)$$

where $[M]_{aq,o}$ is the initial metal concentration, $[M]_{aq,eq}$ and $[M]_{org,\,eq}$ are the metal ion concentration after the extraction in the aqueous and organic phases, respectively. D_M are Fe or Pb distribution ratio.

3. Results and Discussion

The effect of variable concentration of HCl in the aqueous phase containing constant chloride ion concentration (4 mol/L) on the zinc(II) extraction with the studied extractants are presented in Figure 2. It was worth noting that the extraction of Zn(II) increases progressively with the increasing HCl concentration. The extraction of zinc(II) from the acidic chloride solutions also strongly depends on the structure of the studied reagents and the greatest results are observed for E3PC1, E3PC1-Cl and E3PC1-Br.

Other metals are also extracted with noticeable yield, all obtained derivatives are excellent extracting reagents for copper(II), as well as they are suitable for the recovery of lead(II) and iron(III) from strongly acidic solutions. For the alkylpyridylketone and its quaternary salts (K3PC10, K3PC10-Br and K3PC10-Cl) the results of the copper(II) recovery do not depend on the acidity but

depend strongly on the concentration of chloride ion. However, on using 3PC10 and E3PC1 and their quaternary salts, the extraction of Cu(II) strongly depends on acidity of the aqueous phase [11]. The novel reagents have also been studied as the Pb(II) extractants from chloride and chloride/nitrate solutions [8,10]. In this case, also the best ligands were the compounds containing ether group (E3PC1, E3PC1-Br and E3PC1-Cl) which extract Pb(II) in approximately 90%. Furthermore, the ether derivatives have no ability to extract iron(II) but can extract iron(III) from the acidic solutions (%E = 20-60% and depends on the extractant structure).

The stripping efficiency depends on type of metals, extractants and stripping agents, and ranges from 87 to 100% for zinc and copper, 60-98% for iron and 55-57% for lead(II) in double stripping process .

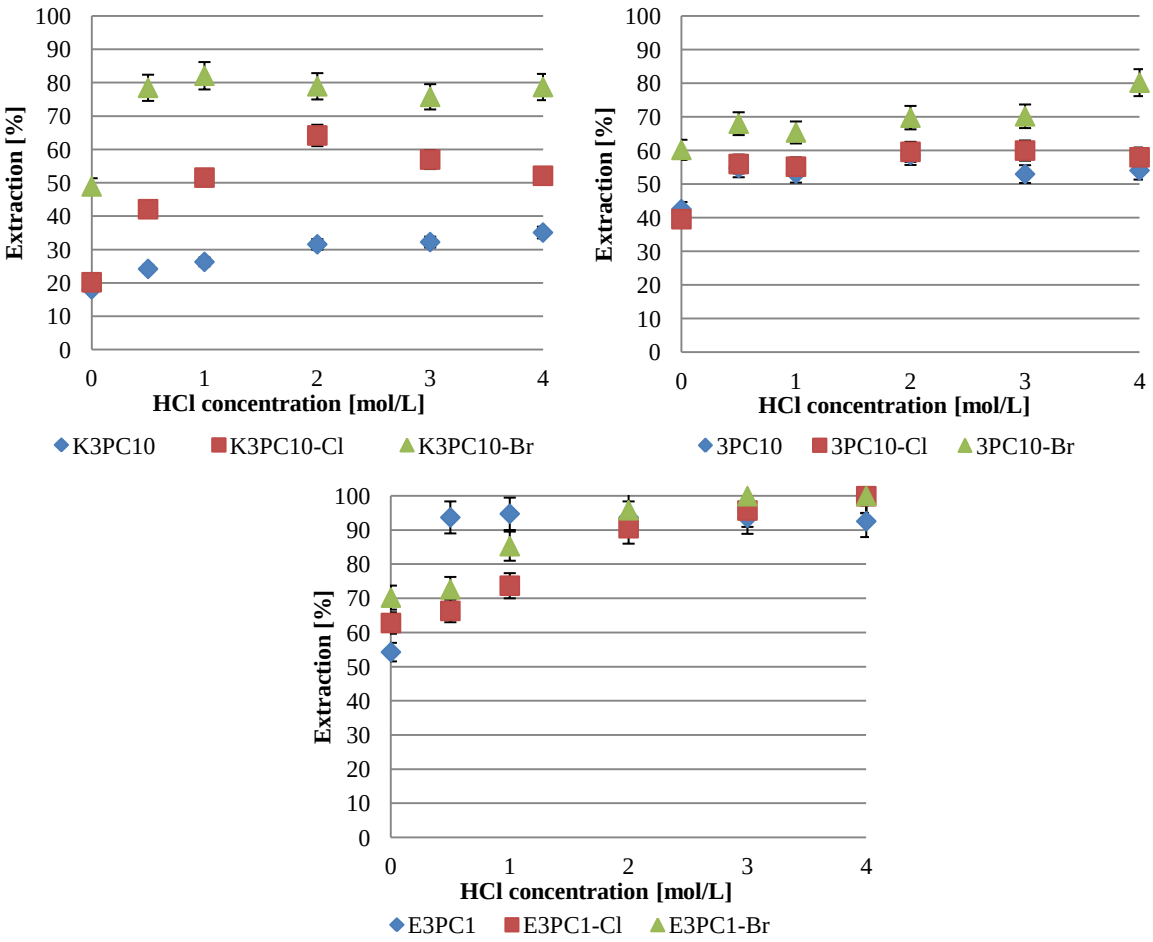

Figure 2. Influence of HCl concentration on zinc extraction

The selective recover of the metal ion from different sources is an important issue in the production of a high-pure metal. The effective recovery of metal ion is possible only if the process (extraction or stripping stage) is sufficiently selective [12,13]. The selectivitity of the extraction from the multimetal aqueous solutions, which contain zinc(II), iron(II) and iron(III), were studied for the solutions containing 4 M Cl^- (NaCl/HCl). The obtained results indicate that the most selective

extractant of zinc(II) over iron are 3PC10 and E3PC1 (Table 1).

Table1. Extraction of zinc(II) from multimetal aqueous solutions with 3PC10, 3PC10-Br, E3PC1 and K3PC10-Br

Composition of aqueous solution	**Extraction [%]**											
	3PC10 [6]			**3PC10-Br**			**E3PC1**			**K3PC10-Br**		
	Zn	Fe(II)	Fe(III)	Zn	Fe(II)	Fe(III)	Zn	Fe(II)	Fe(III)	Zn	Fe(II)	Fe(III)
4M HCl	100	0	0	61.2	0	12.3	100	0	13.9	66.1	0	22.0
2M NaCl /2M HCl	100	0	0	54.8	0	0.9	100	0	29.8	83.1	0	46.5

In the case of lead(II) the selectivity studies of the extraction were performed using the synthetic aqueous solutions containing 1 g/L Zn(II), 1.91 g/L Pb(II), 1.1 g/L Fe(III) (or 1.1 g/L Fe(II)) and 4 mol/L HCl. This level of chloride ion concentration was chosen because at 4 mol/L HCl a maximum extraction of zinc(II) with hydrophobic pyridine derivatives was observed. The studied 3PC10-Cl salt can be used for a selective extraction of Zn(II) over Fe(II) and Fe(III) (extraction below 0.1%), whereas the co-extracted Pb(II) can be removed in the stripping process.

According to the experimental data, a flow sheet has been constructed (Figure 3), in which after the extraction iron(III) ion remained in the feed solutions, but the co-extracted Zn(II) can be first removed by washing with water (100% removal) and then Pb(II) can be stripped with the 1% solution of oxalic acid and sodium oxalate (10:1, w/w).

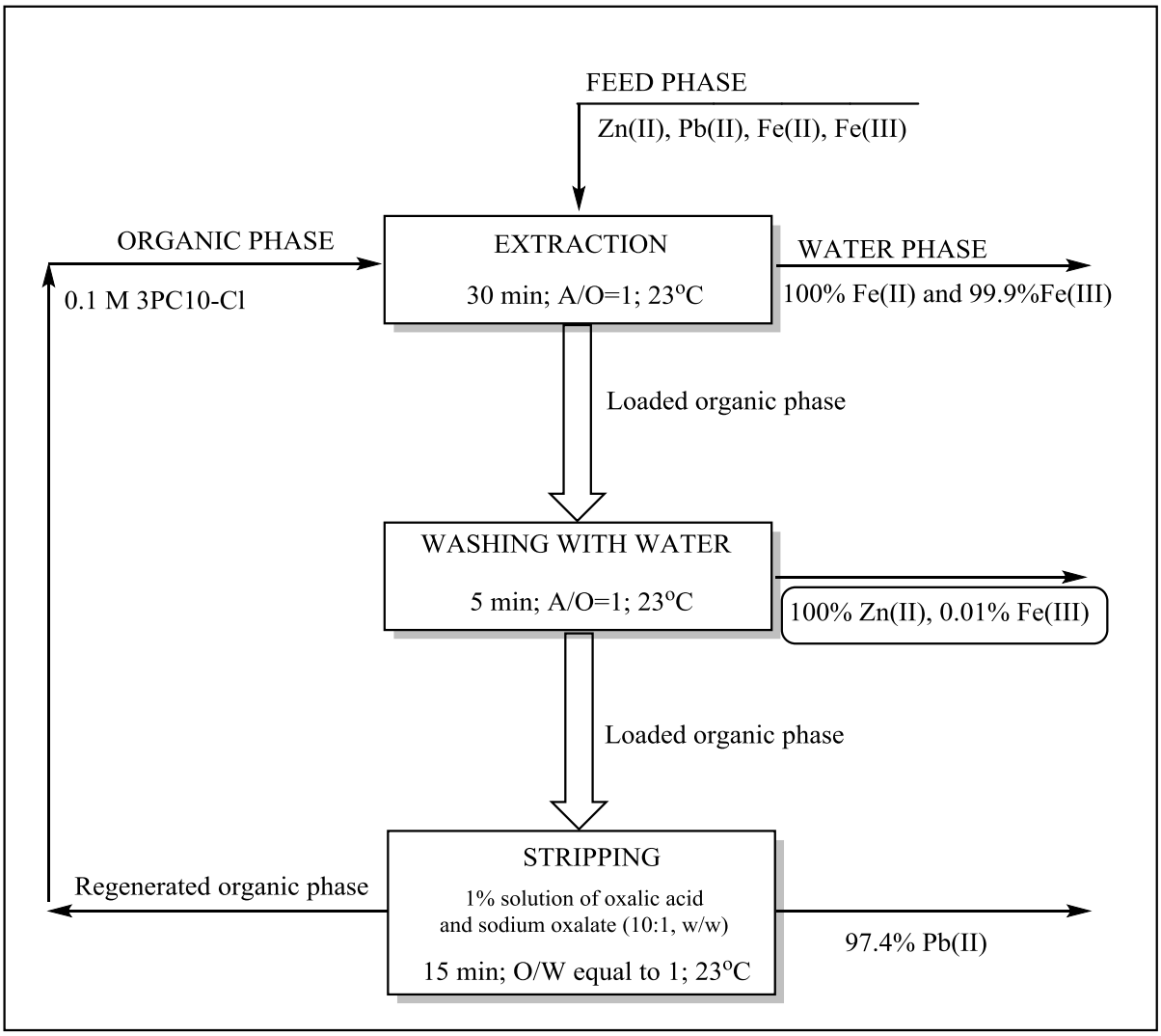

Figure 3. Flow-sheet for recovery of Zn(II) from Zn(II)-Pb(II)-Fe(II)-Fe(III) chloride solution using 3PC10-Cl

4. Conclusion

The obtained results showed that, regardless on the extractant structure, the increase of the chloride concentration increased the extraction of Zn(II). However, at the studied conditions better extraction properties towards zinc(II) demonstrated E3PC1 and its quaternary salts. The extraction and stripping processes kinetic of Zn, Pb and Fe were fast. The stripping process was also proposed as a method enabling the separation of the Zn(II) from the solution containing both Zn-Pb-Fe. Moreover, regardless of the stripping phase composition, the regenerated organic phase can be used frequently without affecting the extraction ability.

Acknowledgement

This study was funded by National Science Center Poland research grant funds according to decision No. DEC-2015/17/N/ST8/00285.

References

1) C.K. Gupta, Chemical Metallurgy-principles and practice, *WILEY-VCH Verlag GmbH & Co. KGaA*, Weinheim (2003).
2) G. Csicsovszki, T. K´ekesi, T. Torok, *Hydrometallurgy*, **77**,19–28 (2005).
3) J.M. Magalhaes, J.E. Silva, F.P. Castro, J. A. Labrincha, *J. Environ.Manage.*, **75**,157–166 (2005).
4) M. Tomaszewska, M. Gryta, A.W. Morawski, *Sep. Purif. Technol.*, **22–23**, 591–600 (2001).
5) K. Wieszczycka, A. Wojciechowska, M. Krupa, R. Kordala-Markiewicz, *J. Chem. Eng. Data*, **58**, 3207–3215 (2013).
6) K. Wieszczycka, *Sep. Purif. Technol.*, **114**,17-23, (2013).
7) K. Wejman-Gibas, K. Wieszczycka, A. Wojciechowska, K. Ochromowicz, P. Pohl, *Sep. Purif. Technol*, **158**, 71-79 (2016).
8) A. Wojciechowska, K. Wieszczycka, I. Wojciechowska, A. Olszanowski, *Sep. Purif. Technol.*, **177**, 239–248, (2017).
9) A. Wojciechowska, K. Wieszczycka, G. Framski, *Modern Organic Chemistry Research*, **2**, 41-47 (2017).
10) A. Wojciechowska, K. Wieszczycka, I. Wojciechowska, *Hydrometallurgy*, **171**, 206-212 (2017).
11) A. Wojciechowska, K. Wieszczycka, I.Wojciechowska, *Sep. Purif. Technol*, **185**, 103-111(2017).
12) G.M Ritcey, *Tsinghua Sci. Technol.*, **11**, 137-152 (2006).
13) F. Fu, Q. Wang, *J. Environ. Manage,*. **92**, 407–418 (2011).

Zinc(II) and Iron(III) Extraction From Chloride Media Using Pyridinecarboximidamides as Extractant

Aleksandra WOJCIECHOWSKA*, Irmina WOJCIECHOWSKA, Karolina WIESZCZYCKA
Poznan University of Technology, Institute of Chemical Technology and Engineering, Berdychowo St. 4, 60-965 Poznan, Poland

The aim of the study was to investigate the extraction properties of new hydrophobic pyridine derivatives - pyridinecarboximidamides. This work was focused on two compounds which are their constituent isomers: *N*'-(2-ethylhexyloxy)pyridine-3-carboximidamide (Eh-3IA) and *N*'-(2-ethylhexyloxy)pyridine-4-carboximidamide (Eh-4IA). The study included determining the effect of initial pH, chloride ion concentration, metal ion concentration and ligand concentration on the extraction efficiency. The ability of both ligands to separate zinc(II) ion from the solution containing iron(III) was also examined.

1. Introduction

Solvent extraction is a separation method based on formation of complex compounds between ligand molecules and metal ions. Liquid-liquid extraction involves intensive contact of an organic phase containing an extractant diluted and charged water phase [1]. During the extraction process, extractant molecules bond metal ions and transfer obtained complex to the organic phase. Metal ions are recovered from an organic phase by reextraction. The final step is to purify the concentrated metal solution, for example by electrolysis [2].

Nowadays, solvent extraction is an important method used in hydrometallurgical processes but also is a method for metal recovery from waste solutions. The development of industry is a source of an increasing volume of wastewaters containing metal ions at various concentrations. Recovery of metal ions from wastewaters is one of the most important tasks due to a depletion of natural resources and the increasing demand for high-purity metal. In addition, it is significant because of the toxic nature of heavy metals to the environment, including plants, animals and humans [3,4].

Ideal extractant should not only provide the purification of wastewaters, but also enable to quick and selective recover of high-purity metals with a considerable efficiency. The study purpose was to define the extraction properties towards Zn(II) and Fe(III) of novel hydrophobic pyridine derivatives: *N*'-(2-ethylhexyloxy)pyridine-3-carboximidamide (Eh-3IA) and *N*'-(2-ethylhexyloxy)pyridine -4-carboximidamide (Eh-4IA, Figure 1).

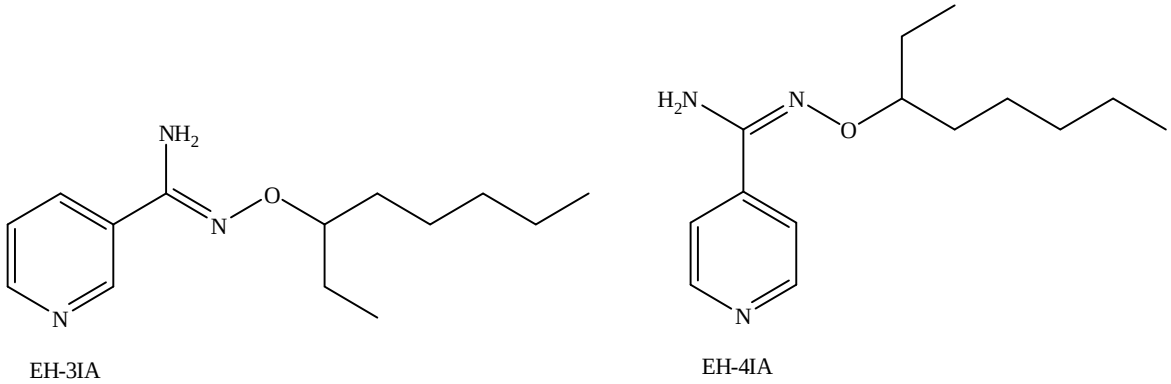

Figure 1. *N'*-(2-ethylhexyloxy)pyridine-3-carboximidamide (Eh-3IA) and *N'*-(2-ethylhexyloxy)pyridine-4-carboximidamide (Eh-4IA)

2. Experimental

2.1 Reagents

All reagents used in this study were of reagent grade. Toluene (99.8%; POCH; Poland) and decan-1-ol (> 99%; Merck; Germany) were used as components of the organic phase. Sodium chloride (ACS reagent; Sigma-Aldrich, Germany), hydrochloric acid (38%) (AR reagent; POCH; Poland), zinc(II) chloride (anhydrous) (ACS reagent; Sigma-Aldrich; Germany) and iron(III) chloride (hexahydrate) (ACS reagent; Sigma-Aldrich; Germany) were used to compose the aqueous phase.

2.2 Extraction procedure

Aqueous feed solutions were prepared by dissolving in ultrapure water appropriate amounts of $ZnCl_2$, $FeCl_3$, HCl and NaCl. Extraction equilibrium studies were carried out at constant ionic strength (I = 4 mol/L) and various HCl and NaCl concentrations (from 0 to 4 mol/L). Another type of the aqueous phase was feed solution prepared with constant mineral acid concentration (HNO_3; 0.5 mol/L), constant a_w = 0.835, constant ionic strength (I = 4 mol/L) and various chloride ion concentrations (from 0 to 4 mol/L). The water activity was adjusted by appropriate addition of NaCl, $NaNO_3$ and $LiNO_3$ (Table 1). The concentrations of the *N'* -alkyloxypyridinecarboximidamides in the organic phase were changed from 0.02 to 0.1 mol/L. Concentration of the metal were changed from 0.02 to 0.12 mol/L. Extraction experiments were carried out in test tubes using equal volumes of both phases (O/W = 1). Both phases were mechanically shaken at room temperature (20-22^{0}C) using Bio-mix BWR 04. The metal concentration in the aqueous phase was analyzed with atomic absorption spectrometry AAS (HITACHI Z-8200 Polarised Zeeman).

3. Results and Discussion

3.1 Zinc(II) and iron(III) extraction

N'-(2-ethylhexyloxy)pyridine-3-carboximidamide (Eh-3IA) and *N'*-(2-ethylhexyloxy)-pyridine-4-carboximidamide (Eh-4IA) were examined for their ability to extract zinc(II) and iron(III) from aqueous solution containg HCl and NaCl. Figures 2 and 3 show the results of the study.

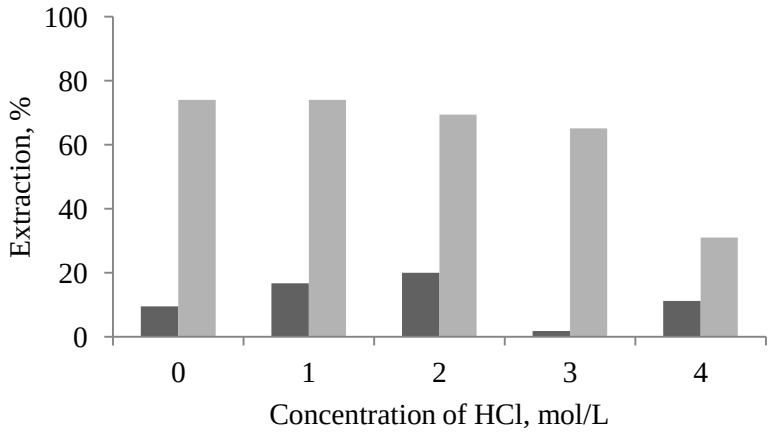

Figure 2. Influence of HCl concentration on extraction of zinc(II) (light grey) and iron(III) (dark grey) using Eh-3IA as extractant ([extractant]=0.1 mol/L; $[Zn^{2+}]$=0.01 mol/L; $[Fe^{3+}]$=0.01 mol/L; $[Cl^-]$=4 mol/L; a_w=0.835)

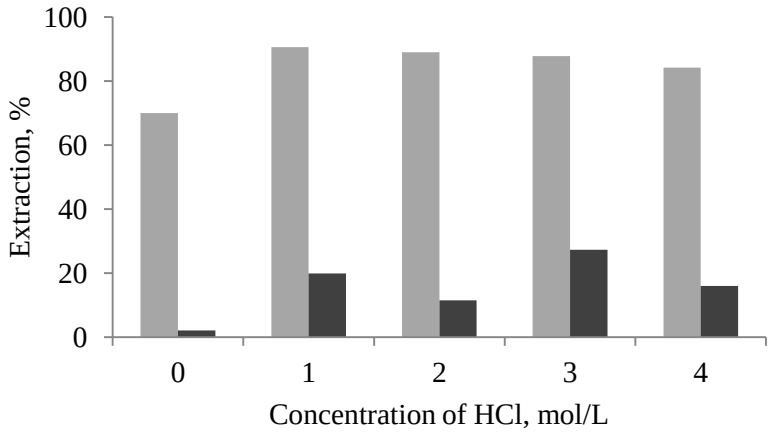

Figure 3. Influence of HCl concentration on extraction of zinc(II) (light grey) and iron(III) (dark grey) using Eh-4IA as extractant ([extractant]=0.1 mol/L; $[Zn^{2+}]$=0.01 mol/L; $[Fe^{3+}]$=0.01 mol/L; $[Cl^-]$=4 mol/L)

The obtained results show that both reagents have good extraction abilities towards zinc(II). At concentration of 1 mol/L HCl, Eh-3IA extracts zinc(II) in 74%, while Eh-4IA in 91% concentration. However, at the same conditions both reagents show much less extraction abilities towards iron(III) (20% and 17% for Eh-4IA and Eh-3IA, respectively). The difference in the extraction properties towards Fe(III) and Zn(II) can enable separation of both metals, especially using as the extractant Eh-3IA and conducting extraction from solution containing 3 mol/L HCl.

3.2 Effect of chloride ion concentration

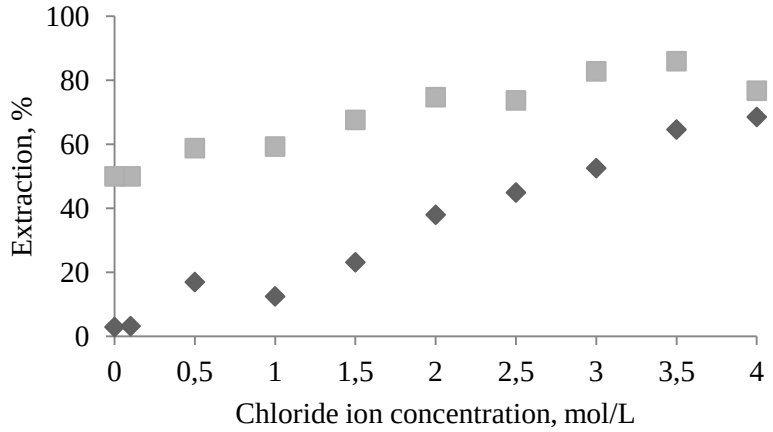

Figure 4. Effect of chloride ion concentration on extraction of zinc(II) with Eh-4IA (light grey) and Eh-3IA (dark grey) ([extractant]=0.1 mol/L; $[Zn^{2+}]$=0.01 mol/L; $[Cl^-]$=0-4 mol/L; a_w=0.835; $[HNO_3]$ = 0.5 mol/L; I = 4 mol/L)

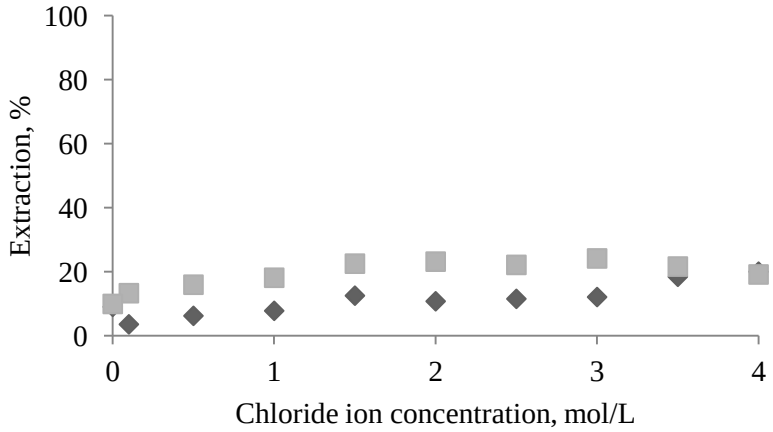

Figure 5. Effect of chloride ion concentration on extraction of iron(III) with Eh-4IA (light grey) and Eh-3IA (dark grey) ([extractant]=0.1 mol/L; $[Fe^{3+}]$=0.01 mol/L; $[Cl^-]$=0-4 mol/L; a_w=0.835; $[HNO_3]$ = 0.5 mol/L; I = 4 mol/L)

The effect of the chloride ion concentration on the zinc(II) and iron(III) extraction was examined using the aqueous solutions containing, besides 0.01 mol/L Zn(II) or Fe(III), a constant mineral acid concentration ($[HNO_3]$ = 0.5 mol/L), constant water activity (a_w = 0.835), constant ionic strength (I = 4 mol/L) and various chloride ion concentrations (from 0 to 4 mol/L NaCl). The obtained results given in Figure 4 show that in the case of both Eh-3IA and Eh-4IA the zinc(II) extraction increases with the increase of the chloride ion concentration. Moreover, results indicate that Eh-3IA is less efficient than Eh-4IA, but the difference decreases when chloride ion concentration increases.

In the case of the Fe(III) the experimental results clearly show that, even after contact with the concentrated chloride solution, the extraction does not exceed 25% (Figure 5).

3.3 Effect of extractant concentration on extraction

The effect of Eh-3IA and Eh-4IA concentration on zinc(II) and iron(III) extraction was studied using the aqueous feed solutions containing the constant concentration of zinc(II) or iron(III) (0.01 mol/L), constant concentration of chloride ion (3.5 mol/L) and the constant concentration of nitric acid (0.5 mol/L). The concentration of Eh-3IA and Eh-4IA in toluene with 10% (v/v) addition of decan-1-ol varied in the range of 0.01 ─ 0.1 mol/L.

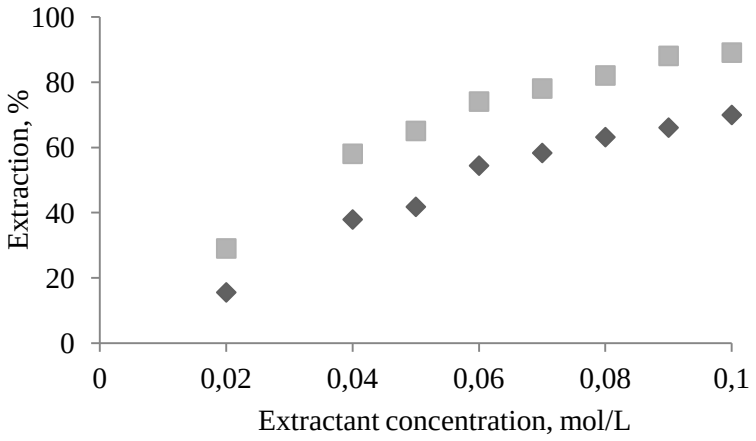

Figure 6. Effect of extractant concentration on extraction of zinc(II) with Eh-3IA (dark grey) and Eh-4IA (light grey) ([extractant]=0.02-0.1 mol/L; $[Zn^{2+}]$=0.01 mol/L; $[Cl^-]$= 3.5 mol/L; a_w=0.835; $[HNO_3]$ = 0.5 mol/L; I = 4 mol/L)

As it can be observed in Figure 6, the increasing concentration of the extractant accelerates the zinc extraction. The observed dependence is comparable for both studied reagents. For example, the reduction of the extractant concentration from 0.1 to 0.5 mol/L causes decrease of the extraction from 89% to 65% for Eh-4IA and from 70% to 42% for Eh-3IA.

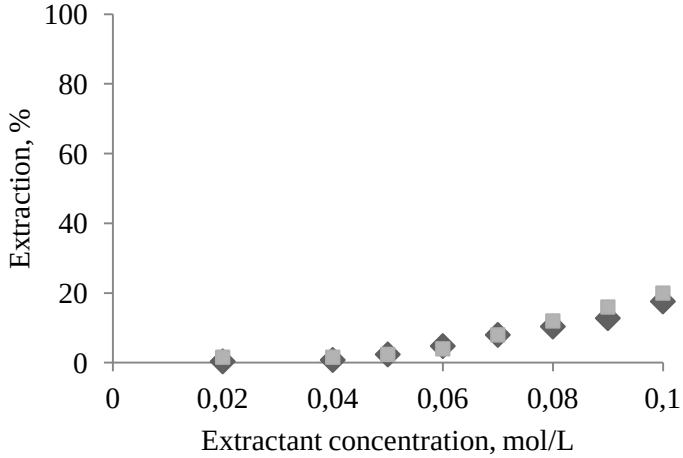

Figure 7. Effect of extractant concentration on extraction of iron(III) with Eh-3IA (dark grey) and Eh-4IA (light grey) ([extractant]=0.02-0.1 mol/L; $[Fe^{3+}]$=0.01 mol/L; $[Cl^-]$=3.5 mol/L; a_w=0.835; $[HNO_3]$ = 0.5 mol/L; I = 4 mol/L)

As Figure 7 shows, the increasing concentration of the extractant causes slightly increase in the iron(III) extraction and it does not exceed 20%.

3.4 Effect of zinc(II) and iron(III) ion concentration

The effect of zinc(II) and iron(III) concentration on the extraction was studied over the range of Zn(II) and Fe(III) 0.01 ─ 0.1 mol/L at the constant concentration of NaCl (4 mol/L) and constant concentration of HCl (0.5 mol/L). In the extraction data presented in Figure 8, regardless on used extractant the increasing Zn(II) concentration decreases the extraction from 95 to 41% for Eh-4IA and from 76 to 35% for Eh-3IA. It was also determined maximum capacities of the studied extractants. In the case of *N'*-(2-ethylhexyloxy)pyridine-4-carboximidamide capacity is approximately 0.49 mol of Zn(II) per 1 mol of the imidamide, while *N'*-(2-ethylhexyloxy)pyridine-3-carboximidamide has ability to extract maximum is 0.41 mol of Zn(II) per mol of the imidamide.

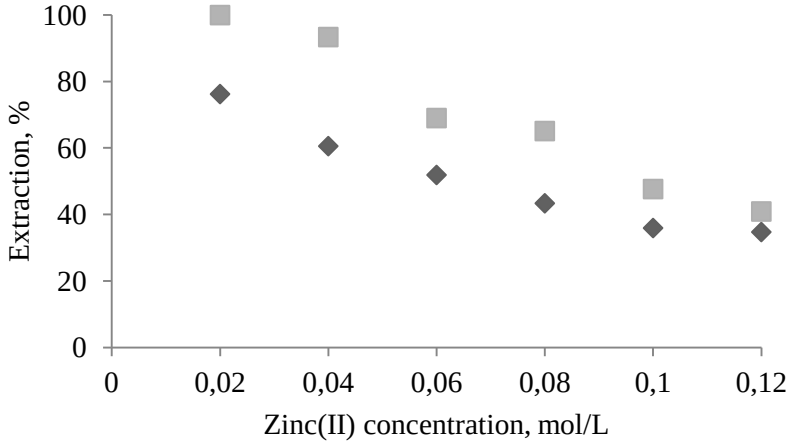

Figure 8. Effect of zinc(II) concentration on extraction with Eh-4IA (light grey) and Eh-3IA (dark grey) ([extractant]=0.1 mol/L; [Zn^{2+}]=0.02-0.12 mol/L; [NaCl]=3.5 mol/L; [HCl]=0.5 mol/L)

The experimental data presented in Figure 9 concern Fe(III) extraction. The results indicate very low extraction, which also decreases with the increase in the Fe(III) concentration.

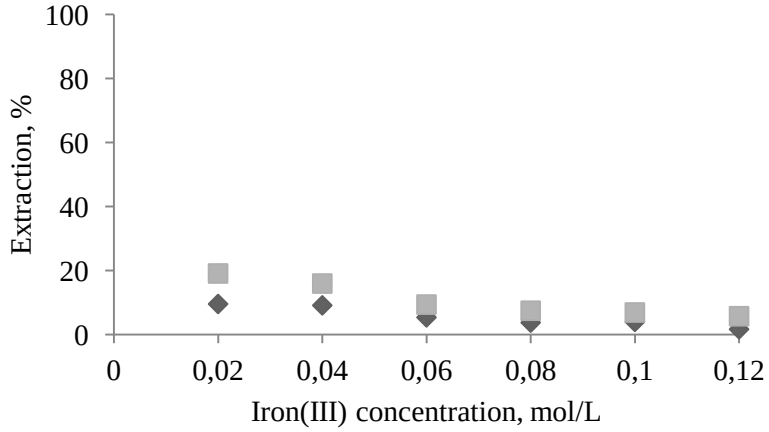

Figure 9. Effect of iron(III) concentration on extraction with Eh-4IA (light grey) and Eh-3IA (dark grey) ([extractant]=0.1 mol/L; [Fe^{3+}]=0.02-0.12 mol/L; [NaCl]=3.5 mol/L; [HCl]=0.5 mol/L)

4. Conclusion

The obtained results confirmed the ability of the studied compounds to extract zinc(II) from acidic solutions, however, their abilities to complex iron(III) and next its transfer to the organic phase were low over the whole concentration range of HCl, extractant and Fe(III). The study confirmed positive influence of chloride and extractant concentrations on the zinc(II) extraction. Furthermore, Eh-4IA appeared as a more effective extractant for zinc(II) and iron(III) than Eh-3IA.

Acknowledgement

This study was funded by National Science Center Poland research grant funds according to decision No. DEC-2015/17/N/ST8/00285. Financial support through the 03/32/DSMK/0720 grant was also acknowledged.

References

1) S.G. Ozcan, N. Satiroglu, M. Soylask, *Food Chem. Toxicol.*,**48**, 2401-2406 (2010).
2) A.M. Wilson, P.J. Bailey, P.A. Tasker, J.R. Turkington, R.A. Grant, J.B. Love, *Chem Soc Rev*, **43**, 123-134 (2014).
3) K. Wieszczycka, *Sep. Purif. Technol*., **114**, 17-23 (2013).
4) A. Parus, K. Wieszczycka, A. Olszanowski, *Sep. Sci. Technol*, **46**, 87-93 (2010).
5) X. Cai, B. Wei, J. Han, Y. Li, Y. Cui, G. Sun, *Hydrometallurgy*, **164**, 1-6 (2016).
6) M.K. Iha, V. Kumar, J.R. Singh, *Solvent Extr Ion Exch*, **20**, 389-405 (2002).

N,N-Dihexyl-*N'*-Hydoxypyridine-2-Carboximidamide as Promising Extractant of Cu(II) and Ni(II) from Sulfate Media

Przemysław AKSAMITOWSKI, Aleksandra WOJCIECHOWSKA*
and Karolina WIESZCZYCKA
Institute of Chemical Technology and Engineering, Poznan University of Technology, Berdychowo St. 4, 60-965 Poznan, Poland

This paper presents studies on the extraction of Cu(II), Zn(II) and Ni(II) from model sulfate solutions using novel reagent: *N,N*-dihexyl-*N'*-hydroxypyridine-2-carboxyimidamide (DH2PIA). The effect of different variables influencing the extraction of the metals ions such as the effect of contact time and the pH of the aqueous phase has been investigated. The studies also covered the determination of selectivity of the extraction of copper(II) over nickel(II) and zinc(II) and further determination of the optimum stripping process condition

1. Introduction

Metals are produced from primary and secondary deposits, and both sources can be treated pyrometallurgically or hydrometallurgically. Nowadays, it can be seen a growing role of solvent extraction in mineral ores processing [1,2]. Leaching is the first chemical step in the hydrometallurgical ore processing. Hydrometallurgical processes generally consist of different steps of pre-treatment, in order to improve metal dissolution rates in the aqueous phase, followed by leaching, purification and finally recovery of different metals from the leach solution. It involves dissolving the metal from ore in leaching reagent. In the leaching step either an acid or a base can be used depending on the material being treated, but still the most frequently used solutions for this purpose are sulfuric acid solutions and an oxidizing agent (e.g.,: $Fe_2(SO_4)_3$, hydrogen peroxide) or bacteria. The effectiveness of the oxidative leaching of sulphide concentrates in sulphuric acid solution is very high [2-5]. Solvent extraction technique is most common used to separate required metal ions from multimetal aqueous solution. In solvent extraction procedure, the solution containing the metal of interest is mixed with an organic solution containing an extractant [6].

Several extractants have been investigated to extract Cu(II) from Ni(II) and Zn(II): organophosphorous extractant (Cyanex 272 [7,8], Cyanex 301 [9], Cyanex 923 [10] and D2EHPA [8]) and LIX84I [10-12]. However, the selective extraction of the metals is still an unsolved problem [9]. Therefore, the present work was to study the extraction of copper(II), zinc(II) and nickel(II) from sulfate solution by novel reagent having extracting properties - *N,N*-dihexyl-*N'*-hydroxy-pyridine-2-carboximidamide (DH2PIA).

2. Experimental

2.1 Reagents

N,*N*-dihexyl-*N'*-hydroxypyridine-2-carboxyimidamide (DH2PIA, Figure 1) was synthesized according to a three-step method described in the previous paper [13]. Purity was determined by thin layer chromatography method (TLC) and quality by FT-IR and NMR (^{1}H and ^{13}C) spectroscopy. Heptane (POCH) was used as diluent to make 0.1M extractant concentration solution. Zinc(II) sulfate heptahydrate (Sigma Aldrich), nickel(II) sulfate monohydrate (Sigma Aldrich), copper(II) sulfate pentahydrate (POCH), sodium sulfate (CHEMPUR), sodium hydroxide (CHEMPUR) and sulfuric(VI) acid (CHEMPUR) was used to make aqueous feed solutions. Aqueous feed solutions had constant concentration of metal ions (0.01M) and sulfate ions (0.01M). pH of the aqueous solution was regulated by an addition of appropriate amounts of sodium hydroxide or sulfuric acid(VI). All used reagents were of analytical-grade.

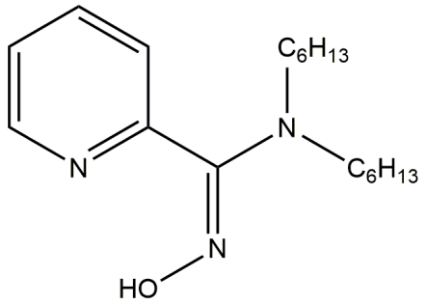

Figure 1. Structure of studied reagent.

2.2 Extraction procedure

The extractant was used at equal volumes of aqueous and organic phases (5 mL) were shaken at room temperature for 5 minutes. After separation of the phases, metal ions concentration and pH of the raffinate were determined.

Concentrations of Cu(II), Ni(II) and Zn(II) ions were determined by Atomic Absorption Spectroscopy using Avanta PM spectrometer (GBC Scientific Equipment) and pH was regulated using T50 titrator (Mettler Toledo) equipped with a DG111-SC combined glass electrode. The content of the metal in the organic phase was calculated from the difference in starting concentrations and concentrations in the raffinate.

Aqueous sulfuric acid solutions were used as reagent enabling a back extraction of metal to the aqueous phase.

3. Results and Discussion

3.1 pH dependency

Figure 2 (A) shows the effect of equilibrium pH on extraction of Cu(II), Zn(II) and Ni(II) from a single metal solution. It has been shown that in the case of Cu(II) the extraction increases with the

increase of pH and the maximum is achieved above pH of 3(~ 100%).

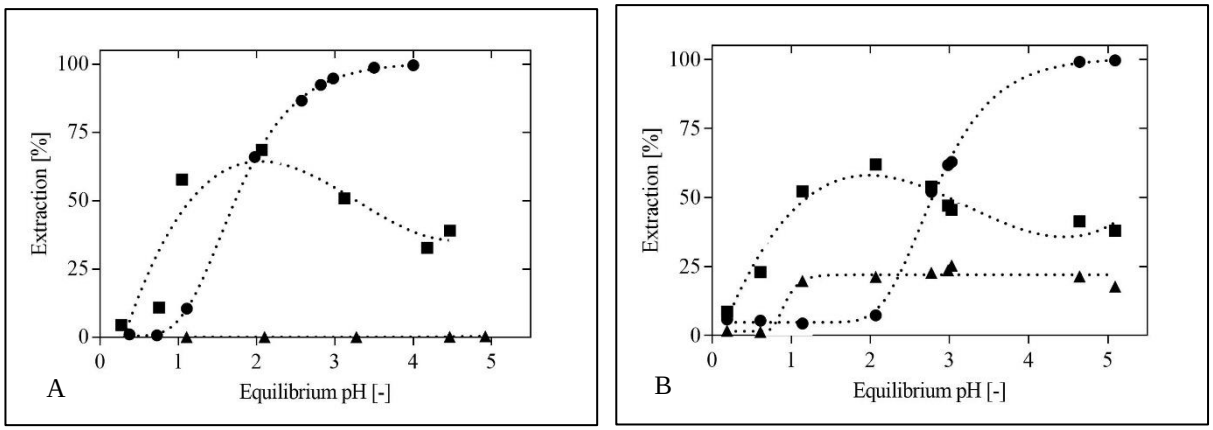

Figure 2. **A**-Effect of equilibrium pH on extraction of Cu(II) - ●, Ni(II) - ■ and Zn(II) - ▲ from single model solutions. **B**- Effect of equilibrium pH on extraction of Cu(II) - ●, Ni(II) - ■ and Zn(II) - ▲ from mixture of metals ions. Dotted line represents approximations.

The different correlation can be observed for Ni(II), when initially the extraction yield increases from 58 to 69% (pH 1-2) and after that decreases up to 39% for pH 5. The Zn(II) extraction is insignificant and observed only at pH of 5. At more acidic conditions all of zinc(II) ions remain in the aqueous phase.

Different results were obtained using mixture of the metals. As it can be observed in Figure 2 (B), the increasing pH also increases Cu(II) extraction, but the most effective removal is observed at pH above 4. It is also observed that Ni(II) is extracted comparably to that obtained for the single metal solutions, but Zn(II) is transported in 20-24%.

3.2 Time dependency

Study of shaking time influence on the extraction was carried out at constant pH equal to 4 for Cu(II) and Zn(II), at pH of 2 for Ni(II), and at a constant concentration of metal ions equal to 0.01 mol/L. The experiment was investigated in the time range of 1-60 minutes.

Figure 3 compares results obtained for Cu(II), Ni(II) and Zn(II), which indicated that equilibrium of the extraction is reached within first 2 minutes and further prolongation of shaking time does not affect the process significantly.

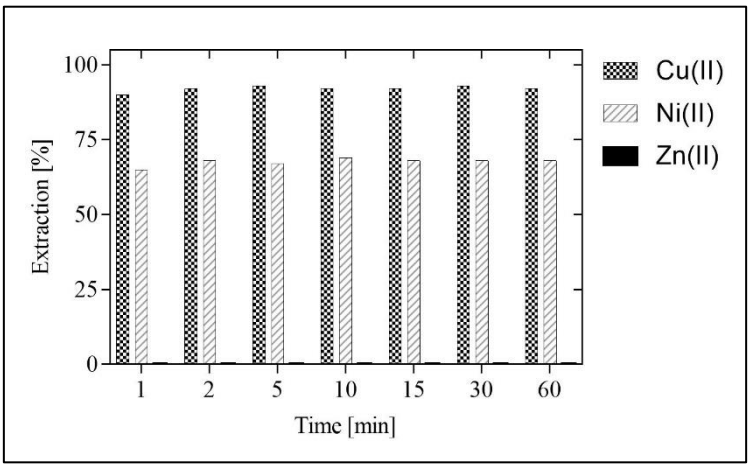

Figure 3. Effect of time on Cu(II), Ni(II) and Zn(II) extraction using DH2PIA as extractant.

3.3 Stripping study

The stripping of Cu(II) and Ni(II) from loaded organic phase was investigated. As a stripping agents water and sulfuric acid solutions were used. It was observed that the co-extracted zinc(II) can be washed out by water, while Cu(II) and Ni(II) require sulfuric acid solution as stripping agent. The optimum concentration of H_2SO_4 for Cu(II) is 3 %, but for the Ni(II) recovery minimum 20% solution allows for the back-extraction of the metal. Moreover, Cu(II) and Ni(II) can be separated conducting extraction at pH 2, and after that the co-extracted copper(II) can be stripped using diluted sulfuric acid.

4. Conclusion

The obtained results indicated the usefulness of the novel reagent DH2PIA as the selective extractant of copper(II) and nickel(II) from acidic sulfate solutions containing also zinc(II). The studied reagent formed complexes according to chelate mechanism, and the complexation was very fast. The selectivity of Ni(II) over Cu(II) depended on the equilibrium pH of the aqueous phase, but co-extracted metal can be washed out by water (Zn(II)) or stripped after shaking with 3% H_2SO_4 (Cu(II)).

Acknowledgement

This study was funded by National Science Center Poland research grant funds according to decision No. DEC-2015/17/N/ST8/00285. This study was also supported by the Polish Grant: 03/32/DSMK/0720.

References

1) A.A. Baba, K.I. Ayinla, F.A. Adekola, M.K. Ghosh, O.S. Ayanda, R.B. Bale, A.R. Sheik, S.R. Pradhan, *Int J Mining Eng Miner. Process.*, **1**, 1-16 (2012).
2) Y. Ghorbani, J.P. Franzidis, J. Petersen, *Miner. Process. Extr. Metall. Rev.*, **37**, 73-119 (2016).
3) H.R. Watling, *Hydrometallurgy*, **140**, 163-180 (2013).
4) A. Oxley, M.E. Smith, O. Caceres, *Miner Eng*, **88**, 53-60 (2016).
5) Y. Li, N. Kawashima, J. Li, A.P. Chandra, A.R. Gerson, *Adv. Colloid Interface Sci.*, **197-198**, 1-32 (2013).
6) M.E. Schlesinger, M.J. King, K.C. Sole, W.G. Davenport, "Extractive metallurgy of copper, Fifth edition", Elsevier, Oxford (2011).
7) N. Begum, F. Bari, S.B. Jamaludin, K. Hussin, *Int J Phys Sci.*, **22**, 2905-2910 (2012).
8) M. Gharabaghi, M. Irannajad, A.R. Azadmehr *Physicochem. Probl. Miner. Process*. **49**, 233−242 (2013).
9) P.E. Tsakiridis. S.L. Agatzini *Hydrometallurgy* **72**, 269-278 (2004).
10) K. Sarangi, P.K. Parhi, E. Padhan, A.K. Palai, K.C. Nathsarma, K.H. Park, *Sep. Sci. Technol.*, **55**, 44-49 (2007)
11) B.R. Reddy, D.N. Priya, *Sep. Sci. Technol.*, **45**, 163-167 (2005)
12) M.K. Jha, D. Gupta, P.K. Choubey, V. Kumar, J. Jeong, J. Lee, *Sep. Purif. Technol.*, **122**, 119-127 (2014).
13) P. Aksamitowski, K. Wieszczycka, A. Wojciechowska, I. Wojciechowska, G. Framski, *MOCR*, **2**, 17-24 (2017).

Interfacial Activity of Pyridine Extractants in Model Extraction System

Aleksandra WOJCIECHOWSKA*, Irmina WOJCIECHOWSKA, Milena KOWALCZYK, Katarzyna STASZAK and Karolina WIESZCZYCKA

Institute of Chemical Technology and Engineering, Poznan University of Technology, Berdychowo St. 4, 60-965 Poznan, Poland

Interfacial tension and surface excess isotherms as well as adsorption parameters for selected pyridine extractants and their chloride and bromide salts in model extraction system were determined and interpreted. Despite their high hydrophobicity, all extractants studied adsorb at the hydrocarbon/water interfaces and decreases effectively the interfacial tension. The interfacial activity of pyridine extractants in model extraction system was affected mainly by the structure of compounds. The highest ability to reduce interfacial tension at the hydrocarbon/water interface was observed for quaternary salts of pyridine extractants.

1. Introduction

Solvent extraction is one of the essential methods used to purify, concentrate, and separate various metals from different aqueous solutions. It is already a mature technology today, though still developing and improving its performance. One of the proposals is to obtain novel, selective and efficient extractants. Interesting examples of such compounds are hydrophobic pyridine extractants and their chloride and bromide salts. These extractants have been studied in our group and proposed as ligands for copper(II), zinc(II), cadmium(II), lead (II) and iron(III) removal using a liquid−liquid extraction technique [1-6] and as carrier in membrane processes realized with the hollow fiber module [7-8].

The hydrophobic-hydrophilic structure of the extractant compounds and as a result their surface activity at the water/organic solvent interface, as well as their significant hydrophobicity (very low solubility in the aqueous phase) causes that the complexation reaction of metal ions in the extraction process probably occurs as a surface reaction [9]. Surface mechanism of the process is preceded by a transfer of extractant molecules from the bulk organic phase to the interfacial area by diffusion. The molecules of extractants form a packed monolayer at the interface or, at the latest literature reports, the bilayer [10]. Therefore, in the study of the mechanism and kinetics of the extraction of metal ions by hydrophobic extractants parameters analysis such as the molecular structure of the extractant, composition of the aqueous phase or the organic solvent type are also important. They affect both the adsorption, as well as diffusion of the extractants molecules between organic solvent and aqueous phase.

The purpose of the present work is to study the interfacial activity and estimate basic adsorption parameters of novel hydrophobic pyridine extractants (ketone and amidoxime derivatives) and their chloride and bromide salts in model extraction systems.

2. Experimental

2.1 Reagents

The novel hydrophobic pyridine extractants (1-(3-pyridyl)undecan-1-one, pyridine-3-carboximidamide, *N'*-alkyloxypyridine derivatives, Figure 1) were synthesized as were described earlier [11,12]. The mixture of toluene with 10% (v/v) of decan-1-ol was used as the organic phase, while the aqueous phase was water obtained from the PURELAB Classic, Elga with resistivity=18.2 MΩ·cm at 25°C. Toluene was supplied by POCh S.A., decan-1-ol was supplied by Merck, and all other reagents necessary to synthesizes were analytical-grade reagents.

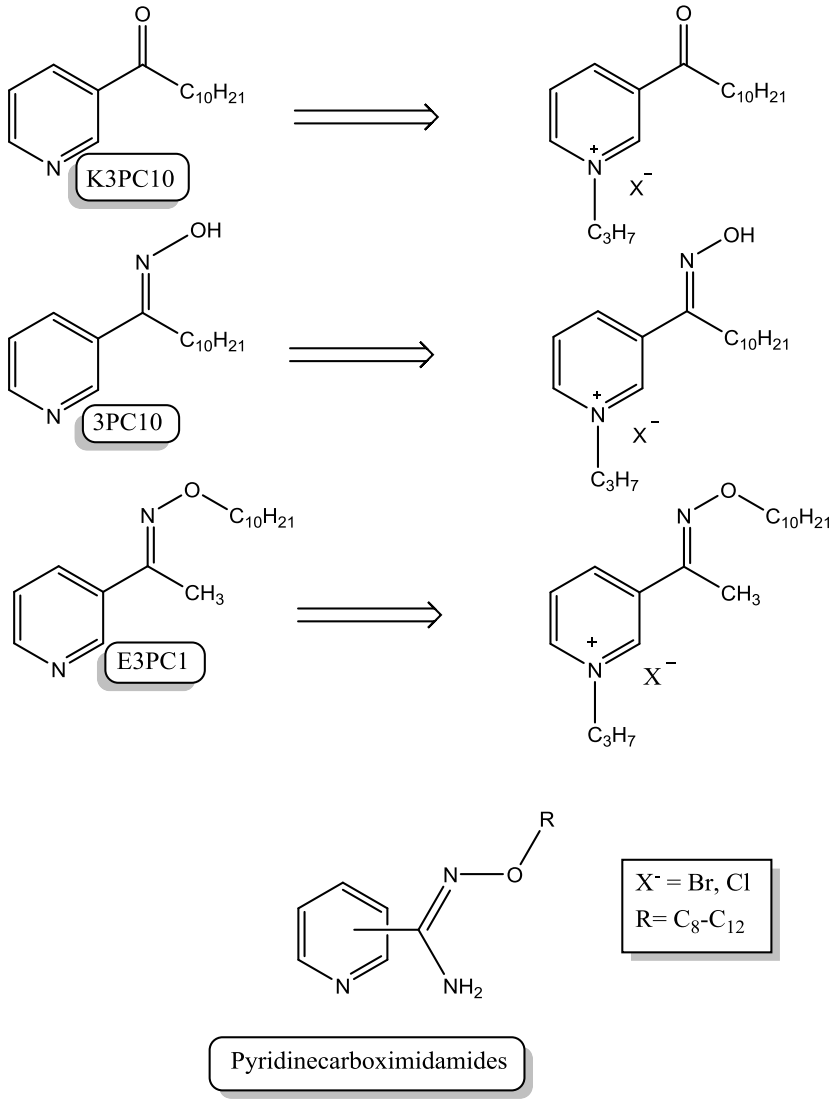

Figure 1 Structure of studied reagents.

2.2 Interfacial tension measurements

The interfacial tension was measured by the Du Noüy ring method with a Krüss tensiometer, with resolution 0.01 mN/m, at a constant temperature 21°C. Measurements were made for the aqueous

solution/organic phase system at the initial concentration of extractants equal 0.1 M, other solutions were obtained by serial dilution method with concentration in the range from 0.1 to 10^{-6} M. The measurements were carried out with presaturated phases, which means that both phases (equal volumes ~10 cm^3) were together mechanically shaken at room temperature for 4 hrs then left for 24 hrs for the complete separation. They were separated directly before measurements. This procedure allows to avoid any transfer of the solvent during the adsorption process.

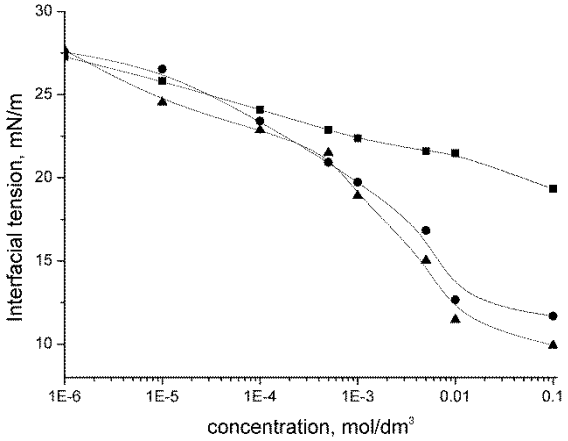

Figure 2 Interfacial tension isotherms for *N*-decyloxy-1-(3-pyridyl)ethanoimine (E3PC1) ■ and its chloride ● or bromide salts ▲ in model extraction sysytem.

2.3 Calculation of adsorption parameters

The interfacial tension data were fitted by the Szyszkowski equation [13]:

$$\gamma^{Sz} = \gamma_0\left[1 - B_{Sz}\ln\left(\frac{c}{A_{Sz}} + 1\right)\right] \quad (1)$$

Adsorption coefficients of the Szyszkowski isotherm (Eq. [1]) can be used to estimate the surface excess at the saturated interface (Γ_∞), the minimum molecular area in the adsorption layer at the saturated interface (A_{min}) and the Gibbs free energy of adsorption (ΔG_{ads}). The following equations are used for these estimations:

$$\Gamma_\infty = \frac{B\gamma_0}{RT} \quad (2)$$

$$A_{\min} = \frac{1}{\Gamma_\infty \cdot N_A} \quad (3)$$

$$\Delta G_{ads}^{Sz} = RT\ln(A_{\min}) \quad (4)$$

In the equations (1)-(4) A_{Sz} and B_{Sz}, γ_0, c, N_A, R, T stand for Szyszkowski adsorption coefficients, interfacial tension for concentration c=0, Avogadro constant, gas constant and temperature, respectively.

3. Results and Discussion

3.1 Interfacial tension isotherms

In Figure 1 exemplary interfacial tension isotherms for *N*-decyloxy-1-(3-pyridyl)ethano- imine and its chloride and bromide salts were presented. Both pyridine extractant and their quaternary salts adsorbed at the liquid/liquid interface and reduced the interfacial tension in model extraction system. However, the obtained results showed a higher interfacial activity of bromide and chloride pyridinium salts compared with pyridine extractants. The values of surface pressure ($\pi=\gamma_0-\gamma_{min}$) in the model extraction system were comparable for the chloride and bromide salts, equal to 16 and 17 mN/m,

respectively, while for pyridine extractant the value of this parameter was twice time smaller. Thus the molecules of the pyridine extractants indicate the lower ability to reduce the interfacial tension. The same relationship was observed for other pyridine extractants as 1-(3-pyridyl)undecan-1-one and 1-(3-pyridyl)undecan-1-one oxime.

3.2 Adsorption properties

The interfacial tension data can be well fitted by various adsorption equations of theoretical, empirical or semiempirical origin. From the physicochemical point of view it is suitable to use the Szyszkowski equation, described in section 2.3. Based on these calculations the exemplary surface excess isotherms for ketone derivates of pyridine extractant and its salt are presented in Figure 2. The interfacial concentration of 1-(3-pyridyl)undecan-1-one at the saturated hydrocarbon/aqueous solution interface was lower in comparison to its chloride and bromide salts. The results obtained suggest that the structures of adsorbed monolayers formed at interfaces considered were different. The molecules of quaternary salts were more densely populated at the saturated interface than those of pyridine extractant. As a result, it may affect the overall rate of the extraction.

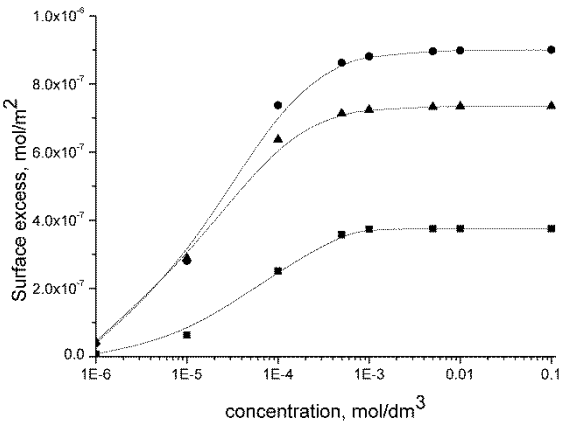

Figure 3 Surface excess isotherms for 1-(3-pyridyl)undecan-1-one (K3PC10) ■ and its chloride ● or bromide salts ▲ in model extraction sysytem.

For all considered extractants and their salt the negative values of free energy of adsorption were estimated, according to equation (4), in the range from -26 to -34 kJ/mol. These results suggest that adsorption process of extractants studied occurs spontaneously.

4. Conclusion

Pyridine extractants exhibits high interfacial activity at the hydrocarbon/water interface. The adsorption properties of extractants studied are significantly dependent on their type. The highest ability to reduce interfacial tension at the hydrocarbon/water interface is observed for quaternary salts of pyridine extractants.

Estimated values of surface excess indicated that structures of adsorbed monolayers formed at model extraction interfaces were different and depended of the extractant used. The negative values of free energy of adsorption for all considered extractants suggested that adsorption process occurs spontaneously.

Acknowledgement

This work was financed within the Polish National Centre of Science funds according to decision No. DEC-2015/17/N/ST8/00285. Financial support through the 03/32/DS-PB/0701 grant was also acknowledged.

References

1) K. Klonowska-Wieszczycka, A. Olszanowski, A. Parus, B. Zydorczyk, *Solvent Extr. Ion Exch*., **27**, 50-62 (2009).
2) A. Parus, K. Wieszczycka, A. Olszanowski, *Sep. Sci. Technol.*, **46**, 87-93 (2011).
3) A. Parus, K. Wieszczycka, A. Olszanowski, *Hydrometallurgy*, **105**, 284-289 (2011).
4) K. Wieszczycka, *Sep. Pur. Technol.*, **114**, 17-23 (2013).
5) A. Wojciechowska, K. Wieszczycka, I. Wojciechowska, *Sep. Purif. Technol.*, **185**, 103-111 (2017).
6) A. Wojciechowska, K. Wieszczycka, I. Wojciechowska, *Hydrometallurgy*, **171**, 206-212 (2017).
7) K. Wieszczycka, M. Regel-Rosocka, K. Staszak, A. Wojciechowska, M.T.A. Reis, M.R.C. Ismael, N.M.L.F. Gameiro, J.M.R. Carvalho, *Sep. Purif. Technol.*, **154**, 204-212 (2015).
8) K. Staszak, A. Wojciechowska, M.T.A. Reis, I. Wojciechowska, K. Wieszczycka, M.R.C. Ismael, J.M.R. Carvalho, *Sep. Purif. Technol.*, **177**, 152-160 (2017).
9) J. Szymanowski, Hydroxyoximes and copper hydrometallurgy, CRC Press, 1993.
10) W. Bu, H. Yu, G. Luo, M.K. Bera, B. Hou, A.W. Schuman, B. Lin, M. Meron, I. Kuzmenko, M.R. Antonio, L. Soderholm, M.L. Schlossman, *J. Phys. Chem. B*, **118**, 10662-10674 (2014).
11) I. Wojciechowska, K. Wieszczycka, A. Wojciechowska, *Sep. Purif. Technol.*, **173**, 372-380 (2017).
12) I. Wojciechowska, A. Wojciechowska, K. Wieszczycka, P. Aksamitowski, J. Zembrzuska, G. Framski, *Chem. Pap*., **71**, 953-960 (2017).
13) D.K. Chattoraj, K.S. Birdi, Adsorption and the Gibbs surface excess, Plenum, New York, 1984.

Application of Microgels for Switchable Phase Separation Behavior to Improve Extraction Processes

Miriam FAULDE[1,*] and Andreas JUPKE[1]

[1] *AVT - Fluid Process Engineering, RWTH Aachen University, Forckenbeckstraße 51, 52074 Aachen, Germany,*

Microgels are innovative deformable polymers. Their most outstanding properties are their switchable structural change and their surface activity. At interfaces microgels deform and act as surface active agents. Their surface activity combined with the switchability makes them promising candidates for the improvement of extraction processes, which suffer from high coalescence of drops. A new concept for the intensification of extraction processes by the application of microgels will be introduced. For the quantitative analysis of the switchable phase separation as response to a temperature shift, experiments in a standardized batch settling cell have been performed. Thereby, a large set of parameters has been tested, including microgel properties as well as process conditions such as ionic strength and pH value. Furthermore, a first investigation of mass transfer through microgel-covered interfaces has been performed. For the mass transfer experiments, a stirred two-phase cell has been utilized.

1. Introduction

The performance of many liquid-liquid extraction processes suffers from strong drop coalescence, leading to a broad drop size distribution. Thus, the drops have different sedimentation velocities and therefore different resident times. Furthermore, the specific mass transfer area varies. All these effects lead to a flat concentration profile and a reduced separation efficiency of the process.

A promising approach to tackle this challenge is the introduction of microgels to extraction processes. Microgels are soft and deformable crosslinked polymer particles with surface-active properties. Their most outstanding characteristic is the response to external triggers, e.g. temperature, by a structural change. Concomitant to the structure and size, the microgel properties change rapidly when exposed to a stimulus. [1, 2]

In this contribution, cross-linked poly(N-isopropylacrylamide) (PNIPAM) microgels are utilized. These microgels show a thermo-responsive behavior which is characterized by a volume phase transition temperature (VPTT) about 34°C which is typical for PNIPAM microgels. Below the VPTT the microgels are in a swollen state containing about 90 Vol-% solvent. Above the VPTT the polymer network collapses leading to a smaller radius and higher polymer content [1]. The interfacial properties of microgels have been investigated by many researchers. Microgels are known to stabilize oil-water [3] and water-air interfaces [4]. Their ability to generate switchable emulsions has been shown qualitatively [1, 3, 5]. Nevertheless, a quantitative investigation on stability and the impact of different parameters is still missing. Furthermore, the arrangement and packing of microgels at liquid interfaces has been

studied intensively [3, 5–8]. Microscopic insights and compression isotherms indicate the formation of a microgel monolayer at the interface [3, 8]. In contrast to rigid particles, microgels have the ability to spread and deform at the interface, the magnitude of spreading is correlated to the degree of crosslinking within the gel and consequently has a big effect on the interfacial behavior [7].

In an extraction column, the switchable interfacial properties will be utilized as follows and illustrated in Figure **1**. Microgels will stabilize the drops suppressing coalescence while passing the active part of the column. At the top of the column, where coalescence is required and phase separation takes place, the microgel properties will be switched by a temperature shift to enable coalescence. Therefore, the switchability of the phase separation behavior by microgels are investigated quantitatively by batch settling experiments [9]. The other important aspect for the application in extraction processes is the impact of the microgel layer on the mass transfer, which is also part of this contribution. The mass transfer trough a flat interface is observed by experiments in a stirred two-phase convection cell [10, 11].

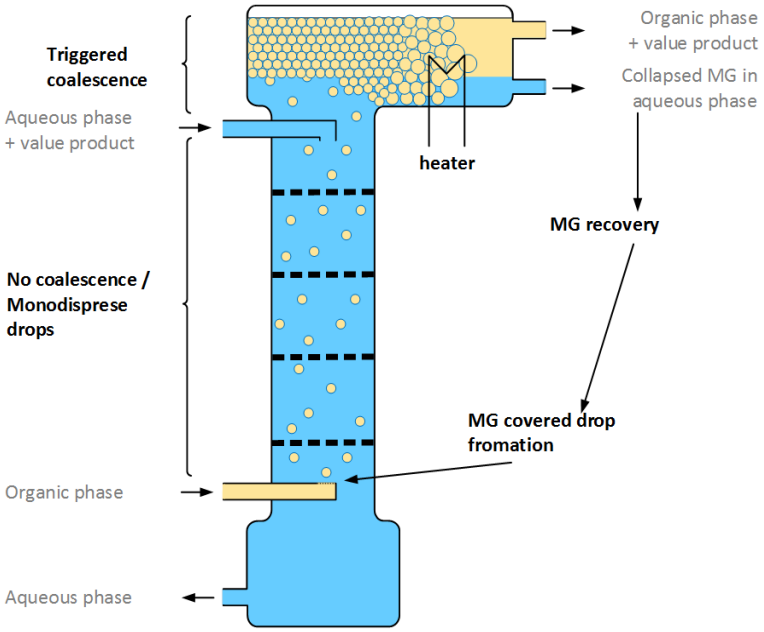

Figure 1. Process concept for an improved extraction process utilizing microgels

2. Experimental work and Simulation

2.1 Temperature responsive phase separation

For the investigation of phase separation and mass transfer through microgel-covered interfaces the standard test system Toluene-Water-Acetone is utilized as recommended by the EFCE [12]. Experiments for the investigation of the phase separation regarding coalescence and sedimentation were performed in a standardized batch settling cell [9]. The experiment is based on the optical evaluation of the settling process over time. Therefore, sedimentation and coalescence of the dispersed drops are observed by means of the heights of the droplet free phases in the cell. In order to investigate the transfer of the temperature-responsive properties of the microgels on the phase separation process temperatures below and above the volume phase transition temperature (VPTT) were tested. Since the VPTT of the PNIPAM microgels is app. 34°C, experiments are performed at 25°C and 40°C respectively. As the microgel properties are part of this investigation, microgels with different crosslinker content have been utilized, 2.5 and 5 mol% BIS respectively, while size and VPTT of the microgels are not affected as can be seen in Figure 2.

Furthermore, the impact of different process parameters such as ionic strength and pH value is

studied. For the adjustment of the ionic strength and the pH value sodium chloride and sodium hydroxide are used. Since the amount of parameters leads to a large number of experiments, a statistical experiment planning (DOE) has been utilized in order to determine the most significant single parameter and interaction effects. Every experiment was repeated at least for four times.

The experiments have been evaluated regarding the overall separation time, which is taken directly from the experiment. Furthermore, the Sauter mean diameter and the coalescence are evaluated utilizing the Henschke model approach [9]. The Sauter mean diameter is determined via a force balance from the slope of the linear part of the sedimentation line. The coalescence parameter is derived from the coalescence line utilizing the settler model approach [9].

2.2 Mass transfer through microgel-covered interface

For the investigation of mass transfer through a microgel-covered interface a stirred two-phase cell is utilized. The total volume of the cell is 500 ml [11]. To ensure the coverage of the interface with microgels preliminary experiments were performed. First, the flow conditions at the interface have been observed with sand particles as a visible model system (mean diameter 148.5 ± 43 µm). Furthermore, the time necessary to cover the interface has been evaluated by variation between 30 minutes and 24 hours. According to the results from the preliminary experiments, the microgel containing solvent system is filled into the cell and stirred slowly for 2 hours allowing the microgels to cover the interface. At the beginning of the measurement acetone is injected to the aqueous phase leading to an initial concentration of about 1.5 w%. The mass transfer is tracked by concentration measurement in the organic phase. The Acetone concentration in the organic phase is determined by gas chromatography.

3. Results and Discussion

3.1 Temperature responsive phase separation

The experimental results obtained at constant temperature show that below the VPTT the microgels stabilize the disperse system extremely well as depicted in Figure 2. While above the VPTT complete separation of the phases was observed for all tested parameters. As an example the experimental results for a system with a low microgel concentration of 0.1 g/L, low crosslinking 2,5 mol% BIS, high ionic strenght 100 mmol/L and low pH value are shown in Figure 2. At 25°C no coalescence can be observed, the drops sediment to a dense packed

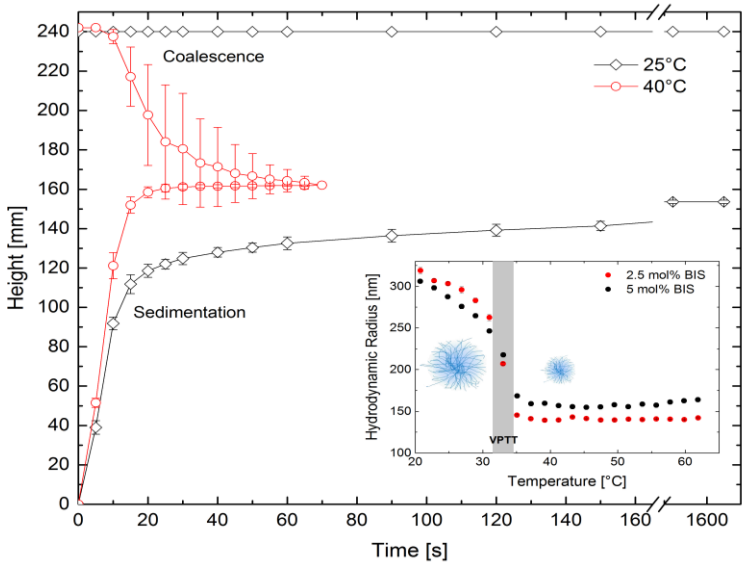

Figure 2. Settling process with microgels at different states (swollen microgels at 25°C, collapsed microgels at 40°C, indicated by the radius measured by DLS at IPC RWTH Aachen) utilized microgels with 2.5 mol% BIS, ionic strength 100 mmol/L, pH 11.

zone. The minor slope of the sedimentation is due to the drainage of continuous aqueous phase from the packed zone. The hold-up of continuous phase in the dense packing decrease from approximately 30 vol-% at 60 s to 11 vol-% after the end of the experiment after 20 min.

For the evaluation of the separation time only the experiments at evaluated temperature are considered. For all tested parameters a complete separation of the phases was observed at 40°C. Nevertheless, the settling time varied in a wide range from 29 s to 91 s depending on the process parameters. For each parameter the averaged settling times for all experiments are determined, whereby it is only distinguished between the state of the regarded parameter. The microgel cross-linking and the pH value were identified to have the most significant impact on the separation time (Figure 3, top). The ionic strength has a minor effect, nevertheless it shows strong interactive effects with crosslinking as well as with the pH value. The coalescence parameter is also predominately affected by the degree of crosslinking (Figure 3, middle). Thereby the magnitude of this single effect is bigger compared to all interaction effects. The Sauter mean diameter (Figure 3, bottom) and subsequently the sedimentation velocity is not substantially affected by any of the investigated parameters. The scattering of the average values is about 10 %. The magnitude of the interaction effects is even minor.

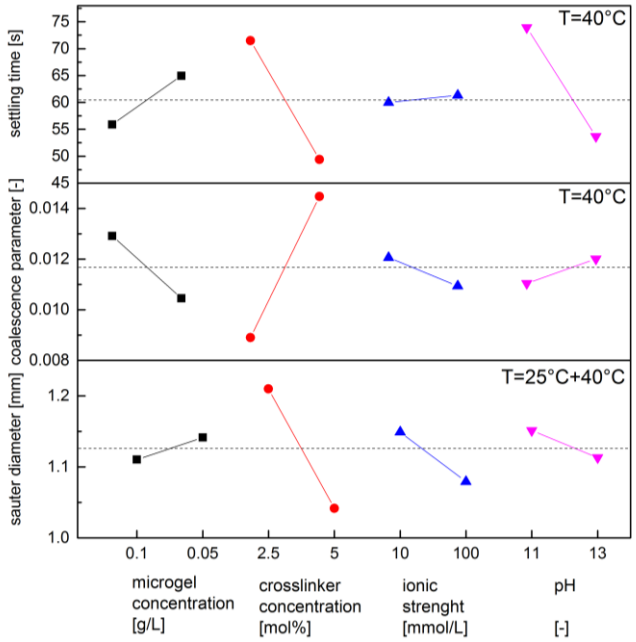

Figure 3. Effects of microgel concentration, crosslinker content, ionic strength and pH on settling time (top), coalescence parameter (middle) and Sauter mean diameter (bottom)

The transfer from the experiments at constant temperature to an operation with temperature-shift, as it would be applied in a future process, is shown in Figure 4. At the beginning of the experiment the microgels form the dens droplet packing, which is stable for 20 min until the heating begins. The coalescence is delayed and approximately 5 times slower as in the experiments at constant temperature. Whereby, the magnitude of time for the microgel collapse is much faster as the observed time range. Thus, a possible

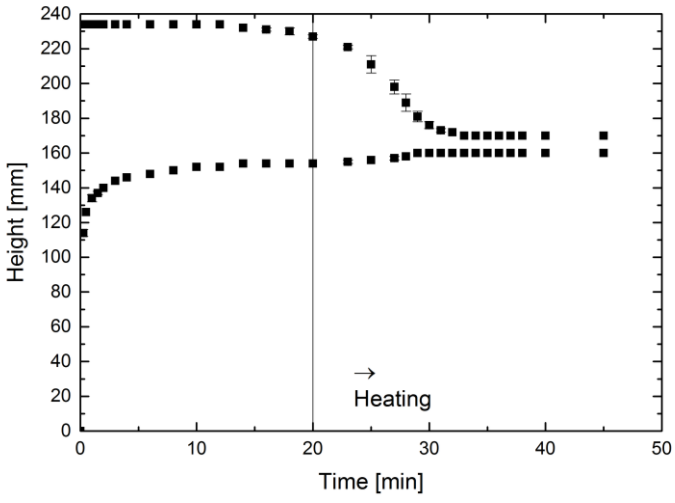

Figure 4. Settling process with subsequent heating, microgel concentration 0.1 g/L with 2.5 mol% BIS ,pH 10.92

explanation for the delay is the heat transfer from the water bath to the solution. Therefore, the heat transfer is the crucial design factor for a future settling unit.

3.2 Mass transfer through microgel-covered interface

As mentioned, besides phase separation also mass transfer could be a critical factor for the applicability of microgel in extraction processes. The partition coefficient determined from liquid-liquid equilibrium experiments at 25°C and 40°C is not affected by the presence of microgels. It was determined to 0.635 $w\%_{org}/w\%_{aq}$ for the pure system and 0.648 $w\%_{org}/w\%_{aq}$ with a microgel content of 1 g/L. The deviation is still within the range of the maximum error of 2 %. The microgels do not affect the partition coefficient, as the particles are suspended but not solved in water and therefore do not contribute to the molar composition of the solvent phase. The dynamic of the mass transfer through the microgel-covered interface was observed by means of a time dependent concentration profile for the organic phase as shown in Figure 5. The calculated mass transfer coefficient obtained from the integral view of the concentration profile is $1.99*10^{-4} \pm 0.4*10^{-4}$ m/s for the pure system and $1.77*10^{-4} \pm 0.9*10^{-4}$ m/s for the microgel containing system (0.25 g/L). Due to the small deviation of the mass transfer coefficients no significant impact of the microgel layer can be detected. Therefore, the microgels do not impede the mass transfer through the interface for the selected test system. It should be noted, that acetone is a very small molecule compared to the microgels. As the gels have a porous structure and a high water content it is assumed, that the transport of small molecules is not hindered.

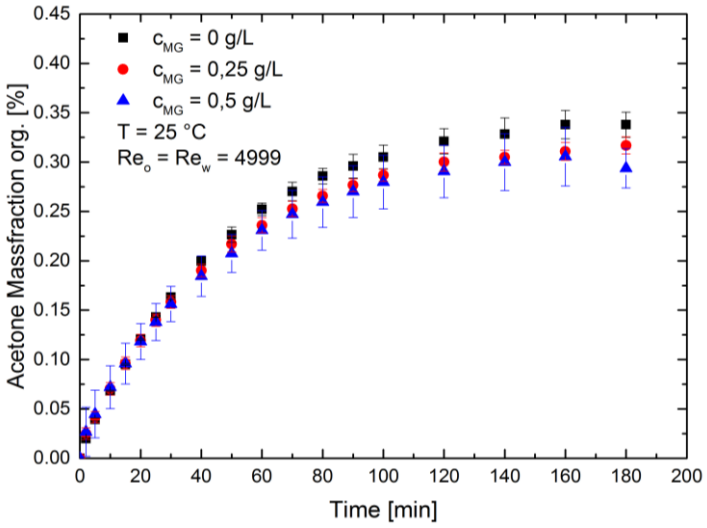

Figure 5. Measured acetone concentration in the organic phase over time, the initial acetone concentration in the aqueous phase was 1.5 w-%, microgels with 5mol% BIS .

4. Conclusion

It has been demonstrated, that microgels allow to switch phase separation by temperature shift. The degree of crosslinking was determined as most effectful parameter. Furthermore it has been shown, that micorgels do not affect the partition coefficient of acetone between water and toluene. The mass transfer experiments indicate that mass transfer of small molecules is not hindered by the interfacial micorgel layer. Nevertheless, more detailed investigation of mass transfer also for larger molecules need to be done to generate a better understanding of mass transfer through the microgel layer at liquid-liquid interfaces.

Acknowledgement

This work was performed as part of the collaborative research center (Sonderforschungsbereich) “SFB 985 – functional microgels and microgel systems”, which is funded by the DFG. Thanks to our project partners Dominik Wöll and Eric Siemes from the IPC RWTH Aachen.

References

1) B. Brugger, W. Richtering, *Langmuir*, **24**, 7769–7777 (2008).
2) W. Richtering, *Langmuir*, **28**, 17218–17229,(2012).
3) K. Geisel, K. Henzler, P. Guttmann, W. Richtering, *Langmuir*, **31**, 83–89 (2015).
4) J. Zhang, R. Pelton, *Langmuir*, **15**, 8032–8036 (1999).
5) B. Brugger, B. Rosen, W. Richtering, *Langmuir*, **24**, 12202–12208 (2008).
6) K. Geisel, L. Isa, W. Richtering, *Langmuir*, **28**, 15770–15776 (2012).
7) O.S. Deshmukh, D. van den Ende, M.C. Stuart, F. Mugele, M. Duits, *Adv. Colloid Interface Sci.,* **222**, 215-227 (2015).
8) K. Geisel, W. Richtering, L. Isa, *Soft Matter*, **10**, 7968–7976, (2014).
9) M. Henschke, *Fort. Berichte VDI*, **379** (1995).
10) W. Nitsch, M. Raab, R. Wiedholz, *Chem. Ing. Tech.*, **45**, 1026–1032 (1973).
11) M.Y. Altunok, M. Kalem, A. Pfennig, *AIChE J.*, **58**, 1346–1355 (2012).
12) T. Míšek, R. Berger, J. Schröter, *EFCE Publ. Ser.*, **46** (1985).

Aliphatic Amine-based Ionic Liquids for Effective Production of Paclitaxel and Related Taxanes in Plant Cell Culture

Shinjiro YAMAMOTO*, Yuka SONODA, Takato KATAOKA, Shuhei HAYASHI, and Hitoshi MIYASAKA

Department of Applied Life Science, Sojo University, 4-22-1 Ikeda, Kumamoto, 860-0082, Japan

We report here hydrophobic ionic liquids (ILs) which enhance the productivity of paclitaxel and the related taxanes of 10-deacetyl baccantin III, baccatin III and cepharomannine with *in situ* extraction from an aqueous medium in suspension cell culture of *Taxus cuspidata* in the IL-medium two phase culture system. Two aliphatic amine-based ILs of N-methyl-n-propyl- piperidinium bis(trifluoromethane-sulfonyl)imide (PP13-TFSI) and N-methyl-n-butylpyrrolidinium bis(trifluoromethanesulfonyl)imide (P14-TFSI) were used. It was found that the two ILs had no cytotoxicity and enhanced productivity of paclitaxel and the related taxanes in the cell culture. In particular, more hydrophobic P14-TFSI, which enhanced the productivity of paclitaxel and the total taxanes by a factor of more than 2 compared to PP13-TFSI, could be an effective extractant.

1. Introduction

Paclitaxel (PX) is an expensive anticancer drug because the conventional semi-synthetic method requires many steps of reactions of precursors such as baccatin III or 10-deacetyl baccatin III extracted from yew tree needles. A culture using callus induced from the needles is one of the promising methods for the cost-effective production of paclitaxel. However, there is a problem of feedback-inhibition of the paclitaxel produced in the culture. In order to reduce the paclitaxel's inhibition, two phase culture system using water-immiscible organic solvents, have been proposed for the *in situ* extraction of hydrophobic paclitaxel from the culture medium [1-2]. Thus, we investigated the use of hydrophobic ionic liquids (ILs) for the *in situ* extraction of paclitaxel from the aqueous medium [3] and reported that 1-hexyl-3-methylimidazolium hexafluorophosphate (HMIN-PF_6) extracted paclitaxel from the aqueous medium [4]. ILs have gained considerable attention as safer solvents in contrast to conventional organic solvents because of their unique properties such as negligible volatility, high thermal stability, and selective solubility. ILs have been applied for extraction and separation of bioactive compounds [5-9]. It is reported that HMIN-PF_6 extracted hydrophobic 3-indole-butyric acid from pea plants [10]. Ferulic acid and caffeine acid found in various plants could be readily extracted with HMIN-PF_6 [11]. Recently, higher extraction efficiencies were obtained for DNA molecules using magnetic ILs such as the benzyltrioctylammonium bromotrichloroferrate (III) ($[(C_8)_3BnN^+][FeCl_3Br^-]$) and 1,12-di(3-hexadecylbenzimidazolium) dodecane bis[(trifluoromethyl)-sulfonyl]imide bromotrichloroferrate (III) ($[(C_{16}BnIM)_2C1_2^{2+}][NTf_2^-$, $FeCl_3Br^-]$) [12]. Though there is a report on enhancement of extraction efficiency of paclitaxel from

biomass taken from the culture broth using a co-solvent made of 1-butyl-3-methylimidazolium tetrafluorophosphate (BMIN-BF_4) and methanol under acidic conditions [13], there is no report on the *in situ* extraction of paclitaxel and the related taxanes of 10-deacetyl baccatin III (10-DAB), baccatin III (BIII) and cepharomannine (CM) in the plant cell culture with the ILs except our study [4]. Figure 1 shows the main metabolic pathway of PX and the related taxanes from geranylgeranyl diphosphate [14].

In the present research the effect of two hydrophobic aliphatic amine-based ILs of N-methyl-n-propylpiperidinium bis(trifluoromethanesulfonyl) imide (PP13-TFSI) and N-methyl-n-butylpyrrolidinium bis(trifluoromethanesulfonyl) imide (P14-TFSI) rather than HMIN-PF_6 on the enhancement of the productivity of PX and the related taxanes of 10-DAB, BIII and CM by the *in situ* extraction in plant cell culture were investigated considering their cytotoxicity.

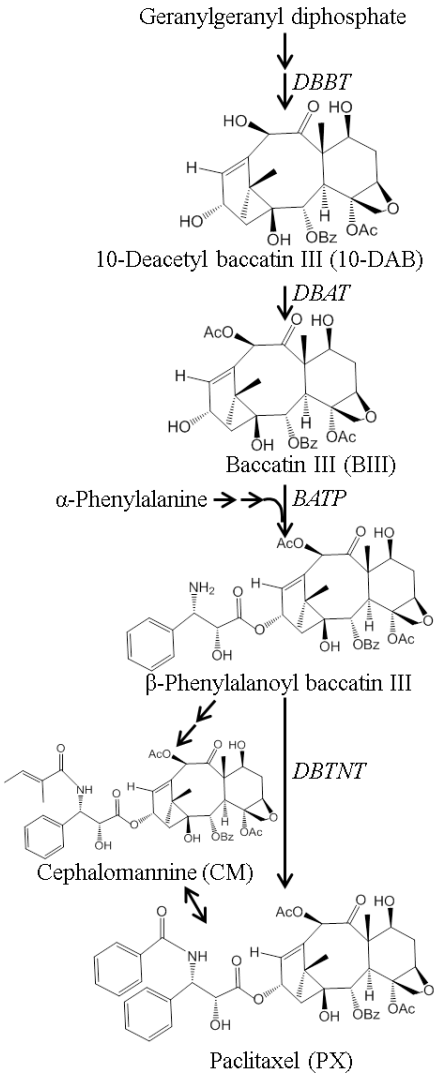

Figure 1 Main metabolic pathway of paclitaxel and the related taxanes from geranylgeranyl diphosphate [14].
DBBT: taxane 2a-O-benzoyl transferase, *DBAT*: 10-deacetyl baccatin III-10-O-acetyltransferase, *BAPT*: baccatin III: 3- amino-3- phenylpropanoylltransferase, *DBTNBT*: 3'-N-debenzoyl-2'-deoxytaxol-N-benzoyltransferase c.

2. Experimental

2.1 Reagents

Two aliphatic amine-based ILs of N-methyl-n-propylpiperidinium bis(trifluoromethanesulfonyl)imide (PP13-TFSI) and N -methyl-n-butylpyrrolidinium bis(trifluoromethanesulfonyl)imide (P14-TFSI) purchased from Kanto Chemical Co. (Tokyo, Japan) were used. Their physical properties and chemical formulas are shown in Table 1. 1-Hexyl-3-methylimidazolium hexafluorophosphate (HMIN-PF_6, TCI, Tokyo, Japan), which was found to enhance the productivity of the taxanes in the previous report [14], was used to compare the effeciency of the taxane production to the two ILs.

2.2 Plant cell culture

Callus induced from the needles of *Taxus cuspidata* and a modified Gamborg's B5 medium [1] were used for the culture. Suspension culture inoculated by the precultured cells was carried out in a 100 cm^3 Erlenmeyer flask containing 20 cm^3 of the B5 medium and 1 cm^3 of the ILs (5 vol%) on a rotary shaker (NR-150, Taitec, Saitama, Japan) at 110 rpm in the dark at 26 ˚C. During the culture the amounts of fresh cells, paclitaxel and the related taxanes in the culture flask were measured.

2.3 Evaluation of cytotoxicity and effectiveness for taxane production of ILs

To examine the cytotoxicity and the effectiveness for the taxanes production of ILs, the suspension cell culture with *in situ* extraction with 5 vol% IL was carried out. The suspension cell culture in the absence of IL was conducted as the control culture.

For examination of the cytotoxicity, relative cell growth rate, R_{FCW}, were defined as follows,

$$R_{FCW}\ [-] = FCW_{IL}/FCW_C \quad (1)$$

where FCW_{IL} and FCW_C are the fresh cell weight in the cultures including IL and that in the control after 7 d culture periods, respectively.

If an IL has cytotoxicity against the cells, the value of R_{FCW} value will be less than 1.

For evaluation of the effectiveness of the IL on the productivity of the taxanes, the specific production rate of the taxane, E_{taxane} was defined as follows,

$$E_{taxane}\ [\mu g/(g\text{-cell}\cdot d)] = \Delta P/(x\cdot \Delta t) \quad (2)$$

where ΔP is the amount of produced taxane (10-DAB, BIII, PX, CM and total amount of these taxanes (total)) during a culture period of Δt, Δt is 7 d and x is fresh cells weight.

Table 1 Chemical formula and properties of ILs used in this reseach

IL	Chemical formula	Abbreviation	Solubility in aqueous medium [mM]	Partition coefficient of paclitaxel in IL-medium two phase system [-]
1-Hexyl-3-methylimidazolium hexafluorophosphate	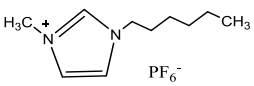	HMIN-PF_6	29.5	160
N-Methyl-n-propylpiperidinium bis(trifluoromethanesulfonyl)imide	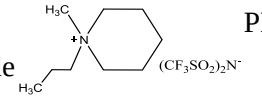	PP13-TFSI	19.9	37.1
N-Methyl-n-butylpyrrolidinium bis(trifluoromethanesulfonyl)imide	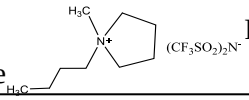	P14-TFSI	16.1	45.4

2.4 Analysis

Cells were harvested from cultures, washed with water, blotted on filter paper to remove excess liquid, and then weighed to determine FCW. The amounts of the paclitaxel and the related taxanes in the medium phase, the IL phase and the cells in all samples were analyzed by using a reversed-phase HPLC system according to the analytical procedures as described previously [2].

3. Results and Discussion

3.1 Cytotoxicity of ILs

The weight of the fresh cells in the culture including each IL after a 7 d culture period is shown in Figure 2. Regardless of the kinds of ILs, the fresh cells weight in the culture with the IL was as similar as that in the contorol culture and the values of R_{FCW} under all the culture conditions were

almost 1, indicating that all the ILs used in the present research have no cytotoxicity.

3.2 Effects of ILs on the productivities of paclitaxel and the related taxanes

Figure 3 shows the effect of ILs on the productivity of PX, P_{PX}, which is defined by Equation (2). The values of P_{PX} in the cultures including the ILs increased compared to that in the control culture. This increase might be causaed by partition of the produced PX into the ILs. The P_{PX} value of P14-TFSI was 2 times higher than that of PP13-TFSI. P14-TFSI was more effecitve to extract and produce PX than PP13-TFSI and HMIN-PF_6 (Figure 3), resulted from its stronger hydrophobicity than PP13-TFSI due to the lowered solubility in the aqueous medium than that of PP13-TFSI (Table 1).

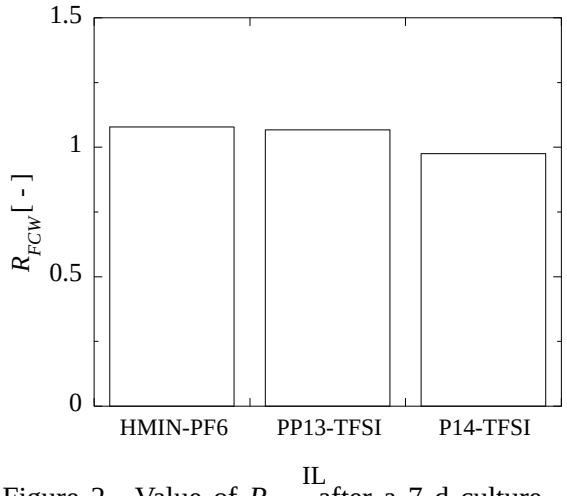

Figure 2 Value of R_{FCW} after a 7 d culture period in the culture including 5 vol% IL.

The ILs might affect the activities of enzymes related to the biosynthesis of PX. Thus, the productivites of the related taxanes of 10-DAB, BIII and CM (Figure 1) in the culture including the ILs were examined. As shown in Figure 3, the productivites of the taxanes in the culture with the ILs were greater than those of the control culture. Greatest productivites of the total taxanes, which mean the total sum of the taxanes, in the culture with P14-TFSI were observed. The value of E_{total} in the culture with P14-TFSI was 2 times greater than that with PP13-TFSI. These results suggest that P14-TFSI could be an excellent extractant of PX and a stimulator for the enzymes related to the metabolic pathway of paclitaxel synthesis in the plant cell culture. Though the reason for the stimulation of the metabolism was still unclear, this should be further studied. An effective method for the back-extraction of the target taxanes from the ILs should be explored. A back-extraction and recovery of the taxanes from the ILs by adjustment of pH was under consideration because adjustment of the medium pH contributed to the efficient back-extraction of hydrophobic ferulic acid and caffeine acid from HMIN-PF_6 [11]

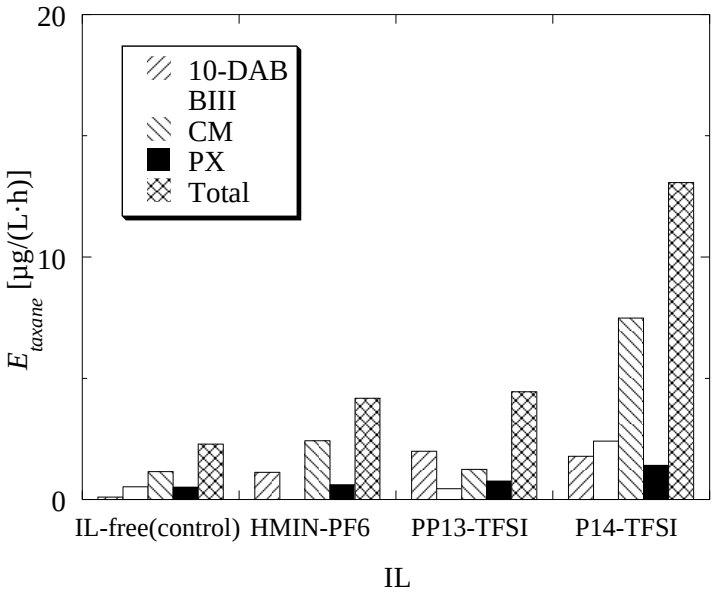

Figure 3 Productivities of 10-DAB, BIII, CM and PX after a 7 d culture period in the culture including 5 vol% IL. "Total" means the productivites of total sum of the taxanes.

4. Conclusion

For effective *in situ* extraction of the anticancer drug, paclitaxel, from the aqueous medium in the suspension cell culture of *T. cuspidata*, two aliphatic amine-based ILs of N-methyl-n-propyl-piperidinium bis(trifluoromethanesulfonyl)imide (PP13-TFSI) and N-methyl-n-butylpyrrolidinium bis(trifluoromethanesulfonyl)imide (P14-TFSI) as extractants were used in the cell culture. The two ILs were found to have no cytotoxicity and increased the productivities of paclitaxel and the related taxanes of 10-DAB, BIII and CM. Greatest productivites of paclitaxel and the total taxanes in the culture with P14-TFSI was observed, suggesting that P14-TFSI could be a excellent extractant and stimulator for the enzymes related to the metabolic pathway of paclitaxel synthesis.

Acknowledgement

This work was supported by JSPS KAKENHI Grant Number JP16K06879.

References

1) S. Yamamoto, K. Ogawa, M. Aochi, K. Nohara, S. Furusaki, *Solvent.Extr. Res. Dev., Jpn.*, **12**, 149-157 (2005).
2) S. Yamamoto, S. Hayashi, S. Furusaki, *Solvent.Extr. Res. Dev., Jpn.*, **20**, 65-70 (2005).
3) S. Yamamoto, T. Morisaki, K. Takayama, Y. Kuriyama, S. Hayashi, H. Miyasaka, *Solvent.Extr. Res. Dev., Jpn.*, **22**, 103-107 (2015).
4) S. Yamamoto, R. Noguchi, A. Hayashi, Y. Kuriyama, S. Hayashi, H. Miyasaka, *Solvent.Extr. Res. Dev., Jpn.*, **23**, 187-192 (2016).
5) J. M. Padró, R. B. P Vidal, M. Reta, *Anal Bioanal Chem*, **406**, 8021–8031 (2014).
6) F.-Y. Du, X.-H. Xiao, G.-K. Li, *J. Chromatogr. A*, **1140**, 56–62 (2007).
7) Z. Du, Y.-L. Yu, J.-H. Wang, *Chem. Eur. J.*, **13**, 2130 – 2137 (2007).
8) W. Bi, M. Tian, J. Zhou, K.H. Row, *J. Chromatogr. B*, **878**, 2243–2248 (2010).
9) B. Tang, W. Bi W, M. Tian, K.H. Row, *J. Chromatogr. B*, **904**, 1–21 (2012).
10) G. Absalan, M. Akhond, L. Sheikhian, *Talanta*, **77**, 407-411 (2008).
11) Y.-Y. Yu, W. Zhang, S.-W. Cao, *Chinese J. Anal. Chem*., **35**, 1726–1730 (2007).
12) K. D. Clark, O. Nacham, H. Yu, T. Li, Melissa M. Yamsek, D. R. Ronning, J. L. Anderson, *Anal. Chem.*, **87**, 1552-1559 (2015).
13) G.-J. Kim. J.-H. Kim, *Process Biochem.*, **50**, 989-996 (2015).
14) Y.-Y. Yu, W. Zhang, S.-W. Cao, *Chinese J. Anal. Chem*., **35**, 1726–1730 (2007).

Aerated Extraction Column for Reactive Extraction from Fermentation Broth

Andreas BEDNARZ[1], Peter SCHERÜBEL[2], Antje SPIEß[3], Andreas PFENNIG[4,*]

[1]RWTH Aachen, AVT – Fluid Process Engineering, Wüllnerstr. 5, 52062 Aachen, Germany; [2]TU Graz, Institute of Chemical Engineering and Environmental Technology, Inffeldgasse 25/C/II, 8010 Graz, Austria; [3]TU Braunschweig. Institute for Biochemical Engineering, Rebenring 56, 38106 Braunschweig, Germany; [4]University of Liège, Department of Chemical Engineering – Product, Environment, and Processes (PEPs), Quartier Agora, Allée du Six Août, 11, 4000 Liège – Sart-Tilman, Belgium

The separation of a product from a fermentation broth can be achieved by reactive extraction. A systematic way to find suitable process conditions based on cascaded option trees has been demonstrated for the example of diamine recovery. Suitable choice of reactive extractant and diluent lead to a high degree of extraction and feasible coalescence characteristics at *p*H values suitable for in-situ extraction. The competing boundary conditions for an efficient process are discussed showing that in general a complex optimization task has to be solved to find the most feasible process conditions. Simulation of extraction-column performance based on single-drop experiments in dedicated lab-scale equipment shows good agreement with pilot-plant experiments up to and including the flooding limit. Finally, to facilitate in-situ removal of a product to avoid product inhibition, an aerated column has been studied, where a dedicated three-phase separator for the top of the column is presented. The results show that even for this challenging task feasible operation conditions can be found.

1. Introduction

The foreseeable feedstock change in chemical industry towards renewable resources will lead to an increased application of bio-reactions for obtaining the product [1,2]. The challenge in an overall process with a biotechnological step is the primary recovery of the product, because typically the product is obtained at low concentration in an aqueous environment. This means that very selective process steps have to be used to achieve directly a significant enrichment of the desired product component(s) and to minimize correspondingly the flowrates in the first separation step. Here, solvent or reactive extraction are feasible options for first downstream steps. The extractant and the reactive agent can be chosen to maximize selectivity and capacity. Another challenge results, if the first separation shall be realized as in-situ extraction. This requires that the boundary conditions for the survival of the microorganisms are taken into account also during the extraction step. Because some microorganisms require continuous supply with oxygen, the extraction process has to be aerated in that case. This leads to the demand to realize a three-phase separation, where already liquid-liquid phase separation alone in many cases results in significant challenges. As an example case the production of diamine by fermentation has been chosen, because it is a component of potential industrial relevance as monomer for polyamide production. Since diamines can be components for high-performance polymers, such a high-added-value component has

the chance to be economically competitive as bio-based product already today.

2. Design of Extraction Process

In the downstream development for diamine removal after fermentation, a variety of options exists to try to solve the challenges mentioned. In order to be able to systematically structure the options, the method of cascaded option trees has been applied [3] as shown in Figure 1. In these option trees all options are collected and the result of evaluation with respect to the relevant criteria is recorded with a color code indicated at the bottom left of Figure 1. Also, unit operations other than extraction had been evaluated but turned out to be obviously less promising than extraction. In further detailing the options physical as well as reactive extraction have been regarded, where different reactive extractants have been considered in various diluents, which were chosen to be characteristic for a variety of solvent classes.

The first criterion considered was toxicity, where the phthalate as diluent has been discarded because of its hormone-like effects on humans. It is obvious that once an option completely fails with respect to one of the criteria, this option does not need to be considered further. Thus, the phthalates do not need to be considered in evaluating the following criteria.

The next challenge to be mastered is the extraction equilibrium, which has to allow efficient and selective removal of the desired product. Reactive selectivity may be especially promising. Figure 2 shows the results obtained for the example extraction of a diamine with D2EHPA (di-(2-ethylhexyl) phosphoric acid) [4]. Equilibration was realized with a mixing device, which allows slow over-head rotation of the sample flasks, which was performed for at least 30 min in a temperature controlled water bath. The phase ratio applied was around 1:1. Plotted is the degree of extraction, which is the fraction of the extracted component, here the diamine, which is transferred into the organic extractant phase at the indicated conditions. Two main parameters are apparently influencing the extraction equilibrium, namely the extractant concentration and *p*H. The *p*H is also relevant when considering in-situ extraction and the extraction concentration directly relates to the capacity of the organic phase.

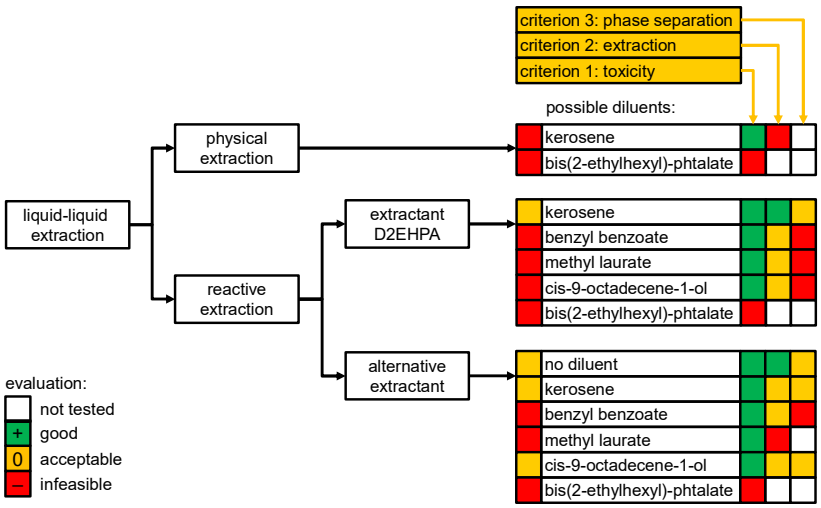

Figure 1. Degree of extraction as basis for extraction-process design

Unfortunately both parameters also simultaneously influence the third criterion evaluated, namely phase separation after extraction [5]. The ease of phase separation is characterized with a standardized settling cell, which was originally proposed by Henschke together with the quantitative evaluation of the coalescence process [6]. The time to settle in that lab-scale equipment is a quantitative measure, which allows direct judgement on feasibility of phase separation. The parameters obtained from the detailed evaluation of videos taken from this experiment with roughly one liter of two-phase system after 30 s of stirring at 800 min^{-1} allow quantitative design of the technical gravity settler. As shown in Figure 3, settling time for this system depends strongly on *p*H as well as on the phase ratio. It is apparent that for biological systems a rather large scatter of the data occurs. As a rule of thumb, settling times below 300 s allow relatively unproblematic phase separation on technical scale, which can be achieved for all phase ratios at suitable values of *p*H [7]. This still holds even if in-situ extraction is performed, i.e. in the presence of cells. Unfortunately, for *p*H-values close to 7, which would be desirable in this case for in-situ extraction, phase separation becomes slightly worse. It should also be mentioned that in a variety of cases the formation of significant crud layer has been observed, e.g. in the case of low *p*H with an aqueous dispersed phase [8].

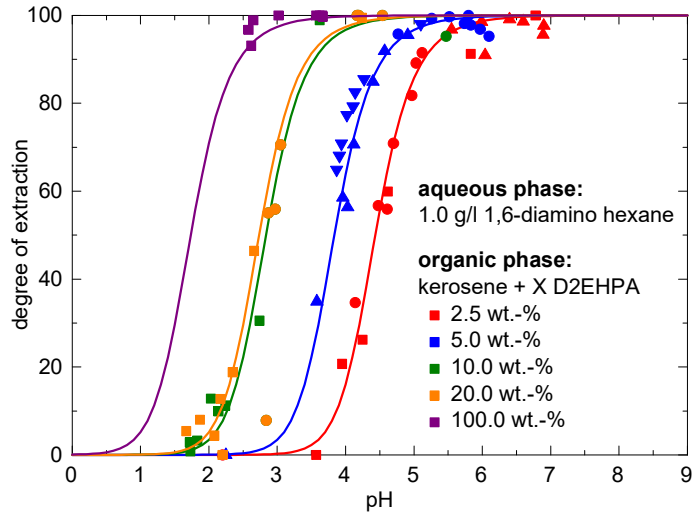

Figure 2. Degree of extraction as basis for extraction-process design at 30°C

Considering these criteria, in overall process optimization a feasible parameter window has to be found. For the example case the following boundary conditions result.

- Good extraction selectivity is characterized via the extraction equilibrium, which is on the one hand side determined by the choice of the reactive extractant, here D2EHPA. Some influence can also be attributed to the diluent, here kerosene. The diluent influence is usually not very pronounced with respect to extraction equilibrium. Finally, in this example *p*H is a major influencing parameter, which strongly affects this ion-exchange equilibrium. Here a sufficiently high *p*H is required to achieve a high degree of extraction, i.e. a sufficient degree of enrichment [4].
- Re-extraction is achieved by adding a base and shifting the *p*H to sufficiently low values so that the diamine in equilibrium can then be found in the aqueous phase. To shift the *p*H, base has to be added leading to salt formation. This back extraction should be possible with as little as possible salt

production. Since the *p*H scale is logarithmic and only small amounts of acid or base are required to shift *p*H around the value of 7, an extractant is desired where the point of inflection in the typical S-shaped curves in Figure 1 is located near this optimal *p*H. In this example, a low extractant concentration is thus desirable.

- A high capacity for the product is on the other hand reached with high extractant concentration.
- In contrast to that, it turns out that good coalescence behavior which allows phase separation in continuous gravity settlers is achieved for low extractant concentrations.
- Crud-formation tendency induced by biomass strongly depends on extractant concentration and *p*H. In the evaluated *p*H-window of 7 and slightly below feasible phase separation has been observed for a variety of phase ratios [5].
- For in-situ extraction, further limitations e.g. on feasible *p*H-range may additionally apply. In the case considered here, a *p*H slightly below neutral is desirable.

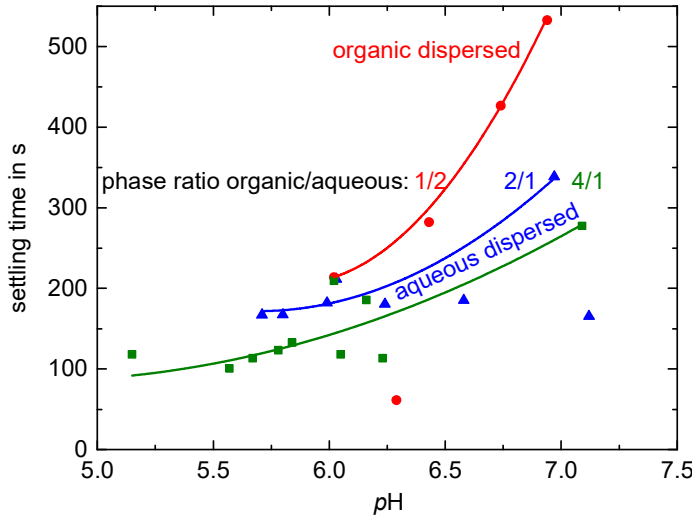

Figure 3. Settling time for the system kerosene with 5 wt-% D2EHPA at 30°C with 0.1g/l diamine, determined with 1 liter of dispersion.

3. Design of Extraction Column

After the extractant has been selected and some basic process parameters defined like *p*H and the choice of the dispersed phase, the extraction equipment has to be designed. An option with high volume-specific separation performance is to use an extraction column. For extraction-column design especially for such complex processes, where during process design only limited amounts of the product are available, drop-based simulation of column performance may be an especially promising approach. In previous work, this method has been developed and it has been shown that even for technical systems, prediction accuracy better than 10% can be expected up to and including flooding limit [9]. This method relies on experiments on lab scale with dedicated equipment to quantify behavior of single drops, e.g. on sedimentation as well as on mass transfer [10,11,12]. The parameters of suitable models are then fitted to these data, which are in turn used in the drop-based column simulation. In the developed tool, ReDrop (REpresentative DROPs), a sufficient number of individual drops can be followed in their behavior, taking sedimentation, mass transfer, breakage and splitting into account, also considering the

swarm effect as well as the interactions with the internals. The tool has been extended to account for chemical reactions in either phase as well as at the interface.

The corresponding single-drop experiments on sedimentation velocity and mass transfer have been performed. Then the ReDrop simulations were compared to experimental results obtained in a pilot-plant scale sieve-tray extraction column of 50 mm diameter. As shown in Figure 4, ReDrop allows describing the transient behavior of the extraction-column performance with good accuracy.

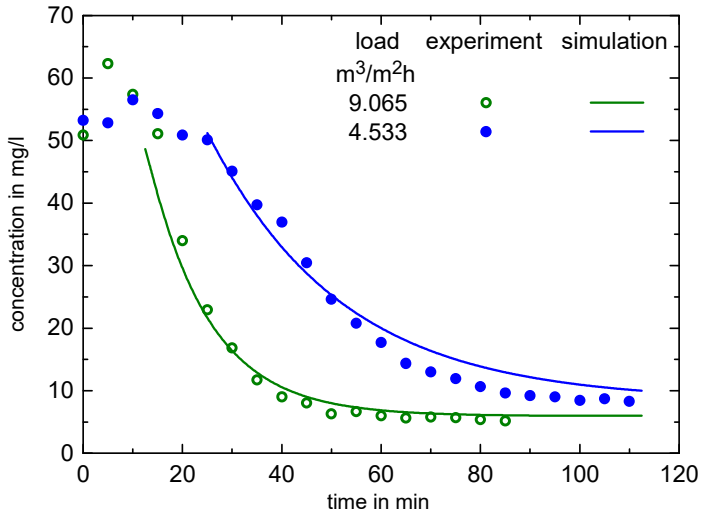

Figure 4. Concentration of diamine at the continuous-phase outlet, organic phase: oleyl alcohol + 5wt-% D2EHPA, aqueous phase: ammonium-phosphate buffer + hexane-1,6-diamine with c_0 =100 mg/l, flow-rate ratio 1/1, pulsation intensity 10 mm/s, 25°C

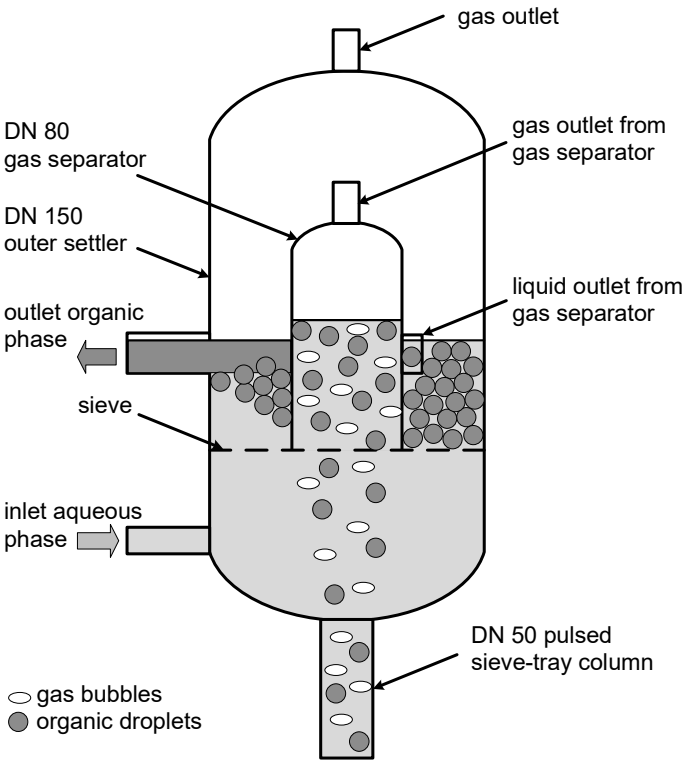

Figure 5. Three-phase separator at extraction-column top for aerated extraction

4. Aerated Column Performance

As mentioned, for in-situ recovery from biotechnological processes e.g. to overcome product inhibition, it is required that the fermentation broth is aerated also during separation. To allow this, the head of the column has been modified with a three-phase separator as shown in Figure 5. All three phases coming from the extraction column – the dispersed phase, gas bubbles and some continuous phase carried along with the dispersed phases – enter the internal gas separator, where the gas is leaving towards the top and the liquids to one side. The liquid phases are then separated in the annular space of the outer separator, where the formerly dispersed phase is exiting to the left.

The results with aeration show that the pulsed sieve-tray column can be operated without problem. The hold-up is significantly increased as compared to the non-aerated case, and the drop size of the organic dispersed phase is reduced, which may even be beneficial for separation performance. The increased hold-up leads to an earlier onset of flooding so that only reduced flowrates are feasible. Since as seen above the degree of extraction of the amine can be approaching essentially unity at reasonable values of *p*H, meaning essentially complete removal in a single theoretical stage, and because of the usually slow reaction kinetics of fermentation, a low flowrate of organic phase may be fully sufficient to ensure sufficient product removal to avoid product inhibition. For any specific case, this of course requires setting up the basic balances, where in this work it has been shown that even aerated extraction columns are a suitable option to realize this primary separation step technically.

References

1) P. Frenzel, R. Hillerbrand, A. Pfennig, *Polymers*, **6**(2), 327-345 (2014).
2) P. Frenzel, R. Hillerbrand, A. Pfennig, *Chem. Eng. Res. Des*., **92**, 2006-2015 (2014).
3) A. Bednarz, B. Rüngeler, A. Pfennig, *Chem. Ing. Techn.*, **86**(5), 611-620 (2014).
4) A. Bednarz, A.C. Spieß, A. Pfennig, *J. Chem. Technol. Biotechnol*., **92**, 1817-1824 (2017)
5) A. Bednarz, P. Scherübel, A.C. Spieß, A. Pfennig, *Chem. Eng. Techn*., accepted, DOI: 10.1002/ceat.201700020 (2017).
6) M. Henschke, L. Schlieper, A. Pfennig, *Chem. Eng. J*., **85**(2-3), 369-378 (2002).
7) A. Pfennig, T. Pilhofer, J. Schröter, in R. Goedecke (Ed.), Fluid-Verfahrenstechnik, Vol. 2, Wiley-VCH, Weinheim, 907-992 (2006).
8) S. Ruckes, A. Pfennig, in F. Valenzuela, B.A. Moyer (Eds.) Proceedings of ISEC 2011 (2011).
9) J. Ayesterán, N. Kopriwa, F. Buchbender, M. Kalem, A. Pfennig, A. *Chem. Eng. Techn.*, **38**(10), 1894-1900 (2015).
10) M. Henschke, A. Pfennig, *AIChE J.*, **45**(10), 2079-2086 (1999).
11) N. Kopriwa, F. Buchbender, J. Ayesterán, M. Kalem, A. Pfennig, *Solvent Extr. Ion Exc.*, **30**(7), 683-723 (2012).
12) F. Buchbender, M. Schmidt, T. Steinmetz, A. Pfennig, *Chem. Ing. Technol.*, **84**(4), 540-546 (2012).

Unique Separation Based on Extraction Kinetics Using a Liquid-liquid Countercurrent Centrifugal Contactor with Taylor Vortices

Masahiko NAKASE[1,*], Yuto MATSUZAWA[2]and Kenji TAKESHITA[2]

[1]*Aqueous Separations and Radiochemistry Department, Idaho National Laboratory, 2525 Fremont Avenue, Idaho Falls, Idaho 83415, United States;* [2]*Laboratory for Advanced Nuclear Energy, Tokyo Institute of Technology, 2-12-1 Ookayama, Meguro-ku, Tokyo, 152-8550, Japan*

We performed a unique separation based on extraction kinetics using a liquid-liquid countercurrent centrifugal contactor that induces Taylor-Couette (TC) flow. Conventional extraction systems typically involve a mixer-settler extractor, which relies on an equilibrium being established. In the case of TC flow, species with faster extraction kinetics can be extracted more efficiently than those with slower kinetics, due to the countercurrent contact of the organic and aqueous phases. In this study, the separation of Fe(III) and Y(III) was achieved by using di(2-ethylhexyl) phosphoric acid (D2EHPA), for which the extraction kinetics are fast forY(III) but slow for Fe(III). Under equilibrium conditions, Fe(III) is more readily extracted than Y(III), but during countercurrent operation with TC flow, the order of extractability is reversed, with Y(III) being more readily extracted than Fe(III). For the condition where the metal ion concentrations are higher than the ligand concentration, which is a more competitive extraction condition for metal ions, the distribution ratio (D) values for both Y(III) and Fe(III) were decreased, but the selectivity for Y ($SF_{Y/Fe} = D_{Y(III)}/D_{Fe(III)}$) increased. Thus, solvent extraction with TC flow may allow the design of effective, efficient separation processes.

1. Introduction

Solvent extraction is one of the most reliable and effective methods for separation of metal ions in solution. Designing ligands with high selectivity for specific ions is important, and for large-scale operations, the design of an appropriate extractor system that provides a sound practical and theoretical basis for a flowsheet is a further requirement. In this study, we investigated effective separation by solvent extraction using a liquid-liquid counter-current centrifugal contactor that induces a series of Taylor vortices inside a narrow region with a high aspect ratio. The contactor consists of an inner rotor and static outer wall and facilitates extraction with multiple theoretical stages due to countercurrent contact between the organic and aqueous phases. To evaluate extraction performance, the oil-water dispersion, extraction/separation behavior, and mechanism of multi-staging were investigated. The flows inside the contactor were observed and measured by the ultrasonic velocity profiler method and the results were verified by numerical simulation of a single-phase flow [1]. A fine dispersion inside the contactor was simulated by altering the volume of the fluid model in the multiphase flow simulation, and the effects of the wetting properties of the inner rotor and interfacial tension were highlighted [2]. Continuous extraction experiments have been performed to study the effects of

operating conditions (e.g., axial flow rates and rotation speed) and extraction systems with fast and slow extraction kinetics (e.g., Zn(II) extraction by di(2-ethylhexyl) phosphoric acid (D2EHPA) and Cs(I) extraction by calix[4]arene-bis(*t*-octylbenzo-crown-6) (BOBCalixC6)) in the presence of certain additives [1,3]. Multi-staging was readily accomplished by D2EHPA-Zn(II) due to its fast kinetics, whereas multi-staging was difficult for BOBCalixC6-Cs due to slow extraction kinetics. However, using a more lipophilic inner rotor resulted in a finer dispersion and some multi-staging was observed. Surface-activating agents, such as sodium di(2-ethylhexyl) sulfosuccinate and sodium dodecyl sulfate, and a surface-protective agent, polyethylene glycol, have also been used in Taylor-Couette (TC) flows under appropriate conditions for phase separation [4]. The effect of synergistic agents on lanthanide extraction have also been studied for *N,N,N′,N′*-tetraoctyl diglycolamide (slow extraction kinetics) in the presence of a water-soluble masking agent and synergist (such as *N,N,N',N'*-tetraethyl-3,6-dioxaoctane-1,8-diamide and nonanoic acid) [5]. Interestingly, such chemicals worked more effectively in TC flows compared with batch extraction. A back extraction has also been performed and the acid concentration needed for the back extraction was greatly minimized [6]. These results suggest that fast extraction kinetics are needed for effective multi-staging in TC flows. Therefore, the effect of extraction rate on separation performance in TC flows was studied for Sm(III)/Eu(III) separation by comparing the distribution ratio (*D*) and the separation factor (*SF*; ratio of distribution ratios, *D*) under equilibrium and non-equilibrium conditions [7]. For separating Sm(III) and Eu(III) by D2EHPA, the extraction rates of Sm and Eu were similar because they are adjacent trivalent lanthanides. For non-equilibrium conditions, the ratio of the gradient of *D* with respect to time, $SF_{Eu/Sm,non\text{-}eq.} = (dD_{Eu}/dt)/(dD_{Sm}/dt)$, was $SF_{Eu/Sm,non\text{-}eq.} < SF_{Eu/Sm,eq}$. Correspondingly, the number of theoretical stages for Sm estimated for extraction at equilibrium was lower than that of Eu, that is, $SF_{Eu/Sm,TC.} < SF_{Eu/Sm,eq}$, where $SF_{Eu/Sm,TC}$ indicates the SF in case of continuous extraction operation with TC flow. If extraction is based on equilibrium conditions, the number of theoretical stages for each metal ion should be the same. In the case of separations with a large difference in extraction kinetics resulting in a large difference in the SF values, that is, $SF_{non\text{-}eq.} > SF_{eq}$, it is expected that separations not governed by the extraction equilibrium may be possible. Under such circumstances, the separation of Fe(III)/Y(III) by D2EHPA has been re-examined. The D2EHPA can extract Fe(III) effectively but the extraction has slow kinetics [8, 9]. Thus, for the Fe(III)/Y(III) system, we compared the extraction kinetics for conventional liquid-liquid extraction performed under equilibrium conditions and continuous extraction with a TC flow.

2. Experimental

2.1 Centrifugal Contactor

A schematic of the centrifugal contactor is given in Figure 2 [7]. When the rotation speed of the inner rotor reaches a critical point, a series of Taylor vortices are induced [10]. The TC flow in this study has a flow region with a high aspect ratio and the rotation speed is high enough to produce stable turbulent Taylor vortices [11]. The dispersed organic phase from the bottom inlet ascends through a series of Taylor vortices and comes into contact with the continuous aqueous phase, which originates from the inlet at the top. The lighter organic solvent (*n*-dodecane) ascends the column because of the difference in specific gravity and overflows from the top outlet. The heavier aqueous phase is pumped

out from the bottom outlet. Phase separation was achieved in the settling zones (intact tube covering the inner rotor, 20 mm in height) at the top and bottom of the contactor.

Table 1. Dimensions of the contactor.

Variable	Symbol	Value	Unit
Radius of inner rotor	D_i	15	mm
Radius of outer wall	D_o	20	mm
Width of fluid region	D_o-D_i	5	mm
Height of fluid region	H_f	200	mm
Radius ratio	D_i/D_o	0.75	-
Aspect Ratio	H_f/d	40	-
Hight of upper settling part	H_u	30	mm
Diameter of inlet hole for aqueous phase	D_a-inlet	3	mm
Diameter of outlet hole for aqueous phase	D_a-outlet	3	mm
Diameter of inlet hole for organic phase	D_o-inlet	3	mm
Diameter of outlet hole for organic Phase	D_o-outlet	3	mm

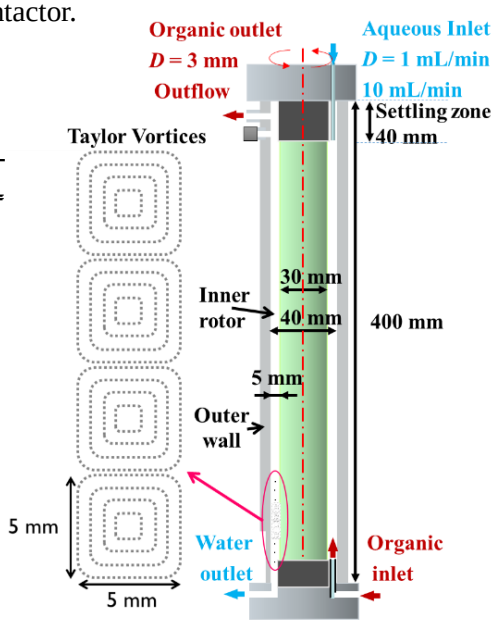

Figure 2. Schematic of contactor

2.2 Solutions and experimental conditions

The experimental conditions for batch extraction and continuous extraction with TC flow are listed in Tables 2 and 3, respectively. The change in the metal ion (Fe(III) and Y(III)) distribution over time was used to assess performance. To compare separation performance in batch extraction and continuous extraction with TC flow, solutions containing various Fe(III) concentrations and a fixed Y(III) concentration were tested. The Fe(III) and Y(III) concentrations in the aqueous phase were measured by inductively coupled plasma atomic emission spectrometry (ICPE-9000, Shimadzu). Several approaches have been described for measuring extraction kinetics, including the batch method [12], the single droplet method [13], stopped-flow apparatus [9], the constant area cell approach [8,14,15], and using specialized equipment [16]. In this study, the batch method was used.

Table 2. Experimental conditions for batch extraction tests.

		value	unit
Operation	Temperature	25	℃
	time	30 - 350000	s
Aqueous phase	volume	3	ml
	Y(III), Fe(III)(single)	5	mmol/L
	HNO_3	0.01	mol/L
	Ionic strength($NaNO_3$)	0.2	mol/L
Organic phase	Volume	3	ml
	Diluent	*n*-dodecane	
	D2EHPA	0.01	mol/L

Table 3. Experimental conditions for continuous extraction tests with TC.

		value	unit
Operation	Ttemperature	25	℃
	Time	60	min
	Rotation speed	1400	rpm
Aqueous phase	flow rate	10	ml/min
	Y(III)	0.5	mmol/L
	Fe(III)	0.3 - 5	mmol/L
	HNO_3	0.01	mol/L
	Ionic strength($NaNO_3$)	0.2	mol/L
Organic phase	Flow rate	3	ml
	Diluent	*n*-dodecane	
	D2EHPA	0.01	mol/L

The extraction equilibrium of trivalent metal ions (M^{3+} = Fe^{3+}, Y^{3+}) with D2EHPA is described as equation (1), where HR and $(HR)_2$ indicate monomeric and dimeric formation of D2EHPA because D2EHPA exists in dimer form in a long-chain hydrocarbon, such as *n*-dodecane. The species with bar and non-bar indicate the species exist in organic phase and aqueous phase, respectively.

$$M^{3+} + \overline{3(HR)_2} \quad \rightleftarrows \quad \overline{MR_3(HR)_3} + 3H^+ \tag{1}$$

The distribution ratio is defined as the ratio of metal ion concentrations in the organic ($C_{org.eq}$) and aqueous ($C_{aq,eq}$) phases at equilibrium, $D = C_{org.eq}/C_{aq,eq}$. In the D2EHPA system, the extraction equation is given by equation (2),

$$K_{ex} = \frac{\overline{[MR_3(HR)_3]}[H^+]^3}{[M^{3+}]\overline{[(HR)_2]}^{*3}} = D\frac{[H^+]^3}{\overline{[(HR)_2]}^{*3}} \tag{2}$$

where the bars indicate "in the organic phase" and $[(HR)_2]^*$ denotes the effective molar concentration of $(HR)_2$ calculated by Alstad's equation [17]. The extraction at equilibrium is described by equation (3),

$$\overline{[(HR)_2]}^* = \gamma^* \overline{[(HR)_2]} \quad , \quad \log\gamma^* = -A\overline{[(HR)_2]}^{1/2} \tag{3}$$

where A = 0.83 for *n*-dodecane [18], and the effective concentration of the D2EHPA dimer is used as shown in equation (4).

$$\log D + 3\log[H^+] = 3\log\overline{[(HR)_2]}^* + \log K_{ex} \tag{4}$$

Equation (4) is derived from equations (2) and (3), and the *log-log* plot gives the extraction coefficient, K_{ex}.

3. Results and Discussion

3.1 Extraction in equilibrium state

Figure 4 shows the results of the slope analysis by the least squares method for a fixed gradient of 3. In the equilibrium state, Fe(III) was more readily extracted than Y(III), namely, $D_{Y(III),eq} < D_{Fe(III),eq}$ was confirmed. The kinetics of the extraction, where there is a contact time dependency for $D_{Y(III)}$ and $D_{Fe(III)}$, by D2EHPA, are shown in Figure 5. Before the extraction reached equilibrium, the order was $D_{Y(III)} > D_{Fe(III)}$. Fe(III) has slow extraction kinetics, but at equilibrium was more readily extractable than Y(III) by D2EHPA. The slope analysis confirmed that the stoichiometries of Y(III)- and Fe(III)-D2EHPA were the same, which implies that the extraction mechanisms for the two metal ions were the same; hence, the difference in extractabilities was attributed to the slow exchange reaction of hydrated water molecules. The rate-determining step for D2EHPA extraction of Fe(III) and Y(III) may be the complexation step at the oil-water interface where the intermediate, MR_2^+ (M: metal ion, R: D2EHPA), is transferred to the organic phase [19-21].

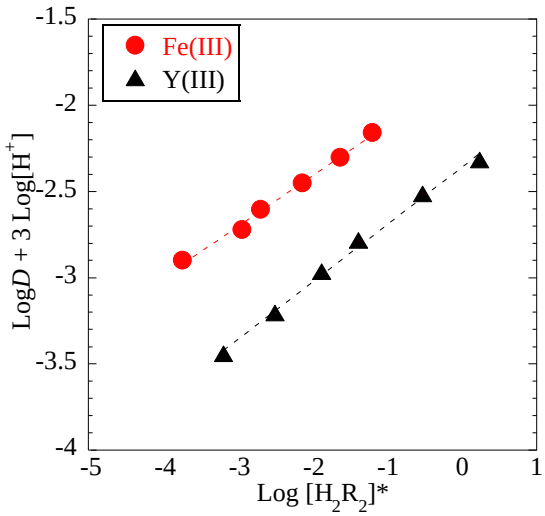

Figure 4. Slope analysis for Y(III)/Fe(III)-D2EHPA extraction systems in nitric acid

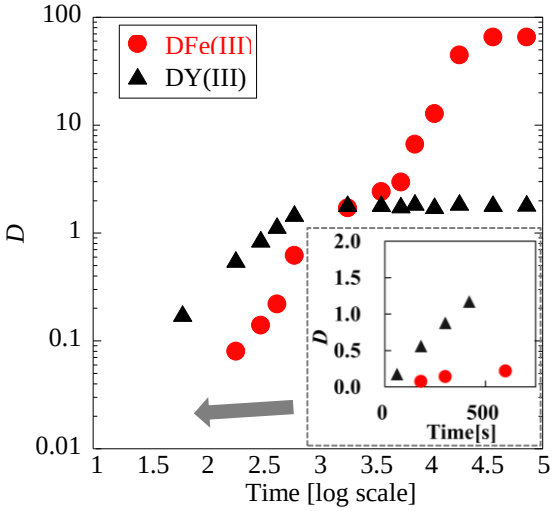

Figure 5. Contact time dependency of $D_{Fe(III)}$ and $D_{Y(III)}$.

3.2 Comparison of batch extraction and continuous extraction by the centrifugal contactor

Figure 6 compares $D_{Y(III)}$, $D_{Fe(III)}$, and $SF_{Y(III)/Fe(III)}$ for (a) batch extraction and (b) continuous extraction with TC flow. In the case of batch extraction, $D_{Y(III),eq} < D_{Fe(III),eq}$ was obtained, and $SF_{Y(III)/Fe(III),eq}$ was less than 1, namely, Y(III) cannot be concentrated from the mixture of Y(III) and Fe(III) using conventional batch extraction. For continuous extraction with TC flow, the order of D was reversed compared with batch extraction, that is, $D_{Y(III),TC} > D_{Fe(III),TC}$, so that $D_{Fe(III)}$ was lower and $D_{Y(III)}$ was higher for the TC extraction experiment. This reversal of order of D term resulted in $SF_{Y(III)/Fe(III),TC}$ being much greater than 1, indicating that Y(III) can be effectively separated from a mixture of Y(III) and Fe(III) based on the extraction kinetics. Furthermore, when the metal/ligand ratio and ratio were high, namely, when extraction of Y(III) and Fe(III) was more competitive, $SF_{Y(III)/Fe(III)}$ was high. This effect is also attributed to the difference in the extraction kinetics of Y(III) and Fe(III) by D2EHPA as a

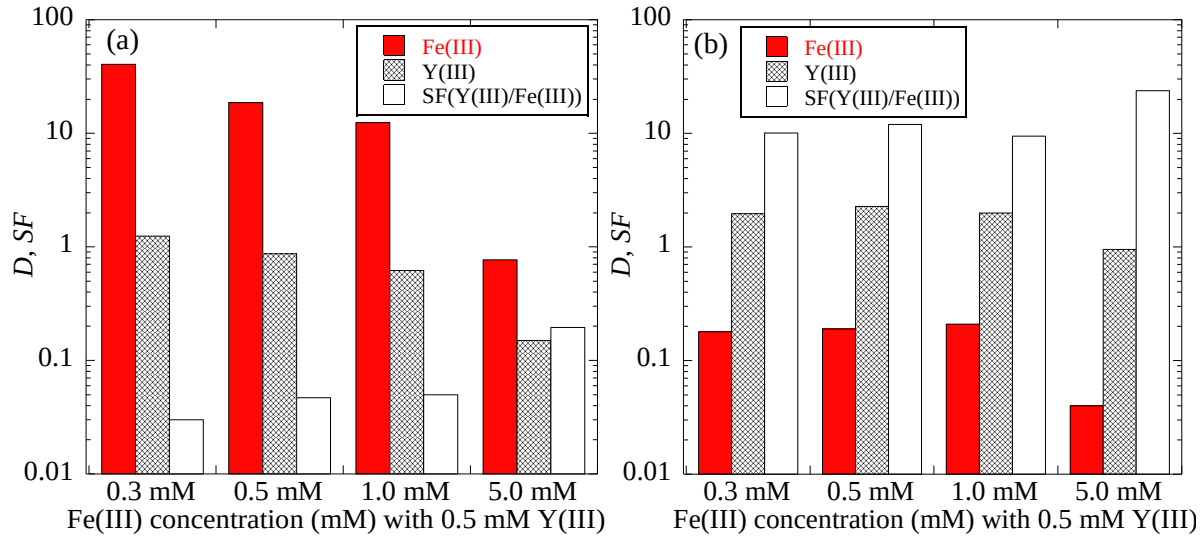

Figure 6. Comparison of D and SF for Fe(III) and Y(III) during (a) batch extraction (equilibrium) and (b) continuous extraction with TC flow (non-equilibrium).

result of high mass transfer due to the countercurrent contact of both phases in a TC flow. Thus, by combining forward and back extractions in a TC flow, much more effective separation can be achieved.

4. Conclusion

A unique separation using a liquid-liquid countercurrent centrifugal contactor was demonstrated by comparing the performance for continuous and batch extractions of Fe(III) and Y(III) by D2EHPA. Separation with countercurrent TC flow was governed by the extraction equilibrium and by the difference in extraction kinetics between the equilibrium and non-equilibrium states. In the batch extraction experiment, Fe(III) was more readily extracted than Y(III) ($D_{Y(III),eq} < D_{Fe(III),eq}$), but for non-equilibrium conditions, Y(III) was more readily extracted than Fe(III) ($D_{Y(III),non\text{-}eq} > D_{Fe(III),non\text{-}eq}$). For continuous extraction with a TC flow, Y(III) was more readily extracted than Fe(III) ($D_{Y(III),TC} > D_{Fe(III),TC}$), For conditions with higher metal/ligand and Y(III)/Fe(III) ratios in the case of continuous extraction with a TC flow, $SF_{Y(III)/Fe(III)}$ was slightly increased. There have been few studies of the differences in extraction kinetics. Further research on extraction kinetics, including the effect of synergistic agents, the effect of masking agents on extraction performance in a TC flow, and relationships between extraction kinetics and separation performance, will provide new extraction/separation methods.

Acknowledgement

This study was supported by a Grant-in-Aid for Scientific Research B (No. 25289352) and Overseas Research Fellowship (434) from the Japan Society for the Promotion of Science.

References

1) M.Nakase, R. Makabe, K.Takeshita, *J Nucl Sci Technol*, 2013, 50, 287-295.
2) M.Nakase, H.Kinuhata and K.Takeshita, *J Nucl Sci Technol*, 2013, 50, 1089-1098.
3) M.Nakase and K.Takeshita, *Procedia Chemistry*, 2013, 7, 288-294.
4) M.Nakase, H.Rokkaku and K.Takeshita, *J Nucl Sci Technol*, 2013, 50, 723-730
5) M.Nakase, Y.Sasaki, K.Takeshita, *Separ Sci and Technol*, 2014, 49, 2478-248
6) M.Nakase and K.Takeshita, *Transactions of the American Nuclear Society*, 2012, 107, 277-278.
7) M.Nakase, M.Tanaka, K.Takeshita, *Energy Procedia*, 2015, 71, 106-111.
8) J.W. Roddy, C. F. Coleman, S. Arai, J Inorg Nucl Chem,1971, 33(4), 1099-1118.
9) H.Matsumiya et al., *Hydrometallugy*, 1990, 24, 37-51.
10) G.I. Taylor, Stability of a viscous liquid contained between two rotating cylinders, *Phil Trans R Soc Lond A*, 1923, 223, 289-343.
11) R.M. Lueptow, Andreas Docter and Kyungyoon Min, Stability of axial flow in an annulus with a rotating inner cylinder, *Phys Fluids A*, 1992, 4, 2446-2455.
12) J.Shibata et al., *Journal of MMIJ*, 1992, 108, 117-121.
13) F.Baumgärtner and L. Finsterwalder, *J Phys Chem*, 1969, 74, 108-112.
14) I.Komasawa, T.Otake, *Ind Eng Chem Fundam*, 1983, 22, 122-126.
15) J.B.Lewis, *Chem Engng Sci*, 1954, 10(3), 248-259.

16) H.Johansson and J.Rydberg, *Acta Chem Scand*,1969, 23, 647-659
17) J.Alstad et al., *Proc Int Solv Extr Conf, Lyon, Society of Chemical Industry*, 1974, 2, 1083-1102.
18) P.R.Danesi and G.F.Vandegrift, *Inorg Nucl Chem Letters*, 1981, 17, 109-115.
19) H.Kim, T.Kanki and T.Asano, *KAGAKU KOGAKU RONBUNSHU*, 1997, 23, 95-102.
20) T.Kanki, et al., *Sep Purif Technol*, 2000, 19(1,2), 93-102.
21) A.Tomita, et al., *Dev Chem Eng Mineral Process*, 2003, 11, 539-555.

Methods for Enhancing the Rates of Dissociation of the *f*-Element / Aminopolycarboxylate Complex for Efficient Differentiation of Trivalent Actinides from Trivalent Lanthanides in the ALSEP Process

Peter R. ZALUPSKI[1,*], Colt R. HEATHMAN[1], Travis S. GRIMES[1] and Santa JANSONE-POPOVA[2]

[1]*Aqueous Separations and Radiochemistry Department, Idaho National Laboratory, Idaho Falls, Idaho, 83415, United States;* [2]*Chemical Sciences Division, Oak Ridge National Laboratory, Oak Ridge, Tennessee, 37831, United States*

Potentiometric and spectroscopic techniques were used to evaluate the coordination behavior and thermodynamic features of trivalent *f*-element complexation by modified aminopolycarboxylate reagents, HEDTTA and DTTA-BuA. Time dependency trends for the forward extraction of trivalent europium present in aqueous environments of HEDTTA or DTTA-BuA are compared with conventional aminopolycarboxylates. The Eu^{3+} distribution patterns show that significant enhancements to the rates of metal extraction may result either from reduction of reagent's polydenticity (HEDTTA) or manipulation of reagent's acid/base chemistry to capitalize on proton–catalyzed dissociation of *f*-element complexes (DTTA-BuA). When translated onto ALSEP chemistry platform, where trivalent americium is back-extracted from organic solvent containing solvating diglycolate extractant TEHDGA and phosphonic acid extractant HEH[EHP], the latter strategy of using a reagent of enhanced total acidity proves promising.

1. Introduction

Actinide Lanthanide Separation (ALSEP) extraction process was developed to isolate trivalent americium from aqueous effluents remaining after the initial recovery of uranium and/or plutonium from dissolved used nuclear fuel [1]. The initial step of the process co-extracts trivalent actinides (An^{3+}) and trivalent lanthanides (Ln^{3+}) from a diverse mixture of fission, activation and corrosion products using a combination of diglycolamide extractant, *N*,*N*,*N*′,*N*′-tetra(2-ethylhexyl)digylcolamide (TEHDGA), and 2-ethylhexylphosphonic acid mono-2-ethylhexyl ester (HEH[EHP]), dissolved in an aliphatic diluent. This ALSEP solvent, when "loaded" with the trivalent *f*-elements, is later equilibrated with an aqueous mixture containing the aminopolycarboxylate complexant to afford a complete differentiation of trivalent An^{3+} from trivalent Ln according to a well-known reversed TALSPEAK concept [2]. Such strategy for An^{3+} back-extraction affords best results when using diethylenetriamine-*N*,*N*,*N*′,*N*″,*N*″-pentaacetic acid (DTPA), capable of octadentate coordination of trivalent *f*-elements [3].

While the octadentate coordination of *f*-elements by DTPA yields efficient An^{3+}/Ln^{3+} separation it is also responsible for slow rate of liquid-liquid mass transfer. The binding pocket contains seven

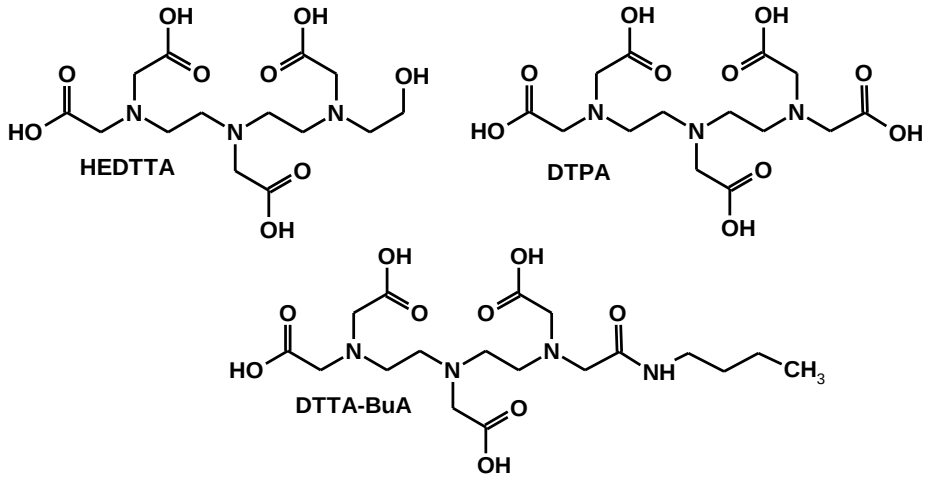

Figure 1. Structures of *N*-hydroxyethyl-*N*,*N*′,*N*′′,*N*′′- diethylenetriaminetetraacetic acid, HEDTTA, *N*-butylacetaamide-*N*,*N*′,*N*′′,*N*′′-diethylenetriaminetetraacetic acid, DTTA-BuA and diethylenetriamine-*N*,*N*,*N*′,*N*′′,*N*′′-pentaacetic acid, DTPA.

stable five-membered chelate rings, with three nitrogens and five oxygens coordinating the metal ion. Accordingly, the metal is well shielded from the interactions with the water molecules, resulting in kinetic inertness. Accordingly, numerous investigations have been focused on structure-function relationships for aminopolycarboxylate aqueous holdback reagents, with an ultimate goal of improving the observed kinetic impediment [4-6].

The interfacial mass transfer of trivalent metal ions in liquid-liquid systems of TALSPEAK-type chemistry is fully controlled by the rate of interfacial chemical reactions, as argued by Danesi and Cianetti [7]. Here, all aqueous species (Eu^{3+}, Eu-hydroxy-carboxylic acid, Eu-aminopolycarboxylate, and complexes with secondary ligand) interact with surface-active liquid cation exchanger at the interface. Accordingly, direct structural modification of molecular species partaking in the interfacial reactions offers one opportunity to enhance the mass transfer.

For the aminopolycarboxylate aqueous holdback complexants, the structural alteration of one or more acetate pendant arms of DTPA molecule may reduce its denticity and/or modify its acid/base chemistry. Such changes to the coordination chemistry offer options for the enhancement of phase transfer kinetics in liquid-liquid systems containing aminopolycarboxylates. Two strategies for structural modification of DTPA to enhance the phase transfer kinetics in liquid-liquid distribution systems designed for efficient An^{3+}/Ln^{3+} differentiation are discussed. First, a replacement of single acetate functionality of DTPA with *N*-hydroxyethyl group (*N*-hydroxyethyl-*N*,*N*′,*N*′′,*N*′′-diethylenetriaminetetraacetic acid, HEDTTA) reduces the coordination sphere of a metal ion. Second, substitution of acetate arm by strongly electron-withdrawing *N*-amide group (*N*-butylacetamide-*N*,*N*′,*N*′′,*N*′′-diethylenetriaminetetraacetic acid, DTTA-BuA), while maintaining an octadentate environment, impacts the protonation equilibria of this reagent. Figure 1 compares the structures of HEDTTA, DTTA-BuA with that of DTPA. Metal ion coordination behavior and the kinetic studies for the distribution of trivalent *f*-elements in liquid-liquid systems containing HEDTTA and DTTA-BuA are presented.

2. Experimental

2.1 Reagents

All chemicals were reagent grade or higher and used without further purification except where noted. Aqueous solutions were prepared using de-ionized water (MilliQ, 18 MΩ). Sodium perchlorate and sodium nitrate (GFS Chemicals) were purified by recrystallization from hot water. The $NaClO_4$ and $NaNO_3$ stock solutions were prepared by dissolving solid salts in HPLC-grade water. The concentrated solutions of $NaClO_4$ and $NaNO_3$ were filtered through a glass fine frit filter to remove undissolved particulates and recrystallized. Resulting crystals were dissolved in 18MΩ H_2O and standardized by ion exchange (Dowex 50X8, H^+ form). The column eluent was titrated with standardized NaOH (triplicate analysis). $Eu(NO_3)_3$ (Molycorp, 99.99%) was used to prepare solutions for Eu^{3+} complexation studies by potentiometry. Aqueous holdback reagents H_5DTPA and H_4EDTA were recrystallized from hot water. Novel aqueous holdback reagents *N*-hydroxyethyl-*N*,*N*′,*N*″,*N*″′-diethylenetriaminetetraacetic acid and *N*-butylacetaamide-*N*,*N*′,*N*″,*N*″′-diethylenetriaminetetraacetic acid were prepared at ORNL as hydrochlorate salts with >97 % purity. Concentrated perchloric (Aldrich, 99.999% trace metal basis) was used to prepare the acid solutions used in potentiometric work. Concentrated reagent grade nitric acid (Aldrich, 70% w/w, ACS reagent grade) and 50% w/w aqueous NaOH (Aldrich) were used for pH adjustment of aqueous mixtures for solvent extraction studies. The extractant 2-(ethylhexyl)phosphonic acid mono-2-ethylhexyl ester (HEH[EHP]) was purchased from Marshallton Laboratories, and *N*,*N*,*N*′,*N*′-tetra(2-ethylhexyl)diglycolamide (TEHDGA) was purchased from Eichrom Technologies. Both reagents were used as received. Radiotracers ^{241}Am, ^{139}Ce and ^{154}Eu were introduced using a working stock mixtures prepared by blending aliquots of stocks purchased from Eckert&Ziegler.

2.2 Potentiometry

Potentiometric titrations were carried out using a Mettler Toledo T-70 Graphix auto-titrator equipped with a Ross Orion semi-micro glass electrode (5 mol·L^{-1} NaCl filling solution). The p[H^+] operational scale for the glass electrode was developed by Gran analysis [4] of a strong acid-strong base titration. All titrations were performed at 25.0 ± 0.1 °C (maintained with a circulating water bath attached to a jacketed beaker). Sodium perchlorate was used to control ionic strength at I = 2.0 mol·L^{-1}. Hydrated nitrogen gas was blanketed over titration solutions to prevent CO_2 absorption. Potentiometric titrations of initially standardized HEDTTA and DTTA-BuA solutions with NaOH were performed in triplicate and analyzed using Hyperquad 2013 software [4] to resolve the acid dissociation constants (K_a) and Eu^{3+} binding stability constants (β_{MHL}).

2.3 Phase transfer kinetic studies

The distribution experiments were measured using equal volumes (0.5 mL) of each phase. Samples were equilibrated using a Glass-Col multi-tube vortexer. Temperature was maintained at 20 ± 0.3°C using sample chamber connected to water circulator. At each time interval the retrieved samples were centrifuged for 30 seconds, and each phase sampled (0.3 mL) for radiometric measurements. Distribution ratios were defined as the quotient of concentration of the metal ion in the non-aqueous phase and the concentration of metal ion in the aqueous phase at equilibrium (D = $[M]_{org}/[M]_{aq}$), as

indicated by the detected radioisotope activity of both phases (cps_{Light}/cps_{Heavy}). Aqueous phases contained holdback complexant in 1 M $NaNO_3$, and were adjusted to $p[H^+] = 3.0$ (HEDTTA, DTPA, EDTA) and $p[H^+] = 2.0$ (DTTA-BuA) using NaOH. Buffers were omitted from the forward extraction experiments in order to slow down the phase transfer equilibrium. This strategy sought to magnify differences for the studied complexants when studied on a kinetic scale. To reduce uncertainty in liquid-liquid distribution the radiotracer ^{154}Eu was introduced into the aqueous mixture before the contact with the organic phase. The concentration of cation exchanger in the non-aqueous phase was chosen to ensure that bulk (>80%) of metal ion was extracted at liquid-liquid distribution equilibrium. Samples were vortexed (motor speed setting: 50), centrifuged, and sampled phases counted on the Packard D5003 Cobra Gamma counter. The 15-300 keV energy window was chosen for radiometric counting of ^{154}Eu.

The non-aqueous solvent used for the back-extraction kinetic studies was 0.05 M TEHDGA, 0.5 M HEH[EHP] in *n*-dodecane. The solvent was pre-equilibrated with 3 M HNO_3 prior to metal loading. After triplicate washing with 0.2 M citrate the three *f*-element radiotracers (^{241}Am, ^{139}Ce, ^{154}Eu) were quantitatively co-extracted from 3 M HNO_3 into the solvent. The back-extraction of ^{241}Am was facilitated using three strip mixtures: a) 0.125 M HEDTTA, pH = 3.0, b) 0.015 M DTTA-BuA, pH = 2.0, c) 0.015 M DTPA, pH = 2.0, all buffered using 0.2 M ammonium citrate. For back-extraction experiments the pH was defined using NIST buffers 4 and 7. The centrifuged, separated phases were counted on an ORTEC GEM50P4 coaxial HPGe detector equipped with DSPEC gamma spectrometer (59.54 keV peak for Am-241, 123.07 keV peak for Eu-154, and 165.86 keV peak for Ce-139).

3. Results and Discussion

3.1 Acid dissociation constants and Eu^{3+} complexation

The influence of *N*-hydroxyethyl- and *N*-butylacetamide- functionalization on the hydrogen ion dissociation equilibria for HEDTTA and DTTA-BuA, respectively, was investigated using potentiometry. Table 1 summarizes the acid dissociation constants for all protonated species quantified using the glass electrode according to equation 1

$$H_{8-n}L^{4-n} \Leftrightarrow H_{7-n}L^{3-n} + H^+ \quad (1)$$

as compared with acid dissociation constants of DTPA generalized by equation 2.

$$H_{9-m}L^{4-m} \Leftrightarrow H_{8-m}L^{3-m} + H^+ \quad (2)$$

The reported acid dissociation constants for HEDTTA match closely with those reported for DTPA in 2.0 M $NaClO_4$ suggesting *N*-hydroxyethane- pendant arm substitution makes minimal inductive impact on the diethylenetriamine backbone. In contrast a clear indication of strong electronic influence of the amide functionality is present for DTTA-BuA, reflected in the enhanced acidity of its amine sites, relative to DTPA.

Table 1. Acid dissociation constants quantified using glass electrode for HEDTTA, DTTA-BuA and DTPA at 25.0 ± 0.1 °C. I = 2.00 M $(H^+,Na^+)ClO_4$. Uncertainties reported at ±3σ.

HEDTTA	n	$-\log_{10}K_a^n$	DTTA-BuA	n	$-\log_{10}K_a^n$	DTPA	m	$-\log_{10}K_a^m$
HL^{3-}	7	9.49 ± 0.02	HL^{3-}	7	9.34 ± 0.01	HL^{4-}	8	9.50
H_2L^{2-}	6	8.19 ± 0.01	H_2L^{2-}	6	6.65 ± 0.01	H_2L^{3-}	7	8.31
H_3L^-	5	4.31 ± 0.02	H_3L^-	5	4.09 ± 0.01	H_3L^{2-}	6	4.38
$H_4L_{(aq)}$	4	2.56 ± 0.02	$H_4L_{(aq)}$	4	2.42 ± 0.02	H_4L^-	5	2.53
H_5L^+	3	2.15 ± 0.02	H_5L^+	3	2.01 ± 0.03	$H_5L_{(aq)}$	4	2.41
H_6L^{2+}	2	-	H_6L^{2+}	2	-	H_6L^+	3	-
H_7L^{3+}	1	-	H_7L^{3+}	1	-	H_7L^{2+}	2	-
					-	H_8L^{3+}	1	-

While the *N*-hydroxyethyl group of HEDTTA does not partake in the metal ion coordination the amidic oxygen of DTTA-BuA chelates the metal ion, completing an octadentate coordination sphere similar to DTPA. Table 2 lists the stability constants for the complexation of Eu^{3+} by the reagents investigated here. The reduction of stability constant for the complexation of trivalent europium by

Table 2. Eu^{3+} complexation constants by HEDTTA, DTTA-BuA and DTPA at 25.0 ± 0.1 °C. I = 2.00 M $(H^+,Na^+)ClO_4$. Uncertainties reported at ±3σ.

$\text{Log}\beta_{mhl}$	m=1, h=0, l=1	m=1, h=1, l=1
HEDTTA	17.92 ± 0.01	20.34 ± 0.02
DTTA-BuA	18.49 ± 0.02	20.40 ± 0.02
DTPA	21.03	22.53

HEDTTA matches the expected weakening due to the elimination of one 5-membered chelate ring from a coordination sphere of the metal ion [6]. The observed decreased value of the β_{101} for Eu^{3+}/DTTA-BuA stems from a significantly lower coordination strength of carbonyl-type oxygen, relative to carboxylic-type. Figure 2 shows the distribution of tracer (10^{-5} M) Eu^{3+} species calculated for a $1 < p[H^+] < 5$ range using the assembled thermodynamic data for HEDTTA and DTTA-BuA. The speciation plot for 0.02 M HEDTTA, when compared to that calculated for DTPA, shows that *N*-hydroxyethyl functionality shifts the reagent's operational complexing scale to higher $p[H^+]$. In contrast, the electron-withdrawing influence of the *N*-butylacetamide group renders the DTTA-BuA more acidic, relative to DTPA, thus enabling the metal ion complexation in regions of higher acidity. The Eu^{3+} speciation plots lay out the foundations to explore two distinct mechanisms for enhancing the rates of metal extraction. First, for HEDTTA, the enhancement may result from the reduction of reagent's polydenticity and weakening of complexant's hold on the metal ion. Second, for

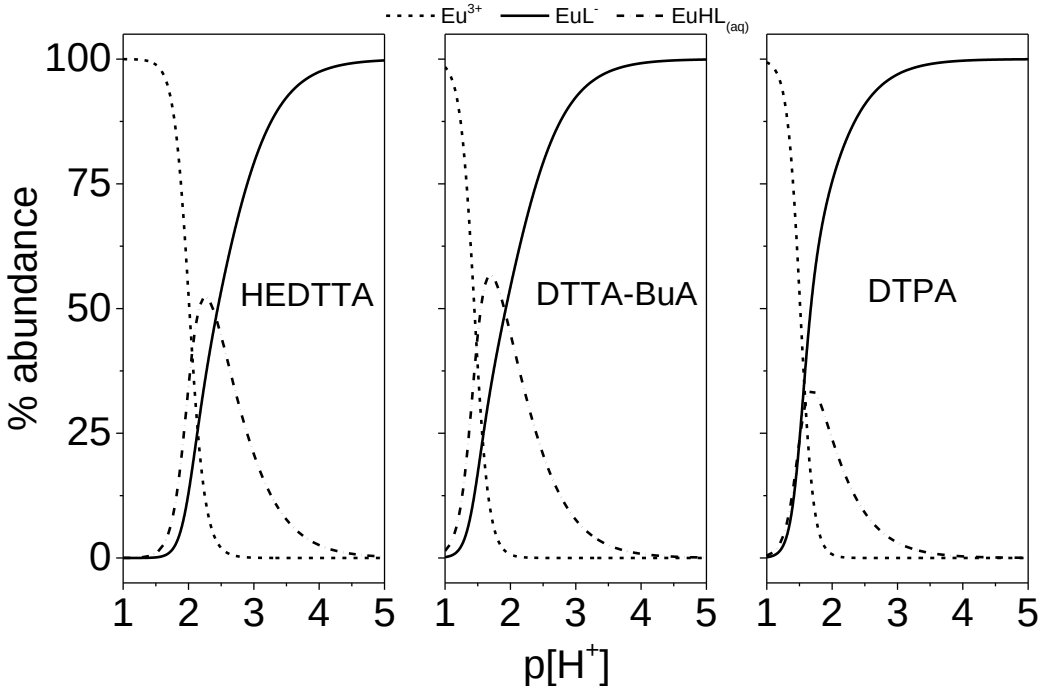

Figure 2. Distribution of species for mixtures of 0.02 M HEDTTA or DTTA-BuA and 10^{-5} M Eu^{3+} plotted as a function of p[H^+].

DTTA-BuA, may capitalize on increased rate of dissociation of *f*-element complexes in regions of higher acidity due to initial complex protonation step [2].

3.2 Forward Eu^{3+} extraction kinetics

Figure 3 compares the Eu^{3+} phase transfer kinetic trends observed for the liquid-liquid systems containing two aqueous holdback complexants considered in this study (HEDTTA and DTTA-BuA) with typical kinetic trends collected when either a hexadentate (EDTA) or octadentate (DTPA) reagent is utilized at p[H^+]. The forward extraction tests did not include buffer in aqueous mixtures to slow down the distribution equilibrium and magnify the time dependencies for various complexants. The distribution of Eu^{3+} for liquid-liquid system containing 20 mM HEDTTA at p[H^+] = 3.0 shows a rapid rate transfer enhancement, relative to

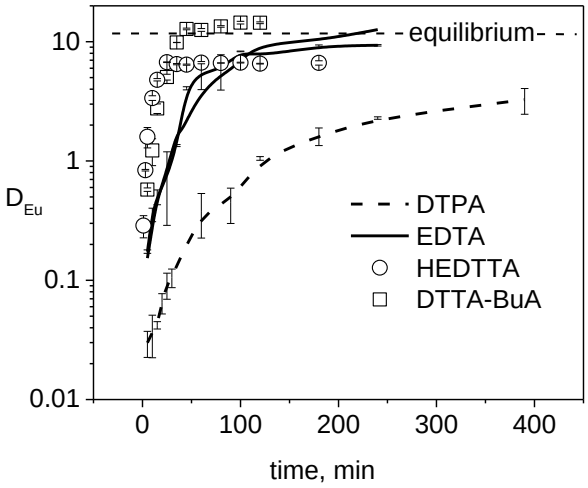

Figure 3. Time-dependent liquid-liquid distribution of ^{154}Eu between aqueous aminopolycarboxylate mixtures and organic solutions of HEH[EHP] in *n*-dodecane. Experimental: (○) 20 mM HEDTTA, p[H^+] 3.0 / 0.065 M HEH[EHP]. (□) 15 mM DTTA-BuA, p[H^+] 2.0 / 0.95 M HEH[EHP]. (--) 5 mM DTPA, p[H^+] 3.0 / 0.3 M HEH[EHP]. (—) 20 mM EDTA, p[H^+] 3.0 / 0.2 M HEH[EHP].

DTPA and EDTA-based chemistries. With a heptadentate coordination environment around the metal a trend intermediate to those observed for hexadentate (EDTA) and octadentate (DTPA) would be expected for mixtures of equivalent acidity. The faster kinetic trend may be attributed to lower concentration of phase transfer reagent required to yield a D_{Eu} ~ 10 at equilibrium. Launiere and Gelis showed that interfacial mass transfer rate for the back-extraction of americium from loaded organic phase containing HEH[EHP] nearly triples when the concentration of the strong cation exchanger is halved [8]. Accordingly, the weakening of the metal ion coordination offers one opportunity to elevate the mass transfer rates in such liquid-liquid distribution systems.

The distribution of Eu^{3+} for liquid-liquid system containing 15 mM DTTA-BuA was studied at p[H^+] of 2.0 to emphasize this reagent's ability to efficiently coordinate Eu^{3+} and delay the competition from the ligand protonation equilibria. From Figure 3, roughly a 10-fold enhancement in the rate of Eu^{3+} extraction observed for DTTA-BuA chemistry, relative to DTPA's trend at p[H^+] of 3.0, follows the expected linear relation between the rate of complex decomposition and concentration of hydrogen ions in solution. Thus, lowering the operational pH scale for complexing the trivalent *f*-elements by aminopolycarboxylate complexants incorporating strongly electron-withdrawing functionalities offers the second avenue for enhancing the phase transfer kinetics, capitalizing on proton-catalyzed mechanism of complex dissociation.

3.3 Am^{3+} back-extraction kinetics

Figure 4 compares the collected time dependent stripping trends for ^{241}Am, which distributes from the initially loaded and washed ALSEP solvent (0.05 M TEHDGA, 0.5 M HEH[EHP]) to aqueous mixtures of HEDTTA or DTTA-BuA or DTPA. This partitioning scenario proceeds much faster, relative to the forward extraction studies designed to slow the mass transfer rates, mainly due to the presence of citrate buffer in the aqueous environment. A weaker coordination of trivalent *f*-elements by HEDTTA explains the elevated distribution of americium ion. Using 0.125 M HEDTTA at pH 3.0 yielded a relatively inefficient stripping of americium (D_{Am} ~ 0.7). The liquid-liquid system containing HEDTTA also showed slowest liquid-liquid partitioning results. In the back-extraction experimental setting the mass transfer rate is not enhanced through modification of the non-aqueous environment.

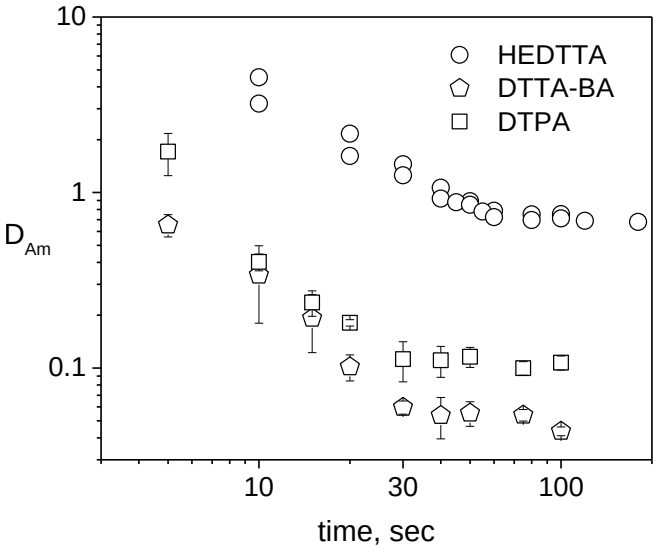

Figure 4. Time-dependent back-extraction of ^{241}Am from 0.05 M TEHDGA / 0.5 M HEH[EHP] in *n*-dodecane using (circle) 0.125 M HEDTTA, pH 3.0, (square) 15 mM DTTA-BuA, pH 2.0, (diamond) 15 mM DTPA, pH 2.0. Buffer: 0.2 M citrate.

The benefit of utilizing a stronger metal complexant, capable of efficient An^{3+}/Ln^{3+} separation in the

aqueous conditions of increased acidity, shows for the back-extraction time-dependent partitioning of Am^{3+} as facilitated by both DTTA-BuA and DTPA at pH of 2.0. Both stripping chemistries reach equilibrium within 30 seconds of phase contact. The partitioning equilibrium for americium is lower for DTTA-BuA (D_{Am} ~ 0.05) as compared to DTPA (D_{Am} ~ 0.11).

4. Conclusion

Potentiometric techniques were used to describe the thermodynamic features of trivalent *f*-element complexation by modified aminopolycarboxylate reagents. One modification replaced a single acetate pendant arm of DTPA reagent with *N*-hydroxyethane functionality, yielding *N*-hydroxyethyl-*N*,*N*′,*N*″,*N*‴-diethylenetriaminetetraacetic acid, HEDTTA. Another structural change substituted the acetate group with *N*-butylacetamide to afford *N*-butylamide-*N*,*N*′,*N*″,*N*‴-diethylenetriaminetetraacetic acid, DTTA-BuA. Time dependency trends for the forward extraction of europium by HEH[EHP] in *n*-dodecane from aqueous environments of HEDTTA or DTTA-BuA are compared with typical trends produced by hexadentate EDTA-type complexants and octadentate DTPA-type complexants. The kinetic studies for the partitioning of Am^{3+} between ALSEP solvent and aqueous mixtures containing HEDTTA and DTTA-BuA are compared with that yielded by DTPA. The Eu^{3+} distribution patterns show that significant enhancements to the rates of metal extraction may result either from reduction of reagent's polydenticity (HEDTTA) or manipulation of reagent's acid/base chemistry to capitalize on proton–catalyzed dissociation of *f*-element complexes (DTTA-BuA). The results of Am^{3+} back-extraction show that HEDTTA is too weak to efficiently balance the thermodynamics imposed by the ALSEP environment, but DTTA-BuA may be regarded as an attractive alternative to DTPA chemistry.

Acknowledgement

The experimental work conducted by TSG, CRH and PRZ at the Idaho National Laboratory was supported by the U.S. Department of Energy, Office of Nuclear Energy, DOE Idaho Operations Office, under contract DE-AC07-05ID14517. The synthetic work by SJ-P was supported by the Fuel Cycle Research and Development Program, Office of Nuclear Energy, U.S. Department of Energy.

References

1) A.V Gelis, G.J. Lumetta, *Ind. Eng. Chem. Res.*, **53**, 1624-1631 (2014).
2) M. Nilsson, K.L. Nash, *Solvent Extr. Ion Exch.*, **25**, 665-701 (2007).
3) B. Weaver, F.A. Kapplemann, *J. Inorg. Nucl. Chem.*, **30**, 263-278 (1968).
4) C.R. Heathman, T.S. Grimes, P.R. Zalupski, *Inorg. Chem.*, **55**, 2977-2985 (2016).
5) C.R. Heathman, T.S. Grimes, P.R. Zalupski, *Inorg. Chem.*, **55**, 11600-11611 (2016).
6) T.S. Grimes, C.R. Heathman, S. Jansone-Popova, V.S. Bryantsev, S. Goverapet Srinivasan, M. Nakase, P.R. Zalupski, *Inorg. Chem.*, **56**, 1722-1733 (2017).
7) P.R. Danesi, C. Cianetti, *Sep. Sci. Technol.*, **17**, 969-984 (1982).
8) C.A. Launiere, A.V. Gelis, *Ind. Eng. Chem. Res.*, **55**, 2272-2276 (2016).

Extraction Behavior of Sr(II) from Nitric Acid Solution using DtBuCH18C6 Containing Ionic Liquid Extraction System and its medical application

Seong-Yun KIM*, Tadayuki TAKAHASHI and Tatsuya ITO

Department of Quantum Science and Energy Engineering, Tohoku University, 6-6-01-2 Aza-Aoba-Aramaki, Aoba-ku, Sendai, Miyagi 980-8579, Japan

4',4'(5")-di-(*tert*-butyl cyclohexano)-18-crown-6 (DtBuCH18C6) as an extractant in combination with three types of ionic liquids, [C_4mim][X] (X = NfO, NTf_2, FAP) as solvents to separate Sr(II) effectively from HNO_3 solution. Under the experimental conditions, within the acidity range studied, the D_{Sr} follows the order of [C_4mim][NfO] > [C_4mim][NTf_2] > [C_4mim][FAP]. In their extraction systems, D_{Sr} decreases with increasing concentration of HNO_3 solution. Thermodynamic parameters for the extraction of Sr(II) tested elements were calculated using the Van't Hoff equation, showing that the reaction is spontaneous and exothermic. Existence of inorganic salts such as KNO_3 usually reduces E_{Sr} for all systems, and the decreasing degree is much larger than that of $NaNO_3$. The extraction systems exhibited high extraction efficiency and high selectivity for Sr(II) from simulated HLLW containing 20 typical elements and 2M HNO_3. From the results, the present system may provide an alternative for extraction of Sr(II) under HLLW conditions.

1. Introduction

In order to minimize the long-term radiological risk and reuse of valuable nuclides in the field of spent nuclear fuel reprocessing, the partitioning of ^{90}Sr and of some specific fission products (FPs) from high-level liquid waste (HLLW) is very desirable [1-3]. The heat-generated elements, ^{90}Sr, having a half-life of 28 years and contributes about 25% of heat generation in HLLW(~1.1 kg/1 tHU, 45 GWd/t) [4] with its daughter nuclide ^{90}Y. Furthermore, ^{90}Y is also expected for the utilization as radioactive material in the medicine field. Therefore the selective separation of ^{90}Sr from HLLW is necessary. A number of recovery methods have been reported in literature for the separation of Sr(II) from HLLW, such as ion exchange [5–9], solvent extraction [10–14] and extraction chromatography [15-16]. Over the last decade, in the ionic liquids extraction has selective extractability to Sr(II) that has been widely used for extraction process. Ionic liquids are composed of heterocyclic organic cations and inorganic anions and have even more advantageous properties, such as nonvolatility, nonflammability, thermal and electrochemical stabilities and conductivity instead of the traditional diluents, enhancement of extraction efficiency, possibly leading to cost-reduction in extraction processes. This evaluation study was carried out based on a novel extraction process for HLLW treatment which was proposed by our group [17]. In this extraction process, the FPs elements PGMs and Cs(I) have been separated from simulated HLLW firstly by [C_4min][NfO] and Calix[4]arene-R14 as an extractant and 1-alkyl-3-methylimdazolium bis(trifluoromethylsulfonyl)amide ([$C_n$mim][NTf_2]) as solvents

successfully.

In this work, the extraction of Sr(II) from HNO_3 solution has been investigated using DtBuCH18C6 as an extractant in combination with three kinds of ionic liquid [C_4mim][X] (X = NfO, NTf_2, FAP) as solvents, where DtBuCH18C6 is 4,4',(5')-di-(*tert*-butyl cyclohexano)-18-crown-6, $[C_4mim]^+$ is 1-butyl-3-methylimidazolium and $[NfO]^-$ is nonafluorobutane-sulfonate, $[NTf_2]^-$ is bis(trifluoro-methyl sulfonyl)amide, $[FAP]^-$ is tris(pentafluoroethyl)trifluorophosphate. The extraction system was studied in detail with regard to different extraction parameters such as the concentration of HNO_3, concentration of extractant, temperature, concentration of inorganic salts, and under coexistence of various metals, on the extraction of Sr(II).

2. Experimental

2.1 Materials

4',4'(5")-di(*tert*-butylcyclohexano)-18-crown-6 (DtBuCH18C6, 90 wt%) was purchased from Sigma-Aldrich Chemical Co. and used without purification. The ionic liquid of [C_4mim][NfO] was synthesized. Its synthesis method was reported in detail by Kozonoi [18]. [C_4mim][NTf_2], [C_4mim][FAP] ionic liquids were purchased from Sigma-Aldrich Chemical Co. The molecular structure of DtBuCH18C6 and [C_4mim][X] (X = NTf_2, NfO, FAP) are shown in Figure 1. Chemical reagents, $NaNO_3$, KNO_3, $AgNO_3$, $Sr(NO_3)_2$, $Ba(NO_3)_2$, $RE(NO_3)_3 \cdot 6H_2O$ (RE = Y, La, Ce, Pr, Nd, Sm, and Gd), $ZrO(NO_3)_2 \cdot 2H_2O$, $(NH_4)_6Mo_7O_{24} \cdot 4H_2O$, $Cr(NO_3)_3$, $Mn(NO_3)_2 \cdot 6H_2O$, $Fe(NO_3)_3 \cdot 9H_2O$, $Ni(NO_3)_2 \cdot 6H_2O$, and $Zn(NO_3)_2 \cdot 6H_2O$ were of analytical grade and supplied by Kanto Chemical Co.

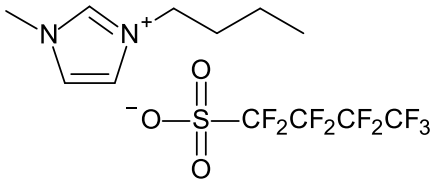

[C_4mim][NfO]

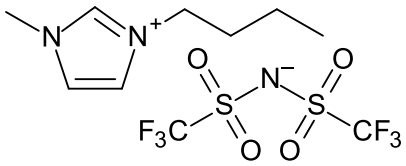

[C_4mim][NTf_2]

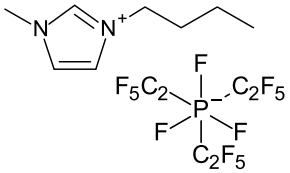

[C_4mim][FAP]

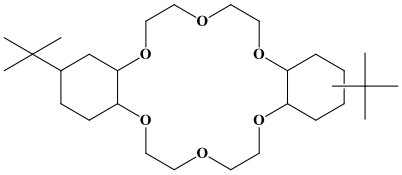

DtBuCH18C6

Figure 1. Chemical structure of the cations $[C_4min]^+$ and anions $[NfO]^-$, $[NTf_2]^-$, $[FAP]^-$ and extractant (DtBuCH18C6).

2.2 Batch extraction method

The extraction behaviors of metal ions for DtBuCH18C6 containing ionic liquid extraction system were estimated by batch methods. An aqueous solution (2 cm^3) containing 5 mM Sr(II) ion was contacted with 2 cm^3 of ionic liquid containing DtBuCH18C6 in a thermostatic bath up to 15 min, which was found to be sufficient for attaining equilibrium. The concentrations of metal ions were

measured using an atomic absorption spectrophotometer (AAS) and inductively coupled plasma atomic emission spectrometer (ICP-AES). The distribution ratios (D_{Sr}) and extraction efficiencies (E_{Sr}) were calculated as follows:

$$D_{Sr} \equiv \frac{C_{IL}}{C_{Aq}} = \frac{C_{0,Aq} \times \frac{V_{0,Aq}}{V_{IL}} - C_{Aq} \times \frac{V_{Aq}}{V_{IL}}}{C_{Aq}} \quad (1)$$

$$E_{Sr} = \frac{100 \times D_{Sr}}{D_{Sr} + \frac{V_{Aq}}{V_{IL}}} \quad (2)$$

where $C_{0,Aq}$ and C_{Aq} represent the initial and final concentrations of Sr(II) in an aqueous solution, $V_{0,Aq}$ and V_{Aq} (cm^3) indicate the volume of the aqueous phase before and after extraction, respectively, and V_{IL} (cm^3) is the volume of the ionic liquid phase after extraction.

3. Results and Discussion

3.1 Extraction kinetics in ILs

In order to evaluate the equilibrium time of Sr(II) for DtBuCH18C6 containing ILs extraction systems, the effect of mixing time on E_{Sr} was examined in the presence of 2 M HNO_3 by the batch method. The E_{Sr} increases with an increase in mixing time and reaches an equilibrium state within 10 min. Under the experimental conditions, the E_{Sr} shows an order of [C_4mim][NfO] > [C_4mim][NTf_2] > [C_4mim][FAP]. The data showed that the extraction capability of Sr(II) decreased with anions under same conditions. This result shows that the extraction capabilities for metal ions have a strong preference for the aqueous phase.

3.2 Effects of HNO_3 solution concentration

To understand the effect of HNO_3 concentration, the extraction behavior of 5 mM Sr(II) into DtBuCH18C6 (10 mM) containing ILs systems were examined at different concentrations of HNO_3 from 0.015 M to 4 M by batch method (Figure 2). As for Sr(II)), a decrease in the D_{Sr} for the [C_4mim][NfO], [C_4mim][NTf_2] systems with increasing concentrations of HNO_3 is observed. In contrast, [C_4mim][FAP] was considerably low in the all range of HNO_3 concentration. Within the acidity range studied, the D_{Sr} values for Sr(II) maintain the order of [C_4mim][NfO] > [C_4mim][NTf_2] > [C_4mim][FAP].

The extraction mechanism with participation of hydrophobic ILs has been continuously studied. Similar results were observed in a study conducted by Luo et al. [19]. Luo has reported that the hydrophobicity of the IL anion has controlling extraction strength. Moreover, several studies have reported that the extraction ratio decreases with an increase in the HNO_3 concentration. Xu et al. has shown that the competition of H^+ might be a leading factor that

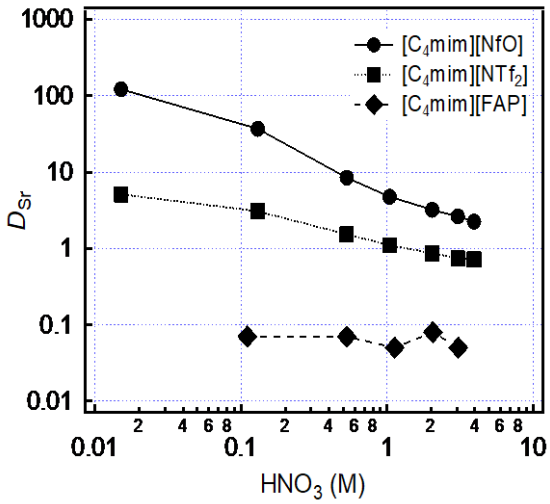

Figure 2. Dependence of D_{Sr} on HNO_3 concentration.

causes an overall decrease in the extraction efficiency [20]. In the same manner, it is possible that competition of H^+ accounts for the decrease in D_{Sr} with an increase in the HNO_3 concentration. These observations suggest that one of the mechanisms for extraction is cation exchange.

3.3 Influence of the DtBuCH18C6 concentration

To understand the extractant effect, the extraction behavior of Sr(II) into DtBuCH18C6 containing ILs systems in a 2 M HNO_3 solution was investigated at different concentrations. Figure 3 shows the relation between E_{Sr} and DtBuCH18C6 concentration in combination with [C_4mim][X]. As shown in Figure 3, E_{Sr} increases with increasing DtBuCH18C6 concentration. The [C_4mim][NTf_2] and [C_4mim][FAP] showed no extraction of Sr(II) in the absence of DtBuCH18C6, *i.e.*, ILs themselves cannot extract Sr(II) in the absence of proper extractants. On the other hand, [C_4mim][NfO] has extraction ability for Sr(II). Kozonoi et al. has shown that [C_4mim][NfO] extract various metal ionic species from the aqueous solution. This observation suggests that [NfO] anion is extractant for Sr(II) in [C_4mim][NfO]. The results in Figure 3 also indicate that the extraction capability of the three selected [C_4mim][X] systems follows the general order of [C_4mim][NfO] > [C_4mim][NTf_2] > [C_4mim][FAP] under given conditions. The [C_4mim][NfO] matches best with DtBuCH18C6 to extract Sr(II).

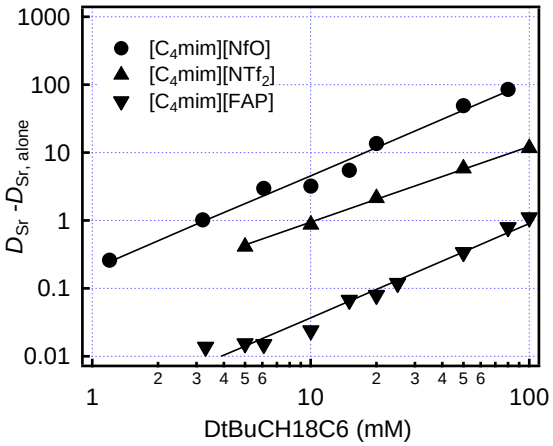

Figure 3. Dependence of D_{Sr} on DtBuCH18C6 concentration.

A linear regression analysis of the D_{Sr} resulted in a straight line with a slope of 1.1, suggesting the involvement of 1 molecule of DtBuCH18C6 during the extraction processes as shown in Eq(3) and (4).

Such a phenomenon has been observed by Dietz and Stepinski while studying the extraction of sodium by crown ether (dicyclohexano-18-crown-6) under low acid conditions [21].

$$Sr^{2+} + DtBuCH18C6 + \overline{2C_4mim^+} \Leftrightarrow \overline{[(Sr \cdot DtBuCH18C6]^{2+}} + 2C_4mim^+ \quad (3)$$

$$Sr^{2+} + 2NO_3^- + \overline{DtBuCH18C6} \Leftrightarrow \overline{[(Sr(NO_3) \cdot DtBuCH18C6]} \quad (4)$$

3.4 Extraction thermodynamics

To understand the temperature effect, the extraction behavior of Sr(II) onto DtBuCH18C6 containing ILs systems in 2 M HNO_3 solution was investigated at different temperatures. In order to gain insight into the thermodynamic nature of the extraction process, several thermodynamic parameters for the present system were calculated. The Gibbs free energy, $\Delta G°$, is the fundamental

criterion of spontaneity. Reactions occur spontaneously at a given temperature if $\Delta G°$ is a negative quantity. The Gibbs free energy of the extraction process is given by the equation as follows

$$\Delta G° = -RT \times \ln D \quad (5)$$

Otherwise, the values of enthalpy change($\Delta H°$) and entropy change ($\Delta S°$) for Sr(II) in the extraction processes can be calculated from the slope and intercept of the plots of ln$D$ *vs.* 1/T by the van't Hoff equation as follows

$$\ln D = \frac{-\Delta H°}{R \cdot T} + \frac{\Delta S°}{R} \quad (6)$$

where R is the gas constant (8.314 J mol^{-1} K^{-1}), T is the absolute temperature in Kelvin, is the distribution ratios (D_{Sr}) on equilibrium state defined as Eq. (1).

The experimental temperature was controlled in the range of 288 to 323 K and the corresponding plots of ln$D$ *vs.* 1/T are depicted in Figure 4. From the plots in Figure 4, all the calculated parameters of the extraction reactions for DtBuCH18C6 containing ILs systems, $\Delta G°$, $\Delta H°$, and $\Delta S°$ are summarized in Table 1. The negative value of $\Delta G°$ means the extraction processes occur spontaneously at a given temperature. The change in $\Delta H°$ for Sr(II) is observed to be negative, confirming the exothermic nature of the extraction processes.

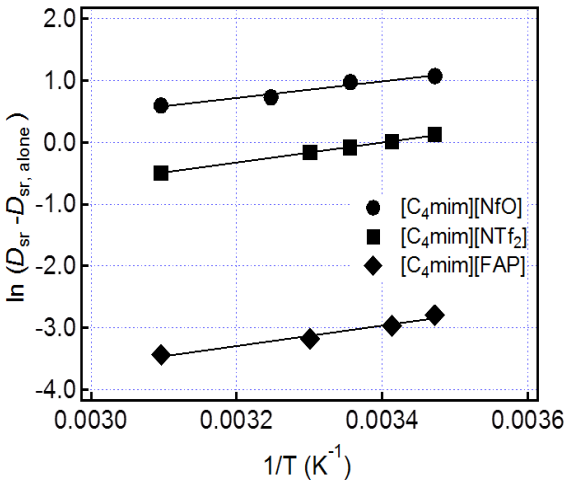

Figure 4. Van't Hoff plots for the extraction of Sr(II) on DtBuCH18C6/ ILs. [HNO_3] = 2.0 M, [DtBuCH18C6] = 10 mM, [Sr] = 5 mM

Table 1. Values of the thermodynamic parameters for extraction of Sr(II) on DtBuCH18C6/ILs

Tem	$\Delta G°$ (kJ mol^{-1})			$\Delta H°$ (kJ mol^{-1})			$\Delta S°$ (kJ mol^{-1} K^{-1})		
(K)	[NfO]	[NTf$_2$]	[FAP]	[NfO]	[NTf$_2$]	[FAP]	[NfO]	[NTf$_2$]	[FAP]
288	-2.59	-0.27	6.81						
293	-	-0.04	7.17						
298	-2.30	0.19	-	-11.15	-13.46	-13.77	-0.030	-0.046	-0.071
303	-	0.42	7.89						
308	-2.00	-	-						
323	-1.55	1.33	9.32						

3.5 Effect of inorganic salts

HLLW containing a large quantity of inorganic salts derived from alkaline liquid waste has an especially large amount of Na(I). To examine the applicability of separation process for HLLW, it is necessary to study the effects of $NaNO_3$ and KNO_3 on the extraction of Sr(II) using DtBuCH18C6 containing ILs systems.

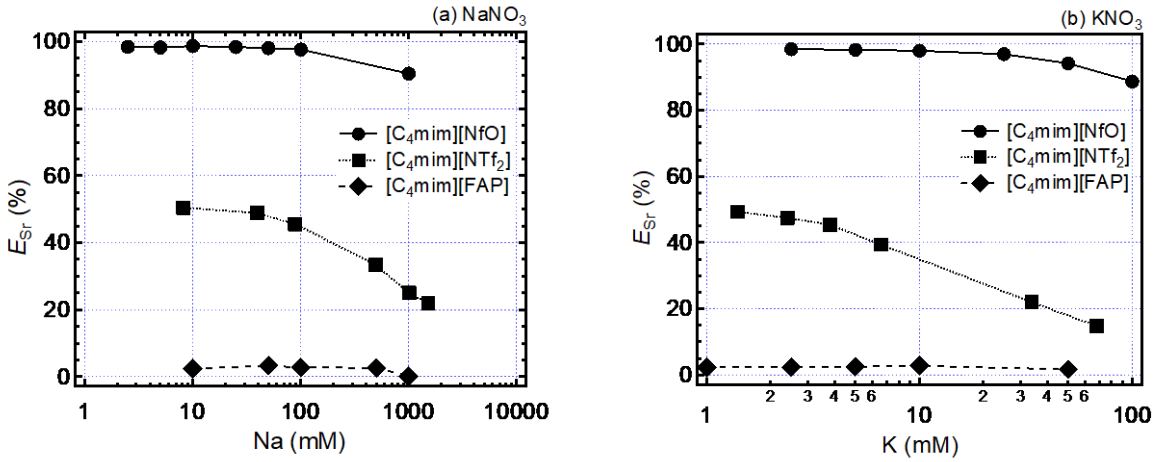

Figure 5. Dependence of the extraction efficiency of Sr(II) in DtBuCH18C6/ILs on the concentration of inorganic salts. ([HNO_3] = 2.0 M, [DtBuCH18C6] = 10 mM, [Sr] = 5 mM, T=295K)

As shown in Figure 5, the addition of the two salts will generally reduce the extraction efficiency of Sr(II); however, the E_{Sr} of solutions containing Na(I) was much larger than that of K(I). This can be explained by the similar ionic radius between K(I) and Sr(II), which causes much more competition with the crown ether complex.

3.6 Separation of Sr(II) for simulated HLLW

The components in HLLW after removing actinides are very complicated. Apart from the ^{90}Sr radioactive nuclide, there are many other coexisting elements such as Cs, Ba, PGMs, rare earths and minor actinide. To understand the separation behavior of Sr(II) as well as other fission products, a group partitioning experiment for a simulated HLLW containing 20 elements and 2 M HNO_3 was performed using the DtBuCH18C6 containing ILs systems at 298 K. The relevant extraction of Sr(II) is illustrated in Figure 6. All extraction systems exhibited a high distribution ratio and high selectivity for separation of Sr(II) and Ba(II) from sHLLW. The separation factor (SF) of Sr from most other elements such as Cs and PGMs is much higher. In addition, the SF of Y(III) is more than 10^3. The results indicate that DtBuCH18C6 containing ILs systems show stronger extraction ability and selectivity for Sr(II) in the HLLW medium.

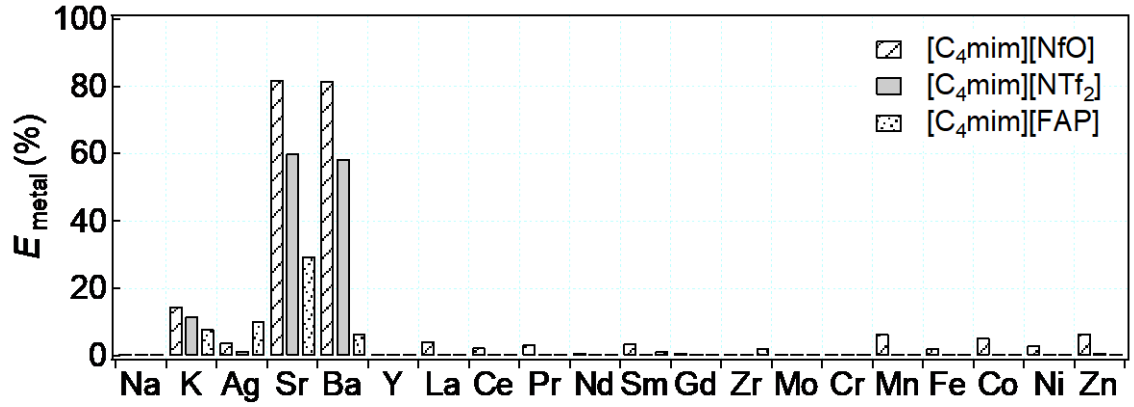

Figure 6. Extraction of Sr(II), Ba(II) from a sHLLW using DtBuCH18C6/ ILs. ([H^+] = 2.0 M, [DtBuCH18C6] = 100 mM, T=298 K)

4. Conclusion

Extraction of Sr(II) ions using DtBuCH18C6 and three ILs as solvents has been investigated. All extraction systems are rapid reactions that reach extraction equilibrium in approximately 10 min. The extractions exhibit a decrease in D_{Sr} with increasing concentration of HNO_3. Within the HNO_3 concentration range studied, the D_{Sr} maintains the order of $[C_4mim][NfO] > [C_4mim][NTf_2] > [C_4mim][FAP]$. The calculated thermodynamic parameters of the extraction of Sr(II) based on Van't Hoff equation indicate that the reaction is spontaneous and exothermic. The existence of inorganic salts such as KNO_3 reduces the E_{Sr} for the three systems, and the degree of decrease is much larger than that of $NaNO_3$; however, the E_{Sr} of solution containing Na(I) was much larger than that of K(I). In the present system, a medium acidity extraction behavior has been revealed, which may provide an alternative method for extraction of Sr(II). This method was observed to effectively separate Sr(II) from the simulated HLLW, avoiding the use of high concentration of HNO_3 when using conventional solvents.

Acknowledgement

This work was supported by JSPS KAKENHI Grant Number 16H02444.

References

1) M. Kubota, K. Okata, I. Yamaguchi, Y. Morita, *Radioact. Waste Manag. Nucl. Fuel Cycle*, **7**, 303–316 (1986).
2) IAEA, *IAEA Technical Report Series*, No. 356, (1993).
3) Atomic Energy Society of Japan (AESJ), *J. At. Energy Soc. Jpn.*, **48**, 327–332 (2006). [in Japanese].
4) Y. Ando, H. Takano, *JAERI-Research 99-004*, (1999). [in Japanese].
5) H. Mimura, T. Kanno, *J. Nucl. Sci. Technol.*, **22**, 284–291 (1985).
6) R. Mori, I. Yamagishi, M. Kubota, *JAERI-M 86-013*, (1986) [in Japanese].
7) H. Mimura, M. Shibata, K. Akiba, *J. Nucl. Sci. Technol.*, **27**, 835–843 (1990).
8) Y. Morita, I. Yamaguchi, T. Fujiwara, H. Koizumi, M. Kubota, *JAERI-Conf 99-004*, 491–497 (1999) [in Japanese].
9) T.M. Nenoff, S.G. Thoma, J.E. Miller, D.E. Trudell, *MRS Proc.*, **412**, 659 (1995).
10) E.P. Horwitz, M.L. Dietz, D.E. Fisher, *Solv. Extr. Ion Exch.*, **8**, 557–572 (1990).
11) J. Chuang, J. Lo, *J. Radioanal. Nucl. Chem.*, 189, **2**, 307-317 (1995).
12) M.L. Dietz, A.H. Bond, M. Clapper, J.W. Finch, *Radiochim. Acta*, **85**, 119–129 (1999).
13) N. Takagi, Y. Izumi, K. Ema, T. Yamamoto, K. Nishizawa, *Solv. Extr. Ion Exch.*, **17**, 1461–1471 (1999).
14) D.R. Raut, P.K. Mohapatra, V.K. Manchanda, *Radiochim. Acta*, **97**, 565–570 (2009).
15) Y. Wu, S.-Y. Kim, D. Tozawa, T. Ito, T. Tada, K. Hitomi, E. Kuraoka, H. Yamazaki and K. Ishii, *J. Nucl. Sci. Technol.*, **49**, 320-327 (2012).
16) S.-Y. Kim, Y. Xu, T. Ito, Y. Wu, T. Tada, K. Hitomi, H. Yamazaki and K. Ishii, *J. Radioanal. Nucl. Chem.*, **295**, 1043-1050 (2013).

17) T. Takahashi, T. Ito, S.-Y. Kim, Asian Nuclear Prospects 2016, Nuclear Fuel Cycle for Sustainable Energy Supply and Human Prosperity, P-21, 1-2 (2016).
18) N.Kozonoi, Y. Ikeda, *Monatshefte fu¨ r Chemie*, **138**, 1145–1151 (2007).
19) H. Luo, S. Dai, P. V. Bonnesen, T. J. Haverlock, B. A. Moyer, A. C. Buchanan III, *Solv. Extr. Ion Exch.*, **24**, 19–31 (2006).
20) C. Xu, X. Shen, Q.D. Chen, H.C. Gao, *Sci. China Ser B-Chem.*, **52**, 1858-1864 (2009).
21) M.L. Dietz, D.C. Stepinski, *Green Chem.*, **7**, 747-750 (2005).
22) L.H. Baetsle, D. Huys, *J. Inorg. Nucl. Chem.*, **30**, 639–649 (1965).

Effect of O/A Ratio on Extraction Performance of Centrifugal Contactor

Atsushi SAKAMOTO[1,2,*], Yuichi SANO[1,2], Masayuki TAKEUCHI[2]
Masayuki WATANABE[1] and Kenji KOIZUMI[1]

[1]*Department of Fukushima Technology Development, Japan Atomic Energy Agency, 4-33 Muramatsu, Tokai-mura, Naka-gun, Ibaraki pref. 319-1194, Japan;* [2] *Fast Reactor Fuel Cycle Technology Development Department, Japan Atomic Energy Agency, 4-33 Muramatsu, Tokai-mura, Naka-gun, Ibaraki pref. 319-1194, Japan*

The PUREX process is widely used in reprocessing plants for spent nuclear fuel. In the process, uranium and plutonium are completely separated in the partitioning stage, and this increases the risk of nuclear proliferation. Japan Atomic Energy Agency (JAEA) has constructed a co-processing process that recovers plutonium with a part of uranium in the partitioning stage. The process requires a higher O/A ratio, which indicates the flow ratio of the organic phase and the aqueous phase, as opposed to a conventional PUREX process. Additionally, JAEA discusses the application of a centrifugal contactor that separates the aqueous and organic phases from a mixed phase by using a strong centrifugal force due to the rapid rotation of the rotor for an advanced solvent extraction process. This study investigates the effects of the O/A ratio on the extraction and back extraction performances of uranium in a centrifugal contactor.

1. Introduction

The PUREX process is a widely used process in present fuel reprocessing plants; the process separates plutonium and uranium in the partitioning stage. However, plutonium isolation increases the risk of nuclear proliferation, and thus, a co-processing process modified PUREX process was developed with the co-recovery of Pu and U [1-3]. The co-processing process reprocesses fuels at a higher O/A ratio, which denotes the flow ratio of the organic phase and the aqueous phase, than the PUREX process.

JAEA has developed an annular type centrifugal contactor for solvent extraction in spent fuel reprocessing, which allows the mixing of the aqueous and organic phases in the annular area and their separation inside the rotor [4-5]. Given these characteristics, a centrifugal contactor offers attractive advantages such as a more compact design and a shorter liquid residence time, when compared to conventional contactors such as a mixer settler or a pulsed column [6-8].

In this study, the effects of O/A ratio on extraction and back extraction performances of a centrifugal contactor were investigated to appropriate the centrifugal contactor for the co-processing process.

2. Experimental

2.1 Equipment

The basic structure of the centrifugal contactor is shown in Figure 1. It comprises a motor, a driving unit, a rotor, and housing. In the study, the centrifugal contactors with a rotor 25 mm in diameter were used. The extraction and back extraction performances were studied by using single stage and four stage centrifugal contactors (Figure 2), respectively. The rotor speed was controlled at 3,500 min^{-1} across all the experiments.

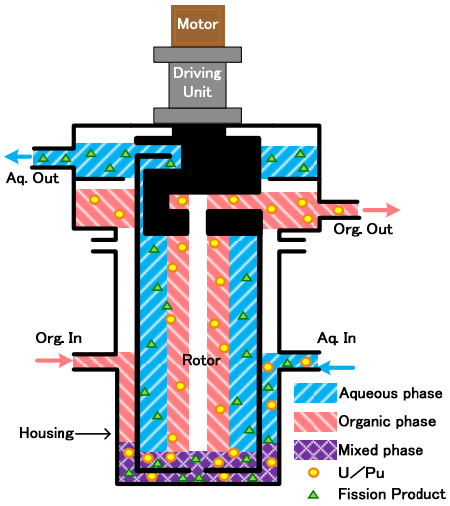

Figure 1. A schematic of the extraction process of a centrifugal contactor

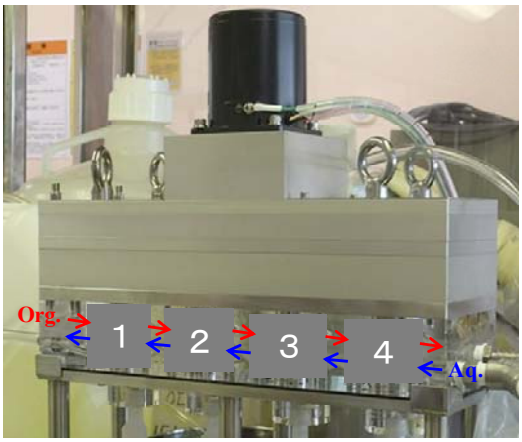

Figure 2. A four-stage centrifugal contactor

2.2 Extraction and back extraction conditions

In the extraction test, 23 g/L uranium nitrate / 3 mol/L HNO_3 solution was prepared as the aqueous phase, and 30 vol%TBP-n dodecane was prepared as the organic phase. Prior to the extraction test, the organic phase was contacted with 3 mol/L HNO_3 solution by using an O/A ratio of 1 for the HNO_3 equilibrium. In the back extraction test, a 0.02 mol/L nitric acid solution was prepared as the aqueous phase, and 30 vol% TBP-n dodecane (including 11 g/L uranium) was prepared as the organic phase. The operational conditions are shown in Table 1. The O/A ratio in the extraction test changed from 0.2 to 30, and then total flow rates were controlled at 2 L/h, 6 L/h, and 12 L/h, respectively. The O/A ratio in the back extraction test changed from 0.03 to 30 at a total flow rate corresponding to 6 L/h. The samples were regularly collected from the contactors during the extraction and back extraction tests. Uranium concentrations of the supplied and discharged solutions were measured by performing a spectroscopic analysis of V-660 (JASCO). In the back extraction test, uranium concentrations were measured at each stage to evaluate the changes in the uranium concentration profile.

Table 1. Operational conditions

Test	O/A ratio	Total Flow rates (L/h)
Extraction	0.2, 0.5, 1, 2, 5, 10, 30	2, 6, 12
Back extraction	0.03, 0.1, 0.2, 0.5, 1, 2, 5, 10, 30	6

2.3 Procedures

Prior to the extraction of uranium, 3 mol/L HNO_3 was supplied to the centrifugal contactor as

the aqueous phase. Subsequently, 30 vol % TBP-n dodecane was supplied as the organic phase. After the stable operation of the centrifugal contactor, the feed of 3 mol/L HNO_3 was replaced by 23 g/L uranium nitrate solution / 3 mol/L HNO_3. The O/A ratio was changed every 10–30 min in the test. The effects of the O/A ratio in the extraction tests were evaluated by stage efficiency determined by the following equation (Murphree efficiency):

$$E = \frac{U_{Aq.feed} - U_{Aq.product}}{U_{Aq.feed} - U_{Aq.product\text{-}in\text{-}equilibrium\text{-}exp.}} \times 100 \quad (1)$$

where E denotes the stage efficiency, $U_{Aq.feed}$ denotes uranium concentration [g/L] in the aqueous feed solution, $U_{Aq.product}$ denotes uranium concentration [g/L] in the discharged aqueous solution, and $U_{Aq.product\ in\ equilibrium\ exp.}$ [g/L] denotes uranium concentration in the discharged aqueous solution after estimating the equilibrium by using batch-wise tests.

In the back extraction test, 30 vol% TBP-n dodecane (including 11 g/L uranium) was supplied (Figure 3 depicts the flowsheet of the back extraction test) after supplying a 0.02 mol/L nitric acid solution to the centrifugal contactor and discharging it from the centrifugal contactor through four stages. The O/A ratio was also changed every 10–30 min. The effects of the O/A ratio on the back extraction tests were evaluated by comparing it with the uranium concentration profiles calculated using MIXSET-X [9].

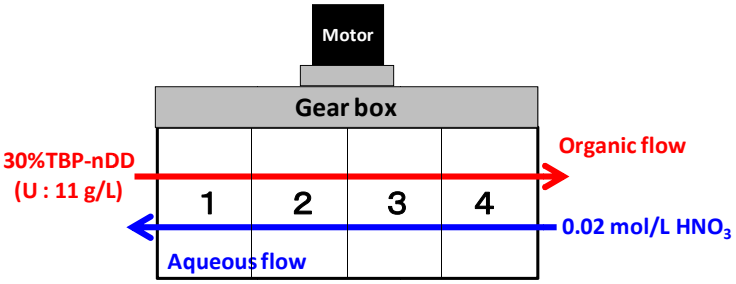

Figure 3. A flowsheet of the back extraction test

3. Results and Discussion

3.1 Extraction performance

Figure 4 depicts the changes in the flow rates and O/A ratios in the extraction test at a total flow rate of 2 L/h. During the operation, the flow rates and the O/A ratios were correctly changed as planned. Additionally, neither overflow nor entrainment was observed, and this implies that the organic and aqueous phases were separated. These results were confirmed across all the extraction tests.

Figures 5, 6, and 7 show the effects of the O/A ratio on stage efficiencies at total flow rates corresponding to 2 L/h, 6 L/h, and 12 L/h, respectively. The stage efficiencies corresponded to approximately 100 % in any condition with the exception of the condition with low flow rate and O/A ratio. The tendencies could be caused by insufficient mixing, which was formed by less liquid volume in the mixing zone, and a few differences in the O/A ratio between the batch-wise tests and the experimental study. Therefore, a total flow rate of 12 L/h (Figure 7) with a sufficient volume for the

organic phase exhibited 100% stage efficiencies in all O/A ratio conditions.

The results indicate that the centrifugal contactor exhibits sufficient extraction performance under a wide range of O/A ratios.

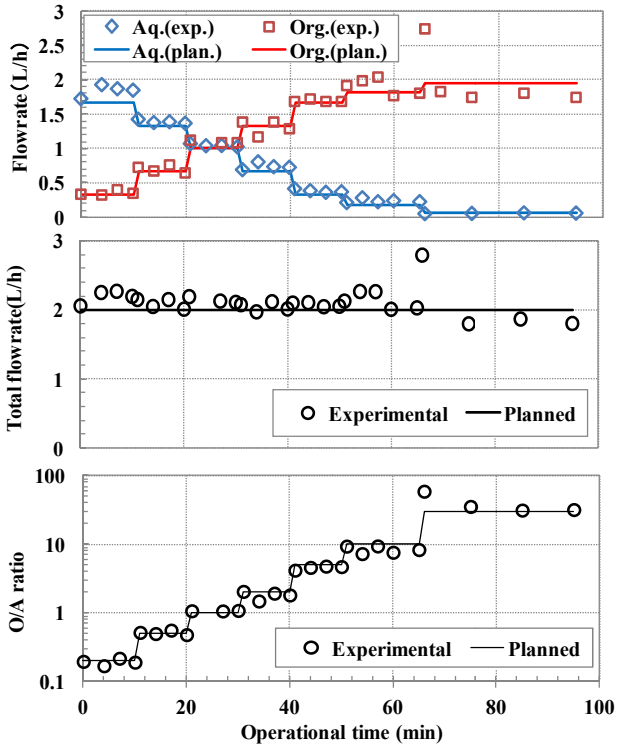

Figure 4. Changes in the flow rates and O/A ratios at a total flow rate of 2 L/h (Extraction tests)

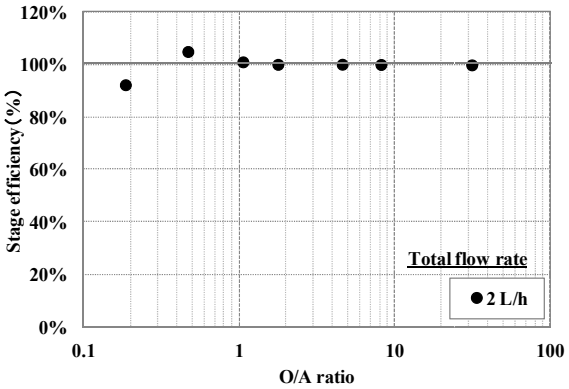

Figure 5. Effect of the O/A ratio on stage efficiency at a total flow rate of 2 L/h (Extraction tests)

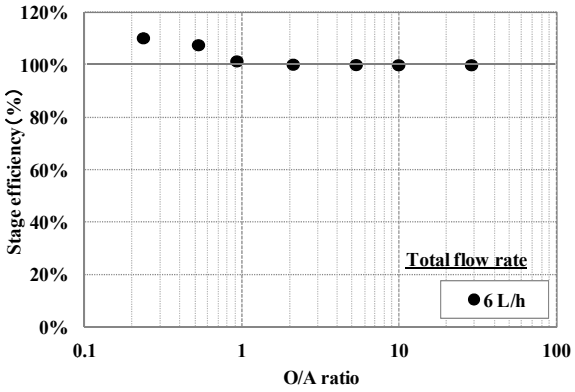

Figure 6. Effect of O/A ratio on the stage efficiency at a total flow rate of 6 L/h (Extraction tests)

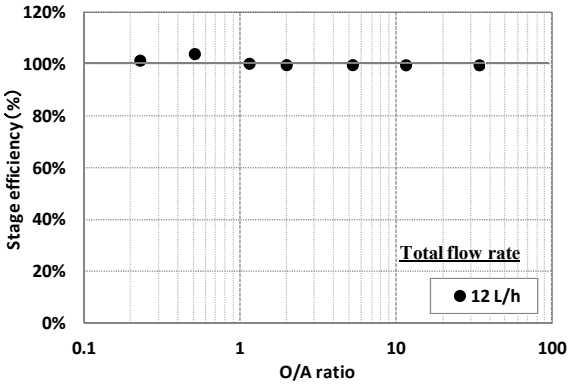

Figure 7. Effect of O/A ratio on the stage efficiency at a total flow rate of 12 L/h (Extraction tests)

3.2 Back extraction performance

Figure 8 depicts the changes in flow rates and O/A ratios in the back extraction test in which the total flow rate corresponded to 6 L/h. The flow rates and the O/A ratios were correctly changed during the operation. However, entrainment was observed at an O/A ratio of 30. It was affected by a lower difference in density between the aqueous phase and organic phase (0.17 g/cm^3) when compared with that of the extraction test (0.30 g/cm^3).

Figure 9 depicts the uranium concentration profile at an O/A ratio of 0.1. The uranium concentration in the organic phase constantly decreased from stage No.1 to stage No. 4. Additionally, uranium concentrations in stage No.3 and stage No.4 were lower than the detection limit of the spectroscopic analysis. This tendency was also confirmed in the conditions with an O/A ratio of less than 0.2.

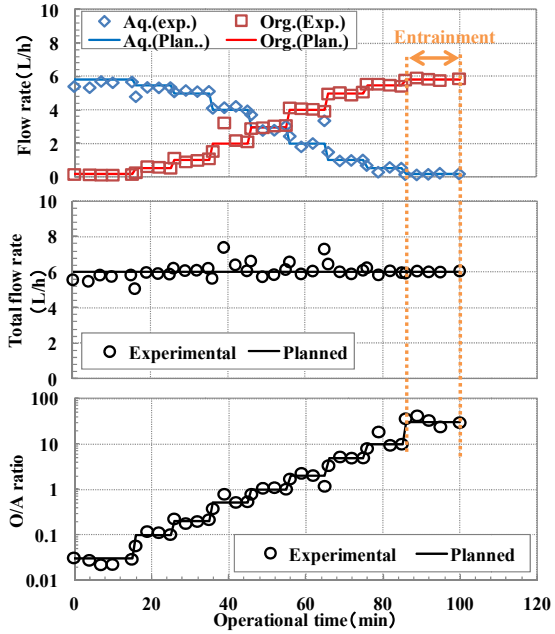

Figure 8. Changes in the flow rates and O/A ratios at a total flow rate of 6 L/h (Back extraction tests)

The O/A ratios of 0.5, 1, and 2 decreased the uranium concentration in the organic phase through the four stage centrifugal contactors (Figure 10 depicts the result at the O/A ratio of 1). With respect to an O/A ratio exceeding 5, the uranium concentration of the organic phase barely decreased through the four stage centrifugal contactors (Figure 11 shows the results for an O/A ratio of 10).

The tendencies are attributed to the transfer of NO_3^- required by the uranium transfer between the organic and aqueous phases as follows:

$$H^+(Aq.) + NO_3^-(Aq.) + 2TBP_{(Org.)} \Leftrightarrow HNO_3 \cdot TBP_{(Org.)} \quad (2)$$

$$UO_2^{2+}(Aq.) + 2NO_3^-(Aq.) + 2TBP_{(Org.)} \Leftrightarrow UO_2(NO_3)_2 \cdot 2TBP_{(Org.)} \quad (3)$$

The reaction from the left side to the right side shows the extraction process, and the reaction from the right side to the left side shows the back extraction process. As shown in the equations, HNO_3 and UO_2 were extracted by forming HNO_3-TBP and UO_2^{2+}-NO_3^--TBP complexes, respectively, in the organic phase. In the back extraction, transfer of NO_3^- from the organic phase to the aqueous phase preceded that of UO_2^{2+} due to a larger mass transfer coefficient of NO_3^- [10]. The phenomenon increased the HNO_3 concentration in the aqueous phase. The influence of the increase in HNO_3 concentration increased at a higher O/A ratio, and thus the back extraction of UO_2 was prevented.

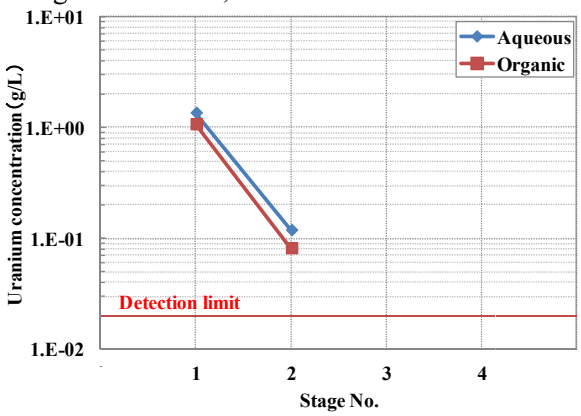

Figure 9. Profile of uranium concentration at a O/A ratio of 0.1
(Back extraction tests)

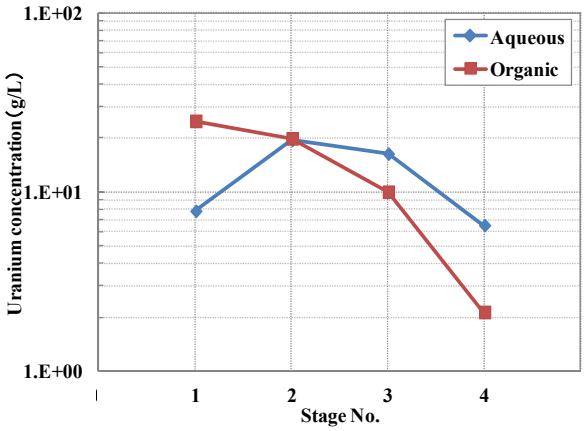

Figure 10. Profile of uranium concentration at a O/A ratio of 1
(Back extraction tests)

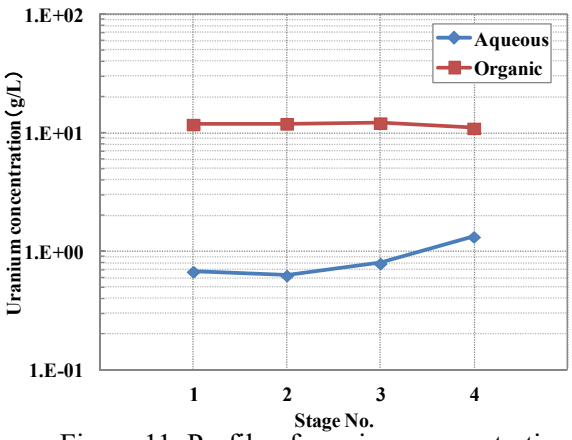

Figure 11. Profile of uranium concentration at a O/A ratio of 10
(Back extraction tests)

The experimental results of uranium profiles were also compared with the MIXSET-X calculation results. It was confirmed that the uranium concentration profiles in the tests at an O/A ratio of less than 2 were in agreement with those calculated by MIXSET-X with 90%–100% stage efficiency (Figure 12 depicts the result at an O/A ratio of 0.1). The tendency was also observed in experiments involving a higher size of the centrifugal contactor such as an 80 mm rotor [5]. In contrast, at an O/A ratio exceeding 5, stage efficiencies were indicated over 100% (Figure 13 shows the result for the O/A ratio of 10). The concentration profiles of HNO_3 at O/A ratios of 0.1 and 10 are shown in the Figures 14 and 15, respectively. The concentration profile of HNO_3 at the O/A ratio of 0.1 was in agreement with that calculated by MIXSET-X with a stage efficiency of 100% (Figure 14). However, at the O/A ratio of 10, the concentration profile of HNO_3 was in agreement with the calculation result with a stage efficiency of approximately 60% (Figure 15). This implies that the transfer of HNO_3 from the organic phase to the aqueous phase was insufficient. This tendency was influenced by a shorter residence time of the centrifugal contactor when compared with the MIXSET-X calculation results.

The results indicate that the centrifugal contactor normally performs the back extraction of uranium with an O/A ratio of less than 2. In this condition, the behavior of uranium is evaluated by MIXSET-X with 90%–100% stage efficiency.

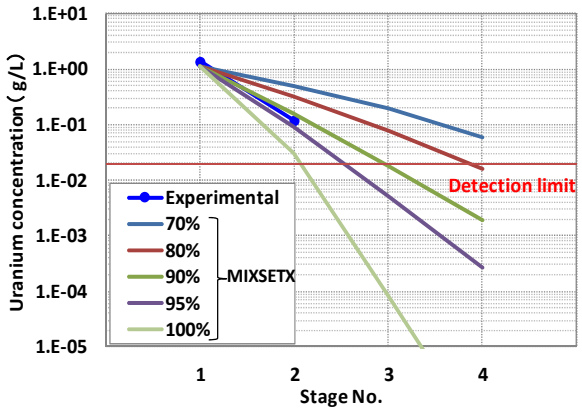

Figure 12. A comparison of uranium concentration in the aqueous phase at a O/A ratio of 0.1 (Back extraction tests)

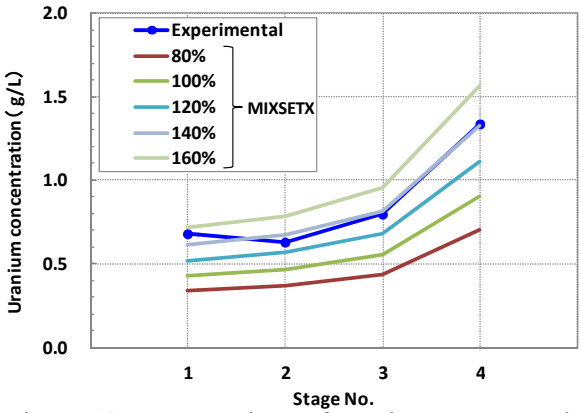

Figure 13. A comparison of uranium concentration in the aqueous phase at a O/A ratio of 10 (Back extraction tests)

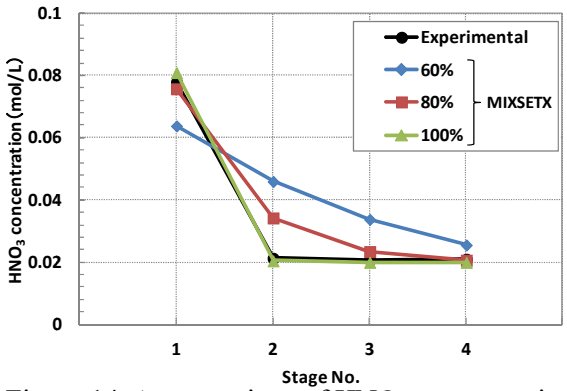

Figure 14. A comparison of HNO_3 concentration in the aqueous phase at a O/A ratio of 0.1 (Back extraction tests)

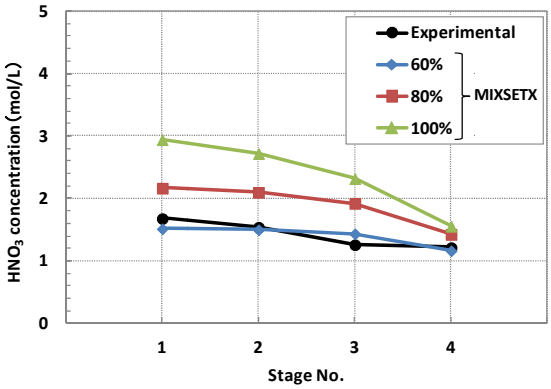

Figure 15. A comparison of HNO_3 concentration in the aqueous phase at a O/A ratio of 10 (Back extraction tests)

4. Conclusion

In this study, the effects of O/A ratio on extraction and back extraction performances of uranium in the centrifugal contactor were investigated to apply the same to the co-processing process. The centrifugal contactor was applied to the uranium extraction process with a high stage efficiency in conditions with a wide range of O/A ratios. The back extraction of uranium was achieved at an O/A ratio of less than 2 by the centrifugal contactor. In this condition, the behavior of uranium was evaluated by MIXSET-X with 90%–100% stage efficiency.

Acknowledgement

This study is the result of "Technology development program of fast breeder reactor international cooperation, etc." entrusted to Japan Atomic Energy Agency (JAEA) by the Ministry of Economy, Trade and Industry (METI).

References

1) M. Nakahara, Y. Koma, Y. Nakajima, *Proc. of GLOBAL2013* (2013).
2) K. Yamamoto, F. Yanagibashi, I. Fujimoto, T. Sato, T. Ohbu, K. Taki, S. Hayashi, *Proc. of GLOBAL2013* (2013).
3) A. Kudo, K. Kurabayashi, F. Yanagibashi, S. Sasaki, T. Sato, I. Fujimoto, T. Ohbu, *Proc. of ICAPP2017* (2017).
4) R. A. Leonard, G. J. Bernstein, A. A. Ziegler, R. H. Pelto, *Sep. Sci. Technol.*, **15**, 925-943 (1980).
5) T. Washiya, M. Takeuchi, H. Ogino, A. Aose, *Proc. of GLOBAL 2005*, 305 (2005).
6) E. R. Irishi, W. H. Reas, *Ind. Eng. AEC Res. Develop. Rep.*, HW-49483A (1957).
7) F. Drain, R. Vinoche, J. Duhamet, *Proc. of WM 03* (2003).
8) J. D. Law, T. A. Todd, *INL/CON-08-15151* (2008).
9) M. Ishida, M. Naito, T. Suto, E. Omori, I. Nojiri, *Proc. of GLOBAL2001* (2001).
10) K. Gonda, T. Matsuda, *PNCT841-82-19* (1982). in Japanese

Solvent Extraction Design for Highly Viscous Systems

Maria Chiara QUARESIMA[1,*], Markus SCHMIDT[2], Andreas PFENNIG[1]
[1]*University of Liège, Department of Chemical Engineering - Product, Environment, and Processes (PEPs), Quartier Agora, Allée du Six Août, 11, 4000 Liège – Sart-Tilman, Belgium*
[2]*RWTH Aachen University, Chair of Fluid Process Engineering, Aachen, Germany*

The change from fossil-based feedstock to bio-based raw materials will lead to changes in the molecular structure of reagents used in the chemical industry. Bio-based raw materials are richer in oxygen, leading to intermediates and products rich in oxygen as well. This will lead to lower vapor pressure and higher viscosity of the systems. Thus liquid-based separations like solvent extraction will increase in importance. Also separation-process design needs to be adapted to properly account for higher viscosities. With drop-based simulation, extraction-column performance can be predicted to better than 10% accuracy, being time and resources saving compared to pilot-plant experiments. In previous work, appropriate models describing all drop phenomena like sedimentation and mass transfer were combined in a simulation tool, called ReDrop (REpresentative DROPs). The models implemented in ReDrop have been largely validated for low-viscous systems. In order to extend the capabilities of ReDrop and describe the entire viscosity range, models have to be tested for a variety of different material system with single-drop lab-scale experiments. In this work mass transfer has been evaluated with single-drop experiments for two systems with different viscosity. The first one is the standard EFCE system composed by water + acetone + butyl acetate. Results were compared with the mass-transfer evaluation for the aqueous two-phase system with higher viscosity composed by water and PEG + albumine + water and phosphate. The results show that the transport of a component between two immiscible phases is strongly influenced by the viscosity of both phases as well as the molecular size of the transferred component. The single-drop results are the basis for validation and extending the applicability of existing models to higher viscosity, which are then introduced into ReDrop.

1. Introduction

The oxygen content in bio-based feedstock is higher as compared to fossil starting material. Thus, intermediates and products of the future chemical industry will be rich in oxygen as well. Polar interactions and hydrogen bonding will be present in mixtures. This in turn will lead to lower vapor pressures and higher viscosity of the systems. Process design has to account for these changes throughout the entire production process, starting from raw-material supply ending at purification and separation steps. The aim of this work is to study some relevant aspects related to liquid-liquid extraction, in order to optimize extraction-column design with a focus on highly viscous systems. The knowledge in the area of solvent extraction in highly viscous systems, as e.g. applied for separation of pharmaceuticals from fermentation broth or extraction of biomaterials from a complex oxygen-containing matrix, is limited.

Thus an investigation on extraction-column behavior for viscous systems is required.

With drop-based lab-scale experiments and simulation, extraction-column performance can be predicted to better than 10% accuracy, being time and resources saving compared to pilot-plant experiments [1]. This is possible, because only a limited number of elementary processes, namely sedimentation, coalescence and splitting, mass transfer, as well as the interactions among the droplets and with the column internals influence the behavior of individual drops of the dispersed phase in the column. In previous work, appropriate models describing these effects were combined in a simulation tool, called ReDrop (REpresentative DROPs). The main idea of ReDrop is to follow the behavior of a sufficiently large number of individual drops along their paths through the column and to solve the population balance accounting for the interconnected phenomena mentioned [1-2]. The appropriate lab-cell measurements are used to derive the corresponding models describing the individual drop behavior with respect to the above-mentioned basic phenomena. The ReDrop simulations have been validated for a variety of systems, mostly standard test systems [3], which have been defined by the EFCE in the past [4], but also for technical systems [1, 7, 8], for which the results of the ReDrop simulations were compared with those of pilot-plant scale experiments. The predictions agreed to better than 10% with the experimental data available. The strength of this drop-based approach is apparent from its ability to even predict the limits of operating the extraction column, namely the flooding point, with similar accuracy. The models implemented in ReDrop have been largely validated for low-viscous systems with viscosities of around 1 mPas [3] and for systems with viscosities of the order of 100 mPas [5]. Since the model parameters even for describing drop sedimentation greatly differ for the different viscosity regimes, the intermediate range has to be investigated to obtain a complete picture. This will result in models and simulation tools capable of describing the entire viscosity range of interest.

2. Experimental

2.1 Material system

Sedimentation velocity and mass transfer of a single drop of dispersed phase rising in the continuous phase has been studied with a sedimentation vessel coupled with a single-drop cell, described in the next section, where a conical glass tube is used to levitate the drop by a counter flow of continuous phase [6].

Before investigating high-viscous systems with the single-drop cell, the equipment for mass transfer measurement, which had been transferred to Liège from TU Graz, Austria, has been validated by analyzing mass transfer and sedimentation behavior of an EFCE standard test system for solvent extraction with low viscosity composed by water, acetone and butyl acetate. The direction of mass transfer has been chosen to be from continuous to dispersed phase. The water has been saturated with butyl acetate, then 5%wt. of acetone were added to the continuous phase. The dispersed phase is composed by *n*-butyl acetate saturated with water.

As an example for viscous systems single-drop behavior previous results obtained for aqueous two-phase systems (ATPS) with a system of phosphate and PEG (polyethylene glycol) are included in this evaluation as well. The investigated system was composed of PEG 2000 at a weight fraction of 13.5 wt% and a phosphate buffer at 8 wt%. The pH of the system was set to 9 by using a mixture of di-

potassium hydrogen phosphate and sodium dihydrogen phosphate at a temperature of 25°C. The physical properties of the system are given in Table 1. Mass-transfer component was the protein albumin with a molecular mass of 65 kDa, which was chosen as a representative for valuable bio-molecules. Mass transfer was from salt-rich continuous phase to PEG-rich droplet phase.

The single-drop results are the basis for validation and extending the applicability of existing models which are introduced in ReDrop. Suitable material systems for solvent extraction with high viscosity are chosen based on the standard test systems proposed by the EFCE [4]. For the first investigations, the aqueous phase is chosen as continuous phase, where the viscosity is increased by adding a suitable polymer like PEG. The dispersed-phase viscosity is increased by dissolving suitable compounds such as paraffin oil in an organic solvent immiscible with water, like e.g. *n*-butyl acetate. Diffusion of the transfer component is influenced by the mass-transfer resistance induced by continuous and dispersed-phase viscosity. Single-drop measurements in viscous systems will allow to understand how viscosity influences the parameters of the model. In previous work [5] the parameters have been fitted for the system composed of water + PEG as continuous phase and toluene + paraffin as dispersed phase. Viscosity of the continuous phase was varied between 80 and 100 mPas and viscosity of the dispersed phase was increased to 64 mPas by adding paraffin oil. Further investigations are thus focusing on the intermediate range of viscosity between 1 mPas and 100 mPas.

Table 1. Physical properties of the investigated ATPS.

phase	density kg/m^3	viscosity mPas	interfacial tension mN/m
continuous	1195.9	2.145	
dispersed	1088.0	9.250	

2.2 Single-Drop Experiments

Sedimentation velocity of single drops has been evaluated in a cylindrical vessel maintained at a temperature of 20°C. The vessel has an inner radius of 4 cm and his height is 40 cm. It can be filled with up to 2010 ml of continuous phase. Inside this vessel, a drop of known volume is produced with the help of a computer driven syringe, which can inject a defined volume of dispersed phase at a defined velocity via a glass nozzle. The glass nozzle is installed in the vessel and connected to the syringe by a PEEK hose of suitable diameter. By finding the right amount of dispersed phase to inject and the right velocity to correctly produce one single drop, individual drops with the drop diameter of interest can be generated. Each drop detaches from the glass nozzle tip and its path is recorded with a video camera. Knowing the numbers of frames, and consequently the time, needed for the drop to rise in the continuous phase through a defined distance, sedimentation velocity can be easily determined.

Single-drop mass-transfer investigations have been carried out in the cell shown in Figure 1. The glass cell has a conical section in the mass-transfer zone. The maximum inner diameter of the cell is 5 cm, and the distance between the drop production point and the collection funnel is 15 cm. All parts of the device consist solely of glass, teflon and stainless steel in order to minimize the influence of contaminants. The cell is maintained at 20°C. The drop is again produced by a computer-driven syringe

and a glass nozzle, with which the right volume of liquid required to produce one drop with chosen diameter is injected. The drop then rises until it reaches the conical part, in which a counter-flow of continuous phase is induced by a pump. It will rise until its sedimentation velocity matches the counter flow of continuous phase, which allows to realize different contact times between the two phases. After the chosen contact time, the counter flow of continuous phase is switched off, the drop can continue its path along the cell, and is collected in a glass funnel. The glass funnel is connected to another syringe which withdraws the exact amount of liquid corresponding to the volume of the drop. After a sufficient number of drops has been withdrawn, typically between 300 and 600 depending on the volume, the sample of dispersed phase can be analyzed. The concentration of transferred component in the drop is determined using UV-Vis spectroscopy, which allows to calculate the dimensionless driving concentration difference of acetone in *n*-butyl acetate drops as a function of the contact time. The dimensionless driving concentration difference is defined as:

$$y^+ = \frac{y(t) - y^*}{y_0 - y^*} \tag{1}$$

where $y(t)$ is the concentration of transferred component in the drop at the residence time t, y^* is the equilibrium concentration of transferred component in the drop and y_0 is the initial concentration of transferred component in the dispersed phase. The dimensionless driving concentration difference is 1 when no mass transfer has occurred and 0 when mass transfer is finished and the concentration of transferred component in the dispersed phase has reached his equilibrium value.

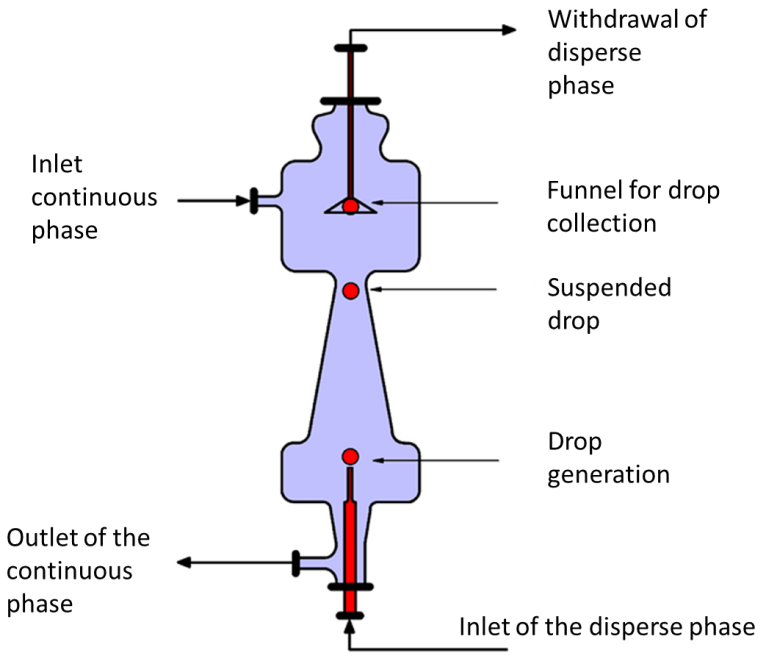

Figure 1. Single-drop cell for single-drop based mass-transfer measurements [6].

3. Results and Discussion

Sedimentation velocity of a single drop as function of its diameter shows typically the behavior

presented in Figure 2. In this work three different drop diameters have been investigated for the system water + acetone + butyl acetate. Figure 2 compares the obtained values for sedimentation velocity with previous results. It is apparent that the new data match almost exactly with the previous data. Drops of *n*-butyl acetate in water behave like rigid spheres for the smallest drop diameter. The larger drops investigated behave as drops with internal circulation, showing a mobile interface. This result shows that the cell is properly working after its transfer to Liège and the methods applied have been validated at the same time.

Mass-transfer results for the standard system water + acetone + butyl acetate are reported and compared with previous data, [6,9], in Figure 3. y^+ decreases from 1, when no mass transfer has occurred and the drop starts with its initial concentration, to 0, when mass transfer ceases. As expected, the dimensionless concentration difference decreases with contact time. The results in Figure 3 show as expected that for drops with smaller diameter faster mass transfer results. This shows that also the mass-transfer cell has been validated and the proper procedures have been established at the University of Liège. As a basis for the future viscous system investigations, previous results related to the aqueous two phase system described above are presented. The results are shown in Figure 4 with the dimensionless driving concentration difference over the residence time of the drops and the drop diameter. The results show, that mass transfer is significantly slower than in the system water + butyl acetate + acetone shown in Figure 3. Reasons for this drastically reduced mass transfer are the higher viscosity of the dispersed phase as well as the size of the mass-transfer component, which is several orders of magnitude larger compared to the acetone in the organic-aqueous system.

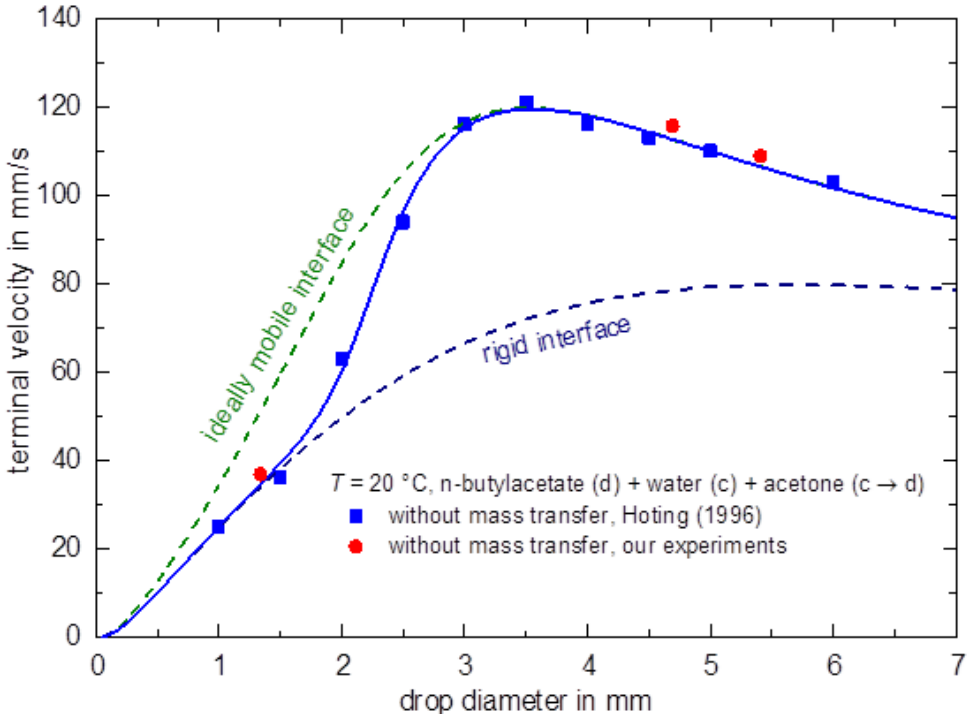

Figure 2. Sedimentation velocity of *n*-butyl-acetate drops in water as a function of the drop diameter.

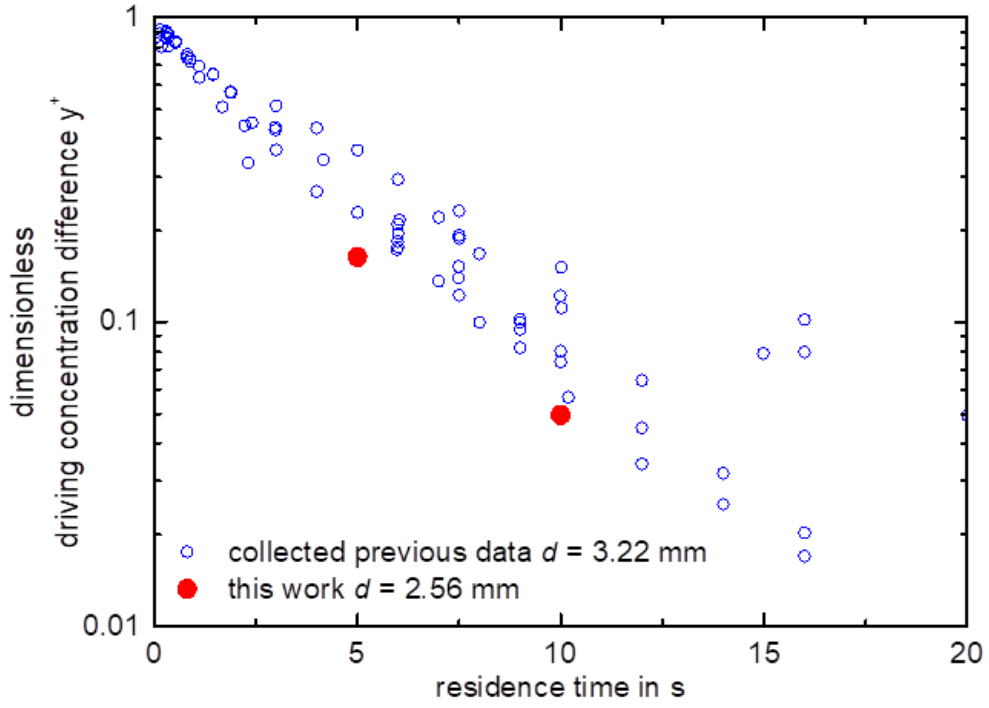

Figure 3. Dimensionless driving concentration difference as a function of residence time.

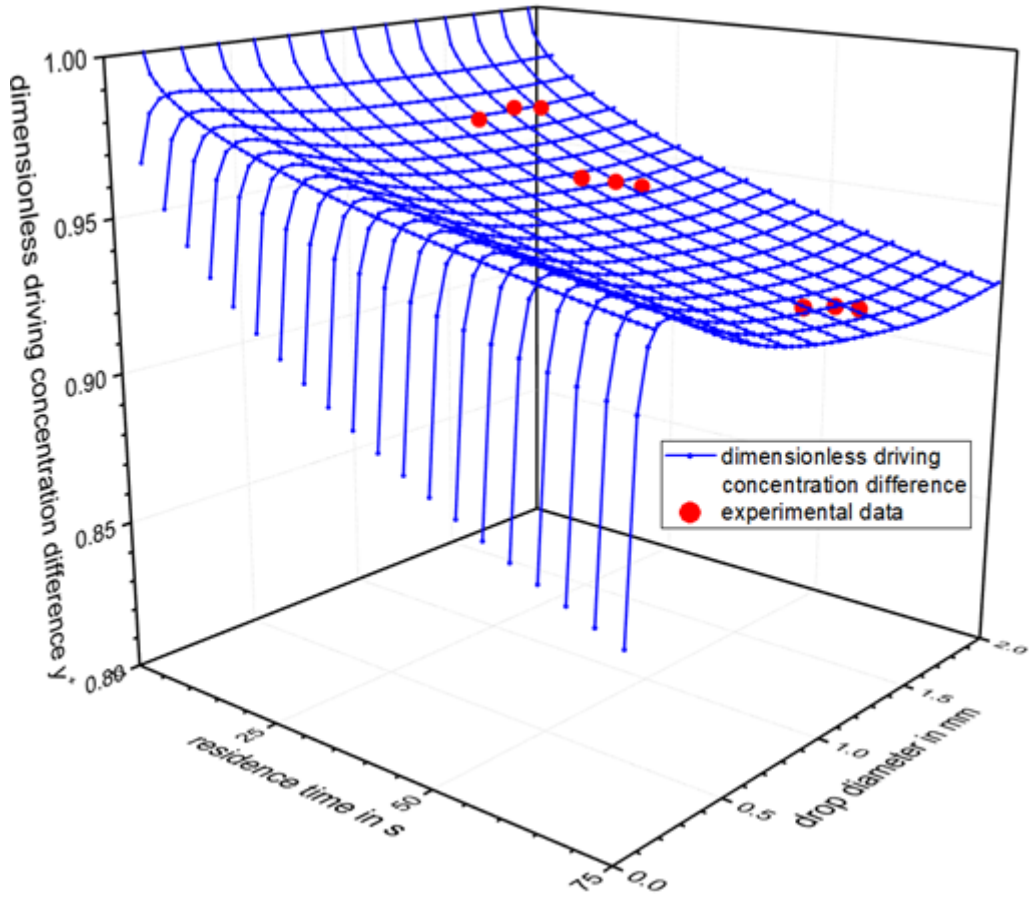

Figure 4. *y*+ as a function of residence time and drop diameter for the aqueous two-phase system.

In the future work, sedimentation and mass transfer will be investigated by changing the properties of the material system, in order to adapt the models to system with increased viscosity in both phases. The influence of the molecular size of the transferred component will be taken also into account as well, since the investigation on ATPS showed that mass transfer is significantly slowed down for large transfer molecules.

4. Conclusion

The validation of the lab-scale equipment to quantify single-drop behavior with the standard test system shows good agreement with previous data. Sedimentation velocity of single drops of *n*-butyl acetate in water without mass transfer agrees with previous data, where small drops behave like a rigid sphere, while with increasing drop diameter sedimentation velocity reaches that of deformed drops with ideally-mobile interface. Mass transfer has been evaluated for three different drop diameters and for different residence times. Results are in good agreement with previous results as well. For an aqueous two-phase system it has been shown that mass transfer is significantly slower than that in low-viscous systems. Thus the basis has been established for investigating systems with increased viscosity in the future. First results are presented at the ISEC2017, Myazaki, Japan.

References

1) M. Altunok, T. Grömping, A. Pfennig, *Comput. Aided Chem. Eng*., **21**, 665-670 (2006).
2) N. Kopriwa, F. Buchbender, J. Ayesterán, M. Kalem, A. Pfennig, *Solvent. Extr. Ion. Exc*., **30 (7)**, 683-723 (2012).
3) M. Henschke, Auslegung pulsierter Siebboden-Extraktionskolonnen. Shaker Verlag, Aachen, *Germany* (2003)
4) T. Misek, R. Berger, J. Schröter, Inst. Chem. Eng. (1985)
5) D. Adinata, Single drop modelling in high viscosity system, PhD Thesis, RWTH Aachen University, *Germany* (2011).
6) M. Henschke, A.Pfennig, *AIChE J.,* **45**, 10 (1999).
7) F. Buchbender, M. Schmidt, T. Steinmetz, A. Pfennig, *Chem. Ing.Tech*., **84**, **(4)** 540-546 (2012)
8) F. Buchbender, F. Onink, W. Meindersma, A. de Haan, A. Pfennig, *Chem. Eng.Sci*., **82**, 167–176 (2012)
9) M. Henschke, A. and Pfennig, *AIChE J.,* **48**, 2 (2002).

Multiphase Loop-Reactor with In-Situ Extraction: CFD Simulation and 2D Compartment Modeling with Population Balances

Benedikt WEBER[1,*], Maximilian von CAMPENHAUSEN,
and Andreas JUPKE[1]

[1]*AVT - Fluid Process Engineering, RWTH Aachen University, Forckenbeckstraße 51, 52074 Aachen, Germany,*

A multiphase loop-reactor, which combines a gas-phase for oxygen supply and an in-situ liquid-liquid extraction for a fermentation process, is developed via CFD simulation. In addition, a two-dimensional compartment model is developed and presented. It applies the results of the CFD simulation to calculate mass-transfer and the local drop distribution in the two-dimensional area of the liquid-liquid extraction part of the reactor. The drop population balances are solved via a n-Monte-Carlo approach. Results of the compartment model show good agreement of the drop motion in comparison with the CFD simulation. In addition, a chemical test-system is used to calculate the mass-transfer in the liquid-liquid extraction area.

1. Introduction

Resulting from the foreseeable shortage of fossil resources and climate change, a feed stock change from fossil resources to renewable educts is inevitable. Therefore, white biotechnology has seen a substantial advancement in recent years. One promising opportunity offer optimized microorganisms from biotechnology combined with efficient processes. However, the separation and purification of products from fermentation media lead to new challenges for process engineers concerning product purity, bio-compatibility and economic as well as ecologic feasibility. Moreover, even if biotechnological processes are on the one hand more selective compared to chemo-catalytic processes they can on the other hand exhibit inhibition at low product concentrations leading to low space time yields.

To overcome product inhibition in aerobe fermentation processes an innovative multiphase loop-reactor was developed [1, 2]. The reactor set-up combines both oxygen supply as well as in-situ liquid-liquid extraction. Thus, the extraction offers the possibility to remove continuously a toxic or inhibitory product and to increase space-time yield of a fermentation. The advantages of the reactor set-up result from locally separated zones of oxygen supply and product separation in one apparatus. The oxygen rich gas-phase induces a loop flow whereas in the outer downcomer the extraction solvent rises counter-currently to the aqueous fermentation broth. The general set-up of the reactor is depicted in Figure 1.

In previous studies we already proposed a possible reactor set-up [2]. The reactor was operated with a test-system composed of water as continuous phase, air and a kerosene fraction (Shellsol T) as

dispersed phase. The experimental results of the fluid dynamics and the performed CFD simulations were in good agreement and proved the performance and functionality of the new rector concept. For comparison the hold-up and an optical evaluation of the flow were used.

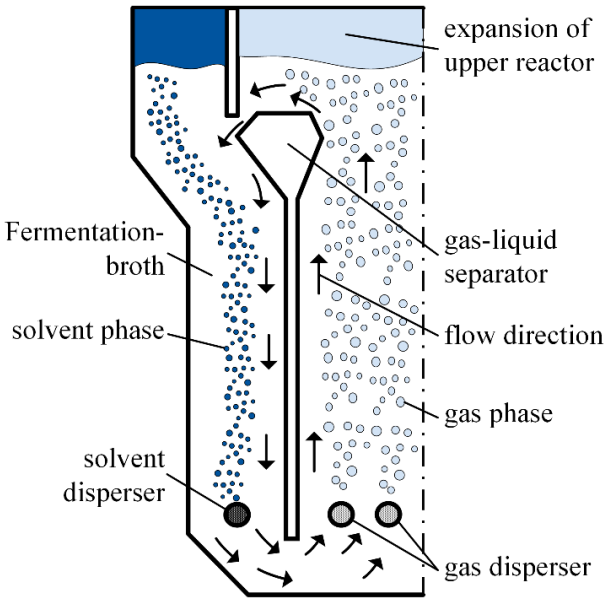

Figure 1. Concept of multiphase loop-reactor

For the description and modeling of the multiphase-loop reactor containing a liquid-liquid extraction part and a bubble column part the drop/bubble size distribution and the mass transfer are of main interest. Depending to the energy input drops or bubbles can coalescence or break. Since simple thermodynamic models like the equation of Kremser [5] do not account for interfacial area and mass transfer, several detailed models were developed. On the one hand, there are one-dimensional models that calculate the drop size distribution with population balances [6, 7]. Due to their one-dimensional set-up, the local flow pattern is calculated with models for axial dispersion along with additional terms including the effects of internals. On the other hand, detailed flow conditions are accessible via CFD simulation [8-10]. A coupling of population balances with CFD leads to a local resolution of drop size distribution and mass transfer according to the local exchange area. This method offers highly accurate results but needs high computational effort since the population balance equations have to be solved for each grid cell. Therefore, researchers have started to use compartment models that combine the advantages of both methods [11]. In the compartment grid, that uses only a small fraction of elements in comparison to the CFD grid, the continuous phase is modeled as ideally mixed and the population balances for the dispersed phase are solved. With a CFD simulation, the local flow characteristics are described neglecting mass transfer and population effects like coalescence and breakage of drops or bubbles. With the flow-data of the CFD simulation the exchange flow between the compartments, the mean convection flow in each compartment and the local energy dissipation are set. The advantages of the compartment model are the employment of detailed flow characteristics based on CFD simulations and less computational effort. Consequently, back-mixing and detailed drop motion is simulated on a physical basis (CFD) without empirical approximations as in one-dimensional population balances. In addition, population balances including drop diameter distribution and mass transfer can be applied with acceptable computational effort.

This methodology has been used with classical population balances for crystallization processes [11], batch reactors [12] and bubble columns [13]. To the best of our knowledge only for crystallization processes, a Monte-Carlo simulation was used to calculate the particle population [14].

In this paper, we present a new compartment model approach for the liquid-liquid extraction part of the recently developed multiphase-loop reactor [2], which solves the population phenomena with a n-Monte-Carlo simulation. Results of the simulation in the multiphase-loop reactor with a chemical test-system are introduced.

2. Experimental work and Simulation set-up

2.1 CFD Simulation

In this study we improved the reactor design via three-phase CFD simulation model as already used and validated in [2]. The properties of the used chemicals are listed in Table 1. The inlet volume flows of Shellsol T (drop diameter 2 mm) as solvent and air (bubble diameter 5 mm) for oxygenation are set constant to 0.034 m³/h and 0.8 Nm³/h. The gaseous phase is dispersed in the center of the reactor and the extraction solvent rises in the gap between inner cylinder and outer reactor wall (Figure 1). The top of the reactor is expanded to include a gas-liquid separator at the top of the internal cylinder. The CFD model includes a two dimensional axisymmetric Euler-Euler approach in combination with a standard k-ε turbulence model. The simulation considers gravitation, drag (model of Schiller and Naumann [3]) and turbulent dispersion (model of Simonin and Viollet [4]) as additional forces. Further information about the simulation set-up can be found in [2]. In addition, a new pilot-reactor has been designed and built in technical scale. The final dimensions of the improved reactor are given in Figure 2.

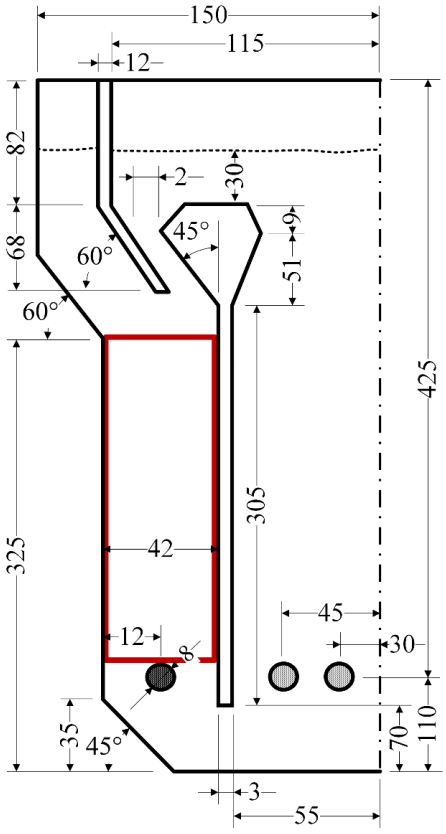

Figure 2. Dimensions of multiphase loop-reactor in mm

Table 1. Chemical properties

	Density [kg/m³]	Dynamic viscosity [Pas]
Shellsol T	780,00	$2{,}40 \cdot 10^{-3}$
Water	993,56	$1{,}03 \cdot 10^{-3}$
Air	1,20	$17{,}10 \cdot 10^{-6}$
Interfacial tension (water – Shellsol T) [N/m]	0,0263	

2.2 Two-dimensional compartment model

The liquid-liquid extraction part of the reactor (marked with a red rectangle in Figure 2) is modelled with a two-dimensional compartment model calculating drop size distributions and mass transfer. At the top of the domain, water loaded with 0.025 kg/kg_{water} of an exemplary transfer

component flows into the extraction area. The unloaded dispersed phase enters at the lower domain at a radius of 0.08 m with a drop diameter of 2 mm. The compartment grid has a resolution of equally distributed compartments (three compartments in radial direction and eight in vertical direction). The performed CFD simulations supply the compartment model with flow characteristics, specifically velocity fields and exchange flows between the compartments as shown in Figure 3. Here the water velocity profile (result of CFD simulation) is shown. Overlapped is the grid in red and the vertical water velocity vectors are added at the boundaries of the compartments. In each compartment, the water velocity is averaged and saved in the model.

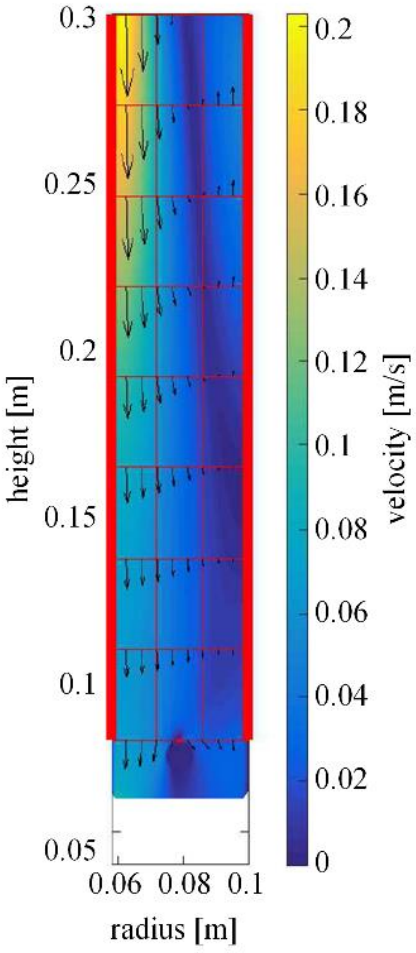

Figure 3. Compartments with velocity vectors at boundaries and velocity

In the compartments, a representative population of the total amount of drops (50 drops per compartment) is calculated with a n-Monte-Carlo simulation approach. The advantage of a n-Monte-Carlo (fixed amount of drops per compartment) in comparison to a v-Monte-Carlo (fixed volume of apparatus) simulation approach is that in case of high droplet breakage the amount of calculated drops is kept constant. Consequently, this model can be used for example for strong dispersing systems.

In the here presented compartment model, sub-models are used for each representative droplet to account for motion, mass transfer and coalescence. The same chemicals as in the CFD simulation are used (Table 1). In the simulations with the compartment model an exemplary transfer component is added that is extracted into the dispersed phase. A sub-model for drop breakage is neglected since the drops can rise freely in the simulated domain. The sub-models of the one-dimensional population balance model ReDrop [6] are transferred into the compartment model and described in more detail in the following paragraphs. The model parameters and physico-chemical properties are given in Table 2. The motion of the drops is simulated with a superposition of the rise-velocity of a single drop and the averaged velocity vector of the continuous phase in one compartment. For the single drop rise-velocity the model of Henschke [6] is applied, which considers different droplet states (rigid, circulating, oscillating and deformed). The transition diameter d_{um} describes the transition of a rigid to a circulation drop. Both, a_{15} and a_{16} parametrize the drop-oscillation and the corresponding reduction of rise-velocity.

The mass-transfer into the drop is given according to the mass-transfer coefficients as

$$\Delta m = \Delta t \cdot \pi d^2 \cdot \frac{1}{\frac{1}{\rho_{\mathrm{d}}\beta_{\mathrm{d}}}+\frac{K}{\rho_{\mathrm{c}}\beta_{\mathrm{c}}}} \cdot (y - Kx) \qquad (1)$$

where Δt is the time step, d the drop diameter, ρ_d and ρ_c the density of the disperse and continuous phase respectively, β_d and β_c the corresponding mass-transfer coefficients, K the distribution coefficient and y and x the concentrations of the disperse and continuous phase. The mass-transfer resistance in the continuous phase is neglected. The mass-transfer coefficient of the dispersed phase is defined by

$$\beta_d = \frac{D_\mathrm{eff}}{d}\sqrt{\frac{4d^2}{\pi D_\mathrm{eff} t} + \pi^4} \tag{2}$$

where D_eff represents an effective diffusion coefficient and t the drop lifespan. It describes an enhancement of the diffusion of the drop due to convection (inner circulation) and is calculated with

$$D_\mathrm{eff} = D_\mathrm{d} + \frac{v_\infty d}{C_\mathrm{IP}\left(1+\frac{\eta_\mathrm{d}}{\eta_\mathrm{c}}\right)} \tag{3}$$

where D_d is the diffusion coefficient of the dispersed phase, v_∞ the rise-velocity, C_IP the mass-transfer enhancement factor and η_d and η_c the viscosities of the disperse and continuous phase respectively.

The idea of the applied coalescence model is that every drop has a statistic lifespan τ_c until it coalesces with another drop. τ_c is determined by

$$\tau_\mathrm{c} = \xi \frac{\eta_\mathrm{c}}{\epsilon \sigma^{1/3} H_\mathrm{cd}^{1/6} (\Delta\rho g)^{1/2}} \tag{4}$$

where ξ is the coalescence parameter, ϵ the hold-up, H_cd the Hamaker coefficient (for organic-aqueous systems $\sim 10^{-20}$ Nm), $\Delta\rho$ the density difference and g the gravitation. The probability Z_c of coalescence of a drop is then calculated with

$$Z_\mathrm{c} = \frac{\Delta t}{\tau_\mathrm{c}}. \tag{5}$$

The drop is marked for coalescence when an equally distributed random number s (between 0 and 1) is $\leq Z_\mathrm{c}$. When two or more drops in one compartment are marked for coalescence randomly these two drops form a new bigger drop. Afterwards the coalescence marker is deleted.

Table 2. Model parameters and physico-chemical properties

single drop sedimentation		mass-transfer	
d_um	7.1 mm	C_IP	9445
a_{15}	1.917	D_d	$2.199 \cdot 10^{-9}$ m²/s
a_{16}	4.5	K	0.9
coalescence		time step size	
ξ	200	Δt	0.1 s

3. Results and Discussion

3.1 CFD Simulation

Figure 4 depicts the volume-fraction of air and solvent for a volume flow of 0.8 Nm³/h air and 0.034 m³/h solvent entering the reactor. The air rises in the center of the reactor and leaves the aqueous phase above the gas-liquid separator. The solvent rises counter currently to the aqueous phase and is not

entrained into the area of the gas phase. The operation in a pilot reactor (dimension in Figure 2) proved the simulated results in a similar manner as already presented in [2]. Therefore, with this setup the reactor can be operated in a preferred manner so that the dispersed phases leave the reactor in different areas.

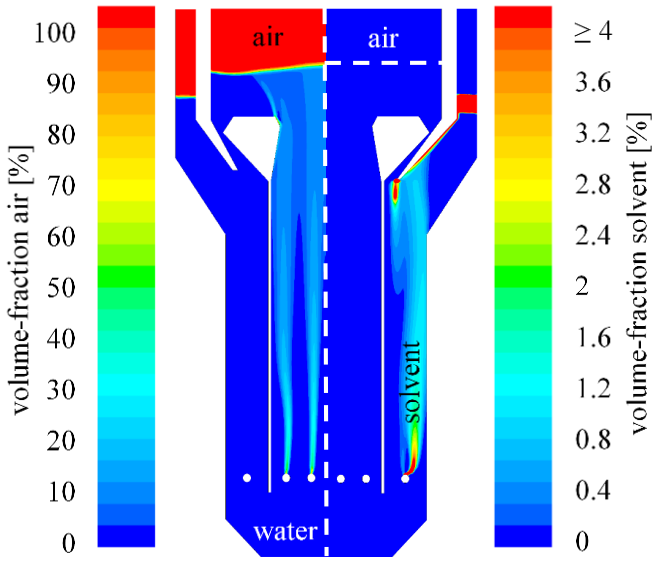

Figure 4. Results of CFD simulation: Volume-fractions in multiphase loop-reactor

3.2 Two-dimensional compartment model

The above explained setup of the two-dimensional compartment model including coalescence and mass-transfer is simulated using a n-Monte-Carlo algorithm for the solution of the drop dispersion. The result after reaching steady state (after 1500 s) is shown in Figure 5. In red the compartment grid is drawn. The drops are marked as circles. The size of the circle represents the drop diameter. The color of the circle represents the amount of transfer component in the drops. During the calculation in each compartment only up to 50 representative drops are considered. Size, concentration and position distribution of the drops are scaled up to the total amount of drops in the reactor. This scaling is also used in Figure 5 so that the drop number represent the hold-up in the reactor.

Considering the drop motion the general flow characteristic of the multiphase flow is captured well by the two-dimensional compartment model. It can be observed that during their rising they move to the outer part of the reactor. This is also shown in Figure 4 in the CFD simulation. The main deviation is found in the first height elements of the compartment grid. In the CFD simulation the drops first move nearly horizontally to the wall, whereas in the compartment model they move directly upwards with a slight motion towards the wall. This is caused by averaging the velocity field of the water phase in each compartment. Especially above the disperser high

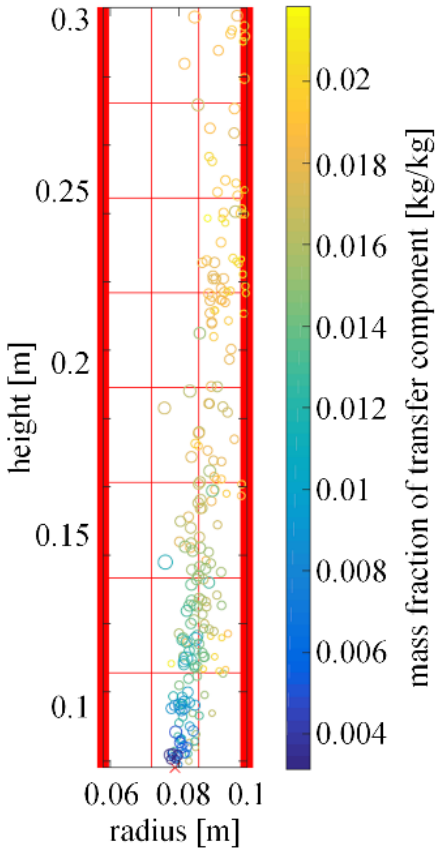

Figure 5. Representative drops in compartment model with position in reactor and concentration of transfer component

local horizontal water velocity vectors exist which are less due to the averaging over the compartment. At the top of the simulation domain in Figure 5, only next to the wall drops are present. However, in the CFD model drops are entrained (Figure 4) into the center of the extraction area. This is missing in the compartment model since the upper area with the backflow is not modeled. During the drop-motion, the transfer component moves into the drops (colored drops in Figure 4). Since only little dispersed phase flows into the reactor only few transfer component is extracted from the continuous phase. Therefore, the concentration of the transfer component in the drops nearly reaches equilibrium when leaving the reactor.

4. Conclusion

The flow direction in the multiphase-loop reactor is modified and improved via CFD simulation in comparison to earlier investigations [2]. A two-dimensional compartment model was successfully developed describing the drop size distribution and mass-transfer into the drops. It uses a n-Monte-Carlo method to solve the population balance calculating only a fixed representative number of drops. It was used for the multiphase flow in the liquid-liquid extraction part of the multiphase-loop reactor. Results show good agreement with the CFD simulation. The advantages of the compartment model are the employment of detailed flow characteristics based on CFD simulations and reduced computational effort when calculating mass transfer, reactions and population balances in comparison to CFD simulations.

In further investigations, a detailed sensitivity analysis regarding number of representative drops and compartment resolution has to be performed. In addition, the whole reactor including an additional gas phase (air) and a bio catalytic reaction will be calculated with the compartment model to investigate the potential of the multiphase-loop reactor. When including models for drop/bubble breakage the two-dimensional compartment model can also be used for different multiphase reactors or extractors like liquid-liquid extraction columns.

Acknowledgement

We would like to thanks the IT-Center of the RWTH Aachen University for the computational resources.

References

1) Bednarz, A., Weber, B., Schmidt, M., Jupke, A., Mehrphasen-Schlaufenreaktor und Verfahren zum Betrieb, EP 16158578 (registered 2016).
2) Bednarz, A., Weber, B., Jupke, A., *Chem. Eng. Sci.*, **161**, 350-359 (2017).
3) Schiller, L., Naumann, Z., *Z. Ver. Deutsch. Ing.*, **77**, 318 (1935).
4) Simonin, O., Viollet, P. L., *Hemisphere Publ. Corp., Waschington, DC,* (1990).
5) Smith, B. D. and Brinkley, W. K., *AIChE Journal*, **6**, 446-450 (1960)
6) Henschke, M, Auslegung pulsierter Siebbodenkolonnen-Extraktionskolonnen. *Dr.-thesis* (2004).
7) Attarakih, M., Al-Zyod, S., AbuKhader, M., Bart, H. *Procedia Engineering*, **42**, 1445-1462.
8) Attarakih, M., Hlawitschka, M. W., Abu-Khader, M., Al-Zyod, S., Bart, H.-J., *Applied Mathematical Modelling*, **39**, 5105-5120 (2015).

9) Bhole, M.R., Joshi, J.B., Ramkrishna, D., *Chemical Engineering Science*, **63**(8), 2267-2282 (2008).
10) Amokrane, A., Charton, S., Sheibat-Othman, N., Becker, J., Klein, J. P., Puel, F., *The Canadian Journal of Chemical Engineering*, **92**(2), 220-233 (2014).
11) Metzger, L., & Kind, M., *Proceedings of the ASME 2014 4th Joint US-European Fluids Engineering Division Summer Meeting*, (2014).
12) Guha, D., Dudukovic, M. P., Ramachandran, P. A., Mehta, S., Alvare, J., *AIChE Journal*, **52**(5), 1836–1846 (2006).
13) Rigopoulos, S., Jones, A., *Chemical Engineering Science*, **58**(14), 3077–3089 (2003).
14) Irizarry, R., *Industrial & Engineering Chemistry Research*, **51**(47), 15484–15496 (2012).

Coalescence in Highly Viscous Systems

David LELEU[1,*], Nicole S. BRUNS[2]
and Andreas PFENNIG[1]

[1]*Department of Chemical Engineering - Products, Environment, and Processes (PEPs), University of Liège, Quartier Agora, Allée du Six Août, 11, 4000 Liège, Belgium;* [2]*AVT - Thermal Process Engineering, RWTH Aachen University, Wüllnerstr. 5, 52062, Aachen, Germany*

A numerical tool based on the ReDrop approach has been developed in order to predict the settling time of liquid-liquid dispersions with a special focus on highly viscous system involving trace components and accounting for drop-size distributions. The model used to describe the coalescence phenomenon was investigated in detail by analyzing separately the different variables involved in the process: the collision frequency, the coalescence time and the contact time. The corresponding coalescence model was integrated in the ReDrop tool, which will be validated with experiments conducted in the Henschke settling cell.

1. Introduction

Molecules of common reactants for obtaining bio-based products contain a larger number of oxygen atoms as compared to fossil resources. Due to the resulting stronger intermolecular interactions, this will induce increased viscosities of the systems. At the same time, separation of liquid-liquid dispersions is a common task in biobased processes. Unfortunately, increased viscosity leads to comparably wide drop-size distributions, which pose additional difficulties in designing a technical settler, e.g. quantitatively predicting the remaining fraction of fine drops found at settler outlet as function of the operating conditions.

Trace components, e.g. ions, considerably influence the settling behavior. The influence varies with the ion type and with their concentration making settling quite unpredictable. Thus, to quantify this influence for any technical systems, settling experiment are required, which can be conducted in a so-called settling cell. With detailed evaluation of such an experiment, the material system can be characterized by a coalescence parameter and by an initial Sauter mean drop diameter [1].

In order to simulate the separation of liquid-liquid dispersions and thus improve the design of equipment, a numerical tool has been developed, which is based on the ReDrop concept (Representative Drops) [1]. Sedimentation and coalescence are evaluated for a sufficiently large ensemble of representative individual drops at each time step. Both elementary processes are depicted by suitable models. Especially coalescence is a major challenge in these simulations.

2. ReDrop concept

The developed ReDrop tool considers each individual drop from a sufficiently large ensemble present in the system. Their individual velocity, obtained from a sedimentation model, is evaluated for each time step in order to determine their individual vertical position in the settling cell. The coalescence frequency is then evaluated between each pair of drops, which are close enough to each other. The horizontal position of the drops is not evaluated, i.e. it is assumed that the drops are randomly distributed horizontally. As a consequence, special care has to be taken to properly evaluate the contact probability of two drops as a basis to quantify correctly the probability of a coalescence event.

The settling cell is divided into height elements which allow the evaluation of the local hold up. The latter influences the sedimentation velocity and is taken into account in the models, e.g. with the approach of Richardson and Zaki [2]. The local hold-up can also be used to get a visual impression of the evolution of the settling as presented in Figure 1.

Real liquid-liquid dispersions may also contain further phases, e.g. gas bubbles, solid particles, which can result e.g. from aeration of a fermentation broth. For that reason, the ReDrop tool allows to deal with liquid-liquid dispersion involving an arbitrary number of further phases in order to approach real dispersion.

The physical properties of the system and the simulation parameters, e.g. density, viscosity, the initial holdup, parameters of the drop -size distribution, simulation time step, etc. are made available to the ReDrop program via input files, which are supplied by the user. The initial drop-size distribution is an important parameter and can be chosen according to various distribution functions, where typically a log-normal drop-size distribution is used.

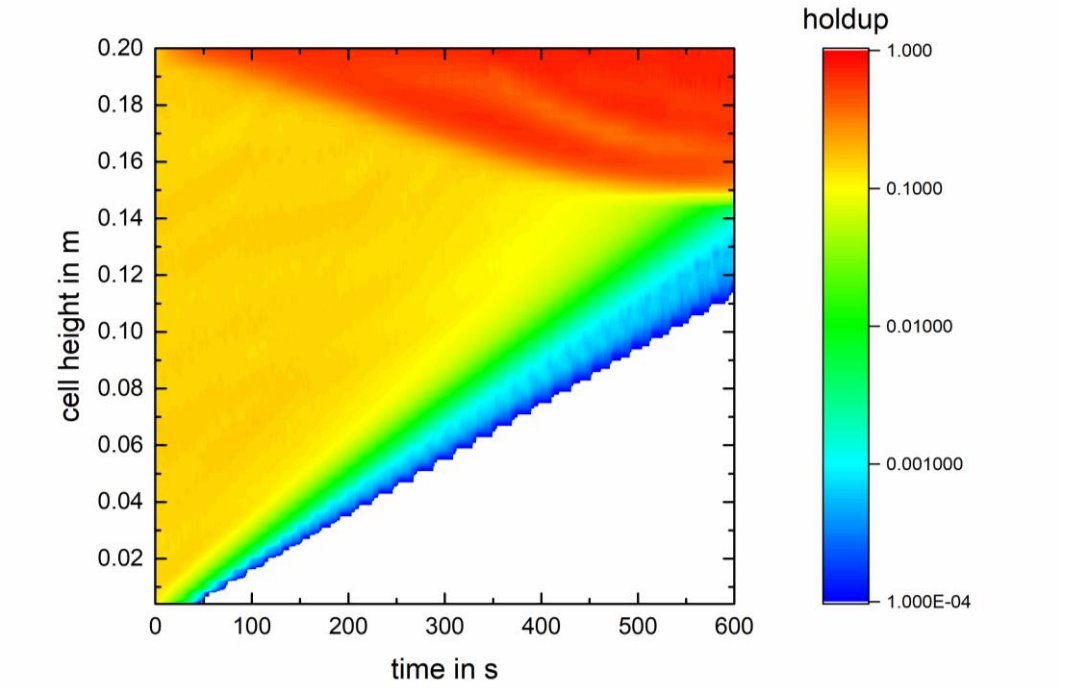

Figure 1. Settling of a liquid-liquid dispersion simulated by ReDrop

3. Coalescence

As shown in Figure 2 the probability that two drops coalesce depends on the frequency with which they meet, defined by the so-called collision rate, and the efficiency with which they coalesce once they met. The coalescence efficiency in turn depends on the time, during which the drops stay in contact and the time they would need to coalesce. Kopriwa [3] showed that extraction columns and settling equipment can be described with the identical model. Kopriwa demonstrated that the frequency with which drops meet and the time they stay in contact depends only on the fluids dynamics of the regarded equipment. The differences in equipment to which this model is applied characterize the fluid dynamics, which thus has to be characterized only once for a dedicated equipment. The time the drops need to coalesce on the other hand only depends on the specific material system used, e.g. solvent, salt type and concentration as well as trace impurities, which makes the prediction of the coalescence time difficult [3-4].

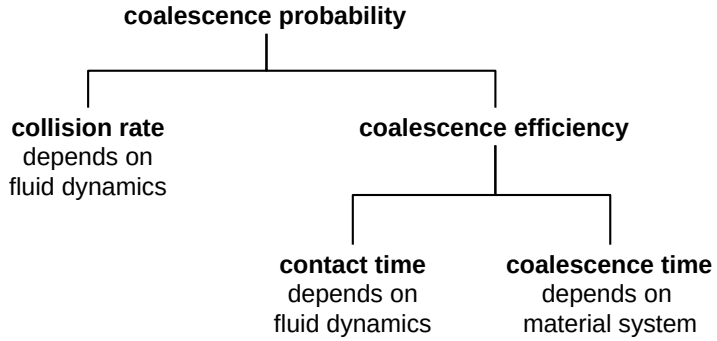

Figure 2. The coalescence model [3]

Pfennig and Schwerin [5] showed that small amounts of salt have a strong influence on the coalescence time, because they influence the interaction between the interfaces. The authors tested different systems with an increased salt concentration and it turns out that the results can be interpreted with the Derjaguin-Landau-Verwey-Overbeek (DLVO) theory. The DLVO theory describes the force resulting from the repulsive ionic and the Van-der-Waals forces acting between two approaching droplets. The DLVO force depends on the salt concentration, as shown on figure 3, and on the different ions present in the system [4].

The DLVO force shows a maximum for a certain salt concentration. At this value, corresponding to 100 mol/m³ in the example presented in Figure 3, the repulsive force between two drops is large and, as a consequence, hinders coalescence, as indicated by Pfennig and Schwerin [5].

In order to include this effect in coalescence modelling, the different terms describing the coalescence probability are investigated separately in order to evaluate their individual effect on the phenomenon. The results will be compared to the models found in the literature and to experimental data. From such experiments, performed in a suitable settling cell, the coalescence time can be evaluated and used for model validation.

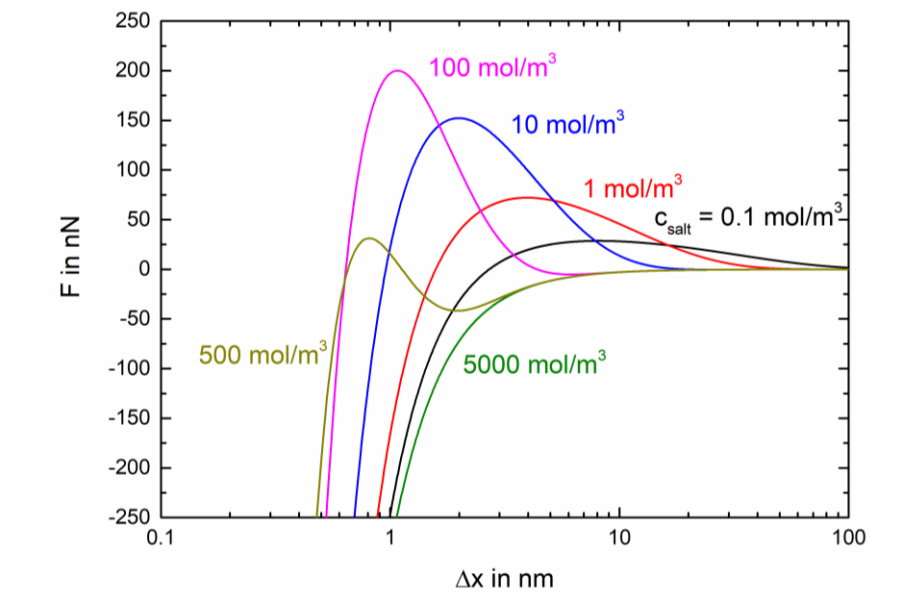

Figure 3. Evolution of the DLVO force with the distance between two drops of a radius of 0.1 mm [5]

4. Material and method

4.1 Experimental set up

The experiments are conducted in the standardized settling cell proposed by Henschke [1], shown on Figure 4. It consists of a double-wall glass vessel with a capacity of 800 ml, with two shafts for stirring with four stirrers on each shaft, each with four tilted blades. They are connected with a gearbox such that they are counter-rotating during stirring in order to stabilize the system in the first seconds after switching off the stirrers without the need of baffles. The gearbox is driven by a stirrer motor. The outer space of the double-wall vessel is connected to a thermostatic bath. The temperature is set to 25°C. The cell is lighted from behind with a LED panel. The vessel is filled from the top with the two-phase system using a funnel. The volumetric phase ratio is easily read from a scale placed at one side of the vessel.

After the cell has been filled with the two-phase system, the stirrers are turned on for 30 s at 800 min^{-1} for generating the dispersion. Once the dispersion is created, the separation can be studied in the same vessel. Alternatively the dispersion can be transferred into a second vessel, placed below the first one, via opening a ball valve. Internals can be placed in this vessel in order to evaluate their effect on the settling behavior. The experiment is finished when half of the interface is covered by a monolayer of drops, which defines the so-called settling time. This definition has been introduced by Henschke to ensure reproducible results, since alternatively waiting until the last drop has coalesced would lead to large scatter due to the stochastic nature of individual coalescence events.

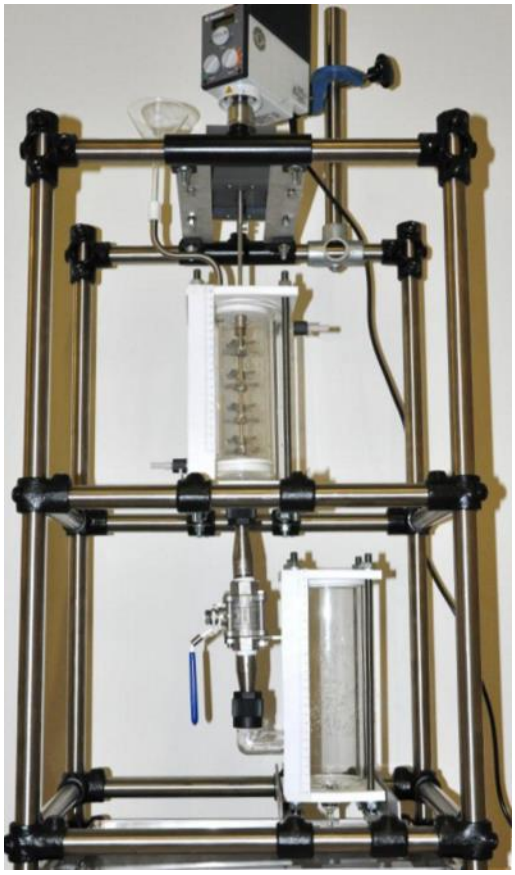

Figure 4. The Henschke settling cell [1]

4.2 Chemicals

The chemicals used during experiments are paraffin oil, water, and salt. As a first step, the paraffin oil is provided by Fauth + Co.KG and has the reference FC2006 (batch number: 64200048). The water used was deionized water directly produced with a deionization cartridge. The salt used was sodium chloride, supplied by VWR (batch number: 12K220010). The concentration of salt during the experiments was 50 mmol/L in the aqueous phase.

Both equilibrium phases were analyzed to determine their density and viscosity with the equipment DSA 5000M combined with Lovis 2000ME of Anton Paar, Graz, Austria. The results are shown in Table 1.

Table 1. Density and viscosity of the saturated phases

		25°C
saturated paraffin oil	density (kg/m³) viscosity (mPas)	819.597 8.48
saturated deionized water + 50 mmol/L of NaCl	density (kg/m³) viscosity (mPas)	999.041 1.030

In the future, different paraffin oils with increased viscosity, to reach a wide drop-size distributions, and varied interfacial interactions introduced by different amounts of salt added will be tested and followed over time. The experimental results will be used to validate the model and the numerical approach.

5. First results

5.1 The Coalescence Model

The first variable investigated which describes the coalescence is the collision rate, $r_{collision}$. It depends on the relative sedimentation velocity of the two considering drops, v_{rel}. In order to take into account the random horizontal position of the drops, the probability of the drops meeting must be evaluated and integrated in the model describing the collision probability. It depends on the surface area of the two studied drops, $\pi(d_1 + d_2)^2$, the separating distance between the two drops, $|h_1 - h_2|$, the horizontal cross-sectional area of the settling cell, A_{cell} and the time step, Δt. Based on this analysis, the collision probability between two drops can be found as:

$$r_{collision} = \frac{\pi(d_1+d_2)^2 v_{rel}\ \Delta t}{A_{cell}\ |h_1-h_2|} \quad (1)$$

The contact time describes the period during which two drops stay in contact while sedimenting. As a first basis to gain a more detailed understanding of the underlying dependencies, the buoyancy and the friction forces acting on the drops were accounted for in the equation of motion of two approaching and meeting drops. The equation was solved assuming that the drops follow their curvature during the contact period. Figure 5 represents the contact time between a first drop with a diameter of 1 mm and a second drop with varied diameter. This approach was developed to get a first impression of the contact time and has to be validated. Further studies will combine this approach with further details of the relative motion, accounting for the fluid dynamics between the drops and the different surface properties [4].

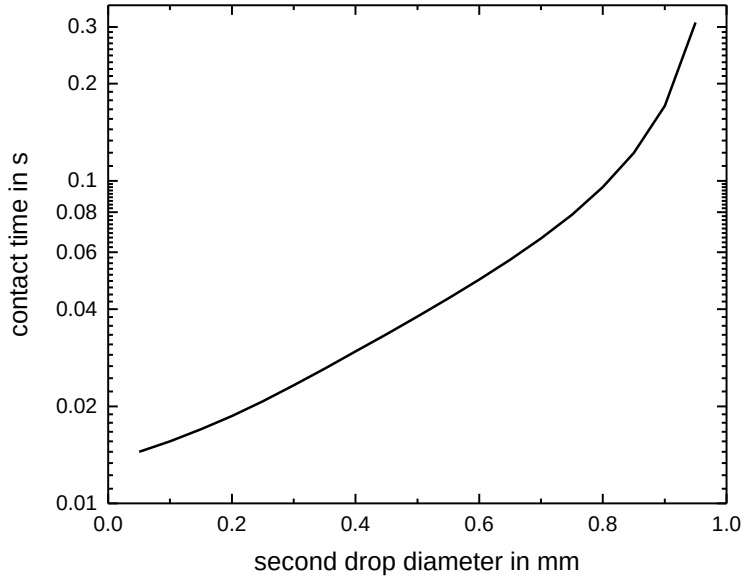

Figure 5. Contact time between a first drop of 1 mm and a second drop with varied diameter

The third parameter, which describes the coalescence probability, is the coalescence time. It corresponds to the time necessary for the acting forces to induce the coalescence between two droplets. Some models exist already, e.g. the Henschke model [1] or the Coulaloglou and Tavlarides model [6], which will to be validated with appropriate experiments as described above.

5.2 ReDrop simulation

The developed ReDrop tool was then used to simulate experimental data. As the modelling of the coalescence curve will be implemented as a next step, here results are shown for sedimentation curve. The parameters of the drop size distribution and of the coalescence were fitted in order to match with experimental data. The results are shown on Figure 6. It is apparent that the coalescence leads to a sedimentation curve being curved upward as in the experiments. Also, some finer droplets remain after the major separation has been completed, which also corresponds to the experimental observation.

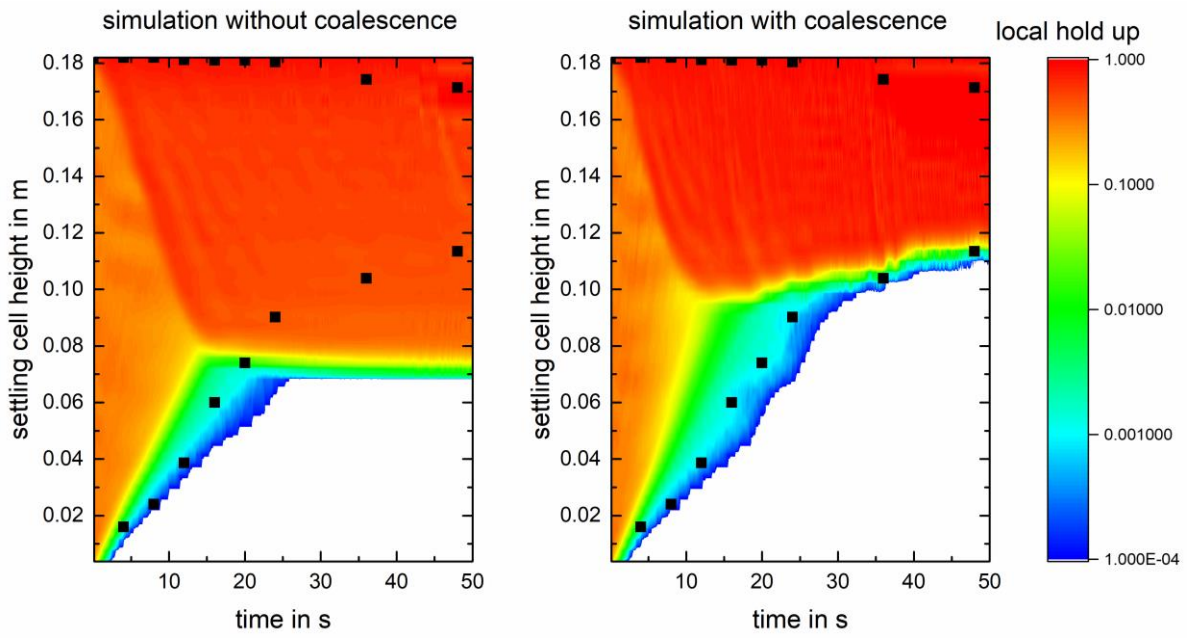

Figure 6: Simulation of settling experiment with the ReDrop tool.

Acknowledgement

The project is partly supported by the Federal Ministry for Economic Affairs and Energy of Germany, project number: 01168585/1.

References

1) M. Henschke, L.H. Schlieper, A. Pfennig, *Chem Eng. J.*, **85**, 369-378 (2002).
2) J.F. Richardson, W.N. Zaki, *Trans. Inst. Chem. Eng.,* **32**, 35-53 (1954).
3) N. Kopriwa, F. Buchbender, M. Kalem, J. Ayesteràn, A. Pfennig, *Solvent Extr. Ion Exch.,* **30**, 683-723 (2012).
4) N. Kopriwa, A. Pfennig, *Solvent Extr. Ion Exch.,* **34**, 622-642 (2016).
5) A. Pfennig, A. Schwerin, *Ind. Eng. Chem. Res.*, **37**, 3180-3188 (1998).
6) C.A. Coulaloglou, L.L. Tavlarides, *Chem. Eng. Sci.*, **32**, 1289-1297 (1977).
7) J. Ayesteràn, N. Kopriwa, F. Buchbender, M. Kalem, A. Pfennig, *Chem Ing. Tech.*, 38, 1894-1900 (2015).
8) T. Tobin, D. Ramkrishna, *Can. J. Chem. Eng.*, **77**, 1090-1104 (1999).
9) J. Kamp, M. Kraume, *Chem. Eng. Sci.*, **126**, 132-142 (2014).

Standardized Settling Cell to Characterize Liquid-Liquid Dispersion

David LELEU*, Andreas PFENNIG

University of Liège, Department of Chemical Engineering - Products, Environment, and Processes (PEPs), Quartier Agora, Allée du Six Août, 11, 4000 Liège – Sart-Tilman, Belgium

Two standardized settling cells, the Henschke and the shaking cells, used to determine the settling time of liquid-liquid dispersion are compared. They are different in terms of dispersion generation and settling-time evaluation. The studied volume also differs and the shaking cell is a closed system unlike the Henschke cell. The aim of this project is to compare the two setups and to characterize their individual advantages and drawbacks in order to finally design an optimal settling cell. Here, the first results of the cells comparison are presented. As a major observation, the Henschke cell is more independent of the operational conditions than the shaking cell.

1. Introduction

Continuous settlers are used for separating liquid-liquid dispersion. In an efficient process, this downstream operation must be sufficiently well designed. Since coalescence depends strongly on trace components, the dispersion needs to be characterized experimentally for each material system of interest, e.g. with respect to settling time. This can be realized in a standardized settling cells at lab scale [1, 2]. Different standardized settling cells have been developed which lead to different characterization procedures and results. It would be desirable to find an optimal standardized settling cell.

In the framework of the project "Energie- und Ressourceneinsparung durch Innovative und CFD basierte Auslegung von Flüssig/Flüssig-Schwerkraft-Abscheidern", called ERICAA, the goal is to design one single standardized settling cell with optimal properties, which allows reliable evaluation of settling behavior and thus also an easier exchange of results between all project partners. One sub-goal of the project is to compare the different standardized equipment present at TU Kaiserslautern, TU Berlin and at the University of Liège in order to build a new equipment which takes all positive aspects into account.

2. Material and methods

2.1 Henschke settling cell

The first studied settling cell, developed by Henschke [1], was available at the Department of Chemical Engineering of the University of Liège. The equipment is shown in figure 1. It consists of a double-wall glass vessel with a capacity of 800 ml, with two shafts for stirring with four stirrers on each shaft, each with four tilted blades. They are connected with a gearbox such that they are counter-rotating during stirring in order to stabilize the system in the first seconds after switching off the stirrers without the need of baffles. The gearbox is driven by a stirrer motor. The outer space of the double-wall vessel

is connected to a thermostatic bath. The temperature is set to 20°C. The cell is illuminated from behind with a LED panel. The vessel is filled from the top with the two-phase system using a funnel. The volumetric phase ratio is easily read from a scale placed at one side of the vessel. After the cell has been filled, the stirrers are turned on for 30 s at 800 RPM for generating the dispersion. Once the dispersion is created, the separation can be studied in the same vessel. Alternatively the dispersion can be transferred into a second vessel, placed below the first one, via opening a valve. Internals can be placed in this vessel in order to evaluate their effect on the settling behavior. The experiment is finished when half of the interface is covered by a monolayer of drops, which is the so-called settling time. This definition has been introduced by Henschke to ensure reproducible results, since alternatively waiting until the last drop has coalesced would lead to large scatter due to the stochastic nature of individual coalescence events. This evaluation method is called visual method in the following. To determine this settling time, a top view of the interface is necessary. At the same time a video recording from the front allows quantitative evaluation of sedimentation and coalescence curve.

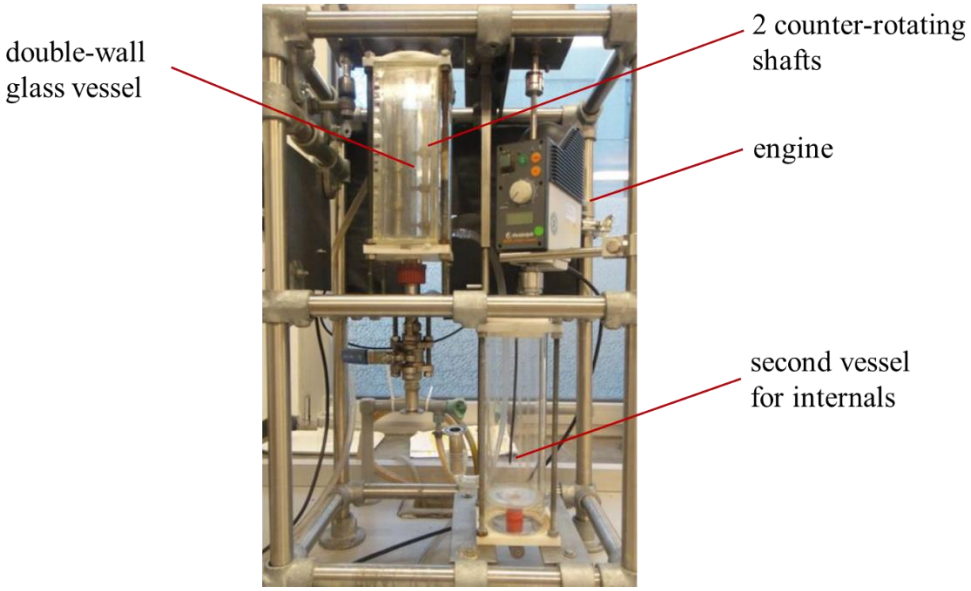

Figure 1. The stirred Henschke settling cell

2.2 Shaking settling cell

The second settling cell was developed at the University of Berlin and is described by Villwock [3]. It has also been used at TU Kaiserslautern. An identical equipment was built in Liège to perform this study, presented in figure 2. Two bottles of 100 ml each are filled with the two-phase system with the identical phase ratio in order to control the repeatability of the experiments. For a practical reason, the flasks are filled with 75 ml of the system which corresponds to the volume to reach the bottle neck. If the bottles were filled above that, the reduction of the bottle diameter in the region of the neck would need to be taken into account in the evaluation of the separation. The two bottles are firmly mounted on a shaking table, which is connected to an electrical motor drive with a rod, which induces a vertical motion of the bottles. The bottles are illuminated from behind with a LED panel. To create the dispersion, the bottles are shaken for 5 s at 650 RPM.

Pictures are then taken in front view of the bottles during the settling experiment at specific times. For the quantitative evaluation of these photos, for each picture of the experiment, an area of interest is selected by the user. For the numerical evaluation, the averaged grey levels of both phases are compared to those of the last picture within this area of interest, resulting in a measure of the difference in grey-scale, which decreases over time. A threshold is set by the user for both phases, which defines when sufficiently clear phases are obtained and the settling time is thus reached. An efficient routine facilitating this quantitative evaluation was written in MATLAB, which requires that the video is uploaded, converted, and then treated with the program. This evaluation method is called the numerical method in the following.

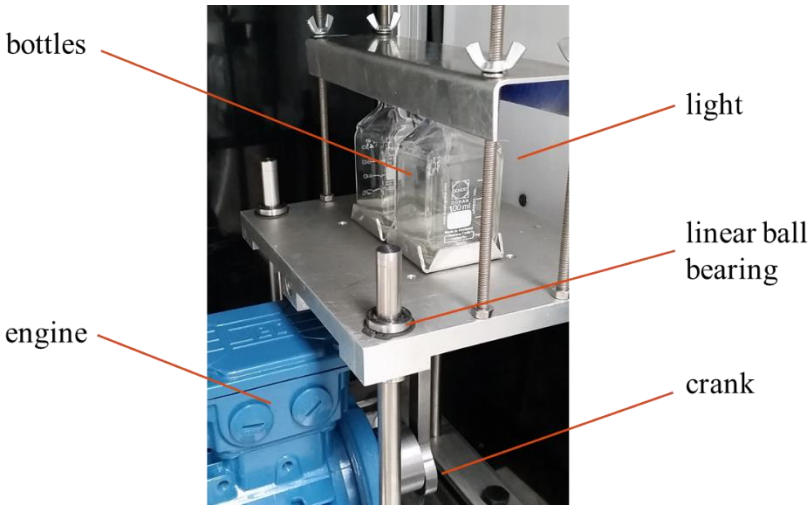

Figure 2. Shaking settling cell

2.3 Chemicals

The chemicals used during experiments are paraffin oil, water, and salt. The paraffin oil is provided by Fauth + Co.KG and has the reference FC2006 (batch number: 64200048). The water used was deionized water directly produced with a deionization cartridge. The salt used was sodium chloride, supplied by VWR (batch number: 12K220010).

The presence of electrolytes in liquid-liquid dispersions influences their separation as shown by Soika [4] and Schwerin [5]. Thus, sodium chloride was added for the experiments for stabilizing separation performance at a concentration of 50 mmol/L in the aqueous phase. Both equilibrium phases were analyzed to determine their density and viscosity with the equipment DSA 5000M combined with Lovis 2000ME of Anton Paar, Graz, Austria. The results are shown in table 1.

Table 1. Density and viscosity of the saturated phases

		20°C	25°C
	density (kg/m³)	822.913	819.597
	viscosity (mPas)	10.06	8.48
	density (kg/m³)	1000.237	999.041
	viscosity (mPas)	1.030	0.924

2.4 Methods

Based on the description of both equipment and the evaluation methods, differences can be pointed out which need to be investigated in order to characterize their effect on the results of settling experiment.

2.4.1 Settling time evaluation

Two different criteria are used to evaluate the settling time, namely the numerical and the visual method described above. The former requires a front view of the settling cell and the latter a top view of the interface. The numerical criterion used to evaluate settling time depends on three parameters: the area of interest, the grey level thresholds for the upper phase as well as that for the lower phase. The sensitivity with respect to these parameters needs to be investigated, the corresponding settling time will then be compared to the one evaluated with the visual criterion for both cells. Different areas of interest (AOI) are tested as represented schematically for both cells in figure 3. The AOIs for the Henschke cell are located between two stirrers to exclude their influence on the evaluation. Nine AOIs are tested. Concerning the shaking cell, AOIs are more restricted due to the presence of the meniscus, so that only three are tested. The thresholds tested will vary between 8 and 12% for the upper phase and 2 and 5% for the lower phase.

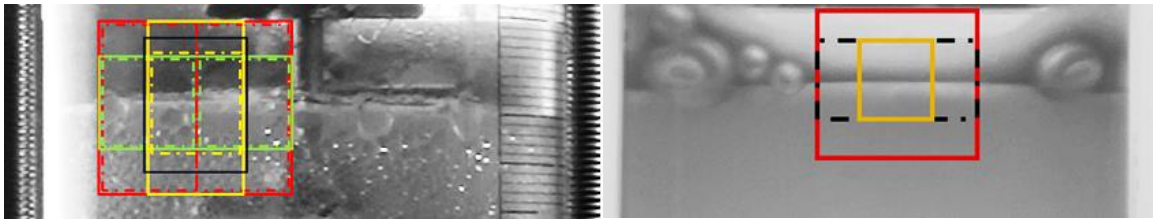

Figure 3. Representation of the different areas of interest (AOI) for both equipments

2.4.2 Air exchange with the environment

The air exchange with the environment is an important parameter influencing the behavior of the separation. It has been observed in previous studies that prolonged air contact can influence the settling behavior significantly, where it has been speculated that this may be due to evaporation of light-boiling fractions of paraffin oil or to dissolution of carbon dioxide leading to a shift in ionic composition in the aqueous phase. The Henschke cell is an open system, while the bottles used with the shaking apparatus must be well closed. In order to investigate the effect of the air exchange on the separation, the bottles of the shaking cell are opened during several hours between two settling experiments.

2.4.3 Dispersion generation

Different speeds and mixing durations are tested. A sensitivity study on these parameters is conducted. The shaking speed varies from 400 to 650 min^{-1} and the shaking time from 5 to 90 s. The stirring speed varies between 500 and 1000 min^{-1} with a mixing time from 5 s to 1 min. The purpose of this variation is to define the experimental parameters ensuring that the system is well mixed but no stable emulsion formed.

2.4.4 Studied volume

The Henschke-cell volume is more than 10 times bigger than the volume used in the shaking-cell bottles. Bottles of 1 L will thus be tested with the shaking-cell apparatus. The mixing protocol of the Henschke cell will be applied to different beakers of different diameters.

Another difference is the air fraction in the cell which influences the studied volume. The Henschke cell can be filled up to 100%, i.e. without any air in the stirred volume. This is not possible for the shaking cell for two reasons. First, the neck-shaped bottle doesn't allow a filling more than 75 ml as explained in section 2.2. Secondly, air must be present to allow efficient dispersion of the two-phase system. The presence of air on the other hand induces the formation of gas bubbles in the dispersion. Different fraction of air volume are tested for both equipments in order to evaluate the effect. A difference of air volume implies a different dispersion height between the experiments. It means that the time needed for the drops too complete sedimentation is shorter, which implies a shorter settling time.

3. Results and Discussion

3.1 Settling time evaluation

For an identical experiment with the Henschke cell, the numerical evaluation method applied to photos taken during the experiment is compared to the visual criterion. The results of this comparison are shown in table 2. In order to characterize the statistical error for the settling time evaluated, each settling experiment is conducted three times. The choice of the AOI and of the thresholds does not affect significantly the settling time. In addition, the visual criterion gives similar results compare to the numerical method.

Table 2. Influence of the parameters of the numerical methods in comparison with the visual criterion for the Henschke cell

	settling time
different areas of interest (AOI)	63 to 74 s
different threshold	64 to 71 s
visual criterion	70 to 77 s

Figure 4 presents the evolution of the difference of the averaged grey scale for the upper and lower phase with respect to the final value over time of one settling experiment performed with the Henschke cell. The evolution of the curves shows a slow but relatively steady decrease of the integrated grey-scale difference over time, where it is obvious that a change of the threshold defining the end of settling will automatically lead to a change of several seconds for the resulting settling time, as indicated in table 2. Both evaluation methods thus lead to settling times in a narrow range as long as the thresholds are fixed to reasonable values, which is less than 12% for the upper phase and less than 5% for the lower phase. The same analysis is performed with the shaking cell, where the method for dispersion generation is different as described above. The results are shown in table 3. The visual criterion is applied to both bottles which gives the same settling time.

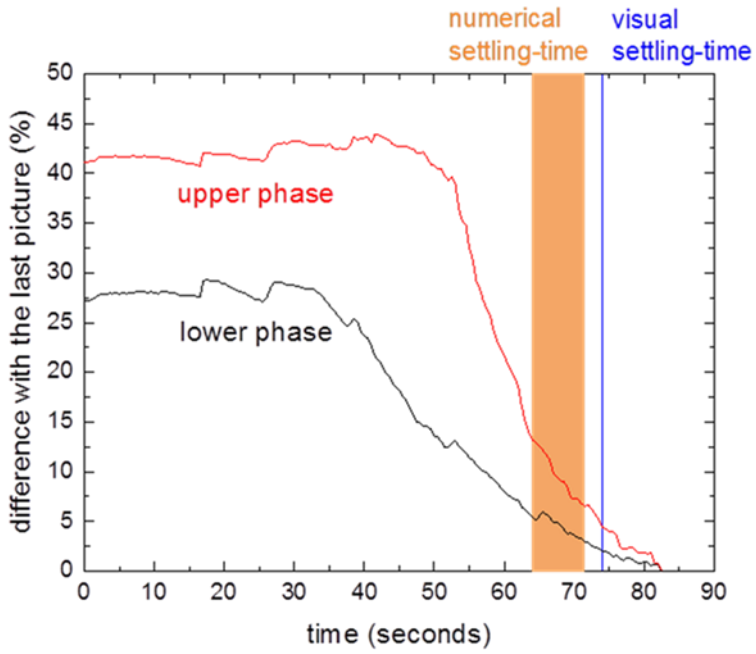

Figure 4. Evolution of the difference of the averaged grey scale for the upper and lower phase

Table 3. Influence of the parameters of the numerical methods in comparison with the visual criterion for the shaking cell

	settling time
different areas of interest (AOI)	196-200 sec
different threshold	196-207 sec
visual criteria	120 sec

It turns out that the choice of the AOI is less important for the shaking cell as compared to the Henschke cell. But even for the Henschke cell, the variation is relatively small. Overall, a change of the threshold values leads to variations in the same range for both equipment. However, the visual criterion results in a significantly differing settling time for the shaking cells because of wall effects of the small bottles. When the interface at the center of the bottles is already cleared of drops, leading to the visual criterion being reached, there are still drops at the wall of the bottles, which strongly influence the numerical evaluation of the settling time. Looking only at the front view of the bottles thus results in misleading data. The visual criterion also has the advantage that it allows to directly measure the settling time "in situ" unlike the numerical evaluation, for which the video needs first to be uploaded and treated with the corresponding MATLAB software. It has to be noted that the visual criterion was applied for all following experiments performed in this study.

3.2 Air exchange with the environment

The air exchange between the system and the environment has a strong influence on the settling behavior as shown in table 4, which compares the settling time between a first closed bottle and second bottle which is opened during 2 hours between two shaking experiments.

Table 4. Influence of the air exchange performed on the shaking cell by opening one bottle between two settling experiments

	settling time
closed bottle	170 sec
bottle open during 2 hours	320 sec

Concerning the Henschke cell, the deviation observed for the settling time doesn't exceed 3% after a delay of 2 hours. The comparison with the shaking cell results presented in table 4 illustrates the stability of the Henschke cell against the air exchange as opposed to the behavior of the shaking cell.

3.3 Dispersion generation

Different mixing times and mixing speeds have been tested with the two settling apparatus. The corresponding settling-time results are presented in figure 5. For slow and short stirring or shaking, below 5 seconds of mixing, the dispersion is not properly generated and experimental settling times are too short. As both parameters are increased, a plateau is reached, within which the settling times remain relatively stable. The plateau of the Henschke-cell data is illustrated by the blue area in the graph. Within this relatively large parameter region the settling time is stable with respect to the mixing parameters. The situation is different for the shaking cell. The red triangle shows the data where the settling time does not vary, the region is significantly more restricted than the Henschke cell. Beyond the triangle, the operational conditions lead to dispersions, which take extremely long to separate or where the settling time cannot be determined because of an excess of very fine drops generated, which impedes visual and numerical evaluation. This infeasible region is indicated by the red area at the top of the graph.

The plateau corresponding to the Henschke cell demonstrates that the mixing parameters do not influence the dispersion characteristic in this region, e.g. drop size distribution, while the two-phase system is well mixed.

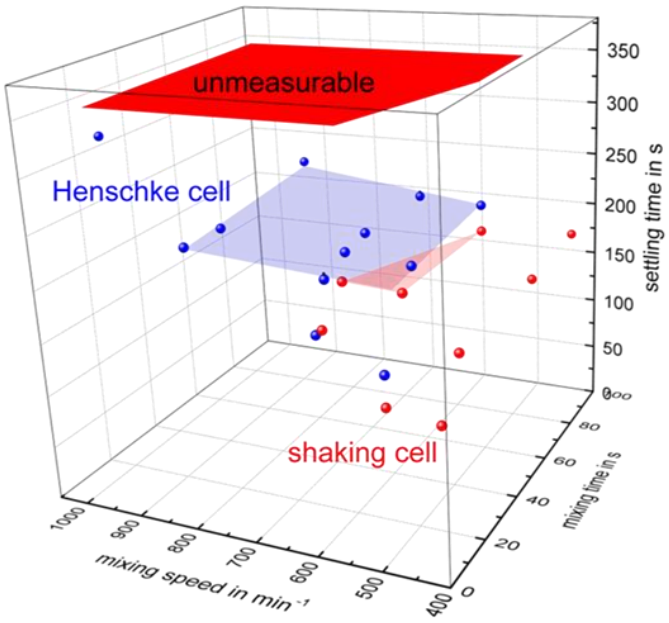

Figure 5. Evolution of the settling time with the the mixing time and the mixing speed

3.4 Studied volume

Different dispersion volumes are tested in order to evaluate the effect of air fraction in the dispersion container on the settling behavior. The results are shown in table 5. As a different filling height implies a different settling time, the experiments with low filling height are predicted with the experimental data of the experiment with high filling height in order to compare the results. The sedimentation and coalescence models are fitted to the experimental sedimentation and coalescence curves of the experiment with high filling height [4]. These parameters are then used to predict the settling behavior for the experiment with low filling height.

Table 5. Air fraction influence on the settling time

	Henschke cell (600 min^{-1}, 30 s)		shaking cell (420 min^{-1}, 15 sec)	
	800 ml	600 ml	75 ml	60 ml
settling time evaluated visually in s	245	238	180	160
settling time based on fitted models in s	232	225	190	168
prediction of the settling time based on the experiment high filling height in s		213		164

The first conclusion is that the visual criterion is in agreement with the settling time evaluated with the fitted settling curves. The predicted settling time of the low height experiment is consistent with the settling time evaluated with the fitted models for both apparatus. It proves that the air fraction does not significantly influence the settling behavior.

4. Conclusion and perspectives

The parameters investigated in this study show significant differences between the two settling cells. First, significant wall effects are observed with the shaking cell, which are responsible for a significant difference between the settling-time evaluation methods. This effect can of course also occur with the Henschke cell. Thus the visual criterion is generally recommended for evaluation of settling time. Secondly, The Henschke cell shows stability against the air exchange and the mixing parameters, e.g. the mixing time and the mixing speed. The last observed parameter, the air fraction in the cell does not seem to influence the settling behavior for both cells. As a general observation, the dispersion studied in the Henschke cell shows a settling behavior more independent of the operational conditions as compared to the shaking cell.

As a perspective, the last difference, related to the dispersion volume, will be compared between the two apparatus in order to confirm the first conclusion of this study. The design of the resulting optimized settling cell will be presented during the ISEC 2017 conference.

Acknowledgement

The project is supported by the Federal Ministry for Economic Affairs and Energy of Germany, project number: 01168585/1.

References

1) M. Henschke, L.H. Schlieper, A. Pfennig, *Chem Eng. J.,* **85**(2-3), 369-378 (2002).
2) L. Schlieper, M. Chatterjee, M. Henschke, A. Pfennig, *AIChE J.*, **50**(4), 802-811, (2004).
3) J. Villwock, F. Gebauer, J. Kamp, H.-J. Bart, M. Kraume, *Chem. Ing. Tech.* **37**(7), 1-10 (2014).
4) M. Soika, A. Pfennig, *Chem. Ing. Tech.*, **77**(7), 905-911 (2005).
5) A. Schwerin, A. Pfennig, *Ind. Eng. Chem. Res.*, **37**, 3180-3188 (1998).
6) N. Kopriwa, A. Pfennig, *Solvent Extr Ion Exc*, **34**, 622-642 (2016).

Single-Drop Experiments for Challenging Conditions as Basis for Extraction-Column Simulations

José Manuel AYESTERÁN JEREZ[1], Florian BUCHBENDER[1], Murat KALEM[2], Eva KALVODA[3], and Andreas PFENNIG[4],*

[1]*AVT - Thermal Process Engineering, RWTH Aachen University, Wüllnerstr. 5, 52062, Aachen, Germany;* [2]*Covestro Deutschland AG, Distillation & Phase Separation, 51365 Leverkusen, Germany;* [3]*TU Graz, Institute of Chemical Engineering and Environmental Technology, Inffeldgasse 25/C/II, 8010 Graz, Austria;* [4]*University of Liège, Department of Chemical Engineering - Product, Environment, and Processes (PEPs), Quartier Agora, Allée du Six Août, 11, 4000 Liège, Belgium*

Different single-drop cells are presented, which allow a very detailed evaluation of sedimentation and mass transfer for a variety of systems. This includes a cell, in which a concentration profile in the continuous phase can be imposed similar to that encountered in real extraction columns. In the cell for investigating stirred extraction columns, a method was implemented to select those drops for analysis, which did not break when passing through the stirred compartments. This allows attributing each mass-transfer result exactly to a defined drop size. Finally, reactive systems have been investigated and the results compared with a Lewis-type mass-transfer cell. It turns out that with these dedicated equipment, which can be integrated into the identical basic experimental rig, a wide variety of experiments are possible, which lead to detailed understanding of the underlying basic drop processes.

1. Introduction

Conventionally, extraction columns are designed based on pilot-plant experiments. This requires a relatively large amount of substance of at least several 100 liters for each phase. The scale-up from a pilot-plant experiment is only possible, if the type of column internals is identical in the technical and pilot-plant equipment. As a consequence, first experience-based column-type selection is required before the pilot-plant experiments can be performed. If it is later realized that the choice of column type was not optimal, significant additional effort is required. Thus a more versatile design method for extraction-column design has been developed in recent years, which is based on drop-based column simulation. This method allows prediction of column performance based on lab-scale experiments with a small amount of original material system. The results of the single-drop experiments are utilized to fit model parameters of corresponding models describing sedimentation, mass transfer, as well as coalescence and splitting, which are then used in the extraction-column simulation. This simulation method has been implemented previously as indicated in Figure 1 based on a Monte-Carlo approach to solve the population balances by regarding a suitably large ensemble of individual drops as they pass through the column [1,2]. The accuracy obtained with such a simulation is typically better than 10%. The consistency of the drop-based approach becomes obvious from its ability to even predict the limit

of operability of the extraction column by flooding with a corresponding accuracy. The drop-based approach has also proven to be accurate for challenging systems like ionic liquids and industrial systems [3,4]. To increase the accuracy of the simulation, quality and scope of the drop models need to be extended.

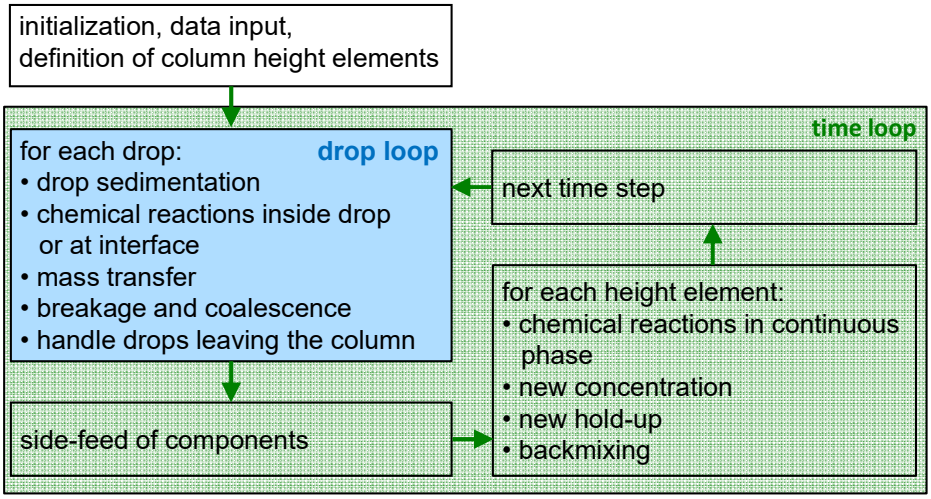

Figure 1. Principal sketch of the ReDrop algorithm.

2. Experimental

The goal of a series of studies was to challenge and extend existing drop models. For example, in typical mass-transfer cells a drop is rising in a tube filled with a continuous phase of given composition and collected after a certain rising height. Alternatively the drop is levitated in a conical cell by a counter-current flow of continuous phase [5]. In both cases the continuous phase has a constant concentration. On the other hand, in extraction columns this is not observed, since the drops instead encounter a continuous phase with a pronounced concentration profile along the column through which the sedimenting droplets pass. Also, it has been found in several studies that sedimentation velocity and mass transfer are strongly linked [6]. Thus it is actually desirable on the one hand to be able to impose a concentration profile in the continuous phase through which the drops are passing and on the other hand facilitate simultaneously measuring mass transfer and sedimentation velocity in detail. Thus a corresponding single-drop cell has been designed as shown schematically in Figure 2. In this cell layers with four different concentrations can be generated, which remain stable for extended periods of time, if the proper order with respect to density is regarded. The drops for the mass-transfer and sedimentation measurement are then produced with a computer-driven syringe and a nozzle of defined inner diameter. If the syringe and nozzle parameters are chosen appropriately, individual drops of very reproducible volume can be generated. At the top of the cell the drops are collected with a drop-collection funnel, which is again connected to a computer-driven syringe. The change in concentration between the produced and collected drops allows quantifying the mass-transfer rate. At the same time the rising drops are recorded with a video camera, which later allows detailed evaluation of sedimentation velocity. The results show that as found previously mass transfer and sedimentation velocity are linked [7,8]. The stronger mass transfer takes place, the slower the drops sediment, which can be explained by mass-

transfer induced instabilities at the interface [9,10]. On the other hand it has been shown that mass transfer can be modelled by a shell model, where an effective diffusion coefficient similar to the previous approach can be used but needs modification to obtain exact description of the experimental data [5].

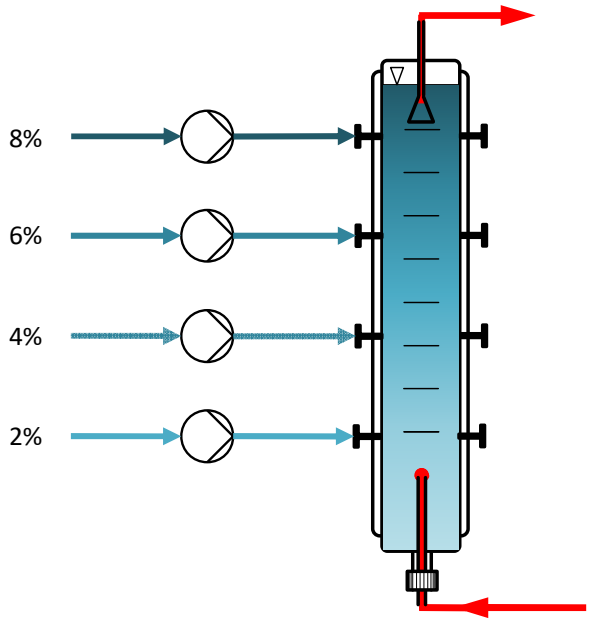

Figure 2. Mass-transfer and sedimentation cell for single-drop experiments with concentration profile

Also the influence of internals on mass transfer needs to be properly depicted by corresponding models in accurate column simulations. This requires corresponding single-drop cells for validating the models. While such cells have already been proposed for sieve trays and packings [5,11], the challenges for rotating internals are especially demanding, because chances are high that a drop will break by interaction with the stirrer or the shear region in its vicinity. To nevertheless be able to attribute an experimental datum to drops of defined diameter, a single-drop cell has been designed, which allows selecting individual drops for the measurement after they passed the internals as shown in Figure 3. In this cell a glass sphere with a conical hole is introduced, which is manually operated. If a drop did not break on its path through the cell, the larger opening of the glass sphere is oriented downward so that the drop is selected and passed into the drop-collection funnel, from where it is again withdrawn with a computer-driven syringe. In case a drop has split into several daughter drops, the opening of the glass sphere is oriented vertically, which guides the daughter drops such that they pass past the drop-collection funnel. Evaluating mass transfer in drops of defined diameter obtained with this mechanism, it turns out that while packings have essentially no influence, mass transfer is slightly enhanced by the stirring.

For modelling sedimentation in columns with rotating internals, the residence times below and above the stirring element as well as in the stirring-element zone together with the corresponding transfer probabilities between these zones have to be characterized experimentally and corresponding models derived [12]. This allows drop-based modelling, where the behavior of the individual drops is described

with a stochastic model accounting for the transfer probabilities between the different regions of the stirred compartment. This model can depict also the residence-time distribution for the drops, where some drops are caught within the compartment for some time, while others pass relatively quickly and move on to the next compartment above. The modelling approach in principle also allows drops from the compartment above to be passed on in downward direction with a certain small probability.

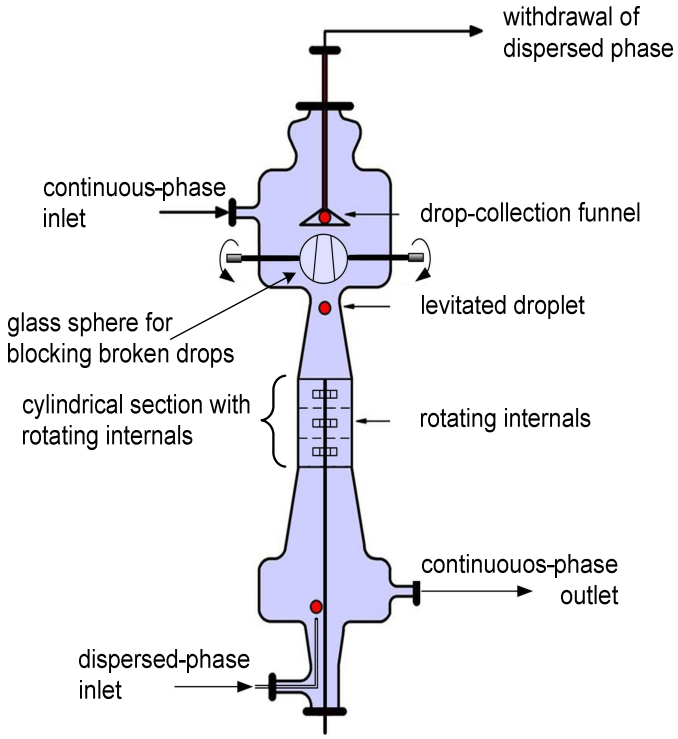

Figure 3. Mass-transfer and sedimentation cell for single-drop experiments with rotating internals

Reaction kinetics may occur on top of the mass transfer induced by Nernst distribution. This needs to be described by corresponding approaches including reaction kinetics [13,14]. If suitable models have been found, the results for drops should compare well with those obtained with a defined flat interface, e.g. for experiments performed in a Lewis-type cell [15]. It turns out that the local reaction kinetics together with the diffusive resistance need to be taken into account to obtain an appropriate description of mass transfer. Nevertheless, in the simulation of an extraction column it is possible to describe mass transfer with an effective diffusion coefficient, which takes the influence of the reactive extractant into account [14].

3. Results and Discussion

Exemplarily here the results obtained with a concentration gradient in the cell shown in Figure 2 are shown in Figure 4. The experiments were performed with the EFCE standard test system for solvent extraction water (c) + n-butyl acetate (d) and acetone as mass-transfer component. The experiments have been performed at room temperature, which varied slightly around 20°C, where for

the evaluation, the exact temperatures have been measured and the physical properties used as interpolated for that temperature. The concentration profile in the continuous phase has been varied in [8] for several characteristic cases, where in Figure 4 the results for an essentially constant slope is shown. As indicated above, the simulation of mass transfer was realized with a shell model, where the mass transfer has been described with the model proposed by Henschke [5], which has been slightly modified for the effective diffusion coefficient of the dispersed phase [8]:

$$D_{d,eff} = D_{phys} + \frac{v_\infty}{C_{prof}\left(1 + \frac{\eta_d}{\eta_c}\right)}$$

where D_{phys} is the physical Fickian diffusion coefficient of acetone in the dispersed phase, v_∞ is the sedimentation velocity of the drop as determined by independent measurements and correlated with the Henschke model as described e.g. in [6], and the η are the viscosities of the dispersed and continuous phase as indicated by the index. C_{prof} is an adjustable system-specific parameter, which has been determined to be 1785000m^{-1}. It has been shown previously that the majority of the mass-transfer resistance is located inside the drop.

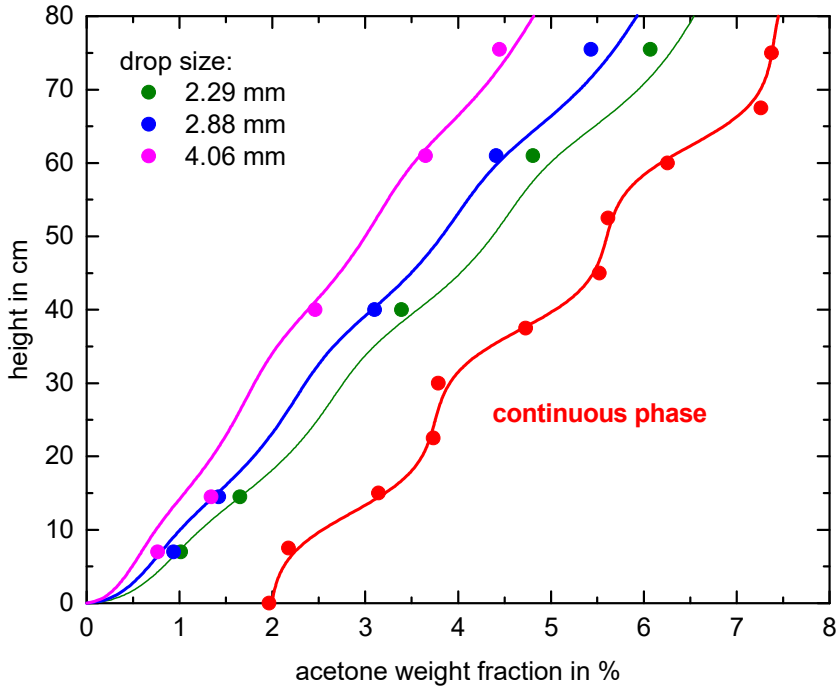

Figure 4. Mass-transfer results obtained with a concentration gradient in the laboratory cell shown in Figure 2 at room temperature for the system water (c) + n-butyl acetate (d) and acetone as mass-transfer component [8]. Model results for the drops are shown as lines.

The investigations also show that the concentration jump, which the drop encounters as it is first contacted with the continuous phase, determines, if interfacial turbulences set in, which lead to an enhancement of mass transfer by a factor of 1.5 in effective diffusion coefficient throughout essentially the entire residence time at least in the laboratory cell shown. In the case shown in Figure 3, the

Marangoni number at the interface divided by the drop diameter lies above the limit for the onset of such turbulences, which has been found to be $2.3 \times 10^{-8} m^{-1}$[8].

Overall, based on these suitably designed single-drop cells and dedicated experiments it thus turns out that conventional models need significant enhancement in order to properly describe the effects addressed, which are encountered in extraction columns under realistic conditions. The structure of such models as well as the model parameters are obtained from experiments in the measuring cells described. Besides deriving improved detailed models, the insights gained can also be used directly to optimize extraction-column performance. Thus, a proposal for reducing the volume of stirred columns without significant effect on drop residence times has been derived and experimentally validated. This optimized stirred compartment is based on the insight that the residence time of drops below the stirrer is short and that this volume can thus be deleted with only little effect on separation performance. This leads to a stirrer position, which not vertically centered in the compartment but closer to its lower stator [12].

References

1) M. Kalem, F. Buchbender, A. Pfennig. *Chem. Eng. Res. Des.,* **89**(1), 1-9 (2011).
2) A. Pfennig, T. Pilhofer, J. Schröter, in R. Goedecke, Fluid-Verfahrenstechnik, Wiley-VCH, Weinheim, 907-992 (2006).
3) F. Buchbender, F. Onink, W. Meindersma, A. de Haan, A. Pfennig, *Chem. Eng. Sci.*, **82**, 167-176 (2012).
4) F. Buchbender, M. Schmidt, T. Steinmetz, A. Pfennig, *Chem. Ing. Techn.*, **84**, 540-546 (2012).
5) M. Henschke, A. Pfennig, *AIChE J*., **48**(2), 227-234 (2002).
6) M. Kalem, M.Y. Altunok, A. Pfennig, *AIChE J.*, **56**(1), 160-167 (2010).
7) E. Cvetkovic, A. Pfennig, Proceedings of the 7th International Berlin Workshop on Transport Phenomena with Moving Boundaries and More, 30th-31st October, Berlin, Germany (2014)
8) E. Kalvoda, Ph.D. thesis, TU Graz, https://diglib.tugraz.at/download.php?id=5891c8d717f30&location=browse, (2016).
9) A. Pfennig, *Chem. Eng. Sci*., **55**(22), 5333-5339 (2000).
10) R. Schott, A. Pfennig, *Mol. Phys*., **102**(4), 331-339 (2004).
11) H.-J. Bart, D. Garthe, T. Grömping, A. Pfennig, S Schmidt, J. Stichlmair, *Chem. Ing. Techn*. **78**(5), 543-547 (2006).
12) F. Buchbender, A. Fischer, A. Pfennig, *Chem. Eng. Sci.,* **104**, 701-716 (2013).
13) M.Y. Altunok, M. Kalem, A. Pfennig, *AIChE J*., **58**(5), 1346-1355 (2012).
14) M. Kalem, Einzeltropfenbasierte Simulation von pulsierten Siebbodenkolonnen für die Reaktivextraktion, Shaker Verlag, Aachen, 2015.
15) E. Bertakis, M. Kalem, A. Pfennig, *Chem. Eng. Sci*., **63**(19), 4881-4887 (2008).

Centrifugal Liquid-Liquid Separation - Experimental Investigation and Simulation of Single Drops and Droplet Swarms

Armin EGGERT[1,*], Stephan SIBIRTSEV[1] and Andreas JUPKE[1]

[1] *AVT - Fluid Process Engineering, RWTH Aachen University, Forckenbeckstraße 51, 52074 Aachen, Germany,*

Fundamentals of the liquid-liquid separation behavior, sedimentation and coalescence, under enhanced force field – the centrifugal field – are investigated experimentally and simulated by detail models. The single drop sedimentation shows an angular deflection against the radial trajectory. Further, a decrease of the sedimentation velocity due to the radial deceleration within the centrifugal force field is determined. The single drop sedimentation, the influences of droplet diameter and rotation speed are presented by radius-angle coordinates and by radius/angle-time coordinates. In addition the liquid-liquid separation with an increased organic droplet hold-up is presented. Compared to the single drop sedimentation a significant lower sedimentation velocity of the droplet swarm is observed. Finally the influence of the droplet swarm on the sedimentation velocity is discussed. Thus, to take the geometric feature of the cylindrical equipment into account of the swarm impact a correlation is developed by a modification of the droplet swarm model.

1. Introduction

Gravity separation of liquid-liquid mixtures - e.g., in settling tanks – is well investigated. Major phenomena of the separation behavior, e.g., the flow pattern, are understood in detail. Thus, sedimentation as well as coalescence effects of single drops and droplet swarms are combined for reliable settler design by a nowadays established experimental lab-scale/model-based approach [1]. However, for centrifugal liquid-liquid separation - e.g., in tube centrifuges, shown by the colored rotor zone of the Annular Centrifugal Contactors (ACC) in Figure 1 - only a few detailed investigations are given in available literature.

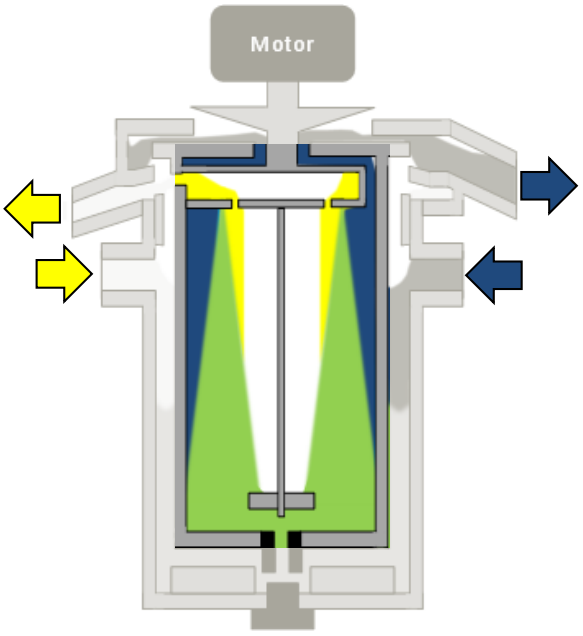

Figure 1. Schematic of an Annular Centrifugal Contactor (ACC), inflow and outflow of the heavy phase (blue), the light phase (yellow) and the centrifugal separation of their mixture (green) within in the rotor-zone.

Despite that an optical validation of the liquid-liquid separation within the rotor of an ACC is not possible Computer Fluid Dynamic (CFD) simulations are investigated by different authors [2–5]. Further a first approach for the determination of the single fluid flow pattern with the particle image velocimetry (PIV) method could be found [6]. An empiric correlation, developed by black box investigation of separation efficiency is given in the general form by Equation (1) [7]. N_{Di} is called the "Dispersion Number" and proposed a relation between the acceleration of a disperse system and the overall separation time t for a fixed geometric $\Delta Z = r_o - r_i$, meaning the outer and inner diameter of the rotor zone.

$$N_{Di} = \frac{1}{t} \cdot \sqrt{\frac{\Delta Z}{a}} = \frac{1}{t} \cdot \sqrt{\frac{r_o - r_i}{a}} \quad (1)$$

More detailed investigation of the drop motion, preferably the motion of droplet collectives and their coalescence behavior within the centrifugal force field is carried out for the Podbielniak differential centrifugal extractor [8–10]. Also, the sedimentation is discussed for monodispersed drop strings [11]. However, a broad knowledge gap exists in the detailed understanding and research of centrifugal continuously liquid-liquid separation in the rotor zone of an ACC. Thus, this contribution focuses on the major liquid-liquid separation effects and their quantification within a centrifugal force field. The single drop sedimentation and the liquid-liquid separation will be characterized by sedimentation, coalescence and the overall separation time as done for the gravitational settling tank. Furthermore, the individual models will be combined for a model-based centrifugal equipment design.

2. Experimental

2.1 Chemical system

For experimental investigations n-butanol/water and toluol/water were chosen as liquid-liquid systems. Their physical properties are summarized in Table 1. N-butanol was provided by Merck, Darmstadt, Germany, with a purity of 99 %. Toluol was provided by CarlRoth, München, Germany, with a purity of 98 %. The aqueous phase was deionized and distillated in a MonoDest3000 distillery from Lenz Glas Instrumente, Wertheim, Germany. Furthermore sodium chloride (NaCl), provided by Merck, Germany, with purity of 99 %, was used for water conditioning – 5 g_{NaCl}/kg_{H2O}.

Table 1. Physical properties of saturated liquid-liquid systems

System		ρ [kg/m³]	η [mPas]	σ [mN/m]	phase state
1	water	987	1,463	1,75	continuous
	n-butanol	846	3,32		dispersed
2	water	999	1,323	3,8	continuous
	toluol	867	2,31		Dispersed

2.2 Experimental setup

Experiments for single drop sedimentation and liquid-liquid separation behavior of droplet

swarms within the centrifugal field are performed with two different experimental set-ups at laboratory scale, as shown in Figure 2. The set-up on the left side (A) enables a single drop induction by a capillary system. The set-up on the right side (B), the stirred centrifugal batch settling cell (SCBSC) [12], enables the mixing and the separation of a liquid-liquid system by a rotor-rotor/stator concept. Both, the centrifugal cell body and the agitator are driven by separate electric motors. Thus, the elements can run synchronously or with a differential rotational speed, $\Delta n = n_C - n_A$. For chemical resistance all components of the SCBSC are made out of stainless steel (1.4401), polypropylene (PP), polytetrafluorethylene (PTFE) and glass.

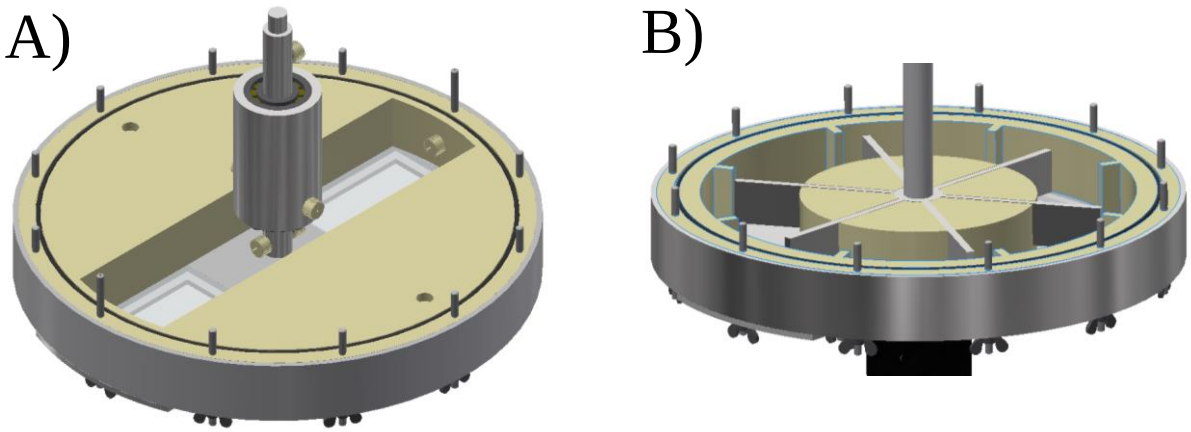

Figure 2. Experimental set-up for A) single drop sedimentation and B) liquid-liquid separation – the SCBSC – investigation within the centrifugal field.

For the optical observation a high speed video camera (type: Os4S1-C-O4, 8 GB DDR working storage, 512 GB SSD intern storage, 1024x1024 pixels, 6.000 frames per second (fps), supplied by Imaging Solutions GmbH, Eningen, Germany) with a camera objective (type: LM16HC, 1'' 16mm/F1.4, supplied by Kowa Optimed Deutschland GmbH, Duesseldorf, Germany) is used. The camera focused on the centrifugal cell front surface with integrated glass windows. The camera is triggered by a laser light barrier and a trigger marker on the cylinder wall. Camera and recording settings are controlled via Ethernet linkage and the Motion Studio PC software (v. 2.12.05). For a sufficient lighting performance, required for short exposure times, a 500 W light emitting diode (LED) is used. The 500 W LED is powered by a direct current (DC) laboratory power supply (type: PS 8360-10 T, 0…360 V, 0…10 A, up to 1,000 W, supplied by Elektro-Automatik GmbH & Co. KG, Viersen, Germany).

2.3 Analytical method

The analytical method is based on the optical observation of the droplet sedimentation and the liquid-liquid separation during the centrifugation process. The sedimentation and separation progress is quantified by path-time coordinates following a radial trajectory to the axis of rotation. Each path coordinate includes a value for the sedimentation (radial, azimuthal) and coalescence progress. In this way, the characteristic separation curves, sedimentation and coalescence, are determined.

3. Simulation

3.1 Model

The theoretical part of this work focuses on the implementation of a single drop motion model for the calculation of the single drop sedimentation velocity v_∞ and further the combination with a droplet swarm correlation for the calculation of the droplet swarm sedimentation velocity v_{DS}.

The particle motion model in the most general form is given in Equation (2) [13], where ρ is the density of the disperse or continuous phase, W the velocity of the droplet, ω the angular frequency, r the radius, V the droplet volume and η the viscosity. In contrast to the gravitational force field the unsteady acceleration is considered by the added mass and Basset history term. From literature work the including constants are set to $\Delta_A = 2.0$ and $\Delta_H = 0.48$ [14]. Especially the estimation and the use of a valid drag force coefficient c_D correlation, as given in Equation (3) [15] as a function of the droplet Reynolds number, was a necessary work before the swarm influence could be focused on.

$\rho_d V_d \frac{dW}{dt} = V_d(\rho_d - \rho_c)\omega^2 r - \frac{1}{2} V_d \rho_c c_D W^2 - \Delta_A \frac{1}{2} V_d \rho_c \frac{dW}{dt}$	
$-\frac{3}{2}\Delta_H {d_d}^2 \sqrt{\pi \rho_c \eta_c} \int_0^t \left(\frac{\left(\frac{dW}{dt}\right)_{t=\tau_1}}{\sqrt{t-\tau_1}} \right) d\tau_1$	(2)
$c_{D,\infty} = 239 / {Re_\infty}^{0.956}$	(3)

For the calculation of the droplet swarm sedimentation velocity the definition of the Reynolds Droplet Swarm Re_{DS} as given in Equation (4) and the empirical model proposed as given in Equation (5) [16] with the organic hold-up ε and the Hadamard-Rybczynski-correction factor are used. For the prediction of the droplet swarm drag coefficient c_{D_DS} Equation (6) is applied.

$$Re_{DS} = \rho_c v_{DS} \Phi_{32,0} / \eta_c \tag{4}$$

$$Re_{DS} = 3zq^2\varepsilon_0 / c_w' q^3 (1-\varepsilon_0) \left(\sqrt{1 + c_w' q^3 (1-\varepsilon_0)^3 / 54 (zq^2)^2 {\varepsilon_0}^2 \, Ar} - 1 \right) \text{ with:} \tag{5}$$

$$q^3 = 5 \left(\varepsilon_0 / 1-\varepsilon_0 \right)^{0,45} K_{HR}^{-3/2}$$

$$zq^2 = \frac{1-\varepsilon_0}{2\varepsilon_0 K_{HR}} \exp\left(2.5\varepsilon_0 / 1-0.61\varepsilon_0 \right) \quad \text{for } 0.06 \le \varepsilon_0 < 0.55$$

$$zq^2 = 2.2 \frac{1-\varepsilon_0}{2\varepsilon_0 K_{HR}} \exp\left(0.44\varepsilon_0 / 1-0.61\varepsilon_0 \right) \quad \text{for } 0.55 \le \varepsilon_0 < 0,74$$

$$c_{D\_DS} = c_{D,\infty}(1-\varepsilon_0)^{-2n} \quad \varepsilon(r_{DS})/\varepsilon_0 \tag{6}$$

Finally, the increase of the initial droplet hold-up is modified and takes into account the geometric influence / radial impact by the correlation as shown in Equation (7).

$$\varepsilon(r_{DS}) = \varepsilon_0 \quad r_0/r_{DS} \tag{7}$$

4. Results and Discussion

4.1 Single drop sedimentation

Figure 3 shows an experimental result of the single drop sedimentation for the toluol/water-system. For illustration and better understanding of the presented radius(y)-angle(x) coordinate pairs an image from the experimental work is given in the figure where drops are marked with withe cycles. The rotational speed is set to n = 1100 rpm. Depending on the used nozzle the centrifugal force leads to a drop diameter of d_T = 0.8 mm. Also the model-based calculated drop trajectory is plotted in the figure. Both, the experiment and the simulation are in good agreement. Moreover, the single drop motion model matches the experimental data quite well. The radius-angle relation shows the Coriolis Effect. Hence, the single drop motion is affected by the drop diameter, the liquid-liquid system properties, especially the density difference and continuous phase viscosity, and centrifugal operating parameters.

The sedimentation progress in radius(y)-time(x) coordinates is shown in Figure 4. It is anticipated that the sedimentation describes a nonlinear sedimentation pathway over the time. This could be observed by a decrease of the radial distance between the drops. This effect is explainable by the centrifugal acceleration based unsteady sedimentation velocity. Thus, the negative gradient of the centrifugal field which leads to a deceleration, affected the drop motion.

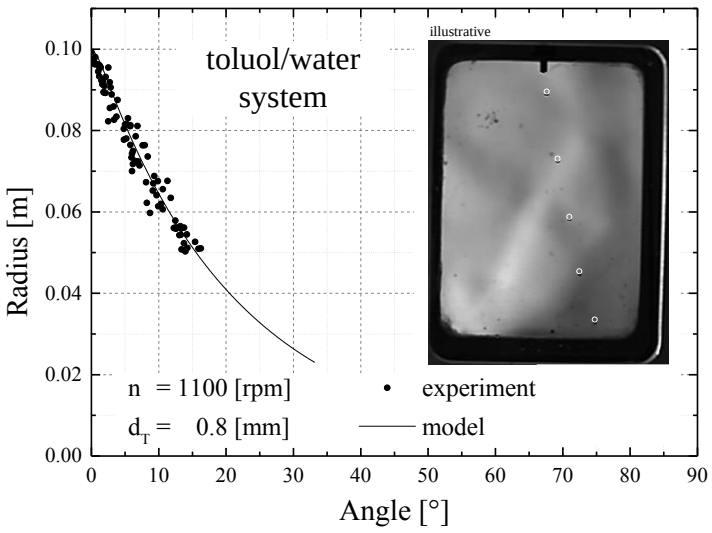

Figure 3.
Single drop investigation - result for droplet (d_T = 0.8 mm) sedimentation at n = 1100 rpm. The diagram shows an experimental evaluation of the droplet trajectory (●) and the simulated drop motion (·····) by radius-angle coordinates. The image shows the experimental evaluation with marked drops.

4.2 Liquid-liquid separation

Figure 4 shows an experimental result of the liquid-liquid separation of the n-butanol/water-system. The differential rotational speed for mixing is set to $\Delta n = 500$ rpm and the rotational speed for separation is set to $n = 1100$ rpm. The phase ratio is $V_{org}:V_{aq} = 1:1$ and thus, the start hold-up is $\varepsilon_0 = 0.5$. For the illustration and better understanding of the experimental result images from different separation times are given in the Figure. Depending on the centrifugal field the organic disperse phase flows from the outer to the inner radius. Opposite the coalescence occurs from inner to outer radius. In the pictures the dispersion band and thus the sedimentation as well as the coalescence front can be identified clearly. Furthermore, the shadow in the bottom shows the displacer of the CSBSC which enables the mixing process without a gas hold-up in the entire volume. Compared to the single drop sedimentation the sedimentation curve describes a nonlinear path way. While sedimentation starts instantaneous the coalescence starts delayed. This phenomenon is explainable by the linear increase of the location-depended centrifugal acceleration. Subsequently, the initial drop hold-up increases along the radial trajectory before coalescence takes place. Thus, the geometric impact needs to be considered in the model approach.

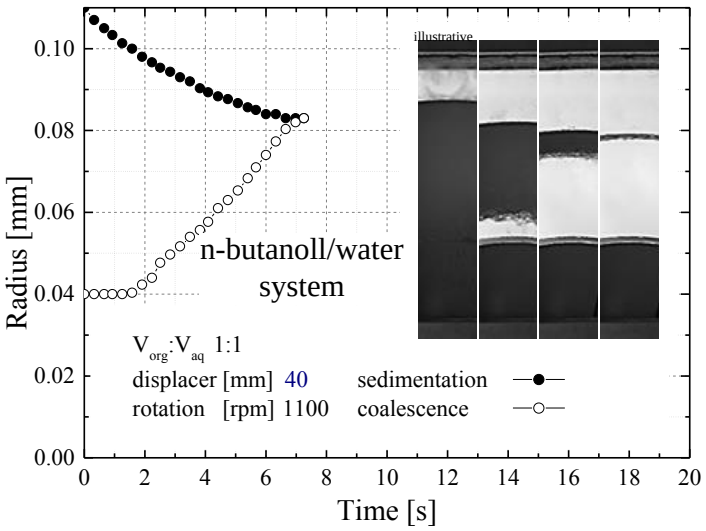

Figure 4. Liquid-liquid separation - droplet swarm sedimentation and coalescence. The picture show an experimental result for the separation progress ($\varepsilon_0 = 0.5$) at $n = 1100$ rpm and the diagram shows an experimental evaluation of the sedimentation (●) and coalescence (○) by radius-time coordinates.

4.3 Swarm impact

Figure 3 shows a simulation result for the single drop and droplet swarm sedimentation behavior. The rotational speed is set to $n = 1100$ rpm and the hold-up is set to $\varepsilon_0 = 0.5$. The drop diameter is $d_d = 0.6$ mm. Based on the simulation results the impact of the drop hold-up is shown qualitatively. The change in radial position is plotted in black lines and the calculated sedimentation velocity in red lines. The single drop results are visualized by the solid lines, the droplet swarm with a constant hold-up by dashed lines and the influence of the geometric impact with an increasing radial hold-up by dotted lines. The droplet swarm influences the free sedimentation by a higher droplet hold-up. Thus, in the shown figure the sedimentation velocity decreases significantly compared to the single drop trajectory. Depending on the slower sedimentation velocity the radial position of the sedimentation

front decreases slower. This results in an increase of the overall sedimentation time. Further, another difference is visualized by the hold-up correction. In the beginning, the initial hold-up and thus the sedimentation velocity are the same, then the theoretical increase of the circumference related hold-up leads to a distinct swarm impact. However, the sedimentation limit depends on the abstraction and model description. As shown in Figure 3 the phase boundary level for the liquid-liquid separation of an entire hold-up of $\varepsilon_0 = 0.5$ and the displacer is up to $r_E > 0.08$ m.

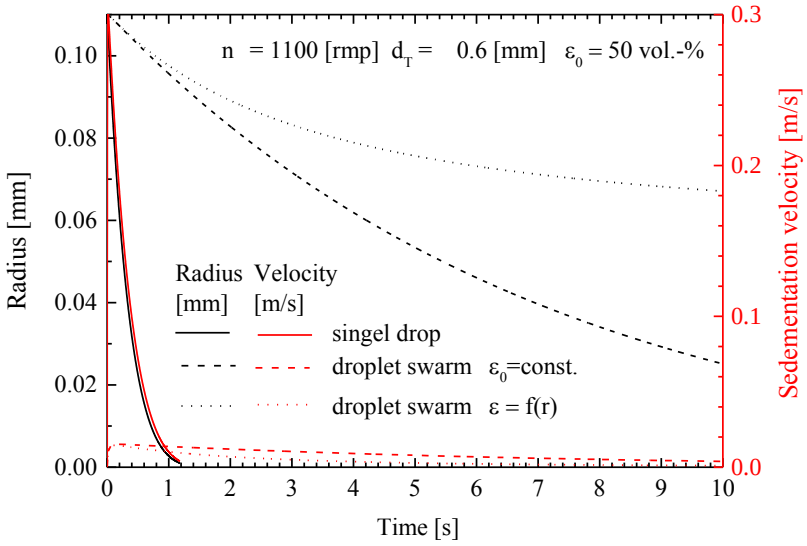

Figure 5.
Simulation results for the radial sedimentation (black) and the sedimentation velocity (red) for a single drop (——) and a droplet swarm with constant hold-up (- - -) and increasing hold-up (· · ·). The rotational speed is n = 1100 rpm, the droplet diameter is $d_T = 0.6$ mm and the start hold-up is $\varepsilon = 0.5$.

5. Conclusion

Centrifugal singel drop sedimentation and liquid-liquid separation investigations were demonstrated sucsessfully. The liquid-liquid separation experiments are characterized by sedimentation, coalescence and the overall separation time. Model approches from gravitational investigations are sucessful implemented and combined for the centrifugal field. A modification of the droplet swarm model considered thecylindric geometirc impact. Thus, a significant decrease of the sedimentation velocity of the droplet swarm in comparison to singel drops is shown.

Acknowledgement

This work was performed as part of the Cluster of Excellence “Tailor-Made Fuels from Biomass”, which is funded by the Excellence Initiative by the German federal and state governments to promote science and research at German universities. Further, the authors thank RWTH Aachen University – department 4.1 Technology Transfer for the assumption of the patent application.

References

1) M. Henschke, *Fort. Berichte VDI*, **379**, (1994).
2) S. Li, W. Duan, J. Chen, J. Wang, *Ind. Eng. Chem. Res.,* **51**, 11245–11253, (2012).
3) N.T. Padial-Collins, D.Z. Zhang, Q. Zou, X. Ma, W.B. VanderHeyden, *Separation Science and Technology*, **41**, 1001–1023 (2006) 1001–1023.
4) J. Patra, N.K. Pandey, U.K. Muduli, R. Natarajan, J.B. Joshi, *Chem. Eng. Commu.*, **200**, 471–493, (2013).
5) S. Vedantam, K.E. Wardle, T.V. Tamhane, V.V. Ranade, J.B. Joshi, *Int. Journal of Chemical Engineering*, **94**, 1-31, (2012).
6) Y. Xu, J.-g. Wang, S.-l. Zhao, Z.-s. Bai, *Chem. Eng. Res. Des.*, **94**, 691-701 (2015).
7) R.A. Leonard, G.J. Bernstein, R.H. Pelto, A.A. Ziegler, *AIChE J.*, **27**, 495-503, (1981).
8) F. Otillinger, *Technical Universität Munich*, (1988).
9) M. Stölting, *Technical Universität Munich*, (1979).
10) R. Schilp, *Technical Universität Munich*, (1979).
11) Y. Jammoal, J. Lee, *Chemical Engineering Research and Design*, **104**, 638-646, (2015).
12) A. Eggert, *German Patent and Trademark Office*, (2016).
13) M.R. Maxey, J.J. Riley, *Physics of Fluids* **26**, 883-889 (1983).
14) D.J. Vojir, E.E. Michaelides, *Int. Journal of Multiphase Flow*, **20**, 547-556, (1994)
15) T. Fukada, S. Takeuchi, T. Kajishima, *Int. Journal of Multiphase Flow*, **85**, 298-313 (2016)
16) T. Pilhofer, D. Mewes, *Verlag Chemie*, (1979).

Adsorption of Indium and Gallium on Natural Banana Fiber

Tetsuto KAJIYAMA[1,*], KensukeARAI[2] and Hisao KOKUSEN[3]

[1]*Jonan Branch, Regional Technology Support Division, Commercialization Support Development, Tokyo Metropolitan Industrial Technology Research Institute, Minamikamata 1-20-20, Ota, Tokyo 144-0035, Japan;* [2]*Division of Physical and Analytical Chemistry, Nihon Pharmaceutical, University, Komuro 10281, Ina, Kitaadachi, Saitama 362-0806, Japan;* [3]*Department of Chemistry, Tokyo Gakugei University, Nukuikitamachi 4-1-1, Koganei, Tokyo 184-0015, Japan*

Adsorption properties of indium and gallium ions were investigated and concentrations of metal ions measured by inductively coupled plasma atomic emission spectroscopy. The adsorption of indium ions by non-treated banana fiber increases with pH. The adsorption percentage of indium ion by non-treated banana fiber increases with increasing of pH. In the pH range between 1.0–2.0 and 3.5–5.0, adsorption of indium ion was 20%–40% and 40%–80%, respectively. For the case of gallium, there was no adsorption of gallium ions by non-treated banana fiber over the pH range 1.0–5.0. Such distinct behavior of these two metal ions raises the possibility of the utilization of banana fibers in the separation and adsorption of metal ions. It should be noted that it is not possible to separate In^{3+} or Ga^{3+} through the use of alkali-treated banana fiber.

1. Introduction

Over a billion banana stalks are thrown away every year. Recently, banana fiber has attracted attention as an inedible natural resource. As a result, the effective use of banana fiber has been studied as a valuable recyclable biomass material. In previous studies, banana fiber/poly(butylene succinate) composites using hexamethylene diisocyanate as a reactive compatibilizer, were investigated [1]. It was found that alkali treatment of banana fibers and an addition of hexamethylene diisocyanate improved the adhesion between banana fibers and poly(butylene succinate). It is therefore both important and interesting to investigate other uses of banana fibers. Several methods have been developed to collect and separate metal ions, including ion-exchange and solvent extraction techniques. In particular, environmentally friendly ion-exchange systems and the use of chelated materials to collect and separate metal ions, have been investigated by many researchers. Gupta et al., reported that banana fibers were used as an adsorbent for the removal of malachite green dye [2]. Haris and Sathasivam reported that banana fibers were used as an adsorbent for the removal of methyl red from aqueous solutions [3–4]. However, as far as it is known, the investigation of banana fibers (or chemically modified banana fibers) for use as an adsorbent for various metal ions, has not been reported. In recent studies carried out by this research group, the adsorption properties of modified and non-modified banana fiber with respect to transition metal ions, rare metal ions and cesium ions have been evaluated [5–7]. Rare metals are important in many fields in particular that of advanced material

science where their application has increased significantly. In the present study, the adsorption properties of banana fibers with respect to indium and gallium were evaluated. Results obtained show the possibility of utilizing banana fibers as an efficient adsorbent for metals ions.

2. Experimental

2.1 Materials

Non-treated banana fiber (Figure 1) was obtained from the Republic of the Philippines and used without further purification or surface treatment. Alkali-treated banana fiber was obtained by treating 100 g of banana fiber with 3.0 dm^3 of 20 wt% NaOH aqueous solution (aq) at room temperature for 2 hours [7]. The resulting alkali-treated banana fiber (Figure 2) was washed with water and dried overnight in a vacuum oven at 70 °C. All chemicals were purchased and used without further purification.

Figure 1. Non-treated banana fiber.

Figure 2. Alkali-treated banana fiber.

2.2 Adsorption of indium and gallium ions by non-treated banana fiber or alkali-treated banana fiber

Non-treated and alkali-treated banana fibers were cut into 5 mm lengths (Figure 3 and 4).

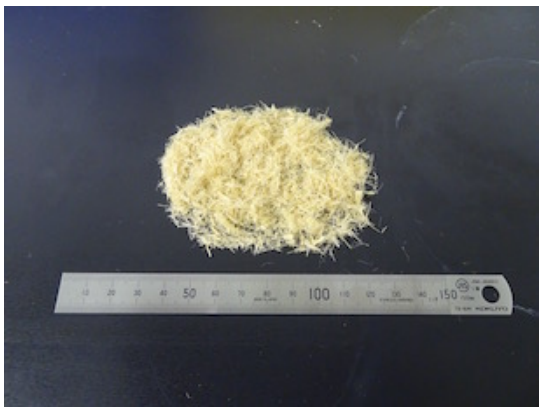

Figure 3. Non-treated banana fiber. The banana fiber was cut into the lengths of 5 mm.

Figure 4. Alkali-treated banana fiber. The banana fiber was cut into the lengths of 5 mm.

Aqueous solutions were prepared containing 1.0×10^{-4} mol dm^3 metal ions (In^{3+} and Ga^{3+}), 1.0×10^{-1} mol dm^3 sodium perchlorate and 1.0×10^{-2} mol dm^{-3} acetic acid. A 30 cm^3 aliquot of each solution, along with 0.3 g of the metal ion adsorbent, was placed into plastic tubes. The tubes were shaken at room temperature for five days. This time length was selected for the purpose of comparison with previously unpublished work completed in this research group. On completion of the reaction, the mixed solutions were filtered. The concentration of the metal ions was then measured by an inductively coupled argon plasma atomic emission spectroscope (ICP-AES). The pH value of the aqueous phase was measured by a pH meter equipped with glass electrodes.

2.3 SEM observation

The surface of the banana fibers was investigated through the use of a scanning electron microscope (SEM).

2.4 Characterization of non-treated and alkali-treated banana fiber

The FT-IR spectra were obtained with the use of a FT-IR spectrometer.

3. Results and Discussion

3.1 Adsorption of indium and allium ions by non-treated banana fiber

Figure 5 shows the percentage adsorption of In^{3+} and Ga^{3+} as a function of pH. The adsorption of In^{3+} increases with pH with 20%–40% adsorption in the pH range 1.0−2.0. Adsorption of 70%–80% was observed in the pH range 3.5–5.0 and maximum adsorption of approximately 90% was seen at pH 3.0. In the case of Ga^{3+} no adsorption was observed over the pH range 1.0–5.0. These results therefore show good separation of In^{3+} and Ga^{3+} ions over the pH range 1.2–5.0. Lignins or other functional group originating from banana fiber are considered to be the adsorption sites of In^{3+} ions.

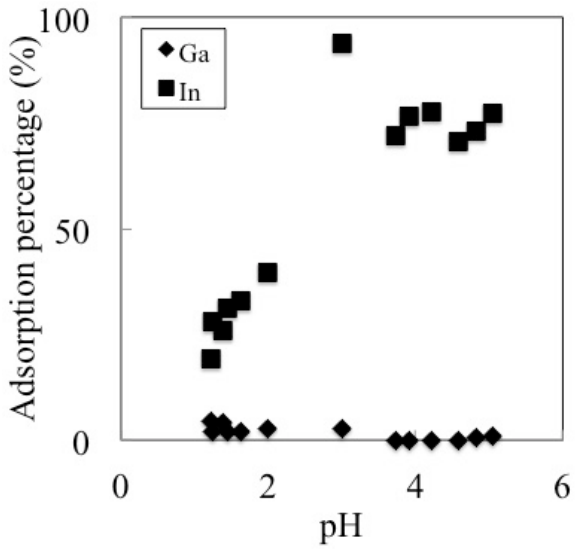

Figure 5. Effectof pH on the adsorption of In^{3+} and Ga^{3+} ions by non-treated banana fiber [9].

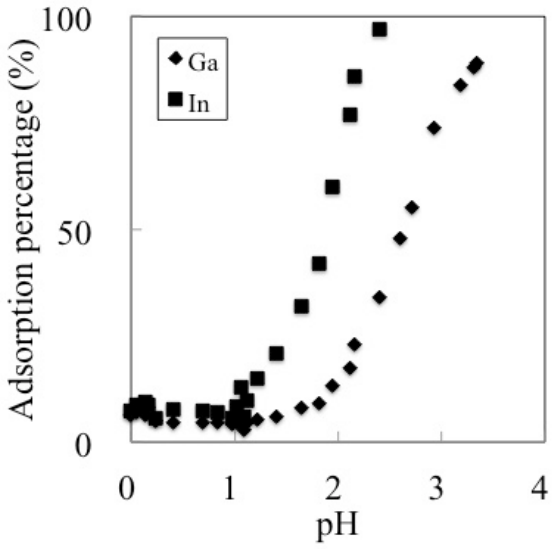

Figure 6. Effectof pH on the adsorption of In^{3+} and Ga^{3+} ions by alkali-treated banana fiber [9].

3.2 Adsorption of indium and gallium ions by alkali-treated banana fiber

Figure 6 shows the percentage adsorption of In^{3+} and Ga^{3+} as a function of pH. Adsorption properties of In^{3+} show approximately 100% adsorption at pH 2.3. A pH of 2.0 corresponds to 60% adsorption, while in the pH range from 0.1 to 1.0, no adsorption occurred. Adsorption properties of Ga^{3+} show approximately 90% adsorption at pH 3.4. A pH of 2.8 corresponds to 50% adsorption, while in the pH range 0.1 to 1.3, no adsorption occurred. These results indicate the possibility of utilizing banana fibers as a rare metal ion adsorbent. Because of the adsorption properties of alkali-treated banana fiber with respect to In^{3+} and Ga^{3+}, this material does not act as an efficient seperater and adsorber of these metal ions.

3.3 Difference between non-treated and alkali-treated banana fibers

The SEM images of the surface of non-treated and alkali-treated banana fibers are shown in Figure 7 and 8. The banana fibers purchased from the Republic of the Philippines were virtually untreated. They were only washed with soap and water thereby leaving much of the lignin and hemicellulose intact. Banana fibers comprise approximately 9% lignin, 39% hemicellulose, 43% cellulose, and many other compounds [8]. The smooth surfaces of the banana fibers transformed into a wavy morphology after alkali treatment and the lignin and hemicellulose originally from the banana fiber were removed by this treatment. Consequently, originated from the cellulose existed on the surfaces of the alkali-treated banana fiber.

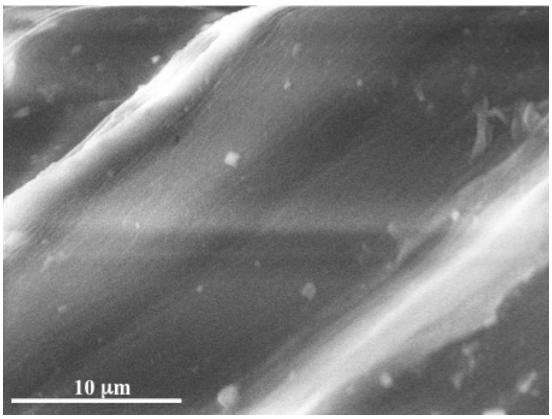

Figure 7. SEM image of non-treated banana fiber.

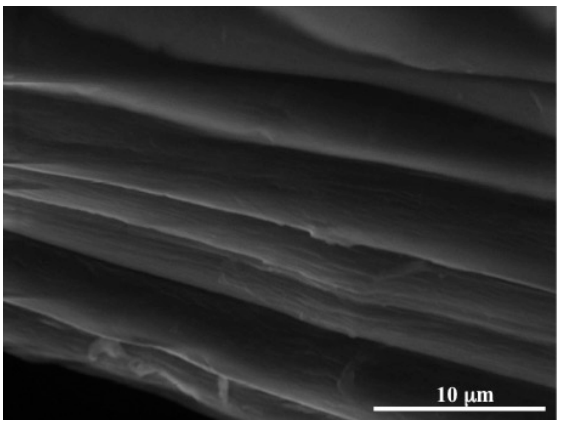

Figure 8. SEM image of alkali-treated banana fiber.

Lignin in banana fiber was identified with FT-IR. Figure 9 shows FT-IR spectra of non-treated and alkali-treated banana fibers. The two spectra show different bands around 1620 cm^{-1} and these are due to C=C groups found in lignin. Lignins or other functional groups originating from banana fiber are considered the adsorption sites of In^{3+} and Ga^{3+}. Almost all lignin present in the banana fiber was removed by sodium hydroxide alkali treatment. This factor is considered to explain the observed differences in the adsorption behavior of non-treated and alkali-treated banana fiber. However, the exact adsorption mechanism of the metal ions into banana fiber could not be analyzed in detail.

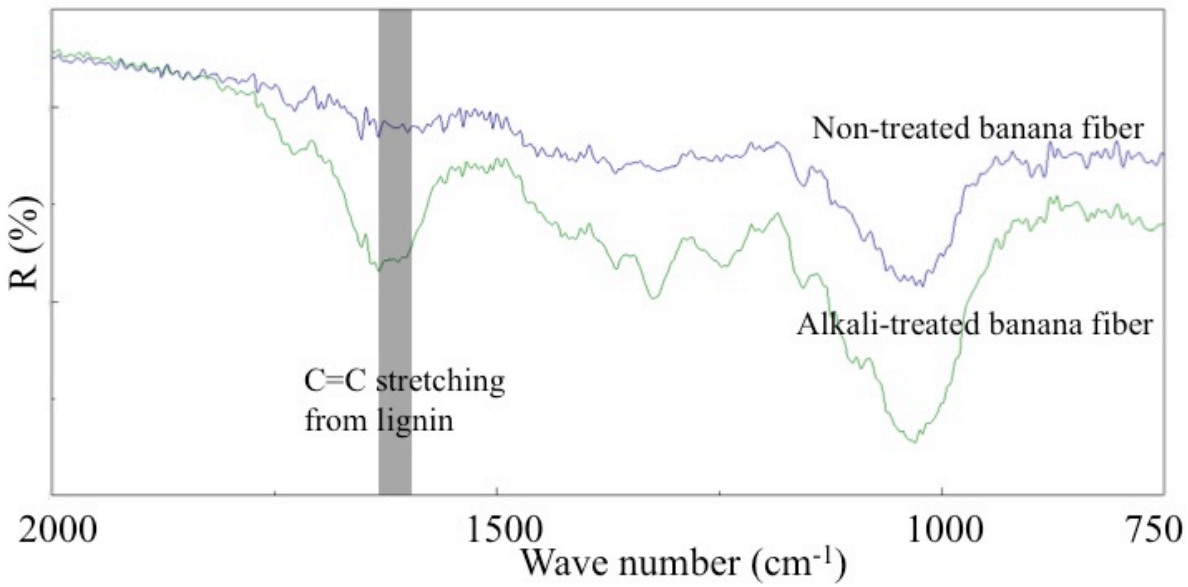

Figure 9. FT-IR spectra of non-treated and alkali-treated banana fibers.

4. Conclusion

The adsorption of indium ions (In^{3+}) by non-treated banana fiber increases with pH. An adsorption of 20%–40% is observed in the pH range 1.0–2.0. For the pH range 3.5–5.0 an adsorption of 70%–80% is seen. A maximum adsorption of 90% is measured at pH 3.0. In the case of gallium ions (Ga^{3+}) and non-treated banana fiber, no adsorption was observed over the pH range 1.0 - 5.0. Due to the different adsorption behavior of untreated banana fiber over the pH range 1.0–5.0 for the ions In^{3+} and Ga^{3+}, the possibility of utilizing this material as an adsorbent and separator for these metal ions is illustrated. Results showed that alkali-treated banana fiber cannot function in a similar manner.

Acknowledgment

This research was supported by the Environment Research and Technology Development Fund (3K143003) of the Ministry of the Environment, Japan.

References

1) T. Kajiyama, T. Yasuda, S. Mimoto, K. Shimizu, K. Hayashi, T. Yamanaka, M. Murakami, *Int. Polym. Process*, **28**, 58–63(2013).
2) N. Gupta, AK. Kushwaha, MC. Chattopadhyaya, *J. Chem.Pharm. Res.*, **3**, 284–296 (2011).
3) MRHM. Haris, K. Sathasivam, *Am. J. Appl. Sci.*, **6**, 1690–1700 (2009).
4) MRHM. Haris, K. Sathasivam, *Arch. Appl. Sci. Res.*, **2**, 209–216 (2010).
5) T. Kajiyama, S. Sakai, J. Inoue, T. Yoshino, S. Ohmuro, K. Arai, H. Kokusen, *J. Ion. Exchange*, **25**, 155–159(2014).
6) T. Kajiyama, S. Sakai, J. Inoue, H. Kokusen, *J. Ion. Exchange*, **27**, 57–62(2016).
7) T. Kajiyama, H. Kokusen, *J. Ion. Exchange*, **27**, 8–12(2016).

8) N. Venkateshwaran, A. Elayaperumal, *J. Reinf. Plast. Comp.*, **29**, 2387–2396 (2010).
9) These data were first presented at IEX 2016.

Solvent Extraction of Electrolyte Compounds in the Recycling of Lithium Ion Batteries

Paul HAAS[1,*], Stefan PFEIFER[1], Jannes MÜLLER[1] and Stephan SCHOLL[1]
[1]*TU Braunschweig, Institute for Chemical and Thermal Process Engineering, Langer Kamp 7, 38106 Braunschweig, Germany*

The extraction of lithium hexafluorophosphate from lithium ion batteries with organic solvents is a promising possibility to remove the conducting salt and recover organic compounds. The influence of temperature onto degradation and extraction was investigated. Multi-stage cross-flow extractions have been performed with dimethyl carbonate as extractant and a combination with a second set of extractions with water. The experiments have been performed in a stirred vessel with 0.5 L volume in inert gas atmosphere. The samples have been analyzed by ion chromatography. After five stage extraction with dimethyl carbonate and three stages with water including drying the fluoride loading in the fine fraction smaller 200 µm was 166 mg fluoride per kg solid material.

1. Introduction

Recycling lithium ion batteries from traction systems is a global challenge with increased importance due to their increasing distribution and limited lifespan. Previous recycling processes focused on the recovery of metals e.g. cobalt, nickel and lithium by hydrometallurgical and pyro metallurgical methods [1–7]. In the collaborative research project LithoRecII, a comprehensive recycling process for lithium ion batteries to recover value compounds and to minimize the risk potential due to the chemical compounds was investigated. The electrolyte is a mixture of conducting salt lithium hexafluorophosphate ($LiPF_6$) and organic carbonates and represents about 20 % of the mass of a single battery cell. These compounds were captured by a solvent extraction with dimethyl carbonate, in following abbreviated as DMC, one of the constituents of the electrolyte mixture. Being a low-boiling organic solvent, it could be removed in a drying process. This allows the subsequent recovery steps to be conducted with reduced risk and effort. The preparation of batteries for extraction in recycling includes the collection, discharging and shredding in nitrogen atmosphere. The solvent is evaporated after extraction by drying and prior to the recovery of precious metals e.g. lithium, cobalt and manganese by mechanical, hydrometallurgical and pyro metallurgical processes. The conducting salt $LiPF_6$ is decomposing in equilibrium reaction and is likely to react to hydrofluoric acid in presence of water as shown in equation 1. [8–18]

$$LiPF_6 \rightarrow LiF + PF_5 \rightarrow LiF + 2\,HF + POF_3 \quad (1)$$

The further hydrolysis of POF_3 results in three equivalents HF and phosphoric acid according to [19,20]. For the recovery of the conducting salt and organic compounds from electrolyte the extraction with super-critical carbon dioxide and combination with solvents e.g. acetonitrile was the only

alternative which has been studied [21].

2. Experimental

2.1 Battery material

The electrolyte compounds of the batteries are the conducting salt and organic carbontes. The cells for characterization experiments have been Panasonic CGR 18650 CH, cylindric cells with electric charge of 2250 mAh and nominal voltage of 3.6 V. After discharging the cells were grinded at the Institute for Particle Technology (TU Braunschweig, Braunschweig, Germany) in the "Battery analysis mill", a modified SM 200 cutting mill (Retsch, Haan, Germany), in nitrogen atmosphere and packaged immediately under inert gas atmosphere. The battery mass of a single cell was 42.64 g on average before the grinding and 37.79 g afterwards. The composition of the batteries was assumed to be a mixture of DMC (40 %), ethylmethyl carbonate (20 %), propylene carbonate (10 %) and ethylene carbonate (EC) (30 %) with 1,18 mol $LiPF_6$/L electrolyte. The salt concentration was determined by the Münster Electochemical Energy Technology centre (MEET) (WWU Münster, Münster, Germany). For each of the experiments in section 3.1 a single cell was used and for the experiment in 3.2 two cells were used.

2.2 Stirred vessel

For the extraction experiments a Versoclave 3 (Büchi Glas Uster, Uster, Switzerland) stirred vessel with 0.5 L was used. The temperature was measured internally by a PT-100, the connected cryostat is a CC 405 (Peter Huber Kältemaschinenbau GmbH, Offenburg, Germany). The stirred vessel was in a housing made of PMMA and alumina profiles. The whole vessel was made from stainless steel. The housing was flushed with nitrogen and the vessel was filled with argon. Most of the experiments were conducted at a pressure of 2 bar absolute or slightly higher. For the extraction kinetics a pneumatic sample system was used to take samples during the experiment from the center of the vessel using internal pressure.

2.3 Ion chromatography

The focus for analysis was the determination of hexafluorophosphate concentration and fluoride, one of the decomposition products. For this reason the ion chromatograph 881 Compact IC pro in combination with a 919 IC Autosampler plus (Deutsche Metrohm GmbH & Co. KG, Filderstadt, Germany) was used. The ion chromatography and accessory was controlled by using Metrohm MagIC Net software. All columns were distributed by Metrohm (Deutsche Metrohm GmbH & Co. KG, Filderstadt, Germany). A linear matrix elimination was integrated with an external 6-port-valve (VICI Vlaco Instruments Co. Inc., Schenkon, Switzerland). The flow rate of eluent was 0.7 mL/min and a temperature of 55 °C was set in the column oven. The composition of eluent was 0.7 L ultrapure water, 0.3 L acetonitrile, 10 mL 1 M sodium carbonate and 2 mL 1 M sodium hydrogen carbonate. The eluent was degassed before use. For the calibration fluoride and phosphate standards (Merck KGaA, Darmstadt, Germany) and $LiPF_6$ salt 1 M dissolved in a mixture of DMC and EC supplied by the MEET (MEET, University Münster, Münster, Germany) were employed. The samples were diluted with DMC for the extract analysis and with ultrapure water. From the anion chromatography result for hexafluoro-phosphate (PF_6^-) the mass of $LiPF_6$ was calculated. The hexafluorophosphate and fluoride mass loading in the fine fraction was analyzed by the dispersion of 0.5 g fine fraction of raffinate in 100 mL ultrapure

water. The fine fraction was produced by drying of the raffinate and sieving with Alpine e200 LS (Hosokawa Alpine AG, Augsburg, Germany) with 200 µm sieve mesh. A sample from solution was taken, filtered and used for ion chromatography.

2.4 Parameters for single stage extraction with DMC

The experiments were performed with solvent to solid mass ratio of 7.5, DMC as solvent and a single Panasonic 18650 cell for each experiment. The stirrer speed was set to 50 rpm. Samples were taken after 1, 3, 5, 10, 15 and 30 minutes. Samples from extract were analyzed by ion chromatography.

2.5 Parameters for multi-stage extraction with DMC

Four cross-flow extraction stages with DMC as extractant have been performed. The extract was separated from stirred vessel after 30 minutes and fresh solvent was added. The temperature was set to 20 °C and the stirrer speed was 50 rpm. The solvent to solid mass ratio for the first stage was 10 and 7.5 for the following stages. The raffinate was dried at 105 °C for three days. Afterwards the fluoride and hexafluorophosphate loading were determined by dissolving the fine fraction in ultrapure water as described in 2.3.

2.6 Settings for combination of multi-stage extractions using DMC and water

The set consisted of five extraction stages with DMC, drying, three extraction stages using water as extractant followed by drying and sieving. The extraction time per stage was 30 min. The temperature for the extractions with DMC was set to 20 °C and for the extractions with water 80 °C were set. The solvent to solid mass ratio for DMC was 5 and for water 10. The stirrer speed was 50 rpm. Two Panasonic 18650 batteries with 84.4 g overall mass have been used for DMC extraction and 30 g from the dried raffinate were used for second part of extractions. Sampling was performed as described in 2.5.

3. Results and Discussion

3.1 Single stage extractions with DMC

In single stage extractions the influence of the extraction temperature was determined. The temperatures were set to 10, 20, 30 and 40 °C. In Figure 1 the mass fractions of the conducting salt $LiPF_6$ in the extract are displayed over extraction time. For 10 °C, 20 °C and 30 °C the $LiPF_6$ mass fraction in the extract increases continuously over time, while for 40 °C it increases in the first 15 minutes and decreases thereafter. Additionally, the extracted $LiPF_6$ content is maximum for 20 °C while it decreases with increasing extraction temperature. While the increase from 10 °C to 20 °C may be attributed to an increase in solubility the drop in the $LiPF_6$ content indicates a degradation of $LiPF_6$ at higher temperatures. While the chromatograms for 10 °C and 20 °C only show minor peaks indicating degradation, the chromatograms for 30 °C and 40 °C showed significant peaks for fluoride and unidentified peaks presumably resulting from decomposition. The following multi-stage extractions with DMC have therefore been performed at 20 °C to achieve the optimum combination of minimum degradation and highest solubility.

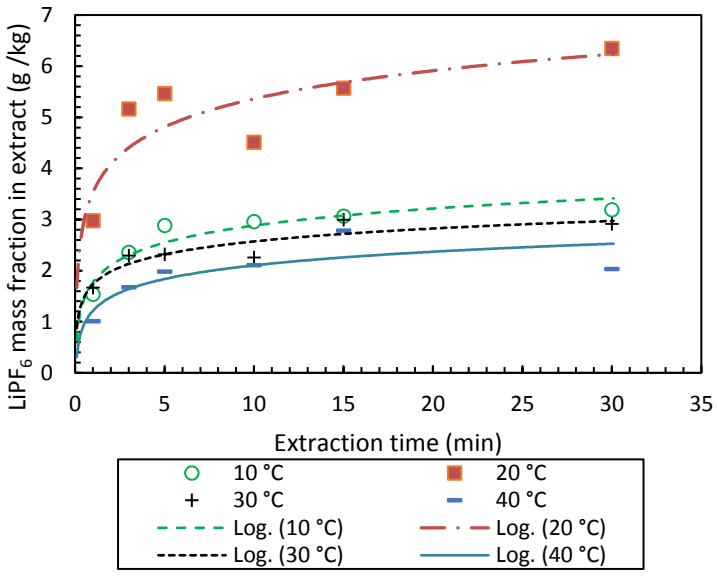

Figure 1. Influence of extraction temperature with logarithmic fits for extraction with DMC.

3.2 Multi-stage extractions with DMC

For the reduction of conducting salt as source for toxic decomposition products multi-stage cross-flow extractions with DMC were used. A four stage extraction was employed to decrease $LiPF_6$ contaminations in solid material for hydrometallurgic processing. The mass fractions for fluoride and $LiPF_6$ in the extract, the cumulated extracted mass of conducting salt and extraction efficiencies are shown in Table 1. Fluoride was only detected in the first stage. The hexafluorophosphate mass fraction decreases after each stage with the maximum mass fraction of 3.106 g PF_6^- per kg extract after first stage and minimum of 0.021 g per kg extract after fourth stage. The extracted mass of $LiPF_6$ after first stage is 1.154 g and after fourth stage 0.007 g. The mass of $LiPF_6$ is calculated based on the composition of the samles and each extract at the end of stage. After fourth stage the cumulated mass of $LiPF_6$ in extract was 1.323 g. The extracted mass per stage decreases significantly and therefore it is assumed that the fresh solvent primarily dilutes the remaining solvent in raffinate. The remaining solvent is approximately 1 kg solvent per kg solid. The extraction efficiency $Y_{extr,\ LiPF6\ in\ solution}$ for dissolved $LiPF_6$ based on the overall mass of conducting salt in extract in reference to overall mass of conducting salt in solution from extract and liquid fraction of raffinate is calculated as shown in equation 2.

$$Y_{extr,\ LiPF_6 in\ solution} = \frac{\sum m_{LiPF_6\ in\ extract}}{\sum m_{LiPF_6\ in\ extract} + m_{LiPF_6\ in\ raffinate\ in\ last\ stage}} \qquad (2)$$

The effect of degradation of conducting salt is included by the mass of $LiPF_6$ in the solid after the drying as shown in equation 3 for the extraction efficiency for overall $LiPF_6$ $Y_{extr,\ LiPF6\ from\ extract\ +\ solid}$. Therefore, the mass of $LiPF_6$ in fine fraction has been included and also the degraded part of the conducting salt from the complete hydrolysis. Equation 4 presents calculation for the mass of $LiPF_6$ in solid. For $LiPF_6$ the mass loading in fine fraction is multiplied with mass of fine fraction. The degradation reaction is also taken into account by calculating the mass of conducting salt assuming complete hydrolysis as described in [19] and complete traceability of fluoride. The fine fraction of solid

from the raffinate has been analysed by extraction with ultrapure water as described in section 2.3 Ion chromatography. No loading with fluoride und hexafluorophosphate was assumed for coarse fraction. For the recovery of high value metal compounds the fine fraction is relevant and therefore the coarse fraction is separated after drying. The sieving with a 200 µm mesh resulted in fractions with similar weight.

$$Y_{extr,\,LiPF_6\ from\ extract+solid} = \frac{\sum m_{LiPF_6\ in\ extract}}{\sum m_{LiPF_6\ in\ extract} + m_{\,LiPF_6\ in\ solid}} \quad (3)$$

$$m_{\,LiPF_6\ in\ solid} = X_{g,LiPF_6} \bullet m_{Fine\ fraction} + X_{g,F^-} \bullet \frac{\widetilde{M}_{LiPF_6}}{6\,\widetilde{M}_{F^-}} \bullet m_{Fine\ fraction} \quad (4)$$

The key parameters for recovery processes of value materials from lithium ion batteries are represented by the fluoride and hexafluorophosphate loading in the fine fraction of raffinate after drying process. The fluoride loading was 3558 mg fluoride per kg fine fraction of solid phase and 233 mg PF_6^- per kg. The remaining PF_6^- was not expected after the extraction and drying for three days at 105 °C. The extraction of dissolved $LiPF_6$ was highly sucessful, while 7 % of the conducting salt remained as $LiPF_6$ or in decomposed form in the solid material. A further reduction of fluoride loading in solid was required and therefore the experiment in section 3.3 was performed.

Table 1 Mass fractions of anions in extract, cumulated extracted mass $LiPF_6$ and extraction efficiencies for four stages at 20 °C.

Extraction stage	Fluoride mass fraction in extract (g/kg)	PF_6^- mass fraction in extract (g/kg)	$LiPF_6$ mass extracted per stage (g)	$LiPF_6$ mass extracted cumulated (g)	Accumulated extraction efficiency based on $LiPF_6$ in solution $Y_{extr,\ LiPF6\ in\ solution}$	Accumulated extraction efficiency based on $LiPF_6$ in extract and solid including degradation $Y_{extr,\ LiPF6\ from\ extract\ +\ solid}$
1	0.047	3.106	1.154	1.154	0.8717	0.8111
2	0.000	0.415	0.138	1.293	0.9762	0.9083
3	0.000	0.078	0.024	1.317	0.9944	0.9253
4	0.000	0.021	0.007	1.323	0.9993	0.9299

3.3 Combination of multi-stage extractions using DMC and water

For the further reduction of fluoride loading in solid material after extraction with DMC and drying a second set of multi-stage cross-flow extractions using water as extractant were performed. The solubility for LiF is higher in water than in DMC [22]. The results for the extraction of LiF with DMC are shown in Table 2 and show similarities to data in Table 1. Fluoride is only detectable in extract from the first stage. The mass fraction of PF_6^- and mass of extracted $LiPF_6$ decrease with rising number of extraction stages. The loading of fluoride was 1093 mg fluoride per kg and 218 mg PF_6^- per kg solid phase after extraction with DMC.

Table 2 Mass fractions of anions in extract, cumulated extracted mass $LiPF_6$ and extraction efficiencies for five stages at 20 °C.

Extraction stage	Fluoride mass fraction in extract (g/kg)	PF_6^- mass fraction in extract (g/kg)	$LiPF_6$ mass extracted per stage (g)	$LiPF_6$ mass extracted cumulated (g)	Accumulated extraction efficiency based on $LiPF_6$ in solution $Y_{extr,\ LiPF6\ in\ solution}$	Accumulated extraction efficiency based on $LiPF_6$ in extract and solid including degradation $Y_{extr,\ LiPF6\ from\ extract\ +\ solid}$
1	0.019	6.646	2.460	2.460	0.8295	0.8125
2	0.000	0.899	0.391	2.852	0.9615	0.9418
3	0.000	0.179	0.075	2.926	0.9867	0.9665
4	0.000	0.058	0.023	2.950	0.9945	0.9741
5	0.000	0.033	0.013	2.963	0.9991	0.9786

The extraction with water was performed with a higher solvent to solid ratio than the extractions with DMC in this section. Table 3 shows the a decrease of fluoride mass in extract with rising number of stages and while after the first stage the mass fraction of hexafluorophosphate decreases the value stays constant for second and third stage. The extraction efficiency for fluoride $Y_{extr,\ F-}$ was calculated as the mass of fluoride in extract in relation to extracted mass of fluoride and fluoride mass in fine fraction as shown in equation 5. The fluoride mass in solid was also determined by the extraction in ultrapure water and in reference to fine fraction of solid.

$$Y_{extr,F^-} = \frac{\sum m_{F^-\ in\ extract}}{\sum m_{F^-\ in\ extract} + m_{F^-\ in\ fine\ fraction\ of\ solid}} \qquad (5)$$

The analysis of the solid material after drying and sieving showed no loading with hexafluoro-phosphate and 166 mg fluoride per kg solid material. Therefore, the reduction of fluoride and PF_6^- was

successfully performed. $LiPF_6$ was degraded completely after drying. The extraction efficiency for fluoride shows the possibility of further reduction.

Table 3 Mass fractions of anions in extract for three stages of extraction with water at 80 °C.

Extraction stage	Fluoride mass fraction in extract (g/kg)	PF_6^- mass fraction in extract (g/kg)	Accumulated extraction efficiency for F^- based on fluoride in extract and in solid
1	0.194	0.018	0.8017
2	0.026	0.005	0.9379
3	0.003	0.005	0.9575

4. Conclusions

The extraction of the conducting salt lithium hexafluorophosphate from lithium ion batteries using the organic extractant dimethyl carbonate is accompanied by degradation at elevated temperatures. The optimum temperature for extraction is 20 °C. The reduction of conducting salt by multi-stage cross-flow extractions with dimethyl carbonate was demonstrated successfully, but traces were still present in raffinate and furthermore higher loadings with fluoride. Therefore, a combination of a set of extractions with dimethyl carbonate, drying and a second set of extractions with water was tested. As a result the conducting salt was completely removed below detection limit. The loading of fluoride was reduced to 166 mg fluoride per kg fine fraction of solid raffinate.

Acknowledgement

This study was part of the joint research project LithoRecII (Reference No. 16EM1024), funded by the Federal Ministry for the Environment, Nature Conservation, Building and Nuclear Safety (BMU) of Germany. We would like to thank the project partners, especially Jan Diekmann, Martin Stoev, André Hartmann, Dr. Martin Bomkamp and Christian Gröber.

References

1) G. Cai, K. Y. Fung, K. M. Ng and C. Wibowo, *Ind. Eng. Chem. Res.*, **53,** 18245–18259 (2014).
2) J. Diekmann, C. Hanisch, L. Froböse, G. Schälicke, T. Loellhoeffel, A.-S. Fölster and A. Kwade, *J. Electrochem. Soc.*, **164,** A6184-A6191 (2016).
3) M. J. Lain, *J. Power Sources*, **97-98,** 736–738 (2001).
4) J. Ordoñez, E. J. Gago and A. Girard, *Renew Sust Energ Rev*, **60,** 195–205 (2016).
5) A. Sonoc, J. Jeswiet and V. K. Soo, *Procedia CIRP*, **29,** 752–757 (2015).
6) F. Treffer, R. Korthauer (Ed.). Berlin, Heidelberg, pp. 345–355 (2013).
7) J. Xu, H. R. Thomas, R. W. Francis, K. R. Lum, J. Wang and B. Liang, *J. Power Sources*, **177,** 512–527 (2008).
8) C. L. Campion, W. Li and B. L. Lucht, *J. Electrochem. Soc.*, **152,** A2327 (2005).
9) A. Guéguen, D. Streich, M. He, M. Mendez, F. F. Chesneau, P. Novák and E. J. Berg, *J.*

Electrochem. Soc., **163,** A1095-A1100 (2016).
10) S. F. Lux, J. Chevalier, I. T. Lucas and R. Kostecki, *ECS Electrochemistry Letters*, **2,** A121-A123 (2013).
11) S. F. Lux, I. T. Lucas, E. Pollak, S. Passerini, M. Winter and R. Kostecki, *Electrochem Commun*, **14,** 47–50 (2012).
12) S. Nowak and M. Winter, *J. Electrochem. Soc.*, **162,** A2500-A2508 (2015).
13) S. E. Sloop, J. K. Pugh, S. Wang, J. B. Kerr and K. Kinoshita, *Electrochem. Solid-State Lett.*, **4,** A42 (2001).
14) K. Tasaki, K. Kanda, S. Nakamura and M. Ue, *J. Electrochem. Soc.*, **150,** A1628 (2003).
15) X.-G. Teng, F.-Q. Li, P.-H. Ma, Q.-D. Ren and S.-Y. Li, *Thermochim Acta*, **436,** 30–34 (2005).
16) L. Terborg, S. Nowak, S. Passerini, M. Winter, U. Karst, P. R. Haddad and P. N. Nesterenko, *Analytica chimica acta*, **714,** 121–126 (2012).
17) L. Terborg, S. Weber, F. Blaske, S. Passerini, M. Winter, U. Karst and S. Nowak, *J. Power Sources*, **242,** 832–837 (2013).
18) H. Yang, G. V. Zhuang and P. N. Ross, *J. Power Sources*, **161,** 573–579 (2006).
19) M. Grützke, V. Kraft, B. Hoffmann, S. Klamor, J. Diekmann, A. Kwade, M. Winter and S. Nowak, *J. Power Sources*, **273,** 83–88 (2015).
20) M. Grützke, X. Mönnighoff, F. Horsthemke, V. Kraft, M. Winter and S. Nowak, *RSC Adv*, **5,** 43209–43217 (2015).
21) X. Mönnighoff, A. Friesen, B. Konersmann, F. Horsthemke, M. Grützke, M. Winter and S. Nowak, *J. Power Sources*, **352,** 56–63 (2017).
22) J. Jones, M. Anouti, M. Caillon-Caravanier, P. Willmann and D. Lemordant, *Fluid Phase Equilibr*, **285,** 62–68 (2009).

Solid-Phase Extraction of Ga^{3+} and In^{3+} with a Hexadentate Chelating Reagent

Tetsuto KAJIYAMA[1,*], Satomi MAKINO[2], Shuhei TAKASE[2], Satoshi OHMURO[2,**], Kensuke ARAI[3], and Hisao KOKUSEN[2]

[1]*Jonan Branch, Regional Technology Support Division, Commercialization Support Development, Tokyo Metropolitan Industrial Technology Research Institute, Minamikamata 1-20-20, Ota, Tokyo 144-0035, Japan;* [2]*Department of Chemistry, Tokyo Gakugei University, Nukuikitamachi 4-1-1, Koganei, Tokyo 184-0015, Japan;* [3]*Division of Physical and Analytical Chemistry, Nihon Pharmaceutical, University, Komuro 10281, Ina, Kitaadachi, Saitama 362-0806, Japan*

[**]*Present Adress: Division of Physical and Analytical Chemistry, Nihon Pharmaceutical, University*

A new adsorption system for divalent and trivalent metal ions have been developed. The indium ion was efficiently separated from an acidic aqueous solution containing Ga^{3+}, In^{3+}, and Zn^{2+}. The adsorption and separation material was synthesized and it was loaded onto silica gel containing chemically bonded ocatadecyl groups (C18). As a ligand, N,N′-bis(5-chloro-2-hydroxybenzyl)-N,N′-bis(2-methyl-pyridyl)ethylenediamine (H_2Clbbpen) was used. The separation material, containing H_2Clbbpen, was able to adsorb Ga^{3+} and In^{3+} from a Zn^{2+} containing acidic solution. In addition, when this adsorption material was applied to the column adsorption method, Ga^{3+} and In^{3+} could be adsorbed from an aqueous acidic solution containing zinc ions. The Zn^{2+} ions did not adsorb onto this separation material. After adsorption, Ga^{3+} could be eluted first using a sodium hydroxide solution. Subsequently, In^{3+} could be eluted with a nitric acid solution.

1. Introduction

Rare earth metals have been abundantly used in the high-tech industry. However, indium is a very rare mineral resource because it can only be mined for several year. Therefore, to secure a stable supply, the recycling and reuse of indium from advanced industrial products is necessary for the construction of a sustainable society. There is an abundant rare metal resource available in our country called the urban mine, which includes used and disposed electronic devices. The development of a technique to efficiently separate and collect rare metals from the urban mine is very important. In the separation and recovery process of rare metals from electronic devices, it is necessary to research separation materials with high selectivity for collecting and separating the desired metal ions. As a method to separate a metal ion from an aqueous solution, the “ion exchange method” and “solvent extraction method” are often used. These methods use the difference in metal valences, ionic radii, and complex formations between a metal ion and the extracting agent to separate metal ions with specificity. In particular, ion exchange methods will be able to support small metal separation systems because the adsorption of metal ions from the aqueous phase to the solid phase does not use harmful

organic solutions. However, the solvent extraction reagent used in the solvent extraction method has superior selectivity over that of a typical ion exchange resin for separating metal ions. Therefore, separation materials impregnated or bonded to a solvent extraction reagent with high selectivity for the separation of metal ion on a solid phase, such as silica gel, resin or natural fiber, were synthesized to study the separation of rare metal ions from an acidic aqueous solution [1–8]. For the establishment of efficient metal ion separation technology, hydrophobic silica gel (silica gel chemically bonded to a long-chain alkyl group) was considered to become a pseudo-organic phase and was used as a carrier for the solvent extraction reagent. A *β*-diketone was chosen as the solvent extraction reagent and the separation material was synthesized. The selectivity of this separation material was better than that of the solvent extraction method using the same loaded extraction reagent [9–11]. In addition, this separation material is available for construction of the pseudo-solvent extraction system in spite of separation system by the ion exchange reaction. Therefore, superior separation ability was developed for metal ions [9–11]. The separation of In^{3+} from Ga^{3+} and Zn^{2+} using the H_2Clbbpen-loaded surface-modified silica gel (C18-H_2L) was studied.

2. Experimental

2.1 Reagents and apparatus

All reagents were used for analytical grade without further purification. Deionized water used throughout was prepared from a Milli-Q Elix Advantage3 water purification system (Millipore). Other organic materials used were obtained from Tokyo Kasei Kogyo. Inductively coupled argon-plasma optical emission spectrometry (ICP-OES) was performed using an Agilent 5100 to determine the concentration of metal ions. The pH values of aqueous solutions were measured using a pH meter (TOA-DKK M-60) equipped with a glass electrode. H_2Clbbpen was synthesized according to Neves *et al.*, as shown in Figure 1 [12].

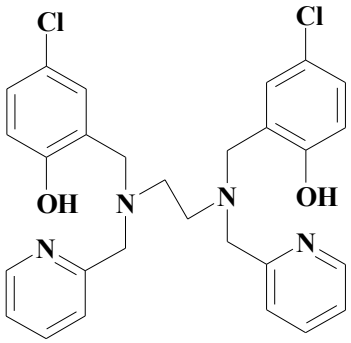

Figure 1. Structure of H_2Clbbpen.

2.2 Preparation of C18-H_2Clbbpen

The non-end-capped ODS was prepared from 60N silica gel (particle size: 40–50 μm, Kanto Chemical Co., Inc.) and octadecyl trichrolosilane according to a standard method. The separation material was prepared according to a previous method: 200 g of ODS was allowed to stand overnight in 1 dm^3 toluene solution containing 0.02 mol H_2Clbbpen [10]. After standing for 24 h at 277 K, the mixed solution was filtrated, washed with methanol and deionized water, and dried in a vacuum at room temperature.

2.3 Adsorption experiment of metal ions

An aliquot of C18-H_2L was shaken with 30 cm^3 of an aqueous phase containing [M^{n+}]:

1.0×10^{-4} mol dm^{-3}, [$CH_2ClCOOH$]: 0.02 mol dm^{-3}, and sodium salt (NaCl, $NaNO_3$, or Na_2SO_4) within 12 days at 25 ± 1 °C. After the reaction was completed, the mixed solutions were filtered. The concentration of metal ions in the aqueous solutions was determined by ICP-OES, and the pH value of the aqueous phase was measured.

2.4 Separation of In^{3+} from Ga^{3+} and Zn^{2+} using the column method

The experimental conditions of the column method is shown: 100 cm^3 of the sample solution containing [M^{n+}]: 5.0×10^{-5} mol dm^{-3}, [NaX] (X^-: Cl^-, NO_3^-, or SO_4^{2-}): 0.1 mol dm^{-3}, [$CH_2ClCOOH$]: 0.01 mol dm^{-3} and adjusted to pH: 3.0. The flow rate was 0.5 cm^3 min^{-1}. Then, metal ions were adsorbed onto the column. The column was rinsed with deionized water. Thereafter, Ga^{3+} were eluted with 0.1 mol dm^{-3} NaOH solution; then, In^{3+} were eluted with 0.2 mol dm^{-3} HCl solution and dispensed in a fraction collector. The concentration of metal ions in the dispensing solution was measured using ICP-OES.

3. Results and Discussion

3.1 Adsorption behavior of the metal ions

Metal ions were adsorbed onto the C18-H_2L separation material. The relations between adsorption ratio of metal ions and pH are shown in Figure 2 and 3.

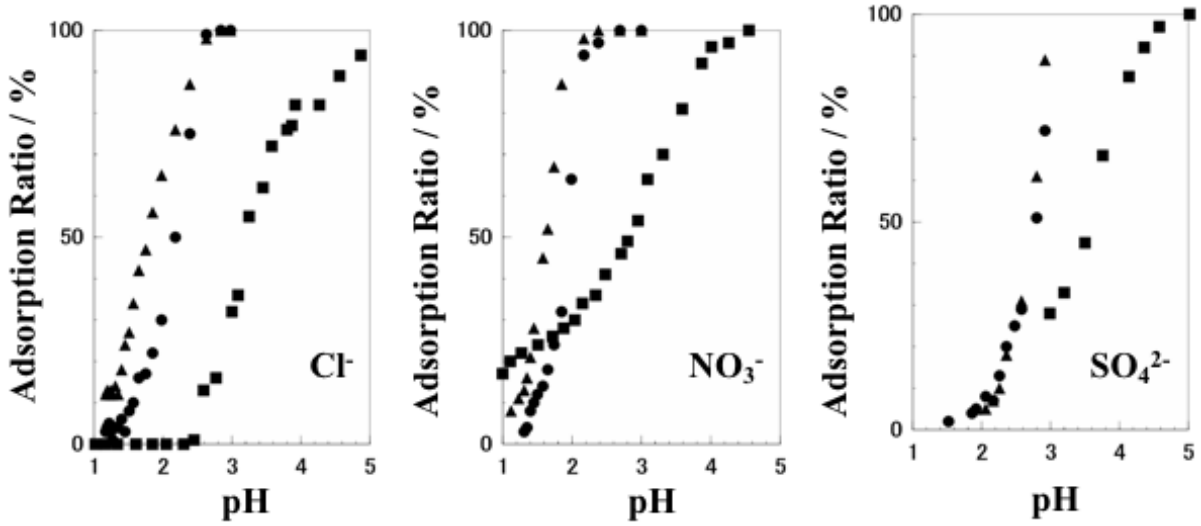

Figure 2. Adsorption ratios of Ga^{3+}, In^{3+}, and Zn^{2+} using C18-H_2L separation material. ▲: In^{3+}, ●: Ga^{3+}, ■: Zn^{2+}, [M^{n+}]: 1.0×10^{-4} mol dm^{-3}, [NaCl], [$NaNO_3$] or [Na_2SO_4]: 0.1 mol dm^{-3}, C18-H_2L: 0.3 g/30 cm^3. Shaking time: 8 days.

The value of adsorption ratio E was defined as follows:

$$E = \{[M^{n+}]_{init} - [M^{n+}]_{eq}\}/[M^{n+}]_{init} \times 100\ (\%) \quad (1)$$

In this equation, $[M^{n+}]_{init}$ was the initial concentration of the metal ion and $[M^{n+}]_{eq}$ was the concentration of metal ions after adsorption. The adsorption behavior of Ga^{3+}, In^{3+}, and Zn^{2+} are shown in Figure 2 and that of Cu^{2+}, Co^{2+}, and Ni^{2+} are shown in Figure 3. In the case of adsorption of Zn^{2+},

Cu^{2+}, Co^{2+} and Ni^{2+} with Na_2SO_4 was already published [13]. In this result, mutual separation of between Ga^{3+} and In^{3+} from the adsorption curves was difficult.

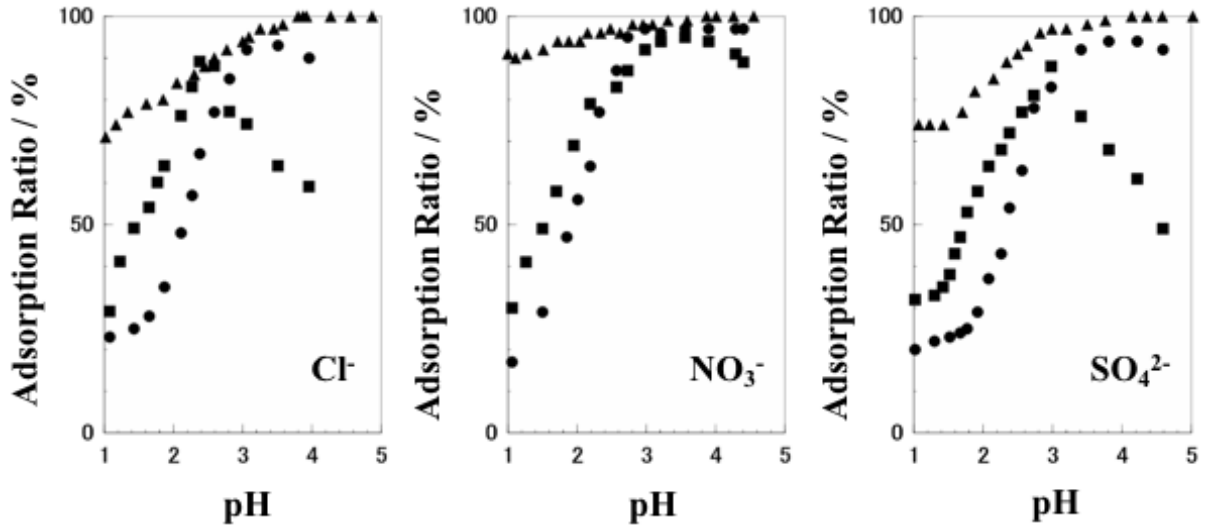

Figure 3. Adsorption ratios of Ni^{2+}, Co^{2+}, and Cu^{2+} using C18-H_2L separation material. ▲: Cu^{2+}, ●: Co^{2+}, ■: Ni^{2+}, $[M^{n+}]$: 1.0 × 10^{-4} mol dm^{-3}, [NaCl], [$NaNO_3$] or [Na_2SO_4]: 0.1 mol dm^{-3}, C18-H_2L: 0.3 g/30 cm^3. Shaking time: 8 days.

Ga^{3+} and In^{3+} were shown to have the same adsorption behavior in the case where $NaNO_3$ was the counter anion. When Cl^- or SO_4^{2-} was used as the counter anion, the adsorption ability of In^{3+} was better than that of Ga^{3+}. The selectivity between Ga^{3+} or In^{3+} and Zn^{2+} with NaCl was better than that with Na_2SO_4. In the future, zinc will be used in the transference electrode for electronic device touch panels. Therefore, the development of mutual separation techniques from acidic zinc solutions containing Ga^{3+} and/or In^{3+} is necessary. On the other hand, Cu^{2+} was adsorbed from the strongly acidic solution with all kinds of counter anions.

The copper ion was adsorbed with all examined counter anions from the acid solution. Adsorption ability at the same behavior was Ga^{3+} and In^{3+}. In the case of a Cl^-, adsorption ability of Ni^{2+} was higher than that of Ga^{3+} and In^{3+}. In the case of a NO_3^-, adsorption ability of Ni^{2+} was lower than that of Ga^{3+} and In^{3+}. In the case of a SO_4^{2-}, adsorption ability of Ga^{3+} and In^{3+} was lower than that of Ni^{2+} and Co^{2+}. The mutual separation of Ga^{3+} and In^{3+} using the batch method was difficult; however, from such a characteristic, thought that mutual separation of the high efficiency construction could be expected by applying separation materials to the column method.

3.2 Separation of In^{3+} from the acid water solution

Acidic solutions containing Ga^{3+}, In^{3+}, and Zn^{2+} were passed through a column filled with the C18-H_2L separation material. Zn^{2+} could not be adsorbed on this separation material under this condition. Ga^{3+} was eluted using 0.1 mol dm^{-3} NaOH solution. The adsorbed Ga^{3+} was completely eluted. Then, In^{3+} was eluted with 0.02 mol dm^{-3} HNO_3 solution. The adsorbed In^{3+} was also completely eluted. The elution curve is shown in Figure 4. When the eluent was passing through the

column, Ga^{3+} was completely eluted approximately 600 cm^3 after the adsorbed metal ions. Under these conditions, In^{3+} was not eluted. Afterward, it was observed that In^{3+} was eluted when a nitric acid solution was passed through the column. In addition, Zn^{2+} was able to set this condition that was not adsorbed by a column from the result of the batch method on this condition. Selective separation of Ga^{3+} and In^{3+} from a simulated urban mine metal-ion-containing solution was accomplished. However, improvements will be necessary because the exchange capacity of the adsorption materials was small and the adsorption rate was also slow.

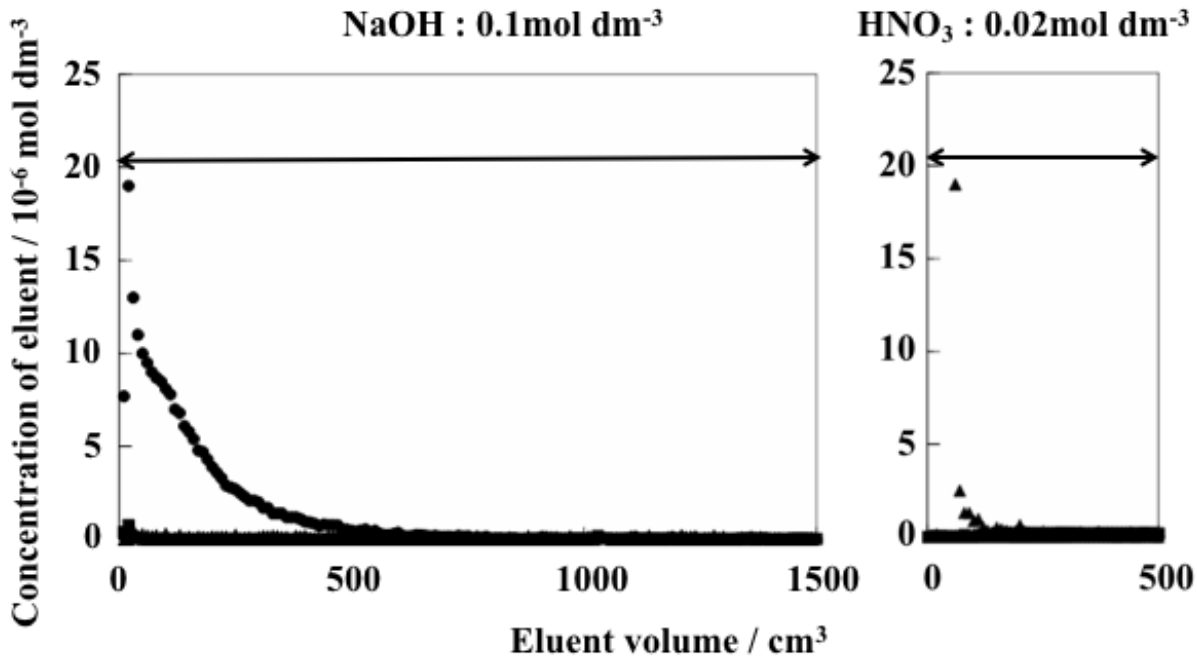

Figure 4. Elution behavior of Ga^{3+} and In^{3+} Coulum : 20cm, internal diameter : 1.0 cm, C18-H_2L : 8.0 g Adsorption condition pH : 3.0 , $[M^{n+}]$: 5.0 x 10^{-5} mol dm^{-3}, Flow rate : 0.5 cm min^{-1} $[Na_2SO_4]$: 0.1 mol dm^{-3}, Flow Volume : 200 cm^3.

4. Conclusion

We have developed a new adsorption system for divalent and trivalent metal ions using the C18-H_2L sorbent, which H_2Clbbpen was directly loaded ODS. Relations between the adsorption ratio E (%) and pH showed that the metal ions could be absorbed from an acidic solution. The C18-H_2L system was found to have good mutual selectivity for In^{3+}–Zn^{2+} for separation. This is important because Zn^{2+} is included in the touch panel of electronic devices.

This new method has an advantage in that a chelating agent can be effectively used to remove metal ions from an aqueous solution without organic solvents. This separation material can be easily synthesized by simply loading the extraction reagent onto hydrophobic silica gel. Therefore, the application of this method is easily possible with many kinds of extraction reagents. The utilization of the extraction reagent with higher selectivity is widely enabled.

References

1) K. Terada, K. Morimoto, T. Kiba, *Anal. Chim. Acta*, **116**, 127-135 (1980).
2) K. Terada, K. Nakamura, *Talanta*, **28**, 123-125 (1981).
3) T. Oshima, S. Ishizaka, H. Morizono, K. Ohe, Y. Baba, *Sep. Purif. Technol.*, **114**, 11-16 (2013).
4) S. Kanemaru, T. Oshima, Y. Baba, *J. Chem. Eng. Jpn.*, **45**, 816-822 (2012).
5) S. Nishihama, K. Kohata, K. Yoshizuka, *Sep. Purif. Technol.*, **118**, 511-518 (2013).
6) F. Guo, S. Nishihama, K. Yoshizuka, *Env. Technol.*, **34**, 1307-1317 (2013).
7) T. Kajiyama, S. Sakai, J. Inoue, H. Kokusen, *J. Ion. Exchange*, **25**, 155-159 (2014).
8) T. Kajiyama, S. Sakai, J. Inoue, T. Yoshino, S. Ohmuro, K. Arai, H. Kokusen, *J. Ion. Exchange*, **27**, 57-62 (2016).
9) M. Iiyama, H. Kokusen, S. Tsurubou, Y. Komatsu, *Trans*. *MRS-J*, **29**(5), 2333-2336 (2004).
10) M. Iiyama, S. Oshima, H. Kokusen, M. Sekita, S. Tsurubou, Y. Komatsu, *Anal. Sci*., **20**, 1463-1464 (2004).
11) M. Iiyama, S. Oshima, H. Kokusen, S. Tsurubou, Y. Komatsu, *J. Ion Exchange*, **16**, 65-69 (2005).
12) A. Neves, M.A. De Brito, G. Oliva, O.R. Nascimento, E.H. Panepucci, D.H.F. Souza, A.A. Batista, *Plyhedron*, **14**. 1307-1314 (1995).
13) S. Ohmuro, K. Fujii, T. Yasui, K. Takada, A. Yuchi, H. Kokusen, *Anal. Sci.,* **32**, 343-347 (2016).

Molybdenum Isotope Fractionation in Basic Aqueous Solution Using Anion Exchange Chromatography

Yu TACHIBANA[1,*], Andri Rahma PUTRA[1], Shin OKUMURA[2], Toshitaka KANESHIKI[2], Masanobu NOGAMI[3], Tatsuya SUZUKI[1] and Masao NOMURA[2]

[1]Department of Nuclear System Safety Engineering, Graduate School of Engineering, Nagaoka University of Technology, 1603-1, Kamitomioka-machi, Nagaoka, Niigata 940-2188, Japan; [2]Laboratory for Advanced Nuclear Energy, Tokyo Institute of Technology, 2-12-1, Ookayama, Meguro-ku, Tokyo 152-8550, Japan; [3]Department of Electric and Electronic Engineering, Kindai University, 3-4-1, Kowakae, Higashiōsaka-shi, Osaka 577-8502, Japan

The Mo(VI) isotope fractionation using well-known anion-exchange resins was investigated in aqueous solutions at 298 K. The weakly basic porous-type WA20 resin (WA20(Cl form)), PA316 resin, which is one of porous-type strongly basic anion-exchange resin (PA316(Cl form)), and benzimidazole-type anion-exchange resin embedded in high-porous silica beads, which has two types of functional groups consisting of 1-methylbenzimidazole and 1,3-dimethylbenzimidazole (AR-01(Cl form)) was used. The adsorption experiments of Mo(VI) species using WA20(Cl form), PA316(Cl form), and AR-01(Cl form) resins were performed by batch-wise techniques to evaluate the distribution coefficients (K_d) of Mo(VI) species in aqueous solutions ranging in pH value from 2.6 to 12.8 at room temperature. As a result, it was found that PA316(Cl form) and AR-01(Cl form) resin have high adsorption ability for Mo(Vl) species in the broad pH range. On the other hand, the K_d values of WA20(Cl form) resin decreased sharply around neutral pH values. This adsorption tendency implies that the Mo(VI) isotope fractionation experiments in adsorption-desorption reactions are available. The isotope separation coefficients per unit mass (ε / $\Delta Mass$) of Mo(VI) species were obtained by using the isotope fractionation curve of Mo(VI) species with WA20(Cl form) resin. The ε / $\Delta Mass$ values were compared with those obtained from acid conditions.

1. Introduction

Tc-99m, a metastable isomer of Tc-99, is of great interest from the viewpoint of the medical use of nuclear diagnostics due to the half-life of $T_{1/2}$ = 6.015 h and 143 keV [1]. It is the fact that our country depends on foreign countries such as Canada, Netherlands, and Belgium, etc. for Mo-99, a raw material of Tc-99m [2]. Nowadays, most Mo-99 is produced by using nuclear research reactors with highly enriched U-235, which has intrinsically some serious worries for nuclear proliferation. These reactors have been getting decrepit and the realistic costs for specialized facilities for chemical treatments, storages, and the disposal of large amounts of highly radioactive wastes are not reasonable [3]. Recently, some researchers have suggested that Mo-99 can be produced using the respective reactions of ^{98}Mo(n, γ)^{99}Mo, ^{100}Mo(n, $2n$)^{99}Mo, and ^{100}Mo(p, x)^{99}Mo [2-4]. Before their nuclear

reactions, it has also been required to enrich Mo-98 or Mo-100 isotope for preparation of the enriched Mo-99 isotope due to comparatively low natural abundance of Mo-98 and Mo-100 isotopes. The geochemists are particularly interested in the Mo isotope fractionation in chemical reaction [5-7]. Our present works which have examined the mechanisms of Mo isotope fractionation in solutions, may contribute to the understanding the nature of the isotope fraction of Mo in the natural world. Some researchers have studied the chemical enrichment of various nuclides by using chromatography [8-24]. In analogy of them, we have also performed some chromatographic isotope separation experiments of hexavalent Mo species using the synthesized benzimidazole-type anion-exchange resin embedded in high-porous silica beads (AR-01(Cl form)) and the weakly basic porous-type WA20 resin (WA20(Cl form)) in hydrochloric acid solutions (see Figure 1) [25] and their effect of different valence states on chromatographic fractionation of Mo isotopes in hydrochloric acid solutions was examined using Sn(II) [23-24]. It has been known that Mo species has various chemical forms in aqueous solutions and seven stable isotopes in nature [23]. In other words, the systematic understanding of adsorption and desorption behavior of Mo species is inevitable, compared with other elements. However, the chemical data on isotope fractionation of medium-heavy elements such as Mo are not well-known. Especially, little information on chromatographic isotope fractionation of Mo(VI) isotopes in basic aqueous solutions is available.

Judging from these viewpoints, we have investigated the Mo(VI) isotope fractionation behavior in the basic aqueous solutions using typical anion-exchange resins such as WA20(Cl form), PA316(Cl form), and AR-01(Cl form) resins.

2. Experimental

2.1 Reagents

$Na_2MoO_4 \cdot 2H_2O$ (Purity: 99.0 %), NaOH (Purity: 93.0 %), HCl (Purity: 35 %) were produced by NACALAI TESQUE, INC., Kyoto, Japan. The foregoing Mo(VI) salts were used without further purification. AR-01(Cl form) resin was synthesized and supplied from Laboratory for Advanced Nuclear Energy, Tokyo Institute of Technology, Tokyo, Japan [20]. Both of WA20(Cl form) and PA316(Cl form) resins were obtained from Mitsubishi Chemical Corporation, Tokyo, Japan and their structural details and chemical properties have been described elsewhere [25]. All chemicals for analyses were of special pure grade.

2.2. Sample preparations

The acidic and basic concentrations in solutions containing 1.0 mM (M = mol/dm^3) Mo(VI) species were adjusted to pH = 2.6 - 12.8 using HCl and NaOH for Mo(VI) adsorption experiments, whereas the concentration of NaOH and HCl was adjusted to 0.5 M for chromatographic experiments. The aqueous solutions with 0.5 M Mo(VI) species was also prepared. By mixing with ultrapure water (Specific electrical resistance: ≥ 18.2 MΩcm, total organic carbon: ≤ 3 ppb (ppb = ng/g)) produced with a Merck Millipore apparatus (Milli-Q Integral 3 Water Purification System), these sample solutions were carefully prepared to prevent any contamination. For Mo(VI) adsorption experiments, AR-01(Cl form), WA20(Cl form), and PA316(Cl form) resins and for Mo(VI) chromatographic

experiments, WA20(Cl form) resin were used. The diameter of silica beads used for AR-01(Cl form) resin was 40 - 60 μm [20]. The quaternization ratio of AR-01(Cl form) resin was 58.8 % [20].

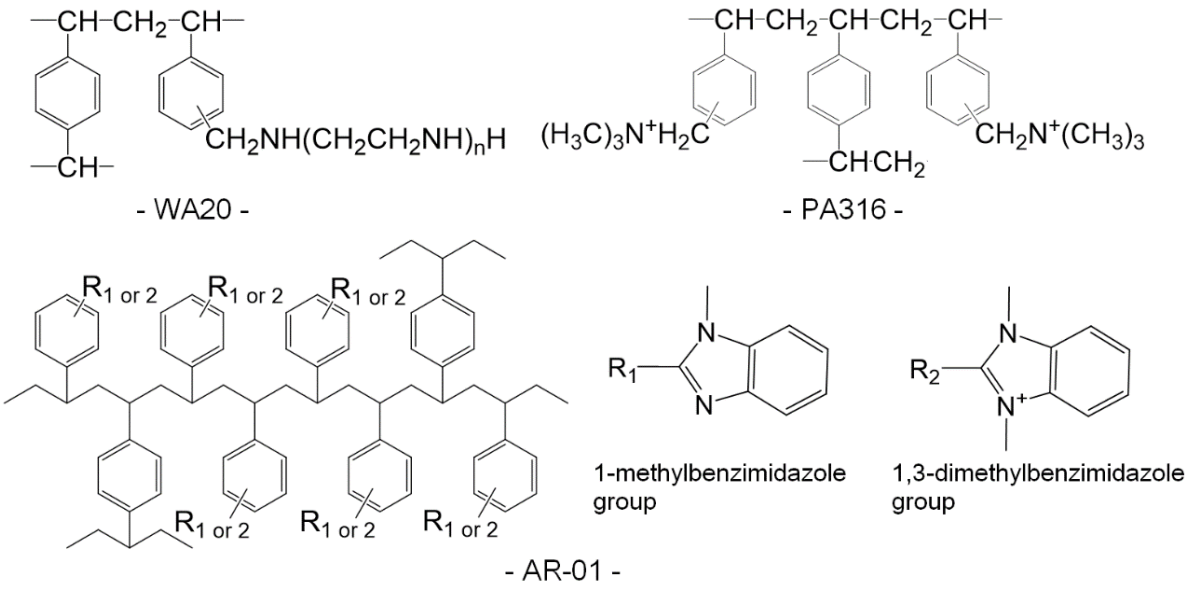

Figure 1. Structural formulas of anion-exchange resins used in the study.

2.3. Adsorption experiments of Mo(VI) species

The adsorption experiments of Mo(VI) species were carried out by batch-wise techniques to evaluate the distribution coefficients (K_d) using AR-01(Cl form), WA20(Cl form), and PA316(Cl form) resins in aqueous solutions of various pH values (pH = 2.6 - 12.8) at room temperature. These resins of 0.10 g were respectively added into 10.0 mL aqueous solutions containing 1.0 mM Mo (VI) species. The shaking time was 24 hours at room temperature. The concentration of Mo(VI) species was measured using ICP/MS (7700x, Agilent) after all samples were passed through a polytetrafluoroethylene-type membrane filter (Sartorius, pore size: 0.45 μm) to remove these resins.

2.4. Chromatography experiments of Mo(VI) species

For the Mo(VI) chromatographic isotope fractionation experiments, seven glass columns connected in series were used. All columns were equipped with water jacket made of glass. The length of one column was 1.0 m and its inner diameter was 8.0 mm. All apparatuses were connected in series with the polytetrafluoroethylene tubes with 2.0 mm inner diameter. The above-mentioned resins were packed into these glass columns. The total weight of WA20(Cl form) resin was 137.3 g. By using the circulator, the reaction temperature was kept constant at 298 K for WA20(Cl form) systems. The column chromatography experiments using aqueous solutions containing 0.5 M Mo(VI) species were performed under constant flow rate of 0.78 mL/min at 298 K. The flow rate was controlled by the high-pressure pump (NP-KX-210, Nihon Seimitsu Kagaku, Co., Ltd.). The order of mobile phase added into the columns was aqueous solution with 0.5 M Mo(VI) species (300 cm^3) and aqueous solution containing 0.5 M NaOH (4000 cm^3). WA20(OH form) resin was converted into WA20(Cl form) resin using 0.5 M HCl aqueous solution. The samples were taken every 10.0 g by using the fraction collector (CHF161RA, Advantech). The Mo(VI) concentration and their isotope ratios were

measured by using ICP/MS described above. By varying the concentration of metal ions and kinds of solvents and their concentration, we have observed the effect of the Mo isotope discrimination in ICP/MS measurements [26]. Hence, the concentration of Mo(VI) species in the sample solutions was adjusted at ca. 10 ppb for the isotope ratio measurements. The 1.0 wt% HNO_3 solution was used as a diluent for all ICP/MS measurements. The Mo(VI) species adsorbed on the resins in the columns were completely removed by using 0.5 M NaOH after the chromatographic experiments.

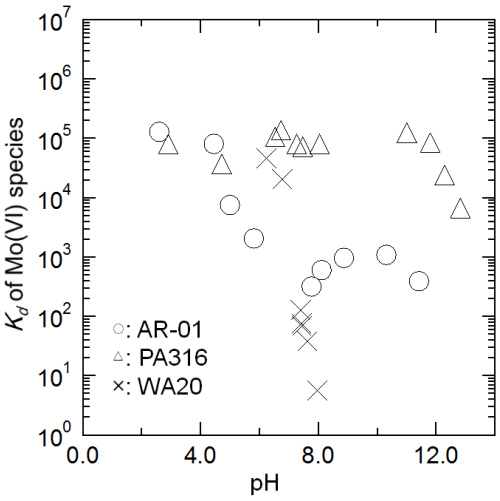

Figure 2. Plots of K_d of Mo(VI) species *vs.* pH at room temperature. [Mo(VI)] = 1.0 mM. Resin = 0.10 g.

3. Results and Discussion

3.1. Adsorption behavior of Mo(VI) species

The adsorption experiments of Mo(VI) species using WA20(Cl form), PA316(Cl form), and AR-01(Cl form) resins were performed by batch-wise techniques to evaluate the K_d values of Mo(VI) species in aqueous solutions in the pH 2.6 to 12.8 region at room temperature. The K_d values were calculated using the following Eq. (1).

$$K_d = \{C_r / C_s \times (V_s / V_r)\} = \{(C_0 - C_s) / C_s\} \times (V_s / V_r) \quad (1)$$

where C_r, C_s, C_0, V_s, and V_r are concentration of Mo(VI) species on resin at adsorption equilibrium, concentration of Mo(VI) species in solution after adsorption equilibrium, initial concentration of Mo(VI) species, volume of solution, and volume of resin, respectively.

As a result, it was found that PA316(Cl form) and AR-01(Cl form) resin have high adsorption ability for Mo(Vl) species in the broad pH range while the K_d values of WA20(Cl form) resin decreased sharply around neutral pH values as shown in Figure 2. In the acidic aqueous solution around pH = 5, Mo(VI) exists as $Mo_7O_{23}^{4-}$, i.e., this Mo(VI) species can strongly adsorb on these resins. In case of pH = 6.5 or above, it was suggested that MoO_4^{2-} forms as a main species. These Mo(VI) species with comparatively high negative valence states such as $Mo_7O_{23}^{4-}$ and MoO_4^{2-} have generally high adsorption ability for these resins. Hence, the decrease of K_d values of Mo(VI) species using WA20(Cl form) and AR-01(Cl form) resins must be attributable to the acid dissociation constants of the functional groups in WA20(Cl form) and AR-01(Cl form) resins because these functional groups such as polyamine and 1-methylbenzimidazole are classified as a weakly basic anion exchange resin [25,27]. This adsorption tendency implied that the Mo(VI) isotope fractionation experiments in adsorption-desorption reactions using WA20(Cl form) resin are available.

Moreover, on the assumption that the 1 : 1 anion-exchange reaction is proceeded, Mo(VI) + WA20(Cl form) ⇌ WA20·Mo(VI) + Cl^- under the conditions; [Mo(VI)] = 1.0 mM, [WA20(Cl form)] = 0.10 g, we have investigated the adsorption mechanisms between WA20(Cl form) resin and Mo(VI) species in aqueous solutions in further detail. The thermodynamic parameters (ΔH, ΔS, and ΔG values) for the adsorption of Mo(VI) species on WA20(Cl form) resin, ranging in Temp. = 278 - 333 K, were calculated from the linear plots of ln K_d against (1/T) using the following Van't Hoff equation (2) [28] and the obtained values were 1.5 ± 0.8, kJ / mol, 34 ± 3 J / (K·mol), and - 8.66 ± 0.01 kJ / mol at 298 K, respectively.

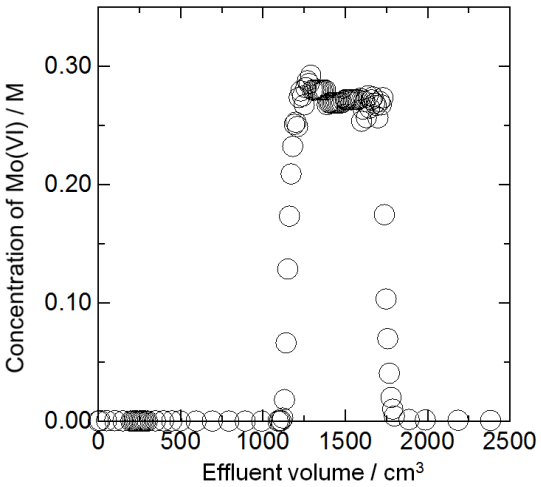

Figure 3. Profile of Mo(VI) concentration in the eluted fraction samples using WA20(Cl form) resin in aqueous solutions.

$$\ln K_d = -\Delta G / R \cdot T = -\Delta H / R \cdot T + \Delta S / R \quad (2)$$

Here, R and T represent gas constant and absolute temperature. This result indicates that the spontaneous adsorption processes between WA20(Cl form) resin and Mo (VI) species occur in aqueous solutions. The positive ΔH values show the endothermic reactions of Mo(VI) species with WA20(Cl form) resin. It can be considered that Mo(VI) species is surrounded by plenty of water in aqueous solutions due to the comparatively high solubility for H_2O. When Mo(VI) species are adsorbed onto WA20(Cl form) resin, the hydration shell of Mo(VI) species must be broken before the adsorption reactions of Mo(VI) species with WA20(Cl form) resin proceed in aqueous solution. Thus, these dehydration processes are expected to require energy. On the other hand, the polyamine-type functional groups in WA20(Cl form) resin are generally regarded as hydrophobic groups. Therefore, it was found that the positive ΔH values become very low, compared with those obtained from different adsorption systems [26]. In addition, the positive values of ΔS also suggest an increase in randomness at the boundary between Mo(VI) species and WA20(Cl form) resin during the adsorption processes. In brief, this tendency implies that the randomness arises due to the destruction of hydration shell of Mo(VI) species superior to the adsorption of Mo(VI) species on the surface of WA20(Cl form) resin. The lower positive ΔH values may cause the high effect of Mo(VI) isotope separation.

3.2. Chromatographic isotope fractionation of Mo(VI) species

The chromatography experiments for Mo(VI) isotope separation were carried out to evaluate the validation of our estimation in aqueous solutions at 298 K. Figure 3 shows the plateau of Mo(VI) concentration in the eluted fraction samples using WA20(Cl form) resin in aqueous solutions at 298 K. The amount of Mo(VI) species calculated from the plateau in Figure 3 is consistent with that obtained from the experimental condition. The typical isotope fractionation of Mo(VI) species is shown in Figure 4. In the figure, the notation of Mo isotope ratio deviation was defined as the isotopic ratios of

Mo-100/Mo-92 over effluent volume. The fractionation behavior of Mo-98/Mo-92 isotope ratio was similar to that of Mo-100/Mo-92 isotope ratio. The original isotope ratios of Mo-100/Mo-92 and Mo-98/Mo-92 were 7.89×10^{-1} and 1.88, respectively. It was found that the 100/92 Mo(VI) isotope ratios decrease sharply with increasing effluent volume and the Mo(VI) isotope ratios eventually approach the original values in case of the front band region. Therefore, this figure indicates that the heavier isotopes are disproportionately enriched in the solution phase. The depletion phenomena of the Mo(VI) isotope ratios were also confirmed in the rear band region. We have confirmed the three steps. In brief, first step exists when the elution volume is around 750 cm^3. Second step is in the range between ca. 1500 - 1600 cm^3, that is, the Mo(VI) original ratio. The effluent volume of third step was confirmed around 1750 cm^3. The existence of three steps indicates that there are three kinds of the Mo(VI) isotope fractionation in aqueous solutions. The chemical form of Mo(VI) species strongly depend on the pH in aqueous solutions [23]. The Mo(VI) species around pH = 5.5 and pH = 6.5 or above, form $Mo_7O_{23}^{4-}$ and MoO_4^{2-}, respectively. MoO_4^{2-} adsorbed on WA20(Cl form) resin was eluted using NaOH. The chemical reactions related to the present separation system can be expressed in the simplified form as follows:

$$Mo_7O_{23}^{4-} + WA20\cdot Cl \rightleftarrows [WA20\cdot Mo_7O_{23}]^{3-} + Cl^- \quad \text{(A-1)}$$

$$^{L}Mo_7O_{23}^{4-} + [WA20\cdot {}^{H}Mo_7O_{23}]^{3-} \rightleftarrows {}^{H}Mo_7O_{23}^{4-} + [WA20\cdot {}^{L}Mo_7O_{23}]^{3-} \quad \text{(A-2)}$$

$$MoO_4^{2-} + WA20\cdot Cl \rightleftarrows [WA20\cdot MoO_4]^- + Cl^- \quad \text{(B-1)}$$

$$^{L}MoO_4^{2-} + [WA20\cdot {}^{H}MoO_4]^- \rightleftarrows {}^{H}MoO_4^{2-} + [WA20\cdot {}^{L}MoO_4]^- \quad \text{(B-2)}$$

$$[WA20\cdot MoO_4]^- + OH^- \rightleftarrows WA20\cdot OH + MoO_4^{2-} \quad \text{(C-1)}$$

$$^{L}MoO_4^{2-} + [WA20\cdot {}^{H}MoO_4]^- \rightleftarrows {}^{H}MoO_4^{2-} + [WA20\cdot {}^{L}MoO_4]^- \quad \text{(C-2)}$$

where superscripts of H and L denote the heavier isotope and the lighter isotope, respectively. The isotope separation coefficients (ε) per unit mass (ε / $\Delta Mass$), which have been frequently used for the analysis of isotope fractionation using ion exchange chromatography and the corresponding height equivalent to a theoretical plate (HETP) derived from the theory of displacement type chromatographic enrichment in the isotopically transient state, are calculated by using the isotope fractionation curve of Mo-98 and Mo-100 in sample solutions. The equation can be expressed by Eq. (3, 4) [15,18,19-24].

$$\varepsilon / \Delta Mass = (\alpha - 1) / (Mass_H - Mass_L) = \Sigma \, (q_i \, |R_i - R_0| / \{Q \times R_0 \, (1 - R_0)\} / (Mass_H - Mass_L) \quad (3)$$

$$\text{HETP} = (\varepsilon / |k_s|) + (1 / k_s^2 \cdot L) \quad (4)$$

Here, α, $Mass_H$, $Mass_L$, q_i, R_i, and Q are the isotope fractionation factor, the mass of heavier isotope, the mass of lighter isotope, the amount of Mo in the fraction sample, the isotopic percentage of Mo, the total amount of adsorbed Mo species on the resin, respectively. The indication of fraction number is i = 0, 1, 2…. As a result, the calculated values of (ε / $\Delta Mass$) of Mo-100/Mo-92 and Mo-98/Mo-92 were found to be 1.0×10^{-4} and 8.7×10^{-5} in the front band region, respectively. These results imply that the (ε / $\Delta Mass$) values of Mo(VI) species are proportional to the reciprocal square of

the atomic weight, which is called mass shift effect [8]. These ε / $\Delta Mass$ values were analogous to those obtained from acid conditions [23,24]. By contrast, as (ε / $\Delta Mass$) values, 1.3×10^{-5} for Mo-100 /Mo-92 ratio and 8.3×10^{-6} for Mo-98 /Mo-92 ratio were calculated from the rear band region. In case of basic condition, the (ε / $\Delta Mass$) values became much smaller. The slope coefficient, k_s value is experimentally determined by plotting of ln (r_i - r_0) against X_{Bi}. The r_0 and X_B values are the original isotopic ratio and the distance from the front boundary. This r value can be defined as Mo-98/Mo-92 and Mo-100/ Mo-92 isotope ratios. The subscripts, i and 0 also denote the fraction number and original sample, respectively. Thus, the k_s values for Mo-98/Mo-92 and Mo-100/Mo-92 isotope ratios in aqueous solutions were calculated to obtain the HETP values and the analytical details of this equation have been described elsewhere [16]. As a result, the obtained HETP values was found to be more than 1.0 mm. The (ε / $\Delta Mass$) values were small and the HETP values were large, much larger (ε / $\Delta Mass$) values is needed to apply the present isotope separation system for nuclear medicine applications.

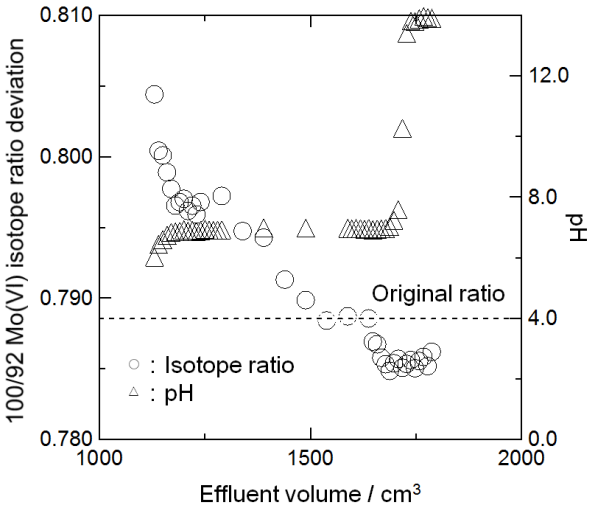

Figure 4. Profiles of Mo(VI) isotope ratios and their pH values in the eluted fraction samples using WA20(Cl form) resin in aqueous solutions.

4. Conclusion

The Mo(VI) isotope fractionation using well-known anion-exchange resins such as (WA20(Cl form)), (PA316(Cl form)), and (AR-01(Cl form)) resins, was investigated in aqueous solutions at 298 K. The adsorption experiments of Mo(VI) species using WA20(Cl form), PA316(Cl form), and AR-01(Cl form) resins were performed by batch-wise techniques to evaluate the K_d of Mo(VI) species in aqueous solutions in the pH 2.6 to 12.8 region at room temperature. As a result, it was found that PA316(Cl form) and AR-01(Cl form) resin have high adsorption ability for Mo(Vl) species in the broad pH range while the K_d values of WA20(Cl form) resin decreased sharply around neutral pH values. This adsorption tendency implied that the Mo(VI) isotope fractionation experiments in adsorption-desorption reactions are available. The ε / $\Delta Mass$ values of Mo(VI) species were obtained by using the isotope fractionation curve of Mo(VI) species with WA20(Cl form) resin. The ε / $\Delta Mass$ values obtained from acidic and basic conditions were compared and we have confirmed that the ε / $\Delta Mass$ values under acidic condition become much larger.

Acknowledgement

This work was partially supported by Nagaoka University of Technology Presidential Research Grant (A) (No. 13).

References

1) M.J. Heeg, S.S. Jurisson, *Acc. Chem. Res.,* **32**, 1053-1060 (1999).
2) Y. Nagai, Y. Hatsukawa, *J. Phys. Soc. Jpn.*, **78**, 033201-1-033201-4 (2009).
3) A. Kimura, Y. Sato, M. Tanase, K. Tsuchida, *IOP Conf. Series: Mater. Sci. Eng.*, **18**, 1-4 (2011).
4) K. Gagnon, F. Bėnard, M. Kovacs, T.J. Ruth, P. Schaffer, J.S. Wilson, S.A. McQuarrie, *Nucl. Med. Biol.,* **38**, 907-916 (2011).
5) J. Barling, A.D. Anbar, *Earth Planet Sci. Lett.*, **217**, 315-329 (2004).
6) T. Golgberg, C. Archer, D. Vance, S.W. Poulton, *Geochim. Cosmochim. Acta*, **73**, 6502-6516 (2009).
7) T. Kashiwabara, Y. Takahashi, M. Tanimizu, *Geochem. J.*, **43**, e31-e36 (2009).
8) J. Bigeleisen, M.G. Mayer, *J. Chem. Phys.*, **15**, 261-267 (1947).
9) Y. Fujii, M. Aida, M. Okamoto, T. Oi., Sep. Sci. Technol., 20, 377-392 (1985).
10) J. Bigeleisen, *J. Am. Chem. Soc.*, **118**, 3676-3680 (1996).
11) M. Nomura, N. Higuchi, Y. Fujii, *J. Am. Chem. Soc.,* **118**, 9127-9130 (1996).
12) I.M. Ismail, M. Nomura, Y. Fujii, *J. Chromatogr. A*, **808**, 185-191 (1998).
13) M.D.A. Matin, M. Nomura, Y. Fujii, J. Chen, *Sep. Sci. Technol.*, **33**, 1075-1087 (1998).
14) S.H. Kim, M. Aida, M. Nomura, M.N. Rifaid, Y. Fujii, *J. Ion Exchange*, **11**, 26-31 (2000).
15) I.M. Ismail, A. Fukami, M. Nomura, Y. Fujii, *Anal. Chem.*, **72**, 2841-2845 (2000).
16) Y. Ban, M. Aida, M. Nomura, Y. Fujii, *J. Ion Exchange*, **13**, 46-52 (2002).
17) C. Marėchal, F. Albarède, *Geochim. Cosmochim. Acta,* **66**, 1499-1509 (2002).
18) K. Hayasaka, T. Kaneshiki, M. Nomura, T. Suzuki, Y. Fujii, *Prog. Nucl. Energ.*, **50**, 510-513 (2008).
19) X. Ding, M. Nomura, T. Suzuki, Y. Fujii, *Prog. Nucl. Energ.*, **52**, 164-167 (2010).
20) T. Suzuki, M. Nomura, Y. Fujii, A. Ikeda-Ohno, T. Takaoka, K. Oguma, *J. Ion Exchange,* **21**, 328-333 (2010).
21) I.M. Ismail, M. Ibrahim, H.F. Aly, M. Nomura, Y. Fujii, *J. Chromatogr. A*, **1218**, 2923-2928 (2011).
22) T. Suzuki, Y. Tachibana, M. Nomura, Y. Fujii, *J. Plasma Fusion Res. Series*, **11**, 45-48 (2015).
23) Y. Tachibana, Y. Yamazaki, M. Nomura, T. Suzuki, *J. Radioanal. Nucl. Chem.,* **303**, 1429-1434 (2015).
24) Y. Tachibana, A.R. Putra, T. Kaneshiki, M. Nogami, T. Suzuki, M. Nomura, *Submitted to Energy Procedia.*
25) Information of structural details and chemical properties of WA20 and PA316 resins. http://www.diaion.com/en/products/ion_exchange_resins/index.html. Accessed 31 July 2017.
26) T. Suzuki, C. Kanzaki, M. Nomura, Y. Fujii, Rev. Sci. Instrum., **75**, 1931-1933 (2004).
27) G. Jerez, G. Kaufman, M. Prystai, S. Schenkeveld, K.K. Donkor, *J. Sep. Sci.*, **32**, 1087-1095 (2009).
28) P. Ilaiyaraja, K. Deb. A.K.S. Sivasubramanian, P.B. Venkatraman, *J. Hazard Mater.*, **250-251**, 155-166 (2013).

Transportation and Separation of Copper (II) and Cobalt (II) Ions Through a Liquid Membrane with Ligands of β-Diketone

Hiroshi MUKAI[1,*], Katsuya KITOH[1], Riu URASHIMA[1], Kouhei SUZUKI[1], Kengo SHINTANI[1], Rie HIROTA[1], Yuuya KOGURE[1], Tomohiro KIMURA[1], Takuya OGINO[1], Yuka KANAZAWA[1] and Yoshiki SOHRIN[2]

[1]Department of Chemistry, Kyoto University of Education, Fukakusa-fujinomori 1, Kyoto 612-8522, Japan; [2]Division of Environmental Chemistry, Institute for Chemical Research, Kyoto University, Gokasho, Uji, Kyoto 611-0011, Japan

Transportation and separation of copper (II) (Cu^{2+}) and cobalt (II) (Co^{2+}) ions through a liquid membrane with ligands of β-diketone types were studied using two types of transportation reaction cells, which were a double tube type and a supported liquid membrane type containing ionic liquid. Almost quantitative transportations of Cu^{2+} and complete separation of Cu^{2+} and Co^{2+} were observed using both of the liquid membrane transportation reaction cells. The control of transportation of Co^{2+} by pH was also achieved in the supported liquid membrane transportation. The electric potential gradient applied between the receiving phase and the suppling phase caused both to short the reaction time and to improve transportation efficiency in the transportation of Cu^{2+}. The transportation mechanisms were discussed.

1. Introduction

The separation and concentration of specific metal ions from an aqueous solution are necessary for analysis of trace metals or recovery of valuable metals. The simple, rapid and high efficient method has been requested. A liquid-liquid extraction is conventionally used for the separation and concentration of metal ions, which is consist of two phases of aqueous and organic phases. This method takes advantage of a phase transfer phenomenon of materials. On the other hand, a liquid membrane transportation method is consist of three aqueous/membrane/aqueous phases, which also utilizes phase transfer as such as the liquid-liquid extraction. The transportation of metal ions are achieved by complexation and dissociation of metal ions with ligands in the organic or membrane phase in both the liquid-liquid extraction and the liquid membrane transportation. By the sequence of complexation and dissociation at the interfaces, the transportation of metal ions is achieved from an aqueous phase to another aqueous phase via a membrane in liquid membrane transportation. The liquid membrane transportation has some advantages such as no phase separation operation, reducing hazardous organic solvent and so on, compared with the liquid-liquid extraction. However, it has several disadvantages such as slow kinetics, lack of innovation due to the basically same mechanism as the liquid-liquid extraction and so on.

Recently, the combination of liquid membrane and electrodialysis was proposed in order to

enhance the efficiency of the transportation and separation of metal ions [1]. The addition of electric potential inclination between two aqueous phases connected by a membrane phase to a liquid membrane transportation system is expected to change the transportation mechanism and kinetics and to improve the efficiency of the transportation and separation of metal ions. The fundamental investigation was carried out in this work in order to evaluate the performance and usability of the liquid membrane transportation system and the effect of electric potential gradient applied between two aqueous phases on the transportation efficiency of metal ions.

Using two types of the liquid membrane cells of a double tube type and a supported membrane type containing ionic liquid, the liquid membrane transportation and separation of the first series transition metal ions of copper (II) (Cu^{2+}) and cobalt (II) ions (Co^{2+}) were investigated. Ion-exchange through metal complex formation by multidentate ligands at interface between two adjacent phases and ionic transportation in each phase are considered to play important role in transportation and separation in phase transfer system. The experimental conditions such as kinds of membranes and ionic liquids and pH levels of aqueous phases were optimized to enhance the performance of liquid membrane transportation and separation of Cu^{2+} and Co^{2+} ions. Furthermore, electric potential gradient was applied between two aqueous phases that are connected by membrane of electrically conductive ionic liquid to promote the phase transportation of metal ions. The effect of electric potential on the phase transportation of metal ions was also investigated.

2. Experimental

2.1 Transportation of metal ions using a liquid membrane of chloroform

An bottomless inner glass tube with 30 mm diameter was set in the inside of an outer glass tube with 46 mm diameter (a 50 mL beaker) at the center, departed from the bottom of the outer tube at the distance of 5 mm (Figure 1a). The liquid membrane (LM) of 25 cm^3 chloroform with 0.1 mol dm^{-3} acetylacetone (acac) was set in the double tubes container [2]. The supplying phase (S) of 5 cm^3 volume of an aqueous solution ([$Cu(NO_3)_2$], [$Co(NO_3)_2$] = 2.0×10^{-5} mol dm^{-3}, [CH_3COONa] = 0.01 mol dm^{-3}, [HCl] = 2.0×10^{-3} mol dm^{-3}, pH 5) was placed in the inner tube on the liquid membrane of the chloroform solution. The recieving phase (R) of 5 cm^3 volume of an aqueous solution ([CH_3COONa] = 0.01 mol dm^{-3}, [HCl] = 0.1 mol dm^{-3}, pH 1) was in the outer tube also on the liquid membrane of the chloroform solution. Three phases were stirred by a magnetic stirrer placed on the bottom of the outer tube at the rotation speed of 270 rpm to transport the metal ions of Cu^{2+} and Co^{2+} from the supplying phase to the receiving phase through the liquid membrane. After a certain period of reaction time the solution of each phase was removed using the 5 mL pipet from the double tubes container, the volume of which was mesured using a volumetric cilinder. The 5 cm^3 chloroform solution as the membrane phase was mechanically shaken with a 5 cm^3 portion of 0.1 mol dm^{-3} HCl in a 30 mL centrifugal tube with a screw cap to strip all of the metal ions from the chloroform solution to the hydrochloric acid. After the pH measurements of the aqueous supplying and receiving phases, the metals in each aqueous phase and the hydrochloric acid after stripping were analized by use of atomic absorption spectrophotometry. The amount of substance and the fraction of metal ions in each phase were calculated from the product of the metal concentration and the volume of each solution.

2.2 Transportation of metal ions using a supported membrane containing ionic liquid

The supported liquid membrane consist of the hydrophobic Durapore membrane filter made with polyvinylidene fluoride (PVDF) with 0.45 μm pores and 47 mm diameter containing ionic liquid of 1-butyl-3-dodecylimidazolium bis(trifluoromethanesulfonyl)imide ($[C_4C_{12}im][Tf_2N]$) or 1-hexyl-3-methylimidazolium bis(trifluoromethanesulfonyl)imide ($[C_6C_1im][Tf_2N]$) with 0.005 mol kg^{-1} 1-phenyl-3-methyl-4-benzoylpyrazol-5-one (PMBP) was set between polyethylene plates with a large hole together with two hollowed silicon rubber sheets at the center of the reaction cell (Figure 1 b) and fixed to the plates by bolts. Before use the membrane filter was soaked in a shallow bath of the ionic liquid containing dissolved PMBP for 24 hours to insorb the liquid. The 25 cm^3 of aqueous supplying phase with metal ions M^{2+} (Cu^{2+}, Co^{2+}) ($[M(NO_3)_2] = 2 \times 10^{-5}$ mol dm^{-3}, $[CH_3COONa]$ = 0.01 mol dm^{-3}) and the 25 cm^3 of aqueous receiving phase without metal ions ($[CH_3COONa]$ = 0.01 mol dm^{-3}) were pored into each part of the reaction cell separated by the membrane at the middle. The pH level of each aqueous phase was controlled by the amount of HCl added to keep the pH level of the supplying phase heigher than that of the recieving one. The magnetic stirrers were set at the bottoms of both containers for the aqueous solutions. Electric potential difference of 1.5 V and direct electric current were applied between two aqueous pahses through the membrane using carbon rods with 5 mm diameter as an electrode dipped at 15 mm deep in each aqueous phase for electrodialysis. After a certain period of reaction time the pH values, the volume and the metal concentration of the supplying and receiving aqueous phases were measured. The amounts of metal ions in membrane and on carbon electrodes were measured by putting these materials in 0.1 mol dm^{-3} HNO_3 and by applying reverse voltage to the carbon electrodes to strip reduced metal on them. The amount of substance and the fraction of metal ions in each phase were calculated from the product of the metal concentration and the volume of each solution.

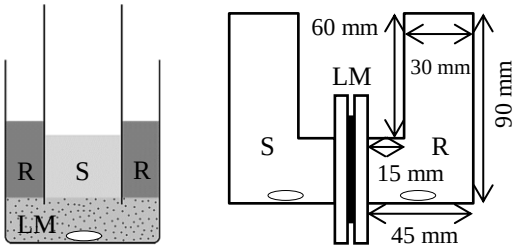

a b

Figure 1. Reaction cells for liquid membrane transportation. A double tube type (a) and a supported liquid membrane type (b). A supplying phase (S), a liquid membrane phase (LM) and a receiving phase (R).

3. Results and Discussion

3.1 Transportation of metal ions using liquid membrane of chloroform

Figure 2 shows the dependence of the fraction of Cu^{2+} of each phase on reaction time at 20 ^oC using a chloroform solution with 0.1 mol dm^{-3} acac as a liquid membrane. The fractions in the figure mean the ratios of the amount of substance of Cu^{2+} in each phase after the transportation for that in the supplying phase before the transportation. The total sums of the amount of substance in each phase well agreed with total amounts before the transportation. The transportation of Cu^{2+} from the supplying phase to the receiving phase could be completely achieved for 4 hours. The fraction of Cu^{2+} of the receiving phase increases gradually although that of the supplying phase decreases rapidly, as

shown in Figure 2. The reaction rate of the transportation from the membrane phase to the receiving one seems to be slower. In order to make the transportation faster, it is needed to fasten the dissociation of a metal complex at the interface between the membrane phase and the receiving one.

Figure 3 shows the time course of the transportation of each metal ion from the supplying phase that contains both Cu^{2+} and Co^{2+} ions. Only Cu^{2+} ions were transported to the receiving phase from the supplying phase because of the smaller complex formation constant of Co^{2+} than that of Cu^{2+} with acac [3]. The almost complete separation of Cu^{2+} and Co^{2+} ions was achieved by use of the liquid membrane transportation system. The transportation reaction rate of Cu^{2+} from the mixture was observed to be slower than that of Cu^{2+} separately transported, as shown Figure 3. This seems to be due to the competition with Co^{2+} ions in the complex formation in the supplying phase.

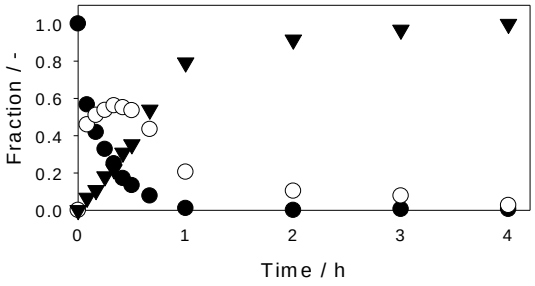

Figure 2. Molar fractions of Cu^{2+} in each phase by use of liquid membrane of chloroform with 0.1 mol dm^{-3} acac. The supplying phase (black circle), the liquid membrane phase (white circle) and the receiving phase (black triangle).

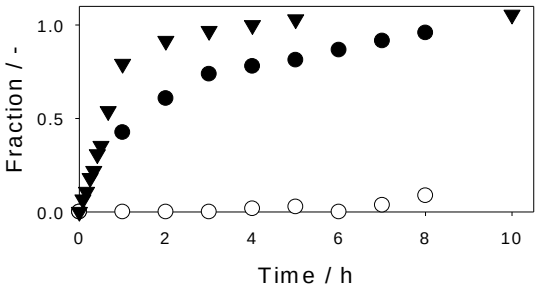

Figure 3. Respective molar fractions of Cu^{2+} and Co^{2+} in the receiving phase by use of liquid membrane of chloroform with 0.1 mol dm^{-3} acac. Cu^{2+} (black circle) and Co^{2+} (white circle) from the mixture and Cu^{2+} separately transported (black triangle).

3.2 Transportation of metal ions using supported membrane containing ionic liquid

Only about 15% of initial amount of Cu^{2+} was transported at maximum for 24 hours using acac with the concentration of 0.855 mol kg^{-1} in ionic liquid in the supported liquid membrane system. The remarkable decrease of the transportation efficiency of Cu^{2+} was observed in this system compared with the liquid membrane system of chloroform.

PMBP with the concentration of 0.005 mol kg^{-1} in $[C_4C_{12}im][Tf_2N]$ was employed as the ligand under the pH levels of the supplying and receiving phases set at 3 and 0, respectively. The results of the liquid membrane transformation of Cu^{2+} and Co^{2+} are summarized in Table 1 by showing the fractions of the metal ions in each aqueous phase for the initial amount of metal ions added in the supplying phase. The transportation efficiency of Cu^{2+} reached to 60% under this condition (No. 1). The transportation efficiency of Cu^{2+} was markedly enhanced using PMBP instead of acac, although the concentration of PMBP in ionic liquid is much lower than that of acac because PMBP is solid compared that acac is liquid at room temperature. Because of the large acid dissociation constant of PMBP (pK_a 3.92) [4-5] the activity of dissociated anion form species that forms a complex with a metal ion can be large even under an acidic condition.

In the transportation of Co^{2+} the transportation and no transportation of Co^{2+} could be

controlled by the adjustment of pH levels of the supplying and receiving phases (Nos. 2 and 3). In the transportation of Cu^{2+} and Co^{2+} from the mixture only Cu^{2+} ions could reach to the receiving phase (No. 4). As the result, Cu^{2+} ions were completely separated form Co^{2+} ions in the receiving phase.

Table 1 Molar fractions of metal ions in aqueous phases and total recovery rates by use of the supported liquid membrane containing ionic liquid of $[C_4C_{12}im][Tf_2N]$ with 0.005 mol kg^{-1} PMBP for 24 hours.

Exp. No.	Metal ion	Supplying phase	Receiving phase	Recovery rate	Final pH Supp. / Rec.
1	Cu^{2+}	0.26	0.60	0.86	2.7 / 0.1
2	Co^{2+}	1.04	0.00	1.04	2.7 / 0.1
3		0.07	0.58	0.65	5.0 / 1.0
4	Cu^{2+}	0.16	0.56	0.72	2.7 / 0.1
	Co^{2+}	1.08	0.00	1.08	2.7 / 0.1

3.3 Effect of electrodialysis

Electrodialysis that cause a direct electric current through the phases was applied to the the supported liquid membrane system by applying voltage of 1.5 V between the aqueous phases. The same experimental conditions as the above except for using $[C_6C_1im][Tf_2N]$ as ionic liquid were employed. Figure 4 shows the dependence of the fraction of Cu^{2+} of each phase on reaction time. The transportation efficiency of 0.72 was obtained for 6 hours. Due to the effect of electric potential gradient, the best efficiency in this system was obtained even for much shorter reaction time.

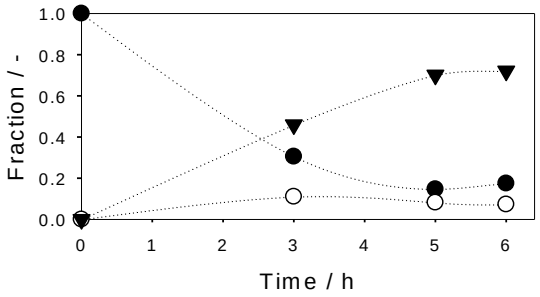

Figure 4. Molar fractions of Cu^{2+} in each phase by use of the supported liquid membrane containing ionic liquid of $[C_6C_1im][Tf_2N]$ with 0.005 mol kg^{-1} PMBP. The supplying phase (black circle), the liquid membrane phase (white circle) and the receiving phase (black triangle).

3.4 Mechanism of transportation

The most possible mechanism of transportation might be ion exchange reactions at the interfaces of the aqueous phases and liquid membrane one. A divalent metal ion and two protons are exchanged when the metal ion and the protons cross the interfaces reversely.

Ion exchange mechanism

$$Cu^{2+}{}_S + 2\,HL_{LM} \leftrightarrow CuL_{2,LM} + 2\,H^+{}_S \qquad \text{S/LM interface}$$

$$CuL_{2,LM} + 2\,H^+{}_R \rightarrow Cu^{2+}{}_R + 2\,HL_{LM} \qquad \text{LM/R interface}$$

Total reaction

$$Cu^{2+}{}_S + 2\,H^+{}_R \rightarrow 2\,H^+{}_S + Cu^{2+}{}_R$$

In the case of electrodialysis caused by electric potential gradient between the supplying and receiving phases using ionic liquid, electron transfer at electrodes and ion transfer due to

electorneutrality are combined.

Electrode reaction

$2\,H^+_R + 2\,e^- \rightarrow H_{2,R}$ cathode in R

$2\,OH^-_S \rightarrow 1/2\,O_{2,S} + H_2O_S + 2\,e^-$ anode in S

Ion transfer

$2\,C^+A^-_{LM} \rightarrow 2\,C^+_R + 2\,A^-_S$

Overall reaction

$$Cu^{2+}_S + 2\,OH^-_S + 4\,H^+_R + 4\,Cl^-_R + 2\,C^+A^-_{LM} \rightarrow 2\,H^+_S + 2\,A^-_S + 1/2\,O_{2,S} + H_2O_S + Cu^{2+}_R + 2\,C^+_R + 4\,Cl^-_R + H_{2,R}$$

The electron transfer at the electrodes could be oxidation and reduction of electrolysis of water or chloride ion. Bubbles on the electrodes generated by electrolysis were not observed because of the small electric current of about 70 μA. In order to keep electroneutrality in each phase, the transfer of cations and anions of ionic liquid into the aqueous phases occurs. The transportation of Cu^{2+} was accelerated under the influence of electric potential. This phenomenon might suggest that the formation and dissociation of a metal complex followed by the transportation of metal ions is promoted due to the effect of the electric field of electric double-layer formed at aqueous/membrane and membrane/aqueous interfaces.

4. Conclusion

The liquid membrane system studied almost completely achieved the transportation of Cu^{2+} and the separation of Cu^{2+} from the mixture with Co^{2+}. It was observed that the combination of ionic liquid and the electric potential gradient in this system accelerated the transportation reaction rate and improved transportation efficiency. The separation of metal ions by use of the liquid membrane system combined with electrodialysis is expected to be investigated further.

Acknowledgement

This study was supported by the Collaborative Research Program of Institute for Chemical Research, Kyoto University (grant # 2014-51, 2015-52, 2016-42 and 2017-41).

References

1) T.Zh. Sadyrbaeva, *J. Membr. Sci.*, **275**, 195–201 (2006).
2) M. Senoo, H. Kise, I. Kobayashi, *Seisankenkyu*, **35**, 281-284 (1983).
3) T. Sekine, M. Katori, R. Murai, T. Saitou, *Bunseki Kagaku*, **33**, E351-E358 (1984).
4) S. Umetani, M. Matsui, *Bull. Chem. Soc. Jpn.*, **56**, 3426-3431 (1983).
5) H. Mukai, S. Miyazaki, S. Umetani, S. Kihara, M. Matsui, *Anal. Chim. Acta*, **239**, 277-282 (1990).

Zinc(II) Membrane-Extraction by *N*-decyloxy-1-(3-pyridyl)ethanoimine Using Pseudo-Emulsion Based Hollow Fiber Strip Dispersion (PEHFSD) Processing

Aleksandra WOJCIECHOWSKA[1]*, M. Teresa A. REIS[2], M. Rosinda C. ISMAEL[2], Karolina WIESZCZYCKA[1], Irmina WOJCIECHOWSKA[1], Jorge M. R. CARVALHO[2]

[1]University of Technology, Institute of Chemical Technology and Engineering, Berdychowo St. 4, 60-965 Poznan, Poland; [2]CERENA – Centre for Natural Resources and the Environment, Department of Chemical Engineering, Instituto Superior Técnico, Universidade de Lisboa, Av. Rovisco Pais, 1049-001 Lisboa, Portugal

The extraction of zinc(II) ions from chloride solutions through pseudo-emulsion based membrane strip dispersion (PEHFSD) using *N*-decyloxy-1-(3-pyridyl)ethanoimine or tributylphosphate as the extractants was investigated. The metal ions transport was investigated as a function of the composition of the organic membrane phase. The overall mass transfer coefficient of permeation was calculated from the experimental data, the values being found in the range of 1.8×10^{-7}–2.3×10^{-6} m/s. The best results in terms of the kinetics of extraction were obtained for the pyridine extractant. The recovery of zinc with pyridine (0.05 M, 0.1 M) and with TBP (1.4 M, 2.9 M) extractants attained values of ~75% and 85–95%, respectively, using water as the strippant. The removal of zinc from aqueous solution exceeded 95% in most cases.

1. Introduction

The *Supported Liquid Membrane* technology (SLM) is a membrane-based solvent extraction method that uses a micro-porous hydrophobic membrane as supporting layer [1]. This membrane, often polypropylene, is impregnated with an organic solvent containing the specific carrier molecules for metal ion extraction [2]. The SLM-technology results, according to the industrial needs, into a strongly reduced disposal of metal waste. This technique not only reduces and avoids waste, but also aims at the recovery of valuable products. The vast majority of industrial effluents and waste water, such as mining water, etching or pickling baths, dilute leach solutions generated during hydrometallurgy, electroplating rinse liquors, etc. may carry Zn(II), Cu(II), Co(II) etc. in low concentrations [3]. SLM membranes also include hollow fiber membranes.

Since many years the scientists have been writing about the advantage of the Pseudo-Emulsion Hollow Fiber Strip Dispersion (PEHFSD) technique offers a potential attractive alternative to the conventional processes because it combines the process of extraction and stripping in a single unit operation. Furthermore, the consumption of the extractant is much smaller than in the classical extraction. An important advantage of hollow fiber membranes is that compact modules with very high membrane surface areas can be formed. The diameter of hollow fibers varies over a wide range,

from 50 to 3000 μm. Pseudo-emulsion system is a very promising method for treatment of liquid waste streams with toxic or valuable metal ions [4].

The aim of this work was to study the possibility of using the non-comercial extractant - *N*-decyloxy-1-(3-pyridyl)ethanoimine (3PC1-OC10) for recovery of Zn(II) from chloride solutions using the PEHFSD technique and compare the results with those obtained with the classical extractant tributylphosphate (TBP).

2. Experimental

2.1 Reagents

N-decyloxy-1-(3-pyridyl)ethanoimine (Figure 1.) was synthesized according procedure described in previous papers [5]. Toluene (ACS reagent, Chem-Lab NV, Belgium) and decan-1-ol (Merck, Germany) were used as components of the organic phase. Sodium chloride (ACS reagent, Panreac, Spain), hydrochloric acid (35%) (AR reagent; VWR, USA), sodium sulfate (ACS reagent, AppliChem, Germany) and zinc(II) chloride (anhydrous) (ACS reagent, Chem-Lab NV, Belgium) were used to compose the aqueous phase.

The organic phase used in the extraction studies contained the synthesized compound (0.05 M or 0.1 M) and toluene (Carlo Erba, France) as a diluent with a 10% (v/v) addition of decan-1-ol (Merck, Germany). Tributyl phosphate (Rhodia, Netherlands) was also used as a carrier being diluted in ShellSol D70 (aliphatic diluent; aromatic content <0.01%, Drogas Vigo, Portugal).

The aqueous solutions before and after tests were analyzed for zinc(II) concentration by AAS using a Perkin Elmer - AAnalyst 200 at 213 nm in the air-acetylene flame.

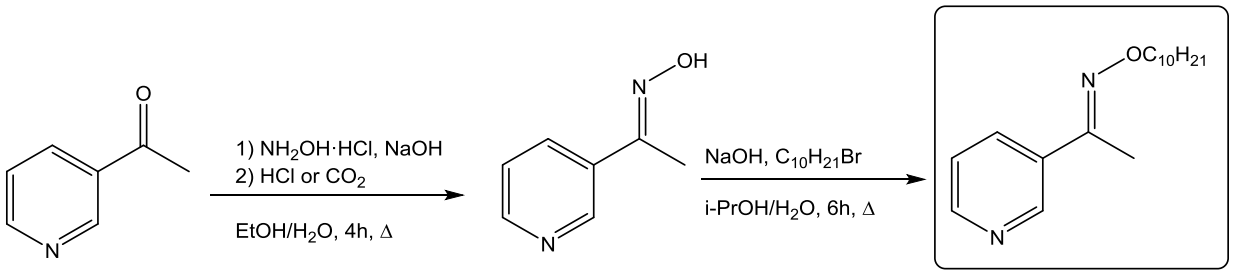

Figure 1. Two-step synthesis of *N*-decyloxy-1-(3-pyridyl)ethanoimine

2.2 PEHFSD experiments

The experimental setup used for carrying out PEHFSD experiments is shown in Figure 2. The HF experiments were carried out in a polypropylene microporous fiber module Liqui-Cel® Extra-Flow (2.5×8 inch) G501, supplied by Celgrad (USA). The module length and diameter were 28 and 7.7 cm, respectively. The module contained ~10,800 fibers with the effective fiber length 15.6 cm and inner and outer diameters of the fibers were equaled to 214 and 300 μm [6].

The volume of the feed solution in the experiments was 800 cm^3 and the same volume of pseudo emulsion, organic and striping solutions (400 cm^3 for each). The organic phase used in the HF studies contained *N*-decyloxy-1-(3-pyridyl)ethanoimine and toluene with 10% (v/v) addition of decan-1-ol or TBP diluted in ShellSol D70. The concentration of the 3PC1-OC10 was 0.05 and 0.1 M,

whereas the concentration of TBP was 1.4 M (40% v/v) and 2.9 M (80% v/v). The feed solution, containing zinc(II) chloride (1.0 g/L of Zn), sodium chloride (1 M) and hydrochloric acid (1 M), was pumped through the hollow fibers. The stripping phase (H_2O) was dispersed into the organic phase, containing the extractant. The pseudo-emulsion flows through the shell side of the membrane module and the aqueous feed phase flows through the tube side. The overpressure on the tube side was in the range of 20-40 kPa to avoid the transport of the organic phase from entering the hollow fibers through the micropores to the feed solution. The flow rate of the aqueous phase was kept at 290-300 mL/min, whereas the flow rate of the pseudo-emulsion phase was kept at 260-270 mL/min. The experiments were conducted at room temperature (typically 23 ºC).

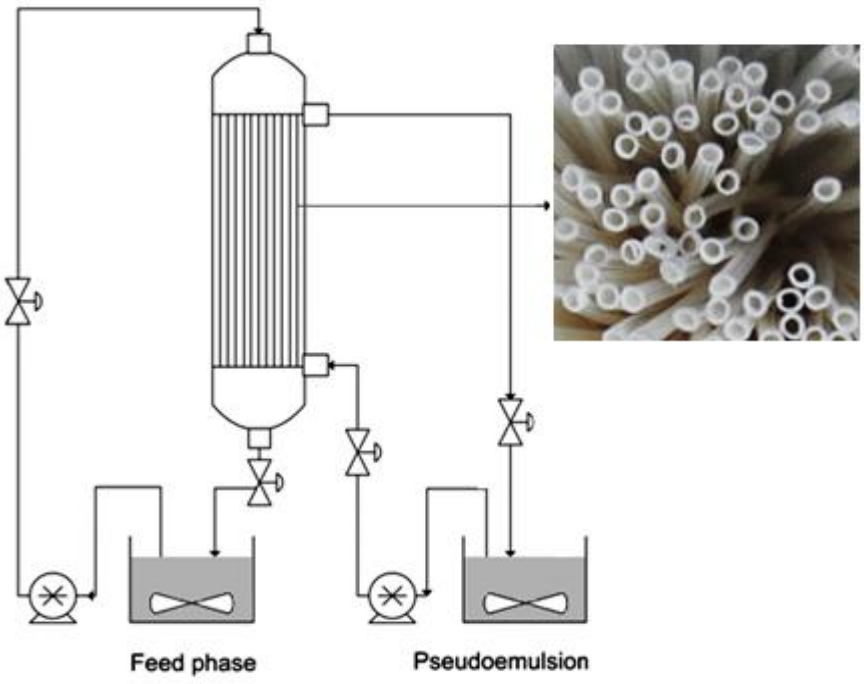

Figure 2. PEHFSD experimental setup

2.3 Calculations

The analysis of the results was made on the basis of the overall mass transfer coefficient of Zn(II) permeation K_P. According to the model for the transport of metal ions in PEHFSD operating in the recycling mode presented in previous studies [7,8], the following linear relationship was derived:

$$V_{aq} \ln \frac{[Zn]_{aq,0}}{[Zn]_{aq}} = St \qquad (1)$$

where V is the volume of the phase, t is the time and aq and 0 refer to the aqueous feed phase and initial value, respectively. Thus, the coefficient K_P can be estimated from the slope S of this linear relationship being given as:

$$K_P = -\frac{u_{aq} r_i}{2L} \ln\left[1 - \left(\frac{S}{Q_{aq}}\right)\right] \quad (2)$$

where u is the linear velocity, Q is the flow rate, r_i is the inner radius of the fiber and L is the fiber length.

3. Results and Discussion

Table 1 summarizes experimental data from PEHFSD experiments using 3PC1-OC1 and TBP as the carriers. Figure 3 illustrates the determination of the overall mass transfer coefficient of zinc permeation from Equations (1) and (2).

Table 1. Exemplary results obtained for aqueous feed solutions containing 1.0 g/L Zn(II), 1 M HCl and 1 M NaCl; strippant: water.

Organic phase	Extraction				Recovery	K_P (m/s)
	15 min	30 min	1 h	2 h		
0.05 M 3PC1-OC10	45%	77 %	96%	-	76%	4.8×10^{-7}
0.1 M 3PC1-OC10	91%	97%	-	-	74%	2.3×10^{-6}
1.4 M (40%) TBP	20%	38%	62%	90%	85%	1.8×10^{-7}
2.9 M (80%) TBP	50%	73%	92%	96%	95%	5.7×10^{-7} [7]

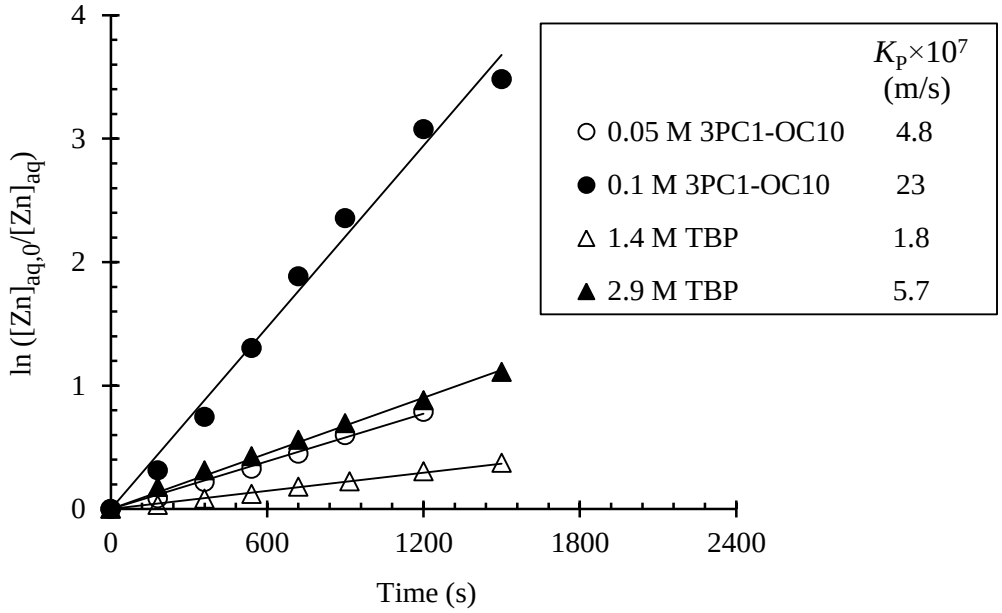

Figure 3. Influence of type and concentration of extractant (3PC1-OC10 or TBP) on zinc transport. Aqueous feed phase: 1.0 g/L Zn(II), 1 M HCl and 1 M NaCl; pseudo-emulsion: (3PC1-OC10 or TBP) and H_2O.

The bests result in terms of mass transfer rate was attained with 0.1 M of 3PC1-OC1. Actually, the extraction efficiency was 97% for 30 min and it was 91% for 15 min of permeation time. The decrease in the concentration of the pyridine extractant from 0.1 M to 0.05 M made the kinetics of the extraction slower, the overall mass transfer coefficient K_P being reduced from 2.3×10^{-6} to 4.8×10^{-7} m/s. It is worth mentioning that the use of 0.05 M 3PC1-OC1 and 80% TBP led to similar kinetics of zinc extraction, as noted from % extraction along time and K_P values (Table 1), as well as from the straight lines depicted in Figure 3. It should be emphasized that in this case the molar concentration of TBP is 58 times higher than that of 3PC1-OC1. The reduction in the concentration of TBP from 80% to 40% decreased the K_P value from 5.7×10^{-7} to 1.8×10^{-7}. Nevertheless, the use of 40% and 80% TBP in the membrane allowed recovering zinc with a very high yield, i.e. 85% and 95%, respectively, after 2 h of permeation. On the other hand, the recovery attained with the pyridine extractant was lower (74-76%), since part of the metal extracted to the organic phase was not stripped with water. However, the stripping process was found more efficient if water was substituted by 5% Na_2SO_4 aqueous solution (data not shown).

4. Conclusion

The novel extractant *N*-decyloxy-1-(3-pyridyl)ethanoimine showed to be a potential carrier of zinc(II) ions from chloride solution using pseudo-emulsion based membrane strip dispersion technique. The efficiency of extraction for a feed phase containing 1.0 g/L of Zn(II) attained very high values (i.e., 96-97%), being comparable to those obtained with the conventional extractant TBP. Nevertheless, the pyridine extractant exhibited a faster kinetics of permeation; the overall mass transfer coefficient of Zn(II) was of the same order of magnitude when the concentration of 3PC1-OC10 in the membrane was much smaller than that of TBP. The recovery of zinc in water (strippant) was found to be in the range of 74-95%. .

Acknowledgement

This study was funded by National Science Center Poland research grant funds according to decision No. DEC-2015/17/N/ST8/00285. Financial support through the project UID/ECI/04028/2013 (FCT, Portugal) is also acknowledged.

References

1) Encyclopedia of Life Support Systems (Eolss): v.1 : *Desalination and Water Resources (Desware): Membrane Processes*. Oxford: EOLSS Publishers Co Ltd. (2010).
2) L. Wang, J. Chen, Y. Hung, N. Shammas, *Membrane and Desalination Technologies*. Springer Science & Business Media (2003).
3) R. Prasad, K. K. Sirkar, Membrane-based solvent extraction, in: W.S.W. Ho, K.K. Sirkar (Eds.), *Membrane Handbook*, Van Nostrand Reinhold, New York, 727–763 (1992).
4) K. Pabby, S.S.H. Rizvi, A.M. Sastre, *Handbook of Membrane Separations*, CRC Press, (2008).
5) A. Wojciechowska, K. Wieszczycka, G. Framski, *Modern Organic Chemistry Research*, **2**(2), 41-47 (2017).

6) *http://www.liquicel.com; Design & Operating Guidelines; 2.5 x 8 EXTRA-FLOW PRODUCT DATA SHEET*
7) K. Wieszczycka, M. Regel-Rosocka, K. Staszak, A. Wojciechowska, M.T.A. Reis, M.R.C. Ismael, M.L.F. Gameiro, J.M.R. Carvalho, *Sep. Purif. Technol*. **154**, 204–210 (2015).
8) S. Agarwal, M.T.A. Reis, M.R.C. Ismael, J.M.R. Carvalho, *Sep. Purif. Technol.*, **127**, 149–56 (2014).

Application of Pseudo-Emulsion Based Hollow Fiber Strip Dispersion (PEHFSD) for Recovery of Zn(II) Using TBP-3PC10 Mixture as Carrier

Aleksandra WOJCIECHOWSKA[1]*, M. Teresa A. REIS[2], Karolina WIESZCZYCKA[1], M. Rosinda C. ISMAEL[2], Joanna BORNIKOWSKA[1], Martyna FRĄCKOWIAK[1], Magdalena REGEL-ROSOCKA[1], Jorge M.R. CARVALHO[2]

[1]University of Technology, Institute of Chemical Technology and Engineering, Berdychowo St. 4, 60-965 Poznan, Poland; [2]CERENA – Centre for Natural Resources and the Environment, Department of Chemical Engineering, Instituto Superior Técnico, Universidade de Lisboa, Av. RoviscoPais, 1049-001 Lisboa, Portugal

The recovery of Zn(II) from chloride solutions using pseudo-emulsion based hollow fiber strip dispersion (PEHFSD) technique with TBP-3PC10 (tributyl phosphate and 1-(3-pyridyl)undecan-1-one oxime) mixture was investigated. The influence of several parameters, among them the concentration of the oxime as modifier of the organic phase was studied. The extractants proposed showed to be appropriate carriers in PEHFSD process and the overall mass transfer coefficient of Zn(II) permeation was found to be 1.0×10^{-6} m/s for the mixtures tested.

1. Introduction

For many years, for industrial scale zinc(II) has been extracted from the hydrochloric acid solution with tributyl phosphate (TBP). Using this type extractant Zn(II) can be extracted in inert chlorocomplex form of $ZnCl_2$ and anionic forms of chlorocomplexes $ZnCl^{3-}$ and $ZnCl_4^{2-}$. Zinc extraction with TBP is affected by many factors such as chloride ions concentration inthe aqueoussolution and the concentration of the extractant in the organic phase. TBP is also a good extractant of organic and inorganic acids, used to regenerate spent nuclear fuel in the PUREX process.

In the case of the Zn(II) extraction from acidic chloride solutions, it is a major disadvantage that TBP co-extracts the mineral acid to the organic solution reducing the extraction of zinc(II) [1]. Due to such extensive use of TBP, it was decided to test the synthesized compound - oxime of 1-(3-pyridyl)undecan-1-one (3PC10) (Figure 1.) as modifier of organic phase to improve TBPextraction properties. The modifier in the extraction process can be defined as a substance whichadded to the organic phase changes the properties of this phase. Modifiers can improve extraction, reduce the surface tension at the interface, so that the extracted compounds can be easier moved to the organic phase. The role of the modifier is also to prevent the formation of third phase [2].

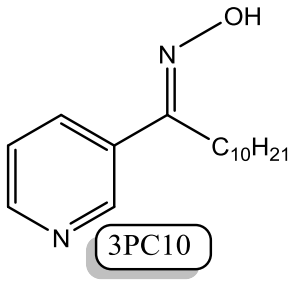

Figure 1. Modifier of TBP- oxime of 1-(3-pyridyl)undecan-1-one

The aim of this work was to study the possibility of using the novel mixture of extractants – TBP-3PC10 for the recovery of Zn(II) from chloride medium using the PEHFSD technique.

2. Experimental

2.1 Reagents

The non-commercial extractant-oxime of 1-(3-pyridyl)undecan-1-one (3PC10) was synthesized in a two stage reaction . In the first stage 1-(3-pyridyl)undecan-1-one was synthesized by treating 3-pyridylcarbonitrile with decylmagnesium bromide in Grignard reaction. In the second stage, the ketone was treated with hydroxylamine hydrochloride in the presence of sodium hydroxide (at pH = 7) [3-5].A purity of the final product-1-(3-pyridyl)undecan-1-one oxime was confirmed by NMR spectroscopy.

1-(3-pyridyl)undecan-1-one oxime (**3PC10**): ^{1}H NMR ($CDCl_3$) δ in ppm: 9.10 (s, 1H, OH); 8.65 (d, 1H, $H_{py}(2)$); 8.30 (d, 1H, $H_{py}(6)$); 8.25 (d, 1H, $H_{py}(4)$); 7.70 (t, 1H, $H_{py}(5)$); 2.80 (t, 2H, CH_2); 1.55 (q, 2H, CH_2); 1.45-1.15 (m, 18H, CH_2); 0.90 (t, 3H, CH_3); ^{13}C NMR ($CDCl_3$) δ in ppm: 157.0 (oxime C=N); 149.3 ($C_{py}(6)$); 147.2 ($C_{py}(2)$); 133.7 ($C_{py}(4)$); 132.2 ($C_{py}(5)$); 122.9 ($C_{py}(3)$); 62.8 (-CH_2(CNOH)); 31.6 (CH_2); 29.8 (CH_2); 29.6 (CH_2); 29.3 (CH_2); 29.1 (CH_2); 26.2 (CH_2); 25.6 (CH_2); 22.5 (CH_2); 14.0 (CH_3).

TBP (Rhodia, Netherlands) and toluene (Carlo Erba, France) were used as components of the organic phase. Sodium chloride (ACS reagent, Panreac, Spain), hydrochloric acid (35%) (AR reagent; VWR, USA); zinc(II) chloride (anhydrous) (ACS reagent, Chem-Lab NV, Belgium) were used to compose the aqueous phase. The organic phase used in the extraction studies contained the synthesized compound in 0.025 and 0.05M and TBP and toluene as the diluents.

The aqueous solutions before and after tests were analyzed for zinc(II) concentration by AAS using a Perkin Elmer - AAnalyst 200 at 213 nm in the air-acetylene flame.

2.2 Pseudo-emulsion based membrane strip dispersion tests

The PEHFSD experiments were carried out in the commercial membrane module, Liqui-Cel® Extra-Flow (2.5×8 inch) produced by CELGARD (USA)[6]. Experimental module system is shown in Figure 2. Further module (contactor G501) details are given in Table 1.

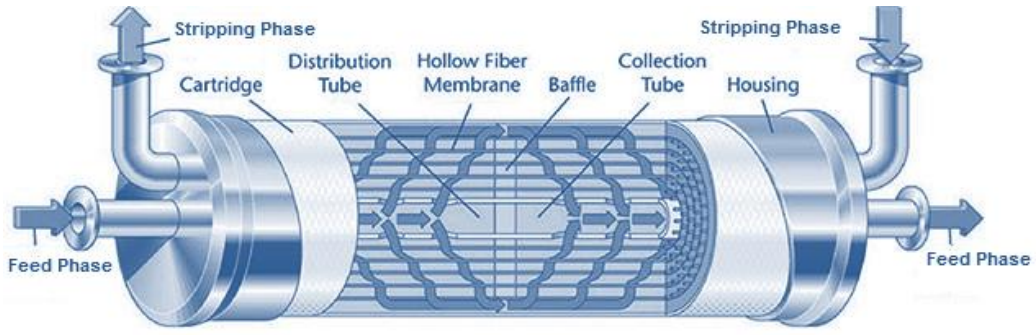

Figure 2. Commercial module hollow fiber

Table 1. Characteristics of hollow fiber membrane module [6,7]

Type of module : G501 (contactor)	
Module length (cm)	28
Module diameter (cm)	7.7
Case inner diameter (cm)	5.55
Centre tube diameter (cm)	2.22
Number of fibers	~10,800
Fiber	X50 – polypropylene
Effective fiber length (cm)	15.6
Inner diameter of the fibers (µm)	214
Outer diameter of the fibers (µm)	300
Pore size (µm)	0.03
Porosity (%)	40
Tortuosity	2.6
Inner interfacial area (m^2)	1.13
Area per unit volume (cm^2/cm^3)	28

The volume of the pseudo-emulsion phase used in the experiments was 800 cm^3, therein 400 cm^3 of the organic solution (0.025 or 0.05M of 3PC10 dissolved in TBP/toluene) and 400 cm^3 of strippant (H_2O). The aqueous phase (800 cm^3) contained zinc(II) in 1 g/L. All tests were carried out for around 2–2.5 h. The samples of the aqueous and pseudo-emulsion phases were collected at regular time intervals, during the process. The overpressure on the tube side was in the range of 20-40 kPa. Both phases were pumped to the module by two pumps capable of variable flows; the flow rate of the aqueous phase was kept at 290–300 mL/min, whereas the flow rate of the pseudo-emulsion phase was kept at 200–280 mL/min. The experiments were conducted at room temperature.

3. Results and Discussion

Several tests using PEHFSD liquid membrane configuration were carried out by varying the composition of the organic phase. Exemplary results are displayed in Table 2. The analysis of the kinetics of the extraction was made on the basis of the overall mass transfer coefficient of Zn(II) permeation K_P. This coefficient was calculated according to the model for the transport of metal ions in PEHFSD operating in the recycling mode presented in a previous study [1]. Figure 3 illustrates the linear relationships obtained, which allow to derive K_p values.

As observed, the addition of a small concentration (0.025–0.05 M) of the non-commercial 3PC10 extractant in the membrane phase, which contains 50% of TBP, strongly increased the extraction rate. In fact, the overall mass transfer coefficient K_P was almost four times higher in the presence of the pyridineketoxime reagent. On the other hand, the mixtures TBP-3PC10 and TBP (100%) led to comparable K_P values ($1.0–1.4 \times 10^{-6}$ m/s). The increase in the concentration of 3PC10 from 0.025 to 0.05 M had no significant effect on the kinetics of zinc extraction, the K_P values being

1.0×10^{-6} m/s. It is worth mentioning that if an organic phase with 0.05 M of 3PC10 (without TBP) was used, the expected value for K_P would be much lower (i.e., 4.9×10^{-7}m/s [8]), which also emphasizes the importance of the presence of TBP in the mixture. Hence, the mixture TBP-3PC10 showed to be a potential carrier of Zn(II) ions from acidic chloride solution. In addition, the recovery of Zn(II) was verified to be very high (95-100%), the overall extraction/stripping performance being more attractive than that of single TBP. As stated before, one major disadvantage of the use of TBP is due to HCl co-extraction to the organic solution reducing the extraction of zinc(II). Therefore, the study ought to be further intensified to optimize the concentration of the oxime modifier in the organic phase, as well as the amount of TBP under various compositions of the feed phase.

Table 2. Exemplary results obtained for aqueous feed solutions containing 1.0 g/L Zn(II), 1 M HCl and 1 M NaCl; strippant: water.

Organic phase	Extraction 15 min	Extraction 30 min	Extraction 1 h	Extraction 2 h	Recovery	K_P (m/s)
1.8 M (50% v/v) TBP	28%	50%	78%	96%	87%	2.8×10^{-7}
3.6 M (100%) TBP	77%	95%	97%	93%	92%	1.4×10^{-6}
0.025 M 3PC10+1.8M TBP	70%	95%	99%	99%	~100%	1.0×10^{-6}
0.05 M 3PC10+ 1.8 M TBP	67%	94%	99%	100%	95%	1.0×10^{-6}

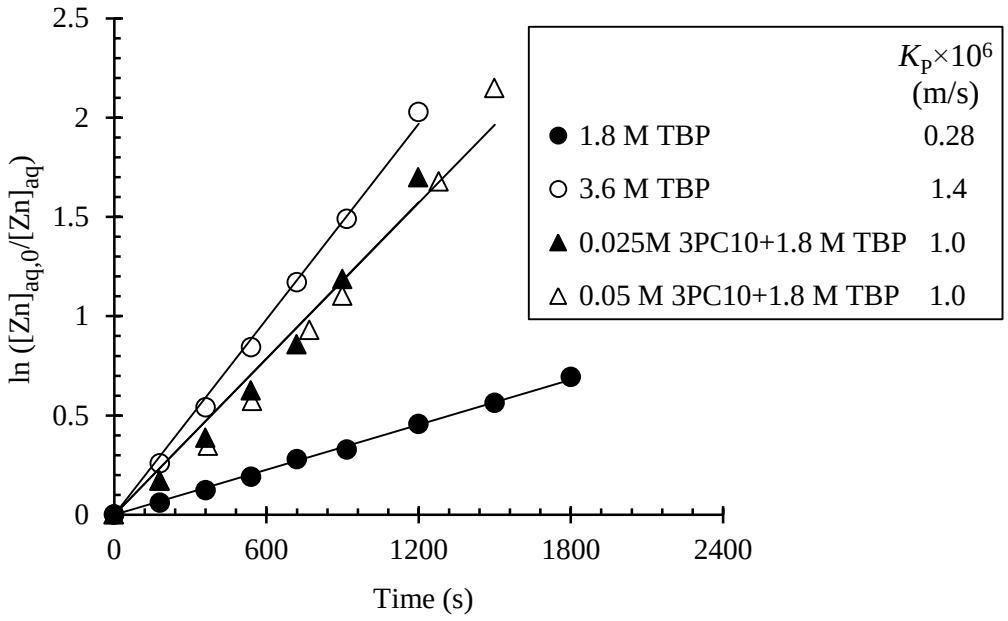

Figure 3. Influence of composition of the organic phase on zinc transport. Aqueous feed phase: 1.0 g/L Zn(II), 1 M HCl and 1 M NaCl; pseudo-emulsion: (3PC10+TBP or TBP) and H_2O.

4. Conclusion

The mixture TBP-3PC10 (tributyl phosphate and 1-(3-pyridyl)undecan-1-one oxime) showed to be a potential extractant of zinc(II) ions from chloride solution using pseudo-emulsion based membrane strip dispersion technique. The recovery of zinc from a feed phase containing 1 g/L of solute attained very high values (i.e., 95-100%) by using 0.025-0.05 M of 3PC10 diluted in TBP/toluene, the yield being higher than that achieved with 100% of TBP in the membrane. In what concerns the kinetics of extraction, the results obtained with the mixtureTBP-3PC10 were found comparable to those obtained with 100% of TBP. Further studies are necessary to optimize the concentration of 3PC10 in the mixture under variable feed compositions.

Acknowledgement

This study was funded by National Science Center Poland research grant funds according to decision No. DEC-2015/17/N/ST8/00285 as well as FCT, Portugal - “Fundação para a Ciência e a Tecnologia” project UID/ECI/04028/2013.

References

1) K. Wieszczycka, M. Regel-Rosocka, K. Staszak, A. Wojciechowska, M.T.A. Reis, M.R.C. Ismael, M.L.F. Gameiro, J.M.R. Carvalho, *Sep. Purif. Technol.*,**154**, 204-210, (2015).
2) F. Habashi, Handbook of Extractive Metallurgy, WILEY-VCH Weinheim, (1997).
3) K. Wieszczycka, A. Wojciechowska, M. Krupa, R. Kordala-Markiewicz, Quaternary pyridiniumketoximes as zinc extractants from chloride solutions, *J. Chem. Eng. Data*, **58**(11),3207–3215 (2013).
4) K. Wieszczycka, Recovery of Zn(II) from multielemental acidic chloride solution with hydrophobic 3-pyridineketoxime, *Sep. Purif. Technol.*, **114**,17–23(2013).
5) A. Wojciechowska, K. Wieszczycka, I. Wojciechowska, A. Olszanowski, Lead(II) extraction from aqueous solutions by pyridine extractants, *Sep. Purif. Technol*.**177**, 239–248 (2017). DOI: 10.1016/j.seppur.2016.12.036
6) *http://www.liquicel.com; Design & Operating Guidelines; 2.5 x 8 EXTRA-FLOW PRODUCT DATA SHEET*
7) A. Wojciechowska, K. Wieszczycka, I. Wojciechowska, M.T.A. Reis, M.R.C., Ismael, M.L.G., Gameiro, J.M.R. Carvalho, Application of Pseudo-Emulsion Based Hollow Fiber Strip Dispersion with Quaternary Pyridinium Salts for the Recovery of Zinc(II) from Chloride Solutions, 43rd International Conference of SSCHE, TatranskéMatliare, Slovakia, May 23–27, (2016).
8) K. Staszak, A.Wojciechowska, M.T.A. Reis, I. Wojciechowska, K. Wieszczycka, M.R.C.Ismael, J.M.R. Carvalho, Recovery ofzinc(II) from chloride solutions using pseudo-emulsion based hollow fiber strip dispersion with pyridineketoxime extractants, *Sep. Purif. Technol.***177**, 152-160 (2017).

Membrane-Based Solvent Extraction for Cobalt(II) Separation Using Cyanex 272

Malgorzata JANISZEWSKA[1], Eugenio BRINGAS[2,*], María F. SAN ROMAN[2], Magdalena REGEL-ROSOCKA[1], Inmaculada ORTIZ[2]

[1]*Institute of Chemical Technology and Engineering, Poznan University of Technology, Poznan, Poland*
[2]*Department of Chemical and Biomolecular Engineering, University of Cantabria, Santander, Spain*

Membrane-based solvent extraction of cobalt(II) from sulfuric waste solutions and model solutions containing nickel(II) and cobalt(II) sulfates was analyzed. Hollow fiber membrane contactor was used for the process. Solvent extraction was conducted using commercial extractant Cyanex 272. Organic phase was passed through the tube side while the acidic feed containing metals was passed through the shell side in counter-current mode. Simultaneous back extraction with sulfuric acid and its influence on the separation process was also tested. Pseudo-emulsion of stripping solution and Cyanex 272 was prepared in a tank and transferred to the membrane contactor.

1. Introduction

The main sources of Ni and Co are located in Ni-Co laterites that contain around 2.5% and 0.15% of each metal, respectively [1]. Both metals are essential for the electronic industry responsible of manufacturing electrodes for lithium ion batteries [2]. Different types of stainless steels contain high quantities of nickel. As a result, as much as 65% of extracted nickel, is consumed in steel production [3]. Some types of steel, made for use in fuel cells are coated with cobalt [4]. Due to their increasing demand, raw metals begin to be insufficient to meet industry needs and therefore, it is crucial to promote the use of secondary materials after the convenient separation process. In this process metals are leached from solid wastes and then are separated from the pregnant leaching liquor to obtain pure products for further reuse. Solvent extraction (SX) allows obtaining high quality products from mixtures of nickel and cobalt, regardless the metal concentration in the solution [5].

For sulfuric waste solutions and pregnant leaching liquors of nickel and cobalt, some commercial extractants have been proposed, including 2-ethylhexyl phosphonic acid mono 2-ethylhexyl ester (PC-88A) [6], bis(2-ethylhexyl)phosphoric acid (D2EHPA) [7] and bis(2,4,4-trimethylpentyl)phosphinic acid (Cyanex 272) [8-10]. The latter currently finding the most interest. Looking for possibilities to reduce the costs of reagents, some synergistic mixtures of extractants have been proposed [11, 12].

2. Experimental

2.1 Materials

Cyanex 272 supplied by Cytec Industries (USA) was used as a metal carrier. Shellsol D70 supplied by Shell Chemicals was a diluent for the organic phase. Sodium hydroxide solutions

(5-10 M) were used to adjust the pH of feed mixtures at 5.2-5.5, which theoretically provides the maximum selectivity. 1 M sulfuric acid was employed as a stripping agent. Model sulfuric solutions were prepared by dissolving cobalt(II) and nickel(II) sulfates in deionized water. Real waste solution was obtained from stainless steel leaching industry. The hollow fiber membrane contactor used for the process was characterized by the parameters presented in Table 1.

Table 1. Parameters characterizing hollow fiber contactor Liqui-Cel (Celgard)

Parameter	Value/Description
Fiber material	Polypropylene
Shell material	Polypropylene
Type of fiber	X-50
Inner diameter (fibers)	240 µm
Thickness (fibers)	30 µm
Average pore size	0.03 µm
Porosity	40%
Effective length (fibers)	0.15 m
Effective membrane area	1.4 m^2
Number of fibers	10200

2.2 MBSX process

Membrane-based solvent extraction (MBSX) using a hollow fiber contactor with an effective membrane area of 1.4 m^2 has been analyzed as a way to improve the conventional SX process employed in the separation of nickel(II) and cobalt(II). This technology combines the advantages of SX, such as facilitated transport and selectivity, with the non-dispersive contact provided by polymeric hollow fibers. Solutions containing cobalt(II) and nickel(II) sulfates (3-15 g/L Co(II) and 3-25 g/L Ni(II)) were treated by MBSX using 0.6 M Cyanex 272 as selective extractant. 1 M solution of sulfuric acid was used as a stripping phase. A magnetic stirrer was used in the feed solution to ensure even distribution of the inflowing solution and added NaOH. A schematic view of the operation system is shown in Figure 1.

Two main issues were investigated: i) kinetics of cobalt(II) extraction and, ii) selectivity of the separation process that is essential to provide high quality products for their further recovery by electrowinning.

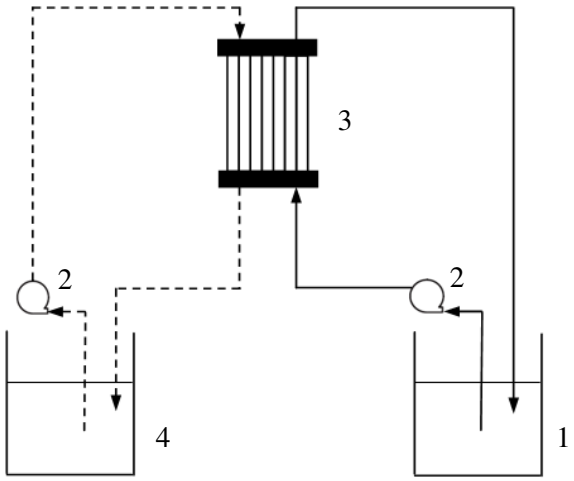

Figure 1. Schematic view of MBSX operation system. (1) Feed solution in the shell side, (2) pump, (3) hollow fiber membrane contactor, (4) organic phase or pseudo-emulsion (solutions of Cyanex 272 and H_2SO_4) in the tube side.

3. Results and Discussion

3.1 Extraction of cobalt and nickel

Preliminary results were obtained with synthetic solutions that contained around 2.5 g/L of cobalt and nickel. As depicted in Figure 2, after two hours of experimental running, cobalt extraction achieved yields above 95%. The extraction of nickel was in the range between 30-36% being this yield higher than the value theoretically expected (<20%) under the selected pH conditions. These differences might be initially attributed to two different reasons: i) the local pH increases as consequence of the non-instantaneous perfect mixing when NaOH was discontinuously dosed to the feed tank and, ii) the uncontrolled pH conditions in the membrane contactor.

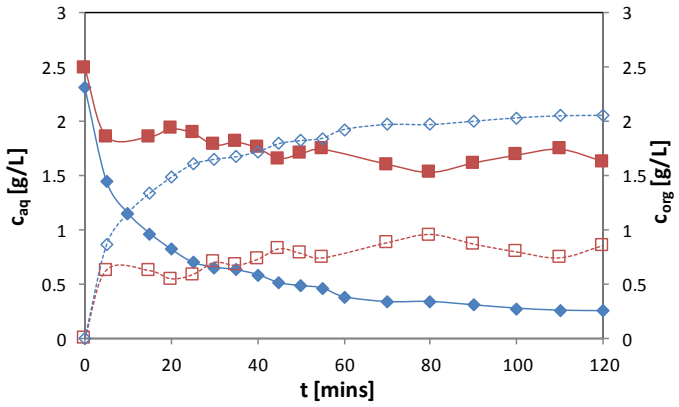

Figure 2. Evolution with time of (◊,♦) cobalt(II) and(□,■) nickel(II) concentration in the aqueous (continuous) and organic phase (discontinuous).

3.2 Influence of simultaneous back extraction

Simultaneous back extraction was conducted by introducing pseudo-emulsion of solutions of Cyanex 272 and sulfuric acid into the tube side of the membrane contactor. Pseudo-emulsion of

organic and stripping solution forms temporarily as long as the mixture is stirred. After stopping the stirrer, phases separates [13]. The volume ratio of organic to stripping phase was 5:1, thus, it allowed to concentrate the resulting aqueous solution. Figure 3 shows that simultaneous back extraction during the process allows to obtain higher yields of cobalt extraction. It also influences the kinetics of the process, which is then quicker than with back extraction conducted outside the system.

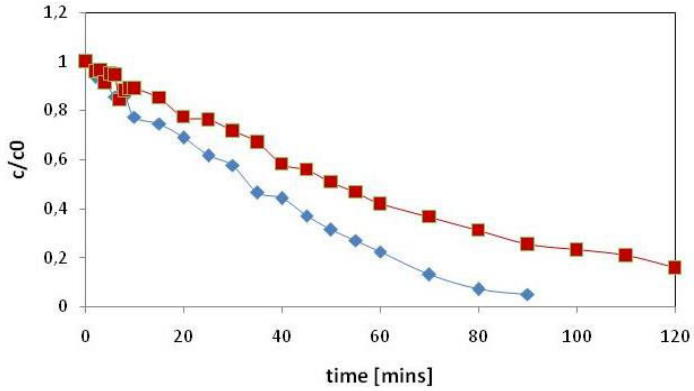

Figure 3. Evolution with time of cobalt(II) concentration in the aqueous solution. Process conducted (♦) with and (■) without simultaneous back extraction.

4. Conclusion

The preliminary results allow to conclude that MBSX ensures high efficiency and selectivity in the removal of cobalt from its sulfate solutions containing nickel(II). Further work will be focused on the improvement of pH controlling, the analysis of the back extraction stage and the evaluation of the stripping requirements to carry out the selective electrochemical recovery of cobalt. Back extraction included in the MBSX process reduces the time needed to achieve the limit of cobalt extraction. It also ensures constant regeneration of the organic phase, thus, influences positively selectivity, reducing co-extraction of nickel to less than 20%.

References

1) M. J. Cracknell, N. H. Jansen, *Aust. J. Earth Sci.*, **63**, 1053-1067 (2016).
2) X. Chen, Y. Chen, T. Zhou, D. Liu, H. Hu, S. Fan, *Waste Manage.*, **38**, 349-356 (2015).
3) B. K. Reck, V. S. Rotter, *J. Ind. Ecol*, **16** (4), 518-528 (2012).
4) H. Falk-Windisch, J. Claquesin, M. Sattari, J-E. Svensson, J. Froitzheim, *J. Power Sources*, **343**, 1-10 (2017).
5) B. Swain, S-S. Cho, G. H. Lee, C. G. Lee, S. Uhm, *Appl. Chem. Eng.*, **26**, 631-639 (2015).
6) V. T. Nguyen, J-C. Lee, J. Jeong, B-S. Kim, B. D. Pandey, *Met. Mater. Int.*, **20**, 357-365 (2014).
7) C. S. Sousa Jr., M. Nascimento, I. O. C. Masson, O. G. C. Cunha, *TMS Annual Meeting*, **1**, 309-316 (2011).
8) F. Xiao, Y. Wang, X. Shen, Z. Li, J. M. Perera, G. W. Stevens, *Hydrometallurgy*, **167**, 36-38 (2017).

9) M. Regel-Rosocka, K. Staszak, K. Wieszczycka, A. Masalska, *Clean Techn. Environ. Policy*, **18**, 1961-1970 (2016).
10) J. Hereijgers, T. Vandermeersch, N. Van Oeteren, T. Breugelmans, W. De Malsche, *Chem. Eng. Res. Des.*, **111**, 305-315 (2016).
11) C. Y. Cheng, K. R. Barnard, W. Zhang, Z. Zhu, Y. Pranolo, *Chinese J. Chem. Eng.*, **24**, 237-248 (2016).
12) D. Darvishi, D. F. Haghshenas, E. K. Alamdari, S. K. Sadrnezhaad, M. Halali, *Hydrometallurgy*, **77**, 227-238 (2005).
13) J. V. Sonavane, A. K. Pabby, A. M. Sastre, *AIChE J.*, **54** (2), 453-463 (2008).

Ethanol Modified Liquid Carbon Dioxide Extraction and Antioxidant Activity of Nobiletin and Tangeretin from Peels of *Citrus Poonensis*

Ryunosuke MITANI[1], Shinichi TOKUNAGA[1], Masashi HARAGUCHI[1], Kenji MISHIMA[1,2*], Tanjina SHARMIN[1,2], Miyuki NAKAMURA[1,2], Takafumi KATO[1], Makoto MISUMI[2], Tadashi SUETSUGU[2], Hideaki ORII[2], Keiichi IRIE[3], Tomomitsu SATHO[3], Takunori HARADA[4]

[1]Department of Chemical Engineering, Faculty of Engineering, Fukuoka University, 8-19-1, Nanakuma Jonan-ku, Fukuoka 814-0180, Japan, [2]Research Center of Composite Material, Fukuoka University, 8-19-1, Nanakuma Jonan-ku, Fukuoka 814-0180, Japan, [3]Faculty of Pharmaceutical Sciences, Fukuoka University, 8-19-1, Nanakuma, Jonan- ku, Fukuoka 814-0180, Japan, [4]Department of Applied Chemistry, Faculty of Engineering, Oita University, 700 Dannoharu Oita-shi, 870-1192, Japan

We extracted nobiletin and tangeretin from the dried peels of *Citrus Poonensis* (Ponkan) using ethanol modified liquid carbon dioxide (CO_2) and determined the best extraction condition. We conducted experiment under temperatures of 5, 20, and 25°C, pressures of 8, 10 and 14 MPa and different modifier (ethanol) mole fractions ($x_{ethanol}$ = 0, 0.06, 0.131, 0.262, 0.390 and 1) in the liquid CO_2 solution for 60 min extraction time. Furthermore, ultrasound with different irradiation power and supercritical CO_2 ($ScCO_2$, 31°C, 10 MPa) were also used for the comparison of the extraction yields of nobiletin and tangeretin. The highest nobiletin and tangeretin contents in dried Ponkan peels were achieved through the ethanol modified liquid CO_2 extraction condition at 25°C, 10 MPa, and mole fraction of ethanol in the liquid CO_2 solution (x_{EtOH} = 0.131) as well as $ScCO_2$ (31°C, 10 MPa).

1. Introduction

A number of citrus fruits are grown plenty in Japan. Most of the fruit is applied to juice processing and the peel has been disposed without any usage. However, these peels contain abundant amount of flavonoids. Methods for extracting flavonoids from citrus fruits have been carried out before. The most common method of them is using organic solvents. However, as many of these organic solvents are toxic and highly flammable, we must be taken to ensure that the solvent applied for the extraction is safe and eco-friendly. Also, the attention should be paid on the disposing of waste which has huge impact on natural environment. Regarding these, nowadays, an extraction method using liquid CO_2 is attracted. CO_2 is biologically friendly, and there is no risk of residual solvents like using harmful organic solvents. Alike other citrus fruits in japan, Ponkan (Citrus poonensis) is one of the high-yield sweet citrus. In this study, dried peels of Ponkan was used as a raw material to extract nobiletin and tangeretin which are expected to have anti-allergic properties by using liquid CO_2. Also the effect of the operating conditions on the extract yield was checked using the single-factor method.

2. Experimental

2.1 Reagents

Ponkan fruits were purchased from local markets in Fukuoka, and the peels dried at room temperature, and ground into a fine powder by using a freezer mill 6750 (SPEX CentriPrep Co. Ltd., New Jersey, USA). Nobiletin with purities >97 wt% were purchased from Sigma-Aldrich, Co, Japan. Tangeretin with purities >95.0 wt% were purchased from Tokyo Chemical Industry Co, Ltd, Japan.

2.2 Apparatus and Procedure

A schematic diagram of the experimental apparatus used for the liquid CO_2 extractions with or without ultrasonic irradiation is shown in Figure 1. The prepared peel powders were placed in an extraction cell (a high-pressure cell) of a liquid CO_2 mixture extraction apparatus (SFC; super200, JASCO Co. Ltd.). The extraction cell was approximately 150 cm3 in volume. The system pressure was controlled by a back-pressure regulator (880-81, JASCO, accurate to 0.1 MPa) and monitored by a digital pressure gauge (Shinwa Electronics Co., model DD-501, accuracy ± 0.3%). The temperature was controlled within ± 0.1 ºC with a water bath. The temperature of the water bath was maintained at 5, 20 and 25 ºC. The optimisation process was conducted under temperatures of 5, 20, and 25°C, pressures of 8, 10 and 14 MPa and different modifier (ethanol) mole fractions (xehanol = 0, 0.06, 0.131, 0.262, 0.393 and 1) in the liquid CO_2 solution for 60 min extraction time. Furthermore, ultrasound with different irradiation power and scCO_2 were used for the comparison of the extraction yields of nobiletin and tangeretin. Finally, the antioxidant activities were evaluated using the quenching activity of the free chromogenic radical, 2,2-diphenyl-1-picrylhydrazyl (DPPH) assay.

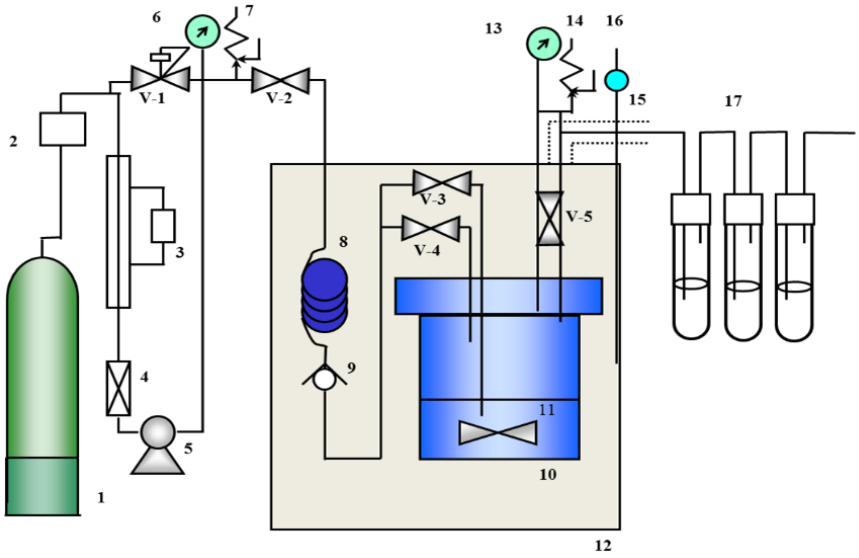

Figure 1. A schematic diagram of the experimental apparatus used for the liquid CO_2 extractions 1: gas cylinder, 2: dryer, 3: cooling unit, 4: filter, 5: pump, 6: pressure gauge, 7: safety valve, 8: preheating piping, 9: stopper, 10: high-pressure cell, 11: stirrer, 12: water bath, 13: pressure gauge, 14: safety valve, 15: heater, 16: thermometer, 17: trap, V-1: back pressure, and V-2–V-5: stop valves.

2.3 HPLC Analysis

The HPLC system consisted of a Tosoh LC-8010 system equipped with a UV detector. The detection wavelength was set at 343 nm and 40°C. Separation of the extract was performed at 40°C and at 1.0 mL/min flow rate. Methanol and 0.1% acetic acid in water were used during the separations. The methanol gradient profile is presented in Table 1.

Table 1. Time course of methanol gradient for HPLC analysis.

Time [min]	0	25	40	50	60	65	75
Methanol [vol%]	5	40	60	90	90	5	5

3. Results and Discussion

The solvent extraction behavior of nobiletin and tangeretin from the Ponkan peel powder was examined using methanol or ethanol at 25 ºC and extraction was performed at several time points. Qualitative and quantitative information was obtained via HPLC. It was found that the mass of extract of isovitexin generally increased over 0-60 min and were then saturated. Therefore, the appropriate time of treatment was set at approximately 60 min.

The effect of three operating parameters, temperature, pressure and the mole fraction of ethanol in a solution of CO_2, on the extraction yield was investigated. The effect of temperature and pressure on the extraction yield is shown in Figure 2. In general, the extraction yield clearly increased with increasing temperature or pressure at a constant temperature or pressure. The yields of both nobiletin and tangeretin are found to be the highest at 25 ºC and at 10 or 14 MPa. For these experimental conditions, the solvent molecular activity induced by the temperature is considered to be more predominant than that induced by the solvent density.

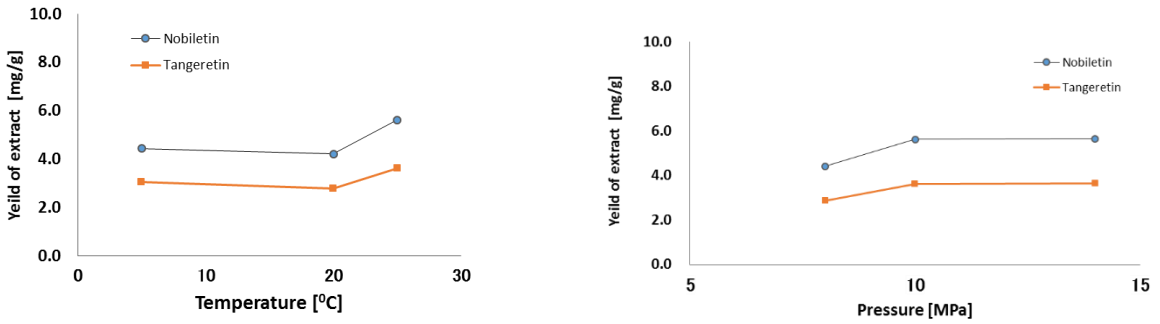

Figure 2. Temperature and pressure dependence of the extract yields using mixtures of liquid CO_2 and ethanol (ethanol mole fraction $x_{ethanol}$=0.131)

To elucidate the effect of changing the mole fraction of ethanol over liquid CO_2 (x_{EtOH}) on the yield, we performed the extraction by using ethanol and liquid CO_2 either solely or in combination. The pressure was set at 10 MPa, the temperature was set at 25ºC, and the extraction was performed for 60 min. The maximum yield was obtained at x_{EtOH} = 0.131. This result implies that lower or higher mole fractions of ethanol reduce the yield.

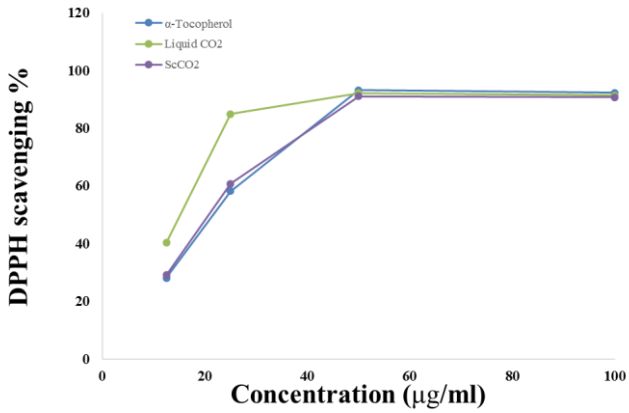

Figure 3. Comparison of the antioxidant activities of the extracts using DPPH

Finally, the antioxidant activities of the extracts were measured and the ethanol modified liquid CO_2 extract exhibited the highest scavenging activity of DPPH free radicals compared with α-Tocopherol (Figure 3). The presence of these activities is attributed to the flavonoid compounds such as nobiletin and tangeretin, revealed in HPLC.

4. Conclusion

Nobiletin and tangeretin were successfully extracted from Ponkan peels using mixtures of liquid CO_2 and ethanol. The yields of nobiletin and tangeretin in the liquid CO_2 extraction were improved by adjusting the operating temperature and pressure (25 ºC, 10 MPa), and mole fraction of ethanol in the liquid CO_2 solution (xethanol = 0.131). Furthermore, ethanol modified liquid CO_2 extract have considerable antioxidant activities value with respect to that of α-Tocopherol. Therefore, our results suggested that the ethanol modified liquid CO_2 extracts can be utilized as an effective and safe antioxidant source in the drug development.

Acknowledgement

This study was supported by the Grant-in-Aid for Scientific Research (No.17K06899 and No.160082) of The Ministry of Education, Science, Sports and Culture of Japan and the Japan Food Chemical Research Foundation, respectively.

References

1) K. Mishima, T. Tokuyasu, K. Matsuyama, N. Komorita, T. Enjoji, M. Nagatani, Fluid Phase Equilib. 144, 299–305 (1998).
2) K. Mishima, S. Yamauchi, M. Ito, M. Ezawa, D. Tanabe, Solvent Extr. Res. Dev., Jpn. 6, 176–181 (1999).
3) Y-H Lee, A. L. Charles, H-F. Kung, C-T. Ho, T-C. Huang, Industrial Crops and Products 31, 59–64 (2010).

Recovery of Copper and Cobalt Contained in a Residue of a Zinc Electrolytic Refinery, and the Synthesis of Semiconductor Nanoparticles

María Guadalupe SÁNCHEZ-LOREDO[1,*], Xóchitl María MACÍAS-RODRÍGUEZ[1], Gladis Judith LABRADA-DELGADO[2], and Zeferino GAMINO-ARROYO[3]

[1]Instituto de Metalurgia/Facultad de Ingeniería, Universidad Autónoma de San Luis Potosí, Sierra Leona 550, 78210 San Luis Potosí; [2]LINAN, Instituto Potosino de Investigación Científica y Tecnológica, Camino a la Presa San José 2055, 78216 San Luis Potosí, [3] Departamento de Ingeniería Química, Universidad de Guanajuato, Noria Alta S/N, 36050 Guanajuato, México

In the hydrometallurgical process for the recovery of zinc, by-products containing elements of interest and economic value are obtained. They are used for further metal recovery, or confined in tailing ponds. In the Zinc Electrolytic Plant in San Luis Potosí, in the various stages of purification, secondary products rich in copper, cobalt and zinc are generated. Particularly the copper cement, by now sold to a copper refining plant, contains mainly copper, but also cobalt in small quantity. In this work, the feasibility of a leach/solvent extraction process for recovery of copper and cobalt from the cement was considered. After stripping, nanoparticles were obtained and characterized.

1. Introduction

More than 80% of the world's zinc production is obtained from zinc sulphide concentrates by the Roasting-Leaching-Purification-Electrolysis process. This process is the main base of operation of the Zinc Electrolytic Plant of Grupo México, S.A. de C.V., in San Luis Potosí, Mexico, which processes more than 200,000 tons of sphalerite (ZnS), with a total zinc recovery of approximately 94.5% [1]. Metal-rich solutions and solids such as jarosite, lead-silver residues, cadmium and copper cements are obtained as by-products. In the stage where the copper cement is obtained, arsenic trioxide and zinc powder are added for precipitation of the prevailing copper and cobalt.

In order to recover metals from residues and by-products, the first step is usually the chemical and mineralogical characterization of the solid, to find out if a washing step with hot water could aid the solubilisation of the desired ions. Otherwise, for dissolving more material, a leaching step using acid solutions at low concentration can be carried out. After that, one of the easiest and more efficient ways to perform the separation and purification of valuable species is the solvent extraction process.

Aldoximes are characterized by their high Cu^{2+} loading capacity, with low affinity for Fe^{3+}. A line of products widely used for copper extraction is Acorga® (Cytec Co.), among them Acorga®M5774 is a well-known reagent for extraction of copper ions [2,3]. On the other hand, the extractant bis(2,4,4-trimethylpentyl)phosphinic acid (Cyanex®272), has a high affinity for Co^{2+}. It has been used for Co^{2+} and Ni^{2+} separation, and was previously used by some of us for the separation of zinc and cadmium [4]. Cobalt extraction takes place at pH≈4, but in solutions containing other metal

ions also susceptible to extraction with Cyanex®272, such as zinc, copper, manganese, cadmium, nickel or magnesium, the extraction is carried out at pH greater than or equal to 6 [5-8].

A nanoparticle is a fundamental component in the manufacture of advanced materials, and its size ranges from 1 to 100 nm. Nanoparticles have different physical and chemical properties compared to the bulk material. The synthesis and modular assembly of nanoparticles allows to exploit their unique properties, leading to new applications in catalysis, electronics, photonics, magnetism, as well as chemical and biological sensors [9-11]. Copper sulphides (Cu_xS_y) nanoparticles are used in the solar cell industry, as superionic conductors, photodetectors, electroconductive electrodes, photothermal conversion devices, gas sensors, etc. They have two different colours, depending on the chemical composition: emerald green in the case of CuS, and reddish brown for Cu_2S [12-14]. The cobalt sulphides family comprises CoS, CoS_2, Co_3S_4, and $Co_{1-x}S_x$ (synthetic material). Cobalt sulphides are used as catalysts in hydrodesulphurization, as part of the cathode in rechargeable lithium batteries, and have been used in electrodes in solar cells, photodetectors and biological labelling [15-18].

In this work, the recovery of cobalt from the copper cement by solubilizing the metal in a washing step is reported, as well as the separation of copper by acid leaching. Both metals were recovered from the aqueous solution using solvent extraction and acid stripping, and the strip solutions were used to synthesize metal sulphide nanoparticles.

2. Experimental

2.1 Reagents

Acorga®M5774 and Cyanex®272 were kindly provided by Cytec Solvay Group. The diluent, Exxsol™ D60, was supplied by Exxon Mobil Co. The copper cement was obtained from the Zinc Electrolytic Plant in San Luis Potosí. Other reagents were analytical-grade reagents.

2.2 Characterization and treatment of the copper cement

The copper cement was analysed by X-ray diffraction (XRD, X-ray Diffractometer Bruker D8) and inductively coupled plasma optical emission spectrometry (ICP- OES Varian 730-ES at IPICyT).

Washing and leaching steps: A mixture of cement (30 g) and deionized water (100 mL) was heated under stirring at 50 °C, for 10 min. The soluble fraction was transferred into solution (solution **S1**). To recover the copper present in the industrial solid, 30 g copper cement was contacted with 1 M H_2SO_4 (100 mL), heated to 65 °C under stirring for 10 min, and filtered (solution **S2**).

2.3 Extraction of cobalt and copper ions

Cobalt extraction was carried out using the **S1** solution and Cyanex®272 (20% in Exxsol™ D60, equilibrium pH values from 1 to 7), and the copper extraction (pH=2) was carried out using the **S2** solution and Acorga®M5774 (20% in Exxsol™ D60). The O/A ratio was 1:1. Counter current experiments with four stages were performed for cobalt in a system of mixers-settlers with size of 3.8×23.3×6.5 cm, stirring section of 3.8×3.8×6.5 cm (equilibrium pH 5.5). To control flows, pumps and valves were used. The metals contained in the organic phases were recovered by contacting with an equal volume of 1 M H_2SO_4.

2.4 Synthesis and characterization of the nanoparticles

For the synthesis of Co_xS and CuS nanoparticles, an aliquot of 3 mL of the stripping solutions

were added dropwise to 2 M ammonium sulphide solution, containing 2% polyvinylpyrrolidone (PVP) as a stabilizer, all of these in a volume ratio 1:1 and under sonication. The powders were washed with water and acetone and characterized using XRD and scanning electron microscopy (SEM FIB Helios Nanolab at IPICyT, San Luis Potosí).

3. Results and Discussion

3.1 Characterization and treatment of copper cement

The residue, according to the X-ray diffraction, contains metallic copper, identified by the card 01-070-3038, cuprite (Cu_2O, 00-005-0667), anglesite ($PbSO_4$, 00-001-0867), as well as arsenolamprite (As°), identified using the card 00-029-0142. The Rietveld structure refinement was performed using the TOPAS software, the cuprite content was found to be 57.4%, Cu° 38.3%, anglesite 2.3% and arsenolamprite 1.97% (Figure 1). Due to the low content, the technique was not able to identify cobalt. During the quantification performed by acid digestion and using ICP-OES, copper was found to be 51.6% of the total mass, cobalt 0.76%, arsenic 4.4%, and zinc 3.0%.

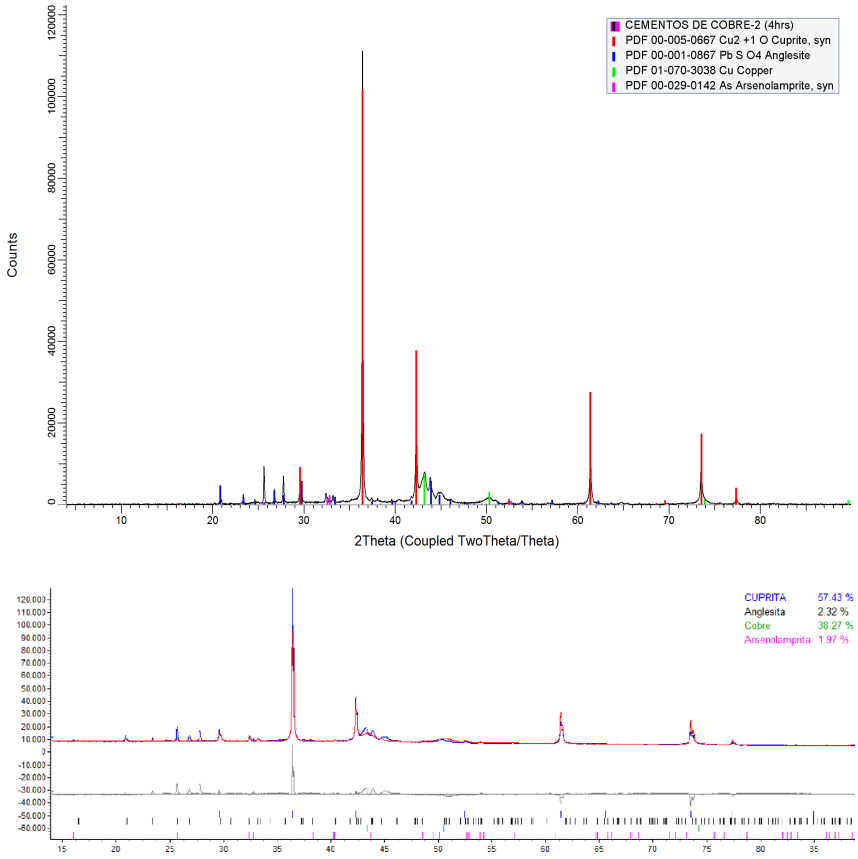

Figure 1. X-ray diffraction and Rietveld refinement of copper cement

After a wash step with hot water, the chemical analysis of the solution **S1** (pH=3.4), showed that it contains mainly cobalt (1034.4 mg/L) and copper (2078 mg/L), as well as small amounts of cadmium, zinc and arsenic (98.8, 35.80 and 1.6 mg/L, respectively). By acid leaching of the cement, solution **S2** was obtained. The metal content was: cobalt (1187.2 mg/L), copper (31.67 g/L), cadmium (108.6 mg/L), zinc (136.3 mg/L) and arsenic (87.4 mg/L).

3.2 Extraction of cobalt and copper ions

Extraction tests at several pH values (from pH 1 to 7) were carried out using **S1** and Cyanex®272. The highest extraction values for cobalt were reached at pH>6, where the metal is extracted almost completely (98.6 %). Experiments were carried out in order to obtain the extraction

isotherm (Figure 2), and to calculate the O/A ratio for the countercurrent extraction tests (equilibrium pH 5.5), which turned out to be 1.3. For the system, a volume of 50 mL was considered, and therefore, the calculated flow for the organic phase was 8.7 mL/s, and for the aqueous phase 11.3 mL/s. The efficiency of the countercurrent cobalt extraction was calculated performing a mass balance by analyzing the amount of cobalt present in the charged organic and the raffinate. The stripping was performed using a concentrated solution of H_2SO_4, and the cobalt concentration was determined. According to the isotherm, the theoretical extraction of cobalt should be 99.9%, but the experimental one in the countercurrent experiments was 92.6%, and the zinc extraction 10.44 %.

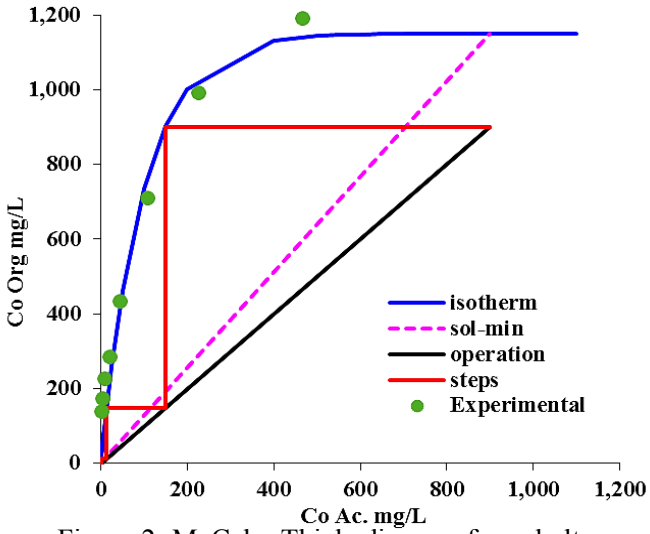

Figure 2: McCabe-Thiele diagram for cobalt extraction from solution **S1** with Cyanex®272 (20% in Exxsol^{TM} D60, equilibrium pH 5.5, 300 s)

As the copper concentration in liquor **S2** was high, copper extraction in a single step was performed (A/O ratio 1:3.5). In this way 99.9% of the copper was extracted, and an organic phase with a concentration of 9048.8 mg/L Cu^{2+} was obtained. The metal was recovered from the organic phase using sulfuric acid, and the both strip solutions were used for the preparation of nanoparticles.

3.3 Synthesis and characterization of the nanoparticles

After precipitation of the sparingly soluble metal sulfides from the stripping solutions, the nanoparticles were characterized using FESEM and XRD (Figure 3). Cobalt sulfide particles are well dispersed and had a size distribution varying from 2 to 20 nm in diameter, with 70% of the particles in the range of 4-10 nm. Characterization using XRD was uncertain because of the amorphous nature of the precipitate, but a possibility is the presence of cattierite (CoS_2, card 01-089-1493), and silica (a compound which can be extracted by the organic phase if present in the feed liquor in the form of colloidal particles) identified with the card 00-001-0357. Even though the presence of silica or other colloidal materials could represent a problem in liquid-liquid extraction since the formation of sludge occurs, the system did not show the formation of emulsions or cruds.

The size range of the copper sulfide nanoparticles varied from 2 to 14 nm, the 70% of the nanoparticles was between 4-9 nm in size. The particles seemed to be agglomerated, but this probably happened during the drying of the sample holder. The diffractogram of the copper sulfide particles showed a crystalline phase identified as copper sulfide ($Cu_{1.8}S$, card 01-089-2073), and covellite (CuS, card 00-001-1281). There is a slight displacement of the peaks because the texture of the sample and also an important peak broadening due to the small size of the crystallites.

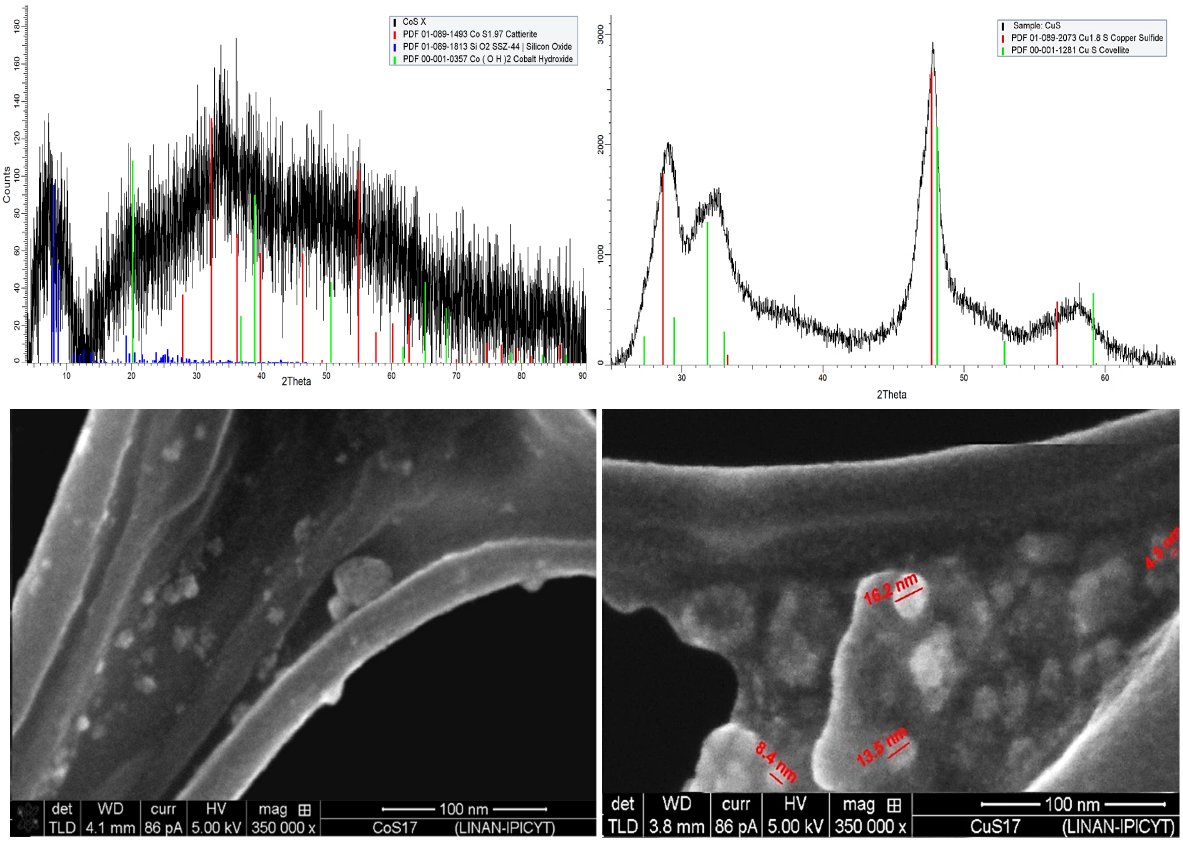

Figure 3: Diffractogram and image of: left, CoS nanoparticles, and right, Cu_xS nanoparticles

4. Conclusion

In this work, most of the cobalt present in the copper cement was obtained by a wash step with water at 50°C, and the charged liquor entered directly to the solvent extraction process, performed at pH=5.5. The efficiency of the counter current extraction was 92.6%. Copper was recovered by acid leaching and the metal was extracted using an organic to aqueous volume ratio of 3.5 to 1 in a single step, with an efficiency of 99.9%. Acidic stripping and a precipitation process allowed the preparation of dispersed nanoparticles of cobalt sulfide (4-10 nm), and copper sulfide (2-14 nm).

Acknowledgements

Xóchitl Macías is grateful to CONACYT for the postgraduate grant. This work was supported by the Fondo Sectorial de Investigación SER-CONACYT México-Argentina de Proyectos Conjuntos en Nanotecnología 2012-13, 191145 “Recuperación de metales de efluentes metalúrgicos para preparar materiales nanométricos, y su uso en sensores ambientales”. We thank Rosa Lina Tovar for the XRD support and Dr. Daniel Bien (Exxon Mobil Co.) for the useful advice and the diluent samples.

References

1) I.M.M.S.A. de C.V., Superintendencia de Área Húmeda, “Manual general del área húmeda”, San Luis Potosí (2013).

2) K. C. Sole, A. M. Feather, P. M. Cole, *Hydromet.*, **78**(1–2) 52–78 (2005).
3) K. C. Sole, M. D. Soderstrom, O. Tinkler, K. Viljoen, B. K. Ferreira, L. Hoffmann, *Can. Metall. Q.*, **47**(3), 285–292 (2008).
4) Xóchitl Macías Rodríguez, Tésis, Universidad de Guanajuato (2015).
5) A. S. Guimarães, P. S. Da Silva, M. B. Mansur, *Hydromet.*, **150**, 173–177 (2014).
6) P. K. Parhi, K. Sarangi, *Sep. Purif. Technol.*, 59(2), 169–174 (2008).
7) R. K. Mishra, P. C. Rout, K. Sarangi, K. C. Natsarma, *Trans. Nonferrous Met. Soc. China*, **26**(1), 301–309 (2016).
8) A. A. Nayl, I. M. Ahmed, M. I. Aly, *Sep. Sci. Technol.*, **49**(2), 290–297 (2014).
9) C. Burda, X. Chen, R. Narayanan, M. A. El-Sayed, *Chem. Rev.*, **105**, 1025–1102 (2005).
10) C. N. R. Rao, A. Müller, A. K. Cheetham, *The Chemistry of Nanomaterials: Synthesis. Properties and Applications*. Wiley-VCH Verlag GmbH & Co., Weinheim, 2004.
11) N. T. K. Thanh, N. Maclean, S. Mahiddine, *Chem. Rev.*, **114**(15), 7610–7630 (2014).
12) X. Rui, H. Tan, Q. Yan, *Nanoscale*, **6**, 9889-9924 (2014).
13) Y. Li, W. Lu, Q. Huang, M. Huang, C. Li, W. Chen, *Nanomedicine*, **5**(8), 1161–1171 (2010).
14) D. H. Ha, A. H. Caldwell, M. J. Ward, S. Honrao, K. Mathew, R. Hovden, M. K. A. Koker, D. A. Muller, R. G. Hennig, R. D. Robinson, *Nano Lett.*, 14(12), 7090–7099 (2014).
15) B. Qu, Y. Chen, M. Zhang, L. Hu, D. Lei, B. Lu, Q. Li, Y. Wang, L. Chen, T. Wang, *Nanoscale*, **4**, 7810-7816 (2012).
16) J. Wang, S. H. Ng, G. X. Wang, J. Chen, L. Zhao, Y. Chen, H. K. Liu, *J. Power Sources*, **159**(1), 287–290 (2006).
17) J. Huo, M. Zheng, Y. Tu, J. Wu, L. Hu, S. Dai, *Electrochim. Acta*, **159**, 166–173 (2015).
18) N. Rumale, S. Arbuj, G. Umarji, M. Shinde, U. Mulik, A. Pokle, D. Amalnerkar, Phys. Status Solidi A, **210**(2), 345–348 (2013).

Controlled Architecture of Glass Fiber/Poly(Glycidyl Methacrylate) Composites via Surface-initiated ICAR ATRP Mediated by Mussel-Inspired Polydopamine Chemistry for Lithium Isotopes Separation

Wenqing WANG[1*], Paziliya JULAITI[1], Gang YE[1], Xiaomei HUO[1] and Jing CHEN[1]

[1] *Collaborative Innovation Center of Advanced Nuclear Energy Technology, Institute of Nuclear and New Energy Technology, Tsinghua University, Beijing, 100084, China*

A new material system, consist of glass fiber/poly(glycidyl methacrylate) composites, was synthesized by integrating surface-initiated atom transfer radical polymerization (SI-ATRP) technique with the mussel-inspired polydopamine (PDA) chemistry. The homogenous PDA layer deposited onto the glass fiber mats (GFMs) facilitated the anchoring of ATRP initiators and controlled growth of poly(glycidyl methacrylate) (PGMA) brushes from the GFMs were then performed by the initiators for continuous activator regeneration (ICAR) ATRP method. Post functionality for GF/PGMA composite (GFPGMAC) was realized by nucleophilic substitution of the abundant epoxy groups and 4'-aminobenzo-15-crown-5 (B15C5). Lithium isotopes separation by GFPGMAC-B15C5 exhibited a maximum adsorption capacity of 6.46 mg g^{-1} and separation factor was 1.307±0.002 in optimal experimental conditions.

1. Introduction

The separation of lithium isotopes has been attracted much attention due to the need for isolated and enriched ^{6}Li and ^{7}Li isotopes in nuclear fusion industry, which supply sufficient energy as well as cleaner production [1]. Normally, ^{6}Li is employed as the nuclear breeding materials in deuterium-tritium fusion power reactors while ^{7}Li is the most ideal heat transfer agent for fusion power reactor and neutral medium of thorium based fused salt reactor [2]. Owing to the same extra-nuclear structure, it is challenging for lithium isotope separation just relying on tiny mass differences. Among current methods, including electrophoresis, membrane, laser, ion exchange, solvent extraction, and chromatography, macrocyclic ligands and ionic liquid (IL) are two main promising candidate for efficient lithium isotope separation by using liquid-liquid extraction or column chromatography method [3-5]. To ameliorate the drawbacks for potential industrial scale utility inherent in the previous methods, such as water solubility, low mass transfer rate, the immobilization of lithium efficient extractants, i.e, crown ether and IL, onto solid supports was developed using a liquid–solid extraction method. Traditionally, porous materials, including mesoporous silica, resins, were chosen as solid support by physical impregnation or chemical grafting [6-8]. In the present study, macrocyclic ligands functionalized glass fiber/poly(glycidyl methacrylate) composites via surface-initiated ATRP [9,10] mediated by mussel-inspired polydopamine chemistry was prepared and the behavior for lithium isotopes separation was evaluated.

2. Experimental

2.1 Reagents

Nonwoven glass fiber mat with 7.0 *wt.*% polyvinyl alcohol (PVA) binder (Craneglass 230) was provided by Crane & Co. Inc (Dalton, MA). 4'-aminobenzo-15-crown-5 (NH_2-B15C5) was synthesized according to previous reports [11]. glycidyl methacrylate (GMA), ethyl 2-bromo-2-methylpropionate (EBiB), 2,2'-azobis(isobutyronitrile) (AIBN), trimethylamine (TEA) etc, were all purchased from J&K Scientific Ltd. (Beijing, China), as analytical-grade reagents. All the solvents, including N,N-Dimethylformamide (DMF), anisole, butylene oxide (THF), anisole, were of highest purity grade and provided by J&K Scientific Ltd. (Beijing, China).

2.2 Preparation of GFPGMAC-B15C5

Glass fiber mats (GFMs) were cut into ca. 2.0 × 1.0 cm pieces, and then added into 90.0 mL water/ethanol (*V:V*=4:3) mixture under magnetic stirring with determined amount of dopamine hydrochloride (pH=8.5, 10 mM) to prepare PDA coated GFMs. BiBB anchored GFMs@PDA were completed in an excess BiBB contained TEA/DMF mixture at room temperature. GFMs@PDA-Br was added in a 50 mL Schlenk flask, followed by adding 3.0 mL anisole, 3.0 mL GMA, 33.0 μL EBiB, 0.74 mL of 1.0 g L^{-1}AIBN/DMF sequentially. The reaction system was sealed and vacuum-argon inflation cycle was operated for several times. In argon protection, 1.0 mL of 1.0 g L^{-1} $CuBr_2$/TPMA (*wt*:*wt*=1:3) dissolved DMF mixture was added to flask through a syringe. The molecular ratio of the reagents was: [GMA]:[EBiB]:[macroinitiator]:[AIBN]:[$CuBr_2$]:[TPMA]=100:1:0.01:0.02:0.02:0.05. The prepared GF/PGMA composite (GFPGMAC) were post functionalized in NH_2-B15C5/DMF solution at concentration of 40 g L^{-1} at 70 ℃ for 6 h. The final product GFPGMAC-B15C5 was rinsed and dried.

2.3 Adsorptive separation of lithium isotopes

Adsorption of lithium was performed under batch mode. Typically, 10.0 mL of Li(I) aqueous solution with particular initial concentrations and pH values was added in a set of 20 mL glass conical flasks, followed by adding 3.0 mg GFPGMAC-B15C5. In a thermostatic oscillator, the mixture of Li(I) and GFPGMAC-B15C5 was agitated for a predetermined time interval. Adsorption capacity (q) was defined as follows,

$$q = \frac{(C_0 - C_e)\cdot V}{m} \times 1000 \qquad (1)$$

where q is the adsorption capacity for lithium, mg g^{-1}; C_0 and C_e are the initial and equilibrium Li(I) concentrations in aqueous phases respectively, mg L^{-1}; V is the volume of the solution, mL; m is the mass of the absorbent, mg.

Lithium isotopes separation was evaluated by the measurement of the lithium isotopes using High Resolution Inductively coupled plasma mass spectrometry (HRICP-MS). The single-stage separation factor (α) for $^6Li/^7Li$ was defined by Eq. (2). The subscripts 's' and 'l' represent the concentrations of lithium isotopes in solid phase and liquid phase, respectively.

$$\alpha = \frac{([^6Li]/[^7Li])_s}{([^6Li]/[^7Li])_l} \qquad (2)$$

3. Results and Discussion

3.1 Preparation of GFPGMAC-B15C5

The digital photos and SEM images for GFPGMAC and the counterparts in the synthesis were shown in Figure 1. Evidently, the morphology of GFMs made an obvious change and preserved the original mat form as well. After surface modification, a core-shell structure was observed, while the pristine fiberglass owned smooth cylindrical shape as the "core" and a polymer "shell" with thickness of 2.1 μm.

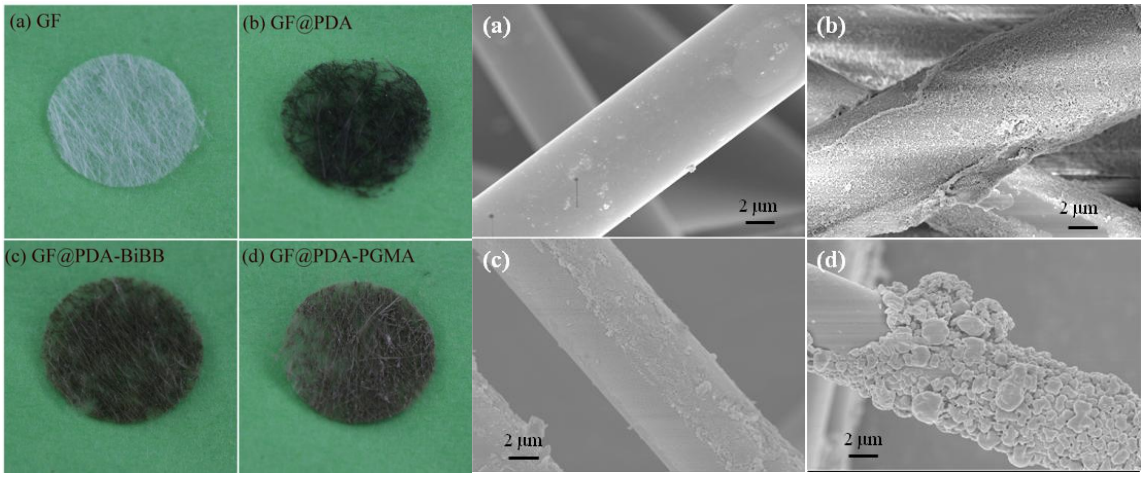

Figure 1. Morphology for GFPGMAC and the counterparts in SI-ATRP synthesis

Table 1 illustrated the compositional analysis results. From XPS analysis, it can be seen that, the carbon content increased with the introduction of organic components on the GFMs. Especially after the ATRP growth of PGMA brushes, *C* Atomic% increases from 52.12 % to 68.55%. For pristine GFMs, there was 13.08% Si content because of the main composition of glass fiber, SiO_2. When PDA coating was deposited onto GFMs, N content obviously increased for the contribution of the amino groups in PDA. After BiBB anchoring, an obvious peak at 76.85 eV could be recognized as the Br 3d adsorption peak, indicating the successful introduction of initiator BiBB with a Br content of 1.85%. Due to the abundant surface epoxy and ester group of GMA monomers, N atomic% relatively reduced but a slight increase (from 0.82% to 0.98%) after NH_2-B15C5 macrocyclic ligands grafted onto the composites' surface.

Table 1 Compositional analysis of the GFPGMAC-B15C5 and the counterparts

Samples	XPS Surface Atomic%				
	Si	Br	C	N	O
GFMs	13.08	Null	52.12	0.10	34.70
GFMs@PDA	2.88	0.06	68.96	7.21	20.89
GFMs@PDA-Br	5.22	1.85	61.21	6.17	25.55
GFPGMAC	Null	0.14	69.6	0.82	29.44
GFPGMAC-B15C5	Null	0.05	68.55	0.98	30.42

3.2 Adsorptive separation of lithium isotopes

Li(I) adsorption selectivity was investigated by static adsorption in Li(I) containing aqueous co-existence with other alkali metal ions, including Na(I), K(I) and Cs(I), at the same concentration of 100 mg g^{-1} in neutral pH and the results were shown in Figure 2a. As shown in Figure 2a, GFPGMAC-B15C5 exhibited selective binding ability towards Li(I) against the other alkali metal ions due to the matched ion size to the macrocyclic ligand diameter. The effect of counter ions for Li(I) uptake was also studied by dissolving different Li(I) salt, i.e, LiI, $LiNO_3$ and CF_3COOLi, into deionized water at Li(I) concentration of 100 mg g^{-1}. Apparently, the adsorption capacity showed an upward trend in the following order: CF_3COO^->NO_3^->I^-. It could be explained by the fact that softer ions have more affinity to organic solvent based on hard and soft acids and bases (HSAB) theory. Solvent influence was also studied by preparing Li(I) aqueous using three kinds of solvents, i.e., water, acetone and acetonitrile and Li(I) adsorption capacity was illustrated in Figure 2c. Li(I) adsorption capacity showed a decrease trend in the following order: acetone>water>acetonitrile. This result violated the previous study. Normally, in the solvents with lower dielectric constants were beneficial for cation, i.e., Li(I), desolvation, and then was helpful for ion mass transfer and adsorption onto solid phase. This results maybe contributed to the adsorbent properties, which against lithium isotope separation in pure liquid-liquid extraction system.

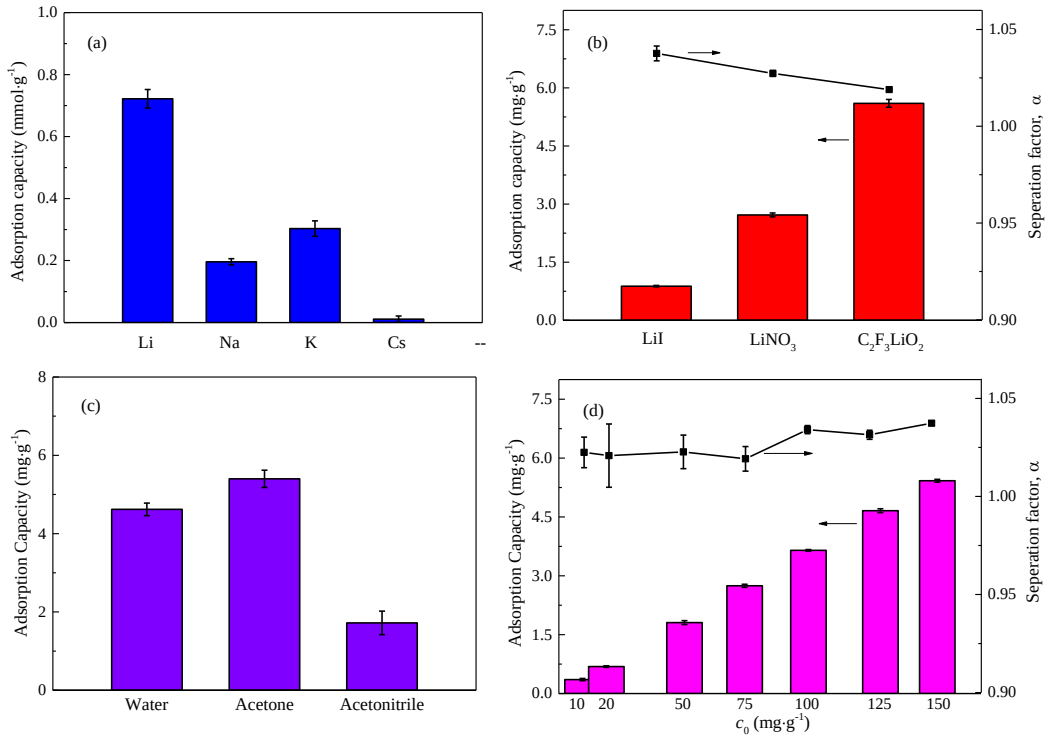

Figure 2. Adsorption and Seperation for ^{6}Li and ^{7}Li by GFPGMAC-B15C5 under different conditions: cations (a); anions (b); solvents (c) and concentrations (d)

Lithium isotope separation was also evaluated and the results were given in Figure 2b and 2d. Evidently, with the increasing of Li(I) concentration, Li(I) uptake and ^{6}Li and ^{7}Li separation factor increased with a maximum separation factor α of 1.037±0.002 in experimental conditions. Another

interesting finding was that the separation factor was counterintuitive to the Li(I) adsorption in different counter ions. The hypothesis was that counter ions would be exchanged to the macrocyclic ligands with the accompany of Li(I) but larger counter ions showed disadvantages for ^{6}Li and ^{7} Li exchange in a confined structured absorbent, leading to a reduced separation efficiency.

4. Conclusion

In this study, a new kind of material system, NH_2-B15C5 functionalized glass fiber/poly(glycidyl methacrylate) (GFPGMAC-B15C5), for lithium isotope separation was prepared using surface initiated ATRP strategy combined with protein inspired polydopamine chemistry. GFMs were considered as ideal support for crown ether stabilization due to their excellent erosion resistance, good strength and easy accessibility. Macrocyclic ligands immobilization was realized through surface initiated ATRP mediated by mussel-inspired PDA chemistry. The good control of PGMA brushes grown from the support, including defined molecular weight and polydispersity, could be beneficial for the post ligands grafting. The behavior of Li(I) uptake onto GFPGMAC-B15C5 and isotope separation was evaluated, in which softer counter ions were beneficial for Li(I) adsorption but separation efficiency inversely. Lithium isotope separation factor of 1.037±0.002 was achieved in optimal conditions. More importantly, this “grafting-from” methodology assisted by polydopamine chemistry opened a new avenue for some other macroscopic support surface modification/functionality for broaden application.

Acknowledgement

This study was financially supported by the Changjiang Scholars and Innovation Research Team in University (IRT13026), the National Science Fund for Distinguished Young Scholars (51425403), National Natural Science Foundation of China under Projects U1430234, 51673109, and 51473087.

References

1) J. R. Black, G. Umeda, B. Dunn, W. F. McDonough, A. Kavner, *J. Am. Chem. Soc.*, **131**, 9904-9905 (2009).
2) Y. A, K. Makhijani, MIT Press: Cambridge, MA, (2000).
3) T. Hoshino, T. Terai, *J. Nucl. Mater.*, **417**, 696-699 (2011).
4) M. Saleem, S. Hussain, M. A. Zia, M. A. Baig, *Applied Physics B*, **87**, 723-726 (2007).
5) A. Ishikawa, M. Sasaki, S. Narita, A. Takeuchi, H. Ohki, K. Yoshino, *Micropor. Mesopor. Mat.*, **248**, 115-121 (2017).
6) Y. Ban, M. Nomura, Y. Fujii, *J. Nucl. Sci. Technol.*, **39**, 279-281 (2002).
7) F. Yan, H. Liu, H. Pei, J. Li, Z. Cui, B. He, *J. Radioanal. Nucl. Ch.*, **311**, 2061-2068 (2017).
8) S. Fujine, K. Saito, K. Shiba, , **20**, 439 −440 (1983).
9) J. Wang, K. Matyjaszewski, *Macromolecules*, **28**, 7901-7910 (1995).
10) M. Kato, M. Kamigaito, M. Sawamoto, T. Higashimura, *Macromolecules*, **28**, 1721-1723 (1995).
11) R. Ungaro, B.E. Haj, J. Smid, *J. Am. Chem. Soc.*, **98**, 5198-5202 (1976).